공학박사 학위논문

Alternative Reinforcement Details for RC Moment Resisting Frames with Limited Ductility Demands

제한된 연성능력을 갖는 철근 콘크리트 모멘트 저항 골조의 대안 철근 상세

2017 년 8 월

서울대학교 대학원

건축학과

김 철 구

Alternative Reinforcement Details for RC Moment Resisting Frames with Limited Ductility Demands

지도교수 박 홍 근

이 논문을 공학박사 학위논문으로 제출함

2017 년 8 월

서울대학교 대학원
건축학과
김 철 구

김철구의 공학박사 학위논문을 인준함

2017 년 8 월

위 원 장 홍 성 걸 (인)

부위원장 박 홍 근 (인)

위 원 강 현 구 (인)

위 원 김 진 오 (인)

위 원 조 강 근 (인)

Abstract

Alternative Reinforcement Details for RC Moment Resisting Frames with Limited Ductility Demands

Kim, Chul-Goo
Department of Architecture and Architectural Engineering
College of Engineering
Seoul National University

Though low-rise buildings with two stories or less account for more than 80% of the total number of buildings in Korea, non-seismic details are generally used without any verification of seismic performance, leading to large earthquake damages in low-rise buildings. Under a Gyeongju earthquake in the magnitude of 5.8 on the Richter scale in September 12, 2016, the structural damages were mainly concentrated on low-rise buildings because the earthquake loading contained high frequency components. As the interest in seismic design of low-rise buildings increased after the earthquake, the enforcement ordinance of domestic Building Law for buildings subject to seismic design was revised in February 2017. The range of buildings for seismic design was changed from buildings more than three stories or gross area of 1000 m^2 to buildings more than two stories or gross area of 500 m^2.

In additions, either Korean Building Code (KBC 2016) for general buildings or Small Building Code for low-rise buildings can be applied for seismic design of low-rise buildings. The current Small Building Code have been established so that non-structural engineers can design reinforcing bar details without any structural calculation, and the details follow complex reinforcement details specified in KBC

2016. However, such complex bar details are not often observed in low-rise buildings because construction supervision is not carried out properly, and relieved non-seismic details are more preferred due to convenient bar placement. Thus, in this dissertation, in order to improve structural safety and construction efficiency of low-rise buildings, reinforcing bar details reflecting characteristics of low-rise buildings were developed, and seismic performance of various bar details was experimentally verified.

The main objective of this dissertation is to evaluate seismic performance and applicability of alternative reinforcing bar details in low-rise buildings. The alternative bar details were developed considering characteristics of low-rise buildings, which can ensure both construction efficiency and structural safety. A number of cyclic loading tests were performed to evaluate seismic performance of columns, beam-column connections, and two-story and two-bay frames. Seismic performance criteria of low-rise buildings were determined as a frame with limited ductility demand (Intermediate moment frame in KBC 2016 and ACI 318). For the comparison with the alternative details, seismic details specified in current seismic codes and non-seismic details used in construction fields without verification were also evaluated. Analytical models for columns and beam-column connections were also discussed. The main findings from experimental and analytical studies are as follows.

Since low-rise buildings generally exhibit a weak-column and strong-beam behavior, anchorage details and spacing of column transverse reinforcement are more significant in seismic performance of the buildings. Thus, seismic performance of column transverse bars with seismic, non-seismic, and alternative details was evaluated to conduct square and rectangular columns with various tie spacing (s = d/2, d/3, and d/4). According to test results, immediately after concrete cover spalling off, premature anchorage failure in 90º hooked and lap-spliced ties occurred, leading to relatively less ductility of columns when compared to the column with 135º hooked hoops. Also, since the shear strength of concrete V_c was gradually degraded as shear deformation increased, the shear strength V_n under inelastic deformation was significantly influenced by shear resistance of transverse reinforcement V_s. Based on this result, shear strength degradation model for columns was proposed and verified through a number of present and existing test data.

Furthermore, since lap splices of column bars are generally used in the bottom of columns where potential plastic hinges may form in low-rise buildings, adequate splice length and splice details of column bars are determined by considering seismic performance such as load and ductility capacities, and energy dissipations. Thus, reversed cyclic load tests of spliced columns were performed with various splice length ($l_s = 30d_b \sim 50d_b$) and details (Bottom offset bar splice, Top offset bar splice, and Splice without offset bend). In spliced column with $l_s = 50d_b$ satisfying ACI 318 requirement, the nominal flexural strength was attained with ductile behavior; however, when provided lap splice length was decreased to $40d_b$ or $30d_b$, inelastic deformations and energy dissipations of spliced columns were degraded due to early bond failure with severe splitting cracks along splice regions. Further, lap splice details also significantly affected seismic performance: Bottom offset bar splice showed lower flexural strength but greater ductility and energy dissipation with flexural failure mode; on the other hand, top offset bar slice and splice without offset bend showed greater flexural strength but lower ductility and energy dissipation with bond splitting failure. Since tensile stresses significantly vary along splice regions in columns, average bond demands of spliced bars decrease with increasing moment gradient. Thus, a modified lap splice length model for lap-spliced columns considering moment gradient along splice regions was proposed to reduce splice length required in current design codes. The reduced splice length correlated well with the present and existing cyclic test results of columns with lap splices.

In low-rise buildings with small sizes of columns and joints, insufficient shear capacity of joints without shear reinforcement has resulted in joint shear failure before adjacent beams and columns are subjected to flexural yielding. Also, since it is difficult to secure anchorage length of 90º hooked beam bars, attention should be paid to the joint reinforcement details. In this dissertation, cyclic load tests of beam-column connections with small effective joint area were conducted to investigate the effect of joint shear reinforcement ratio, anchorage length of beam bars, joint types (interior and exterior), and U shaped bars. The joint shear strength was increased proportionally with the increase of joint shear reinforcement ratio. However, when the anchorage length of beam bars was not secured, the joint shear strength was not proportional to joint shear reinforcement due to bond deterioration of beam bars. Based on present and existing test results of exterior joints with shear failure, shear strength model was empirically presented considering joint shear reinforcement ratio.

In order to evaluate the effect of anchorage directions of beam bottom bars on beam-column connection behaviors, exterior connections with only beam bottom bars bent away from the joints were compared to those with both top and bottom beam bars bent inside the joints. Since shear forces in exterior joints without shear reinforcement were transmitted only by a diagonal strut mechanism, the joint behaviors were affected by anchorage directions of beam bottom bars. On the other hand, joint shear forces in exterior joints with shear reinforcement are transferred by both a diagonal strut mechanism and a truss mechanism, so the effect of anchorage directions of beam bottom bars is not significant.

Finally, two-story and two-bay frame tests were performed to verify the applicability of reinforcing bar details verified by member tests, and to investigate the overall seismic behavior of low-rise buildings in system level. Seismic behavior and a role of a shear wall in a frame were also examined. In moment frames without a shear wall, plastic hinges were formed at both ends of 1st columns, leading to weak-column and strong-beam behaviors and bond failure with severe splitting cracks along splice regions. Exterior joints with U-bars showed satisfactory seismic performance. In a moment frame with a shear wall, on the other hand, sliding failure was occurred horizontally in the upper part of shear wall at top floor. In order to prevent such sliding failure, dowel reinforcement should be additionally provided between a wall and a beam (or a slab) to secure a sufficient shear friction strength.

Various member tests and frame tests were carried out to evaluate seismic performance of alternative bar details for low-rise buildings. Based on experimental results, analytical models for columns and exterior joints were developed. Also, for the newly revised Small Building Code, the design criteria and commentary on the alternative bar details in columns and beam-column joints are presented.

Keywords : Low-rise building; Alternative detail; Limited ductility;
Transverse reinforcement detail; Lap splice;
Joint shear reinforcement; Anchorage detail of beam bar;
Two-story and two-bay frame

Student Number : 2013-30931

Contents

List of Tables

List of Figures

List of Symbols

a	Shear span, equal to distance from center of concentrated load to face of support for cantilevered members, mm
A_{ch}	Cross-sectional area of a member measured to the outside edges of transverse reinforcement, mm^2
A_g	Gross area of concrete section, mm^2
A_j	Effective cross-sectional area within a joint, mm^2
A_{sh}	Total cross-sectional area of transverse reinforcement, mm^2
A_v	Area of shear reinforcement within spacing s, mm^2
b	Width of compression face of member, mm
b_c	Cross-sectional dimension of member core measured to the outside edges of the transverse reinforcement, mm
c_b	Lesser of (a) the distance from center of a bar to nearest concrete surface, and (b) one-half the center-to-center spacing of bars being developed, mm
C_s	Seismic response coefficient
d	Distance from extreme compression fiber to centroid of longitudinal tension reinforcement, mm
d_b	Nominal diameter of bar, mm
d_{bL}	Diameter of longitudinal bar, mm
d_{bT}	Diameter of transverse bar, mm
E_c	Modulus of elasticity of concrete, MPa

f_c'	Specified compressive strength of concrete, MPa
f_u	Ultimate strength for nonprestressed reinforcement, MPa
f_y	Specified yield strength for nonprestressed reinforcement, MPa
f_{yd}	Design value of yield strength of steel, MPa (EC8)
f_{yt}	Specified yield strength of transverse reinforcement, MPa
h	Overall height or depth of member, mm
h_b	Beam depth, mm
h_c	Column width, mm
h_{min}	Minimum column dimension, mm
h_x	Maximum center-to-center spacing of longitudinal bars, mm
H_o	Clear length of column, mm
I_E	Important factor for earthquake loading
I_g	Moment of inertia of gross concrete about centroidal axis, mm^4
K_{eff}	Effective stiffness of members, N/mm
K_{tr}	Transverse reinforcement index
l_{al}	Provided anchorage length of beam bars in exterior joints, mm
l_b	Length of beam from column centerline to the roller support, mm
l_c	Length of column from loading point to bottom hinge, mm
l_{dh}	Development length in tension of deformed bar with a standard hook from critical section, mm

l_o	Length measured from joint face along axis of member, over which special transverse reinforcement must be provided, mm
l_p	Anchorage length of reinforcement for bond stress, mm
l_s	Lap splice length, mm
l_{sm}	Modified lap splice length, mm
M_b	Applied moment at base, N-mm
M_{cr}	Cracking moment, N-mm
M_n	Nominal flexural strength at section, N-mm
M_{nb}	Nominal flexural strength of beam framing into joint, N-mm
M_{nc}	Nominal flexural strength of column framing into joint, N-mm
M_s	Applied moment at end of lap splices, N-mm
M_L	Richter local magnitude of earthquake
M_W	Moment magnitude of earthquake
N, N_d	Axial force, N
P_{nb}	Nominal joint shear strength due to beam flexural yielding, N
P_{nc}	Nominal joint shear strength due to column flexural yielding, N
P_{nc}^{C}	Nominal joint shear strength in conforming detail, N
P_{nc}^{NC}	Nominal joint shear strength in non-conforming detail, N
R	Response modification coefficient
s	Center-to-center spacing of transverse reinforcement, mm
S_{DS}	Design spectral acceleration at short periods

T	Fundamental period of a structure
T_b	Tensile force of a beam longitudinal bar at a peak load, N
u	bond stress, MPa
V	Base shear, N
V_c	Nominal shear strength provided by concrete, N
V_{jn}	Nominal joint shear strength, N
V_n	Nominal shear strength, N
V_p	Shear contribution of axial load, N
V_s	Nominal shear strength provided by shear reinforcement, N
V_u	Applied shear force at section, N
W	Total weight of a structure
δ	Drift ratio (= Δ / a)
δ_y	Yield drift ratio
δ_u	Ultimate drift ratio
Δ	Measured horizontal displacement, mm
Δ_f	Horizontal displacement by flexural deformation, mm
Δ_s	Horizontal displacement by shear deformation, mm
Δ_{sl}	Horizontal displacement by slip deformation, mm
Δ_y	Yield displacement, mm
Δ_u	Ultimate displacement, mm
ε_y	Yield strain of steel bars, mm/mm

θ_f	Rotation angle by flexure behavior
θ_s	Rotation angle by shear behavior
θ_{slip}	Rotation angle by bar slip
η	Reduction factor addressing decrease in concrete shear strength
μ	Ductility (= δ_u / δ_y) or coefficient of friction
ρ_b	Ratio of beam bottom reinforcement
ρ_j	Ratio of joint shear reinforcement
ρ_t	Ratio of beam top reinforcement
ρ_v	Ratio of tie reinforcement area to area of contact surface
ρ''	Volume ratio of joint shear reinforcement

Chapter 1. Introduction

1.1 Motivation of Research

Seismic safety requirements for low-rise buildings have been recently increased since a Gyeongju 912 earthquake in Korea with the magnitude M_L of 5.8 on Richter scale (moment magnitude M_W of 5.4) occurred in September 12, 2016 (See Figure 1-1). The Gyeongju earthquake included high frequency components, resulting in much damage to low-rise buildings compared to middle- and high-rise buildings. As the low-rise buildings (one or two story buildings) were not mandatory to apply seismic design under the domestic Building Law and Korean Building Code, most low-rise buildings had been designed by general architects, not structural engineers, without the verification of structural safety under earthquake. After Gyeongju earthquake, the enforcement decree of the Building Law was revised to target buildings higher than two stories or greater than a total area of 500 m^2, which should be built considering seismic design codes in February 4, 2017.

In the study of Lee et al. (2016), under the Gyeongju earthquake, required yield strengths of structures were increased in the short period zone less than 0.2 sec. In particular, low-rise buildings with low ductility demand (μ = 1.5 and 2.0) required higher strength under Gyeongju earthquake, when compared to El Centro earthquake (M_w = 6.9). This indicated that the Gyeongju earthquake, in which the energy of the seismic wave was concentrated in the high frequency band, could cause serious damage to the low-rise buildings where low ductility demand is required in general. Thus, seismic design codes for low-rise buildings need to be revised in order to enhance structural safety.

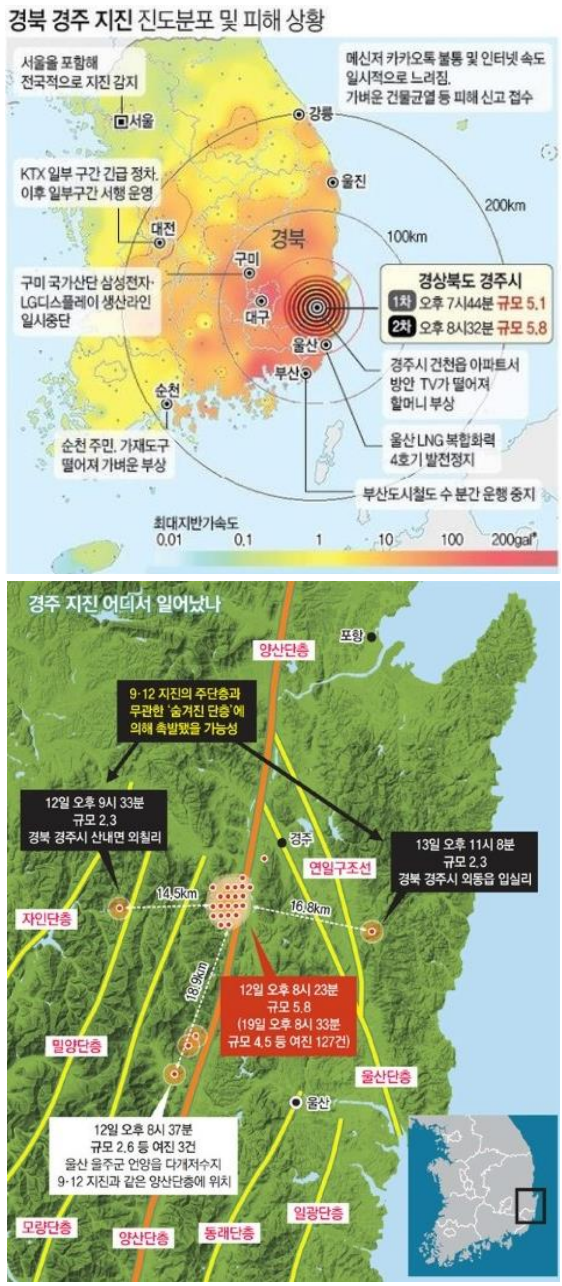

Figure 1-1 Gyeongju 912 earthquake in Korea with the magnitude of 5.8 on Richter scale

1.2 Characteristic of Low-rise Buildings

Seismic design codes should be developed considering characteristics of low-rise buildings. Since the current seismic design codes are primarily established to secure the seismic safety of middle- and high-rise buildings, it is difficult to be directly applied to low-rise buildings. In other words, if seismic design of low-rise buildings is carried out using the current design codes, structure members in the buildings can be overdesigned, resulting in reducing economy and construction efficiency. Therefore, the seismic design code for low-rise buildings should be developed considering following characteristics of low-rise buildings.

1) Since relatively low gravity load is applied in low-rise buildings, column elements are designed to be smaller than beam elements. Thus, the low-rise buildings are subjected to weak-column and strong-beam behavior under earthquake as shown in Figure 1-2(a) and (b). Under such behavior, as plastic hinges can be formed at both ends of columns, more attention should be paid to the reinforcing bar details of columns. Further, because of low axial load applied in columns, columns are designed to prevent brittle shear failure rather than loss of axial load carrying capacity after the formation of plastic hinges at columns.

2) Under weak-column and strong-beam behavior in low-rise buildings, plastic hinges are scarcely formed in beam ends; thus, reinforcing bar details used in beams can be relieved compared to requirements in current seismic design codes.

3) For convenient bar placements in construction fields of low-rise buildings, various reinforcing bar details are used, even not specified in seismic design codes. For instance, transverse reinforcements with non-seismic details (Figure 1-2(c)) are used as shear reinforcements in columns, and lap splices of column longitudinal bars are applied to the bottom of columns where plastic hinges are expected (Figure 1-2(d)). Such non-seismic members may have lower seismic performance (strength and deformation capacities) than those designed by seismic design codes.

4) Since a beam-column joint in a RC frame is a primary member that transmits moment and shear forces between adjacent beams and columns, sufficient strength and deformation capacities should be secured in the joint. However, joint

shear reinforcement is hardly used in low-rise buildings due to difficult bar placement and steel congestion in beam-column joint regions. If shear reinforcement is not provided in the joint, force transfer mechanism is quickly lost, resulting in brittle shear failure in the joint as shown in Figure 1-2(e) and collapse of an entire structure under earthquake. In low-rise buildings, joint shear reinforcement is very significant for satisfactory seismic performance.

5) In low-rise buildings, shear walls are generally used for perimeter walls excluding an entrance, and space partitions in residential buildings. Shear walls can resist most of lateral forces due to their high stiffness; thus, reinforcement details of beams and columns in the frame can be relieved when shear walls are used in a frame structure.

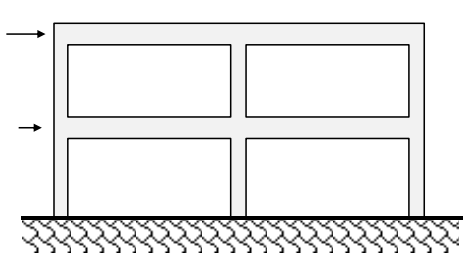

(a) A two story moment frame

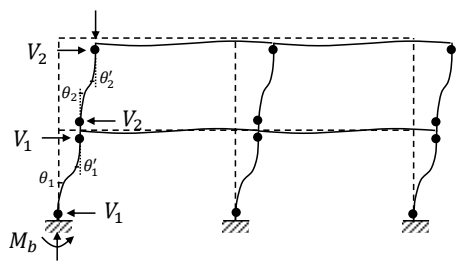

(b) Weak column and strong beam mechanism

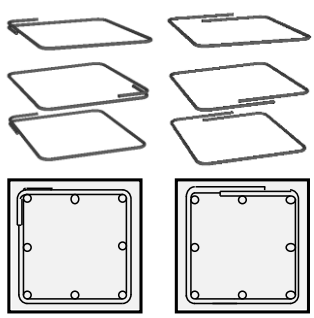

(c) Non-seismic tie details

(d) Lap splices of column bars

(e) Joint shear failure in an unreinforced exterior joint

Figure 1-2 Characteristics of low-rise buildings

1.3 Seismic Design Philosophy of Low-rise Buildings

Uncertainty exists in selecting analytical models of low-rise buildings, and in characteristics of earthquake ground motions. Through "capacity design" approach developed in New Zealand in 1976, such uncertainty can be significantly reduced.

Paulay and Priestley (1992) introduced the simple concepts of capacity design philosophy with a chain shown in Figure 1-3. If brittle links were designed to have the same nominal strength as the ductile link, the failure would primarily occur in a brittle link so the entire chain has no ductility. However, if brittle links were designed to have greater nominal strength than the ductile link, failure of brittle links would be prevented, resulting in adequate ductility for the entire chain. As the ductility of the ductile link (μ_2) affects the ductility of the entire chain (μ), the inelastic deformation capacity of the ductile link is significant factor in overall ductility.

Capacity design procedure of structures against earthquake is as follows. The primary lateral force resisting elements (ductile links) are selected, and detailed for attaining ductile response. In the elements, sufficient strength is provided for other possible failure modes (e.g., shear failure by flexural overstrength M_o of the elements) throughout the post-elastic deformations. Then, all other structural elements (brittle links) are then designed to resist strength corresponding to development of maximum strength in the potential plastic hinge regions (ductile links).

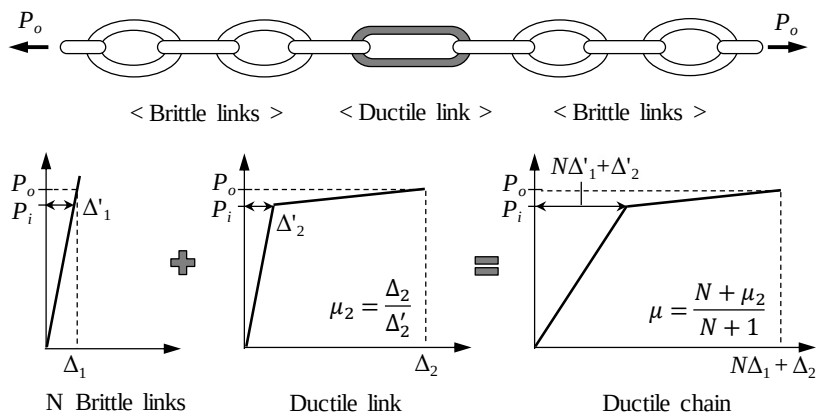

Figure 1-3 Concept of capacity design philosophy (Paulay and Priestley, 1992)

In the capacity design, seismic performance of entire buildings varies depending on failure mechanism of structural elements. In the case of tall buildings presented in Figure 1-4(a), plastic hinge rotations θ_1 in beam sidesway mechanism are much smaller than those in column sidesway mechanism (θ_2) for the same roof displacement Δ. In other words, the column sidesway mechanism requires the much larger rotational capacity in first-story columns. Such mechanism may result in soft story failure, leading to the total collapse of tall buildings during earthquakes. Furthermore, large interstory sway caused by plastic hinges of columns will introduce problems of instability, which reduce the gravity load carrying capacity of the buildings. The major objective of capacity design in tall buildings is to prevent a soft story mechanism and to ensure that only beam sidesway mechanism can develop.

On the other hand, in small buildings given in Figure 1-4(b), the rotational demand θ_4 on plastic hinges of first-story columns is moderate even with column sidesway mechanism; thus, limited ductility is required for columns. Further, the secondary effect ($P-\delta$ effect) is insignificant due to relatively low axial load applied in columns ($0.1A_g f_c^{'} \sim 0.2A_g f_c^{'}$). For this reason, Standards New Zealand (2004) specifies that a column sidesway mechanism is permitted for one or two story frames.

For seismic design of low-rise buildings, capacity design approach is applied with allowing column sidesway mechanism because increasing the size of columns for beam sidesway mechanism is practically difficult. Thus, we mainly focused on shear design of columns (ductile links) where potential plastic hinge occurred. In shear design of columns, the required shear strength is to be calculated based on the flexural strength of columns (capacity design), not factored shear forces by lateral load analysis (1^{st} mode).

In addition to capacity design, a joint shear reinforcement is a major consideration in seismic design of low-rise buildings. In the case of a moment frame under only gravity loading (Figure 1-5(a)), shear force is primarily transmitted between beams and columns. On the other hand, when lateral loads are applied, moment plays an important role in load transfer in a joint, which is subjected to high joint shear force attributed to moment reversal (Figure 1-5(b)). For resisting such high joint shear force, sufficient joint shear reinforcement is required, especially in low-rise buildings where effective joint area is small.

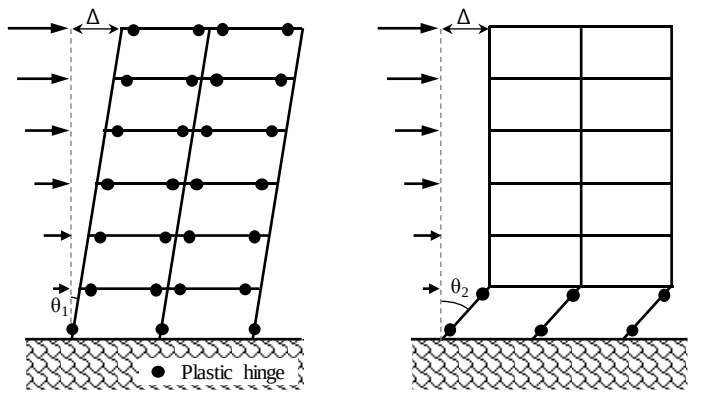

< Beam sidesway mechanism > < Column sidesway mechanism >

(a) Failure mechanisms in tall buildings

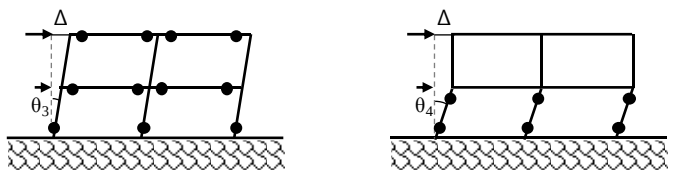

< Beam sidesway mechanism > < Column sidesway mechanism >

(b) Failure mechanisms in small buildings

Figure 1-4 Rotation demands according to failure mechanisms of tall or small building

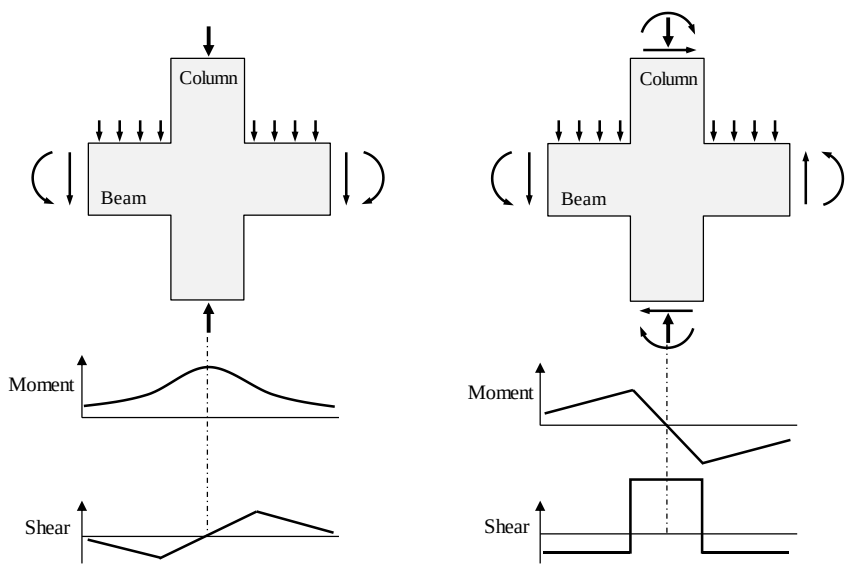

(a) Gravity loading (b) Gravity and lateral loading

Figure 1-5 Moment and shear diagrams of beam-column joints

1.4 Objective and Scope of Research

The primary objective of this dissertation is to verify the application of alternative reinforcing bar details in low-rise buildings. The alternative bar details were developed considering characteristics of low-rise buildings, which can ensure both construction efficiency and structural safety. A number of cyclic loading tests were performed to evaluate seismic performance of columns, beam-column connections, and two-story and two-bay frames. Seismic performance criteria of low-rise buildings were determined as a frame with limited ductility demand (Intermediate moment frame in KBC 2016 and ACI 318). For the comparison with the alternative details, seismic details specified in current seismic codes and non-seismic details used in construction fields without verification were also evaluated. Detailed research objectives through the experimental study are as follows.

1) Since low-rise buildings exhibit a weak-column and strong-beam behavior, bar details and spacing of column transverse reinforcement play an important role in seismic performance of the buildings. Thus, seismic performance of seismic and non-seismic tie details in columns was verified with test parameters of tie spacing (s = d/2, d/3, and d/4) and column section types (Squares and Rectangles).

2) Column longitudinal bars are often lap-spliced at the bottom of the first story columns where potential plastic hinges are formed; thus, seismic resistance of such lap spliced columns should be verified. Through cyclic tests, the effect of lap splice details and lengths of column longitudinal bars was evaluated considering moment gradient along splice regions.

3) Seismic performance of alternative U-shaped bars, which were developed for convenient bar placement in joints, was verified through cyclic tests of the beam-column connections with small effective joint area. The main test variables include joint shear reinforcement details, shear reinforcement ratio, and provided anchorage lengths of beam bars.

4) Seismic resistance of exterior beam-column connections is mainly influenced by anchorage length and details of beam longitudinal bars into joint regions. The effect of such anchorage directions and length of beam bars on joint

behaviors was evaluated by performing cyclic tests of exterior connections with beam bars bent inside the joints or beam bottom bars bent away from the joints.

5) Two-story and two-bay frame tests were performed to evaluate reinforcing bar details verified by member tests, and to investigate the overall seismic behavior of low-rise buildings in system level. Slabs with the effective slab width were used to consider the slab effect and to sustain steel blocks as much as the gravity load. A shear wall was also planned to investigate the effect of the shear wall in a frame.

Another major objective of this dissertation is to develop analytical models for columns and exterior connections on the basis of present and existing test results. From analysis of test variables in experimental studies, three analytical models were developed, such as a shear strength degradation model of RC columns, a lap splice length model of column longitudinal bars considering moment gradient, and a shear strength model of RC exterior beam-column connections as follows.

1) A post yield deformation capacity of columns was mainly influenced by the ratio of the shear resistance by shear reinforcement V_s to the applied shear force V_u owing to the degradation of concrete shear resistance V_c by increasing inelastic deformations. Thus, a post-yield shear strength degradation model for columns was proposed based on test results of columns with various tie details and spacing.

2) An average bond demand of lap spliced bars decreases in increasing moment gradient along splice regions in columns because tensile stresses of the spliced bars significantly vary along splice length. Thus, a modified lap splice length model for columns considering moment gradient along lap splice zones was proposed based on test results of a number of lap-spliced columns with various lap splice length l_s and shear span length a.

3) Current seismic codes (ACI 318 and NZS) define joint shear capacity only for the case when satisfying the amount of joint shear reinforcement required in the codes. The experimental study, however, showed that the joint shear strength was proportionally increased to joint shear reinforcement ratio ρ_j even when the amount of joint shear reinforcement is less than the code requirements. Accordingly, a shear strength model for connections was empirically presented on the basis of present and existing test results of exterior connections with joint shear failure.

1.5 Organization of Dissertation

The research manuscript is organized in eight chapters. Chapter 2 ~ Chapter 6 deal with experimental and analytical studies on each research topic discussed above (section 1.4). Since the chapters cover slightly different subjects, each chapter presents literature reviews of current design codes and exiting studies, test programs, test results, and test analysis. A flow chart of experimental and analytical studies in Chapter 2 ~ Chapter 6 is illustrated in Figure 1-6.

In Chapter 2, experimental and analytical studies were conducted to evaluate seismic performance of square and rectangular columns with various tie details. The effects of anchorage details and spacing of ties on failure modes and displacement ductility were mainly investigated by a number of cyclic test results of columns. Furthermore, based on present and existing column test results, a post-yield shear strength degradation model for columns was proposed.

Chapter 3 deals with experimental and analytical studies on lap splice of column longitudinal bars at plastic hinge regions. Based on test results, the effects of lap splice length and splice details on flexural strength, deformation capacity, and energy dissipation were examined. In additions, a modified lap splice length model for lap-spliced columns considering moment gradient (shear span length) along lap splice regions was proposed to reduce splice length required in current design codes.

Chapter 4 presents the effect of the amount of joint shear reinforcement on shear capacity in exterior and interior beam-column connections with small effective joint area. Through exterior test results, seismic performance of alternative U-shaped bars in exterior joints was also verified. Further, a shear strength model for exterior connections was empirically presented by parameter analysis with present and existing test results.

In Chapter 5, the effect of anchorage directions of beam bottom bars on beam-column connection behavior was evaluated by performing cyclic tests of exterior connections. Exterior connections with only beam bottom bars bent away from the joints were compared to those with top and bottom beam bars bent inside the joints in Chapter 4. Force transfer mechanism according to anchorage directions of beam

bars was investigated on the basis of load and displacement curves and failure modes.

In Chapter 6, two-story and two-bay frame tests were performed to verify the application of reinforcing bar details verified by column tests (Chapters 2 and 3) and beam-column connection tests (Chapters 4 and 5). The overall seismic behavior of low-rise buildings was also investigated in system level whether the buildings were controlled by beam sidesway mechanism or column sidesway mechanism. The seismic behavior and role of a shear wall in a frame were also examined.

Chapter 7 presents design codes and commentaries of alternative reinforcing bar details for low-rise buildings, which is reflected in a newly revised structural design code for low-rise buildings (Small Building Code). On the basis of research data in Chapter 2 ~ Chapter 6, design considerations for reinforcing bar details were proposed.

Finally, Chapter 8 presents summary and conclusion of this dissertation.

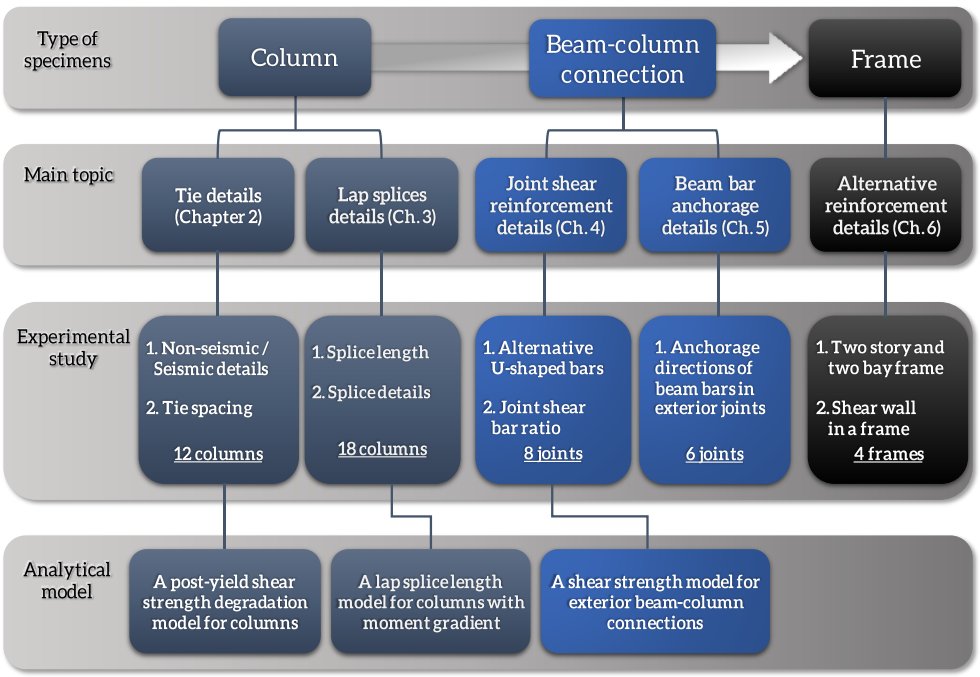

Figure 1-6 A flow chart of experimental study and analytical model

Chapter 2. Effects of Tie Details on Columns

2.1 Introduction

2.1.1 General problems in tie details on columns

In low-rise moment frame structures of less than three stories built in low and moderate seismic zones, their beams and columns are primarily designed for gravity load, rather than earthquake load. In such a case, seismic demands of the beams and columns are not significant, and hence strict requirements for the detailing of transverse reinforcement, specified in ACI 318-14 Chapter 18 (Earthquake resistance structures), have not been applied. Instead, the detailing of transverse reinforcement for the columns and beams are determined in accordance with ACI 318-14 Chapter 25 (Reinforcement details). However, concerns about the structural safety of such members and structures are raised as follows.

1) Under gravity load, generally, columns in low-rise moment frames are subjected to small axial compression force and bending moment while beams are subjected to large bending moments at their ends and mid-span. It means that the cross section of the columns is usually smaller than that of the beams. Accordingly, such moment frames may show a weak column-strong beam behavior with limited ductility during earthquake loading. In such a case, special attention should be paid to the transverse reinforcement details of the columns (including the beam-column connection) rather than the beams. Figure 2-1 illustrates the weak column-strong beam behavior of a two-story moment frame designed for gravity load. Since the columns are loaded in double curvature under earthquake load, bending moments and shear forces acting on the columns are increased. The increased shear demand of the columns can be determined by hinging moments at the top and bottom. Furthermore, the deformation demand at such plastic hinge regions is increased. Under such condition, the columns with ties spaced at the least dimension of the cross section (h_{min}) according to ACI 318-14 Chapter 25 can hardly resist against the

increased shear force and deformation demands.

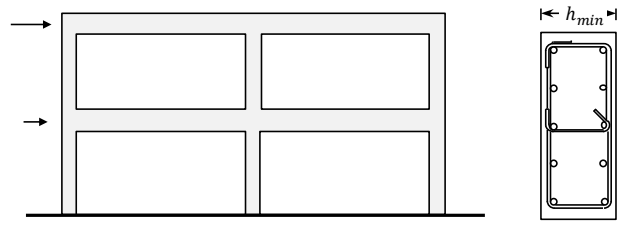

(a) A two-story and two-bay frame

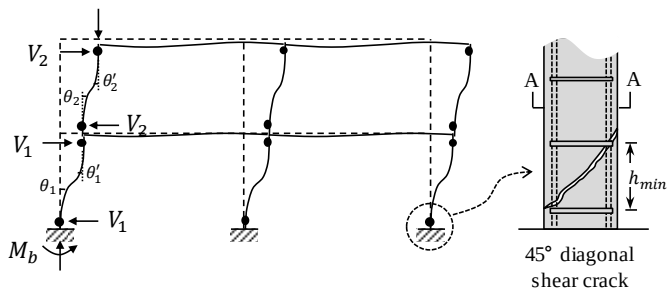

(b) A weak column-strong beam mechanism

Figure 2-1 A weak column-strong beam behavior of a two-story and two-bay frame

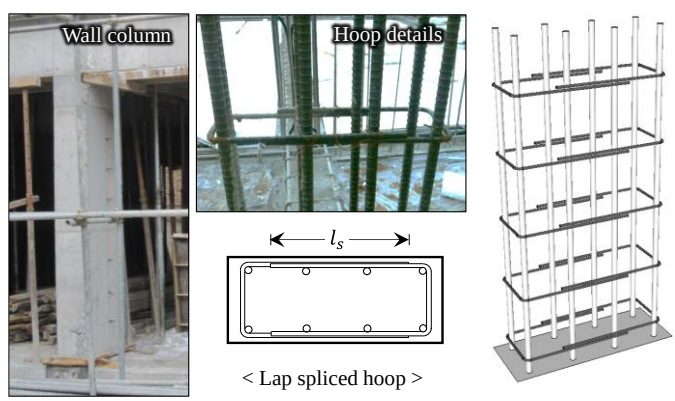

Figure 2-2 Lap spliced U-bars for wall columns

2) Figure 2-2 shows lap-spliced rectilinear ties for columns used in a construction field of low-rise buildings. Despite superior anchorage performance of 135° end hooks, such alternative details are preferred in the construction field due to easier installation of the ties. In particular, two-piece lap-spliced U-bars are very convenient for the long and narrow rectangular cross section of wall-columns. The shear resistance and confinement effect given by the lap-spliced ties can be developed without anchorage failure, provided that the lap splice is embedded and anchored in the core concrete with the sufficient lap splice length. However, as shown in Figure 2-2, the ties are spliced in the cover where severe flexural cracks occur in the inelastic deformation. The resistance of such ties to the confinement of concrete, buckling of longitudinal bars, and shear force is questionable. Accordingly, the performance of the lap-spliced ties needs to be verified by experimental studies.

Special seismic provision specified in ACI 318-14 Chapter 18 requires closely-spaced hoops with 135° seismic hook anchorage. However, in low- and moderate-seismic zones, the detailing of transverse bars in beams, columns, and beam-column joints may not necessarily conform to the special seismic provision of ACI 318-14 because the seismic demands such as shear force and ductility are relatively low. This is also the case for the beams and columns of gravity load-dominated buildings designed and constructed in the past before modern seismic provisions were included in design codes. In such old members, poorly detailed transverse reinforcements such as 90°-hooked ties, lap-spliced ties, and lap-spliced U-bars, shown in Figure 2-3, could be used for convenience in bar placement. Particularly for long and narrow column sections or wall column sections, the lap-spliced U-bars are mostly preferred to conventional seismic hoops with 135º hook anchorage.

However, in columns with poorly detailed ties, the ductility might be limited as follows. First, the poorly detailed ties are vulnerable to premature bond or anchorage failure at the lap splice or 90º hook anchorage particularly after spalling of the cover concrete. Second, if the moment frame is designed primarily for gravity load, the moment frame might show a weak column – strong beam behavior because the column cross section is smaller than the beam cross section. In such case, plastic hinge occurs in the columns rather than in the beams and consequently, the shear and ductility demands of the columns can be increased. Therefore, the effects of the

poorly detailed ties on the column failure mode and ductility need to be investigated in depth.

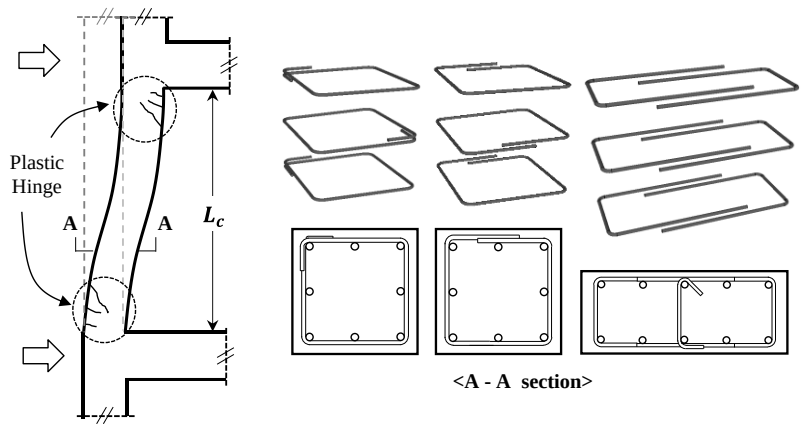

Figure 2-3 Behavior and reinforcement details of columns in gravity load-dominated moment frames

2.1.2 RC Column failures in past earthquakes

Under past earthquakes, lightly reinforced concrete columns with inadequate transverse bar details or insufficient transverse bar ratio have experienced severe damages with partial or total collapse of RC frames and bridges. Figure 2-4 ~ Figure 2-9 show damage cases of the past earthquakes such as San Fernando, California, 1971 (M= 6.6); Gualan, Guatemala, 1976 (M= 7.5); Bucharest, Romania, 1977 (M= 7.19); Kobe, Japan, 1995 (M= 6.69); Izmit, Turkey, 1999 (M= 7.4); and Chi-Chi, Taiwan, 1999 (M= 7.6). The photos of the damaged columns have been collected from the library of NISEE in the UC Berkeley (https://nisee.berkeley.edu/elibrary/).

The buildings constructed before 1970's were of concern because most buildings were designed only for gravity load. Thus, such buildings were vulnerable to lateral loading, especially earthquakes. As shown in Figure 2-4 ~ Figure 2-9, under past earthquakes, the damaged structures underwent weak-column and strong beam behavior. Especially, columns located in first stories were failed due to lack of column confinement, deficient shear resistance, and buckling of longitudinal reinforcement. The major reason of such column failures was attributed to lightly reinforced concrete columns with inadequate tie details or insufficient transverse reinforcement. In this chapter, therefore, various transverse reinforcement details of columns were investigated to prevent partial collapse of columns and total collapse of RC frames and bridges.

Figure 2-4 Damage to lightly reinforced concrete columns in the San Fernando, California earthquake, 1971 (Courtesy of NISEE, University of California, Berkeley)

Figure 2-5 Confinement failure of columns in the Gualan, Guatemala earthquake, 1976 (Courtesy of NISEE, University of California, Berkeley)

Figure 2-6 Confinement failure of columns in the Bucharest, Romania earthquake, 1977 (Courtesy of NISEE, University of California, Berkeley)

Figure 2-7 Collapsed bridges damaged by the Kobe, Japan earthquake, 1995 (Courtesy of NISEE, University of California, Berkeley)

Figure 2-8 Severe column damages by the Izmit, Turkey earthquake, 1999 (Courtesy of NISEE, University of California, Berkeley)

Figure 2-9 Severe column damages by the chi-chi, Taiwan earthquake, 1999 (Courtesy of NISEE, University of California, Berkeley)

2.1.3 Comparison of current design codes for column tie details

2.1.3.1 ACI318-14

The ACI standards assume that a structure will respond inelastically in a severe earthquake, and reduce the elastic design base shear by response modification factor R for different types of reinforced concrete structures; RC special moment frames (R = 8.0), RC intermediate moment frames (R = 5.0), RC ordinary moment frames (R = 3.0).

(1) Columns in special moment resisting frames

Limits on longitudinal reinforcement area

The area of longitudinal reinforcement is required to be greater than $0.01A_g$ or smaller than $0.06A_g$, where A_g is the gross area of the column cross section. The lower limit is defined to control time dependent deformations and to have the yield moment exceeding the cracking moment M_{cr}, and the upper limit is defined to reduce steel congestion and prevent high shear stress generated by high flexural strengths of column at both ends.

Spacing of transverse reinforcement

The spacing of transverse reinforcement over plastic hinge zone is limited to the smallest of one-quarter of the minimum column dimension $h_{min}/4$, six times the diameter of the largest longitudinal bar $6d_{bL}$, $(100+(350-h_x)/3)$, where h_x is maximum center-to-center spacing of longitudinal bars laterally supported by corners of crossties or hoop legs around the perimeter of the column. These requirements are to ensure that the spacing is close enough to prevent premature buckling of longitudinal bars, to confine the compressed concrete, and to resist vertical shear forces.

Confinement of concrete

To confine the compressed concrete in the potential plastic hinge regions of columns, transverse bars should be greater than:

For columns with rectangular hoops

$$A_{sh} \geq 0.3 \frac{sb_c f_c^{'}}{f_{yt}} \left(\frac{A_g}{A_{ch}} - 1 \right) \tag{2-1}$$

$$A_{sh} \geq 0.09 \frac{sb_c f_c^{'}}{f_{yt}} \tag{2-2}$$

where, s is hoop spacing, b_c is core dimension of tied column, outside to outside edge of transverse reinforcement bars, and A_{ch} is area of column core measured from outside edge to outside edge of hoop.

This provision is intended to limit the axial strength loss of the columns after concrete cover spalling off.

Shear reinforcement

Transverse reinforcement over the plastic hinge region shall be designed to resist shear assuming $V_c = 0$ if the earthquake-induced shear force is at least one-half of the maximum required shear strength or if the factored axial compressive force P_u including earthquake effects is less than $A_g f_c^{'}/20$.

Anchorage of transverse reinforcement

The transverse reinforcement in columns of ductile frames is required to have hoops with 135º hooks. Cross ties are required for longitudinal bars to exceed 150 mm clear spacing without support. The cross tie should engage a longitudinal bar at both ends with a 135º hook at least at one end (See Figure 2-10).

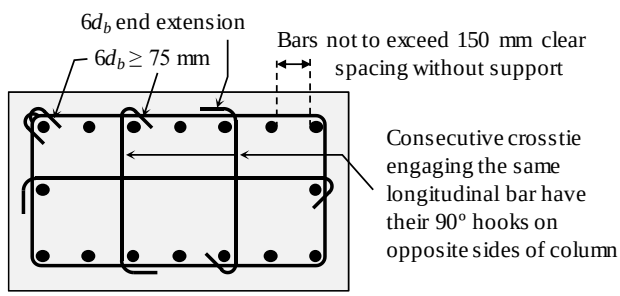

Figure 2-10 Transverse reinforcement in columns

(2) Columns in intermediate moment resisting frames

At the joint faces of the column over plastic hinge zone, the spacing of the transverse reinforcement is relaxed to the smallest of one-half the minimum column dimension $h_{min}/2$, 8 times the diameter of the smallest longitudinal bar enclosed $8d_{bL}$, 24 times the diameter of the transverse reinforcement $24d_{bT}$, 300 mm. Between the areas of plastic hinge zone, ties with 90º hooks are permitted at a smallest spacing of the minimum column dimension h_{min}, 16 times the diameter of the smallest longitudinal bar enclosed $16d_{bL}$, 48 times the diameter of the transverse reinforcement $48d_{bT}$. The spacing and details of transverse reinforcement of columns in special, intermediate, and ordinary moment frames are illustrated in Figure 2-11.

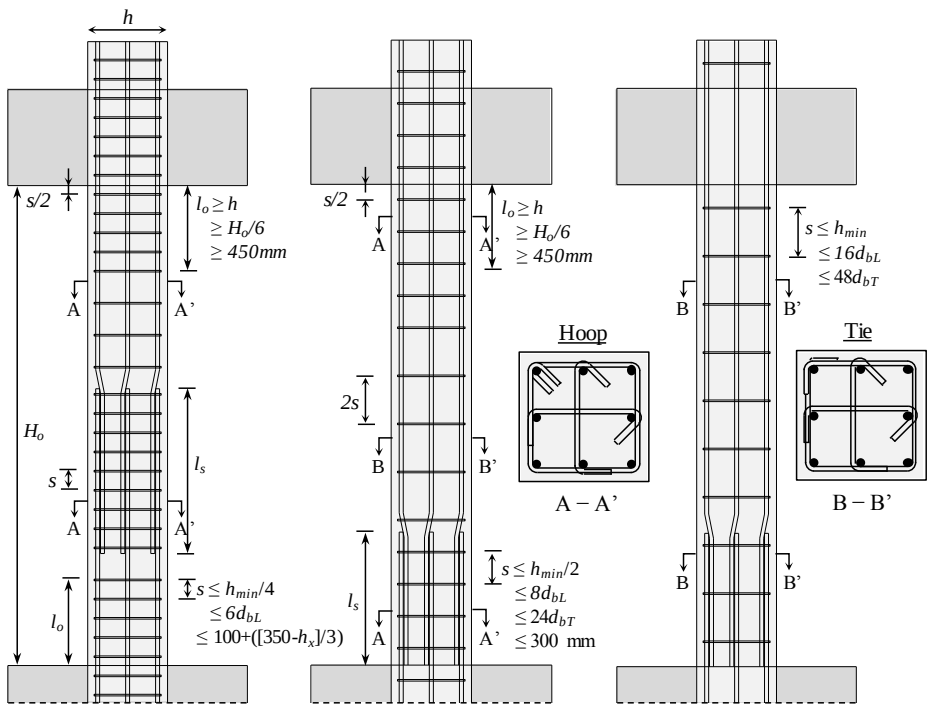

(a) Special moment frame (b) Intermediate moment frame (c) Ordinary moment frame

Figure 2-11 Spacing and details of transverse reinforcement of columns

2.1.3.2 EC 8

In EC 8, there are three Ductility Classes (DC); DC High (H), Medium (M), and Low (L). DC L amounts to design essentially for strength with no ductility and limited to low seismicity cases (similar to ordinary moment frames in ACI 318). DC M is slightly easier to design for and achieve at the site and may provide better performance in moderate earthquakes (similar to intermediate moment frames in ACI 318). DC H may give better performance under motions stronger than the design seismic action (similar to special moment frames in ACI 318). The design and detailing rules of columns are summarized in Table 2-1 for Ductility Classes H, M, and L.

Table 2-1 Detailing and dimension of columns according to EC8

Ductility Class	DC H	DC M	DC L
Critical region	$\geq 1.5h_c$, $1.5b_c$, 600, $l_c/5$	$\geq h_c$, b_c, 450, $l_c/6$	$\geq h_c$, b_c
Longitudinal bars			
ρ_{min}	1%		$0.1N_d/A_c f_{yd}$, 0.2%
ρ_{max}	4%		4%
Bars per side	3		2
Spacing between restrained bars	≤ 150 mm	≤ 200 mm	−
Transverse bars			
Outside critical regions			
spacing s	$\leq 12d_{bL}$, $0.6h_c$, $0.6b_c$, 240 mm		$\leq 20d_{bL}$, h_c, b_c, 240 mm
At lap splices, s	$\leq 12d_{bL}$, $0.6h_c$, $0.6b_c$, 240 mm		
Within critical regions			
spacing s	$\leq 6d_b$, $b_o/3$, 125 mm	$\leq 8d_b$, $b_o/2$, 175 mm	−
ω_{wd} 1)	≥ 0.08	−	
$\alpha\omega_{wd}$ 2)	$\geq 30\mu_\varphi \varepsilon_{yd} \nu_d b_c/b_o - 0.035$	−	
In critical region at column base			
ω_{wd}	0.12	0.08	−
$\alpha\omega_{wd}$	$\geq 30\mu_\varphi \varepsilon_{yd} \nu_d b_c/b_o - 0.035$		−

1) ω_{wd} is the ratio of the volume of confining hoops to that of the confined core to the centerline of the perimeter hoop, times f_{yd}/f_{cd}.
2) α is the "confinement effectiveness" factor.

2.1.3.3 NZS 3101

Limits on maximum column longitudinal reinforcement area

The area of longitudinal reinforcement should be greater than $0.008A_g$ or greater than $18A_g/f_y$. The minimum number of bars is eight. In ductile detailing lengths for columns with rectangular cross sections, the center-to-center spacing of longitudinal bars should be less than the smaller of one-quarter of the adjacent lateral dimension of the column section or 200 mm.

Spacing of transverse reinforcement in columns

Transverse reinforcement in columns is required to prevent buckling of longitudinal bars and provide confinement of concrete. The maximum spacing is limited to the smaller of one third of least lateral dimension of the column $h_{min}/3$ or 10 times longitudinal bar diameters $10d_{bL}$. In ductile and limited ductile detailing lengths, the permitted spacing of transverse reinforcement is reduced. For ductile detailing lengths, the maximum permitted spacing of transverse reinforcement is taken as the smaller of one quarter of the least lateral dimension of the column $h_{min}/4$ or 6 times longitudinal bar diameter $6d_{bL}$.

Transverse reinforcement to prevent of premature buckling of bars

The transverse reinforcement should provide an adequate restraining force to the restrained reinforcement to prevent longitudinal bars from buckling. In columns with rectangular hoops, the area of transverse bars A_{te} in the direction of potential buckling of the longitudinal bars should be greater than

$$A_{te} = \frac{\Sigma A_b f_y s_h}{135 f_{yt} d_b} \tag{2-3}$$

where ΣA_b is the sum of the areas of the longitudinal bars restrained by the tie leg, and s_h is the spacing of hoops measured along the column.

Confinement of concrete

In rectangular columns, the minimum area of transverse reinforcement A_{sh} required to provide confinement of the concrete within a longitudinal spacing s_h is given by:

$$A_{sh} = \frac{(1.0 - p_t m) s_h h''}{3.3} \frac{A_g}{A_c} \frac{f_c'}{f_{yt}} \frac{N}{\phi f_c' A_g} - 0.0065 s_h h'' \qquad (2\text{-}4)$$

where h'' is the dimension of the confined core measured outside to outside of ties perpendicular to the direction of the reinforcement A_{sh}.

Anchorage of transverse reinforcement

The transverse reinforcement should be anchored by at least a 135º bend around a longitudinal bar and a specified extension into the core or be welded. Welding of reinforcing bars, if used, should be carried out strictly controlled conditions, since it can lead to brittleness of the reinforcement.

2.1.3.4 NBCC 2005 and CSA A23.3-04

The NBCC (National Building Code of Canada, 2005) and CSA (Canadian Standards Association, 2004) have two force modification factors, a ductility-related force modification factor R_d and an overstrength-related force modification factor R_o. The factor R_d ranged from 1.0 to 4.0 for RC structure types reflects the capability of energy dissipations through inelastic deformations. The factor R_o ranged from 1.0 to 1.7 accounts for reserved strength according to structure types. Table 2-2 summarizes the values of R_d and R_o for RC moment-resisting frames.

Table 2-2 Summary of design and detailing requirements for moment-resisting frames

Type of seismic force resisting system (SFRS)	R_d	R_o	Design and detailing requirements in CSA
Ductile moment-resisting frames	4.0	1.7	- Beams capable of flexural hinging with shear failure and bar buckling avoided. - Beams and columns must satisfy ductile detailing requirements. - Columns properly confined and stronger than beams. - Joints properly confined and capable of transmitting shears from beam hinging.
Moderately ductile moment-resisting frames	2.5	1.4	- Beams and columns must satisfy detailing requirements for moderate ductility. - Beams and columns to have minimum shear strengths. - Joints must satisfy moderate ductility detailing requirements and must be capable of transmitting shears from beam hinging.
Moment resisting frames with conventional construction	1.5	1.3	- Beams and columns must have factored resistances greater than or equal to factored loads. - Beams and columns must satisfy design and detailing requirements for conventional construction. - Joints must have factored shear resistances greater than or equal to shears from factored loads.

Design and detailing requirements in CSA are similar to ACI318. Design provisions for ductile moment resisting frames (similar to special moment frame in ACI318) are summarized as follows. Spacing and detailing of transverse reinforcement of columns and beams are illustrated in Figure 2-12.

Potential plastic hinge regions in columns

Closely spaced transverse reinforcement shall be provided over potential plastic hinge regions (l_o) where flexural yielding may occur as a result of inelastic lateral displacement of the frame.

(1) where $P \leq 0.5\phi_c f_c' A_g$, l_o shall be greater than either 1.5 times the largest columns cross sections 1.5h or on-sixth of the clear span of the column $H_o/6$.

(2) where $P > 0.5\phi_c f_c' A_g$, l_o shall be greater than either 2 times the largest columns cross sections 2h or on-sixth of the clear span of the column $H_o/6$.

Limits on longitudinal reinforcement area

The area of longitudinal reinforcement shall be greater than 0.01 and smaller than 0.06 times the gross area A_g of the column section.

Spacing of transverse reinforcement

Transverse reinforcement shall be spaced at distance not exceeding

(1) one-quarter of the minimum column dimension $h_{min}/4$

(2) Six times the diameter of the smallest longitudinal bar $6d_{bL}$

(3) (100+(350-h_x)/3), where h_x is maximum horizontal center-to-center spacing between longitudinal bars on all faces of the column that are laterally supported by seismic hoops or crosstie legs.

Confinement of concrete

Transverse reinforcement for confinement in the potential plastic hinge regions of columns is specified. The total effective area in each of the principal directions of the cross section within spacing s of rectangular hoop shall be greater than the larger of the amounts required by the following.

$$A_{sh} = 0.2 k_n k_p \frac{A_g}{A_{ch}} \frac{f_c'}{f_{yh}} s h_c \qquad (2\text{-}5)$$

$$A_{sh} = 0.09 \frac{f_c'}{f_{yh}} sh_c \qquad (2\text{-}6)$$

where $k_n = n_l / (n_l - 2)$, $k_p = P_f / P_o$ and f_{yh} shall not be taken as greater than 500 MPa. If the thickness of the concrete cover outside the confining transverse reinforcement exceeds 100 mm, additional transverse reinforcement shall be provided within the cover at a spacing not exceeding 300 mm.

Anchorage of transverse reinforcement

The transverse reinforcement is provided by hoops with seismic hooks and seismic crossties. A seismic crosstie is a single bar with a seismic hook at one end and a hook not less than 90º with at least $6d_b$ end extension at the other end. The hooks must engage peripheral longitudinal bars. The 90º hooks of successive crossties along the same longitudinal bar shall be alternated end for end.

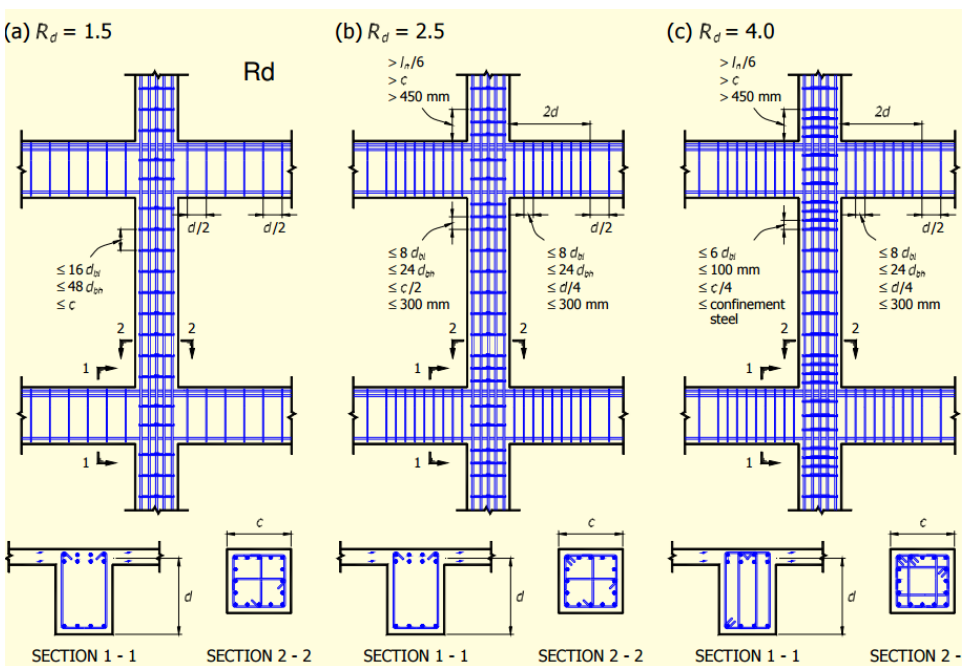

Figure 2-12 Spacing and details of transverse reinforcement of columns and beams (NBCC)

2.1.4 Review of previous studies

2.1.4.1 Anchorage details of column transverse reinforcement

Several previous researches were performed to evaluate the anchorage details of transverse reinforcement in RC columns subjected to monotonic and cyclic loading. The effectiveness of various types of crossties and perimeter ties has been investigated in some studies as below.

Moehle and Cavanagh (1985) tested RC columns under concentric compression with cross ties with 90° and 135° end hooks or cross ties with 180° end hooks as shown in Figure 2-13. Though the columns using 90° and 135° end hooked cross ties were slightly less than those using 180° end hooks, differences in confinement effectiveness appeared not to be significant. This conclusion was derived from analytical studies on monotonic flexural responses of assumed column sections.

Saatcioglu and Ozcebe (1989) tested RC columns subjected to constant axial load and incrementally increasing lateral load reversals. Those columns had the transverse reinforcement details A to C as shown in Figure 2-14.Crossties linking the intermediate longitudinal bars were highly effective in confining the core concrete. Crossties with 90° and 135° end hooks perform as satisfactorily as those with 135° hooks at both ends.

Tanaka (1990) tested RC columns under simulated severe seismic loading. Those columns had the transverse bar details shown in Figure 2-15. He reached the following conclusion based on the test results.

(1) Satisfactory behavior was observed for perimeter hoops with 135° end hooks, interior cross ties of 'J' bars with a tension splice of $24d_b$ in the core concrete, and interior cross ties of 'U' bars with a tension splice of $24d_b$ in the core concrete. The tension splices of the 'J' and 'U' bars were not affected by concrete cover cracking.

(2) For interior cross ties with 90° and 180° end hooks (Figure 2-15(b)), the 90° end hooks commenced to open, and the effectiveness of those end hooks was gradually reduced beyond a displacement ductility factor of 8. The same conclusion

was achieved for interior cross ties with 90° and 135° end hooks.

(3) The effectiveness of perimeter ties with 'U' bars lapped with a tension splice of $17d_b$ in the cover concrete degraded rapidly after concrete cover spalling. This transverse bar detail is definitely to be discouraged.

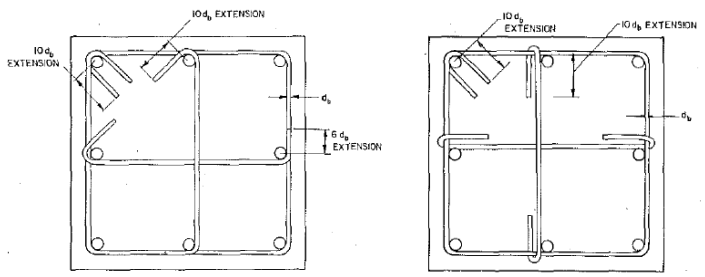

(a) 90° and 135° cross tie (b) 180° end hook

Figure 2-13 Cross tie details used in tests of Moehle and Cavanagh (1985)

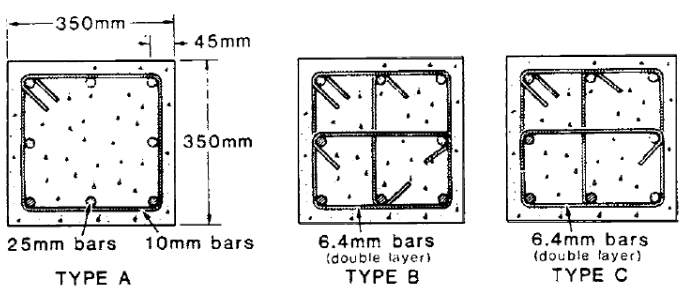

Figure 2-14 Column sections used in tests of Saatciglu and Ozcebe (1989)

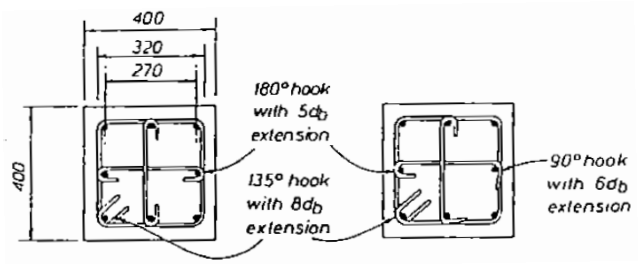

(a) 180° end hooked cross tie (b) 90 ° - 180° end hooked cross tie

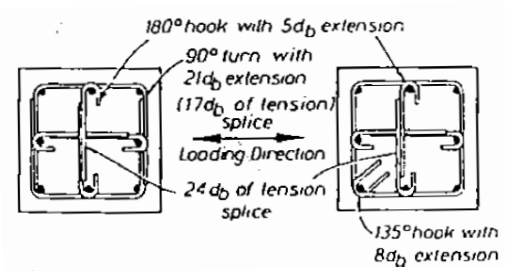

(c) 'J' cross ties & 'U' hoops (d) 'J' cross ties & 135° hooked hoops

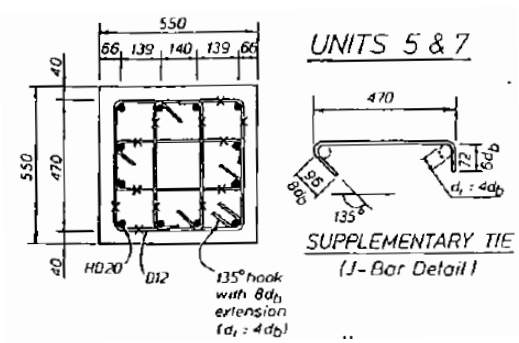

(e) 90 ° - 135° end hooked ('J' bars) cross tie

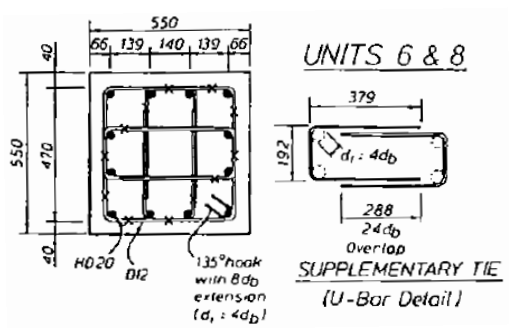

(f) 'U' bars (cross ties) with tension splices

Figure 2-15 Transverse bar details used in tests of Tanaka (1990)

Mo and Wang (2000) tested RC columns with a new configuration of transverse bars with alternate ties shown in Figure 2-16(c). The proposed configuration of transverse bars provided comparable or improved seismic performance in terms of member ductility and energy dissipation capacity to typical configuration usually used in construction (Figure 2-16(a) and (b)).

Lam et al. (2003) tested columns specimens under cycles of lateral load and subjected to high axial loads. The specimens had low lateral confinement and two configurations of transverse bars, 135° and 90° hooks shown in Figure 2-17. The use of 90° hook for transverse bars resulted in a substantial reduction in the drift capacity with a 40% reduction compared to 135° hook.

Lukkunaprasit and Sittipunt (2003) tested moderately confined RC columns to investigate the effectiveness of hook-clips in improving the performance of conventional 90° hooked transverse bars. The hook-clips shown in Figure 2-18(a) were found to be effective in improving the performance of the 90° hooked transverse bars and even superior to the 135° hooked transverse bars.

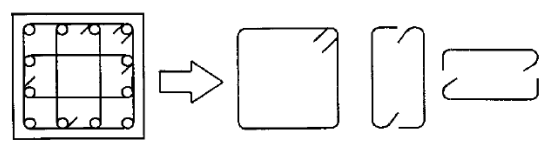

(a) C1 tie shape

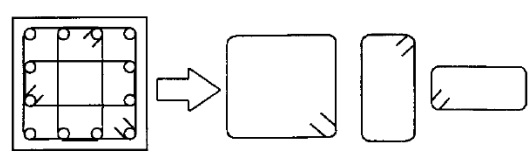

(b) C2 tie shape

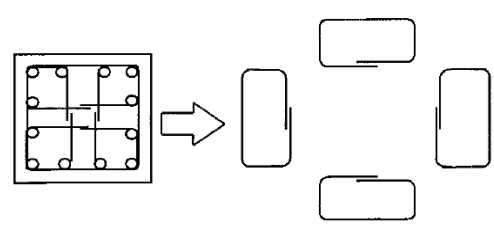

(c) C3 tie shape

Figure 2-16 Tie configuration used in tests of Mo and Wang (2000)

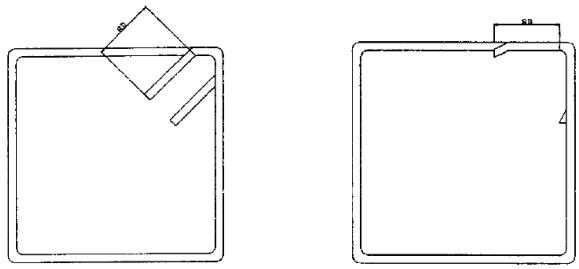

(a) 135° hook (b) 90° hook

Figure 2-17 Detailing of 135° hook and 90° hook (Lam et al., 2003)

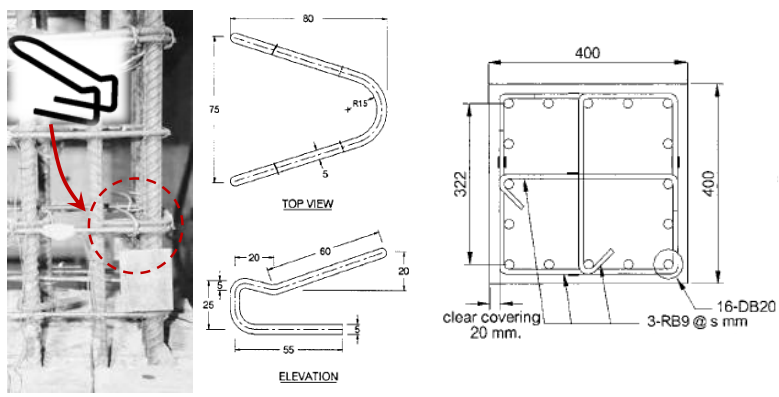

(a) Details of hook-clip (b) Column reinforcement details

Figure 2-18 Details of hook-clip used in tests of Lukkunaprasit and Sittipunt (2003)

2.1.4.2 Shear strength degradation model of columns

According to previous test results of RC columns, the columns showed shear strength degradation in the post-yield deformation, which affects seismic performance of columns. For example, Figure 2-19 illustrates lateral load-drift ratio relations and failure mode of a cantilever column. Figure 2-19(a) shows a failure sequence of tested column corresponding to critical points 1 to 3 in the load-drift loop. Until drift ratio of 2.5% (Point 1), the load carrying capacity remained constant even after flexural yielding. While reaching to drift ratio of 3.5%, however, the load was abruptly degraded due to severe diagonal shear cracks along the whole column shown in Figure 2-19(b) because shear strength was significantly degraded in a large post-yield deformation.

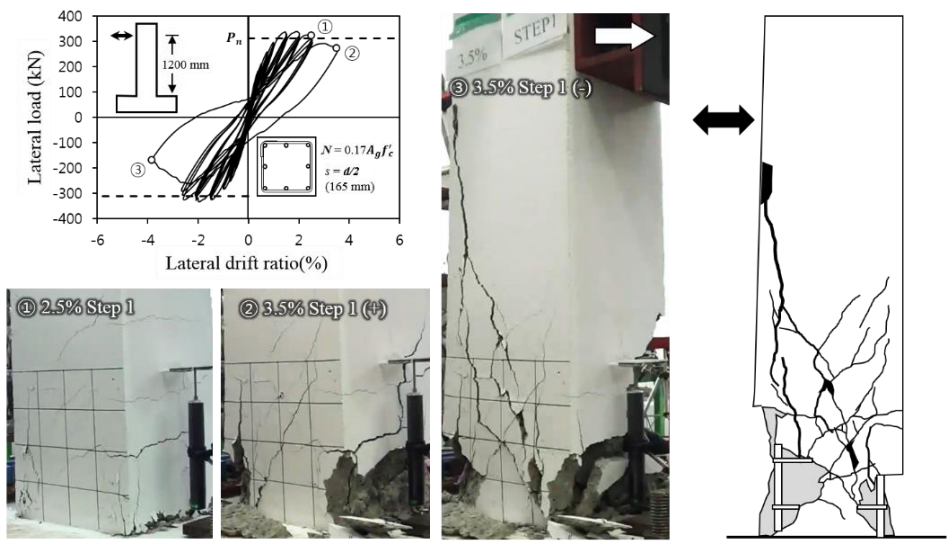

(a) Failure sequence of RC column specimen (b) Final failure

Figure 2-19 Test result of RC column with shear failure after flexural yielding

Many researchers observed such shear strength degradation of columns, and proposed shear strength degradation models. In empirical models, shear strength is expressed as $V_n = V_c + V_s$ or $V_n = V_c + V_s + V_p$, in which V_c indicates contribution of concrete, V_s indicates contribution of transverse reinforcement, V_p indicates contribution of axial load. In most shear strength degradation models, the concrete contribution V_c is only degraded as post-yield deformation increases. On the other

hand, several models (Sezen and Moehle, 2004) decrease both V_c and V_c based on degradation of the overall shear resisting mechanism.

Wight and Sozen (1973) developed the analytical model used for a quantitative analysis of the observed change in the shear-resisting mechanism of column specimens for monotonically increasing deflection. The change in the shear capacity of the concrete was evaluated for varying steel longitudinal bar strengths, reinforcement ratio, and shear span to depth ratio. Figure 2-20(a) shows the variation of shear strength contribution of concrete and stirrup depending on displacement ductility. The contribution of concrete was gradually decreased after peak load, while that of stirrup remained constant. As the shear capacity of concrete was degraded after displacement ductility of 3.0 shown in Figure 2-20(b), a transverse reinforcement ratio large enough to carry all of the shear applied to the column was provided to prevent unstable behavior at large deflection.

Ghee et al. (1989) suggested that a model for shear strength degradation with increasing flexural ductility could be developed (see Figure 2-21). At flexural displacement ductilities $\mu>2$, the shear strength degraded gradually with increasing ductility, and the inclination to the longitudinal axis of diagonal compression struts of the truss mechanism decreased.

Ascheim and Moehle (1992) suggested that continued inelastic loading causes an overall reduction in shear resistance due to accumulated plastic elongation of the stirrups and subsequent dilation of the surrounding concrete. The dilation and criss-cross cracking pattern resulted in a series of irregular concrete blocks with reduced load carrying capacity as shown in Figure 2-22(a). Cycling loading action also resulted in degradation of bond and anchorage mechanisms (see Figure 2-22(b)). The net result was an overall reduction in shear resistance with increased cyclic loading.

Ichinose (1992) explained flexural shear failure mode using Figure 2-23: as inelastic rotation of the hinge region was increased, the shear strength was decreased, while the flexural strength was constant. Shear failure was occurred at the crossing point. The shear strength degradation was attributed to the reduction of aggregate interlocking in hinge regions due to widening of flexural shear cracks and that of the effective compressive strength of concrete in hinge regions due to densely intersecting large flexural shear cracks.

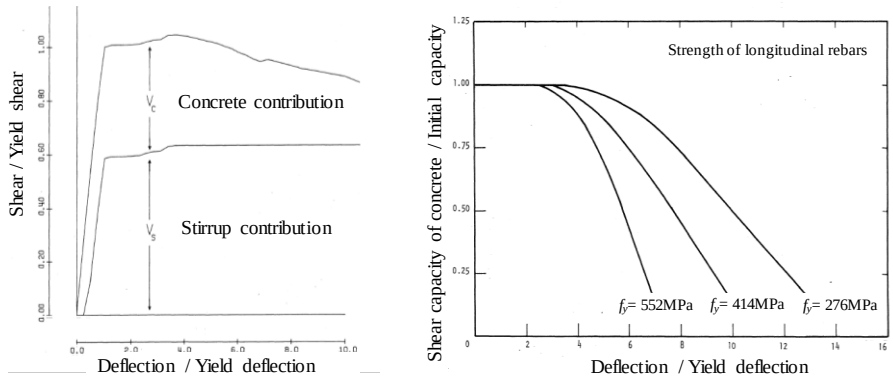

(a) Variation of shear contribution (b) Degradation of concrete contribution according to f_y

Figure 2-20 Variation of shear contribution and degradation of concrete contribution in test results of Wight and Sozen (1973)

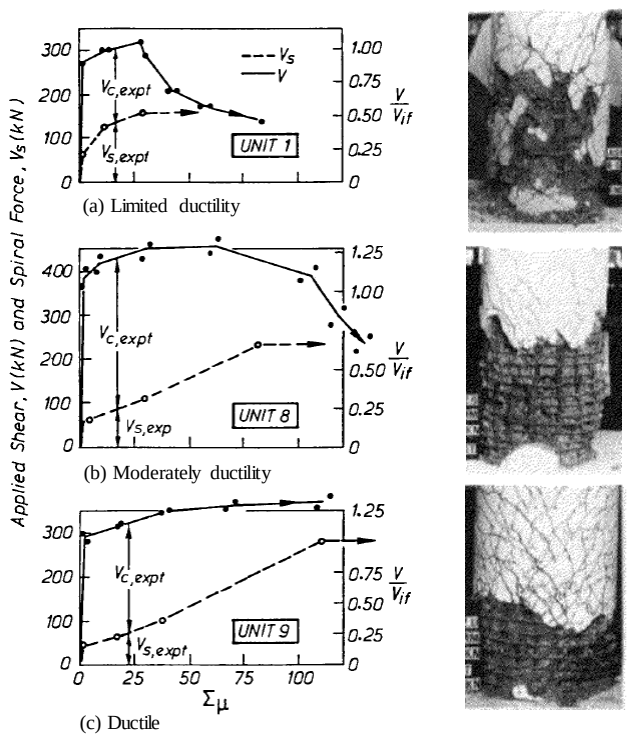

(a) Limited ductility

(b) Moderately ductility

(c) Ductile

Figure 2-21 Influence of cumulative ductility factor on components of shear resistance (Ghee et al., 1989)

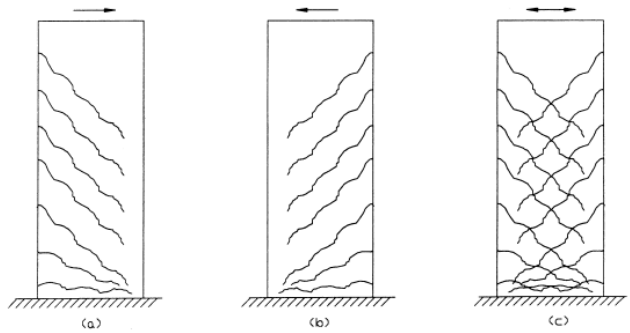

(a) Diagonal cracking under load reversal

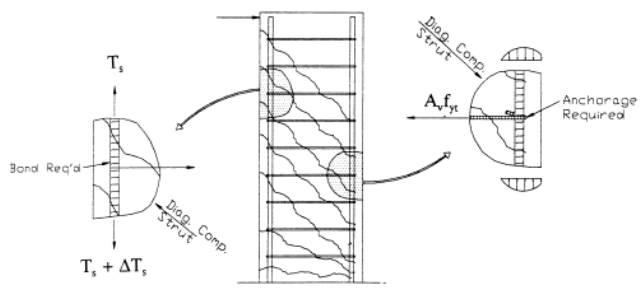

(b) Regions requiring anchorage and bond

Figure 2-22 Effects of earthquake loading on shear strength degradation (Ascheim and Moehle, 1992)

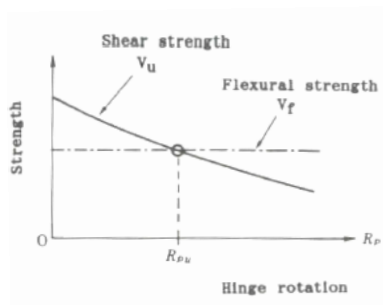

Figure 2-23 Decrease of shear strength (Ichinose, 1992)

Priestley et al. (1994) proposed a model capable of representing the interaction between flexural ductility and shear strength. The strength of the concrete component is reduced as flexural displacement ductility increases due to the reduction in aggregate interlock as cracks widen (see Figure 2-24). The proposed method, in which the contributions of concrete, truss mechanism, and axial load mechanism were separately considered, was shown to provide significantly improved correlation with experimental results.

Lee and Watanabe (2003) proposed a method to predict the ductile capacity of RC beams failing in shear after flexural yielding by considering the degradation of the diagonally compressed concrete due to the axial elongation of the beam and a decrease in the effective compressive strength of the concrete (see Figure 2-25). The shear deterioration of RC beams was predicted by using a compatibility-aided truss model RA-SRM taking into account the axial strain at the center of the beam's cross section.

Sezen and Moehle (2004) proposed shear strength equation including contributions of concrete and transverse reinforcement corresponding to displacement ductility demand. As shown in Figure 2-26, the proposed model decreased both concrete and transverse reinforcement contributions based on statistical evaluation of predicted and actual shear strengths. The proposed model was adopted for shear strength V_n of columns in ASCE41-13.

Park et al. (2012) developed analytical model to evaluate the shear strength degradation and the deformation capacity of slender columns subjected to cyclic loading. After flexural yielding, the shear capacity of the compression zone decreases with inelastic flexural deformation because inelastic deformation reduces the depth of the compression zone and increases the area of the concrete subjected to compressive softening shown in Figure 2-27.

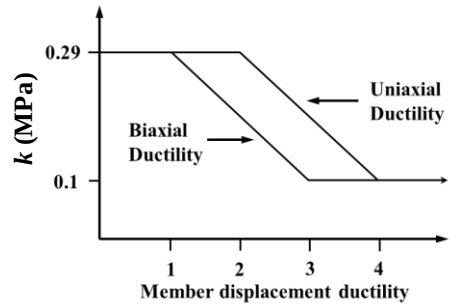

Concrete component

$$V_c = k\sqrt{f_c'}\,0.8A_{gross}$$

Truss mechanism component

$$V_s = A_v f_{yh} D' / s \cot 30$$

Axial load component

$$V_p = P\tan\alpha = P(D-c)/2a$$

Figure 2-24 Degradation of concrete shear strength with ductility in Priestley et al. (1994)

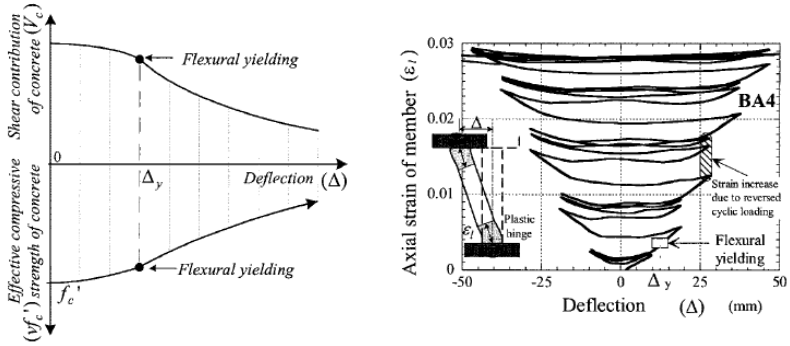

(a) Decreased shear contribution of concrete with increasing deflection

(b) Axial strain versus deflection of a specimen failing in shear after flexural yielding

Figure 2-25 Shear strength degradation and axial strain increment of a beam specimen (Lee and Watanabe, 2003)

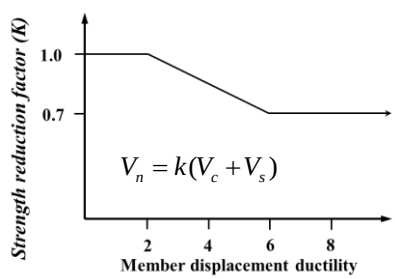

Concrete contribution

$$V_c = \frac{0.5\sqrt{f_c'}}{M/Vd}\sqrt{1+\frac{N_u}{0.5\sqrt{f_c'}A_g}}\,0.8A_g$$

Transverse reinforcement contribution

$$V_s = A_v f_y d / s$$

Figure 2-26 Shear strength degradation with displacement ductility (Sezen and Moehle, 2004)

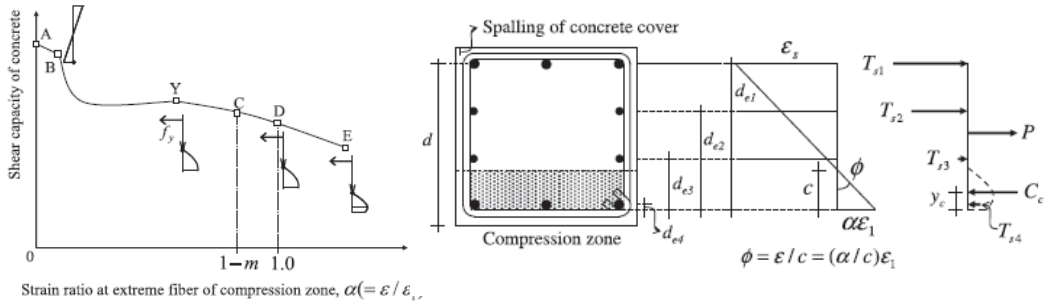

Figure 2-27 Variations of shear strength capacity with the progress of flexural deformation (Park et al., 2012)

2.1.4.3 Lightly reinforced RC columns

Moehle, Elwood, and Sezen extensively investigated the cyclic behavior of lightly reinforced columns with 90°-hooked ties (i.e. non-seismic details) which do not conform to the special seismic requirements. On the basis of the test results by Sezen (2002) and Sezen and Moehle (2006), Sezen and Moehle (2004) proposed a shear strength model addressing the effects of axial load and displacement ductility. Elwood and Moehle (2005a) evaluated the deformation capacity at shear failure. Further, by using a shear friction concept, they proposed an axial load-carrying capacity model for shear-damaged columns and estimated the deformation capacity at axial failure (Elwood and Moehle, 2005b). Elwood and Moehle (2006) developed an idealized backbone model for existing columns with non-seismic transverse reinforcement, defining the damage states of flexural yielding, shear failure, and axial load failure. On the basis of the studies by Moehle, Elwood, and Sezen, a shear strength model for columns was introduced in ASCE 41-13 Chapter 10 (a guideline for seismic evaluation and retrofit of existing buildings).

(1) Sezen (2002) and Sezen and Moehle (2006)

Sezen and Moehle tested four full-scale RC columns in double bending under uni-directional lateral load with test variables of magnitude and history of axial and lateral loads. As the major objective of the research was to identify main factors contributing to shear failure and axial failure of lightly reinforced concrete columns, column responses vary considerably with magnitude and history of axial and lateral loads as shown in Figure 2-28. Specimen 1 (control specimen) had constant compressive axial load of $0.15A_g f_c'$ and standard lateral displacement history. Specimen 2 had higher axial load of $0.6A_g f_c'$ and standard lateral displacement history. Specimen 3 had axial load varying with applied lateral load in Figure 2-28. Specimen 4 had constant compressive axial load of $0.15A_g f_c'$ with standard lateral displacement history until yield displacement followed by monotonic lateral displacement to failure.

Lightly reinforced concrete columns were influenced by magnitude and history of axial and lateral loads. In the case of low axial load applied, shear failure occurred with strength degradation after beam flexural yielding. However, axial failure did not occur until large inelastic displacement. In the case of high axial load applied, brittle shear compression failure and loss of axial load capacity immediately after shear failure. The column with varying axial load showed different behavior in tension and compression, resulting in failure under compressive loading. The deformation capacity under monotonic loading was larger than that under cyclic loading.

With a database of more than fifty columns with shear failure, a model to predict shear strength of columns was developed, a strength reduction factor was proposed for design and assessment purposes. Further, based on test results, simplified analytical procedures were developed to model flexural and shear behaviors, and longitudinal bar slip under monotonic lateral loading with three springs to combine individual monotonic displacements.

Details of test specimens, test results, and the analytical model are presented in a doctoral dissertation by Sezen (2002).

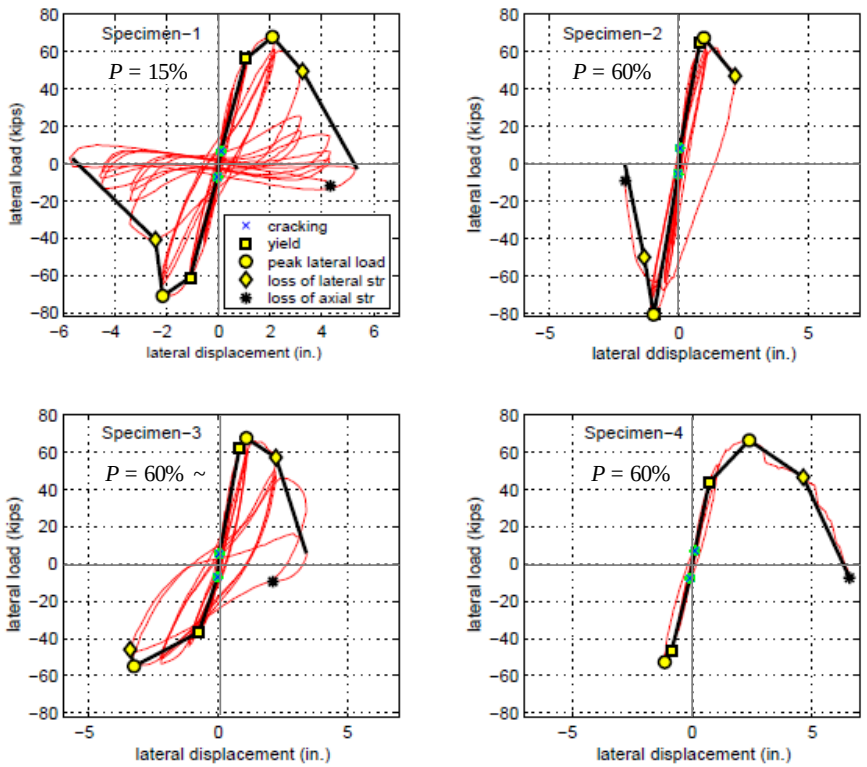

< Load and displacement relationship >

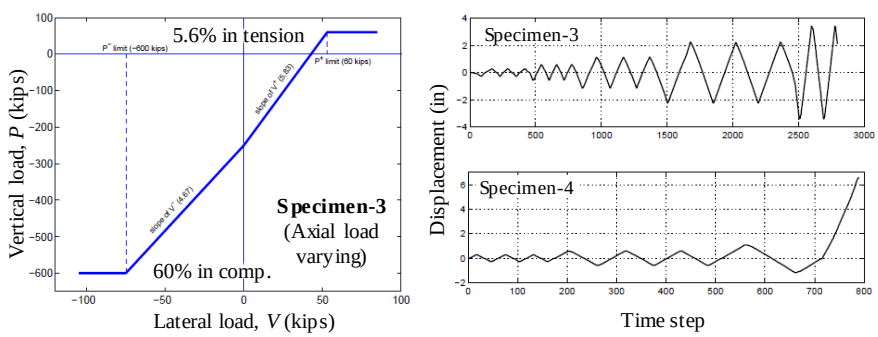

< Axial and lateral load relations > < Applied displacement histories >

Figure 2-28 Test results of lightly reinforced columns with various axial loads (Sezen, 2002)

(2) Shear strength model proposed by Sezen and Moehle (2004)

Sezen and Moehle (2004) proposed an alternative shear strength model considering the effects of column aspect ratio, axial load, amount of transverse reinforcement, and deformation ductility demand. In the proposed shear strength model, diagonal tension capacity is considered to estimate concrete contribution. It is assumed that onset of diagonal tension cracking in an element under uniform stress can be represented to the nominal principal tension stress.

$$\sigma_1 = \frac{\sigma_x + \sigma_y}{2} + \sqrt{\left(\frac{\sigma_x - \sigma_y}{2}\right)^2 + \tau^2} \tag{2-7}$$

where, σ_x and σ_y are normal tension stress in the x and y directions, respectively. τ is shear stress acting on the faces. In a RC column, it will be assumed that σ_x is zero since the confinement effect of poorly detailed ties on σ_x is very small. As σ_x is normal stress parallel to the column longitudinal axis, $\sigma_x = -P/A_g$. Assuming that tensile cracking occurs when σ_1 attains the nominal tensile strength $f_{ct} = 0.5\sqrt{f_c'}$, the shear stress at the onset of diagonal tension cracking can be defined as follows.

$$\tau = 0.5\sqrt{f_c'}\sqrt{1 + \frac{P}{0.5\sqrt{f_c'}A_g}} \tag{2-8}$$

As flexural cracking becomes more predominant with larger aspect ratio a/d, the aspect ratio is considered. The contribution of concrete to shear strength using an effective concrete area of $0.8A_g$ is defined as follows.

$$V_c = \frac{0.5\sqrt{f_c'}}{a/d}\sqrt{1 + \frac{P}{0.5\sqrt{f_c'}A_g}}0.8A_g \tag{2-9}$$

Transverse reinforcement contribution is defined as $V_s = \alpha\, A_v f_y\, d/s$ using traditional truss models. The effective value α is taken as 1.0 similar to ACI 318 and FEMA 273 on the basis of plotting ($V_{test} - V_c$) and ($A_v f_y d/s$) relations with 51 previous test results.

Several researchers proposed shear strength model considering reduced contribution with increasing displacement ductility (Aschheim and Moehle, 1992 and Priestley et al. 1994). To evaluate the effect of displacement ductility on shear strength of columns, normalized shear strength is plotted as a function of the displacement ductility with previous test results in Figure 2-29. The graph showed that shear strength is decreased with increasing displacement ductility.

Ascheim and Moehle (1992); Priestley et al. (1994); and FEMA 273 (1997) considered reduction factor only for the concrete contribution based on the understanding that a large crack opening resulted in degradation of concrete contribution, but the transverse reinforcement contribution does not degrade. On the other hand, Sezen and Moehle (2004) proposed a ductility related factor *k* to reduce shear contributions of both concrete and transverse reinforcement with increasing displacement ductility demand. They insisted that concrete damages in columns had led to loss of anchorage of transverse reinforcement and reduction of bond capacity of longitudinal and transverse reinforcements. Since the degree of degradation in concrete and transverse reinforcement contributions was difficult to be clearly identified, same ductility related factor *k* was proposed for contributions of concrete and transverse reinforcement as shown in Figure 2-29.

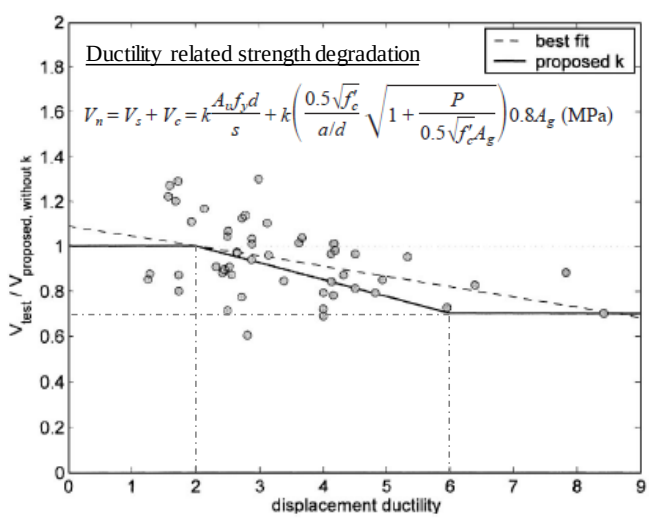

Figure 2-29 Shear strength degradation model with displacement ductility by Sezen and Moehle (2004)

(3) Elwood and Moehle

Elwood and Moehle (2005a) proposed new drift capacity model of RC columns with light transverse reinforcement considering transverse reinforcement ratio ($\rho^{"}$), shear stress demand ($v/\sqrt{f_c'}$), and axial load ratio ($P/[A_g f_c']$). Based on a least-squares fit to the data of 50 shear-critical columns, the following empirical expression is proposed to estimate the drift ratio at shear failure.

$$\delta_s = \frac{3}{100} + 4\rho^{"} - \frac{1}{40}\frac{v}{\sqrt{f_c'}} - \frac{1}{40}\frac{P}{A_g f_c'} \geq \frac{1}{100} \quad \text{(MPa units)} \tag{2-10}$$

Figure 2-30 compares Equation (2-10) with the test results from the database. The mean value is 0.97 and the coefficient of variation is 0.34.

The way to assess seismic behavior of a column is presented in Figure 2-31. The figure includes the idealized elastic and perfectly plastic flexural response of specimen 1 in Figure 2-28, Sezen's shear-strength model, and the proposed drift capacity model. Comparing the Sezen model, it is apparent that the shear demands are in a range where shear distress should be expected. An important point is that the drift capacity model should be used only for columns exhibiting shear failure after flexural yielding.

Figure 2-32 shows the effect of axial load and transverse reinforcement ratio on the drift capacity at shear failure by the proposed drift capacity model. As shear strength varies with axial load and transverse reinforcement, the limits in Equation (2-10) are able to shift with changes in axial load and transverse reinforcement ratio. The proposed model indicates that the drift ratio at shear failure is decreased when axial load is increased and transverse reinforcement ratio is decreased.

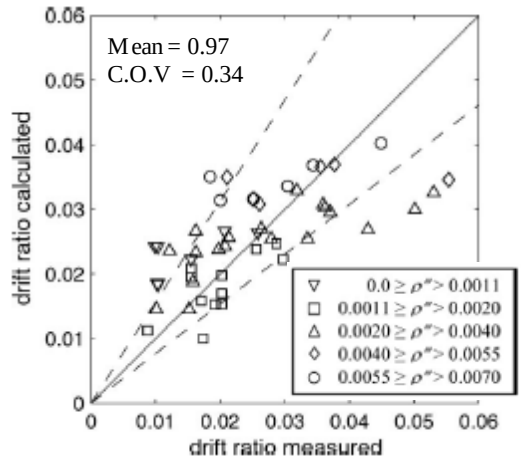

Figure 2-30 Comparison of calculated drift ratio at shear failure by Elwood and Moehle (2005a)

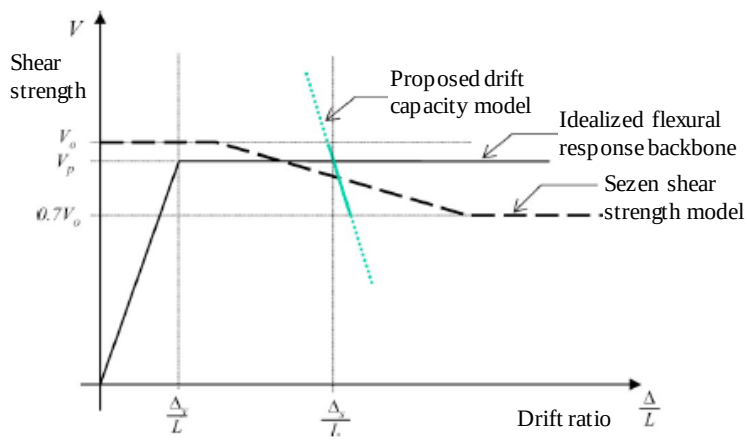

Figure 2-31 Comparison of Sezen shear strength model and the proposed drift capacity model for specimen 1 in Figure 2-28

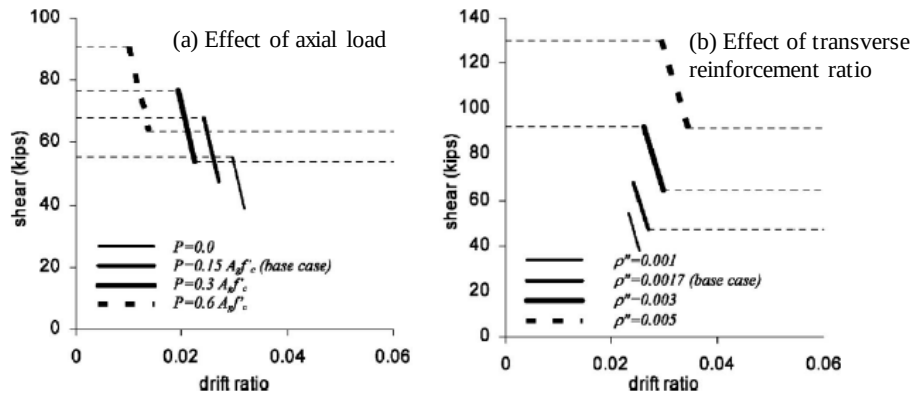

Figure 2-32 Effect of axial load and transverse reinforcement ratio on drift ratio at shear failure by proposed drift capacity model

Elwood and Moehle (2005b) proposed axial capacity model for shear-damaged columns using shear friction concept. The mean ratio of the measured to calculated drift at axial failure with following proposed equation is 0.97 with the coefficient of variation of 0.26.

$$\left(\frac{\Delta}{L}\right)_{axial} = \frac{4}{100}\frac{1+(\tan\theta)^2}{\tan\theta + P\left(\frac{s}{A_{st} f_{yt} d_c \tan\theta}\right)} \qquad (2\text{-}11)$$

where θ was assumed to be 65º. Figure 2-33 shows the axial capacity model with a single curve and test data denoted with squares.

The results from the model are agreeable with the observation in experimental tests that the drift ratio at axial failure is directly proportional to transverse reinforcement ratio and inversely proportional to the applied axial load. The model suggested that for low axial loads or high transverse reinforcement ratio, a shear-damaged column can maintain its axial load beyond a drift ratio of 2.0%.

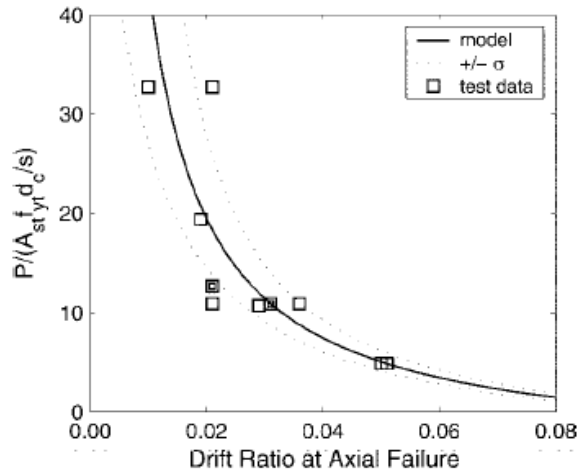

Figure 2-33 Comparison of axial capacity model and test results

Elwood and Moehle (2006) developed idealized backbone model for existing RC columns with light transverse reinforcement. The drift capacity model and axial capacity model presented above can be incorporated into an idealized backbone response for RC columns. The model approximates the envelope curve from test data by capturing flexural yielding, shear failure, and axial load failure during cyclic loading. Idealized backbone response can be developed as shown in Figure 2-34.

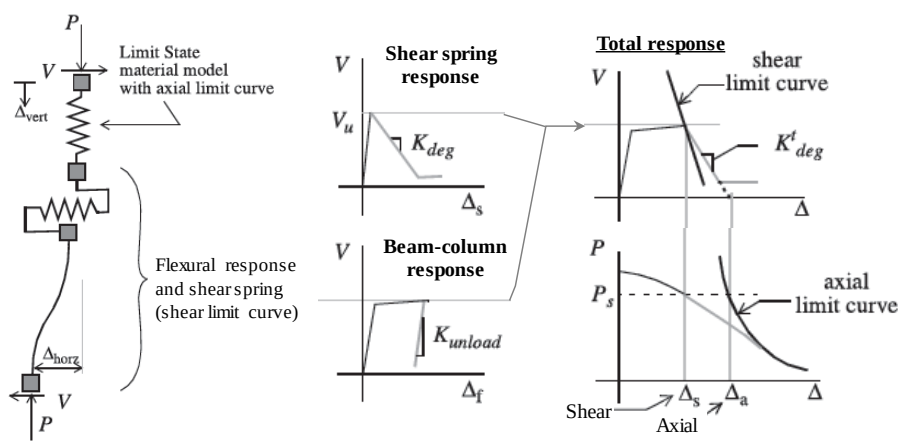

Figure 2-34 Flexural and shear response with shear and axial limit curves

2.2 Test Program of Various Tie Details

2.2.1 Major design parameters

Table 2-3 shows the test parameters of square and rectangular column specimens, such as the spacing and anchorage detail of transverse rebars. Figure 2-35 and Figure 2-36 show the reinforcement details of six square columns (**SAd2**, **SBd2**, **SBd4**, **SCd2**, **SDd2**, and **SDd4**) and six rectangular columns (**REd2**, **RFd2**, **RFd3**, **RGd2**, **RHd2**, and **RHd3**), respectively. In the specimen names, the first letters 'S' and 'R' denote square and rectangular cross-sections, respectively; the second letters 'A' through 'H' denote types of the tie details; and the last two letters 'd2', 'd3', and 'd4' denote the tie spacings, $d/2$, $d/3$, and $d/4$, respectively (d = effective depth of the column section). Since a weak column-strong beam behavior can occur in columns subjected to a low or moderate axial compression load, shear resistance is critical in the design of such columns. For this reason, the tie spacings of the column specimens were determined to be not greater than $d/2$.

Table 2-3 Test variables of column specimens

Specimen	Section type	Transverse reinforcement		
		Type[1)]	Spacings (mm)	Ratio ρ_v[2)]
SAd2	Square	A	165	0.39
SBd2		B	165	0.39
SBd4		B	82	0.77
SCd2		C	165	0.39
SDd2		D	165	0.39
SDd4		D	82	0.77
REd2	Rectangles	E	105	0.32
RFd2		F	105	0.32
RFd3		F	70	0.48
RGd2		G	105	0.32
RHd2		H	105	0.32
RHd3		H	70	0.48

1) Details of transverse bars and crossties are shown in Figure 2-35 and Figure 2-36.

2) $\rho_v = A_v / (bs)$, where A_v is the total cross-sectional area of transverse reinforcement including crossties, s is spacing of transverse reinforcement, and b is width of column.

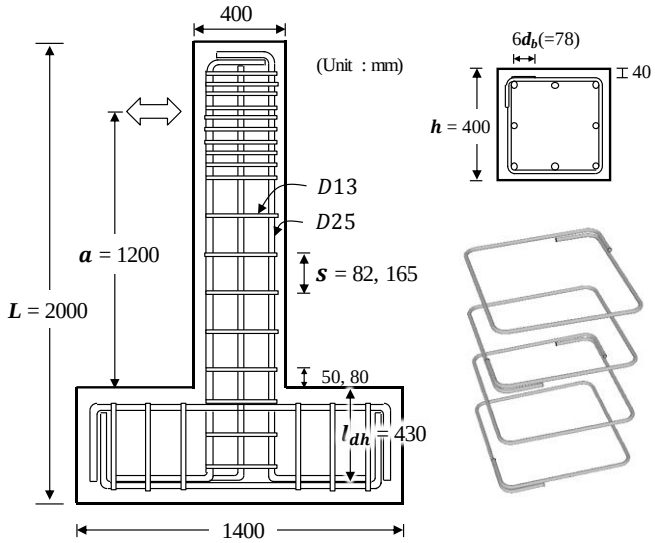

(a) Reinforcement details

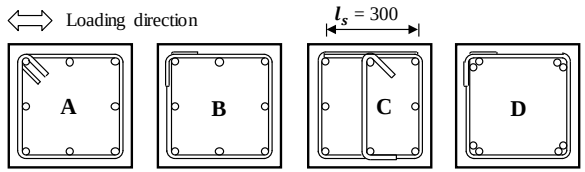

(b) Types of transverse bars

Figure 2-35 Reinforcement details of square columns

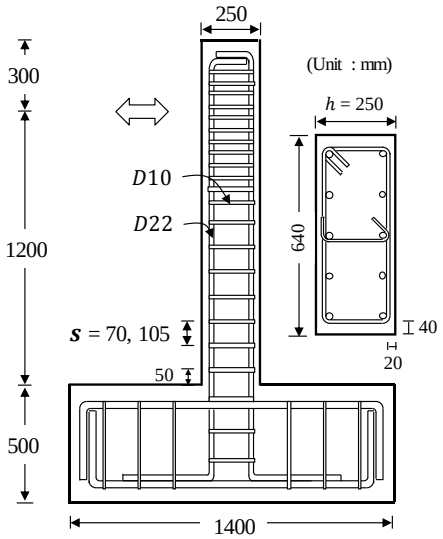

(a) Reinforcement details

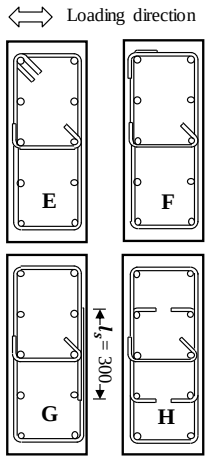

(b) Types of transverse bars

Figure 2-36 Reinforcement details of rectangular columns

2.2.2 Test specimens

In Figure 2-35 and Figure 2-36, the dimensions of the column section were 400 mm × 400 mm for the square columns and 250 mm × 640 mm for the rectangular columns. Thus, the cross-sectional area A_g (=160,000 mm^2) of the square and rectangular columns was the same. The net column height from the base to the lateral loading point was a = 1200 mm, and the aspect ratios (= a/h) were 3.0 for square columns (h = 400 mm) and 4.8 for rectangular columns (h = 250 mm). In the rectangular columns, lateral load was applied to create bending about the weak axis because the weak column-strong beam mechanism can occur in that direction.

Figure 2-35(b) shows four types of transverse rebars and crossties used for the square columns, **Types A** through **D**. **Types A** and **B** indicate the conventional ties with 135° and 90° hook anchorages, respectively. In **Type C**, the rectangular one-piece tie is lap-spliced at an edge of the column section (lap splice length l_s = 300 mm) and, in the lap splice, a crosstie is used to support the longitudinal bar laterally. The crosstie was placed perpendicular to the loading direction so as not to contribute to the shear resistance of column. In **Type D**, bundles of two bars are placed at the corners of the rectilinear ties with 90° hook anchorage. By using the bundled bars, the column flexural strength increases, and at the same time, bar placement becomes easier because crosstie is not necessary. As shown in Figure 2-35(a), the anchorage hooks and lap splices of the ties were alternated end for end.

In the square columns, D25 bars (bar diameter d_b = 25.4 mm and yield strength f_y = 571 MPa) and D13 bars (d_b = 12.7 mm and yield strength f_{yt} = 500 MPa) were used for the longitudinal and transverse reinforcements, respectively. In **SAd2** (refer to Table 2-3), conventional hoops with 135° seismic hook anchorage (**Type A**) were placed at a spacing of 165 mm (= $d/2$). Crosstie was not used because the distance between two adjacent longitudinal bars was not greater than 150 mm. In **SBd2** and **SBd4**, conventional ties with standard 90° hook anchorage (**Type B**) were placed at spacings of 165 mm and 82 mm, respectively. In **SCd2**, lap-spliced ties (**Type C**) were used with crossties at a spacing of 165 mm. In **SDd2** and **SDd4** (**Type D**), rectangular ties with 90° hook anchorage were used at spacings of 165 mm and 82 mm, respectively, along with bundles of two D25 bars at the corners of the ties. The first tie and crosstie were placed at a height of 80 mm from the column base for **SAd2**, **SBd2**, **SCd2**, and **SDd2** or at a height of 50 mm for **SBd4** and **SDd4**.

Figure 2-36(b) shows the four types of transverse ties and crossties used for the rectangular columns, **Types E** through **H**. In **Types E** and **F**, the conventional ties with 135° and 90° hook anchorages, respectively, are used. In **Type G**, the one-piece ties are lap-spliced at the longer edge of the column section (l_s = 300 mm). On the other hand, in **Type H**, the two-piece U-bars are produced by lap-splicing two U-bars, each of which has 90° end hooks with $6d_b$ extensions embedded in the confined core. In all types of transverse reinforcement, crossties are used to support the intermediate longitudinal bars, complying with the requirements of ACI 318-14 25.7.2.3.

In the rectangular columns, D22 bars (d_b = 22.2 mm and f_y = 566 MPa) and D10 bars (d_b = 9.7 mm and f_{yt} = 530 MPa) were used for the longitudinal and transverse reinforcements, respectively. In **REd2**, the conventional hoops with 135° hook anchorage (**Type E**) were placed at a spacing of 105 mm (= d/2). In **RFd2** and **RFd3**, the conventional ties with 90° hook anchorage (**Type F**) were placed at spacings of 105 mm and 70 mm, respectively. In **RGd2**, the one-piece ties lap-spliced at the longer edge of the column (**Type G**) were used at a spacing of 105 mm. In **RHd2** and **RHd3**, two U-bars with 90° hooks at both ends were used as the lap-spliced two-piece U-bars (**Type H**). The tie spacings for **RHd2** and **RHd3** were 105 mm and 70 mm, respectively. The first tie and crosstie of each column were placed at a height of 50 mm from the column base.

2.2.3 Specimen construction

Construction procedures of the test specimens are illustrated in Figure 2-37. Steel cages were assembled with manufactured rebars. Strain gauges were attached on the longitudinal rebars and transvere rebars at the location specified in Figure 2-38. Since the flexural and shear damages were accumulated in the plastic hinge zone of columns, the attached gauges were concentrated in such plastic hinge zone. To minimize the effect of construction joint between column and pedestal, concrete was poured at the side of column specimens.

Before curing concrete, the steel rods were inserted in the specimens to install measuring equipment (LVDT, Linear Variable Differential Transformer) as shown in Figure 2-39. The specimens were steam cured for 3 days prior to stripping their molds for attaining target concrete strength. The column tests were conducted in 30 days after concrete placing.

<Manufactured re-bars>

<Assembling steel cages>

<Manufacturing molds>

<Placing concrete>

Figure 2-37 Construction procedures of column specimens

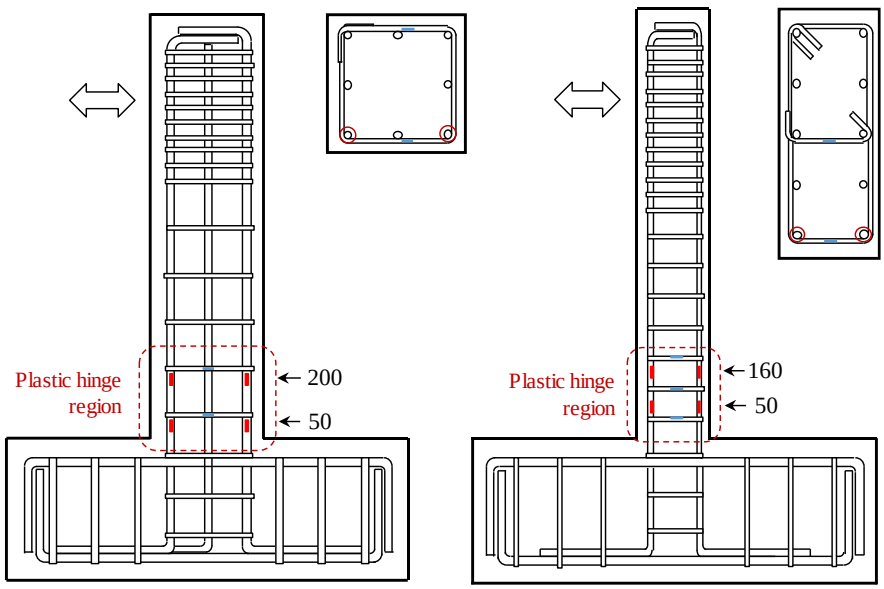

Figure 2-38 The locations of strain gauges in plastic hinge region of columns

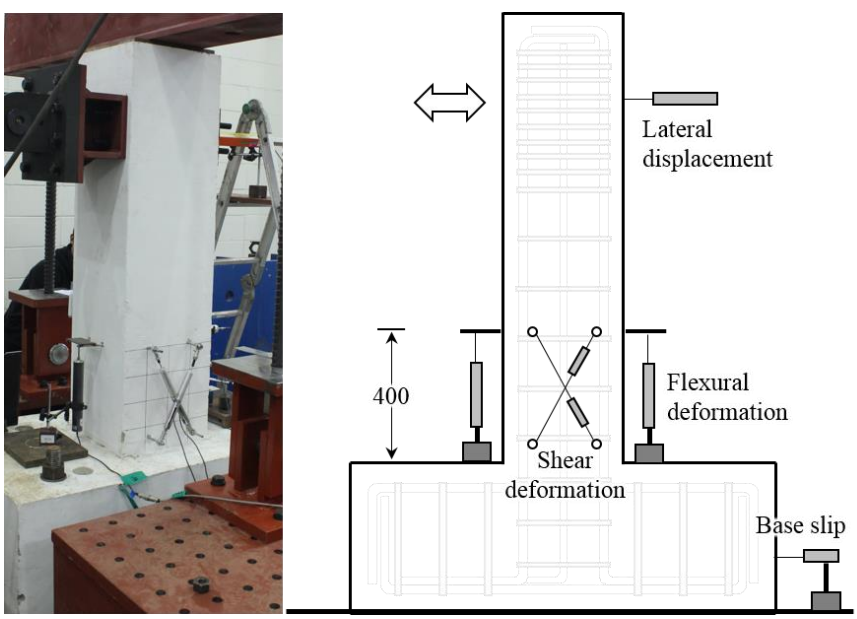

Figure 2-39 Measuring equipments for displacement and deformations

2.2.4 Material strengths

Table 2-4 shows the mix proportioning of the concrete. The maximum aggregate size was 25 mm. Six concrete cylinders of diameter 100 mm × height 200 mm were prepared for compression test. The compression test was performed on the first day of the column tests. The compressive strength of the concrete was f_c' = 32 MPa on average.

Table 2-5 and Figure 2-40 show the properties and strain-stress relations of steel reinforcing bars, respectively. The yield strengths of D22 and D25 longitudinal bars were f_y = 566 MPa and 571 MPa, respectively. The yield strengths of D10 and D13 transverse bars were f_{yt} = 530 MPa and 500 MPa, respectively.

Table 2-4 Mix design of concrete

Compressive strength	W/C	Unit weigh, kgf/m^3							Slump
		W	C	FS	S	FA	CA	SP	
32 MPa	55.5%	155	153	56	70	923	950	1.95	120 mm

Note: W = water; C = cement; FS = fly ash; S = blast furnace slag; FA = fine aggregate; CA = coarse aggregate; SP = superplasticizer,

Table 2-5 Properties of steel reinforcing bars

Type		d_b (mm)	f_y (MPa)	f_u (MPa)	E_s (GPa)	ε_y (mm/mm)
Longitudinal reinforcement	SD500 D22	22.2	566	678	204	0.00277
	SD500 D25	25.4	571	700	200	0.00285
Transverse reinforcement	SD400 D10	9.53	530	591	205	0.00259
	SD400 D13	12.7	500	645	200	0.00250

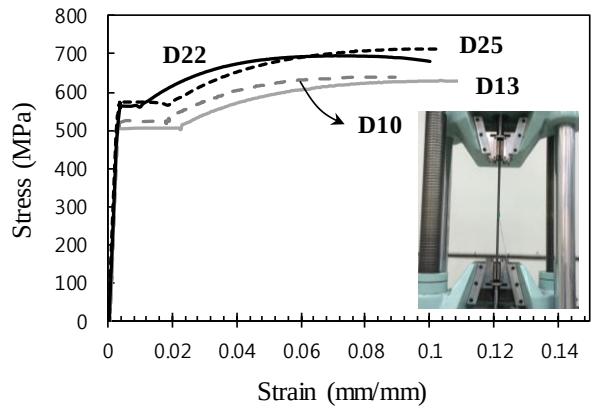

Figure 2-40 Stress and strain curves of steel reinforcing bars

2.2.5 Test setup and loading plan

Figure 2-41 and Figure 2-42 show the test setup for the lateral and axial loading. The cyclic lateral loading was performed by controlling the displacement of the actuator (maximum stroke ± 250 mm) placed at a height of 1200 mm from the column base. Figure 2-43 shows the displacement history for the cyclic lateral loading. Load cycles were repeated three times at each displacement step. The loading protocol was planned with increasing of 1.25 ~ 1.5 times previous drift ratio and three steps at every drift ratio specified in ACI 374.1. The lateral displacement of the columns was increased from 0.25% in the elastic range to the drift ratio at 80% of peak loads in the descending branch.

Axial loads N of $0.10\,A_g f_c'$ and $0.17 A_g f_c'$ were applied to the columns by post-tensioning two high-strength Dywidag bars (diameter = 47 mm) (see Figure 2-41). For the post-tensioning, a steel beam was placed on top of the concrete column, and two hydraulic jacks with a capacity of 1000 kN were then placed on the steel beam. During cyclic lateral loading test, the axial load was maintained uniformly. To eliminate the contribution of the Dywidag bars to the column strength and stiffness, pin joints were placed at the bottom of the Dywidag bars (see Figure 2-41). The axial load created by the Dywidag bars always acts at the geometric center of the column because both the column and Dywidag bars are displaced simultaneously. Therefore, the second-order effect can be ignored in the lateral load-displacement relationship.

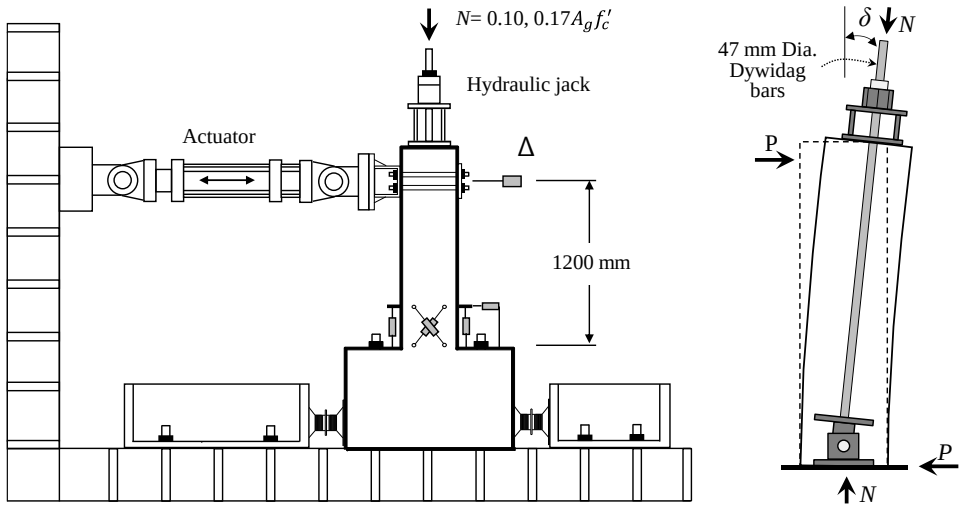

Figure 2-41 Schematic test setup of RC column

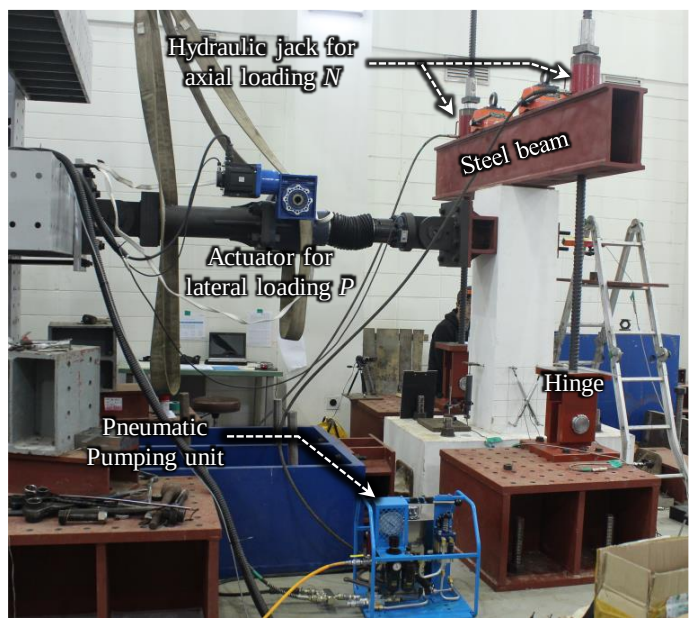

Figure 2-42 Photograph of the test setup

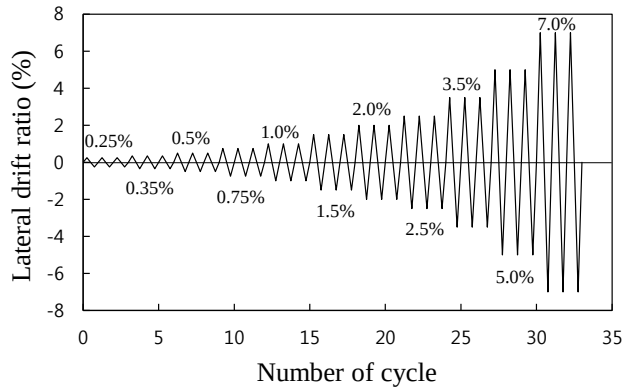

Figure 2-43 Displacement history for cyclic lateral loading

2.3 Test Results and Observations

2.3.1 Cyclic behavior and failure mode of square columns

Figure 2-44 shows the lateral load-drift ratio (P-δ) relationships of the square columns, **SAd2**, **SBd2**, **SBd4**, **SCd2**, **SDd2**, and **SDd4**. The drift ratio δ was calculated by dividing the net lateral displacement at the loading point by the shear span (a =1200 mm). The maximum load P_u of each column is denoted with circles. For comparison, the nominal flexural strengths P_n (=M_n /a) calculated by section analysis are denoted as horizontal dashed lines. Figure 2-45 shows concrete damages at δ = 3.5% and failure modes at the end of the tests.

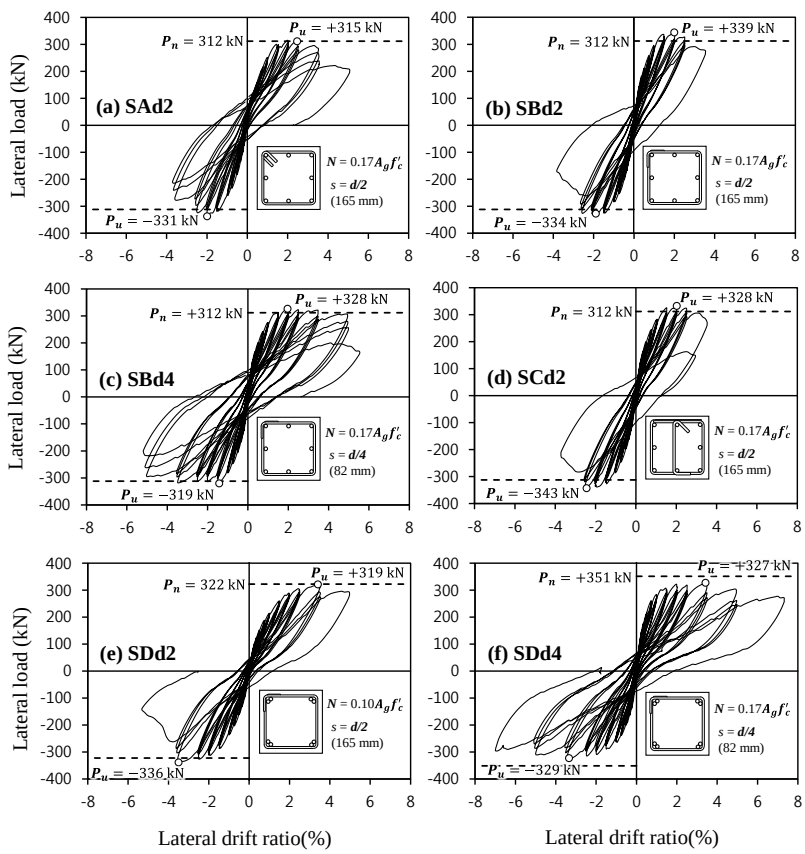

Figure 2-44 Lateral load and drift ratio relationships of square columns

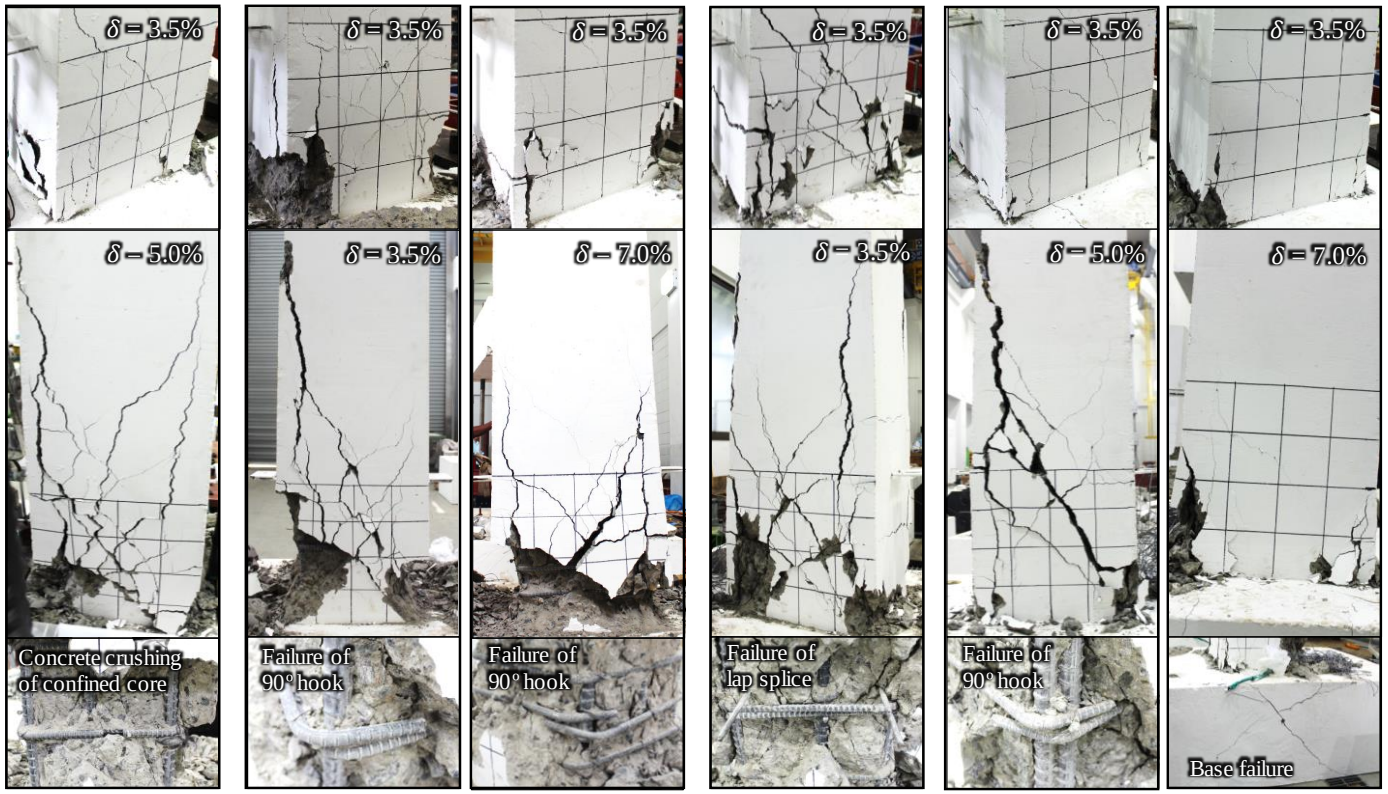

(a) SAd2 (b) SBd2 (c) SBd4 (d) SCd2 (e) SDd2 (f) SDd4

Figure 2-45 Failure modes of square columns

In **SAd2** using conventional hoops with 135° seismic hook anchorage (see Figure 2-44(a)), at δ = 2.0% ~ 2.5%, the maximum loads (P_u = +315 kN and -331 kN) were reached and the spalling of the cover concrete occurred. At δ = 3.5%, a significant strength degradation occurred, and then, the column failed at the first load cycle to δ = +5.0%. As shown in Figure 2-46, the failure mode of **SAd2** was excessive web shear cracking and subsequent concrete crushing (i.e. shear failure after flexural yielding). Despite the severe damage in the cover concrete, anchorage failure did not occur in the hoops.

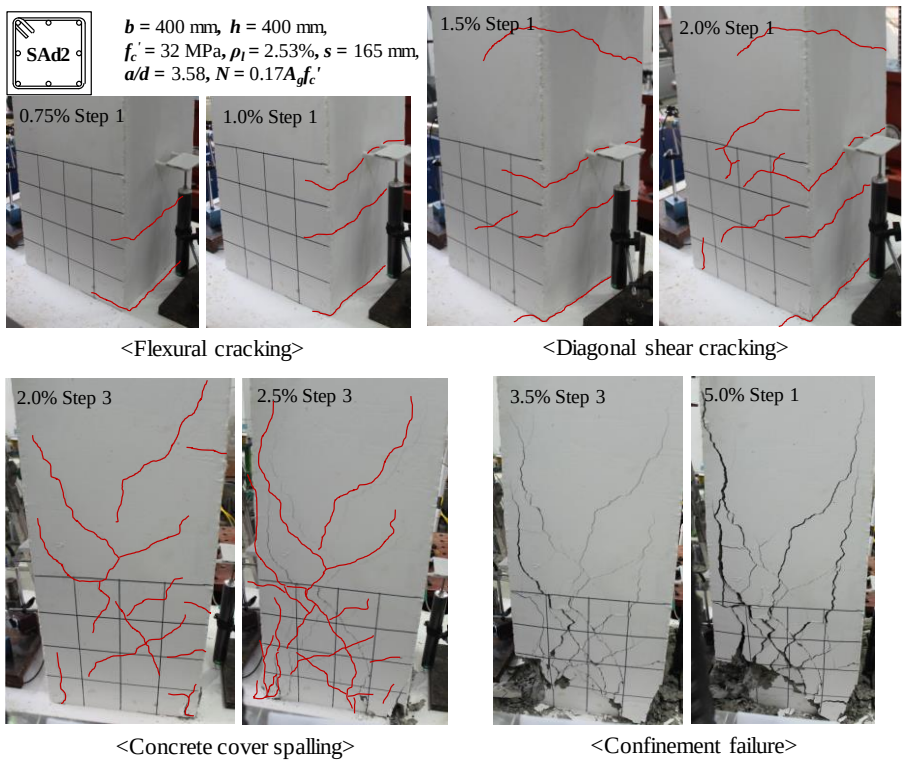

Figure 2-46 Failure sequence of specimen SAd2

In **SBd2** using conventional ties with 90° standard hook anchorage (see Figure 2-44(b) and Figure 2-45 (b)) and **SCd2** using lap-spliced one-piece ties (see Figure 2-44(d) and Figure 2-45(d)), the maximum loads P_u were equivalent to those of **SAd2**; however, post-yield shear failure occurred at δ = 3.5%, which was earlier than in **SAd2** failed at δ = 5.0%, due to the excessive web shear cracking and the anchorage failure of the ties.

On the other hand, in **SBd4** using conventional ties with 90° standard hook anchorage at the reduced spacing $d/4$ (see Figure 2-44(c) and Figure 2-45(c)), shear cracking in the web was limited at δ = 3.5%, and consequently a ductile behavior was observed without significant strength degradation until the first load cycle at δ = 5.0%. **SBd4** eventually failed at the third load cycle at δ = 5.0% due to the anchorage failure of the ties and subsequent concrete crushing in the confined core.

In **SDd2** using conventional ties with 90° hook anchorage along with longitudinal bundled bars (see Figure 2-44(e)), the maximum loads P_u occurred at δ = 3.5% and then post-yield shear failure followed at the first load cycle to δ = -5.0%. The failure mode was excessive shear cracking in the web and anchorage failure at the 90° hook (see Figure 2-45(e) and Figure 2-47). When compared to the cyclic curves of **SAd2** and **SDd2**, the area enclosed by a full load cycle (i.e. hysteretic energy dissipation) was significantly decreased in **SDd2**. The decreased hysteretic energy dissipation might be attributed to the bond-slip of the bundled bars occurring in the plastic hinge region where concrete damages were concentrated.

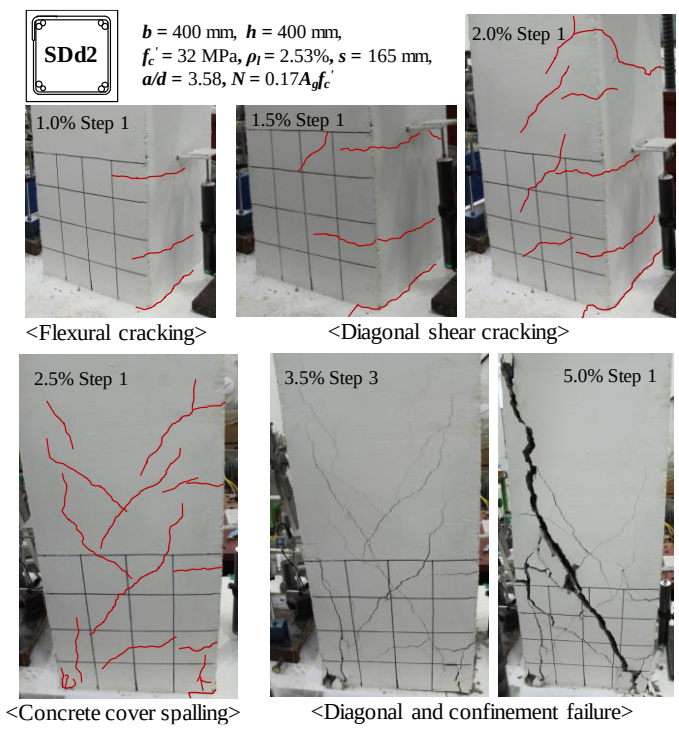

Figure 2-47 Failure sequence of specimen SDd2

Figure 2-44(f) and Figure 2-45(f) show the test results of **SDd4** using conventional ties with 90° hook anchorage at the reduced spacing $d/4$, along with longitudinal bundled bars. The maximum loads P_u occurred at δ = 3.5% and then load-carrying capacity were maintained until the first load cycle at δ = 7.0%. Only in **SDd4**, unlike the other square columns, the maximum load P_u was 6.9% less than the predicted nominal strength P_n. This indicates that yielding of the bundled bars and the resulting bond slip might have occurred within the base slab, rather than in the column with the closely-spaced ties ($s = d/4$). As shown in Figure 2-45(f), diagonal cracks were observed at the side of the base slab, while concrete damages in the column were relatively limited. As shown in Figure 2-48, in **SDd4**, the strains of the longitudinal bundled bars (i.e. **RU**, **RD**, **LU**, and **LD**) measured in the column did not reach the yield strain (ε_y = 0.00285 mm/mm), while in **SBd4**, the strains of the distributed bars exceeded the yield strain. It is noted that, in Figure 2-48, the lines indicate the envelope curves connecting the maximum tensile strain of the longitudinal bars at each drift level. Such observations demonstrate the yielding of bundled bars occurred within the base slab.

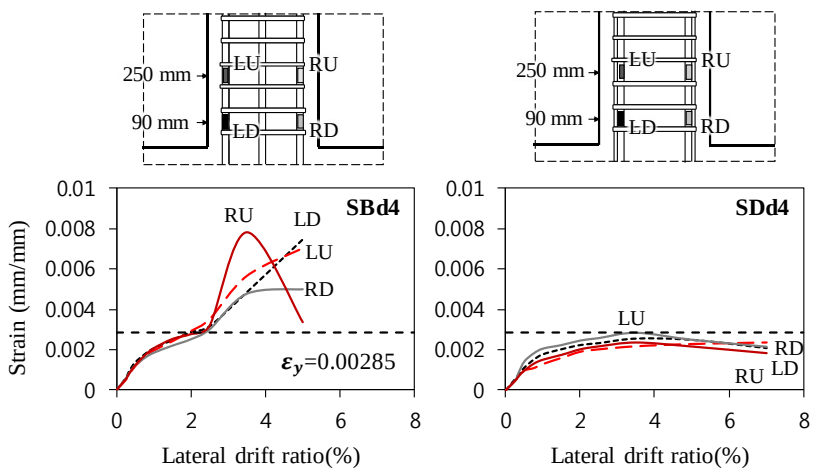

Figure 2-48 Strains of longitudinal bars in SBd4 and SDd4

2.3.2 Cyclic behavior and failure mode of rectangular columns

Figure 2-49 and Figure 2-50 show the *P*-*δ* relationships and failure modes of the rectangular columns, **REd2**, **RFd2**, **RFd3**, **RGd2**, **RHd2**, and **RHd3**. The maximum loads P_u and nominal strengths P_n are denoted as circles and horizontal dashed lines, respectively. Since the columns were subjected to the weak axis bending moment, the maximum loads were less than those of the square columns. The nominal flexural strengths P_n agreed well with the test maximum loads P_u.

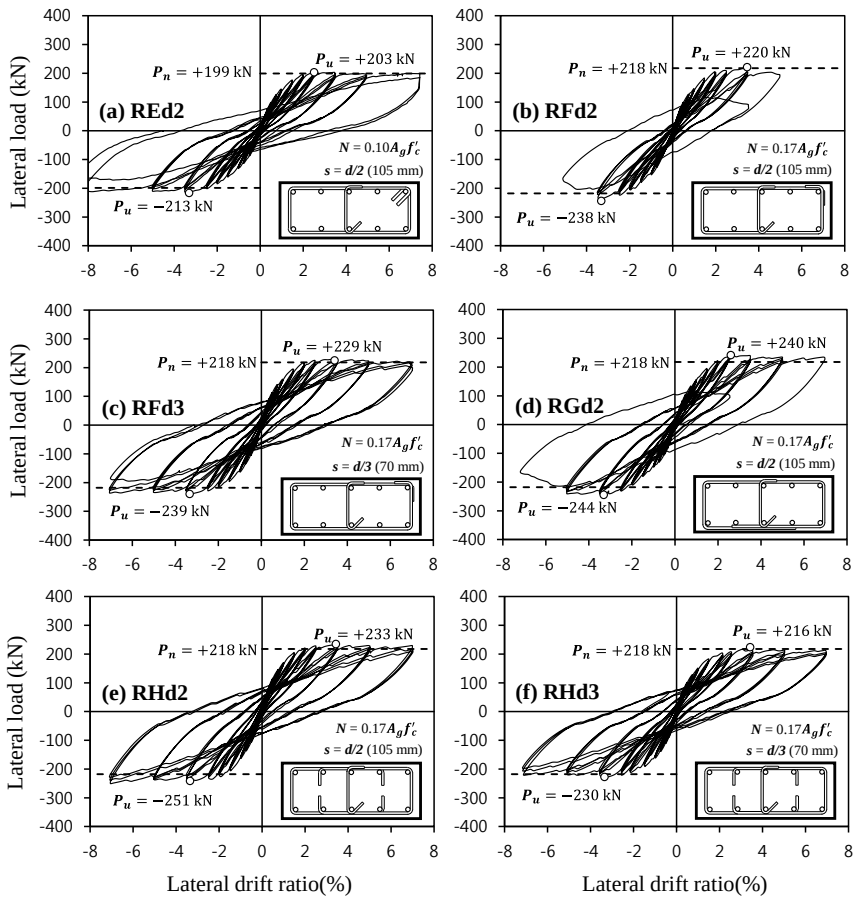

Figure 2-49 Lateral load and drift ratio relationships of rectangular columns

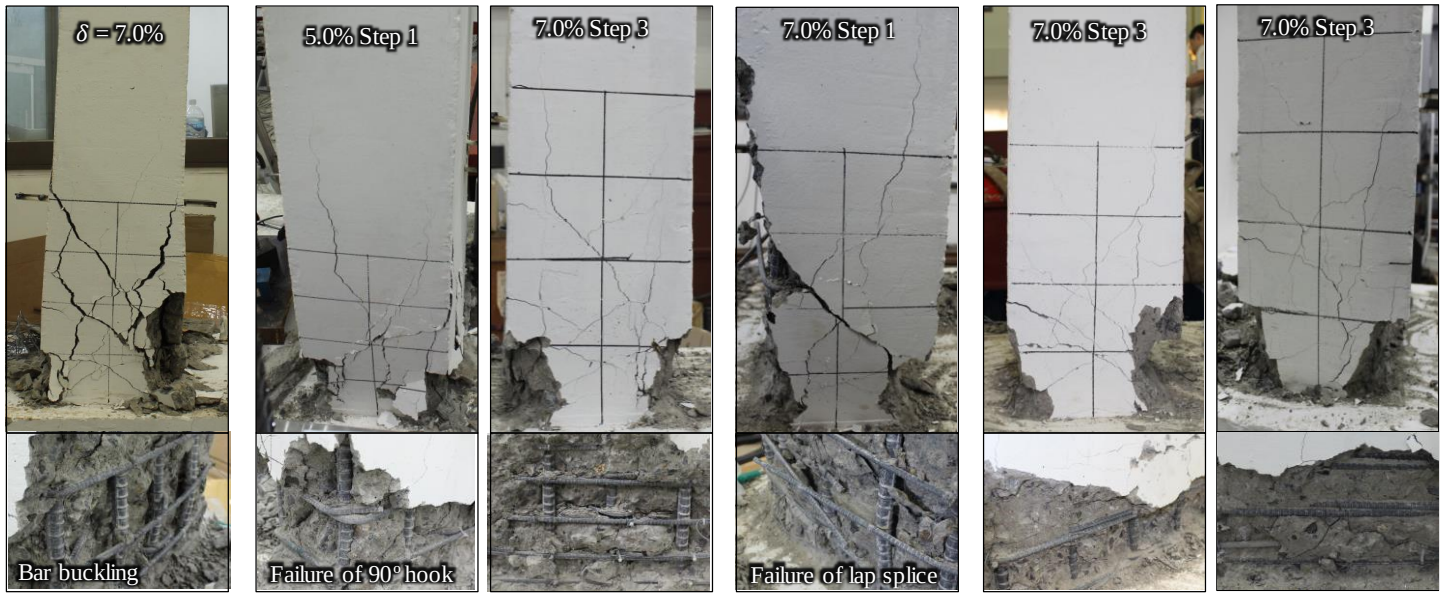

(a) REd2 (b) RFd2 (c) RFd3 (d) RGd2 (e) RHd2 (f) RHd3

Figure 2-50 Failure modes of rectangular columns

In **REd2** using conventional hoops with 135º standard hook anchorage (see Figure 2-49(a) and Figure 2-50(a)), the maximum loads occurred at $\delta = 2.5\% \sim 3.5\%$. The load-carrying capacity was maintained until δ = 7.0% without significant strength degradation. The failure mode of **REd2** was excessive concrete crushing and subsequent longitudinal bar buckling. Although the axial load $N = 0.10A_g f_c'$ was applied, excessive web shear cracking occurred at δ = 5.0% as shown in Figure 2-51.

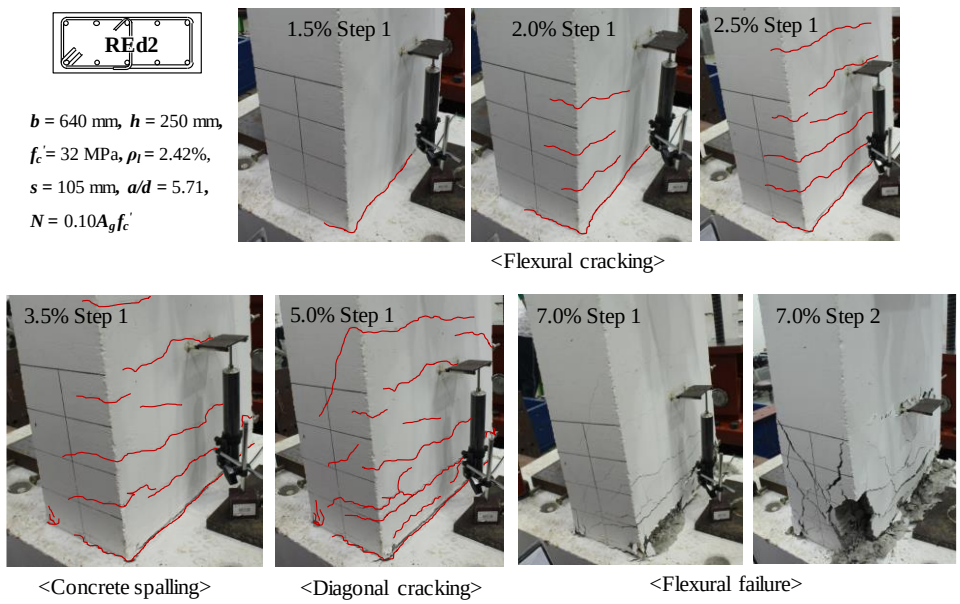

Figure 2-51 Failure sequence of specimen REd2

RFd2 using conventional ties with 90° standard hook anchorage (see Figure 2-49(b) and Figure 2-50(b)) showed a ductile behavior until the first load cycle at δ = 5.0%. Failure occurred at the second load cycle to δ = +5.0% due to the anchorage failure of the ties. In **RFd3** with the reduced tie spacing of 70 mm (= d/3) (see Figure 2-49(c) and Figure 2-50(c)), the load-carrying capacity was maintained until the third load cycle at δ = +7.0%, which was equivalent to **REd2**. Because of the lack of the actuator stroke, the test was ended at δ = +7.0%. Even at such large deformations, web shear cracking was limited.

In **RGd2** with lap-spliced one-piece ties (see Figure 2-49(d) and Figure 2-50(d)), failure occurred at the first load cycle to δ = -7.0%. After spalling of the cover concrete, bond failure occurred at the lap splice due to out-of-plane lateral

displacement of the buckled longitudinal bars. In contrast, in **RHd2** and **RHd3** using lap-spliced U-bars with 90° end hooks (see Figure 2-49(e) ~ Figure 2-49(f) and Figure 2-50(e) ~ Figure 2-50(f)), failure did not occur even after the third load cycle at δ = 7.0%; because of the lack of the actuator stroke, the tests were terminated at δ = +7.0%. In **RHd2** and **RHd3**, web shear cracks were limited. None of lap-spliced U-bar failure, excessive concrete crushing in the confined core, or longitudinal bar buckling occurred. These results indicate that the hooked U-bars performed well even at large inelastic deformations.

2.3.3 Energy dissipation

Figure 2-52 shows the cumulative energy dissipation which indicates the total energy absorption during cyclic loadings. The cumulative energy dissipations of square and rectangular columns showed similar trend regardless of the tie details until δ = 2.0% ~ 2.5% in which maximum loads were attained. However, after peak loads, the cumulative energy dissipations differed. The 90° hook specimens, **SBd2** and **RFd2**, which failed by loosening hook anchorages had least energy dissipation capacities. On the other hand, the 135° hook specimens (**SAd2** and **REd2**) and lap spliced U-bars with 90° hook specimen (**RHd2**) had superior energy dissipations by preventing the anchorage failure.

Since the rectangular columns showed greater inelastic deformations in ultimate state, the rectangular columns dissipated more energy than the square columns. It means that rectangular columns with ductile behavior can be more advantageous to seismic loading in terms of energy dissipation in spite of less load carrying capacity.

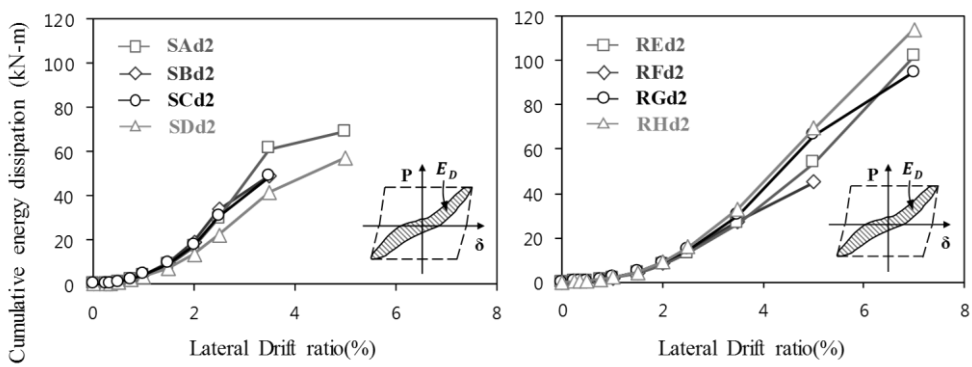

Figure 2-52 Cumulative energy dissipation of columns

2.4 Nonlinear Modeling for Various Tie Details

Behavior characteristic, such as stiffness, loading capacity, and deformation capacity, should be defined to evaluate seismic performance of columns using non-seismic tie details. ASCE41-13 about seismic evaluation and retrofit of existing buildings was used to analyze effective lateral stiffness and nonlinear modeling parameters to define deformation capacity.

2.4.1 Effective stiffness

The effective lateral stiffness (K_e) of test results can be defined from load and displacement envelope curves with proposed methods from several researchers. In this study, K_e is calculated with the secant stiffness at the applied load equal to 60% of the effective yield strength of columns. The effective stiffness values (K_{eff}) without experimental data can be calculated as follows.

$$K_{eff} = \begin{cases} 0.3E_cI_g\left(\frac{3}{a^3}\right) & for \ \frac{P}{A_g f_c'} < 0.1 \\ \left(\frac{P}{A_g f_c'} + 0.2\right)E_cI_g\left(\frac{3}{a^3}\right) & for \ 0.1 \le \frac{P}{A_g f_c'} < 0.5 \\ 0.7E_cI_g\left(\frac{3}{a^3}\right) & for \ \frac{P}{A_g f_c'} \ge 0.5 \end{cases} \quad (2\text{-}12)$$

where, E_c = Modulus of elasticity of concrete (= $8500\sqrt[3]{f_c'}$), f_c' = Compressive strength of concrete, I_g = Moment of inertia of gross concrete about centroidal axis, a = Shear span of a cantilever column (= 1200 mm). Equation (2-12) represents flexural rigidity of cantilever column

Table 2-6 shows the effective lateral stiffness (K_e) from test results and the effective stiffness values (K_{eff}) from Equation (2-12). The specimen **SDd4** was

excluded due to deficient load carrying capacity by unexpected anchorage failure. The ratio of experimental stiffness to predicted stiffness (K_e / K_{eff}) is 0.64 ~ 0.94 in the square columns (a/h = 3.0) and 0.83 ~ 1.18 in the rectangular columns (a/h =4.8). The average ratio (K_e / K_{eff}) of flexural dominated rectangular columns is 0.98, while that of flexural-shear dominated square columns is 0.81. Effective lateral stiffness from ASCE41-13 can be applied to define effective stiffness of columns using non-seismic tie details proposed in this study.

2.4.2 Maximum deformation

Nonlinear load and deformation relationship should be obtained to evaluate initial stiffness, strength, and deformation capacity of test results. Nonlinear modeling procedures specified in ASCE41-13 were discussed as follows and compared to test data from square and rectangular columns in this study.

The failure conditions i ~ iii are obtained from the classification into flexural, flexural-shear, and shear failure according to transverse reinforcement details and shear capacity ratio (V_p / V_o) in Table 2-7 and Table 2-8. Transverse reinforcement details include 135° hook, 90° hook, and lap-spliced transverse reinforcement. V_p is the plastic shear demand at flexural yielding of plastic hinge and V_o is nominal shear strength with Equation (2-13).

$$V_o = \frac{A_v f_y d}{s} + \lambda \left(\frac{0.5\sqrt{f_c'}}{M/Vd} \sqrt{1 + \frac{N_u}{0.5\sqrt{f_c'} A_g}} \right) 0.8 A_g \qquad (2\text{-}13)$$

where M / Vd is the largest ratio of moment to shear times effective depth under design loadings for the column but shall not be taken greater than 4 or less than 2. d is the effective depth (= 0.8h). A_g is the gross cross sectional area of the column.

Modeling parameters a ~ c are computed from failure conditions (i ~ iii), axial load (P / $A_g f_c'$), shear reinforcement ratio ($\rho = A_v / b_w s$), and design shear force (V / $b_w d\sqrt{f_c'}$) in Table 10-8 specified in ASCE41-13. As shown in Figure 2-53(a), modeling parameter a provides the plastic rotation at the point of a 20% or greater

reduction in the lateral loading capacity from the peak load. Modeling parameters *b* and *c* provide an estimate of the plastic rotation at the axial load failure and residual strength ratio after reduction of lateral force resistance.

Figure 2-53(b) and (c) compare nonlinear load and deformation relationship predicted from ASCE41-13 with the test results. In the predictions, the initial lateral stiffness K_{eff} in Equation (2-12) was used and the maximum strength was estimated by sectional analysis. The lateral deformations were determined by nonlinear modeling parameters $a \sim c$ in Table 2-7. Seismic hoop details with 135° hook(A and E), and non-seismic tie details with 90° hook(B, D, and F) are relevant to the failure condition ⅱ, while alternative tie details (C, H, and G) are applicable to the failure condition ⅲ. Specimen **RHd3** with the tie detail of H and $s = d/3$ was classified into the failure condition ⅱ due to increase nominal shear strength V_o.

As shown in Figure 2-53, the initial stiffness and maximum strength showed great agreement with the test results, whereas the lateral deformations did not because the specimens using the alternative tie details (**SCd2**, **RHd2**, and **RGd2**) did not apply plastic deformation after maximum strength due to modeling parameter $a = 0$ from failure condition ⅲ. Therefore, the modeling parameter for alternative tie details, such as lap spliced, and U-bars, should be revised to similar deformation capacity with 90° hook detail in ASCE41-13 in the case of applying axial load of below $0.17 A_g f_c'$.

Table 2-6 Effective stiffness and ductility ratio of column specimens

Speci-men	Positive direction						Negative direction					
	K_e [1] (kN/mm)	K_{eff} [2] (kN/mm)	K_e/K_{eff}	Δ_y [3] (mm)	Δ_u [4] (mm)	Δ_u/Δ_y	K_e (kN/mm)	K_{eff} (kN/mm)	K_e/K_{eff}	Δ_y (mm)	Δ_u (mm)	Δ_u/Δ_y
SAd2	24.6	38.5	0.64	12.36 (1.03)[5]	50.88 (4.24)	4.1	27.7	38.5	0.72	11.64 (0.97)	46.92 (3.91)	4
SBd2	36	38.5	0.94	9.24 (0.77)	44.04 (3.67)	4.8	34.7	38.5	0.9	9.36 (0.78)	37.08 (3.09)	4
SBd4	34.7	38.5	0.9	9.24 (0.77)	61.68 (5.14)	6.7	35.3	38.5	0.92	8.88 (0.74)	60.36 (5.03)	6.8
SCd2	33.6	38.5	0.87	9.48 (0.79)	44.04 (3.67)	4.6	32.8	38.5	0.85	10.2 (0.85)	40.20 (3.35)	3.9
SDd2	20.7	31.2	0.66	15.12 (1.26)	77.04 (6.42)	5.1	23.1	31.2	0.74	8.4 (0.7)	51.96 (4.33)	6.2
REd2	14.4	12.2	1.18	13.92 (1.16)	89.04 (7.42)	6.4	10.8	12.2	0.89	19.68 (1.64)	95.16 (7.93)	4.8
RFd2	13.8	15	0.92	15.72 (1.31)	59.88 (4.99)	3.8	13.3	15	0.89	17.28 (1.44)	61.32 (5.11)	3.5
RFd3	16.2	15	1.08	13.92 (1.16)	84.00 (7.00)	6	14.7	15	0.98	15.72 (1.31)	84.72 (7.06)	5.4
RGd2	16.8	15	1.12	13.56 (1.13)	83.88 (6.99)	6.2	14.4	15	0.96	16.92 (1.41)	78.84 (6.57)	4.7
RHd2	13.6	15	0.91	17.28 (1.44)	83.76 (6.98)	4.8	12.5	15	0.83	18.96 (1.58)	86.28 (7.19)	4.6
RHd3	14.6	15	0.97	14.28 (1.19)	83.64 (6.97)	5.9	15.8	15	1.05	14.04 (1.17)	85.44 (7.12)	6.1

1) K_e : Effective lateral stiffness from test curves
2) K_{eff} : Effective stiffness value from Equation (2-13) of ASCE41-13
3) Δ_y : Yield displacement
4) Δ_u: Ultimate displacement
5) ( ) : Lateral drift ratio , Δ/L (%)

Table 2-7 Nonlinear modeling parameters of column specimens

Specimen	V_o (kN)	V_p (kN)	$\frac{V_p}{V_o}$	Tie detail	Failure condition [1]	Spacing (mm)	ρ_{tie}	Axial load ratio	$\frac{V}{b_w d\sqrt{f_c'}}$ [2]	Modeling parameter [3]		
										a	b	c
SAd2	449	312	0.69	135º	ii	165	0.39	0.17	0.41	0.0182	0.0354	0.172
SBd2	449	312	0.69	90º	ii	165	0.39	0.17	0.41	0.0182	0.0354	0.172
SBd4	728	312	0.43	90º	ii	82	0.77	0.17	0.41	0.0249	0.0528	0.172
SCd2	449	312	0.69	Lap splice	iii	165	0.39	0.17	0.41	0	0.0346	0
SDd2	424	322	0.69	90º	ii	165	0.39	0.1	0.42	0.0201	0.0402	0.2
REd2	317	199	0.63	135º	ii	105	0.32	0.1	0.26	0.0216	0.035	0.2
RFd2	332	218	0.66	90º	ii	105	0.32	0.17	0.29	0.0189	0.031	0.172
RFd3	445	218	0.49	90º	ii	70	0.48	0.17	0.29	0.024	0.044	0.172
RGd2	332	218	0.66	Lap splice	iii	105	0.32	0.17	0.29	0	0.029	0
RHd2	332	218	0.66	U-bar	iii	105	0.32	0.17	0.29	0	0.029	0
RHd3	445	218	0.49	U-bar	ii	70	0.48	0.17	0.29	0.024	0.044	0.172

1) Failure condition: refers to Table 2-8
2) $V / b_w d\sqrt{f_c'}$: Design shear force
3) Modeling parameter: refers to Table 10-8 in ASCE41-13

Table 2-8 Condition according to transverse reinforcement details

Shear capacity ratio	135-degree hooks	90-degree hooks	Other (Lap-spliced transverse reinforcement)
$V_p / V_o \leq 0.6$ 1)	i	ii	ii
$0.6 < V_p / V_o \leq 1.0$	ii	ii	iii
$V_p / V_o > 1.0$	iii	iii	iii

1) V_p : Plastic shear demand at flexural yielding of plastic hinge,
V_o : Nominal shear strength in Equation (2-13)

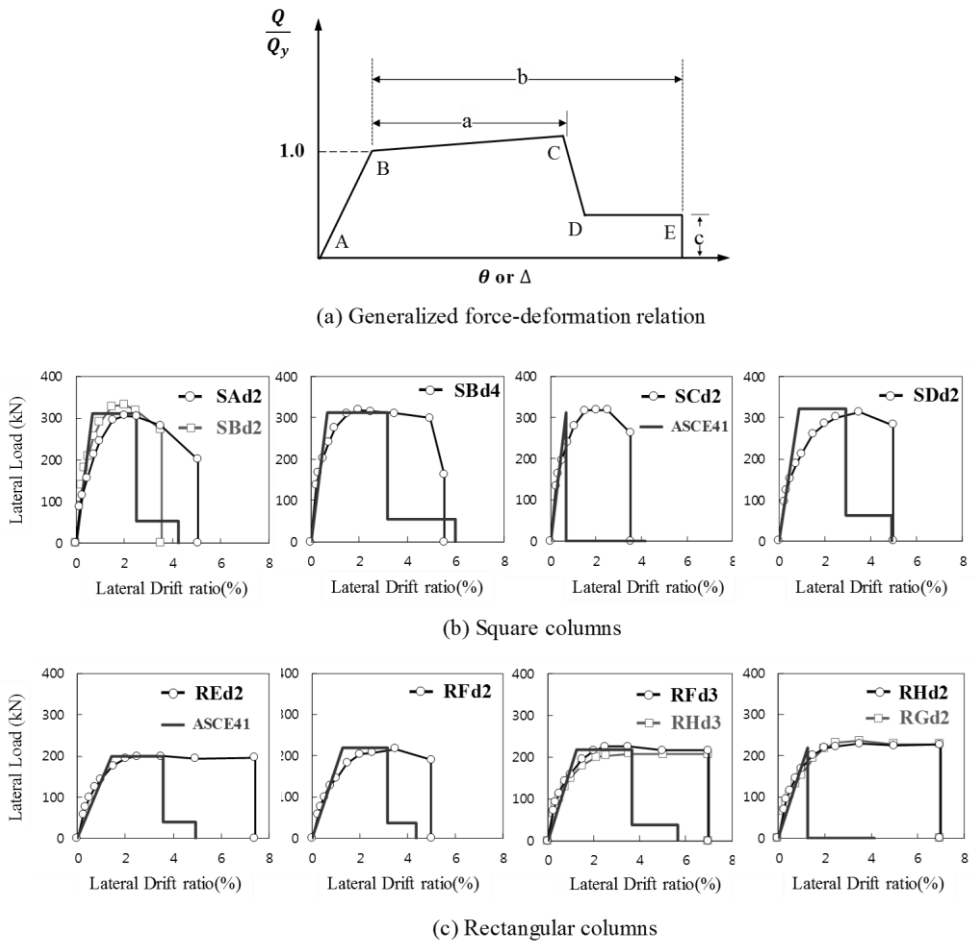

(a) Generalized force-deformation relation

(b) Square columns

(c) Rectangular columns

Figure 2-53 Comparison of backbone curves specified in ASCE41-13 and test curves

2.5 Factors Affecting Deformation Capacity

2.5.1 Degradation of shear strength

Table 2-9 compares the shear demand V_u (or test strength) and nominal shear strength V_n of the column specimens. V_u is the mean of the positive and negative maximum loads P_u. V_n was calculated as the sum of the shear contributions of concrete (V_c) and transverse reinforcement (V_s), in accordance with ACI 318-14: $V_c = 0.17(1+N/[14A_g])\sqrt{f_c'}bd$ and $V_s = A_v f_{yt} d/s$, where N = applied axial compression load, b and d = width and effective depth of the column section, and f_{yt} and s = yield strength and spacing of the transverse reinforcement.

For square columns, the nominal shear strength V_n (= $V_c + V_s$) was greater than the shear demand V_u by factors of 1.33~2.27. Thus, flexural yielding occurred prior to web shear failure, except for **SDd4** where yielding of the bundled bars occurred within the base slab. As shown in Table 2-9, in **SBd4**, the shear strength contribution V_s (= 554 kN) of the transverse reinforcement alone was greater than the shear demand V_u (= 324 kN). As a result, the web shear cracking was limited until the first load cycle at δ = 5.0%. On the other hand, in **SAd2**, **SBd2**, **SCd2**, and **SDd2** where V_s was less than V_u (i.e. V_s/V_u = 0.82 ~ 0.85), web shear failure occurred at relatively low drift ratios, δ = 2.5% ~ 3.5%. Thus, it seemed that the shear strength resisted by the transverse reinforcement alone (V_s) was a primary factor that significantly affected the post-yield shear failure and deformation capacity of the columns.

The shear failure mechanism after flexural yielding can be explained by existing shear strength degradation models (Watanabe and Ichinose, 1991; Ascheim and Moehle, 1992; Priestley et al., 1994; Sezen and Moehle, 2004; Park et al., 2012; ASCE 41-13). When columns are subjected to inelastic deformation after flexural yielding, the shear resistance of the concrete gradually decreases. Such post-yield shear strength degradation is mostly attributed to concrete rather than transverse reinforcement. The shear resistance of concrete V_c decreases further during cyclic loading as crack-opening and closing are repeated. However, the shear resistance of transverse reinforcement V_s gradually increases or remains uniform during repeated load cycles at large inelastic deformation as strains of the ties and crossties continue to increase.

The decreased post-yield shear strength V_{nr} of columns can be defined as follows.

$$V_{nr} = \eta V_c + V_s \tag{2-14}$$

where η (≤ 1.0) is a reduction factor addressing the decrease in the concrete shear strength during the post-yield ductile behavior. If V_{nr} is less than the shear force demand, post-yield shear failure occurs in the columns.

In Equation (2-14), it is difficult to determine the coefficient η directly from the test results because the exact values of V_c and V_s are not known. In this study, the coefficient η was investigated using the test results as follows. For clarity, the calculation process was explained for **SAd2** (see Table 2-9). First, V_{nr} was determined as the test strength V_u: V_{nr} = 323 kN. Then, by assuming $V_c = 0.17(1+N/[14A_g])\sqrt{f_c'}bd$ and $V_s = A_v f_{yt} d/s$ (ACI 318-14), the coefficient η was calculated as $\eta = (V_{nr} - V_s)/V_c$ (see Equation (2-14)): V_c = 180 kN, V_s = 275 kN, and η = 0.267. Table 2-9 shows the η values of **SBd2**, **SCd2**, and **SDd2**, calculated in the same manner. The calculated η values varied from 0.267 to 0.344 and the mean value was 0.321. This indicates, in the square columns, the concrete resisted only 32% of its nominal strength V_c at the point of the post-yield shear failure (δ_u = 2.49% ~ 5.03%).

The post-yield shear strength degradation also occurred in the rectangular columns with $V_s < V_u$, such as **RFd2**, **RGd2**, and **RHd2** (see Table 2-9). **RFd2** and **RGd2**, showing anchorage failure at the 90° hook and lap splice, retained $0.022V_c$ at δ_u = 4.20% and $0.095V_c$ at δ_u = 5.0%, respectively. **RHd2** without anchorage failure of U-bars had $0.095V_c$ at δ_u = 7.02%. When compared to the square columns, the residual shear strength of the concrete was relatively less in the rectangular columns because the lateral drift ratios at failure were greater (see Table 2-9)).

Table 2-9 Shear strengths, ductility, and failure mode of specimens

Specimen	Test strength	Nominal strength			Strength ratios			Ductility			Failure mode [3]
	V_u (kN)	V_c (kN)	V_s (kN)	$V_n (=V_c+V_s)$	V_n/V_u	V_s/V_u	$\eta = (V_u-V_s)/V_c$	δ_y [1] (%)	δ_u [2] (%)	$\mu = \delta_u/\delta_y$	
SAd2	323	180	275	456	1.41	0.85	**0.267**	0.8	3.5	**4.38**	WS
SBd2	337	180	275	456	1.35	0.82	**0.344**	0.78	2.67	**3.42**	AF and WS
SBd4	324	180	554	734	2.27	1.71	-	0.74	5.03	6.80	AF and WS
SCd2	336	180	275	456	1.36	0.82	**0.338**	0.79	2.92	**3.69**	AF and WS
SDd2	328	159	275	435	1.33	0.84	**0.333**	1.16	3.58	**3.09**	AF and WS
SDd4	328	180	554	734	2.24	1.69	-	-	-	-	Bar anchorage
REd2	208	158	225	383	1.84	1.08	-	1.16	7.42	6.40	BB and WS
RFd2	229	179	225	403	1.76	0.98	**0.022**	1.31	4.58	**3.50**	AF
RFd3	234	179	337	516	2.21	1.44	-	1.16	7.0	6.03	Not failed
RGd2	242	179	225	403	1.67	0.93	**0.095**	1.41	6.0	**4.26**	AF (U bars)
RHd2	242	179	225	403	1.67	0.93	**0.095**	1.44	7.08	**4.92**	Not failed
RHd3	223	179	337	516	2.31	1.51	-	1.19	6.97	5.86	Not failed

1) $\delta_y = P_u/K_y$, where P_u = the maximum load and K_y = the secant stiffness connecting the origin and the pre-peak point of $0.6P_u$ (ASCE 41-13 Chapter 7).

2) δ_u was defined as the smaller of the positive and negative maximum drift ratios corresponding to 80% of the maximum load or as the drift ratio at the end of tests.

3) WS, AF, and BB indicate the failure modes of web shear failure, anchorage failure of transverse bars, and bar buckling, respectively.

It should be noted that, columns showing ductile behavior after flexural yielding do not always fail due to the post-yield shear-strength degradation. Rather, the post-yield shear failure can occur only in the columns where the shear strength of the transverse reinforcement alone is less than the maximum load (i.e. $V_s < V_u$). For example, as shown in Figure 2-45 and Figure 2-50, **SBd4**, **SDd4**, **REd2**, **RFd3**, and **RHd3** satisfying $V_s > V_u$ were failed due to the excessive concrete crushing at the cover and confined core without significant web shear cracking, which is the typical flexure-compression failure mode in columns subject to axial compression. Thus, such column specimens were excluded from the calculation of η in Table 2-9.

2.5.2 Anchorage details of ties

As shown in Figure 2-44 and Table 2-9, the deformation capacity of **SAd2** using seismic hoops with 135º hook anchorage, δ_u = 3.5%, was clearly greater than those of **SBd2** and **SCd2** using 90°-hooked and lap-spliced ties. This indicates that such poor anchorage details caused premature anchorage failure of ties as the stress of the transverse bars increased close to the yield stress, as follows.

Figure 2-54 shows the transverse bar strains measured from the square columns, **SAd2**, **SBd2**, **SBd4**, and **SCd2**. In **SBd2** and **SCd2** with poorly detailed ties, the transverse bars underwent the yield strain (ε_{yt} = 0.0025 mm/mm) at δ = 2.5%, and then anchorage failure of ties occurred at δ = 3.5%. On the other hand, **SAd2** with 135º hook anchorage, hoop failure did not occur even after the yielding of the transverse bars, and consequently the deformation capacity and energy dissipation capacity were increased. In **SBd4** with 90° hook anchorage ties at the reduced spacing d/4, the transverse bars did not reach the yield strain; thus, despite the poor anchorage detail of the ties, the deformation capacity was increased to δ = +5.0%.

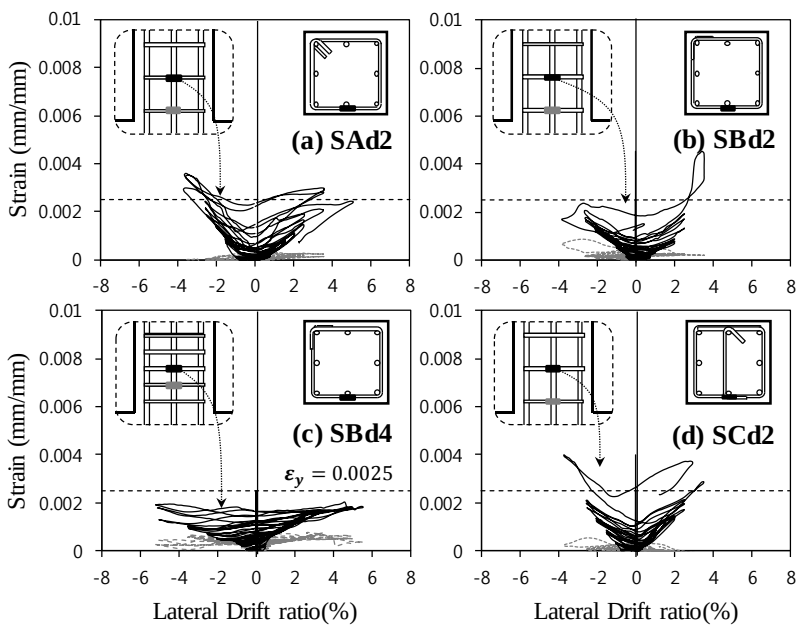

Figure 2-54 Strains of transverse bars in square columns

Similar results were observed in the rectangular columns. In **RFd2** and **RGd2** with poor tie anchorage details (see Figure 2-55(b) and Figure 2-55 (c)), the transverse bars reached the yield strain at δ = 5.0% and 7.0%, respectively, and anchorage failure of ties then occurred. On the other hand, in **REd2** using conventional one-piece ties with 135º hook anchorage and **RHd2** using two-piece U-bar with 90º end hooks embedded in the confined core (see Figure 2-55(a) and Figure 2-55(d)), the anchorage failure of ties did not occur even at δ = 7.0%.

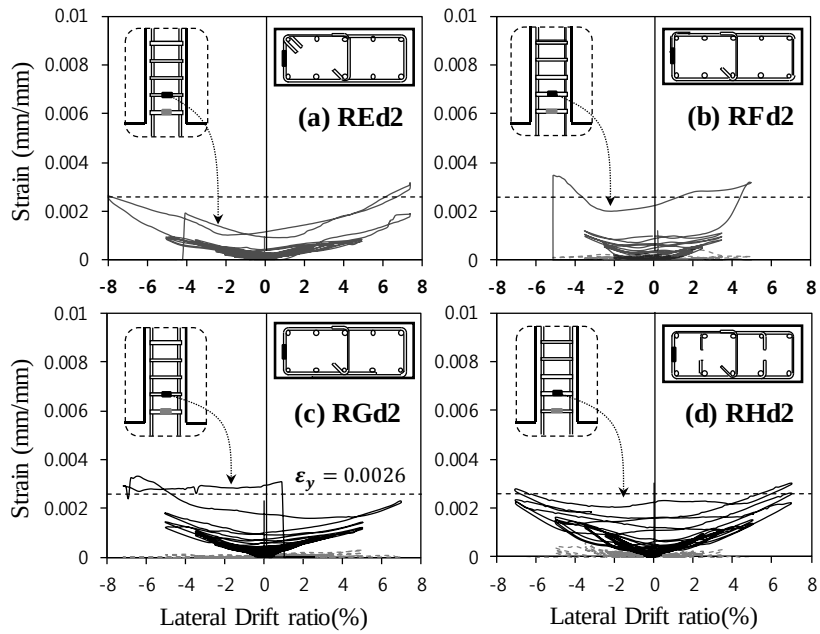

Figure 2-55 Strains of transverse bars in rectangular columns

2.6 Post-yield Shear-strength Degradation Model

2.6.1 Proposed shear-strength degradation model

By modifying the existing model developed by Priestley et al. (1994) and from the test results, a post-yield shear-strength degradation model was developed as follows (see Figure 2-56).

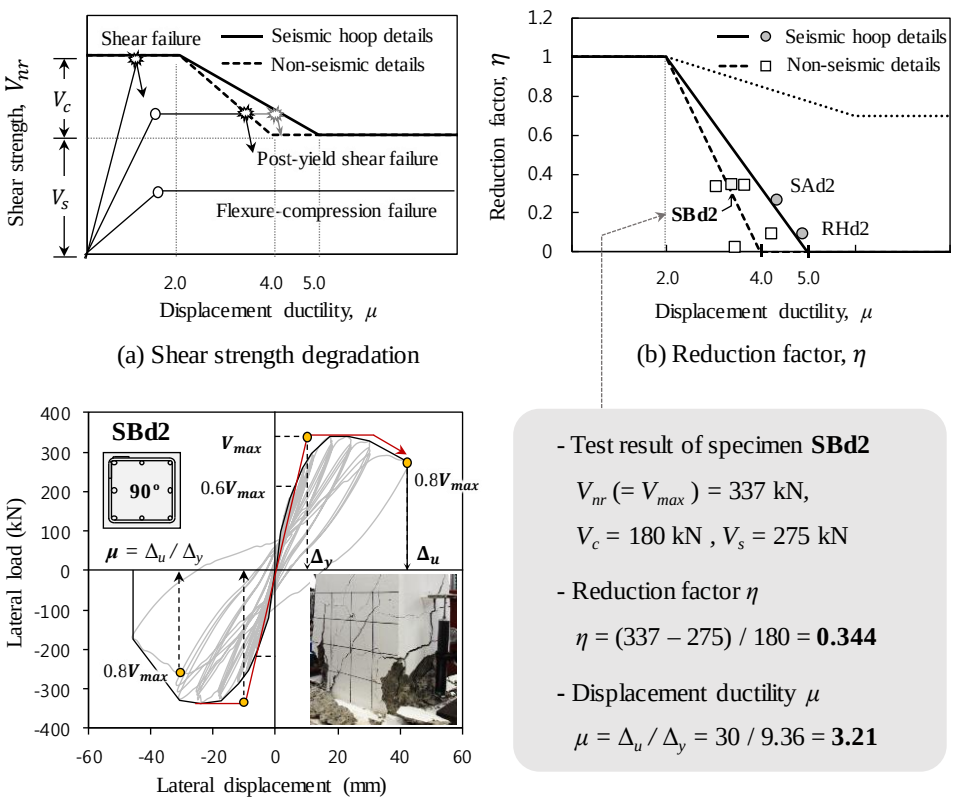

(a) Shear strength degradation

(b) Reduction factor, η

(c) Reduction factor η and displacement ductility μ of specimen SBd2

Figure 2-56 Shear strength degradation according to displacement ductility

$$\eta = \begin{cases} 1.0 & \text{for } \mu \le 2 \\ (5-\mu)/3 & \text{for } 2 < \mu \le 5 \\ 0.0 & \text{for } \mu > 5 \end{cases} \quad \text{for well detailed ties} \qquad (2\text{-}15)$$

$$\eta = \begin{cases} 1.0 & \text{for } \mu \le 2 \\ (4-\mu)/2 & \text{for } 2 < \mu \le 4 \\ 0.0 & \text{for } \mu > 4 \end{cases} \quad \text{for poorly detailed ties} \qquad (2\text{-}16)$$

In Equation (2-14), V_{nr} is the reduced post-yield shear strength of columns at a displacement ductility μ (see Figure 2-56(a)); η ($\le$ 1.0) is the reduction factor for the concrete shear strength (see Figure 2-56(b)); and V_c (= $0.17(1+N/[14A_g])\sqrt{f_c'}bd$) and V_s (= $A_v f_{yt} d/s$) are the nominal shear strengths of the concrete and transverse reinforcement, respectively (ACI 318-14). In Equation (2-15) and Equation (2-16), conventional hoops with 135º seismic hook anchorage and continuously wound ties are classified as the well detailed ties. On the other hand, ties with 90º standard hook anchorage and lap-spliced ties are classified as the poorly detailed ties. Of course, the lap-spliced ties with 90º end hook embedded within the confined core such as the type H tie can be classified as the well detailed ties.

Figure 2-56(a) shows the envelope curve of V_{nr} corresponding to the displacement ductility μ. The column shear capacity V_{nr} decreases as μ increases. If the decreased V_{nr} becomes the same as the column shear demand, which is maintained as almost constant after flexural yielding, a post-yield shear failure occurs. However, if V_{nr} is always greater than the shear demand, other failure modes such as flexure-compression failure can occur.

Figure 2-56(b) shows the proposed η - μ relationships depending on anchorage details of ties. The reduction factor η decreases linearly from 1.0 at μ = 2.0 to zero at μ = 5.0 for well detailed ties or to zero at μ = 4.0 for poorly detailed ties. In Equation (2-14) and Equation (2-16), the η values were determined so that the shear strength degradation can be more pronounced in the columns with poorly-detailed ties such as 90º-hook and lap-spliced ties (e.g. **SBd2**, **SCd2**, **SDd2**, **RFd2**, and **RGd2**), as discussed in the previous section.

For verification, the values of η and μ for columns using well-detailed ties and poorly-detailed ties are plotted with grey circles and white squares in Figure 2-56(b), respectively. The η and μ values of the columns are shown in Table 2-9. The ductility of the columns was calculated as $\mu = \delta_u / \delta_y$, where δ_u and δ_y are the maximum drift ratio at failure and yield drift ratio, respectively; δ_u was determined as the smaller of the positive and negative maximum drift ratios corresponding to 80% of the maximum load as shown in Figure 2-56(c) or as the drift ratio at the end of tests; and δ_y was calculated as P_u / K_y, where P_u is the maximum test strength and K_y is the secant stiffness connecting the origin and the pre-peak point of $0.6P_u$ (ASCE 41-13 Chapter 7). As shown in Figure 2-56(b), the proposed η - μ relationships agreed reasonably with the test results.

2.6.2 Verification of proposed model

The proposed model was also compared with the existing test results of columns. The existing test results were obtained from the PEER structural performance database (www.ce.washington.edu/~peera1/). The PEER structural performance database provides the cyclic test results of more than 300 columns, 80 lightly reinforced columns of which were used for the verification. Such columns were chosen for verification because the shear strength of transverse reinforcement (V_s) was less than the column shear demand by test (V_u). The ranges of the design parameters used in the 80 columns are 20 MPa $\leq f_c' \leq$ 116 MPa, $1.16 \leq a/d \leq 5.6$, $0.1 \leq s/d \leq 1.15$, $0.07\% \leq \rho_v \leq 1.62\%$, 255 MPa $\leq f_{vt} \leq$ 1126 MPa, 325 MPa $\leq f_y \leq$ 510 MPa, and $0 \leq N/A_g f_c' \leq 0.8$.

Properties and test results of 12 columns (Gill, 1979; Soesianawati, 1986; Nagasaka, 1982; Muguruma et al., 1989; Ono et al., 1989; Sakai et al., 1990; Sezen and Moehle, 2006; Esaki, 1996) are shown in Table 2-10 and Figure 2-57(b); the results of the remaining 68 columns are shown in Figure 2-58. In Figure 2-57 and Figure 2-58, the test setups for axial compression differed. Thus, for fair comparison of the test results, the second order effect was variously addressed considering the loading conditions. In Figure 2-60, the existing column specimens were classified into three categories, cases 1 ~ 3, according to the axial-loading method. Here, P and N denote the lateral load and axial load applied externally, respectively, and Δ denotes the lateral displacement at the point of lateral loading. V is the shear demand at the bottom of the column. For case 1, the second-order effect was ignored: $P = V$.

For cases 2 and 3, the shear demand V was amplified by the second-order effect (see the equations in Figure 2-60). In Figure 2-57 and Figure 2-58, the strengths predicted by the shear degradation model were determined by shear strength (V) subtracted from the force by the second-order effect (NΔ/L) to compare the test cyclic loads (P).

For comparison, the existing shear-strength degradation model specified in ASCE 41-13, defined as Equations (2-17) to (2-19), was also plotted in Figure 2-57 and Figure 2-58.

$$V_{nr} = k\,(V_c + V_s) \tag{2-17}$$

where,

$$k = \begin{cases} 1.0 & \text{for } \mu \le 2 \\ 1.15 - 0.075\mu & \text{for } 2 < \mu \le 6 \\ 0.7 & \text{for } \mu > 6 \end{cases} \tag{2-18}$$

$$V_c = \frac{0.5\sqrt{f_c'}}{M/(Vd)}\left(1 + \frac{N}{0.5\sqrt{f_c'}A_g}\right)^{0.5} 0.8A_g \tag{2-19}$$

In Equation (2-19), $M/(Vd)$ should be not greater than 4. It should be noted that, in the ASCE model, the reduction factor k, not less than 0.7, should be applied to both V_c and V_s and any modification for poorly detailed ties are not given.

In Figure 2-57 and Figure 2-58, ultimate drift ratios corresponding to 80% of the maximum test loads are indicated with circles, and the predicted values by ASCE 41-13 and the proposed model are marked with rectangles and squares, respectively. For comparison of the proposed model and the ASCE equation, predicted displacement and experimental displacement relations ($\Delta_{pred} - \Delta_{test}$) were plotted in Figure 2-59. The proposed model predicted more accurately with the mean value of 0.88 and the standard deviation of 0.47 compared to the ASCE equation with the mean value of 1.44 and the standard deviation of 0.95. The proposed model agreed reasonably with the test results (displacement at shear failure after column flexural yielding).

Table 2-10 Geometric and material properties of existing column specimens

Specimen		d (mm)	a (mm)	a/d	f_c' (MPa)	$N/A_g f_c'$	f_{yt} (MPa)	s (mm)	A_v (mm^2)	Δ_y (mm)
Gill	No. 3	488	1200	2.46	21.4	0.42	297	75	314	3.54/ -2.72
Soesianawati	No. 3	372	1600	4.30	44	0.30	364	100	154	5.98/ -8.19
Nagasaka	HPRC10-63	176	300	1.70	22	0.17	344	35	48	0.99/ -0.79
Muguruma et al.	BL-2	179	500	2.8	116	0.42	328	35	113	2.68/ -2.49
Ono et al.	CA025C	170	300	1.76	26	0.26	426	70	113	1.27/ -1.38
	CA060C	170	300	1.76	26	0.62	426	70	113	0.94/ -0.98
Sakai et al.	B1	215	500	2.32	100	0.35	774	60	79	2.43/ -2.38
	B3	215	500	2.32	100	0.35	344	60	95	3.43/ -2.26
	B4	215	500	2.32	100	0.35	1126	60	79	2.59/ -2.02
Sezen & Moehle	No. 1	368	1473	4.0	21	0.15	476	305	243	24.65/ -22.54
	No. 2	368	1473	4.0	21	0.60	476	305	243	13.22/ -13.1
Esaki	H-2-1/3	175	400	2.29	23	0.33	364	40	52	1.60/ -1.73

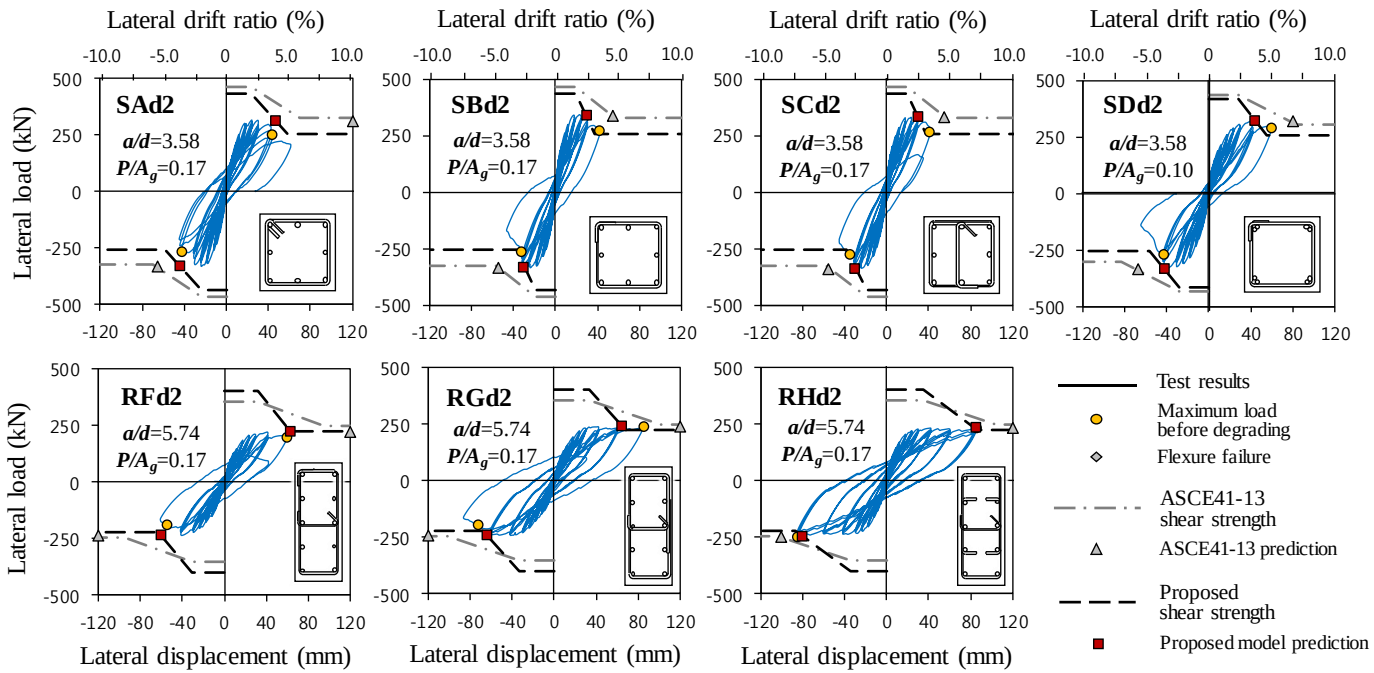

(a) This study

Figure 2-57 Comparisons of proposed model and ASCE 41-13 shear strength with test results

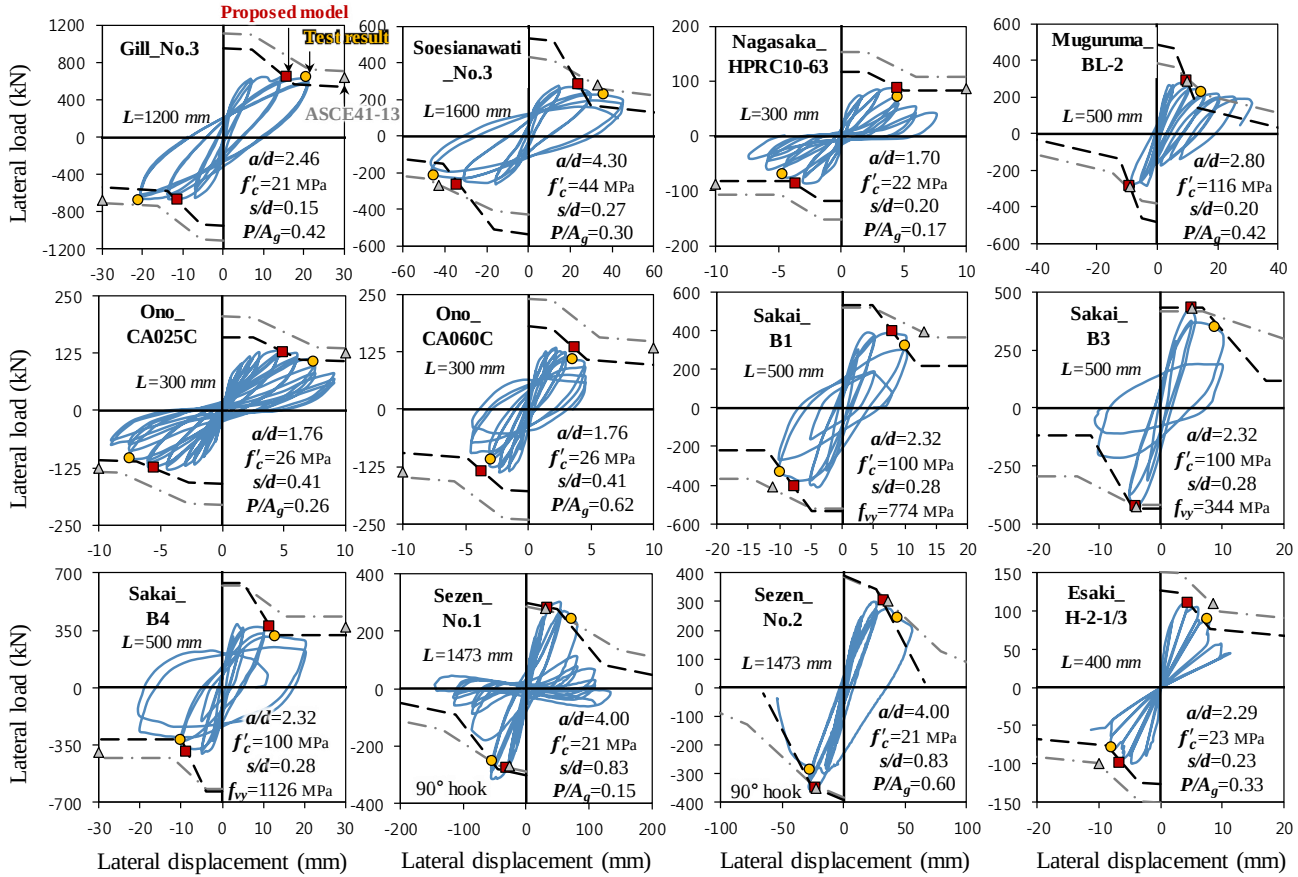

(b) PEER structural performance database

Figure 2-57 Comparisons of proposed model and ASCE 41-13 shear strength with test results

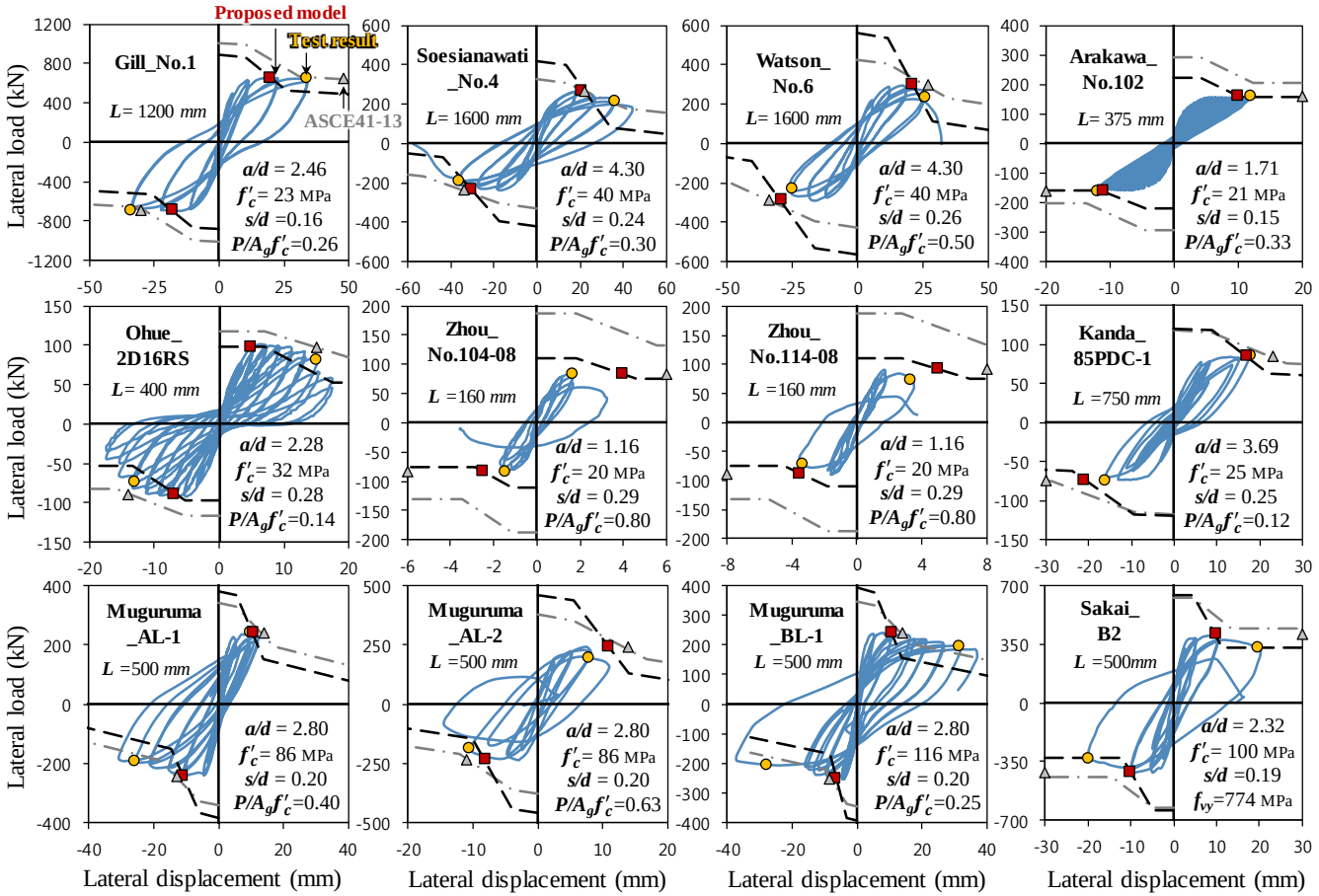

Figure 2-58 Comparisons of proposed model with test results (PEER structural performance database) (Continued)

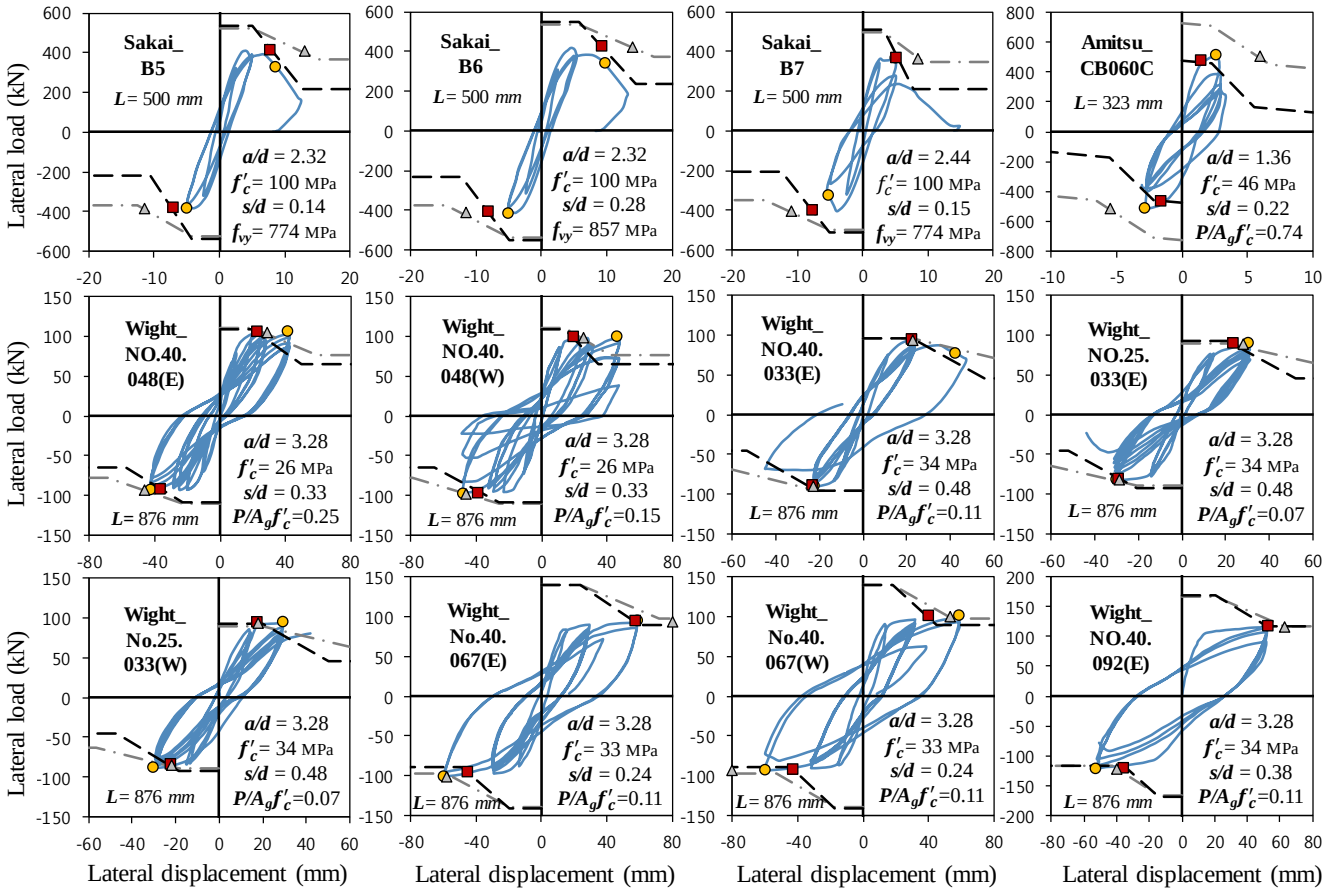

Figure 2-58 Comparisons of proposed model with test results (PEER structural performance database) (Continued)

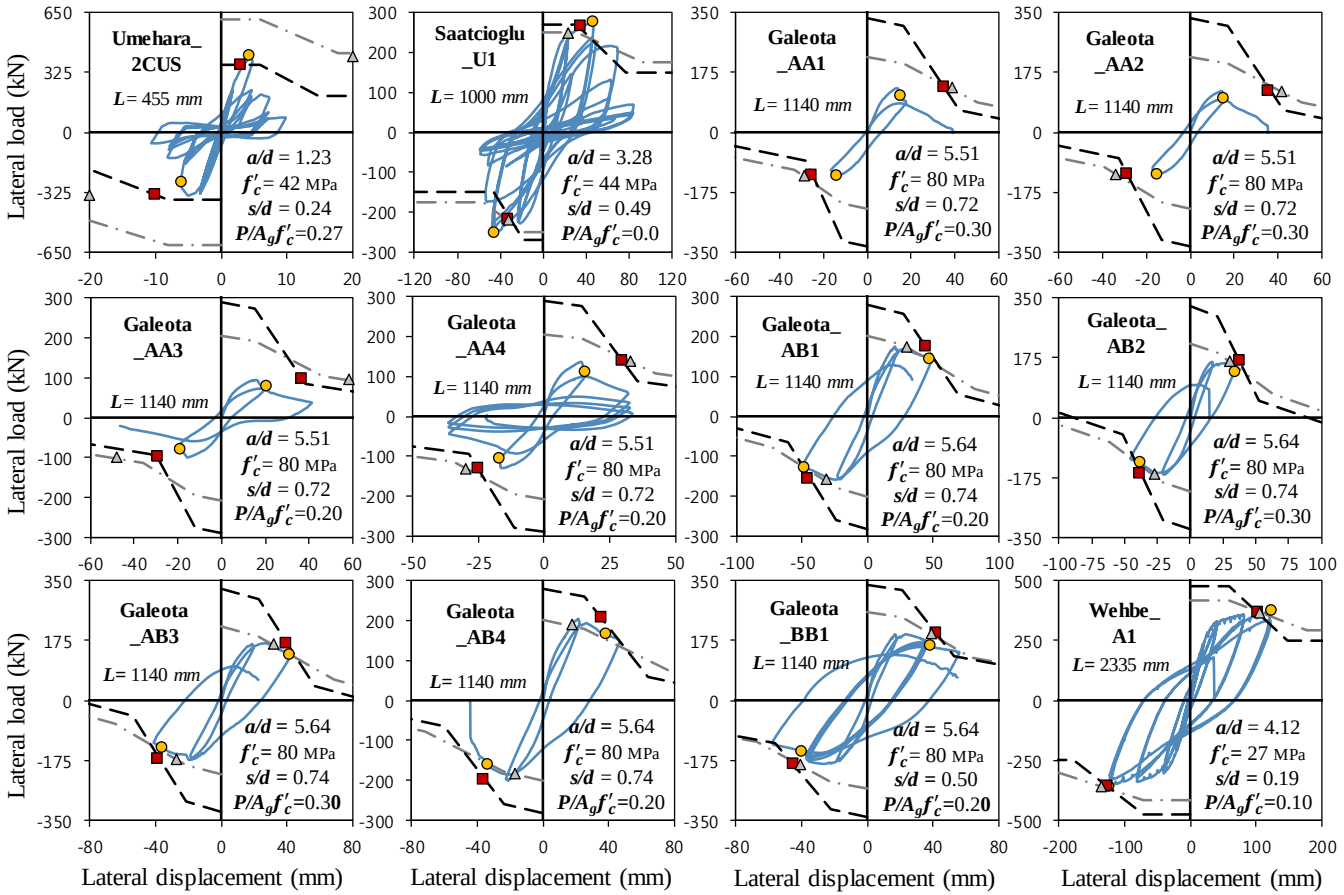

Figure 2-58 Comparisons of proposed model with test results (PEER structural performance database) (Continued)

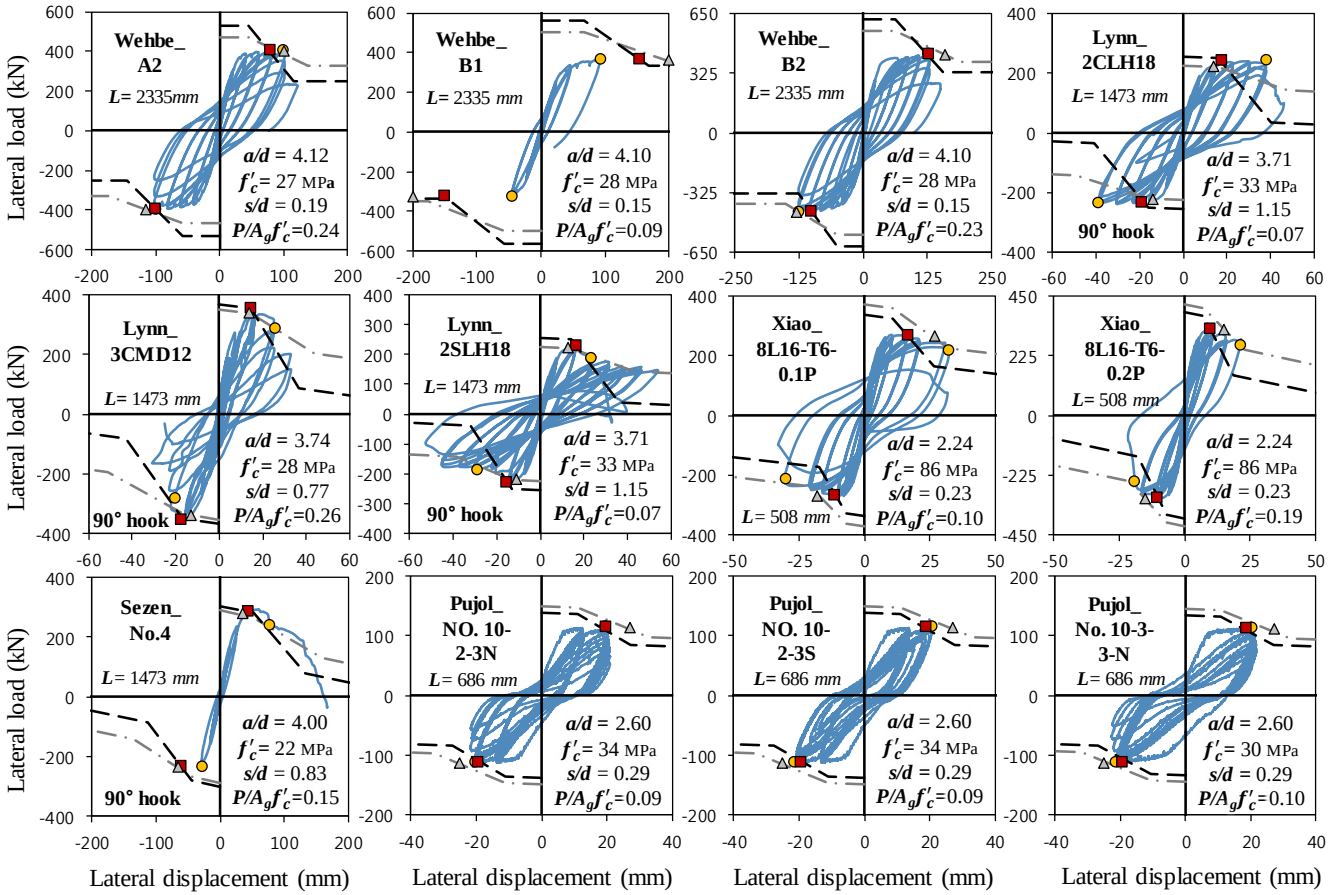

Figure 2-58 Comparisons of proposed model with test results (PEER structural performance database) (Continued)

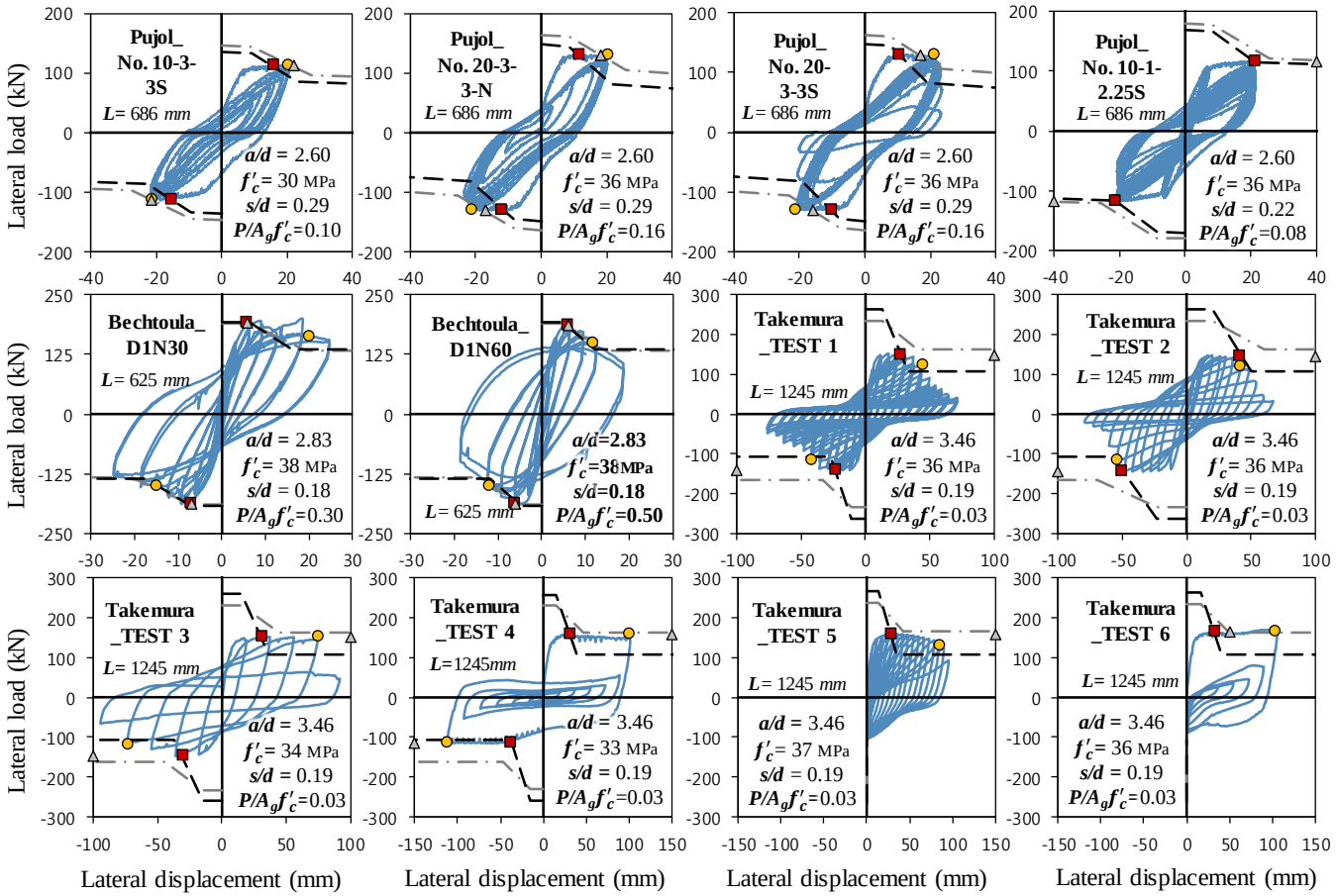

Figure 2-58 Comparisons of proposed model with test results (PEER structural performance database) (Continued)

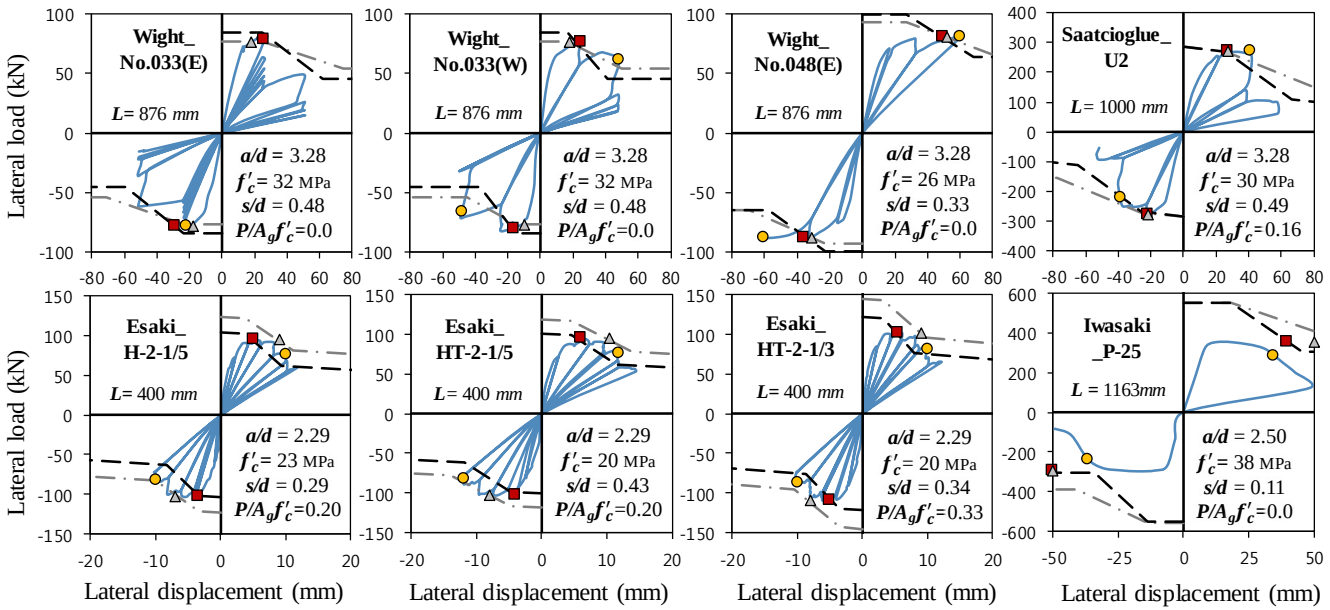

Figure 2-58 Comparisons of proposed model with test results (PEER structural performance database)

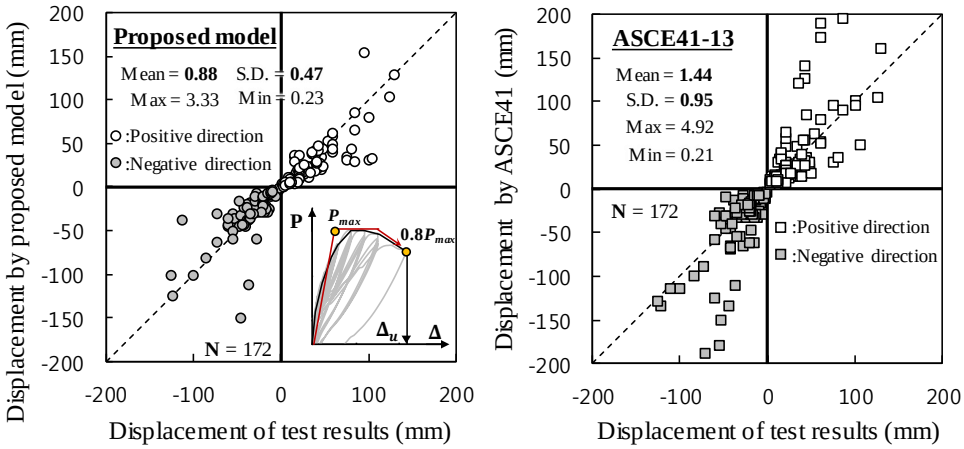

Figure 2-59 Verification of proposed model and ASCE41-13 with test results

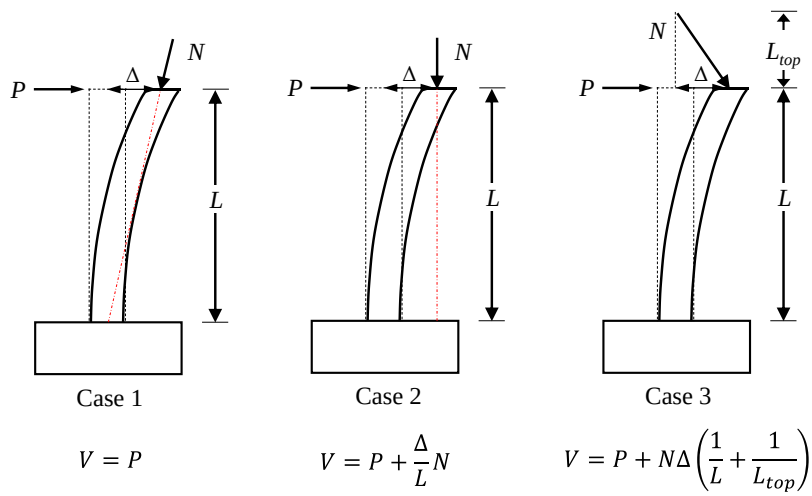

Figure 2-60 Second-order effect on the behavior of columns with different loading conditions

2.7 Discussion

Cyclic loading tests were performed for lightly reinforced square and rectangular columns with alternative tie details. On the basis of the test results, the effects of the spacing and anchorage details of the ties on the failure mode and deformation capacity of the columns were investigated. Further, a post-yield shear-strength degradation model for lightly reinforced columns was proposed. The major findings of this study are summarized as follows.

1) The post-yield failure mode and deformation capacity of the columns were significantly affected by the ratio of the shear strength by transverse reinforcement V_s to the applied shear force V_u. In the columns with $V_s / V_u < 1.0$, post-yield column failure occurred primarily due to excessive web shear cracking. On the other hand, in the columns satisfying $V_s / V_u \geq 1.0$, web shear cracking was limited even at large inelastic deformations.

2) The anchorage details of the ties significantly affected the ductility of columns. In the columns confined with 90°-hooked and lap-spliced ties, premature anchorage failure of perimeter ties occurred after spalling of the cover concrete, consequently the column ductility was relatively less when compared to the column with 135°-hooked hoop. However, in the column using lap-spliced U-bars with 90° end hooks embedded in the confined core, the column ductility was comparable to that of the well detailed hoop with 135° hook.

3) The post-yield shear failure of the columns occurred due to the degradation of concrete shear resistance. In this study, from the test results, the degraded shear strength of the columns was defined as $V_{nr} = \eta V_c + V_s$, where η ($0 \leq \eta \leq 1$) is the reduction factor depending on the column ductility μ and anchorage detail of perimeter ties. The proposed model was compared with the present and previous test results of columns. The results showed that the proposed model predicted the post-yield strength degradation and deformation capacity of the columns with reasonable precision.

Chapter 3. Effects of Lap Splice Details on Columns

3.1 Introduction

3.1.1 General problems in lap splice details on RC columns

In low-rise buildings designed primarily for gravity load in low and moderate seismic zones, a weak column - strong beam behavior can occur under earthquakes due to relatively small column size. In such buildings, severe damages and plastic deformations are concentrated in columns rather than in beams. Thus, to secure the seismic safety of those buildings, attention should be paid to the reinforcement detailing of columns. Particularly, at the bottom of the 1st floor columns, longitudinal bars are often lap-spliced (refer to Figure 3-1) and ties with 90° standard hook anchorage are used at a large spacing of the minimum column dimension (= h_{min}) in low-rise buildings.

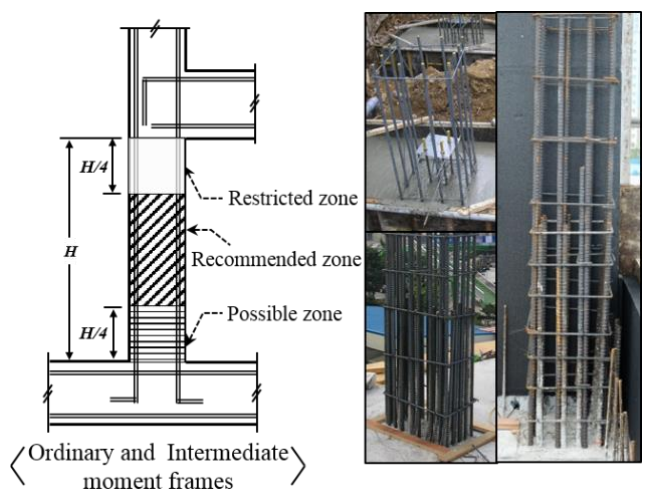

Figure 3-1 The location of lap splices in reinforced concrete columns

The seismic resistance of RC columns is degraded when lap splices of longitudinal reinforcing bars are located at the plastic hinge zone. For this reason, in ACI 318-14, lap splices are not permitted in potential plastic hinge zones of special moment frames. On the other hand, such requirement is not imposed for ordinary and intermediate moment frames. Thus, in low and moderate seismic regions, for convenience of rebar placement, lap splices of longitudinal rebars are usually located at the bottom of columns, which is a plastic hinge zone.

When lap splices of longitudinal rebars are used at the plastic hinge zone of columns, the strength and ductility of columns are affected by various design parameters. First, lap-splice length affects the strength and ductility of columns. Table 3-1 shows the required tension splice length (l_s) specified in ACI 318-14, EC2 (Eurocode2), and CSA (similar to ACI318). Figure 3-2 shows the required tension splice length (l_s) specified in ACI 318-14 and EC2. The horizontal and vertical axes denote the concrete compressive strength ($f_c' = 18 \sim 30$ MPa) and the required splice length-to-bar diameter ratio (l_s/d_b), respectively. In ACI 318-14, the lap-splice length is defined as $l_s = 1.3l_d = 1.3\cdot(0.9d_b f_y/\sqrt{f_c'})/([c_b+K_{tr}]/d_b)$ for Splice Class B. In EC2, the lap-splice length is defined as $l_s = \alpha_6 l_{bd} = \alpha_2\alpha_6(d_b f_{yd})/(4f_{bd})$, where f_{yd} is the design yield stress of the spliced bar, f_{bd} is the concrete bond strength ($= 2.25f_{ctd} = 0.47f_{ck}^{(2/3)}$), and α_2 is coefficient of concrete minimum cover. The coefficients α_1, α_3, α_4, and α_5 are assumed to be 1.0. The definitions of other parameters are given in the codes. When lap splices of column longitudinal rebars are placed at the same location (α_6 =1.5), the splice lengths of ACI 318-14 and EC2 are $l_s/d_b = 38.0$ and 52.3 for $f_y = 400$ MPa and $l_s/d_b = 48.0$ and 65.4 for $f_y = 500$ MPa, respectively.

Table 3-1 Development length and lap splice length specified in design codes

Design code	Development length (l_d)	Lap splice length (l_s)
ACI 318	$l_d = \frac{0.9 d_b f_y}{\lambda\sqrt{f_c'}} \frac{\alpha\beta\gamma}{(c + K_{tr})/d_b}$	Class A : 1.0 l_d Class B : 1.3 l_d
Eurocode 2	$l_d = \alpha_1\alpha_2\alpha_3\alpha_4\alpha_5 \frac{d_b f_y}{4 f_{bd}}$ $(f_{bd} = 2.25\eta_1\eta_2 f_{ctd})$	$l_s = \alpha_6 l_d$
CSA	$l_d = 1.15 \frac{k_1 k_2 k_3 k_4 f_y A_b}{(d_{cs} + K_{tr})\sqrt{f_c'}}$	Class A : 1.0 l_d Class B : 1.3 l_d

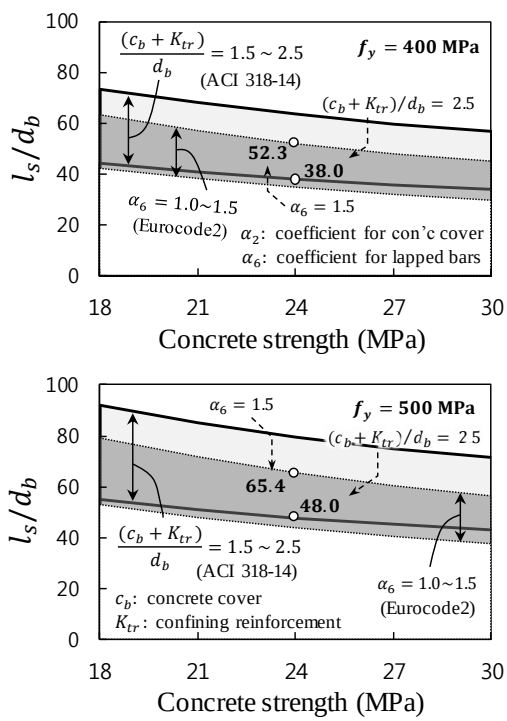

Figure 3-2 Comparison of lap splice lengths by ACI 318-14 and Eurocode 2

Second, the strength and ductility of columns are affected by lap-splice details. Figure 3-3(a) ~ (b) and Figure 3-4(a) ~ (b) show two offset-bar details specified in ACI 315: bottom and top offset bar splices. In the bottom offset bar splice, the bottom bars from the lower story are offset inside. In the top offset bar splice, on the other hand, the top bars are offset inside. As the bottom bars are located inside the core concrete, the moment-carrying capacity of the column with the bottom offset bar splice is less. However, the columns with the bottom offset bar splice show better displacement ductility owing to the thicker concrete cover of the bottom offset bar. For this reason, in current seismic design codes, the bottom offset-bar splice is recommended (ACI 318-14 10.7.5).

Such offset bar splices are required to bend relatively large size of longitudinal rebars with the slope of inclined portion not exceed 1 to 6. Therefore, in low-to-moderate seismic zone especially for low-rise buildings, the splice without offset bend (Figure 3-4(c)) is alternatively used due to construction efficiency, which were not specified in current design codes.

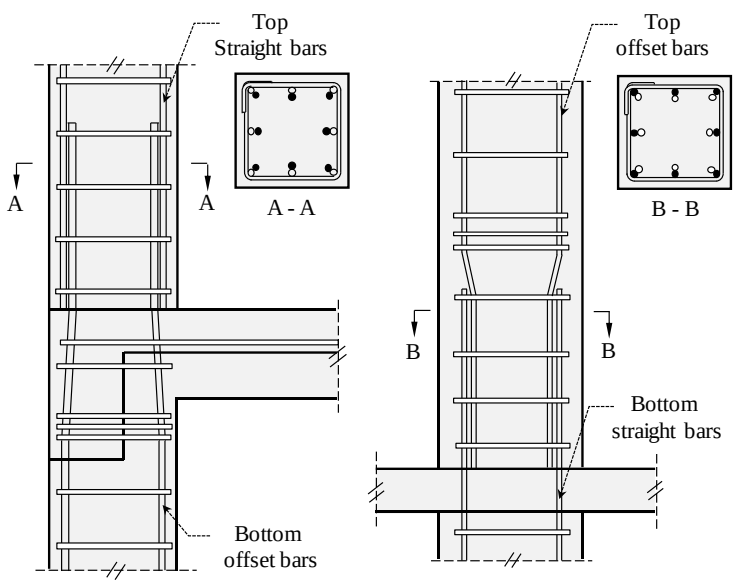

(a) Bottom offset-bar splice (b) Top offset-bar splice

Figure 3-3 Lap splice details using offset bars specified in ACI 315

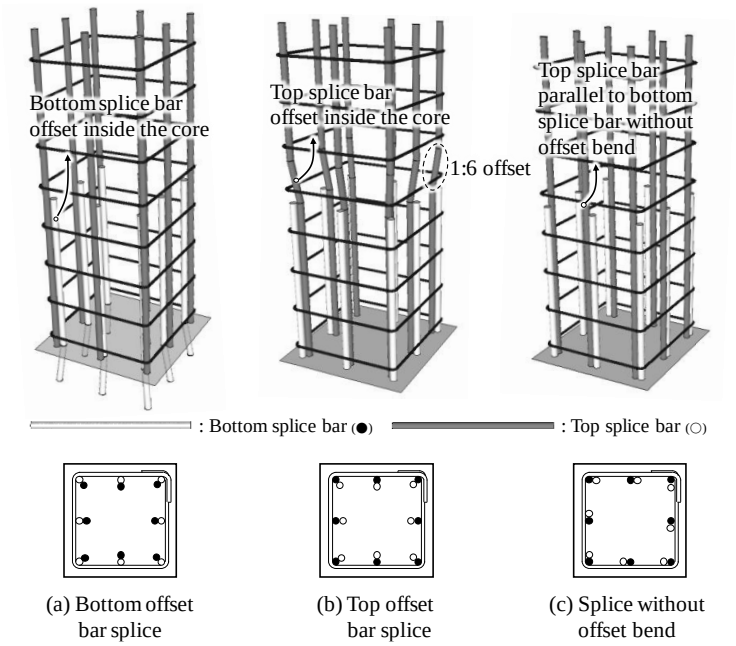

Figure 3-4 Possible lap splice details for column longitudinal bars

Third, the performance of lap splices is significantly affected by the distributions of flexural moment and shear force along the length of columns (Paulay, 1982; Ferguson and Krishnaswamy, 1971). The lap-splice length of ACI 318-14 was developed considering uniform bond stresses based on the test results for beams with uniform moment (Figure 3-5(a)). On the other hand, in columns subjected to lateral loading (Figure 3-5(b)), the demand of bond stress varies along the splice length according to the moment gradient. However, bond-splitting cracks in the lap-splice region become severe owing to the presence of shear force, particularly after diagonal shear cracking. Repeated cyclic loading may also result in bond deterioration in the plastic hinge zone. Ferguson and Krishnaswamy (1971) evaluated the performance of lap splices under moment gradient for bearing walls. They reported that the performance of lap splices was affected by the average stress of two spliced bars, which was less than the yield stress because of the moment gradient of the lap-splice region. They proposed a reduction factor of $(1+k)/2$, ranging from 0.75 to 1.0, where k is the ratio of the less of two spliced bar stresses to the yield stress. As no data for $k < 0.5$ were available, the reduction factor for splice length was limited to not less than 0.75.

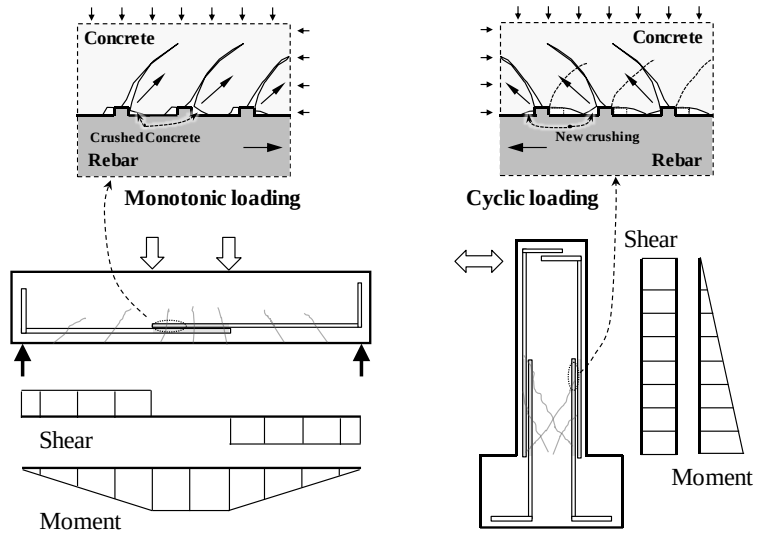

(a) Beams without moment gradient (b) Columns with moment gradient

Figure 3-5 Bending moments and shear forces at lap splice region

In the present study, cyclic loading tests of columns with lap-spliced longitudinal bars at the plastic hinge region were performed. The lap-splice length of the column bars, and the shear-span length (i.e., moment gradient and shear force) were taken into account as the primary test variables. With the results of the cyclic loading tests, the strength, ductility, and failure mode of the columns were investigated and the effects of the test variables on the column performance were discussed. Based on the results, the lap-splice length of column rebars was evaluated.

3.1.2 Lap splice failure of columns in past earthquakes

In past earthquakes, lap splice failure occurred at plastic hinge region of columns due to severe damages accumulated in the lap splice regions. Figure 3-6 ~ Figure 3-8 show failure cases of lap spliced columns by past earthquakes such as Kobe earthquake, Japan, 1995 (M= 6.69); Izmit earthquake, Turkey, 1999 (M= 7.4); and Chi-Chi earthquake, Taiwan, 1999 (M= 7.6), respectively. The photos of the damaged RC columns have been collected from the library of NISEE in the UC Berkeley (https://nisee.berkeley.edu/elibrary/).

In the case of Kobe earthquake damage, large damages occurred in the plastic hinge zone of columns (Piers of bridges), and failure occurred due to loss of axial load capacity. Confinement failure occurred due to lack of lateral confinement with buckling of column longitudinal bars. Similar failure patterns were observed in the Izmit earthquake. Large damages accumulated at the plastic hinge zone of columns, and confinement failure occurred due to loss of axial load carrying capacity with buckling of column longitudinal bars. In the Chi-Chi earthquake, lap splice failure occurred with diagonal shear cracks due to lack of transverse reinforcement in the lap splice zone.

In this chapter, seismic performance of RC columns with lap splices in the plastic hinge zone was evaluated with various parameters. Based on test results, attention was paid to the application of lap splice in the plastic hinge zone of columns.

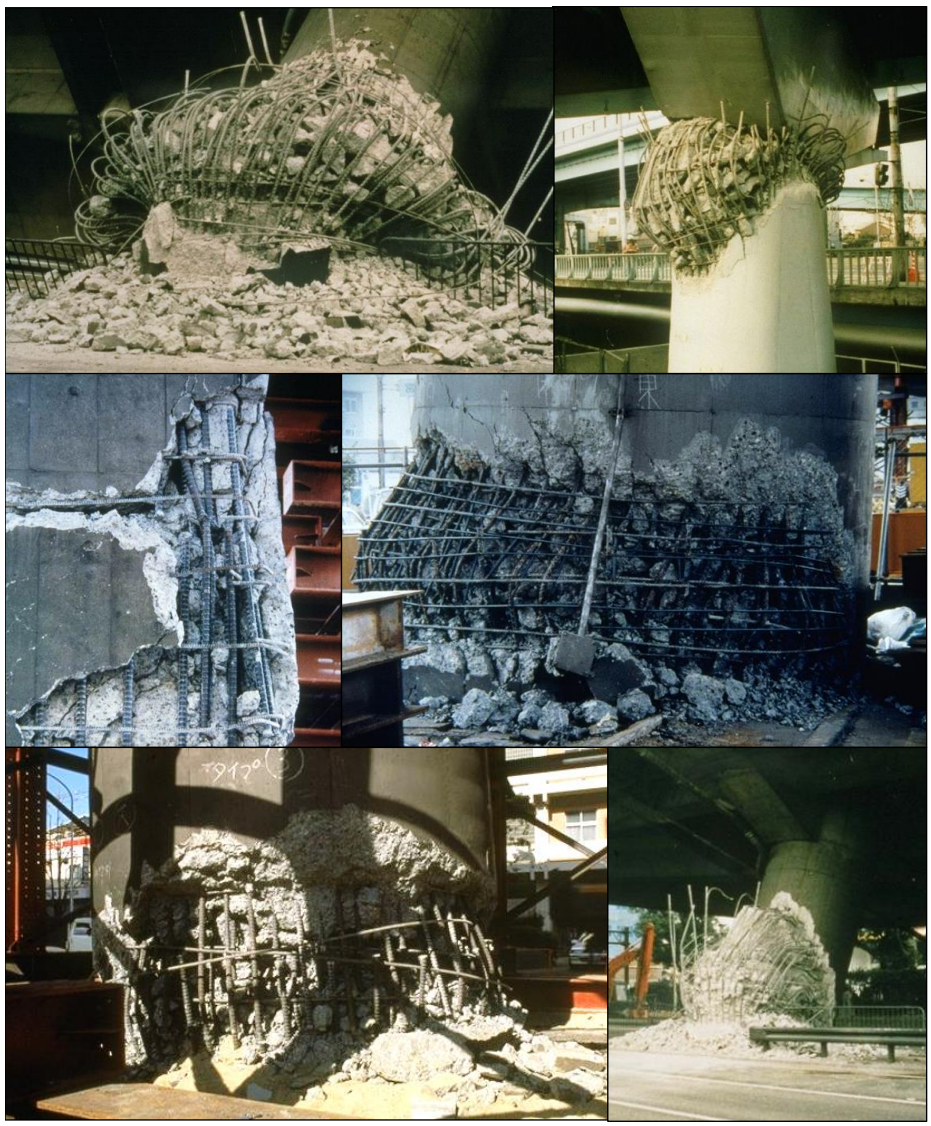

Figure 3-6 Severe damage to RC column by lap splice failure in the Kobe, Japan earthquake, 1995 (Courtesy of NISEE, University of California, Berkeley)

Figure 3-7 Severe damage to RC column by lap splice failure in the Izmit, Turkey earthquake, 1999 (Courtesy of NISEE, University of California, Berkeley)

Figure 3-8 Severe damage to RC column by lap splice failure in the Chi-Chi, Taiwan earthquake, 1999 (Courtesy of NISEE, University of California, Berkeley)

3.1.3 Comparison of current design codes for lap splice of bars

ACI 318 has different permitted lap splice locations depending on structure types. In special moment frames where the inelastic deformation demand is large, lap splicing in the plastic hinge zone is prohibited. On the other hand, in intermediate or ordinary frames with relatively small deformation demand, as shown in Figure 3-1, it is possible to use lap splices not only in the center half of the column height (recommended zone) but also in the plastic hinge zone at the bottom of the column (possible zone).

EC8 specifies spacing and required area of the shear reinforcement along lap splice zone as shown in Table 3-2. Other provisions about lap splices of bars are referred to EC2. In EC2, the transmission of the forces from one bar to the next is assured. Lap splices between bars should not be located in areas of high moments / forces (e.g. plastic hinges).

Similarly, in NZS 3101, CSA, and AIJ, lap splices in ductile moment resisting frames are permitted only within the center half of the column height where both the member stress and existing stress in the reinforcing bar are small. Requirements for lap splice of longitudinal bars in moment-resisting frames are summarized in Table 3-2.

In plastic hinge zones, since the flexural cracks are greatly enlarged and concrete covers are spalled off after flexural bar yielding, the bond capacity of lap spliced bars is significantly decreased. Thus, most current design codes allow lap splices in columns except plastic hinge zone where cross sections of members are subjected to high stresses. However, ACI 318 and AIJ specify that lap splicing can be used in the plastic hinge zone of columns exceptionally in intermediate or moderately ductile moment frames where large inelastic deformations are not required.

Table 3-2 Requirements for lap splice of longitudinal bars in moment frames

Design code	Lap splice of longitudinal bars in moment-resisting frames
ACI 318	[**Special** moment frame] Lap splices are only permitted within the center half of the column story height. In addition, lap splices must be enclosed with transverse reinforcement with seismic hook. [**Intermediate** / **ordinary** moment frames] There are no limitations placed on the locations of lap splices, and special transverse reinforcement in not required at lap splices.
EC8	- The spacing s of the transverse reinforcement in the lap splice zone shall not exceed $\boldsymbol{s = \min(h/4, 100)}$, where h is the minimum cross-section. - The required area of transverse reinforcement A_{st} within the lap splice zone of the longitudinal bar of columns spliced at the same location may be calculated from $\boldsymbol{A_{st} = s(d_{bL}/50)(f_{yld} / f_{ywd})}$, where A_{st} is the area of one leg of the transverse reinforcement, d_{bL} is the diameter of the spliced bar, s is the spacing of the transverse reinforcement, f_{yld} and f_{ywd} are the design value of the yield strength of the longitudinal reinforcement and the transverse reinforcement, respectively.
NZS 3101	In a column, the center of a splice is required to be within the middle quarter of the column story height, except where capacity design Method A (regular/ordinary frames) provides a high level of protection against plastic hinging at the ends of members.
CSA	[**Ductile** moment resisting frame] Lap splices are permitted only within the center half of the member length and shall be designed as tension lap splices, and shall be enclosed within transverse reinforcement conforming to the column confinement requirements.
AIJ	Lap splices shall be located at a region where both the member stress and existing stress in the reinforcing bar are small. The lap splice joint for ensuring the serviceability limit against long-term loading and for the damage control limit against short-term loading are to satisfy $\boldsymbol{\sigma_t d_b/(4l) \le f_a}$ for a tension reinforcing bar, where σ_t is existing stress in a tension reinforcing bar at a lap splice joint, and the value may be reduced to 2/3 if the standard hook is arranged at the end of the bar. f_a is allowable bond stress, and values for top reinforcements (similar design equation of EC2 of Table 3-1)

3.1.4 Review of previous studies

Since the 1990s, cyclic tests of columns with short lap splices ($l_s = 20 \sim 40d_b$) have been conducted by several researchers. Figure 3-9 shows the cross-sections and bar offset details of the columns tested in the previous studies. In the figure, the column bars extending from the top and bottom are denoted as void and solid circles, respectively. Most of researchers tested columns with bottom offset bar splice (Lynn et al., Melek and Wallace, Aboutaha et al., Haroun and Elsanadedy, Harries et al., and ElGawady et al.), while Boyes et al. tested columns with top offset bar splice, and Harajli, Bournas and Triantafillou tested columns with splice without offset bend.

Lynn et al. (1996) and Melek and Wallace (2004) studied the performance of the columns with a lap splice length of $l_s = 20d_b$ (d_b = bar diameter). The bottom bars extending from the base were offset toward the column core. According to the tests, the ductility increased in the columns with closely-spaced ties at the lap splice, but decreased in the column under high axial compression loads. In the columns tested by Boyes et al. (2008) where the column bars extending from the top were offset, the same trends as those of the column tests by Lynn et al. (1996) and Melek and Wallace (2004) were observed. Other researchers such as Aboutaha et al. (1999), Haroun and Elsanadedy (2005), Harries et al. (2006), ElGawady et al. (2010), Harajli (2008), and Bournas and Triantafillou (2009) studied the cyclic behavior of the lap-spliced columns ($l_s = 20 \sim 40d_b$) where the plastic hinge region was strengthened with fiber reinforced polymer or steel jacketing. The tests showed that the strength and ductility of the columns significantly deteriorated due to the bond failure between the lap-spliced bars and surrounding concrete, regardless of the bar offset details. However, by using the fiber reinforced polymer or steel jacketing, the column strength and ductility were enhanced.

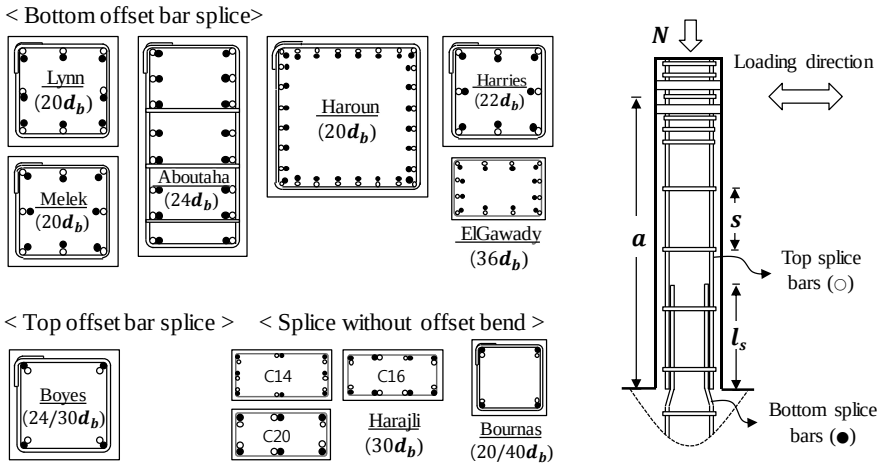

Figure 3-9 Lap splice details used in previous studies

(1) Lynn et al. (1996)

Lynn et al. performed reversed cyclic tests of RC columns with typical details used in pre-1970's construction including light transverse reinforcement and lap-splices at the bottom of the column. As show in Figure 3-10, where column was governed by shear (**3CLH18** and **3SLH18**), axial failure occurred soon after loss of lateral force resistance. Where column was initially governed by lap-splice deterioration and gravity load was light (**2SLH18**), axial load resistance was maintained until shear failure occurred. Where column was predominantly governed by flexural yielding (**2CLH18**), axial load capacity was maintained to relatively large displacement.

If the transverse reinforcement was insufficient (s/H = 1.0), the splice resistance decreased with increasing displacement after yielding of spliced bars, resulting in loss of load carrying capacity at the end of lap splices. On the other hand, if the transverse reinforcement was relatively sufficient (s/H = 0.67), the lap splices could maintain the yield forces through large inelasitc displacement. In all cases, splitting cracks along the splices occurred, thereby leading to shear failure with inclined shear cracks.

(2) Melek and Wallace (2004)

Melek and Wallace tested full scale cantilever columns with lap splices of $20d_b$ (67% of $l_{s,ACI}$) to constant axial load with test variables of axial load, moment to shear ratio, and loading history. Maximum moments (M_{max}) reached during tests at 97% to 103% of the calculated moment strength (M_{cal}), which indicates that actual bond stresses were higher than those from ACI 318-02. When compared with bond stress of $0.66\sqrt{f_c'}$(MPa) from ACI 318-02, Average bond stresses from the tests were $0.88\sqrt{f_c'}$ with a standard deviation of $0.13\sqrt{f_c'}$.

Loss of lateral load capacity initiated between drift ratios of 1.0 % and 1.5% for all specimens as shown in Figure 3-11. Strength degradation occurred due to bond deterioration between lap spliced bars and the surrounding concrete. The variation of axial load had only a marginal impact on the lateral load when bond deterioration initiated, and did impact the energy dissipation capacity modestly. The rate of strength degradation was affected mainly by the applied displacement (loading) history.

(3) Boyes et al. (2008)

Boyes et al. tested gravity RC columns with insufficient transverse reinforcement and lap splices in the plastic hinge region. As shown in Figure 3-12, the columns with inadequate transverse reinforcement were vulnerable to loss of axial load capacity at drift ratio of 2.0% due to high axial load ratio of $0.3A_g f_c'$. The lap splice length did not affect the drift capacity of RC columns, but did affect the rate of strength degradation and concrete damages.

(4) Aboutaha et al. (1999)

In the study of Aboutaha et al., rectangular RC columns with short lap splice length ($l_s = 24d_b$) and without axial load were tested to investigate seismic repair of lap splice failures in damaged columns. The unretrofitted columns (**FC4** and **FC5**) in Figure 3-13 exhibited a brittle splice failure before column flexural yielding, so the columns displayed low ductility and low energy dissipation due to the pinched hysteretic loops.

(5) Bournas and Triantafillou (2009)

Bournas and Triantafillou tested old type RC columns with limited capacity due to bar buckling or due to bond failure at lap splice regions to evaluate the effectiveness of seismic retrofitting with textile reinforced mortar or FRP jacketing. Unretrofitted columns **L20d_C** and **L40d_C** developed significant longitudinal and horizontal splitting cracks along the lap splice regions at drift ratio of 1.56% and 2.5%, respectively. As drift ratio increased, the bond between splice bars and concrete was deteriorating and the cover concrete was spalling off, thereby degrading substantial lateral strength after peak load (See Figure 3-14).

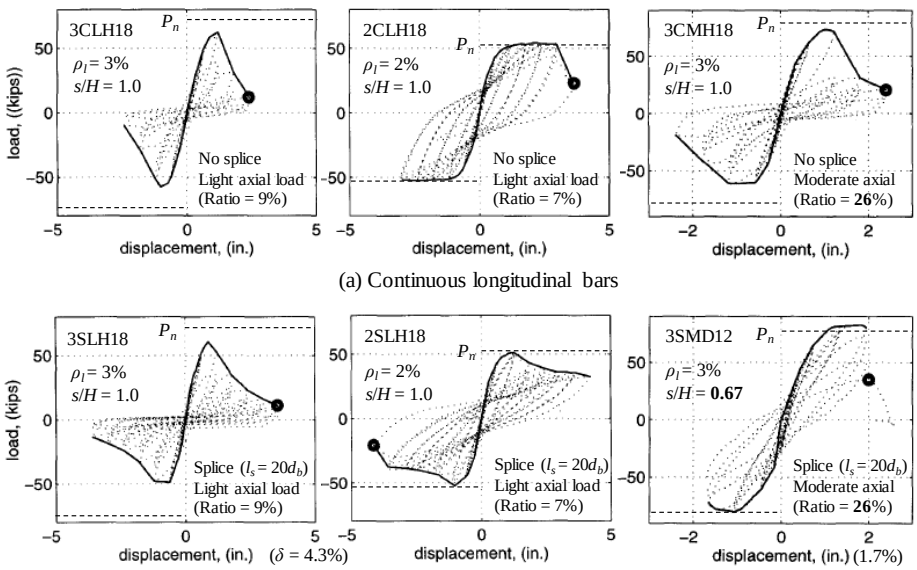

Figure 3-10 The effects of short splice length, axial load, and tie spacing in the test results of Lynn et al. (1996)

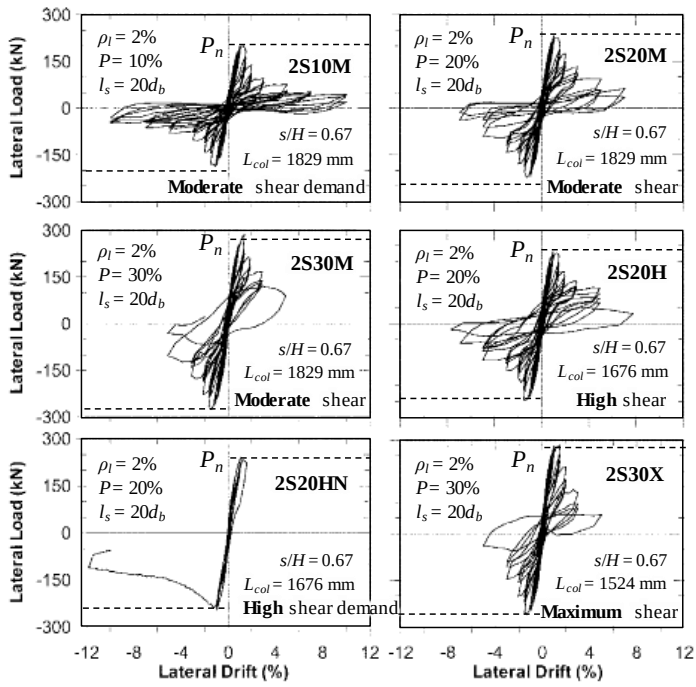

Figure 3-11 The effects of axial load, moment to shear ratio, and loading history in the test results of Melek and Wallace (2004)

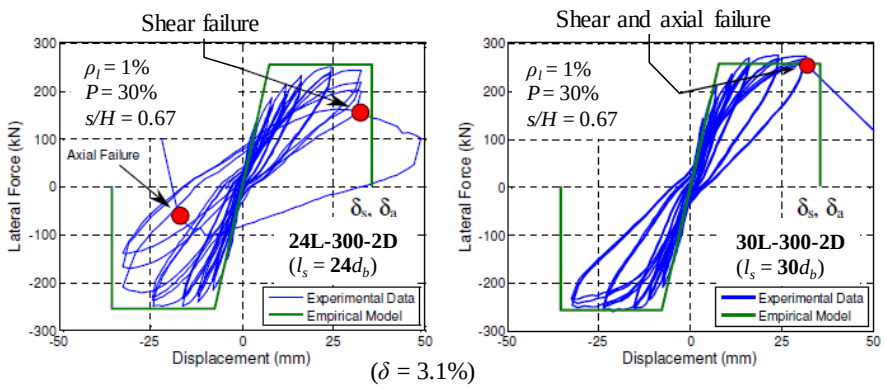

Figure 3-12 The effect of lap splice length in the test results of Boyes et al. (2008)

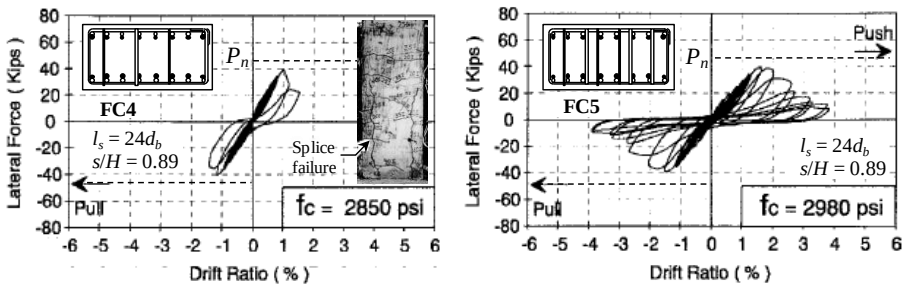

Figure 3-13 The effect of transverse bars in the test results of Aboutaha et al. (1999)

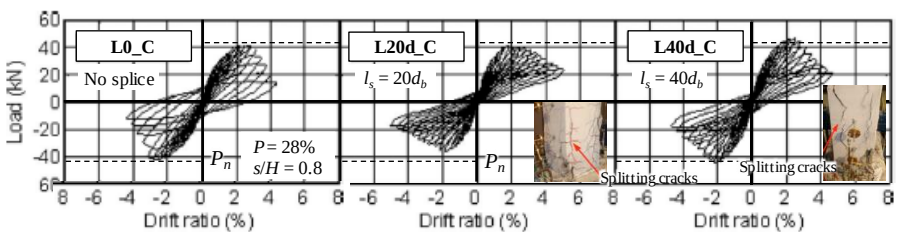

Figure 3-14 The effect of lap splice length in the test results of Bournas and Triantafillou. (2009)

3.2 Test Program of Lap Splice Details on RC Columns

3.2.1 Major design parameters

Table 3-3 presents the test parameters of square and rectangular columns, such as shear span length (a), lap splice length (l_s), and lap splice details. Figure 3-15 and Figure 3-16 show the reinforcement details of thirteen square columns with bottom offset bar splice (**SL00S1B ~ SL50S2B-1**) and top offset bar splice and splice without offset bend (**SL30S2T ~ SL50S2S**), and five rectangular columns (**RL00S1B ~ RL40S2B**), respectively. In the specimen names, the first letter 'S' and 'R' denote the square and rectangular cross-sections, respectively; the following letters 'L00', 'L30', 'L40', and 'L50' denote the length of lap splices, l_s =0, 30d_b, 40d_b, and 50d_b, respectively; 'S1' and 'S2' denote the shear span, 1200 mm and 2400 mm, respectively; and the last letters 'B', 'T', and 'S' denote the offset details of column bars, Bottom offset bar splice, Top offset bar splice, and Splice without offset bend, respectively.

Table 3-3 Test variables of column specimens

Specimen[1)]	Section type	Test No.	Shear span length (a)	Splice length (l_s)	Lap splice details
SL00S1B	Square Column (400 x 400)	1	1,200 mm (a/h = 3.0)	N/A	Bottom offset bar splice
SL30S1B		1		30d_b	
SL40S1B		1		40d_b	
SL30S2B		2	2,400 mm (a/h = 6.0)	30d_b	
SL40S2B		2		40d_b	
SL50S2B		4		50d_b	
SL40S2B-1[2)]		4		40d_b	
SL50S2B-1[3)]		3		50d_b	
SL30S2T		2		30d_b	Top offset bar splice
SL40S2T		2		40d_b	
SL50S2T		3		50d_b	
SL40S2S		3		40d_b	Splice without offset bend
SL50S2S		3		50d_b	

RL00S1B	Rectangular Column (250 x 640)	1	1,200 mm (a/h = 4.8)	N/A	Bottom offset bar splice
RL30S1B		1		$30d_b$	
RL40S1B		1		$40d_b$	
RL30S2B		2	2,400 mm (a/h = 9.6)	$30d_b$	
RL40S2B		2		$40d_b$	

1) **S**(Section type)/ **L00** (Lap splice lengths)/ **S1** (Shear span lengths)/ **B** (Splice details)

2) SL40S2B-1 : Longitudinal bar size increased to D29 (d_b = 28.6 mm)

3) SL50S2B-1 : Tie spacing increased to 1.0d (s = 330 mm)

3.2.2 Test specimens

In Figure 3-15, the cross-sectional dimension of the square columns was 400 mm x 400 mm (h = 400 mm). The shear span lengths were a = 1200 mm (a/h = 3.0) or a = 2400 mm (a/h = 6.0). SD500 D25 and D29 bars were used for the longitudinal reinforcement. In all specimens except **SL40S2B-1**, the straight column bars were lap spliced at the plastic hinge region with the bottom offset-bars of the same diameter extended from the base, while in **SL40S2B-1**, the diameter of the bottom offset-bars was increased to D29 to make up for a moment strength reduction due to the bottom bar offset. The lap splice lengths of the column bars varying from $30d_b$ to $50d_b$ were equivalent to 56% ~ 108% of the required minimum splice lengths calculated by ACI 318-14 using actual material strengths.

The lap-spliced column bars were confined by transverse bars with 90° end hooks for anchorage. SD400 D13 ties were used at a spacing of s = 165 mm (= 0.5d where d is the effective depth of the column tension bars), except for **SL50S2B-1** with s = 330 mm (=1.0d). The first tie was placed at a height of 80 mm from the base. As shown in Figure 3-15, the 90º hook anchorage of the ties was alternated end for end in accordance with ACI 318-14.

Figure 3-16 shows the reinforcement details of the rectangular columns (**RL00S1T ~ RL40S2T**). The dimension of the rectangular column section was 250 mm × 640 mm (h = 250 mm). Thus, the square and rectangular columns had the same cross-sectional area A_g (=160,000 mm^2). The net column heights from the base to the lateral loading point were a = 1,200 mm (a/h = 3.0) or 2,400 mm (a/h = 6.0). The typical lap splices were located in the plastic hinge zone with the length of 30 ~

$50d_b$, which were 56 ~ 85% of the splice length specified in ACI 318-14 based on nominal material strength.

The conventional ties with 90° hooked anchorages in rectangular column was placed at the spacing of 105 mm (0.5*d*). The first perimeter tie and crosstie were placed at a height of 50 mm. The anchorage hooks of the transverse reinforcement were placed in an alternate manner to restrain early loosening of the ties. Crossties were used to support the intermediate longitudinal bars, complying with the requirements of ACI 318-14 25.7.2.3. The lateral load was applied perpendicular to the weak axis of the column, because the weak column-strong beam mechanism can be occurred in that direction under earthquake.

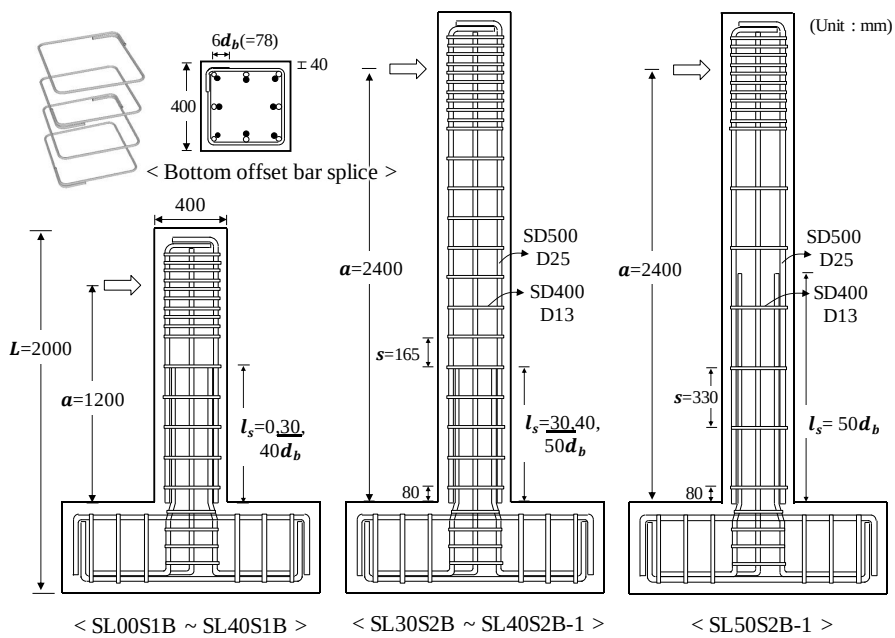

(a) Bottom offset bar splice

Figure 3-15 Dimensions and reinforcement details of square columns (Continued)

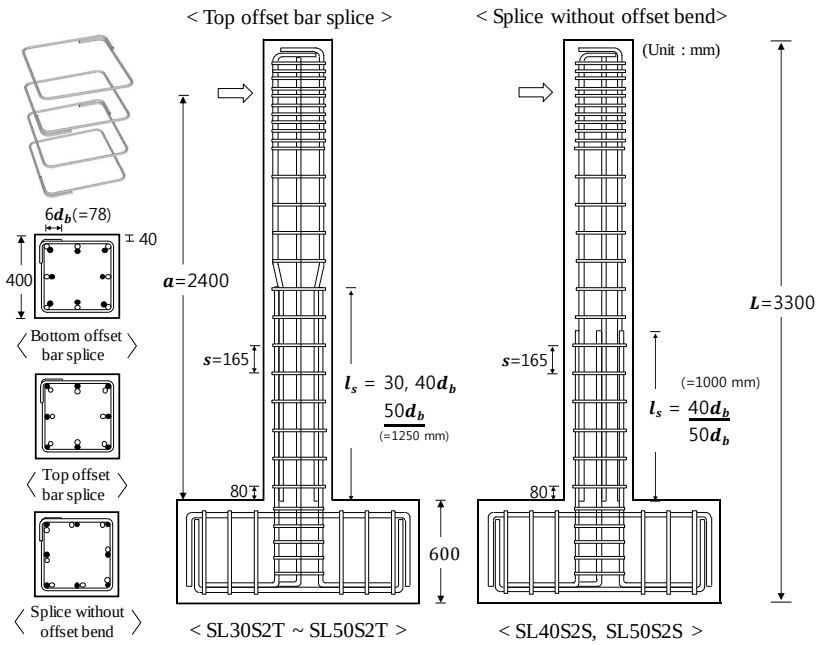

(b) Top offset bar splice and splice without offset bend

Figure 3-15 Dimensions and reinforcement details of square columns

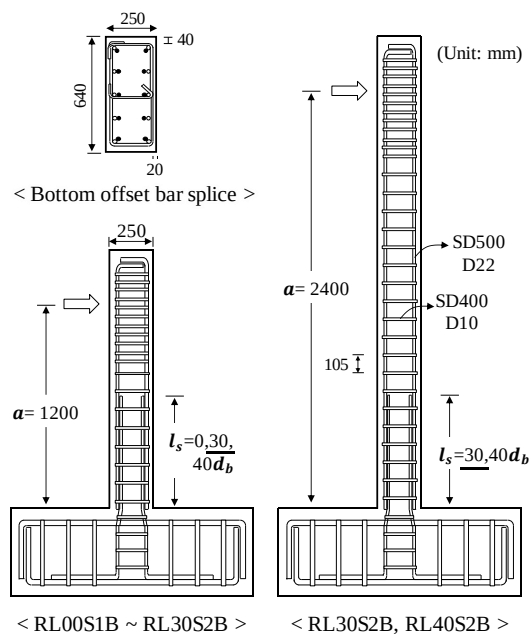

Figure 3-16 Dimensions and reinforcement details of rectangular columns

3.2.3 Specimen construction

Construction procedures of the lap spliced column specimens are illustrated in Figure 3-17. Steel cages were assembled with manufactured rebars. Strain gauges were attached on the longitudinal rebars and transvere rebars at the location specified in Figure 3-18. To investigate the stress transfer between top and bottom splice bars through concrete bond, strains of lap spliced bars were measured at the locations of 300 mm, 600 mm, 1000 mm (or 750 mm in $l_s = 30d_b$), 1250 mm from the pedestal depending on lap splice length. Strains of transverse bars were also measured.

Concrete was poured at the side of column specimens. The specimens were steam cured for 3 days prior to stripping their molds for attaining target concrete strength. The column tests were conducted in 30 days after concrete placing. Before curing concrete, the steel rods were inserted in the specimens to install measuring equipment (LVDT, Linear Variable Differential Transformer) same as Chapter 2 (Figure 2-39).

<Manufactured re-bars>

<Assembling steel cages>

<Manufacturing molds>

<Placing concrete>

Figure 3-17 Construction procedures of lap spliced column specimens

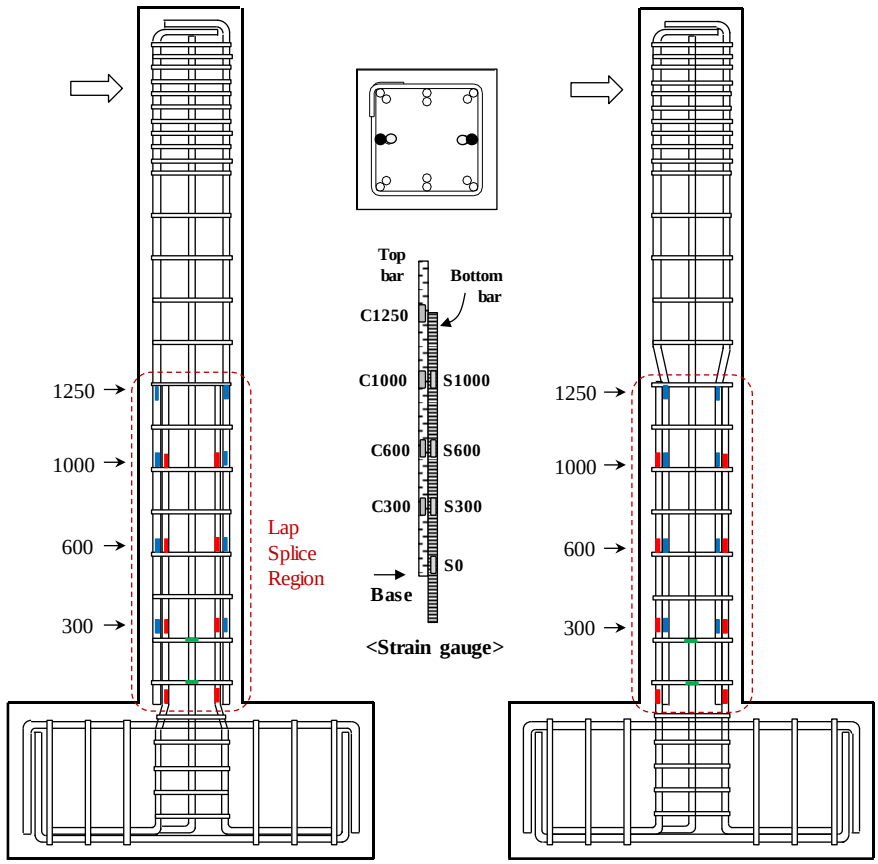

Figure 3-18 The location of strain gauges in lap splice region of columns

3.2.4 Material strengths

Table 3-4 shows the yield and tensile strengths (f_y and f_u, respectively) of the reinforcing steel bars used for test columns. For the columns, cyclic tests were performed four times. Thus, as shown in Table 3-4, f_y (= 475 ~ 590 MPa) and f_u (= 591 ~ 707 MPa) of D10 to D29 bars used in each test were differed. In the table, SD400 and SD500 denote the nominal yield strength grades of deformed bars, 400 and 500 MPa, respectively, and D10, D13, D22, D25, and D29 denote the diameters of deformed bars, d_b = 9.53, 12.7, 22.2, 25.4, and 28.6 mm, respectively. The yield and tensile strengths in Table 3-4 are average values of three of reinforcing bars.

Table 3-5 shows the mix proportioning of the concrete. The maximum aggregate size was 25.4 mm. In each column test, three concrete cylinders of a diameter 100 mm and a height 200 mm were prepared and the compression tests of the cylinders were performed on the first day of testing. The compressive strengths of the concrete were f_c' = 25 ~ 37 MPa on average. Material test results of two concretes (Test No. 2 & 3) are shown in Figure 3-19.

Table 3-4 Properties of steel reinforcing bars

Test No.	Bar type	d_b (mm)	f_y (MPa)	f_u (MPa)	ε_y (mm/mm)
1	SD400 D13	12.7	500	645	0.0025
	SD500 D25	25.4	571	700	0.00286
	SD400 D10	9.53	530	591	0.00265
	SD500 D22	22.2	566	678	0.00283
2	SD400 D13	12.7	481	607	0.00241
	SD500 D25	25.4	550	685	0.00275
	SD400 D10	9.53	552	682	0.00276
	SD500 D22	22.2	565	694	0.00283
3	SD400 D13	12.7	528	656	0.00264
	SD500 D25	25.4	588	702	0.00294
4	SD400 D13	12.7	475	659	0.00238
	SD500 D25	25.4	590	707	0.00295
	SD500 D29	28.6	521	671	0.00261

Table 3-5 Mix design of concrete

Test No.	Compressive strength	W/C	Unit weigh, kgf/m^3							Slump
			W	C	FS	S	FA	CA	SP	
1	32 MPa	55.5%	155	153	56	70	923	950	1.95	120 mm
2	25 MPa	46.2%	173	243	56	75	807	887	2.24	150 mm
3	27 MPa	53.5%	159	149	74	74	907	893	1.78	120 mm
4	37 MPa	44.8%	168	319	56	-	832	915	2.25	150 mm

Note: W = water; C = cement; FS = fly ash; S = blast furnace slag; FA = fine aggregate; CA = coarse aggregate; SP = superplasticizer

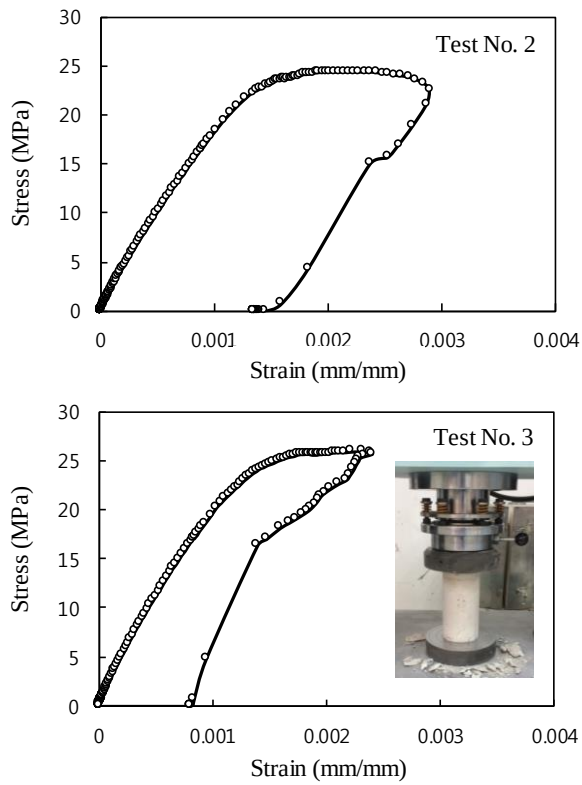

Figure 3-19 Stress and strain curves of concrete cylinders

3.2.5 Test setup and loading plan

Figure 3-20 and Figure 3-21 show the test setup for the lateral and axial loading. The cyclic lateral loading was performed by controlling the lateral displacement of the actuator (maximum stroke ± 250 mm) placed at a height of 1200 mm or 2400 mm from the column base. The displacement history for the cyclic lateral loading was identical to Figure 2-43 (in Chapter 2). Load cycles were repeated three times at each displacement step.

Axial loads N were applied to the columns by post-tensioning two high-strength Dywidag bars (diameter = 47 mm) (see Figure 3-20). For the post-tensioning, a steel beam was placed on top of the concrete column, and two hydraulic jacks with a capacity of 1000 kN were then placed on the steel beam. During the cyclic lateral loading, the axial load was kept as constant by maintaining the hydraulic pressure of the jacks uniform. To eliminate the contribution of the Dywidag bars to the column strength and stiffness, pin joints were placed at the bottom of the Dywidag bars (see Figure 3-20). The axial load of the Dywidag bars always acts along the center line of the column because both the column and Dywidag bars are displaced simultaneously. Therefore, the second-order effect can be ignored in the lateral load-displacement relationship.

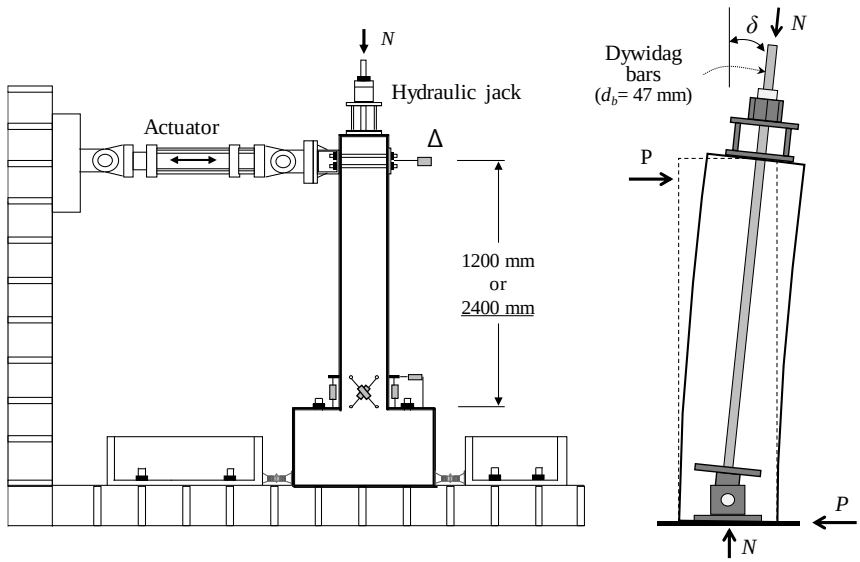

Figure 3-20 Schematic test setup for RC columns with lap splices

Figure 3-21 Photograph of test setup for RC columns with lap splices

3.3 Test Results

3.3.1 Square columns with bottom offset bar splices

3.3.1.1 Cyclic behavior and failure mode

Figure 3-22 shows the base moment and lateral drift ratio (M-δ) relationships of the square columns. For a consistent strength comparison between columns with different shear spans, the base moment M (= Pa where P is the lateral load of the actuator and a is the shear span of the column) were compared, instead of the lateral load P. The lateral drift ratio δ was calculated by dividing the lateral displacement at the loading point by the shear span. The maximum moments M_u were denoted as white circles, while the predicted moment strengths M_n were denoted as horizontal dashed lines. M_n of each specimen was calculated from the section analysis considering the applied axial load N, actual material strengths, and displaced location of the bottom offset-bars from the base.

In **SL00S1B** without lap splices, the maximum loads (M_u = +407 and -400 kN·m) were greater than the nominal strengths (M_n = ±374 kN·m). A strength degradation was observed at δ = 2.0% as the spalling of concrete cover occurred at the bottom of the column. Ultimately at δ = 3.5%, the load-carrying capacity was significantly decreased due to anchorage failure at 90º hook, as shown in Figure 3-23(a). Despite the presence of the applied axial load of N = 870 kN, web shear cracking and concrete strut failure occurred excessively in the plastic hinge region.

In **SL30S1B** with the lap splice $l_s = 30d_b$, the maximum loads (M_u= +350 and -354 kN·m) were 13% less than those of **SL00S1B** without lap splice. However, M_u was slightly greater than the nominal strengths (M_n = ±340 kN·m) calculated for the displaced bottom offset-bars. Ultimately, failure occurred at δ = 3.5% due to excessive concrete crushing in the column bottom, as shown in Figure 3-23(b). Although excessive bond splitting cracking was not observed in the lap splice region, the relatively poor behavior of **SL30S1B** was attributed to the insufficient splice length (i.e. 63% of the minimum splice length required by ACI 318-14). In **SL40S1B** with the increased splice length $l_s = 40d_b$, unlike **SL30S1B**, the maximum loads (M_u= +393 and -417 kN·m) were significantly increased and thus equivalent to those of

SL00S1B without lap splice. The enhanced behavior of **SL40S1B** might be attributed to the increased splice length. Cover concrete spalling began to occur at δ = 2.0%. The load-carrying capacity of **SL40S1B** was significantly degraded during the first load cycle to δ = -5.0% due to excessive concrete crushing at the cover and core along with web shear cracking, as shown in Figure 3-23(c).

Figure 3-22(d) and Figure 3-22(e) show the cyclic behaviors of **SL30S2B** and **SL40S2B** with the increased shear span a = 2400 mm. The maximum loads were about 95% of the nominal strength (M_n = 294 kN·m), which indicates that the performance of the lap splices was not successful. Despite the insufficient strengths, a ductile behavior until δ = 7.0% was observed. The column shears in **SL30S2B** and **SL40S2B** were significantly reduced due to the increased shear span length, compared to those of **SL30S1B** and **SL40S1B** with the less shear span. Thus, as shown in Figure 3-23(d) and Figure 3-23(e), diagonal shear cracking in the web was insignificant even at large inelastic deformations of δ = 5.0% or greater. However, bond splitting cracks occurred due to the insufficient splice lengths (i.e. 57% and 76% of the required splice length) and propagated along the spliced bars as inelastic deformations increased. When comparing the test results of **SL30S2B** and **SL40S2B** with those of **SL30S1B** and **SL40S1B**, it is obvious that the increased shear span length (a) affected the failure mode and ductility of the columns with lap splice by decreasing the applied shear force.

In **SL50S2B** with $l_s = 50d_b$, the maximum loads (M_u = +364 and -377 kN·m) were significantly increased and thus equivalent to the nominal strengths (M_n = ±367 kN·m). Since the provided splice length was greater than the minimum splice length required by ACI 318-14, the strength degradation during repeated load cycles was limited and the energy dissipation capacity was significantly enhanced compared to other columns with $l_s = 30d_b$ and $40d_b$. **SL50S2B** did not fail until δ = 7.0% and the test was forced to end due to lack of the actuator stroke. As shown in Figure 3-23(f), bond splitting cracking was not significant in **SL50S2B**. This indicates that the stress transfer between the spliced bars through concrete bond was successful.

In **SL40S2B-1** with the bottom offset bars of a greater bar size D29 ($l_s = 40d_b$ and d_b = 28.6 mm), as shown in Figure 3-22(g), the maximum loads (M_u = +342 and -383 kN·m) were less than the nominal strength (M_n= ±393 kN·m). This might be because the lap splice length $l_s = 40d_b$ was not sufficient to develop the full yield

strength of D29 offset-bars with the increased bar diameter. However, since the spliced bars were confined well by the transverse bars of a spacing s = 0.5d, the strength degradation was limited and the hysteretic energy dissipation was significant. On the other hand, in **SL50S2B-1** with the increased perimeter tie spacing s = 1.0d, the maximum loads (M_u = +347 and -337 kN·m) were greater than the nominal strengths (M_n = ±312 kN·m). This indicates that the lap splice length l_s = 50d_b was sufficient to develop the full yield strength of D25 offset-bars. However, it seemed that the tie spacing s = 1.0d was not sufficient to ensure a post-yield ductile behavior of the column. Thus, as the lateral drift ratio increased to δ = 2.0% or greater, bond splitting cracks significantly occurred along the lap splice, as shown in Figure 3-23(h). Consequently, the ductility and energy dissipation capacity of **SL50S2B-1** were significantly degraded.

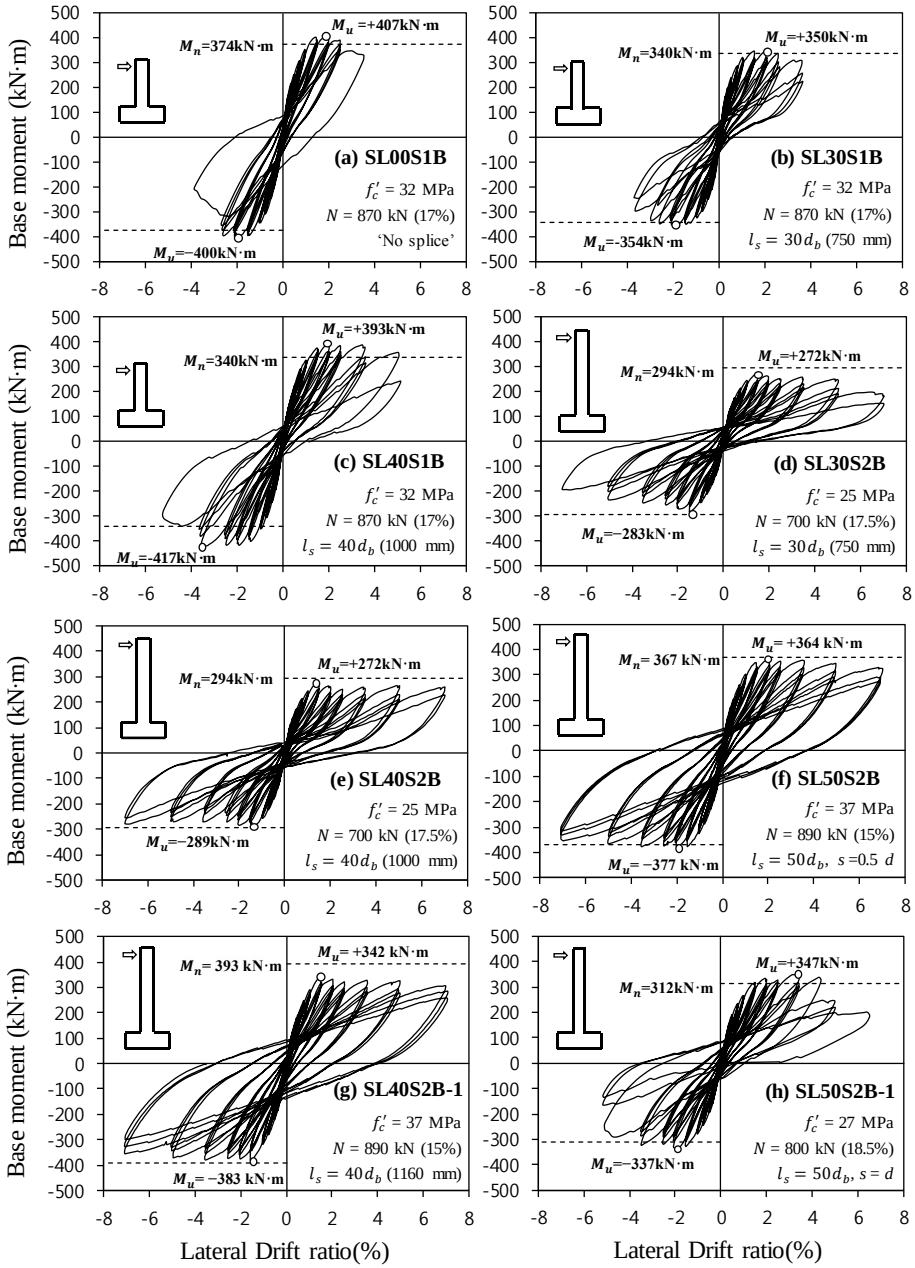

Figure 3-22 Base moment and lateral drift ratio relationships of square columns with bottom offset bar splices

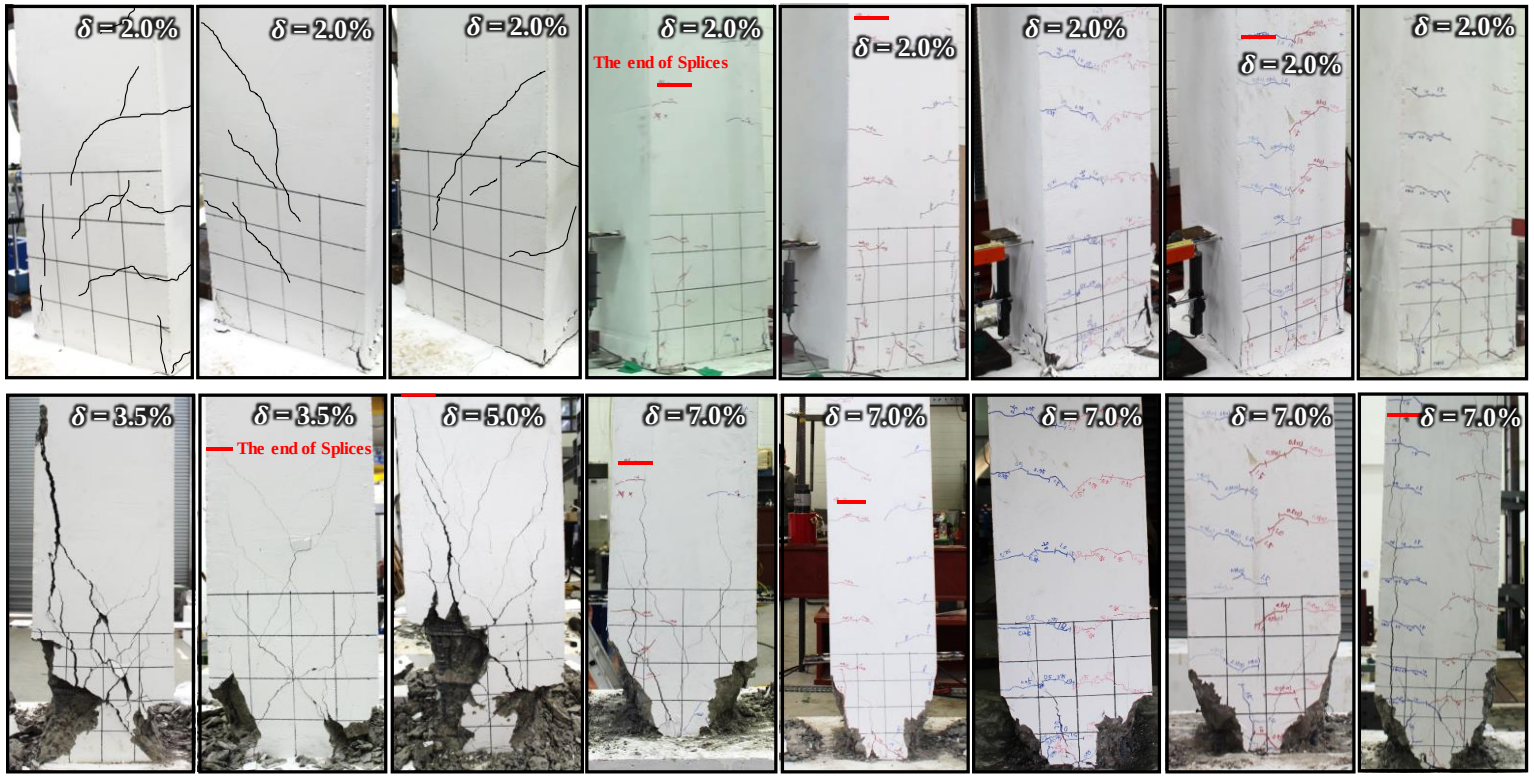

(a) SL00S1B (b) SL30S1B (c) SL40S1B (d) SL30S2B (e) SL40S2B (f) SL50S2B (g) SL40S2B-1 (h) SL50S2B-1

Figure 3-23 Failure modes of square columns with bottom offset bar splices

3.3.1.2 Strains of lap-spliced bars

To investigate the stress transfer between the straight column bars and the offset bars extended from the base through concrete bond, strains of lap-spliced bars were measured. Figure 3-24 shows the strains of the spliced bars measured from **SL30S2B**, **SL40S2B**, **SL50S2B**, **SL40S2B-1**, and **SL50S2B-1.** In each specimen, the strains of the straight and offset bars are plotted in the right and left figures, respectively. The horizontal and vertical axes, respectively, denote the bar strains and the height from the base where the strains were measured. The bar strains in Figure 3-24 were the maximum values that each spliced bar underwent during the load cycles repeated at each lateral drift ratio. For clarity, the bar strains corresponding to δ = 0.25%, 0.5%, 1.0%, 1.5%, 2.0%, and 2.5% are denoted with bars, crosses, triangles, diamonds, circles, and squares, respectively.

As shown in Figure 3-24, at every lateral drift ratio, the strains of the bottom offset-bars extended from the base decreased as the height from the base increased, while the strains of the straight column bars did not vary significantly along the lap splice length. In addition, the bar strains were much greater in the bottom offset-bars than in the straight column bars. These measurements indicate that the tensile stress of the bottom offset-bars extended from the base was transferred to the straight column bars through bond with the surrounding concrete, and the bond demand was much greater in the bottom offset-bars than in the straight column bars.

The magnitudes of the bar strains were significantly affected by the lap splice length. The bar strains of **SL30S2B** ($l_s/l_{s,ACI}$ = 0.57) and **SL40S2B** ($l_s/l_{s,ACI}$ = 0.76) in Figure 3-24(a) and Figure 3-24(b) were relatively small and not greater than the yield strain (ε_y= 0.00275) since the concrete cover spalled off at the bottom early at δ = 1.5% ~ 2.0%. This indicates that due to the short splice lengths, the stress of the bottom offset-bars was not fully transferred through concrete to the top straight bars. In addition, overall, the bar strains of **SL40S2B** with the greater splice length were greater than those of **SL30S2B** with the less splice length.

In **SL50S2B** ($l_s/l_{s,ACI}$ = 1.08) and **SL50S2B-1** ($l_s/l_{s,ACI}$ = 0.93), on the other hand, by increasing the lap splice lengths the bar strains were significantly increased. Particularly, the strains of the bottom offset-bars exceeded the yield strains (ε_y= 0.00295 or 0.00299) at the bottom of columns, which indicates that the stress transfer

between the spliced bars was sufficient to develop the full column strength. As similar strain distribution was observed in **SL40S2B-1** (l_s / $l_{s,ACI}$ = 1.01) though the size of the bottom bars extended from the base was increased to D29 (d_b=28.6 mm).

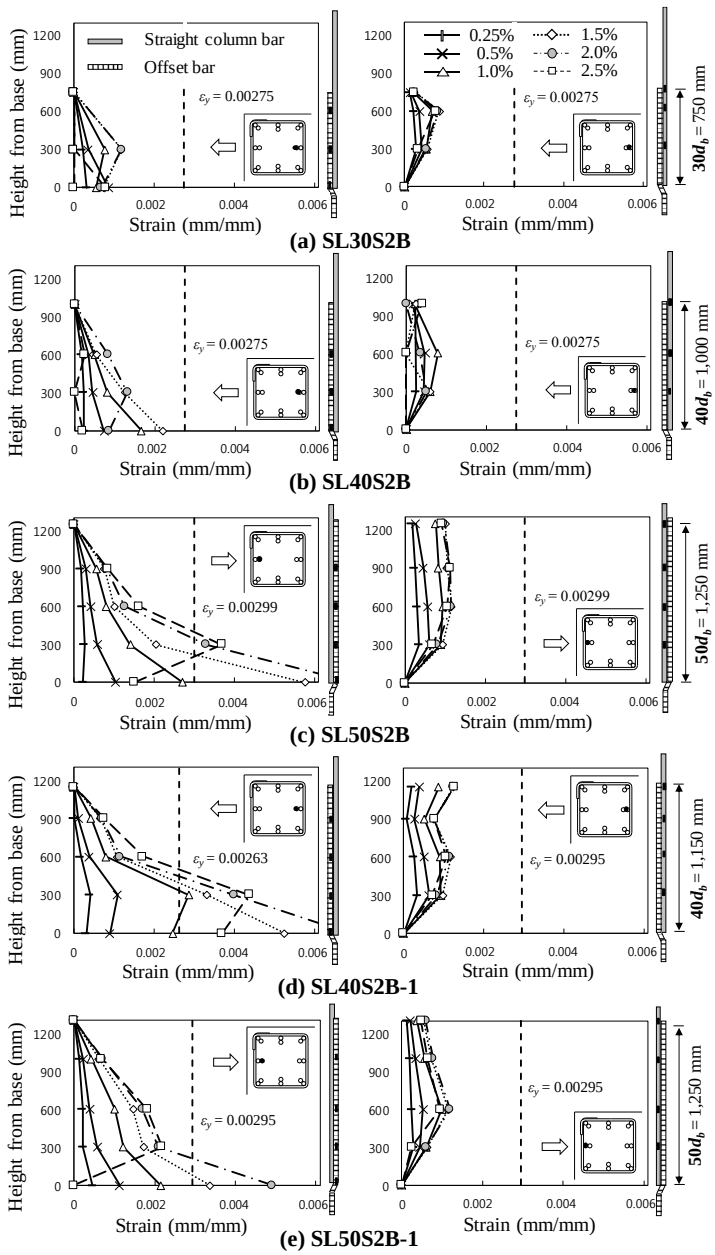

Figure 3-24 Strains of spliced bars of bottom offset bar splices

3.3.2 Square columns with different offset bar splice details

3.3.2.1 Cyclic behavior and failure mode

Figure 3-25 shows the lateral load and lateral drift ratio (V-δ) relationships of the columns. The lateral drift ratio δ was calculated by dividing the lateral displacement at the loading point by the shear span (2400 mm). The maximum load V_u were denoted as white circles, while the predicted strengths V_n (=M_n/a) were denoted as horizontal dashed lines. Moment strength M_n of each specimen was calculated from the section analysis considering the applied axial load N, actual material strengths (f_c' and f_y in Table 3-4 and Table 3-5), and displaced location of the offset bars from the base. In the bottom offset bar splice (Figure 3-25(a) ~ Figure 3-25(c)), since the longitudinal bars from the base are located relatively inside the concrete core, the predicted strength V_n is approximately 10% smaller than other splice columns. In the specimens where bond splitting failure occurred, the points at initial vertical cracking and splice failure were marked with white and grey squares, respectively. The failure modes at δ = 2.0% when maximum lateral load was applied and at the end of tests were shown in Figure 3-26.

Figure 3-25(a) ~ Figure 3-25(c) show the cyclic behaviours of **SL30S2B**, **SL40S2B**, and **SL50S2B** with bottom offset bar splice, which were explained again to compare to the other offset bar splice details. In the columns with bottom offset bar splice at a potential plastic hinge zone, a ductile behaviour was observed until δ = 7.0% without significant strength degradation except **SL30S2B** in which short lap splice was used (l_s / $l_{s,req}$ = 0.57). In **SL30S2B**, initial vertical cracking and splice failure along lap splice length were occurred at 2nd cycle of δ = 5.0% and 1st cycle of δ = 7.0%, respectively. On the other hand, in **SL40S2B** and **SL50S2B**, bond splitting failure was not observed at the end of tests as shown in Figure 3-26(b) and Figure 3-26(c). The tests were terminated without failure due to lack of the actuator stroke. **SL50S2B** with bottom offset bar splice and l_s / $l_{s,req}$ of 1.08 showed the greatest cyclic behaviour in terms of strength, ductility, and energy dissipation. However, **SL30S2B** and **SL40S2B** showed about 95% of the nominal strength (V_n = 123 kN) due to deficient splice lengths (i.e. 57% and 76% of the required splice length).

Figure 3-25(d) ~ Figure 3-25(f) show the cyclic behaviours of **SL30S2T**, **SL40S2T**, and **SL50S2T** with top offset bar splice. In the columns with top offset

bar splice at a potential plastic hinge zone, a brittle behaviour was observed especially in **SL30S2T** and **SL40S2T** with short lap splices ($l_s / l_{s,req}$ = 0.56 and 0.74). The deformation capacity increased as lap splice length increased. In **SL30S2T** and **SL40S2T**, initial vertical cracking and splice failure along lap splice length were occurred at 1st cycle of δ = 2.5~3.5% and 1st cycle of δ = 3.5~5.0%, respectively. In **SL50S2T** with top offset bar splice and $l_s / l_{s,req}$ of 1.08, the initial vertical cracking and splice failure along lap splice length were occurred at 1st and 2nd cycle of δ = 5.0%, respectively. As shown in Figure 3-26(d) ~ Figure 3-26(f), the columns with top offset bar splice experienced concrete crushing in the compression zone at δ = 2.0% when maximum load was applied, and cover spalling of concrete and severe bond splitting failure along lap splice region at the end of tests. The stress transfer between top and bottom splice bars was limited after initial vertical cracking, and the brittle failure was occurred with the relatively low deformation capacity.

In **SL40S2S** and **SL50S2S** with splice without offset bend, similar cyclic behaviours were observed on the comparison of columns with top offset bar splice. Despite different lap splice details in **SL50S2T** and **SL50S2S**, the maximum strength, deformation capacity, and failure mode were almost identical. As the location of bottom splice bars extended from the base to resist flexural moment is same in **SL50S2T** and **SL50S2S**, the maximum loads (V_u = 175 ~ 187 kN) were 9% greater than the nominal strength (V_n = 166 kN), and the splice failure were occurred at 2nd cycle of δ = 5.0%. When short lap splice length is used in **SL40S2S** ($l_s / l_{s,req}$ = 0.87), the maximum loads (V_u = 171 ~ 193 kN) were 10% greater than the nominal strength (V_n = 166 kN), but brittle failure occurred right after peak load: initial vertical cracking and splice failure along lap splice region were occurred at 1st cycle of δ = 2.5% and 1st cycle of δ = 3.5%, respectively.

These results indicate that cyclic behaviour of spliced columns are mainly affected by the location of bottom splice bars as well as lap splice length. Bottom offset bar splice resulted in lower strength but greater ductility and energy dissipation. On the other hand, top offset bars splice and splice without bend gave rise to greater strength but lower ductility and energy dissipation.

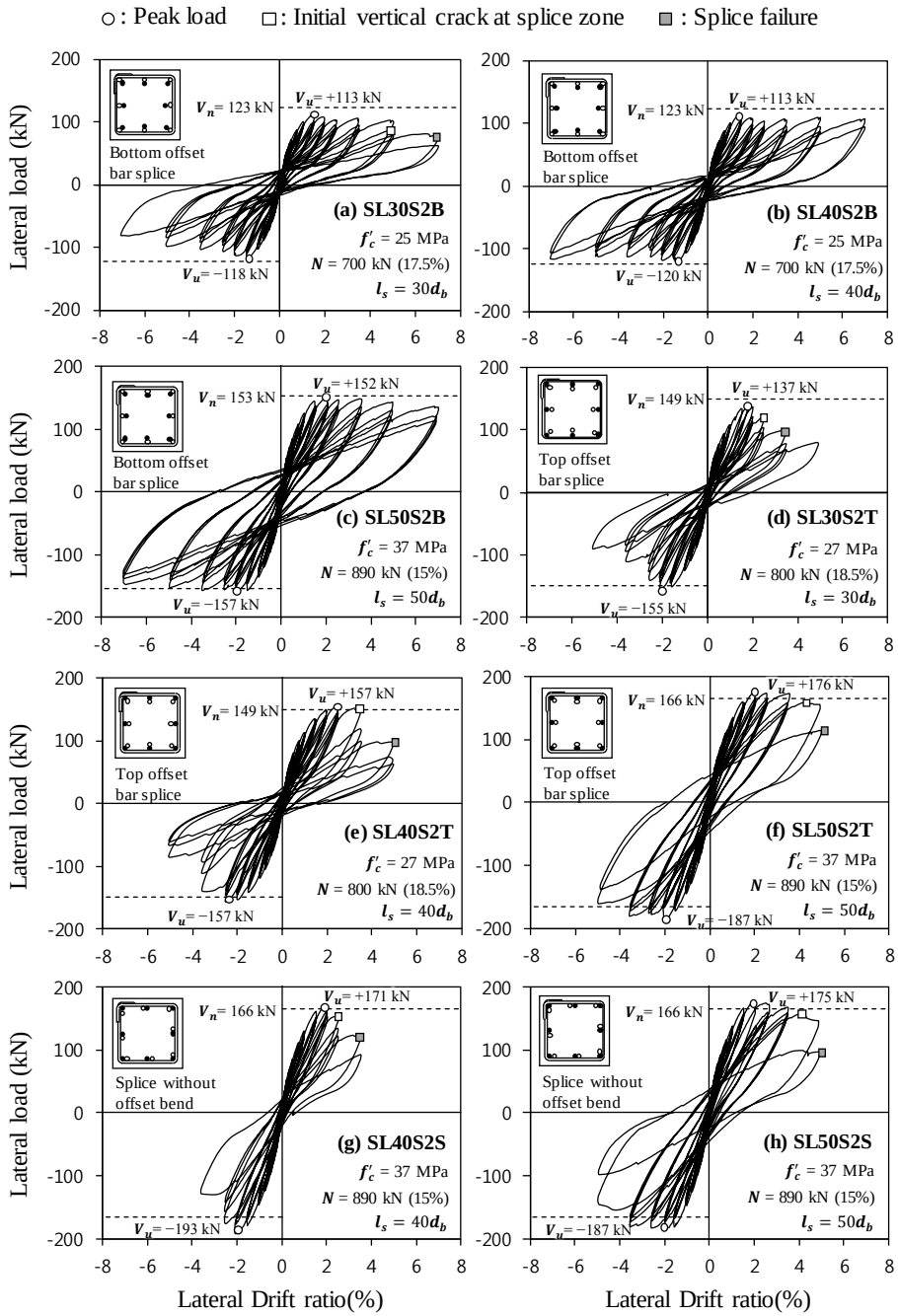

Figure 3-25 Lateral load and drift ratio relationships of columns with different lap splice details

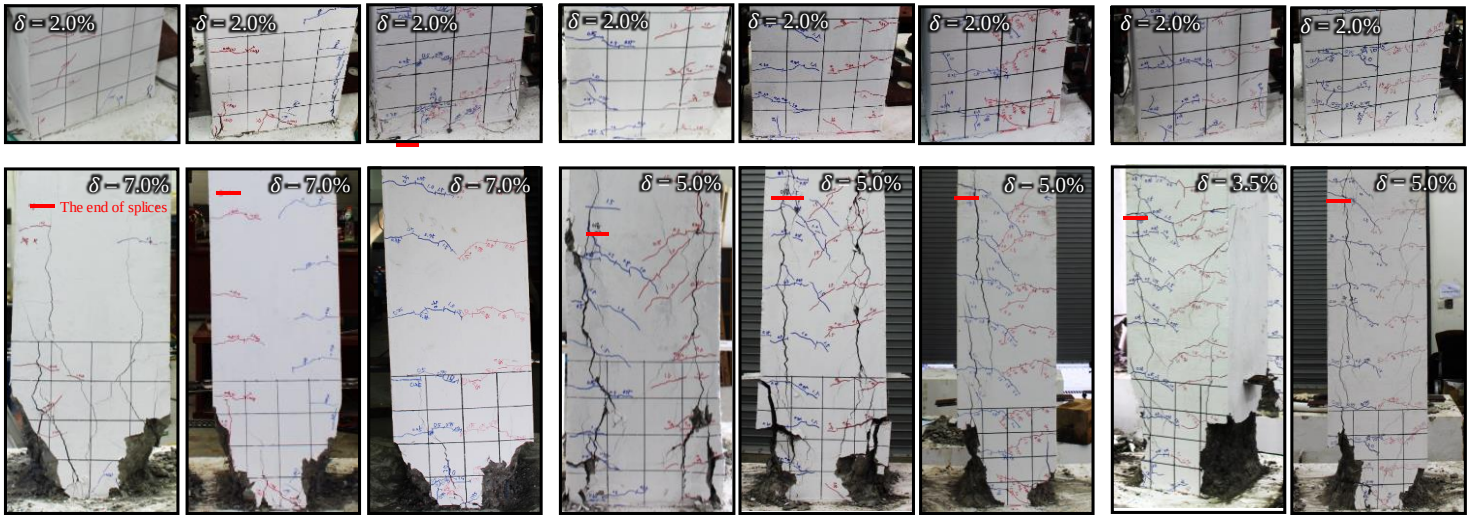

(a) SL30S2B (b) SL40S2B (c) SL50S2B (d) SL30S2T (e) SL40S2T (f) SL50S2T (g) SL40S2S (h) SL50S2S

Figure 3-26 Failure modes of square columns with different lap splice details

3.3.2.2 Failure sequence depending on offset bar splice details

The failure patterns varied according to the lap splice details of the column longitudinal bars. The columns with bottom offset bar splice exhibited typical flexural failure behavior, but the columns with top offset bar splice or splice without offset bend showed splice failure with severe splitting cracks at the lap splice regions after flexural yielding. In order to investigate the failure mode in detail, crack patterns observed at drift ratio of 2.0%, 2.5%, 3.5%, and 7.0% (or 5.0%) of columns with lap splice length of $50d_b$ were illustrated in Figure 3-27.

In the bottom offset bar splice, the concrete crushing occurred in the compression zone at a drift ratio of 2.0% when the maximum load was attained. As the drift ratio increased after flexural reinforcement yielded at 2.0%, the concrete cover in the plastic hinge zone was gradually spalled off. At a drift ratio of 7.0%, the cross-sectional area of the concrete at the bottom of the column was greatly reduced, but the load reduction was marginal.

The top offset bar splice showed similar behavior to splice without offset bend. At a drift ratio of 2.0%, when maximum load was reached, the concrete crushing occurred in the compression zone, and the concrete cover was gradually dropped at the bottom of columns. At a drift ratio of 3.5%, initial vertical splitting cracks occurred, and they propagated along the lap splice zone. Ultimately, the splice failure occurred with severe splitting cracks at a drift ratio of 5.0%. In the top offset bar splice and splice without offset bend, vertical cracks were observed on the side of columns due to the large tensile forces applied in the bottom offset bars located at the outermost cross section.

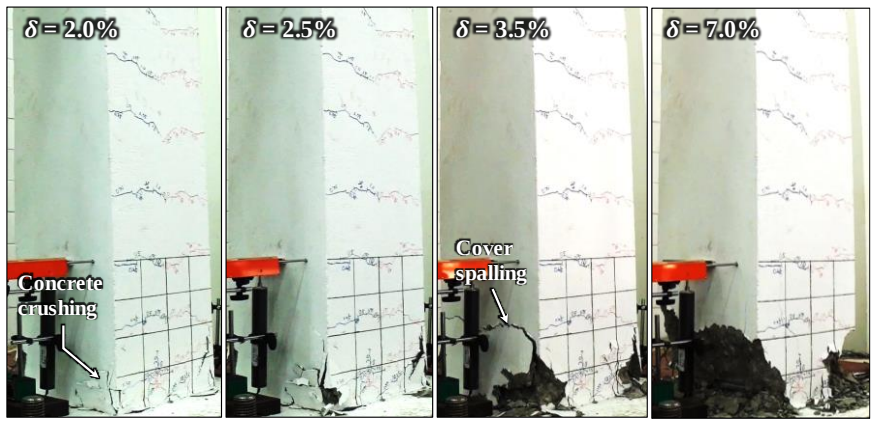

(a) Bottom offset bar splice (SL50S2B)

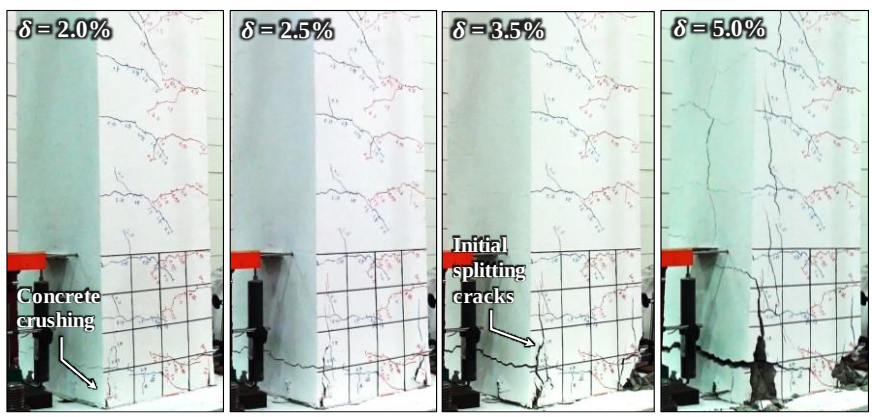

(b) Top offset bar splice (SL50S2T)

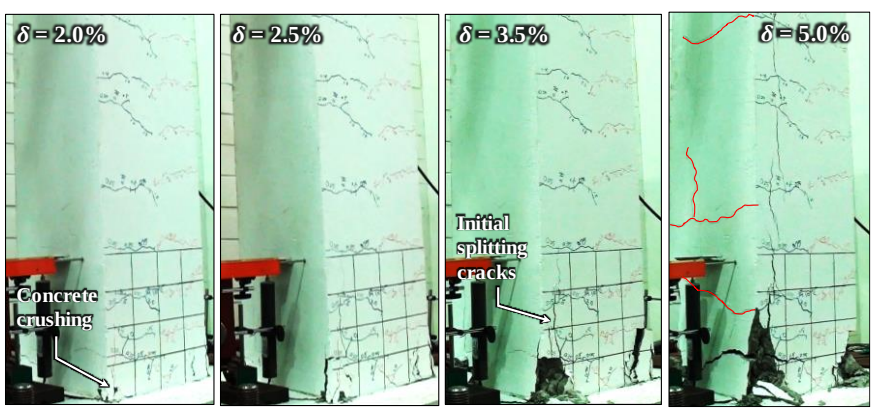

(c) Splice without offset bend (SL50S2S)

Figure 3-27 Failure sequences of lap spliced columns

3.3.2.3 Energy dissipation

Figure 3-28 shows the cumulative energy dissipation, which defines as total energy absorption (E_D, the enclosed area of load and displacement relationships) during cyclic loadings. Columns with lap splice lengths of $30d_b$, $40d_b$, and $50d_b$, are indicated with triangles, squares, and circles, respectively. When compared to columns with top offset bar splice and splice without offset bend, energy absorbing capacity in columns with bottom offset bar splice was similar until δ = 5.0% (see grey circles); however, additional energy was dissipated at δ = 7.0% only in bottom offset bar splice. Therefore, in columns with the bottom offset bar splice, despite lowest load carrying capacity, the greatest cumulative energy dissipation could be attained due to greatest deformation capacity.

The cumulative energy dissipation of spliced columns differs among the lap splice lengths, $30d_b$, $40d_b$, and $50d_b$. As shown in Figure 3-28(a), in the columns with bottom offset bar splice at δ = 5.0%, the cumulative energy dissipation of **SL50S2B** was 46% greater than those of **SL30S2B** and **SL40S2B**. Similarly, in the columns with top offset bar splice at δ = 3.5% (refers to Figure 3-28(a)), the cumulative energy dissipation of **SL50S2T** was 39% greater than those of **SL30S2T** and **SL40S2T**. Despite different maximum strengths (V_u) in same lap splice details due to different material strength, the gap in energy dissipation among the lap splice lengths was significant. Failure mode of spliced columns, such as splitting cracks and bond slip developed along lap splices, were main reason for different energy dissipations. A column with short lap splice length applying higher bond demand along lap splices is prone to bond slip, thereby reducing energy dissipation during cyclic loading.

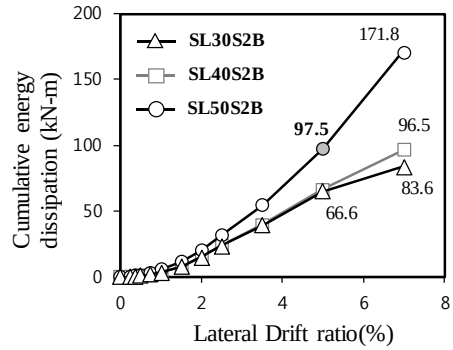

(a) Bottom offset bar splice

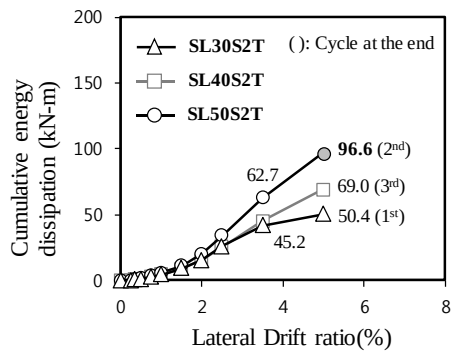

(b) Top offset bar splice

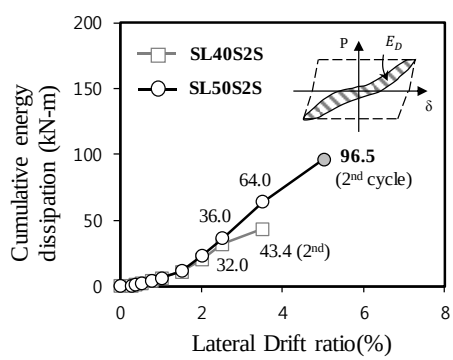

(c) Splice without offset bend

Figure 3-28 Cumulative energy dissipation of square columns with different lap splice details

3.3.2.4 Strains of lap spliced bars

To investigate the stress transfer between the top splice bars and the bottom splice bars extended from the base through the lap splice, strains of lap-spliced bars were measured along the lap splice length. Figure 3-29 shows the strain distributions of spliced bars measured from all the tested columns varying with the height from the base. In each specimen, the strains of the top splice bars and bottom splice bars are represented in the left and right figures, respectively. The horizontal and vertical axes, respectively, denote the bar strains and the height from the base where the strains were measured. The bar strains in Figure 3-29 were the maximum values that each spliced bar underwent during the load cycles repeated at each lateral drift ratio. For clarity, the bar strains corresponding to δ = 0.25%, 0.5%, 1.0%, 1.5%, 2.0%, and 2.5% are denoted with bars, crosses, triangles, diamonds, circles, and squares, respectively.

In all specimens shown in Figure 3-29, at each lateral drift ratio, the strains of the bottom splice bars increased as the strains were closer to the base, while the strains of the top splice bars did not vary significantly along the lap splice length. In addition, the strains were much greater in the bottom splice bars than in the top splice bars in large lateral drift ratio. These strain measurements indicate that the tensile stress of the bottom splice bars extended from the base was transferred to the top splice bars through bond with the surrounding concrete, and the bond demand was much greater in the bottom bars than in the top bars.

In **SL40S2T**, **SL50S2T**, **SL40S2S**, and **SL50S2S**, in which peak lateral loads were greater than nominal strengths, the maximum strain of bottom splice bars could be reached to yield strain of the bars (ε_y= 0.00294 ~ 0.00299). Especially, in **SL50S2T**, and **SL50S2S** with lap splice length greater than required splice length in ACI 318 (l_s / $l_{s,req}$ = 1.08), due to sufficient stress transferring along lap splices, the strains in bottom splice bars attained the yield strain (ε_y) at δ = 1.0 ~ 1.5%, and large plastic strain (2.3ε_y ~ 3.9ε_y= 0.006983 ~ 0.011565) at δ = 2.5%. Similar strain result was observed in **SL40S2S** though splice length was smaller than the required splice length (l_s / $l_{s,req}$ = 0.87). Also, the measured strain in **SL 40S2T** (l_s / $l_{s,req}$ = 0.74) was reached to yield strain at δ = 2.5%. On the other hand, the measured strain in **SL30S2B**, **SL40S2B**, and **SL30S2T** could not reach to yield strain, and suddenly decreased after δ = 1.5 ~ 2.0%; thus, the maximum strength V_u was less than the

nominal strength V_n, indicating that stress transfers in specimens with short lap splice length was limited after development of bond cracks along lap splices.

From the measured strain distribution of top and bottom splice bars in the splice zone, moment diagram and corresponding flexural stress diagram in tension zone of columns can be demonstrated as shown in Figure 3-30. Under lateral loading applied in columns, linear moment gradient exists from the base (M_b) to the end of lap splices (M_s). In the meantime, the total flexural tensile stresses, summating the stresses applied in top and bottom splice bars, are increased closer to the base. The flexural tensile stress in the bottom splice bars is significantly increased closer to the base, while the stress in the top splice bar remains constant along the lap splice length.

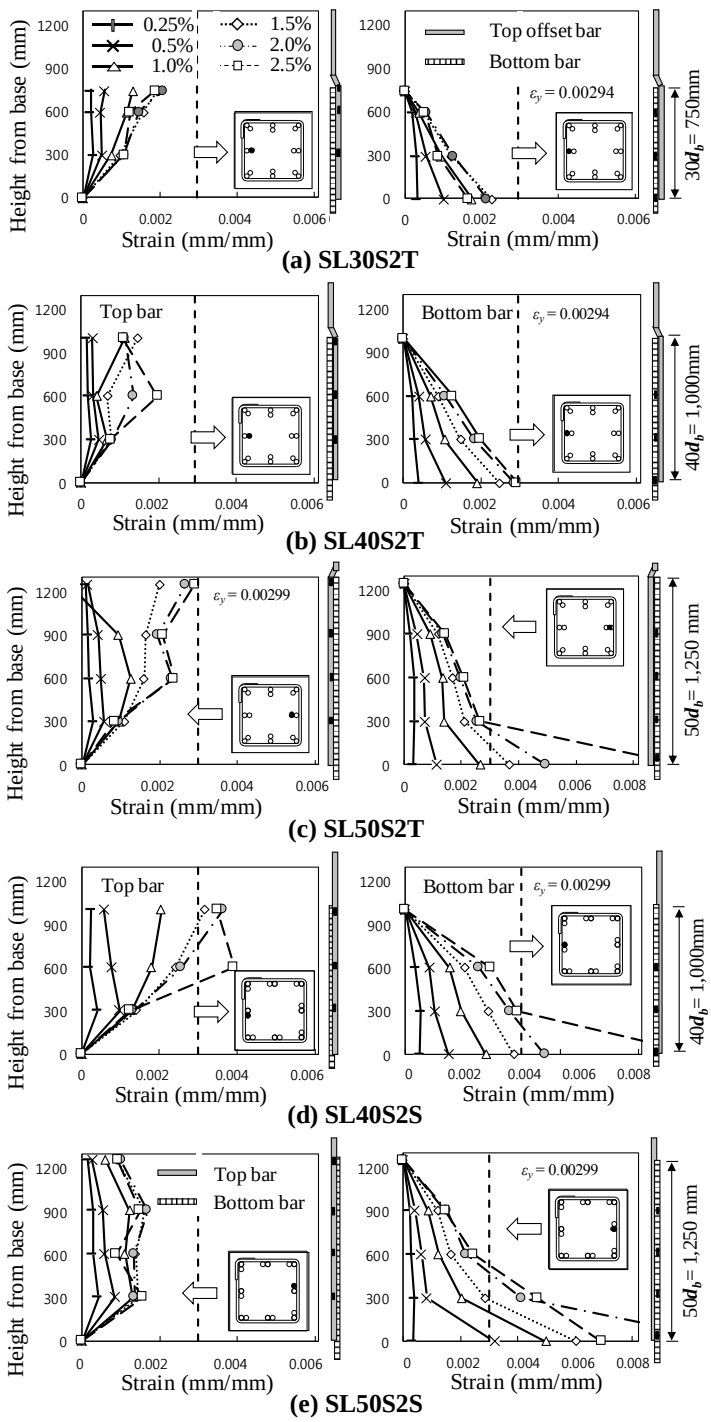

Figure 3-29 Strains of spliced bars of different lap splice details

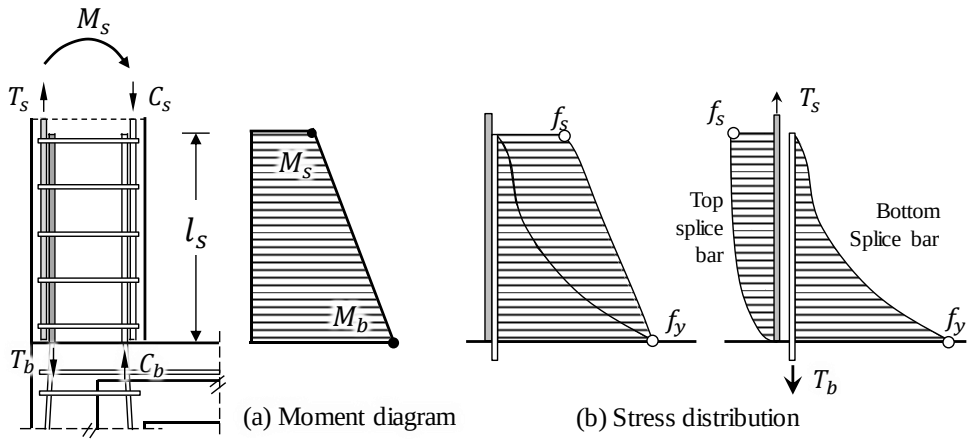

Figure 3-30 Moment gradient and spliced bar stress distributions

3.3.3 Rectangular columns with bottom offset bar splices

3.3.3.1 Cyclic behavior and failure mode

Figure 3-31 shows the base moment and lateral drift ratio (M-δ) relationships of the rectangular columns. The deformation capacities of rectangular columns except **RL00S1B** were improved with δ = 7.0% due to larger aspect ratios (a/h) of 4.8 and 9.6 compared to square columns (a/h= 3.0 and 6.0). In **RL00S1B** without lap splices, the maximum moments (M_u= +264 kN·m and -285 kN·m) were greater than nominal strength (M_n= ±262 kN·m). Load carrying capacity is significantly decreased at δ = 5.0% with the anchorage failure of 90° hooks shown in Figure 3-32(a). Shear failure occurred after flexural yielding.

On the other hand, other specimens **RL30S1B** and **RL40S1B** with lap splices of $30d_b$ and $40d_b$ showed flexural failure mode without significant strength degradation until δ = 7.0%. As the bottom offset bars resisting flexural moment are located inside concrete core, the load carrying capacity (shear demand) showed 10% reduction of **RL00S1B**. Thus, in lap spliced columns, diagonal shear cracks and anchorage failure were limited until δ = 7.0%. Only concrete cover in the plastic hinge zone was spalled off.

In **RL30S1B** and **RL30S2B** with short lap splice length (l_s / $l_{s,req}$ = 0.63 and 0.56), the maximum moment (M_u= 227 kN·m and 191 kN·m) were greater than nominal strength (M_n= 208 kN·m and 183 kN·m), respectively. **RL40S1B** and **RL40S2B** with the variation of axial loads were also satisfied with the moment capacity by sectional analysis on the basis of the location of bottom splice bars and the strength of material test results. It means that flexure dominated columns applied relatively small shear demand show great seismic performance though provided lap splice length is not satisfied with ACI318.

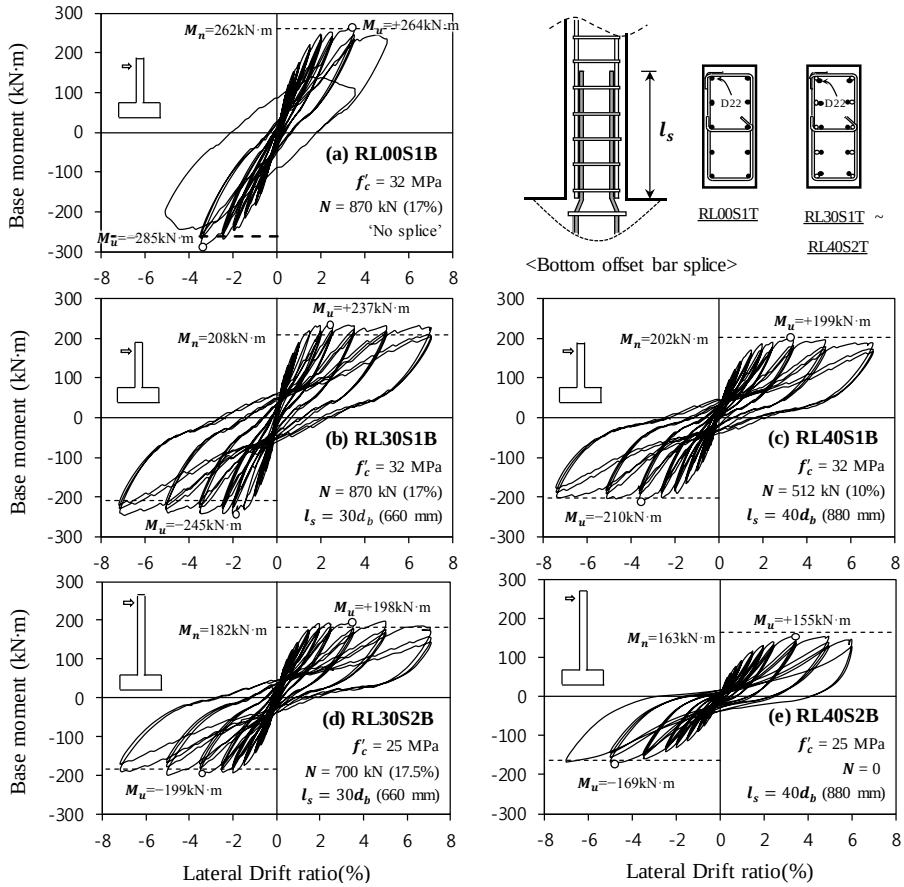

Figure 3-31 Moment and drift ratio relations of rectangular columns with bottom offset bar

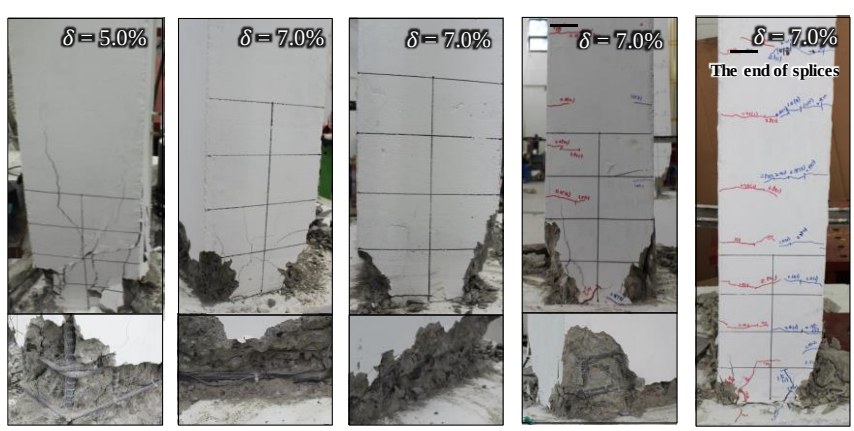

(a) RL00S1B (b) RL30S1B (c) RL40S1B (d) RL30S2B (e) RL40S2B

Figure 3-32 Failure modes of rectangular columns with bottom offset bar splices

3.3.3.2 Strain distribution of longitudinal reinforcement

Strain gauges were attached on top and bottom splice bars along the splice regions to investigate stress transfer mechanism between lap splices. Figure 3-33 shows measured strain distribution of longitudinal reinforcements in **RL30S2T** and **RL40S2T**. The left and right sides of graphs in each specimen represent strains measured on top and bottom bars, respectively. Horizontal and vertical axes indicate the maximum strain at each drift ratio and the location of strain gauges from basement.

Bottom splice bars anchored in the basement show maximum strain at the base (right graphs); on the other hand, top splice bars anchored in the top of columns show similar strain along the lap splice zone (left graphs). The strains of bottom splice bars were much greater than those of top splice bars. The stress transfer mechanism between top and bottom bars can be verified with the distributions of top and bottom bar strains. The strains of bottom bars in **RL30S2T** and **RL40S2T** ($M_u > M_n$) were reached to yield strain at δ= 1.5~2.0%.

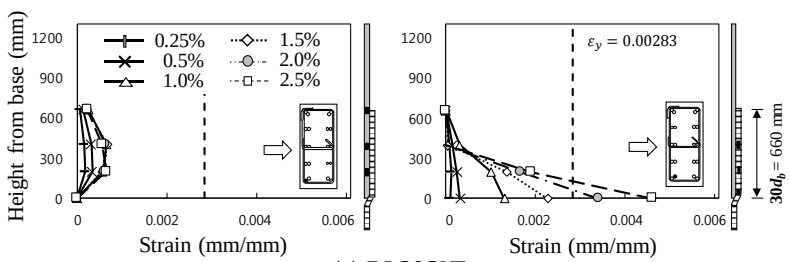

(a) RL30S2T

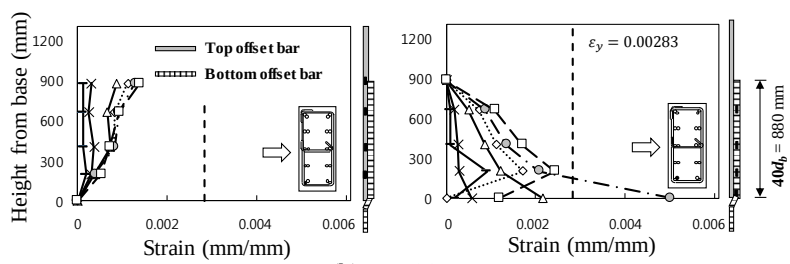

(b) RL40S2T

Figure 3-33 Strains of spliced bars of rectangular columns

3.4 Factors Affecting Performance of Lap Splice

3.4.1 Moment gradient

As shown in Figure 3-22 and Figure 3-23, the performance of the columns with lap splice at the plastic hinge was significantly affected by the shear span length. In **SL30S1B** and **SL40S1B** with the smaller shear span length a = 1200 mm (a/h = 3) (refer to Figure 3-22(b) and (c)), the maximum loads M_u were greater than the nominal strengths M_n, though the lap splice lengths l_s were only 63% or 83% of minimum splice lengths $l_{s,ACI}$ specified in ACI 318-14. In contrast, in **SL30S2B** and **SL40S2B** with the greater shear span length a = 2400 mm (a/h = 6) (refer to Figure 3-22(d) and (e)), the maximum loads M_u were less than the nominal strengths M_n. The poor performance of the lap splices in **SL30S2B** and **SL40S2B** might be attributed to an increase in the bond demand of spliced bars, which involved in the moment gradient in the lap splice region, as follows.

The moment gradients in the lap slice region are depicted in Figure 3-34. The tensile stress gradients of the spliced bottom offset-bars and top straight bars along the lap splice length are also illustrated in the same figure. Solid and dot lines denote the gradients of the column moments and spliced bar stresses corresponding to a = 1200 and 2400 mm (a/h = 3.0 and 6.0), respectively. The bond demand over the entire lap splice length can be defined as the sum of the tensile stress f_{sO} of the bottom offset-bars at the base level and the tensile stress f_{sS} of the straight column bars at the top end of the lap splice region. As shown in Figure 3-34, the moment gradient becomes less as the shear span length increases from 1200 mm to 2400 mm. Thus, although the moment demand at the base level is the same as M_u, the moment M_s at the top end of the lap splice region is less in a = 1200 mm than in a = 2400 mm. A greater M_s results in a greater f_{sS} of the top straight column bars. Thus, the bond demand over the lap splice length (= $f_{sO} + f_{sS}$) was smaller in **SL30S1B** and **SL40S1B** (a/h = 3.0) than in **SL30S2B** and **SL40S2B** (a/h = 6.0). For this reason, the column flexural strength was fully developed at the lap splice region in **SL30S1B** and **SL40S1B** with a = 1200 mm though the provided splice lengths l_s were less than the required $l_{s,ACI}$.

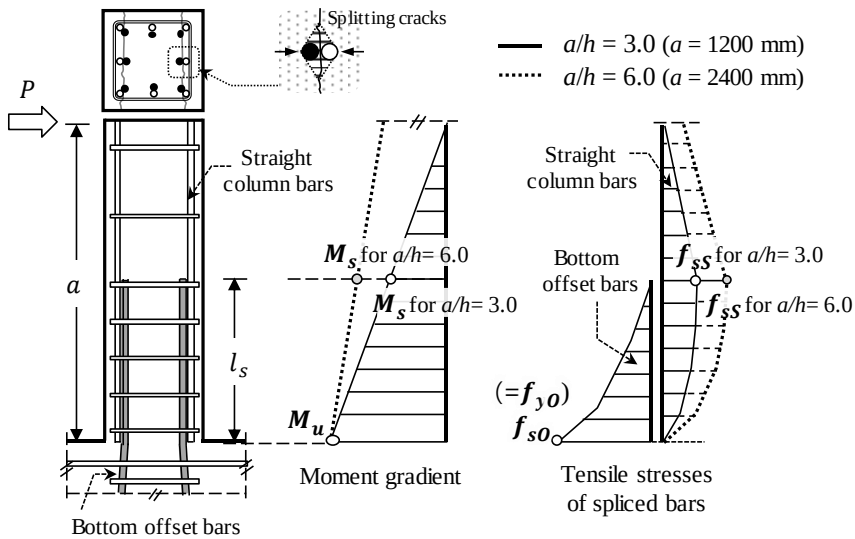

Figure 3-34 Moment gradient and spliced bar stresses

3.4.2 Shear force and transverse reinforcement

Shear force also affected the column performance such as failure mode and deformation capacity. The maximum shear force V_u acting on **SL40S1B** was about twice greater than that of **SL40S2B** because the shear span length of **SL40S1B** was only a half. Thus, in **SL40S1B**, due to the increased shear force, excessive shear cracks occurred in the web (refer to Figure 3-23(c)). Particularly, in **SL00S1B**, **SL30S1B**, and **SL40S1B**, with a = 1200 mm, the maximum shear forces V_u during the tests were 13% ~ 30% greater than the shear resistance V_s (= $A_v f_{yt} d/s$) carried by the transverse bars of a spacing of $s = 0.5d$ (i.e. V_s / V_u= 0.77 ~ 0.88). As the shear resistance of the concrete was decreased significantly after the spalling of the concrete cover occurred around δ = 2.0% ~ 2.5%, the transverse bars alone were not sufficient to prevent the excessive web shear cracks at large inelastic deformations. Consequently, the deformation capacities of **SL00S1B**, **SL30S1B**, and **SL40S1B** were limited to δ = 3.5 ~ 5.0%.

In contrast, in **SL30S2B**, **SL40S2B**, **SL50S2B**, and **SL40S2B-1**, with a = 2400 mm, the V_s / V_u ratios were decreased to 1.59 ~ 2.17 and the transverse bars of a spacing of $s = 0.5d$ were sufficient to prevent web shear cracking. Thus, as shown in the failure modes of Figure 3-23(d) ~ (g), the web shear cracking was not

significant and consequently the deformation capacities were equivalent to or greater than $\delta = 7.0\%$, even in **SL30S2B** and **SL40S2B** where the provided lap splice lengths ($l_s = 30d_b$ and $40d_b$) were less than $l_{s,ACI}$. It is noted that, in **SL50S2B-1** where the tie spacing was increased to $s = d$ and thus the V_s / V_u ratio (= 0.96) were smaller than 1.0, web shear cracks occurred and vertical bond splitting cracks propagated along the spliced bars. Consequently, the deformation capacity was decreased to $\delta = +3.5\%$ and -5.0%.

The test results of **SL50S2B** and **SL50S2B-1** shown in Figure 3-22 and Figure 3-23 show the effects of the transverse bar spacing on the performance of the lap splice. In both specimens, since the lap splice length l_s of $50d_b$ was used, the maximum loads M_u were equivalent to or greater than the nominal strengths M_n. However, in **SL50S2B-1** with the large transverse bar spacing $s = d$, vertical bond splitting cracks propagated along the spliced bars after the maximum loads occurred (refer to Figure 3-23(h)). It seemed that in **SL50S2B-1**, bond splitting cracks initiating at the bottom propagated rapidly along the lap splice length during repeated load cycles, and consequently limited the deformation capacity of the columns. Thus, closely-spaced ties should be used to increase the column ductility. As illustrated in Figure 3-34, the confining transverse bars are to develop a clamping force across the splitting crack.

3.4.3 Lap splice detail

Figure 3-35(a) and (b) show final failure modes and the spliced bar location of bottom and top offset bar splice columns, **SL50S2B** and **SL50S2T**, respectively. The crack patterns of each column were significantly different from the location of bottom splice bars. In the columns with bottom offset bar splice, in which the bottom splice bars were located inside the concrete core, the flexural cracks along the column height and concrete cover spalling in the plastic hinge zone were occurred without significant strength degradation until $\delta = 7.0\%$. On the other hand, in the columns with top offset bar splice, in which the bottom splice bars were located beside the concrete cover, the brittle failure mode with the vertical splitting cracks along lap splice length were observed at $\delta = 5.0\%$ after concrete cover spalling in plastic hinge zone. Similar failure mode was observed in the columns with splice without offset bend.

Such failure mode and large deformation capacity in the columns with bottom offset bar splice are related to concrete bond demand along lap splice zone. As shown in Figure 3-35(c), concrete bond demand along spliced bars is caused by stress variations in top and bottom splice bars. Thus, larger concrete bond demands regardless of lap splice type are required in bottom splice bars where higher stresses are applied (Figure 3-24 and Figure 3-29).

In Figure 3-36, the bond force transfer region between spice bars and surrounded concrete is compared according to lap splice details. As the bottom splice bars are located inside concrete core in the column with bottom offset bar splice, larger effective concrete area for bond transfer after concrete cover spalling off can be attained. Therefore, the column with bottom offset bar splice, in which the bottom splice bars located in the un-cracked concrete section, are preferred to limit concrete bond cracking along lap splice length and improve the deformation capacity of columns. As shown in Figure 3-25(b) ~ (c), **SL40S2B** and **SL50S2B** with bottom offset bar splice retained constant flexural moment strength in large inelastic deformation δ = 7.0% without bond failure along the lap splice region.

In the columns with the top offset bar splice and the splice without offset bend, as the bottom splice bars were located beside the cracked concrete cover, bond failure with severe vertical splitting cracks was occurred at δ = 2.5 ~ 5.0%. When larger lap splice length is used, deformation capacity can be increased. However, it is hard to avoid vertical splitting cracks along lap splice length because initial splitting cracks developed after concrete cover spalling at the plastic hinge zone have resulted in bond failure of spliced columns with increasing bond demand of upper lap splice region, consequently. For this reason, **SL50S2T** and **SL50S2S** with lap splice length of $50d_b$ were failed with severe splitting cracks along the lap splice region at δ = 5.0% (see Figure 3-26(f) and (h)).

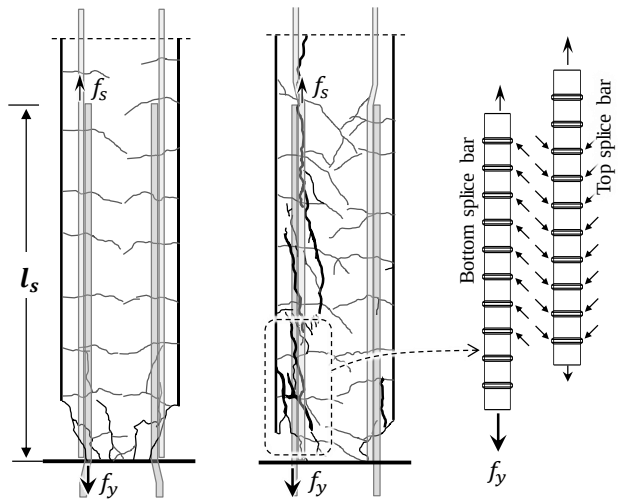

Figure 3-35 Failure mode and stress transfer between spliced bars via surrounding concrete

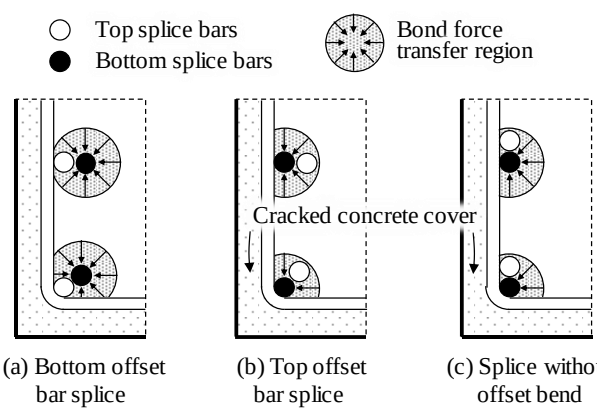

Figure 3-36 Effective concrete area for bond transfer after concrete cover spalling

3.4.4 Lap splice length

The moment gradients and the tensile stress gradients of the spliced bars along the lap splice region are shown in Figure 3-37. Dot lines with grey circles and solid lines with white circles indicate the gradients of spliced bar stresses corresponding to $l_s = 40d_b$ and $50d_b$, respectively. The bond demand over the lap splice region can be defined as the average value of the tensile stress f_y of bottom splice bars extended from the base and the tensile stress f_s of top splice bars at the end of lap splices. Thus, when compared to a column specimen and a beam specimen with lap splices, the smaller bond demand ($\approx [f_y+f_s]/2 < f_y$) along splice length is applied in the column specimen due to moment gradient. In the case of **SL40S2B**, **SL40S2T**, and **SL40S2S** with $l_s = 40d_b$ (1000 mm) and shear span of 2400 mm, the bond demand of the column specimen, where $(f_y + f_s)/2 \approx (1+(a - l_s)/a)\, f_y/2 = 0.79f_y$, is 79% smaller than that of the beam specimen ($= f_y$) due to moment gradient. Such decreased bond demand along lap splice in the column specimen corresponds with lap splice length. For example, **SL40S2B** and **SL40S2T** with $l_s/l_{s,ACI} = 0.76$ and 0.74 could not reach yield strain in the bottom splice bars at the base; on the other hand, **SL40S2S** with $l_s/l_{s,ACI} = 0.87$ exceeded the yield strain, showing successful lap splice performance. These results indicate that the current lap splice length equation in ACI 318 ($l_{s,ACI}$) can be conservative to the column lap splice due to moment gradient.

As shown in Figure 3-37, according to lap splice length, the spliced columns have same moment gradient but different tensile stress distribution along column height. Since the total tensile stresses of top and bottom splice bars corresponding to moment diagram are same regardless of lap splice length, the tensile stress (f_s^4) at the top of lap splice zone in the column with $l_s = 40d_b$ is greater than that in the column with $l_s = 50d_b$ (f_s^5). Thus, higher bond demand $(f_y + f_s)/2$ is required in columns with short lap splice length with $l_s = 40d_b$.

Furthermore, according to the study of Chung and Shah (1989), since lap splice length can be affected by the loading rate, further study on the effect of loading rate is needed.

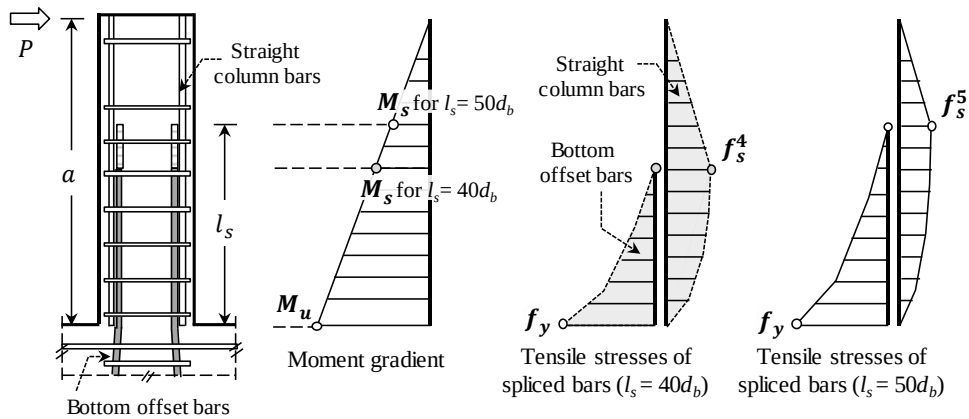

Figure 3-37 Variation of tensile stresses of spliced bars depending on lap splice length

3.5 Lap Splice Length Model Considering Moment Gradient

As discussed in the previous section, because bond demand of spliced bars decreases in columns where a moment gradient exists, the lap splice length can be reduced. The bond demand over the lap splice length is the sum of the tensile stress of the offset-bars extended from the bottom (f_{sO}) and straight column bars from the top (f_{sS}). The strength f_{sO} can be taken as the yield strength f_{yO} of the offset-bars at the bottom. On the other hand, f_{sS} of the straight column bars which is less than the yield strength f_{yS} can be approximated as follows (refer to Figure 3-34).

$$f_{sS} = \left(1 - \frac{M_s}{M_n}\right) f_{yO} = \left(1 - \frac{l_s}{a}\right) f_{yO} \le f_{yS} \tag{3-1}$$

where M_n = nominal moment strength at the bottom of the column, M_s = moment demand at the top of the lap splice (= $M_n \cdot (l_s/a)$), a = shear span length of the column, and l_s = length of the lap splice. It is noted that, in Equation (3-1), f_{sS} of the straight column bars does not depend on f_{yS}, but on f_{yO} of the bottom offset-bars.

By replacing f_y in ACI 318-14's Class B lap splice length equation with the average bond demand $(f_{yO} + f_{sS})/2 = f_{yO}(1 - l_s/[2a])$, the modified lap splice length l_s in columns can be obtained as follows.

$$l_s = 1.3\left(1 - \frac{l_s}{2a}\right) l_{dO} \tag{3-2}$$

$$l_s = \left(\frac{2}{1.54 + l_{dO}/a}\right) l_{dO} \tag{3-3}$$

where l_{dO} = development length of the bottom offset-bars specified in ACI 318-14. In Equation (3-3), the modified l_s varies between $0.87 l_{dO}$ to $1.3 l_{dO}$ depending on the moment gradient. The shear span length a can vary depending on the moment distribution shape along the column height. Thus, it is recommended that the shear span a of columns equals to half of the column height ($0.5H_o$) under the strong-column and weak-beam behavior and conservatively the column height ($1.0H_o$) under the weak-column and strong-beam behavior.

For verification, the modified splice length was compared to the test results of the present and existing studies. Figure 3-38 shows the lap splice and offset details used in the existing column specimens considered for the verification. The test results of the present and existing studies are summarized in Table 3-6 and Table 3-7, respectively. Twenty-six columns were collected from ten studies. The test parameters varied in ranges of 19.7 MPa $\leq f_c' \leq$ 41.4 MPa, 315 MPa $\leq f_y \leq$ 617 MPa, 12.5 mm $\leq d_b \leq$ 31.8 mm, 105 mm ($0.21H_{min}$) $\leq s \leq$ 457.2 mm ($1.0\ H_{min}$), and 280 mm ($20d_b$) $\leq l_s \leq$ 880 mm ($40d_b$).

Figure 3-39 shows the relationships between the maximum load-to-nominal strength ratio (M_u/M_n) and the provided-to-predicted lap splice length ratio (l_s/l_{sm}), where l_{sm} is the modified lap splice length calculated by Equation (3-3). In general, the M_u/M_n ratios show a growth trend as the l_s/l_{sm} ratios increased. In all columns with l_s/l_{sm} ratios not less than 1.0, except **SL40S2B-1** with different bar diameters between the spliced bars, the M_u/M_n ratios were equal to or greater than 1.0. This indicates that Equation (3-3) can give reasonable lap splice lengths required for the development of nominal strength in columns with moment gradient.

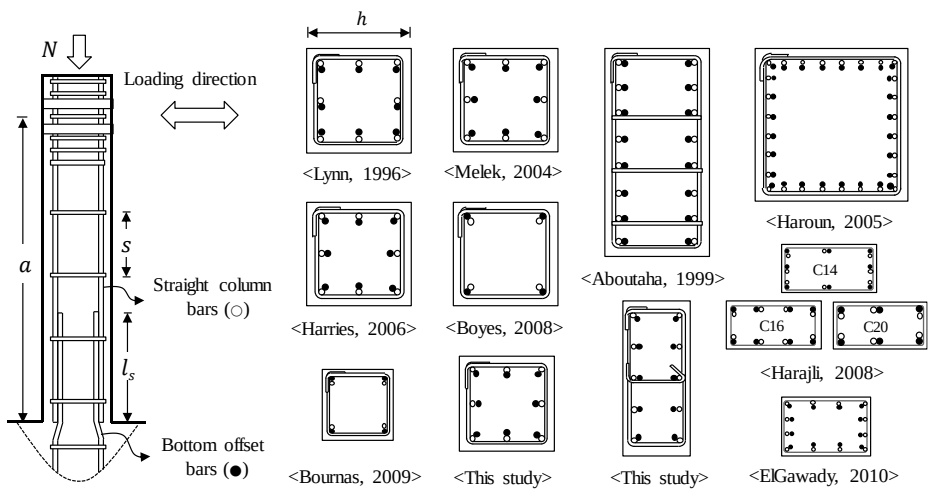

Figure 3-38 Lap splice and offset details of existing column specimens

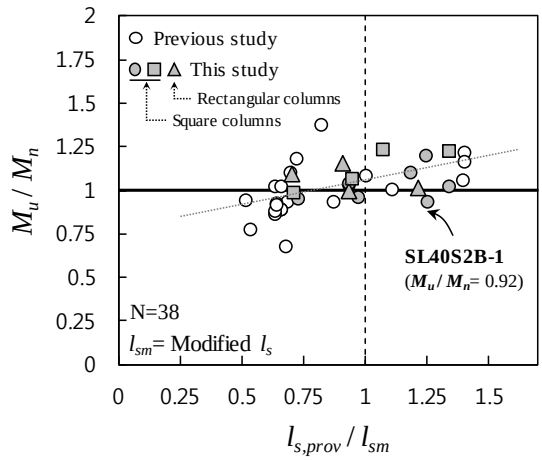

Figure 3-39 Moment strength ratio and lap splice length ratio relationship

Table 3-6 Summary of test results of columns with lap splices

Specimen	f_c' (MPa)	Lap splice length						M_u [3] (kN·m)	M_n (kN·m)	M_u/M_n	Failure mode [4]
		l_s	l_s/d_b	$l_{s,ACI}$ [1]	$l_s/l_{s,ACI}$	l_{sm} [2]	l_s/l_{sm}				
SL00S1B	32	-	-	-	-	-	-	404	374	1.08	Flexure Shear
SL30S1B	32	750	30	1200	0.63	799	0.94	352	340	1.04	Flexure Shear
SL40S1B	32	1000	40	1200	0.83	799	1.25	405	340	1.19	Flexure Shear
SL30S2B	25	750	30	1308	0.57	1027	0.73	278	094	0.94	Bond Splitting
SL40S2B	25	1000	40	1308	0.76	1027	0.97	281	294	0.95	Flexure Yielding
SL50S2B	37	1250	50	1153	1.08	1050	1.19	371	367	1.01	Flexure Yielding
SL40S2B-1	37	1160	40	1146	1.01	929	1.35	363	393	0.92	Flexure Yielding
SL50S2B-1	27	1250	50	1345	0.93	925	1.25	342	312	1.10	Bond Splitting
SL30S2T	27	750	30	1345	0.56	1050	0.71	351	358	0.98	Bond Splitting
SL40S2T	27	1000	40	1345	0.74	1050	0.95	376	358	1.05	Bond Splitting
SL50S2T	37	1250	50	1153	1.08	929	1.35	436	398	1.09	Bond Splitting
SL40S2S	37	1000	40	1153	0.87	929	1.08	436	398	1.10	Bond Splitting
SL50S2S	37	1250	50	1153	1.08	929	1.35	434	398	1.09	Bond Splitting

Specimen	f_c' (MPa)	Lap splice length						M_u [3] (kN·m)	M_n (kN·m)	M_u/M_n	Failure mode [4]
		l_s	l_s/d_b	$l_{s,ACI}$ [1]	$l_s/l_{s,ACI}$	l_{sm} [2]	l_s/l_{sm}				
RL00S1B	32	-	-	-	-	-	-	275	262	1.05	Flexure Shear
RL30S1B	32	750	30	1040	0.63	725	0.91	241	208	1.16	Flexure Yielding
RL40S1B	32	1000	40	1040	0.85	725	1.21	205	202	1.01	Flexure Yielding
RL30S2B	25	750	30	1174	0.56	943	0.70	199	182	1.09	Flexure Yielding
RL40S2B	25	1000	40	1174	0.75	943	0.93	162	163	0.99	Flexure Yielding

1) Length of Class B lap splice specified in ACI 318-14
2) Modified lap splice length in Equation (3-3)
3) Average of positive and negative maximum loads
4) Flexure Shear and Bond Splitting, respectively, denote web shear failure after flexural yielding, bond splitting failure along lap splice length. Flexure Yielding indicates that flexural yielding occurred but the tests were ended without failure due to lack of the actuator stroke.

Table 3-7 Summary of existing tests of columns with lap splices

Specimen		Specimen properties							Lap splice length			Moment strength		
		h	f_c'	f_y	$N/A_g f_c'$	a	s/h	d_b	l_s	l_{sm}	l_s/l_{sm}	M_u	M_n	M_u/M_n
Lynn (1996)	3SLH18	457	25.6	331	0.09	2946	1.0	31.8	635	1141	0.56	415	449	0.92
	2SLH18		33.1	331	0.07	2946	1.0	25.4	508	772	0.66	454	333	1.36
	3SMD12		25.5	331	0.28	2946	0.67	31.8	635	1091	0.58	590	505	1.17
Aboutaha (1999)	FC4	457	19.7	414	0	2743	0.89	25.4	610	1141	0.53	488	553	0.88
	FC5		19.7	414	0	2743	0.89	25.4	610	1141	0.53	488	553	0.88
Melek (2004)	2S10M	457	36	510	0.1	1829	0.67	25.4	508	966	0.53	371	432	0.86
	2S20M		36	510	0.2	1829	0.67	25.4	508	966	0.53	427	492	0.87
	2S30M		36	510	0.3	1829	0.67	25.4	508	966	0.53	522	514	1.02
	2S20H		35	510	0.2	1676	0.67	25.4	508	953	0.53	452	492	0.92
	2S20HN		35	510	0.2	1676	0.67	25.4	508	953	0.53	448	492	0.91
	2S30X		35	510	0.3	1524	0.67	25.4	508	926	0.55	519	514	1.01
Haroun (2005)	RF-A1	610	41.4	443	0.054	3429	0.21	19.0	381	895	0.43	0.832	1089	0.76
Harries (2006)	L0	458	27.6	414	0.26	2440	0.78	22.2	490	873	0.56	426	389	1.09

Specimen		Specimen properties							Lap splice length			Moment strength		
		h	f_c'	f_y	$N/A_g f_c'$	a	s/h	d_b	l_s	l_{sm}	l_s/l_{sm}	M_u	M_n	M_u/M_n
Harajili (2008)	C14	400	39	550	0	1400	0.5	1.0	420	591	0.71	111	119	0.93
	C16		40	528	0	1400	0.5	16.0	480	629	0.76	135	132	1.02
	C20		32	617	0	1400	0.5	20.0	600	1040	0.58	122	183	0.67
Boyes (2008)	24L-300-2D	450	33.6	315	0.3	1624	0.67	25.4	600	667	0.90	406	406	1.00
	30L-300-2D		33.9	315	0.3	1624	0.67	25.4	750	664	1.13	426	406	1.05
Bournas (2009)	L20d_C	250	27.8	523	0.28	1600	0.8	14.0	280	668	0.42	62	67	0.93
	L40d_C		25.8	523	0.28	1600	0.8	14.0	560	688	0.81	72	67	1.08
ElGawady (2010)	AB-1	381	31	331	0.07	1803	0.33	12.5	445	401	1.11	135	112	1.21
	AB-2		31	331	0.07	1803	0.33	12.5	445	401	1.11	130	112	1.16
Unit		mm	MPa	MPa	-	mm	-	mm	mm	mm	-	kN·m	kN·m	-

3.6 Recommendations for Seismic Design of Columns with Lap Splice

Based on the present and previous test results, the following considerations for the design and evaluation of the splice length are recommended for ordinary and intermediate moment frames.

1) When the lap splice length satisfies the requirements of ACI 318-14, a lap splice of longitudinal bars can be used in the plastic hinge zone of columns, provided sufficient transverse reinforcement is used along lap splice regions.

2) In the columns with offset longitudinal rebars for lap splice, because the flexural strength can be decreased owing to the location of the bottom offset rebars, the nominal flexural strength should be calculated considering the locations of the offset rebars in the cross-section.

3) For moment frames with limited ductility, top offset splice details or splice without offset bend can be available for lap splice of column longitudinal bars. In a large inelastic deformation, bond failure with severe splitting cracks may occur along lap splice region, so attention should be paid in a design stage.

4) To avoid premature bond failure, lap-spliced rebars should be confined by closely spaced transverse reinforcement. In this study, $s = 0.5d$ (or 165 mm) is recommended for Grade 500 MPa D25 longitudinal re-bars (Bar diameter = 25.4 mm); Otherwise, the deformation capacity and energy dissipation are significantly decreased, even with the splice length specified in ACI 318-14.

5) When the shear span is short ($a/h = 3.0$), a short splice length ($l_s = 30d_b \sim 40d_b$) is acceptable, unless a very large deformation capacity is required. In this study, considering moment gradient, a reduced lap-splice length was proposed as a function of the shear span length.

3.7 Discussion

Cyclic loading tests of columns with lap splices were performed. Based on the test results, the effects of lap splice length and details, moment gradient, and transverse reinforcement on the failure mode and deformation capacity were investigated. Further, a modified lap splice length for columns with moment gradient was proposed. The major findings of this study are summarized as follows.

1) In the specimens with lap splice length (l_s = 30d_b or 40d_b) less than the requirement of ACI 318-14, when the shear span ratio was a/h = 3.0 (**SL30S1B** and **SL40S1B**), the test strength reached the nominal flexural strength, despite the short splice length. On the other hand, when the shear span ratio was a/h = 6.0 (**SL30S2B** and **SL40S2B**), the test strength was less than the nominal strength (M_u = 0.95M_n); however, ductile behavior was maintained until large inelastic deformation.

2) In the specimen **SL50S2B** (l_s = 50d_b), with the lap splice length satisfying the requirement of ACI 318, despite the lap splice being located in the plastic hinge zone, the test strength reached the nominal flexural strength and the ductile behavior occurred. However, in the specimen **SL50S2B-1**, with a greater spacing of ties (s = 1.0d), the deformation capacity was decreased.

3) Top offset bar splice showed similar seismic behavior to splice without offset bend. In the specimens **SL30S2T** and **SL40S2T** (l_s = 30d_b and 40d_b), the nominal strength was attained despite the short lap splice length, but a brittle failure occurred with severe splitting cracks at drift ratio of 2.5 ~ 3.5%. On the other hand, the specimen **SL50S2T** with the lap splice length satisfied in ACI 318 attained the nominal flexural strength and ductile behavior until a drift ratio of 5.0%.

4) Cyclic behavior of spliced columns is mainly affected by the location of bottom splice bars as well as lap splice length. Bottom offset bar splice resulted in lower strength but greater ductility and energy dissipation. On the other hand, top offset bar splice and splice without offset bend gave rise to greater strength but lower ductility and energy dissipation.

5) For columns with moment gradient, a reduced lap splice length was proposed as a function of the shear span length a. The reduced splice length

correlated well with the present and existing test results of columns with lap splice.

6) When lap splice is used in the plastic hinge zone, it is recommended that the spliced bars extended from the bottom be offset inside and the moment strength at the lap splice be calculated using the actual location of the bottom splice bars. In addition, to ensure a ductile behavior without splitting failure at the lap splice, the shear strength of the transverse reinforcement alone needs to be not less than the shear demand ($V_s > V_u$) and the spacing of the transverse bars confining the spliced bars should be not greater than *d/2*.

Chapter 4. Effects of Reinforcement Details on Joints

4.1 Introduction

4.1.1 General problems in joint reinforcement details

One or two story low-rise buildings generally show weak-column and strong-beam behaviors under seismic loads because smaller columns are architecturally preferred and only gravity load is considered in a structural design. In low-rise buildings, joint shear reinforcements were seldom used in beam-column joints due to difficult rebar placement. In such conditions, the joints could be vulnerable under earthquake loading, thereby decreasing structural safety. The lack of joint shear reinforcement is attributed to absence of proper design codes for low-rise buildings and difficulty in placing rebars in the joints.

In order to clarify the definitions of joint and connection, a beam-column **joint** is defined as the column within the depth of the beam that frames into the column, and a beam-column **connection** is composed of the joint, columns, beams, and slabs.

As columns in low-rise buildings are subjected to small axial compression force, column width (h_c) is relatively smaller than beam depth (h_b) as shown in Figure 4-1. Further, in the case of parking garages where long and narrow columns are used to secure a parking space, the column width (h_c) framing into the joint can be smaller. Such smaller column decreases a size of beam-column joint. The smaller column and joint have several detrimental effects on structural system and performance as follows.

1) A weak column-strong beam behavior can be attained more likely by load reversals during earthquake loading. Under such behavior, inelastic deformation capacity of a whole structure may be reduced, thereby forming plastic hinge in columns that leads complete collapse of the structure with softy story mechanism.

2) Owing to low shear strength of smaller beam-column joint, the joint failure can occur before plastic hinges form in adjacent framing members. Concrete shear cracks and damages in the joint result in brittle failure of the whole structure with decreasing axial load-carrying capacity of columns.

3) In an exterior beam-column connection, beam longitudinal reinforcing bars terminate in 90º standard hooks within the joint. With smaller joint size, it is difficult to secure necessary development length of the beam bars into the joint.

When the depth of beam-column joints is small, the reinforcement details in beam-column connections may need special attention. Further, in the regions of high seismicity, beam-column joints should be designed with sufficient joint shear reinforcement to transmit shear and moment among beams and columns. However, since a number of old buildings were constructed before adoption of seismic design and beam-column joints in modern buildings have not been designed to resist seismic loading, beam-column joints do not have joint shear reinforcement or have it in lesser quantities. Thus, in this study, the effect of joint shear reinforcement was evaluated by performing beam-column connection tests with relatively small joint size.

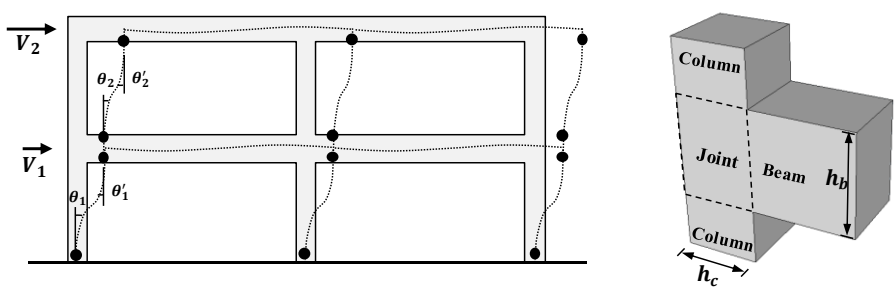

(a) A two story moment frame (b) Beam-column connection

Figure 4-1 Beam-column connection in a two story moment frame

4.1.2 RC Beam-Column joint failures in past earthquakes

In past earthquakes, exterior beam-column joint damages occurred due to insufficient shear reinforcement ratio in the joints. Figure 4-2 ~ Figure 4-6 show damage cases of the past earthquakes such as Caracas earthquake, Venezuela, 1967 (M= 7.5); San Fernando earthquake, California, 1971 (M= 6.6); El Asnam earthquake, Algeria, 1980 (M= 7.7); Izmit earthquake, Turkey, 1999 (M= 7.4); and Chi-Chi earthquake, Taiwan, 1999 (M= 7.6); Bhuj earthquake, India, 2001 (M= 7.7); Yogyakarta earthquake, Indonesia, 2006 (M= 6.3). The photos of the damaged RC exterior joints have been collected from the library of NISEE in the UC Berkeley (https://nisee.berkeley.edu/elibrary/).

In the buildings built before the seismic design codes were provided, the beam-column joints do not have joint shear reinforcement. Thus, the severe damage can be occurred at the joint where the forces from beam and column are transmitted under seismic loading. As such joint damage and failure resulted in the whole building to collapse as shown in Figure 4-5, the exterior connections should be reinforced with adequate joint shear reinforcing bars.

In the past, shear reinforcement was hardly placed in beam-column connections because of the reinforcing bar congestion with the column longitudinal bars as well as the hook anchorage of the beam bars into the exterior joints. Figure 4-2 and Figure 4-4 shows the failure mode of the unreinforced exterior joints. The severe cracks and damages were concentrated only on joints as compared to beams and columns adjacent to the joints.

In this chapter, seismic performance of unreinforced exterior and interior connections, and improved seismic performance through joint reinforcement were evaluated. Furthermore, we discussed the performance of U-shaped bar which can be easily applied to the exterior joint where reinforcing bar congestion may occur.

Figure 4-2 Damage to RC exterior beam-column joints in the Caracas, Venezuela earthquake, 1967 (Courtesy of NISEE, University of California, Berkeley)

Figure 4-3 Damage to RC exterior beam-column joints in the California and Algeria earthquakes (Courtesy of NISEE, University of California, Berkeley)

Figure 4-4 Severe damages of RC exterior beam-column joints by the Izmit, Turkey earthquake. 1999 (Courtesy of NISEE, University of California, Berkeley)

Figure 4-5 Severe damages of RC exterior beam-column joints by the chi-chi, Taiwan earthquake. 1999 (Courtesy of NISEE, University of California, Berkeley)

Figure 4-6 Damage to RC exterior beam-column joints in the India and Indonesia earthquakes (Courtesy of NISEE, University of California, Berkeley)

4.1.3 Comparison of current design codes for beam-column joint

Integrity of beam-column joints is essential for force (moment and shear) transfer from beams to columns in moment frames during earthquakes. Current design code requirements are specified based on capacity design concept to prevent brittle failure of the joints. Joint design requirements are summarized by each design code, ACI 318 / ACI 352 (USA), EC8 (Europe), NZS (New Zealand), and AIJ (Japan). ACI 352 is an ACI committee report on beam-column connections in which more reinforcing bar details are described compared to ACI 318.

4.1.3.1 Capacity design approach

The capacity design concept was developed in New Zealand in 1976 to reduce uncertainty of the seismic load characteristics, and the selection of the analytical model of the structure in the structural design. Such uncertainty is considerably reduced through capacity design. As special requirements for seismic load and displacements are applied only to identified members where they are needed, the capacity design approach results in more economical design. Further, the seismic performance may vary depending on the details selected by the structural designer.

The procedure of the capacity design is as follows.

1) Assign where plastic hinges occur in members.
2) Determine the reinforcement details so that sufficient strength can be exerted in the plastic hinge region through the structural analysis.
3) Design should be made so that sufficient strength is exhibited for other possible failure modes throughout the post-elastic deformations.

In NZS (New Zealand Standards, 2004), the desirable mechanism for moment frames is a beam sidesway mechanism with strong-column and weak beam behavior (See Figure 4-7(a)). A column sidesway mechanism with weak-column and strong beam behavior is not permitted except for one or two story frames (See Figure 4-7(b)). The column sidesway mechanism in high-rise buildings can require very large demands on ductility at plastic hinge region of columns, resulting in the collapse of the buildings during earthquakes.

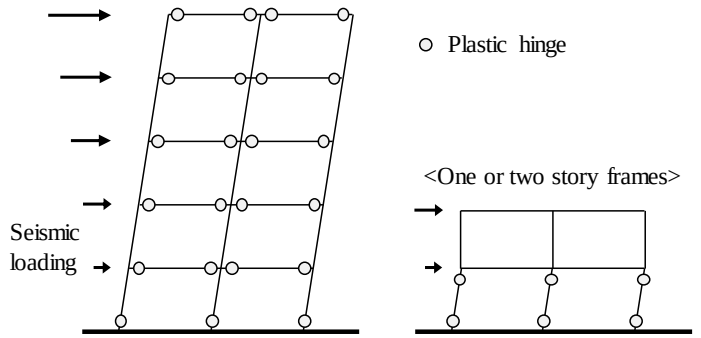

(a) Beam sidesway mechanism (b) Column sidesway mechanism

Figure 4-7 Desirable sidesway mechanism of moment frames under large inelastic deformations during seismic loading according to New Zealand standard

Capacity design concepts are used to design RC joints in moment frames to encourage formation of plastic hinges in the beams rather than the columns and development of large inelastic rotations at the ends of beams. For strong-column and weak-beam behavior, each design code specifies flexural capacities of beams and columns as follows.

$$\sum M_{nc} \geq 1.2 \sum M_{nb} \quad \text{in ACI 352} \tag{4-1}$$

$$\sum M_{Rc} \geq 1.3 \sum M_{Rb} \quad \text{in EC8} \tag{4-2}$$

$$M_c = \omega \varphi_o M_E \quad \text{in NZS 3101} \tag{4-3}$$

where, ΣM_{nc} and ΣM_{Rc} are the sum of nominal flexural strength of the columns at the joint faces, and ΣM_{nb} and ΣM_{Rb} are the sum of nominal flexural overstrength values of the beams. According to NZS at the ultimate limit states, the joint should be able to support the strengths of the members without loss of strength under seismic loadings. The terms ω and φ_o are the dynamic magnification and overstrength factors, respectively.

4.1.3.2 Joint shear strength

In **ACI 352**, the joint shear strength V_{jn} is taken as

$$V_{jn} = 0.083\gamma\sqrt{f_c'}A_j \qquad \text{in ACI 352} \qquad (4\text{-}4)$$

where, A_j is the effective cross-sectional area of the joint (effective joint width times the column depth). Effective joint dimensions are summarized in section 4.1.3.3. γ is a factor that depends on the connection classification as shown in Figure 4-8. A beam framing into a joint is considered to provide confinement to the joint at least three-quarters of the width of the column. According to the ACI 352 classification of beam-column connection type, a 'Type 1' connection can resist loading without significant inelastic deformation; on the other hand, a 'Type 2' connection can sustain deformation reversals into the inelastic range. Type 2 connection is required for special moment frames used in high seismic zones.

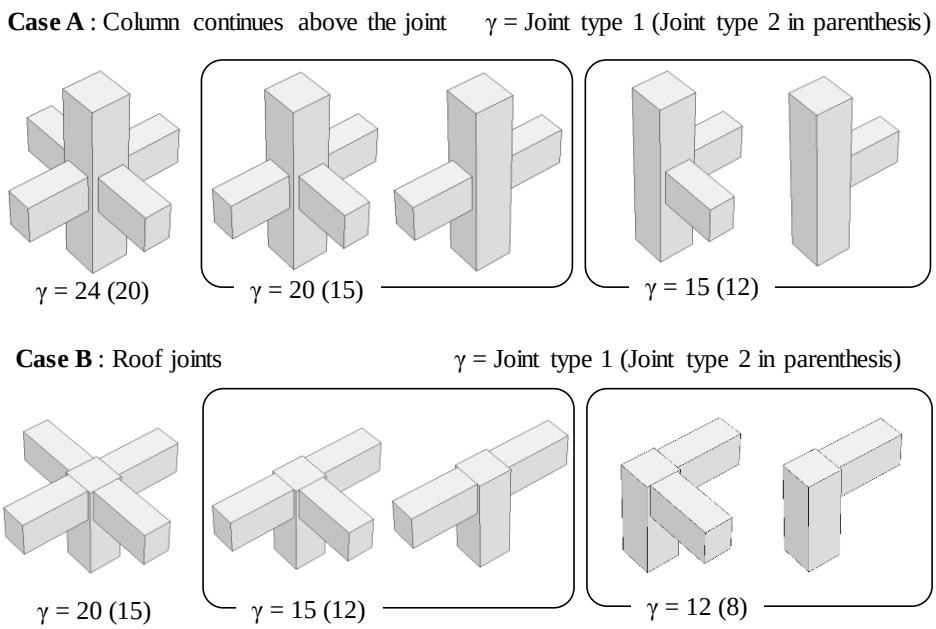

Figure 4-8 γ-values for Type 1 and Type 2 connections (ACI 352)

In **EC8**, the diagonal compression induced in the joint by the diagonal strut mechanism shall not exceed the compressive strength of concrete in the presence of transverse tensile strains.

For interior beam-column joints

$$V_{jhd} \le \eta f_{cd} \sqrt{1-\frac{v_d}{\eta}} A_j \qquad \text{in EC8} \tag{4-5}$$

For exterior beam-column joints

$$V_{jhd} \le 0.8\eta f_{cd} \sqrt{1-\frac{v_d}{\eta}} A_j \qquad \text{in EC8} \tag{4-6}$$

where, η accounts for the strength reductions of the diagonal compression strut in the joint due to diagonal tension cracking (= 0.6[1−f_c'/250]). A_j is the effective joint area, v_d is the normalized axial force in the column above the joint, and f_{cd} is the design concrete strength in MPa.

In **NZS 3101**, to prevent premature diagonal crushing of the concrete in the joint region, the horizontal design shear force across a joint V_{jh} shall not exceed the smaller of $0.20f_c'A_j$ or $10A_j$.

$$V_{jh} \le \min(0.2 f_c' A_j, 10A_j) \qquad \text{in NZS} \tag{4-7}$$

In **AIJ 2010**, the joint shear strength V_{ju} is estimated from

$$V_{ju} = \kappa \cdot \phi \cdot F_j \cdot A_j \qquad \text{in AIJ} \tag{4-8}$$

where, κ is shape coefficient depending on the joint type (κ = 1.0 for interior joints, κ = 0.7 for intermediate exterior or roof joints, κ = 0.4 for knee joints), ϕ is reduction coefficient depending on the degree of confinement (ϕ = 1.0 for joints having transverse beams on both sides, ϕ = 0.85 for all other cases), and F_j is nominal joint shear strength which is calculated from $F_j = 0.8\sigma_B^{0.7}$ (σ_B : the cylinder compressive strength of concrete).

4.1.3.3 Effective joint dimensions

The effective joint area A_j is expressed by multiplying the effective joint depth h_j by the effective joint width b_j. In all cases, the effective depth of the joint area h_j is taken equal to the effective depth of the column h_c. The effective joint width b_j is different from each design code. Table 4-1 and Figure 4-9 present definition of effective joint width and dimensions related to effective joint area.

Table 4-1 Definition of effective joint width according to desgin codes

Geometry	ACI 318	ACI 352	EC8, NZS 3101	AIJ 2010
$b_c > b_b$ [1)]	$\min(b_b+h_c, b_b+2x)$	$\min(b_b/2+b_c/2, b_b+\Sigma m h_c/2, b_c)$ [2)]	$\min(b_c, b_b+0.5h_c)$	$b_b + b_{a1} + b_{a2}$ [3)]
$b_c < b_b$	b_c		$\min(b_b, b_c+0.5h_c)$	

1) b_c and b_b are the column and beam width section, respectively.
2) m = 0.3 where the eccentricity between the beam centerline and the column centroid exceeds $b_c/8$, m = 0.5 for all other cases.
3) $b_{ai} = \min(b_i/2, h_c/4)$ where b_i is the distance from the side of the beam cross section to the side of the column parallel to the beam.

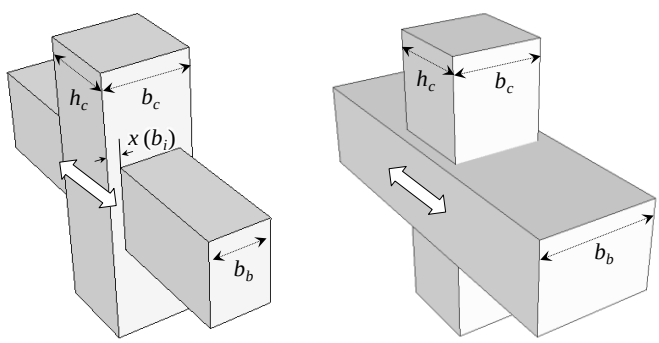

(a) $b_c > b_b$ (a) $b_c < b_b$

Figure 4-9 Dimensions related to effective joint area

4.1.3.4 Transverse reinforcement

In **ACI 352**, the joint reinforcement is intended for confinement of the diagonal compressive strut that forms an essential part of the force transfer mechanism of the joint. Thus, reinforcement details from the adjacent critical regions of the column are extended inside the joint. The total cross-sectional area of rectangular hoops or stirrups is as follows.

$$A_{sh} \geq 0.3 \frac{s b_c f_c^{'}}{f_{yt}} \left(\frac{A_g}{A_{ch}} - 1 \right) \qquad \text{in ACI 352} \qquad (4\text{-}9)$$

$$A_{sh} \geq 0.09 \frac{s b_c f_c^{'}}{f_{yt}} \qquad \text{in ACI 352} \qquad (4\text{-}10)$$

where, s is hoop spacing, b_c is core dimension of tied column, outside to outside edge of transverse reinforcement bars, and A_{ch} is area of column core measured from outside edge to outside edge of hoop. Further, required hoop spacing is 100 mm < s < min (h_c/4, 6$D_{b,min}$, 100+[350-h_x]/3), where $D_{b,min}$ is the diameter of column longitudinal bars to be restrained, and h_x is maximum center-to-center spacing of longitudinal bars laterally supported by corners of crossties or hoop legs around the perimeter of the column.

In **EC8**, it is required that adequate confinement (both horizontal and vertical) of the joint should be provided, in order to limit the maximum diagonal tensile stress of concrete to f_{ctd} (characteristic tensile strength). In the absence of a more precise model, this requirement may be satisfied by providing horizontal hoops such that:

$$\frac{A_{sh} f_{ywd}}{b_j h_{jw}} \geq \frac{\left(V_{jhd} / b_j h_{jc} \right)^2}{f_{ctd} + \nu_d f_{cd}} - f_{ctd} \qquad \text{in EC8} \qquad (4\text{-}11)$$

where, A_{sh} is the total area of the horizontal hoops, h_{jw} is the distance between the top and the bottom reinforcement of the beam, h_{jc} is the distance between extreme layers of column reinforcement, and ν_d is the normalized design axial force of the column ($\nu_d = N_{Ed} / A_c f_{cd}$).

As an alternative to the above clause, integrity of the joint after diagonal cracking may be ensured by horizontal hoop with the following total area.

$$A_{sh} f_{ywd} \geq \gamma_{Rd} (A_{s1} + A_{s2}) f_{yd} (1 - 0.8 v_d) \quad \text{in interior joints} \qquad (4\text{-}12)$$

$$A_{sh} f_{ywd} \geq \gamma_{Rd} A_{s2} f_{yd} (1 - 0.8 v_d) \quad \text{in exterior joints} \qquad (4\text{-}13)$$

where, γ_{Rd} is equal to 1.2. In exterior joints, it is required that they enclose the ends of beam bars bent towards the joint.

The distance between consecutive longitudinal bars engaged by hoops does not exceed 200 mm. At least one intermediate vertical column bar shall be provided at each side of a joint. It is also required that the vertical reinforcement of the column passing through the joint should be provided.

$$A_{sv,i} \geq (2/3) A_{sh} h_{jc} / h_{jw} \quad \text{in EC8} \qquad (4\text{-}14)$$

where, A_{sh} is the required total area of horizontal hoops and $A_{sv,i}$ denotes the total area of the intermediate bars placed in the relevant column faces between corner bars of the column.

In **NZS**, superposition of a concrete mechanism and a truss mechanism for horizontal and vertical joint shear transfer results in nominal shear forces being transferred across the joint core as follows.

$$V_{jh}^{*} \leq \phi V_{jh} = V_{ch} + A_{jh} f_{yh} \quad \text{in NZS} \qquad (4\text{-}15)$$

$$V_{jv}^{*} \leq \phi V_{jv} = V_{cv} + A_{jv} f_{yv} \quad \text{in NZS} \qquad (4\text{-}16)$$

where, V_{ch} and V_{cv} are the horizontal and vertical shear forces transferred across the joint core by the diagonal compression strut mechanism, respectively, and $A_{jh}f_{yh}$ and $A_{jv}f_{yv}$ are the horizontal and vertical shear forces transferred across the joint core by the truss mechanism, respectively.

In the joint zone of moment frames designed to be ductile or limited ductile, the V_{ch} and V_{cv} values are not explicitly defined; instead, the required amounts of horizontal and vertical reinforcements are specified as follows.

Horizontal joint shear reinforcement for interior joints

$$A_{jh} = \frac{6V_{jh}^{*}}{f_c' b_j h_c}\left(\frac{\alpha_i f_y A_s^{*}}{f_{yh}}\right) \geq 0.4\frac{V_{jh}^{*}}{f_{yh}} w \tag{4-17}$$

where, $0.85 \leq 6V_{jh}^{*}/(f_c' b_j h_c) \leq 1.20$ and $\alpha_i = (1.4\text{-}1.6C_j N_o^{*}/[f_c' A_g])\alpha_n$; α_n is 0.85 where the curvature ductility in the adjacent plastic region is equal or less than for a limited ductile region, and 1.0 where the curvature exceeds this limit. A_s^{*} is the greater of the area of top or bottom beam reinforcement passing through the joint; C_j is the ratio of the horizontal joint shear force in the direction being considered to the sum of the joint zones shear forces on the two axes.

Horizontal joint shear reinforcement for exterior joints

$$A_{jh} = \frac{6V_{jh}^{*}}{f_c' b_j h_c}\left(\frac{\beta f_y A_s}{f_{yh}}\right)\left(0.7 - \frac{C_j N_o^{*}}{f_c' A_g}\right) \geq 0.4\frac{V_{jh}^{*}}{f_{yh}} \tag{4-18}$$

where, $0.85 \leq 6V_{jh}^{*}/(f_c' b_j h_c) \leq 1.20$, β is the ratio of area of compression beam reinforcement to area of tension beam reinforcement but not taken greater than 1.0.

Vertical joint shear reinforcement

The vertical joint shear reinforcement shall consist of intermediate column bars placed between the corner bars, or vertical stirrups or other special bars adequately anchored to transmit the required tensile forces within the joint. There shall be at least one intermediate column bar in each side of the column in that plane. The required area of vertical joint shear reinforcement is as follows.

$$A_{jv} = a_v A_{jh}\frac{f_{yh} h_b}{f_{yv} h_c} \tag{4-19}$$

where, $a_v = 0.7 / (1+N_o^{*}/[f_c' A_g])$.

In **AIJ**, transverse reinforcement area ratio is specified regardless of the joint type from the relationship.

$$\rho_{jw} = \frac{\sum A_{jw}}{b_c j} \qquad \text{in AIJ} \qquad (4\text{-}20)$$

where, ΣA_{jw} is the total cross sectional area of transverse reinforcement, b_c is the column width, and j is the distance between beam top and bottom reinforcement layers.

In general, the maximum spacing of the joint shear reinforcement is the same as that of the transverse reinforcement of adjacent columns. The recommended spacing of horizontal and vertical transverse reinforcement is presented in Table 4-2.

Table 4-2 Recommended spacing of horizontal and vertical transverse reinforcement

Code	Spacing of horizontal transverse bars		Spacing of vertical bars
ACI 318	$s = \min(h_c/4, 6d_b, s_x)$ [1]		≤ 150
EC8	$s = \min(b_o/2, 175, 8d_{bL})$ [2]	$\min(b_o/3, 125, 6d_{bL})$	≤ 150
NZS	$s = \min(10d_b, 200)$		$s = \min(h_c/4, 200)$

1) $s_x = 100 + [(350 - h_x)/3]$ where h_x is maximum hoop spacing for shear resistance.
2) b_o is width of confined core in a column for DC M

4.1.3.5 Development length of bars in tension

Since longitudinal bars in a beam and a column penetrate a joint or are fixed to a joint, the development length of the bars in tension is significant factor for seismic performance of the joint. Figure 4-10 compares behavior of three beam-column joints with different values of h_c/d_b. As joints with smaller values of h_c/d_b had greater bar slip within the joint, interior connection stiffness was reduced and more pinching occurred, thereby reducing energy dissipation capacity. Therefore, most current seismic design codes specify the limitation of the ratio h_c/d_b for interior beam-column joints and development length l_{dh} for exterior beam-column joints. The ratio h_c/d_b and l_{dh} of current design codes were summarized in Table 4-3. More complicated expressions are given as alternatives in NZS 3101, as well as in EC8.

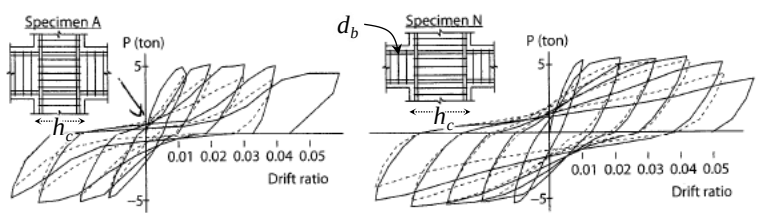

$(a)\ \frac{h_c}{d_b} = 18.8$ $(b)\ \frac{h_c}{d_b} = 28.0$

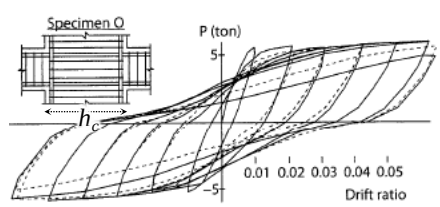

$(c)\ \frac{h_c}{d_b} = 37.5$

Figure 4-10 The effect of development length of beam bars in joints (Kaku and Asakusa, 1991)

Table 4-3 Anchorage requirements within the joint according to various design codes

Code	Joint type			
	Interior joints		Exterior joints	
ACI 318	$h_c \geq 20\ d_b$ (normal-weight concrete) $h_c \geq 26\ d_b$ (light-weight concrete)		$l_{dh} = \dfrac{f_y d_b}{4.2\sqrt{f_c'}}$	
ACI 352	Wide Column	Wide Beam	Type 1	Type 2
	$\dfrac{h_{col}}{d_b} \geq 20\dfrac{f_y}{420} \geq 20$	$\dfrac{h_{col}}{d_b} \geq 24\dfrac{f_y}{420} \geq 24$	$l_{dh} = \dfrac{f_y d_b}{4.2\sqrt{f_c'}}$	$\dfrac{f_y d_b}{6.2\sqrt{f_c'}}$
EC 8	$\dfrac{d_{bL}}{h_c} \leq \dfrac{7.5 f_{ctm}}{\gamma_{Rd} f_{yd}} \dfrac{1+0.8v_d}{1+0.75k_D\rho'/\rho_{\max}}$		$\dfrac{d_{bL}}{h_c} \leq \dfrac{7.5 f_{ctm}}{\gamma_{Rd} f_{yd}}(1+0.8v_d)$	
NZS	With seismic actions	Without seismic actions	$l_{dh} = 0.24\alpha_b\alpha_1\alpha_2 \dfrac{f_y d_b}{\sqrt{f_c'}}$ 3)	
	$\dfrac{d_b}{h_c} = 4a_f \dfrac{\sqrt{f_c'}}{f_y}$ 2)	$6a_f \dfrac{\sqrt{f_c'}}{\left(f_y\left(1+f_s/f_y\right)\right)}$		
AIJ	$\dfrac{d_b}{h_c} \leq \dfrac{2.8}{1+\alpha_b}\left(1+\dfrac{P}{A_g f_c'}\right)\dfrac{(f_c')^{2/3}}{f_y}$ 4)			

1) f_{ctm} is the mean value of the tensile strength of concrete; f_{yd} is the design value of the yield strength of steel; k_D is the factor reflecting the ductility class equal to 1 for DCH and to 2/3 for DCM; ρ' is the compression steel ratio of the beam bars passing through the joint; ρ_{max} is the maximum allowed tension steel ratio; γ_{Rd} is the model uncertainty factor on the design value of resistances, taken as being equal to 1.2 or 1.0 for DCH or DCM, respectively.
2) $\alpha_f = 0.85$ where beams pass through a joint in two directions, as in two-way frames, or $\alpha_f = 1.0$ for one-way frames.
3) $\alpha_b = A_{sr} / A_{sp}$, $\alpha_1 = 0.7$ for 32 mm bars or smaller with side cover ≥ 60 mm, and cover on the tail extension of 90º hooks ≥ 40 mm, 1.0 for all other cases.
$\alpha_2 = 0.8$ where confined by hoops spaced at $6d_b$ or less and which satisfy the relationship $A_{tr}/s \geq A_b/1000$, 1.0 for all other cases.
4) α_b is ratio of areas of beam tension reinforcement to compression reinforcement, but not more than 1.0.

4.1.3.6 Typical seismic resistant joint details

Since a beam-column connection consists of column longitudinal bars, hook anchorage of beam longitudinal bars, and joint transverse reinforcement, there is a great difficulty in placing steel reinforcing. Thus, member sizes of beams and columns should be carefully selected and reinforcing steel adequately arranged to avoid reinforcement congestion.

In ACI 315-99, a U-shaped bar is suggested as a joint transverse reinforcement when the adjacent beam width b_b is equal to or greater than the column width b_c for regions of moderate seismic risk (See Figure 4-11(b)). For high seismic risk with $b_b < b_c$, closed hoops are used for a joint transverse reinforcement and U-shaped bars are used to confine intermediate column bars(See Figure 4-11(a)). When such U-shaped bars are used, sufficient anchorage length should be secured inside the beam.

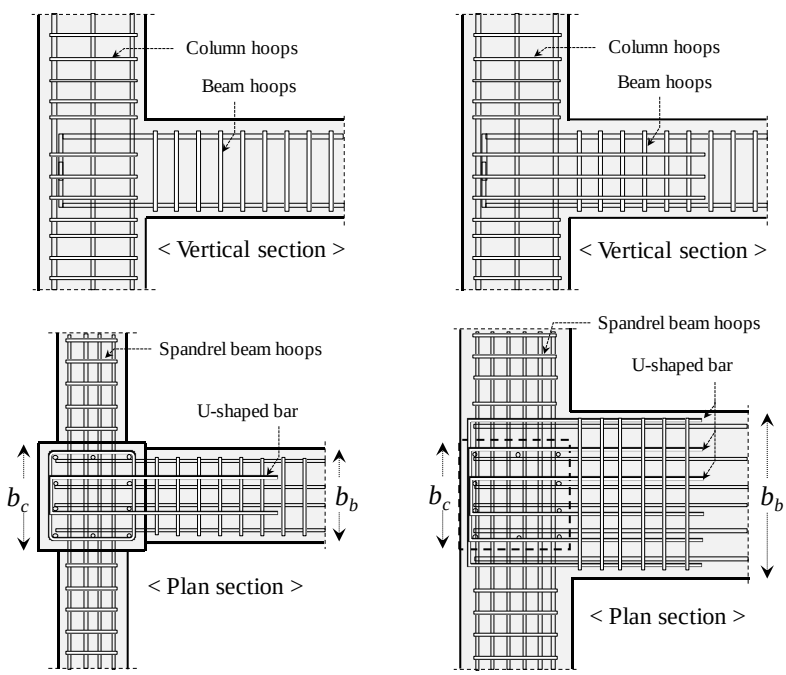

(a) For regions of high seismic risk ($b_b < b_c$)

(b) For regions of moderate seismic risk ($b_b \geq b_c$)

Figure 4-11 Typical seismic resistant joint details (ACI 315-99)

4.1.4 Previous studies for RC beam-column connections

4.1.4.1 Experimental studies of exterior beam-column connections

Murty et al. (2003) tested exterior beam-column connections in preseismic code/gravity-designed RC frame to evaluate the effect of joint shear reinforcement details and anchorage details of beam longitudinal bars. As main test parameters, joint shear reinforcement details (hairclips same as U-bars and closed ties) and anchorage details of beam bars (U-bars, 90º hook, full anchorage, and gravity design detail) were considered as shown in Figure 4-12. The horizontal line indicates beam flexural strength when steel stress reaches $1.25f_y$, and specimens variables illustrated in Figure 4-12.

All the test specimens exhibited joint shear failure before beam flexural yielding except for specimens **Q2**, **R2**, and **R3** in which maximum positive load reached to beam flexural capacity. Since the beam bottom bars in type **S** had short anchorage length without hooks, specimens of type **S** attained larger asymmetric lateral strengths (H_u^+/H_u^- = 1.63 in specimen **S1**) and severe pinching of hysteretic curves. On the other hand, specimens of type **P** with U-bars for beam longitudinal reinforcement showed most symmetric lateral strengths (H_u^+/H_u^- = 1.09 in specimen **P1**); however, the specimens resulted in not only low average initial lateral stiffness but also low displacement ductility. This is attributed to the spread of stress from the tension field to the compression field of the U-bars. Type **R** specimens with full anchorage of bars provided the satisfied anchorage performance to have largest strength and ductility. Type **Q** specimens showed a similar performance as Type **R** specimens. For joint shear reinforcement details, hairclips (U-bar) are the most effective. The use of hairclips acts as additional longitudinal reinforcement of beams, resulting in shifting the inelastic actions in the beam away from the face of columns.

Since the anchorage length of beam longitudinal bars (l_{dh} = $10d_b$) was insufficient due to the small column size (h_c= 250 mm), anchorage failure and joint shear failure occurred before beam flexural yielding though the sufficient joint shear reinforcement (ρ_{hoop} = 0.72%) was used in type 2 and type 3 specimens. This results indicated that anchorage length of beam bars should be secured within the confined core column using hook anchorage.

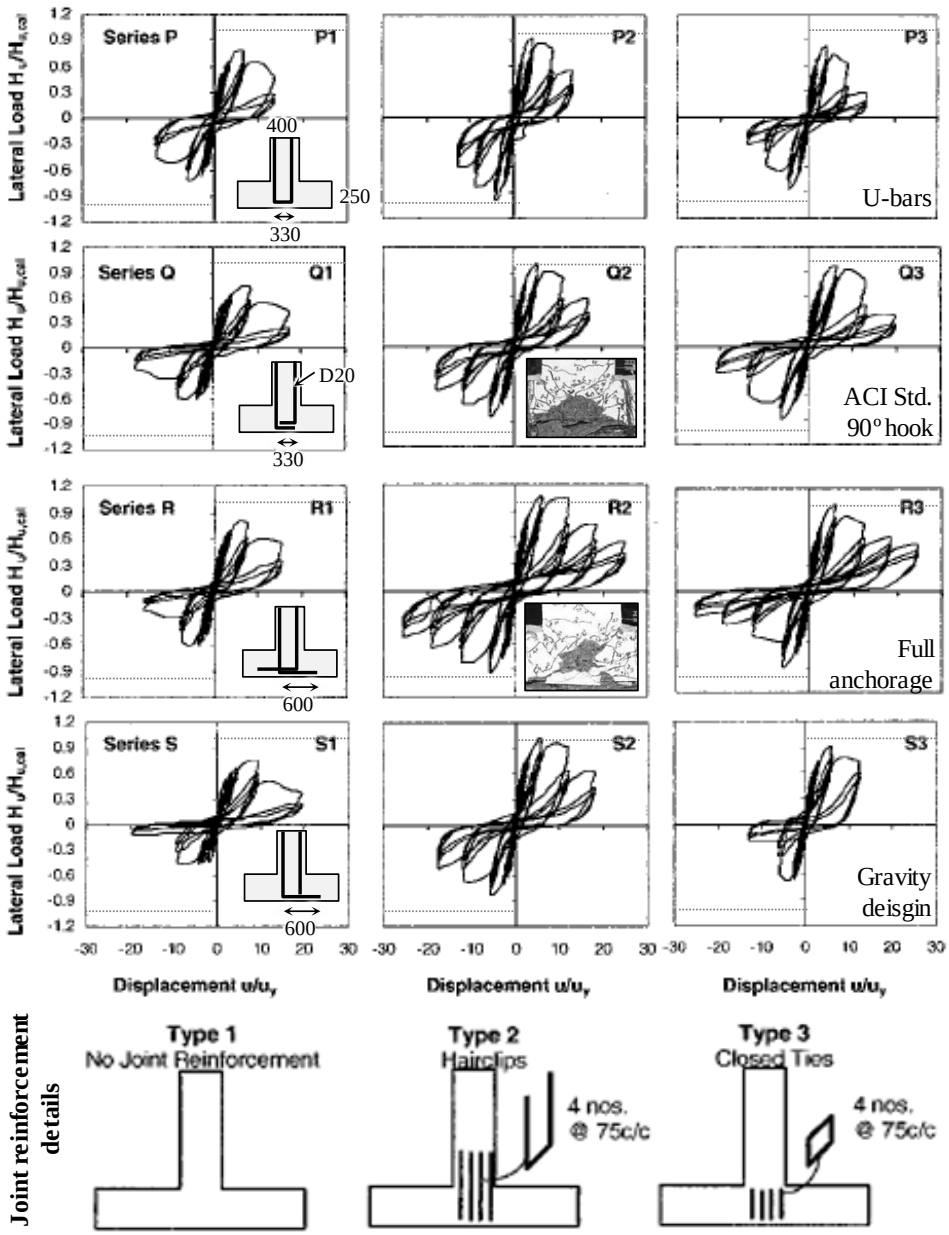

Figure 4-12 The effect of joint shear reinforcement details and anchorage details of beam bars in non-seismic exterior joints in the study of Murty et al. (2003)

Hwang et al. (2005) investigated the effect of joint shear reinforcement on the shear strength of exterior beam-column connections under seismic loading. The test parameters include the amount and details of the joint shear reinforcements. The test results showed that the major function of the joint shear reinforcement is to carry shear force as a tension tie and to control the crack width. From the side of the joint shear reinforcement as confining the concrete core, the ACI requirements are unnecessary and very difficult for construction. The less joint shear reinforcement with wider spacing up to 300 mm could be used without significantly affecting the performance of joints. The exterior connection without joint shear reinforcement can exhibit satisfactory seismic behavior when the joint is provided with adequate shear strength according to softened strut and tie model.

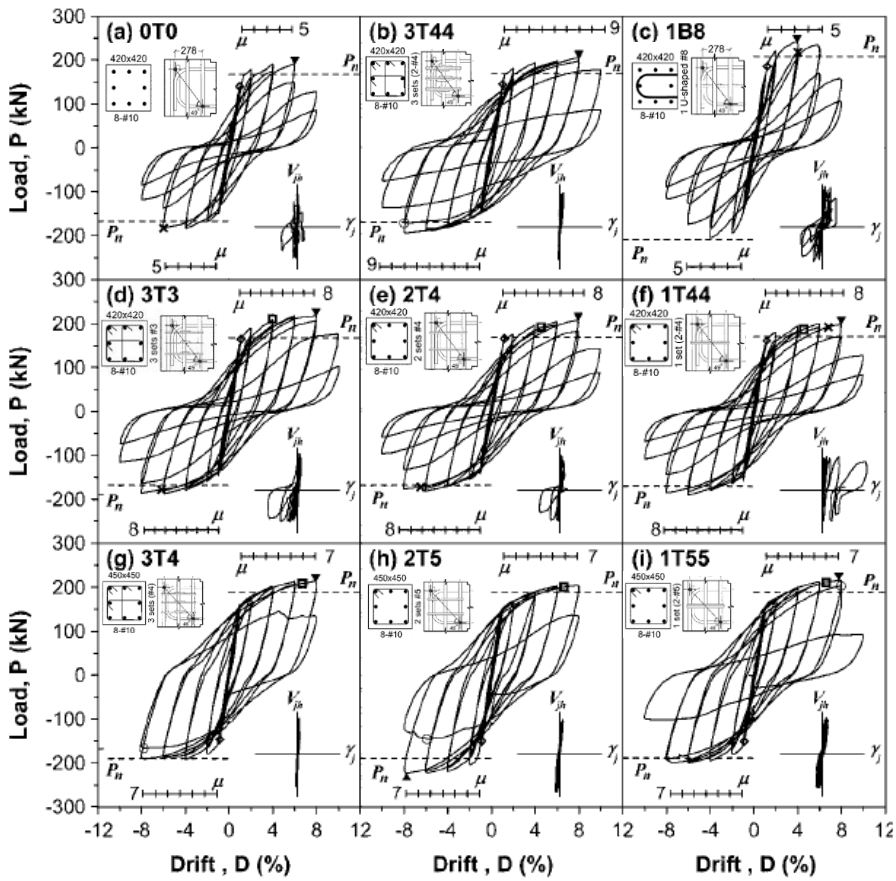

Figure 4-13 The effect of joint shear reinforcement ratio and details in the exterior beam-column connections in the study of Hwang et al. (2005)

Wong and Kuang (2008) performed full-scale RC exterior beam-column connection tests to evaluate the effects of the beam-column depth ratio and intermediate column longitudinal bars. The beam-column depth ratio has a significant effect on the strength and ductility of beam-column connections. The joint shear strength decreases as the joint aspect ratio (beam depth to column depth ratio) increases. When the aspect ratio is greater than 2.0, however, further obvious decrease in the joint shear strength cannot be attained. Intermediate column bars enhanced the joint shear strength and improved the hysteretic behavior of connections. Upper limits of the intermediate bar ratio and the corresponding overall longitudinal bar ratio in columns for increasing the joint shear strength are recommended to be 0.8% and 4%, respectively: The joint shear strength is increased by 33% in this study. Such intermediate column bars did not significantly improve the hysteretic behaviors and horizontal shear strength of a connection.

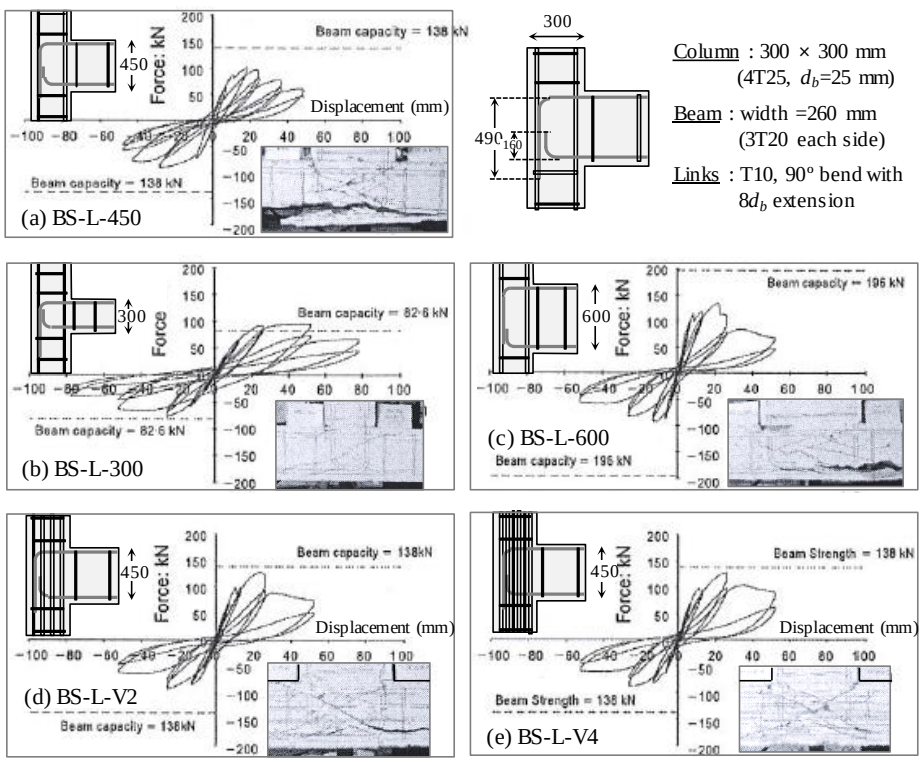

Figure 4-14 The effect of joint aspect ratio and intermediate columns bars in the study of Wong and Kuang (2008)

Kuang and Wong (2013) tested exterior beam-column connections with non-seismic details to evaluate the effect of joint shear reinforcement ratio. The main test parameters considered are joint shear reinforcement ratio (ρ_{hoop} = 0, 0.14%, 0.27% in **BS-450** and 0.13%, 0.26% in **BS-600**) and beam depth (beam flexural strength). The left and right graphs in Figure 4-15 show load and displacement relations of test specimens with beam depth of 450 mm and 600 mm, respectively. The horizontal dashed line indicates beam flexural strength, and final failure modes are presented with the graphs. All the test specimens exhibited joint shear failure prior to beam flexural yielding except for positive direction in specimen **BS-450-H2T10**. The top and bottom beam longitudinal bars were the same as 3T20 (d_b= 20 mm), but the maximum positive loads were about 10 ~ 40% larger than the maximum negative loads. In the negative direction (bottom beam bars in tension), it seems that bond deterioration reduced the joint shear strength because the 90º hook tails of the beam longitudinal bars were relatively short.

Since the effective joint area ($b_b \times h_c$ = 260 mm × 300 mm) of all the specimens was the same, but the number of joint shear reinforcement (joint shear reinforcement ratio $\rho_{hoop} = A_{sj} / [b_c \times h_b]$) differed, the effect of joint shear reinforcement directly on joint shear strength can be evaluated. Test results showed that the joint shear strength is proportional to the joint shear reinforcement ratio until ρ_{hoop} = 0.4% (see Figure 4-16), and the energy dissipation capacity was increased by reducing the pinching effect.

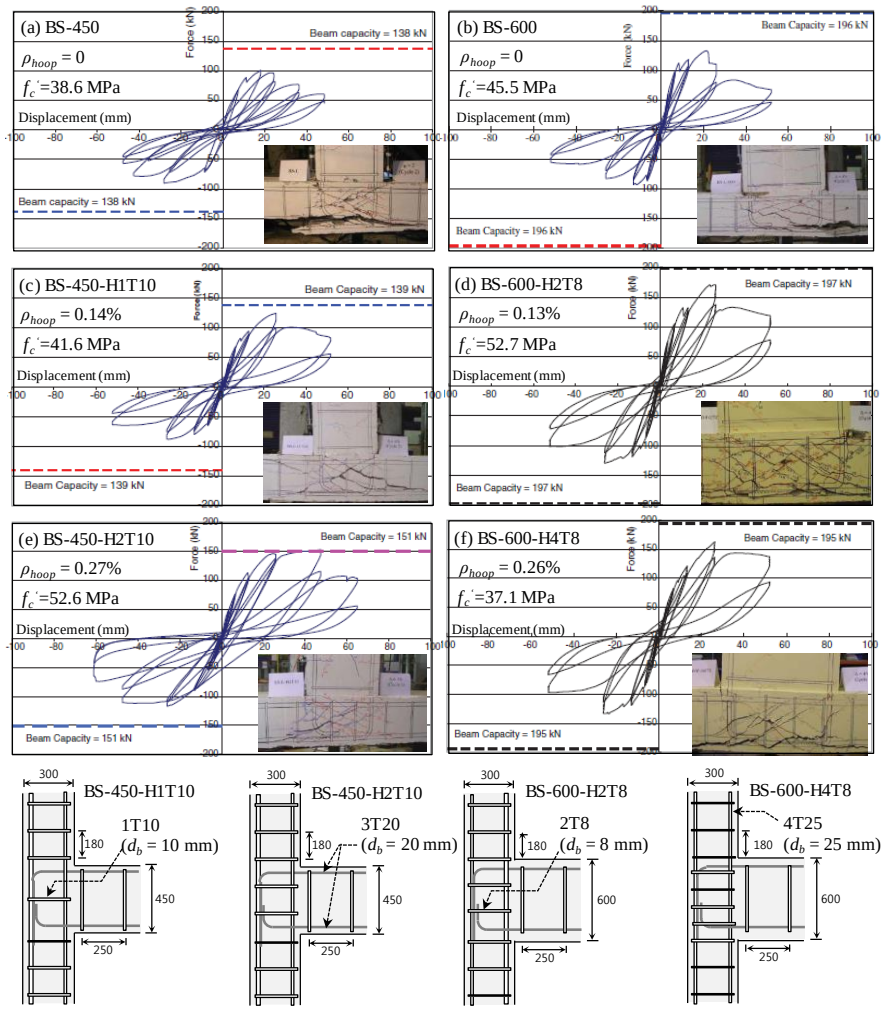

Figure 4-15 The effect of joint shear reinforcement ratio in non-seismic exterior joints in the study of Kuang and Wong (2013)

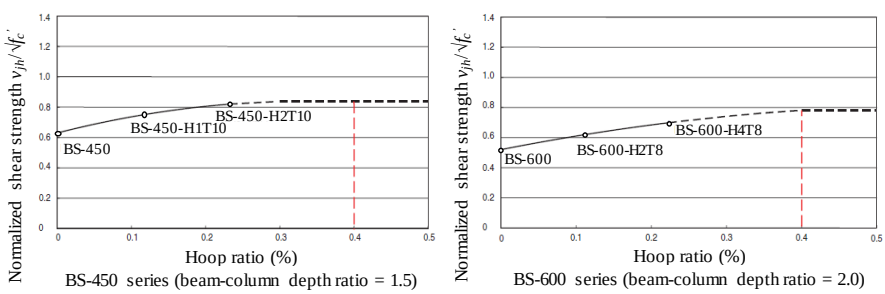

Figure 4-16 Shear strength and joint hoop ratio relations (Kuang and Wong, 2013)

Chun and Shin (2014) tested exterior beam-column connections to evaluate the effect of joint aspect ratio (beam depth to column depth ratio) and the required amount of transverse reinforcement. Recently, as the number of long-span structures increases, deeper beams are required to control the beam deflection. The joint aspect ratio can be more than 1.5, and sometimes greater than 2.5 in low-rise buildings. In this study, therefore, the exterior joints with aspect ratio of 0.7 to 2.5 were tested. The shear reinforcement and the beam anchorage (90º hook / headed bar) were also considered as test parameters.

As shown in Figure 4-17, the joint specimens with aspect ratio of 0.7 and 1.0 reached the drift ratio of 7.5% without decreasing lateral load capacity. After beam flexural yielding, the compressive concrete was crushed, but significant joint damage was not occurred. On the other hand, the beam-column connection specimens with aspect ratio greater than 1.5 developed extensive diagonal shear cracks in joints accompanied by beam flexural yielding. As the joint aspect ratio increased, the joints was severely damaged, but the beam damage was relatively decreased. Joint shear strength was also affected by the joint aspect ratio.

The influence of joint aspect ratio can be explained by Strut and Tie modeling. There are two paths of shear force transfer developed from the beam longitudinal bar as shown in Figure 4-18. The first is direct path through ST1 and the second is indirect path through ST2-T-ST2. In low aspect ratio, direct transfer of the joint shear force is effective because strut angle is small. In high aspect ratio, on the other hand, since the strut angle is large, direct path using only ST1 is inefficient. Thus, the joints with high aspect ratio need more joint shear reinforcement to transfer joint shear force effectively.

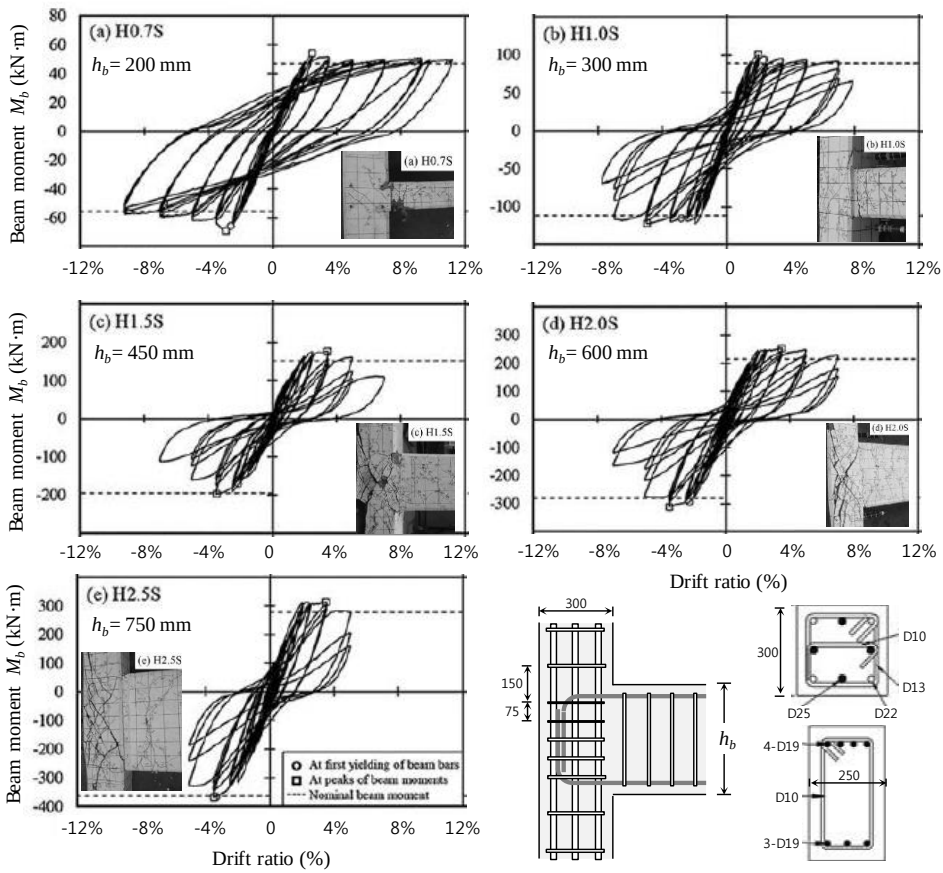

Figure 4-17 Shear strength according to joint aspect ratio in the study of Chun and Shin

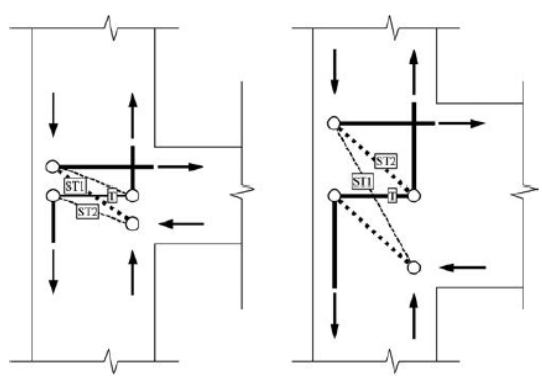

(a) Low aspect ratio (b) High aspect ratio

Figure 4-18 Strut and tie models for joint shear transfer according to joint aspect ratio by Chun and Shin (2014)

4.1.4.2 Design of beam-column joints for seismic resistance

The recommended approaches for the design of beam-column joints in each country may vary significantly. United States and New Zealand design procedures for beam-column joints often lead to different amounts and arrangement of transverse reinforcement in joints. Such differences are of major interest to designers, particularly since problems are often experienced during construction in placing the large amount of reinforcement required by the codes in joint regions with steel reinforcement congestion.

After ACI 352-76 report was published, designers became aware that, in spite of large number of experimental data, design recommendations in each country were not consistent. Many of differences were attributed to interpretation of test data under different loading histories, performance demand of RC joints, sophistication of design rules, and complexity and cost of construction.

In an effort to resolve the differences between design codes and test interpretations, seventeen participants representing the U.S., Japan, and New Zealand discussed the design approach used in each country and initiated a collaborative research from 1984 to 1989. Through cooperative research effort, ACI special report, Design of beam-column joints for seismic resistance (Jirsa, 1991) was published in 1991. The report is divided into the following groups.

Group 1: Tests conducted on specimens designed using current codes
but with the same general geometry and a specified loading history
Group 2: Design recommendation – Japan
Group 3: Influence of joint geometry on strength and
deformation characteristics
Group 4: Influence of bond on joint performance
Group 5: Joints in precast systems and with high-strength materials

For helping understand the report, the results of the researches presented in the report were briefly summarized.

(1) Tests of Beam-Column-Slab subassemblages using each code

To evaluate the seismic behavior of beam-column-slab connections designed using code requirements for each country, the full-scale subassemblages were tested under quasi-static and bidirectional cyclic loading. The test specimen details are presented in Figure 4-19.

In New Zealand tests, the superior performance of specimens was attributed to large quantity of joint shear reinforcement and the use of small diameter longitudinal bars to avoid excessive slip through the joint. No evidence was observed during tests that the presence of slabs or transverse beams provided significant confinement to the joint during bidirectional loading. Although the joint remained in the elastic range, the contribution of joint shear deformations to total deformations was significant (20 ~ 26%). Because of slab reinforcement, the lateral load of test specimens was increased up to 39% higher than that calculated using the effective flange widths in tension. The strengths and stiffness reduced when bidirectional loading was applied, due to changes in contributions of slab reinforcement.

In United State tests, all specimens failed in joint shear at drift ratio of 4.0% after beam flexural yielding, and exhibited higher strength than calculated for a beam hinging mechanism. The slab participation generally increased with increased drift ratio. Beam moment capacities calculated assuming 60% of the slab width to be effective resulted in good agreement with measured maximum beam moments. The strengths predicted by the ACI 352 underestimated the maximum load by 10 ~ 35%. The NZS produced the most conservative predictions (40 ~ 80% below the maximum load) due to the most conservative estimation of the concrete contribution of joint shear strength. The AIJ provided similar predictions to ACI 352.

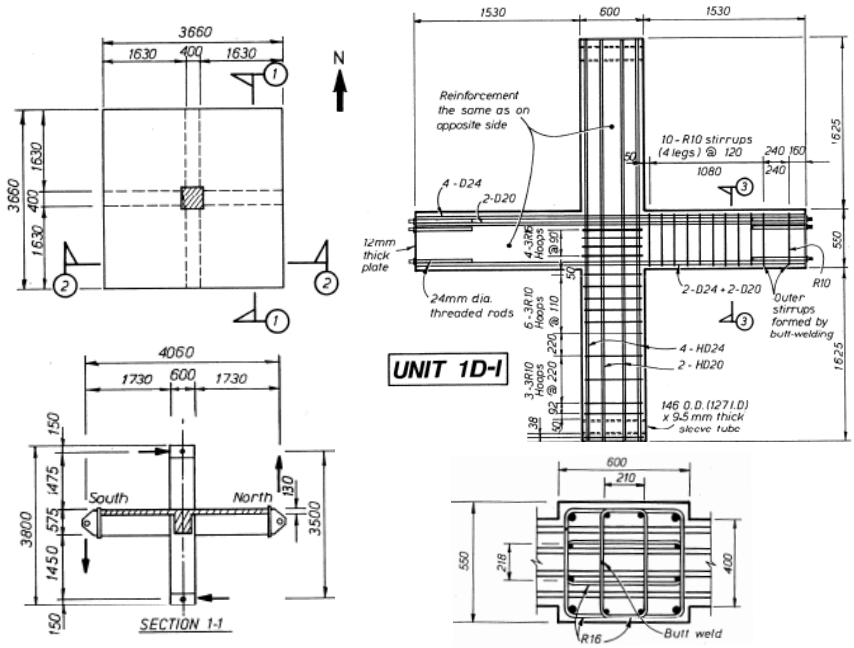

(a) New Zealand tests on RC Beam-Column-Slab subassemblages (Cheung, Paulay, and Park)

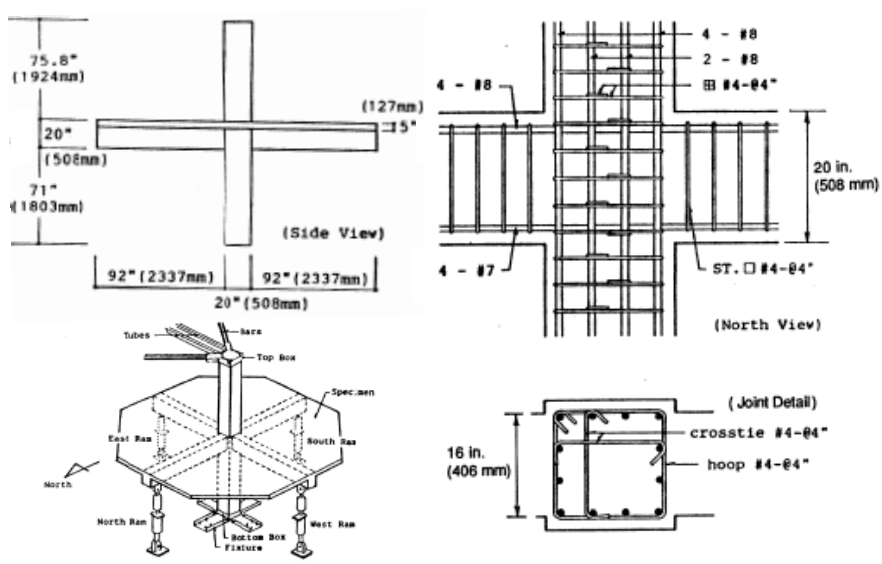

(b) United State tests on RC Beam-Column-Slab subassemblages (Kurose et al.)

Figure 4-19 Specimen details tested in New Zealand and United state

(2) Development of Japanese design criteria for RC interior joints

The development of Japanese seismic design criteria for RC interior joints are briefly summarized. Design provisions were suggested in order to maintain the performance to a story drift ratio of 2.0%, or to a beam ductility factor of 4.

(a) The ratio of the column width to the beam bar diameter should be limited as $h_c/d_b \geq f_y / (9\sqrt{f_c'})$.
(b) The joint shear stress v_u should be limited as $v_u / f_c' \leq 0.25$.
(c) A minimum lateral reinforcement ratio of 0.4% is recommended. This required value may be reduced if the joint shear stress is sufficiently lower than $0.25f_c'$.
(d) The nominal shear strength of a joint may be increased up to $0.33f_c'$, if beams frame into four vertical faces of the joint and if at least two-thirds of each joint face is covered by framing beams.
(e) Column axial stress smaller than $0.3\,f_c'$ does not exhibit beneficial effect on the bond resistance along the beam reinforcement within a joint, and that smaller than $0.5\,f_c'$ does not influence the joint shear strength.

(3) The AIJ proposal of ultimate strength design requirements for joints

The Architectural Institute of Japan (AIJ) published “Design guidelines for Earthquake Resistant Reinforced Concrete Buildings based on Ultimate Strength Concept” in 1988, as a first attempt to develop an ultimate strength design procedure in Japan. Based on experimental evidence, the required joint shear reinforcement is significantly reduced from the ACI requirements. The AIJ guidelines require that the beam-column joint shall not be potential plastic hinge because the joint should sustain gravity load, large energy dissipation and large deformation capacity are difficult to achieve in the joint, and the joint is difficult to repair after an earthquake. A joint should be designed to avoid joint shear failure and to avoid anchorage failure of beam and column reinforcement.

Vertical joint reinforcement is not required because at least one intermediate column longitudinal bar is placed in a column section.

Anchorage of beam reinforcement

For exterior joint tests, it is often difficult to distinguish a shear failure and an anchorage failure; however, the anchorage failure often exhibits bearing crushing of concrete at the bend, or splitting along the reinforcement. The anchorage failure resulted in a sudden loss of load resistance and poor energy dissipations.

The horizontal projection length before the bend is important: The extension of the bar beyond $12d_b$ from the bend is not effective for anchorage. Thus, the straight portion of the bar before the bend should be as long as possible.

There have been several proposals to evaluate the anchorage resistance of reinforcement with 90º hook. The bond stress transfer would be lost along the horizontal portion at an early stage, and that the anchorage resistance would be attained when the bearing stress along the bend reached the concrete bearing strength f_{bear} and proposed the expression as shown in Figure 4-20.

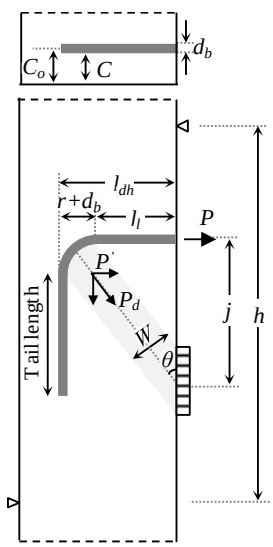

$P = P' \, h / (h - j)$

$P' = P_d \sin\theta = w \, d_b \, f_{bear} \sin\theta$

$P = w \, d_b \, f_{bear} \sin\theta \, h / (h - j)$

in which

$w = 1.41\beta \; r \cos(\pi/4 - \theta)$

$\theta = \tan^{-1}(l_{dh} / j)$

$l_{dh} = l_l + r + d_b$

$\beta = (r/3\, d_b) - 0.84$

$f_{bear} = \alpha \, \gamma \sqrt{f_c'}$

$\alpha = 16.1 \; C_c / d_b$

$\gamma = 1 + 30 A_s / (l_l \, s)$

Figure 4-20 Anchorage mechanism of 90º hook

(4) Ductility estimation of exterior joints in RC frames

When joint shear failure precedes the beam flexural yielding (J failure), the joint shear strengths are very effective. However, when beam flexural yielding precedes the joint shear failure, the beam fail in flexure (B failure) or the joint shear failure occurs prior to beam flexural failure (BJ failure). Thus, some other criterion should be established to evaluate the performance of joints with BJ failure. The ductility of a joint is more effective than the joint shear strength for the evaluation of the performance of joints with BJ failure.

Though the ratio of shear stress at beam flexural yielding to joint shear strength V_{ju} / V_{jn} was less than 0.5, ten of eighteen specimens failed due to joint shear after beam flexural yielding. Ductility of exterior joints is increased by the increase of column axial compressive force and joint shear reinforcement ratio and the existence of column intermediate bars. The critical cumulative displacement ductility factor, at which the value of joint shear distortion reaches 0.8%, was quantified as a function of the experimental variables, and very effective in estimating seismic performance of exterior joints.

(5) Bond and anchorage of bars in joints

For seismic design of RC beam-column joints, bond and anchorage of longitudinal bars is the most significant factor together with joint shear capacity.

Bend bar anchorage in exterior joint

When $l_{dh}/d_b > 10$, M_{max} is greater than M_y, and a deformation capacity is greater than drift ratio of 2.0%.

When the confinement of hooked bar is poor, the influence of inner radius and tail extension on the anchorage capacity of hooked bar is significant. However, in common practice, as the hooked bars are located within a joint core, the influence appears to be less apparent.

If pull-out or splitting failures along with the bar are not occurred, the anchorage mechanism approaches to shear transfer mechanism in joint. Thus, the requirement for development length is significant not only for bond in lead-in length zone but also to guarantee the area to resist joint shear force.

4.1.4.3 Analytical model for RC beam-column joints

The role of joint shear reinforcement and mechanism of shear transfer in beam-column joint are still in discussion. Significant collaborated research program as mentioned in section 4.1.4.2 (United States, New Zealand, and Japan) has been made, but design method (philosophy) of beam-column joints still differs from each design code.

New Zealand (NZS 3101 standards) incorporates both diagonal strut mechanism and truss mechanism, which assumes adequate bond of reinforcing bars in joint so that shear forces are transferred to the joint core (See Figure 4-21(a) and (b)). Relatively large amounts of joint shear reinforcement are required to transfer tension force by the truss mechanism in joint. On the other hand, in United States (ACI 318 and ACI 352), severe bond deterioration of the reinforcing bars in joint is assumed, so joint shear forces are only transferred by a diagonal strut of concrete (See Figure 4-21(a)). The role of joint shear reinforcement in the diagonal strut of concrete is to confine the core concrete.

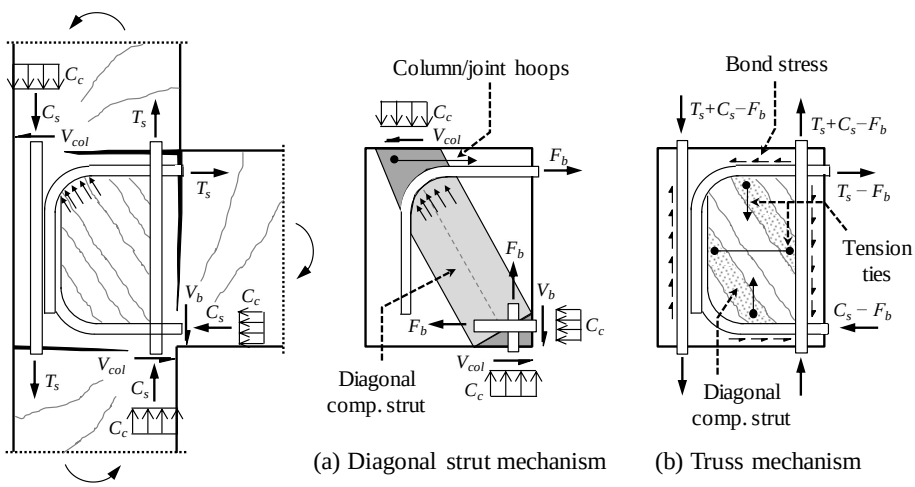

Figure 4-21 Force transfer mechanism in exterior beam-column joint

(1) Joint model proposed by Paulay, Park, and Priestley (New Zealand)

Paulay et al. (1978) proposed analytical models for interior beam-column joints under seismic actions. The total shear force applied to a joint core should be divided into concrete diagonal strut and truss mechanism. The shear resistance of joint core concrete is primarily due to the contribution from the diagonal compression strut. When plastic hinges form in the adjacent beam, the shear transfer by the diagonal strut is decreased by flexural cracking at the face of the column and by yield penetration. The shear resistance provided by reinforcement is due to the contribution from truss mechanism. Both horizontal and vertical shear reinforcement is required such as horizontal shear reinforcement and column intermediate bars.

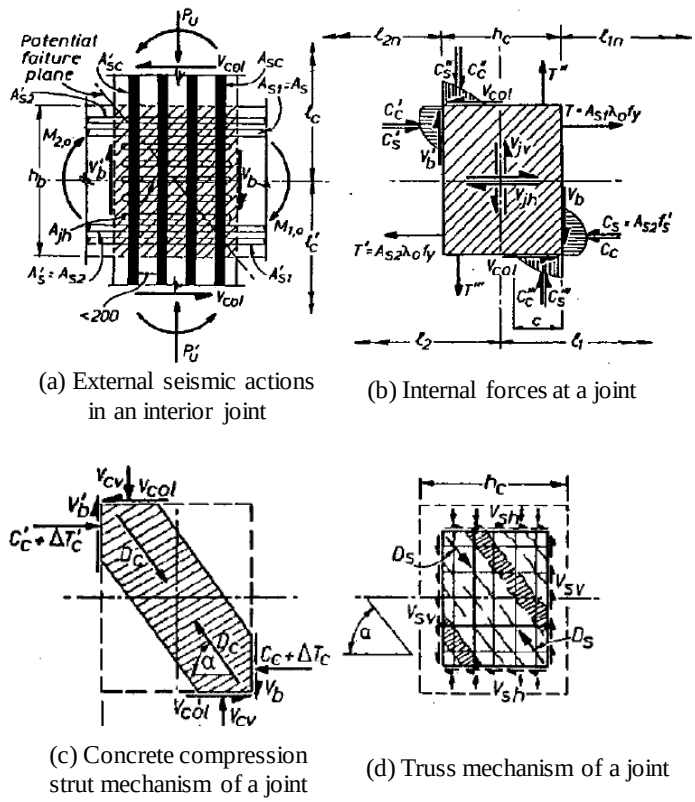

(a) External seismic actions in an interior joint

(b) Internal forces at a joint

(c) Concrete compression strut mechanism of a joint

(d) Truss mechanism of a joint

Figure 4-22 External actions and internal stress at a joint in the study of Paulay et al. (1978)

(2) Softened Strut and Tie Model

Hwang and Lee (1999) proposed a softened strut and tie model for shear strength of exterior beam-column joints. The model is derived from the concept of strut and tie, and it satisfies the three basic mechanics principles: equilibrium, compatibility, and material constitutive laws. The basic assumption is that the bond deterioration of beam reinforcement should be tolerated, resulting in a diagonal strut to resist joint shear (Diagonal mechanism in Figure 4-23(a)). Additional struts are associated with joint shear reinforcement and column intermediate bars (Horizontal and vertical mechanisms in Figure 4-23(b) and (c)).

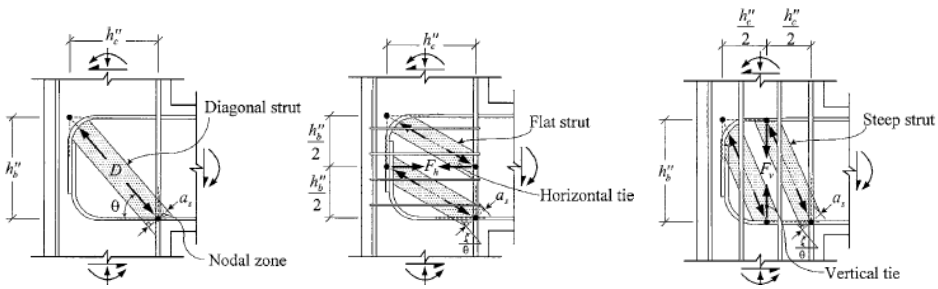

(a) Diagonal mechanism (b) Horizontal mechanism (c) Vertical mechanism

Figure 4-23 Joint shear resisting mechanisms in the study of Hwang and Lee (1999)

(3) Quadruple flexural resistance model

Shiohara (2001) proposed a new concept of quadruple flexural resistance in RC beam-column joints. Failure models using the truss mechanism or the strut mechanism determine joint shear failure as yielding of joint shear reinforcement or compressive failure of the diagonal concrete strut, respectively. In new model, however, shear deformation in the joint is assumed primarily due to the rotation of the four triangular concrete segments and the crack opening as shown in Figure 4-24. The rotational deformation of each segment causes uneven opening of the cracks. As shown in Figure 4-24(b), the vertical and horizontal springs connecting the segments prevent them from breaking into pieces, similar to longitudinal bars in a beam and a column in a conventional beam-column joint.

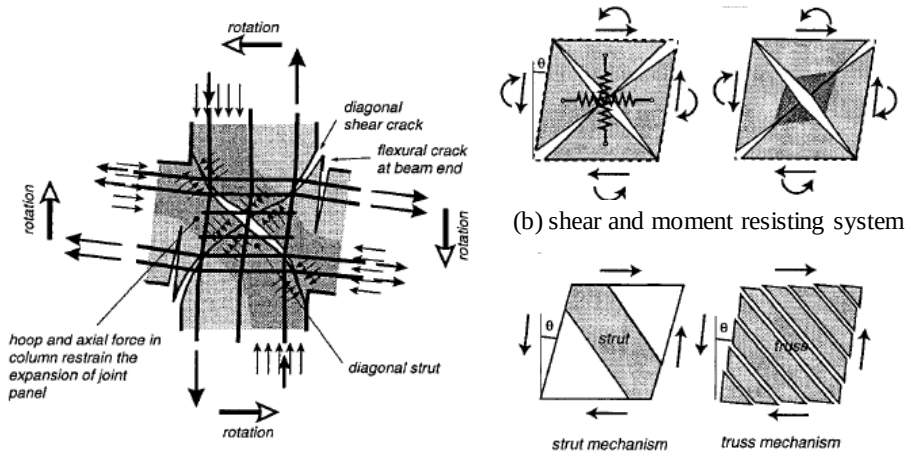

(a) Quadruple flexural resistance model

(b) shear and moment resisting system

(c) Shear resisting system

Figure 4-24 Quadruple of flexural resistance in the study of Shiohara (2001)

(4) Model for unreinforced exterior joints

Park and Mosalam (2012) proposed an analytical model to predict the shear strength of RC exterior joints without joint shear reinforcement (denoted as unreinforced) using two inclined compressive struts in the joint as shown in Figure 4-25. The two inclined struts are assumed to resist the horizontal joint shear force in parallel, and the fraction of each strut contribution is formulated using the bond resistance of the concrete surrounding the beam longitudinal bars within joint region. The proposed model is validated by many test results.

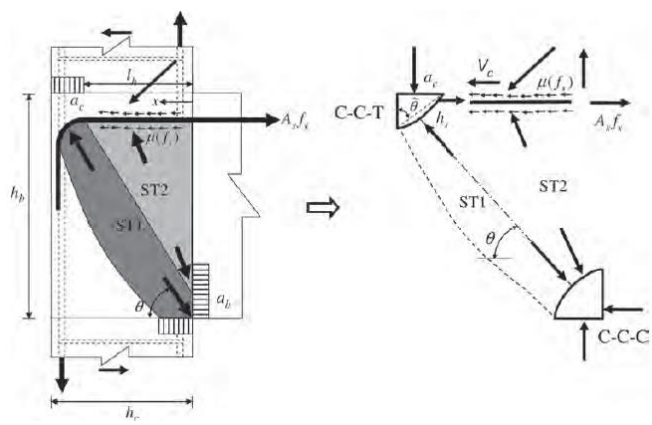

Figure 4-25 Assumed SAT model in exterior joints by Park and Mosalam (2012)

4.1.4.4 Shear strength degradation models

(1) Priestley (1997)

Priestley proposed a model for principal tension strength degradation as drift ratio increases as shown in Figure 4-26. This model distinguishes the two cases of beam bars bent-in and bent-out from the joint with different principal tension stress.

Priestley suggested that comparatively small amounts of joint shear reinforcement greatly improve the joint behavior and reduce joint dilation, thereby delaying concrete cover spalling of the joint. When the beam bar hooks are restrained from straightening, integrity of the diagonal compression strut is maintained.

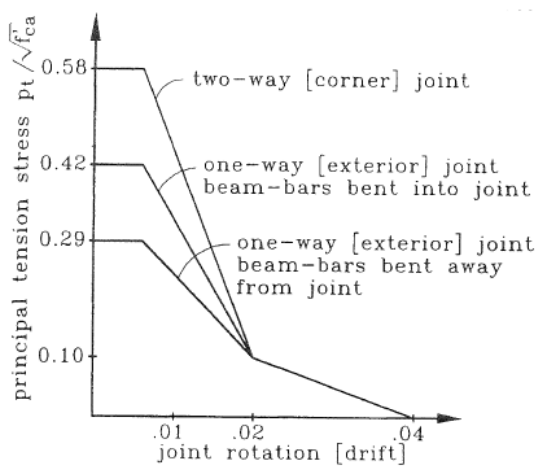

Figure 4-26 Strength degradation model for joints proposed by Priestley (1997)

(2) Park (1997)

The nominal joint shear stress by the concrete diagonal compression strut in the joint without shear reinforcement has been experimentally found to reduce with increase in ductility. The values of *k* in Figure 4-27 are for one-way frames, which are expected to be conservative for two-way frames.

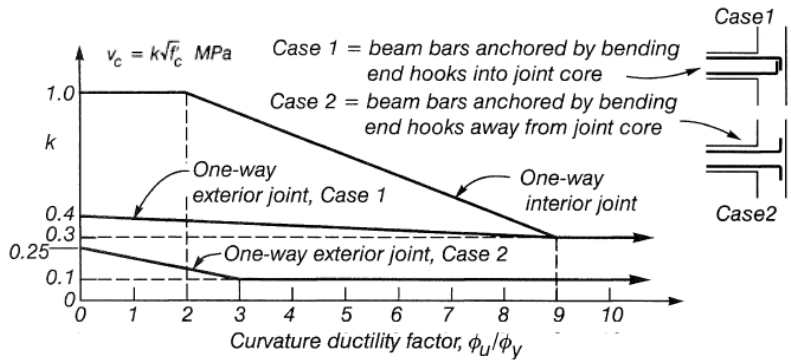

Figure 4-27 Degradation of the joint shear stress resisted by strut mechanism with curvature ductility factor in the study of Park (1997)

(3) Hakuto et al. (2000)

Since the diagonal tension cracking of the joint core in alternative directions during seismic loading will reduce the diagonal compressive strength of the concrete, the joint shear strength may degrade as the displacement ductility factor increases. Based on previous test results, a model in Figure 4-28 is proposed for the shear strength degradation of interior joints without joint shear reinforcement.

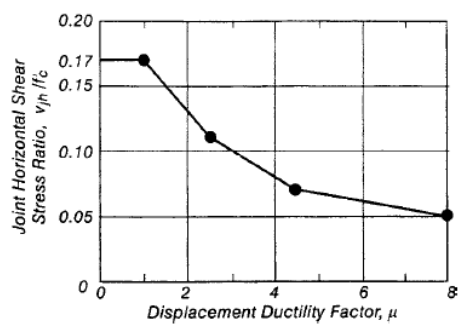

Figure 4-28 Model for strength degradation with imposed displacement ductility factor by the study of Hakuto et al. (2000)

4.2 Test Program of Reinforcement Details on Joints

4.2.1 Major design parameters

Table 4-4 presents the test parameters of beam-column connections including types of the beam-column joints, joint shear reinforcement details, and the number of joint shear reinforcements. Figure 4-29 and Figure 4-30 present reinforcement details of six exterior beam-column connections and two interior beam-column connections, and details of joint shear reinforcement, respectively. In the specimen names, the first letter 'E' and 'I' denote the Exterior and Interior connection types, respectively; the following letters 'U', 'U2', and U4' denote the number of joint shear rebars used in the joints; 'N', 'R', and 'U' denote the joint shear rebar details, no shear reinforcement, 90º hook, and U-bar details, respectively; and the letter 'C' denotes the different column size used in the specimen **EU4UC**. Since anchorage length for 90º standard hook of beam longitudinal rebars within the joint affects seismic performance of beam-column details, two different sizes of beam top and bottom rebars, D25 (d_b = 25.4 mm) and D19 (d_b = 19.1 mm), are used in the test specimens, **EUN** ~ **EU2U** and **EU4R** ~ **IU**, respectively.

Table 4-4 Test variables of beam-column connection specimens

Specimen[1)]	Type	Joint shear rebar details	Number of joint shear rebars	Column size $b_c \times h_c$ (mm×mm)	Beam top and bottom rebars
EUN	Exterior	N/A	-	350×350	4D25 & 2D25
EU2R		90º	2		
EU2U		U-bar	2		
EU4R		90º	4		7D19 & 4D19
EU4U		U-bar	4		
EU4UC		U-bar	4	350×450	
IN	Interior	N/A	-	350×350	7D19 & 4D19
IU		U-bar	5		

1) **E**(Exterior)/ **U**(Upward) /**2**(Number of joint bar)/ **U**(Type of joint shear rebar, U-bar)

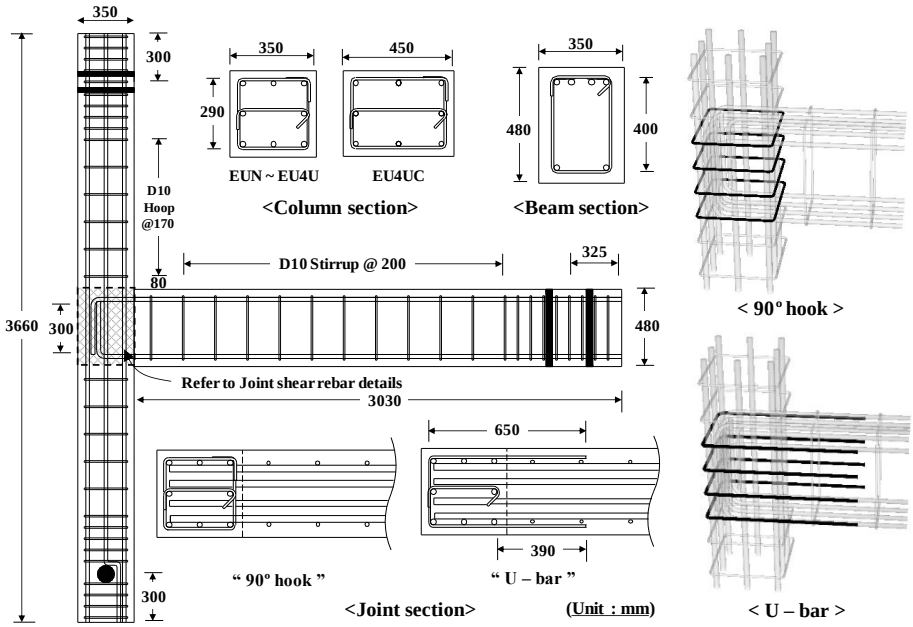

(a) Exterior beam-column connection

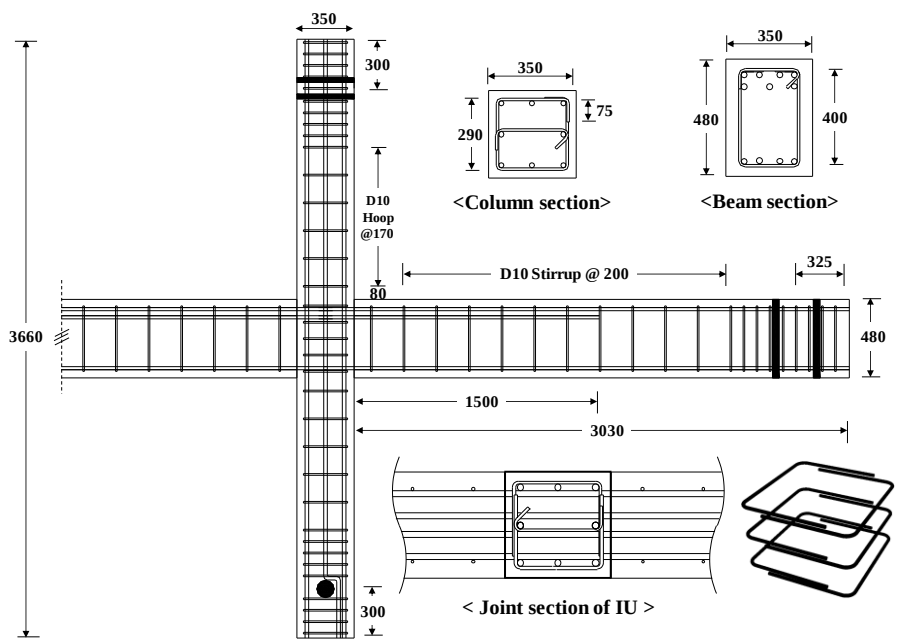

(b) Interior beam-column connection

Figure 4-29 Dimensions and reinforcement details of beam-column connections

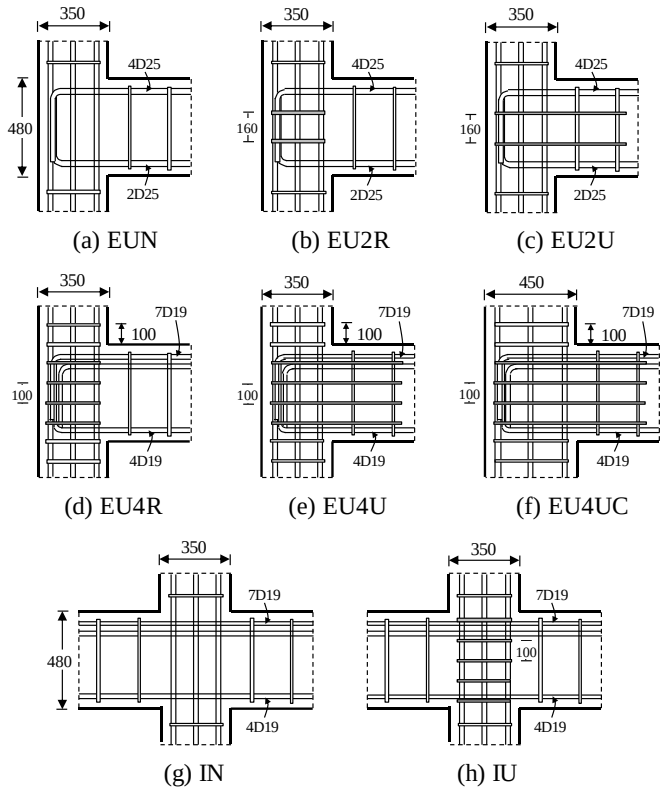

Figure 4-30 Details of joint shear reinforcement

4.2.2 Test specimens

In Figure 4-29, the dimension of the column section was $b_c \times h_c$ = 350 mm × 350 mm and that of the beam section was $b_b \times h_b$ = 350 mm × 480 mm except for **EU4UC** (column section $b_c \times h_c$ = 350 mm × 450 mm). All specimens were designed to have beam depth h_b (=480 mm) greater than column depth h_c (=350 mm or 450 mm). Nonetheless, in the exterior connection specimens, the sum of column moments ΣM_{nc} was larger than a beam moment M_{nb} from one side, which indicates that strong column-weak beam actions were expected. On the other hand, in the interior connection specimens, the sum of column moments ΣM_{nc} was less than 0.7 times that of beam moments ΣM_{nb} from both side. Weak column-strong beam behavior was made in **IN** and **IU**.

Figure 4-29(a) shows two types of joint shear rebar details used for the exterior connections, 90º hook and U-bar details. The U-bar was used for convenient joint rebar placement on behalf of the closed tie with 90º hook by enclosing column longitudinal bars after beam and column cages constructed. To secure bond performance, a development length of U-bar greater than $30d_b$ should be anchored into the beam. In the interior connection, lap spliced U-bars were used for joint shear rebars as shown in Figure 4-29(b). This detail can also relive rebar placement in beam-column joints.

Table 4-4 and Figure 4-30 present joint shear rebar details. Specimens **EUN** and **IN** did not have joint shear reinforcement as control specimens. On the other hand, in specimens **EU2R**, **EU4R**, and **IU**, the closed rectilinear ties (D13) and cross ties (D10) were placed in the joints. **EU2R** and **EU4R** had ties with 90º hooks for anchorage, but **IU** had lap spliced U-bars to improve constructability of rebar placement as shown in Figure 4-29. As alternative joint shear reinforcement details, specimens **EU2U**, **EU4U**, and **EU4UC** used U-bars anchored into adjacent beams without hook anchorages at the end.

In the exterior connections, the beam longitudinal rebars anchored in the column by standard 90º hook are bent into the joint to improve development of a diagonal compression strut across the joint. In ACI318-14 and JSCE, beam and column bars should be firmly anchored to the joint of beam and column members with a standard hook. Hooked anchorage length of beam longitudinal rebars from

the face of column was greater than $12d_b$ (300 mm for D25 and 228 mm for D19) with concrete cover thickness over 50 mm.

Figure 4-29 shows dimensions and reinforcement details of beam and column connections. Except for **EU4UC**, column reinforcement details are identical in all specimens. Eight D22 bars (bar diameter d_b = 22.2 mm and yield strength f_y = 565 ~ 577 MPa) and D10 bars (d_b = 9.53 mm and yield strength f_{yt} = 552 ~ 576 MPa) were used for the longitudinal and transverse reinforcements, respectively. In **EU4UC**, four D22 bars and four D25 bars (bar diameter d_b = 25.4 mm and yield strength f_y = 550 ~ 588 MPa) were used for the longitudinal reinforcement to make up for the increased column section (h_c = 450 mm). For top and bottom reinforcement in beams, four D25 bars (ρ_t = 1.21%) and two D25 bars (ρ_b = 0.60%) were used in **EUN**, **EU2R**, and **EU2U** and seven D19 bars (bar diameter d_b = 19.1 mm, yield strength f_y = 550 MPa, and ρ_t = 1.20%) and four D19 bars (ρ_b = 0.68%) were used in **EU4R**, **EU4U**, **EU4UC**, **IN**, and **IU**, respectively.

4.2.3 Specimen construction

Construction procedures of the beam and column connection specimens are illustrated in Figure 4-31. Steel cages were assembled with manufactured rebars. Strain gauges were attached on the longitudinal rebars and transvere rebars at the location specified in Figure 4-32. To investigate yielding of members and yield penetration into the joint, a number of strains were measured in the plastic hinge region of beam and column, and the beam-column joint. Strains of transverse bars were also measured.

After manufacturing molds and placing steel cages, concrete was poured at the side of beam-column connection specimens. The specimens were steam cured for 3 days prior to stripping their molds for attaining target concrete strength. The tests were conducted in 35 days after concrete placing. Before curing concrete, the steel rods were inserted in the specimens to install measuring equipment (LVDT, Linear Variable Differential Transformer) as shown in Figure 4-33 and Figure 4-34. Shear deformations of joints, columns, and beams were computed by diagonally placed LVDTs. Flexural deformations were evaluated by horizontal or vertical LVDTs.

<Manufactured re-bars>

<Assembling steel cages>

<Manufacturing molds>

<Placing concrete>

Figure 4-31 Construction procedures of beam-column connection specimens

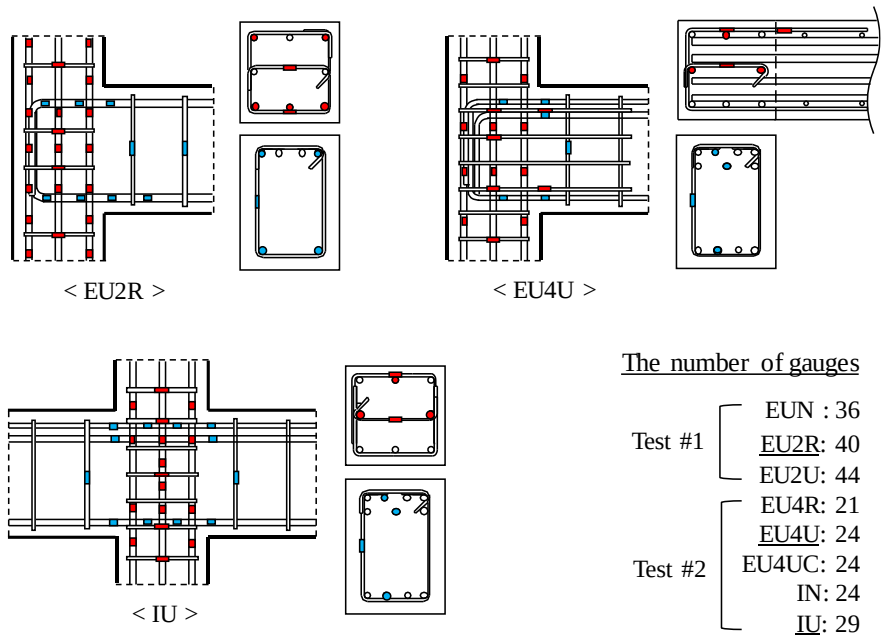

Figure 4-32 The locations of strain gauges in beam-column connection specimens

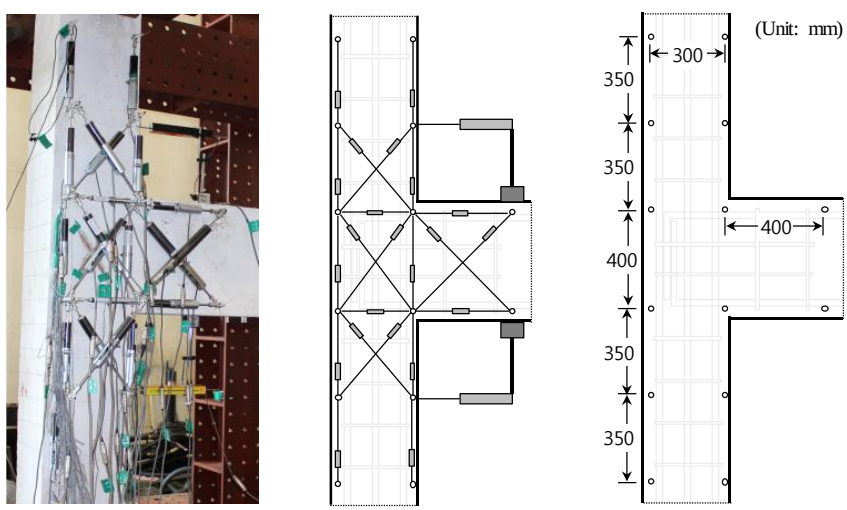

Figure 4-33 LVDT locations for measuring deformations in exterior connections

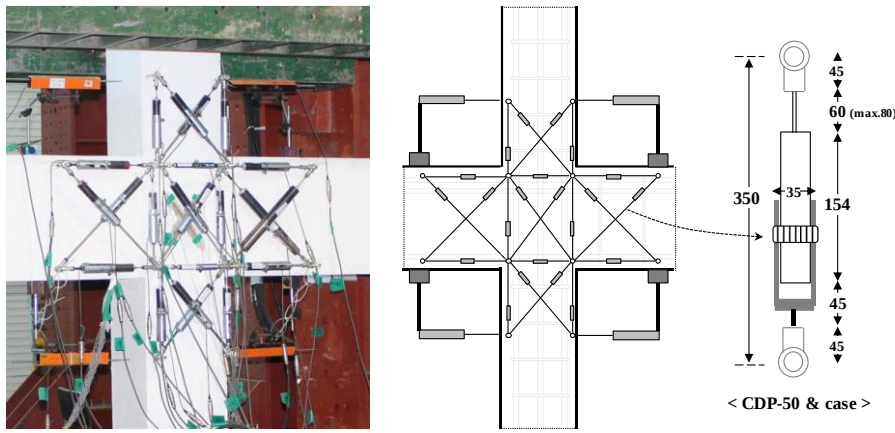

Figure 4-34 LVDT locations for interior connections and LVDT case details

4.2.4 Material strengths

Table 4-5 presents the yield and tensile strengths (f_y and f_u) of the reinforcing steel bars used for beam and column connection specimens. For the specimens, cyclic tests were performed two separate times. Thus, as shown in Table 4-5, f_y (= 481 ~ 588 MPa) and f_u (= 605 ~ 720 MPa) of D10 to D25 bars used in each test were differed. In the table, SD400 and SD500 denote the nominal yield strength grades of deformed bars, 400 and 500 MPa, respectively, and D10, D13, D19, D22, and D25 denote the diameters of deformed bars, d_b = 9.53, 12.7, 19.1, 22.2, and 25.4 mm, respectively. The yield and tensile strengths in Table 4-5 are average values of three test results of reinforcing bars. Figure 4-35 presents stress and strain curves of longitudinal and transverse bars used in Test No. 2 specimens (**EU4R**, **EU4U**, **EU4UC**, **IN**, and **IU**).

Table 4-6 shows the mix proportioning of the concrete. The maximum aggregate size was 25.4 mm. In each material test, three concrete cylinders of a diameter 100 mm and a height 200 mm were prepared and the compression tests of the cylinders were performed on the first day of testing. The compressive strengths of the concrete were f_c' = 20 ~ 31 MPa on average. Material test results of concretes (Test No. 2) are shown in Figure 4-36.

Table 4-5 Properties of steel reinforcing bars

Test No.	Bar type	d_b (mm)	f_y (MPa)	f_u (MPa)	ε_y (mm/mm)
1	SD400 D10	9.53	552	676	0.00276
	SD400 D13	12.7	481	605	0.00241
	SD500 D22	22.2	565	688	0.00283
	SD500 D25	25.4	550	664	0.00275
2	SD400 D10	9.53	576	689	0.00288
	SD400 D13	12.7	528	656	0.00264
	SD500 D19	19.1	550	685	0.00275
	SD500 D22	22.2	577	720	0.00289
	SD500 D25	25.4	588	702	0.00294

Note: Test No. 1 contains specimens **EUN**, **EU2R**, and **EU2U**,
Test No. 2 contains specimens **EU4R**, **EU4U**, **EU4UC**, **IN**, and **IU**

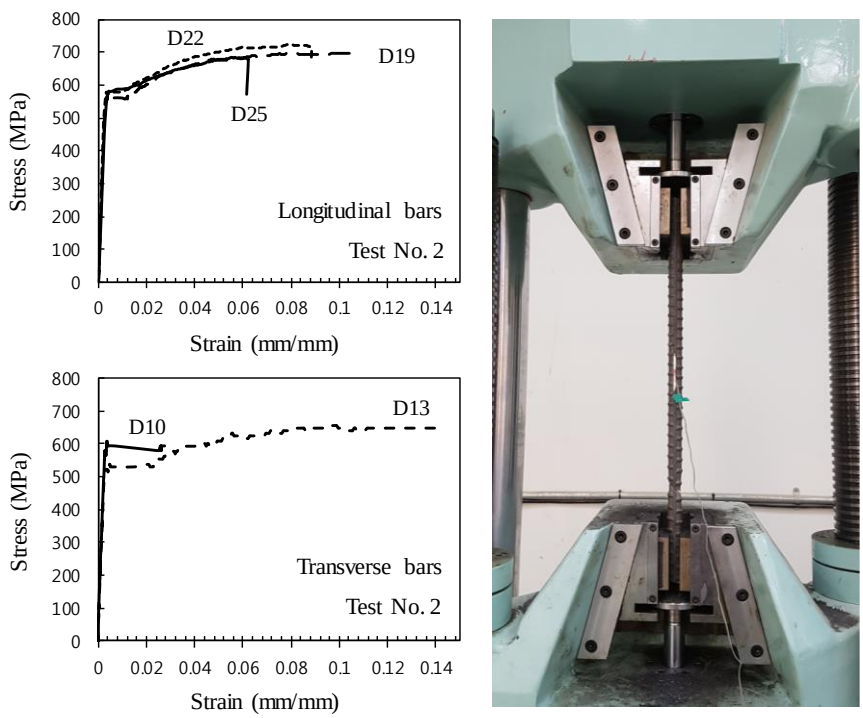

Figure 4-35 Stress and strain curves of steel reinforcing bars

Table 4-6 Mix design of concrete

Test No.	Compressive strength	W/C	Unit weigh, kgf/m^3							Slump
			W	C	FS	S	FA	CA	SP	
1	20 MPa	54.2%	167	200	46	62	873	806	1.54	120 mm
2	31 MPa	48.4%	155	192	64	64	904	909	2.24	120 mm

Note: W = water; C = cement; FS = fly ash; S = blast furnace slag; FA = fine aggregate; CA = coarse aggregate; SP = superplasticizer

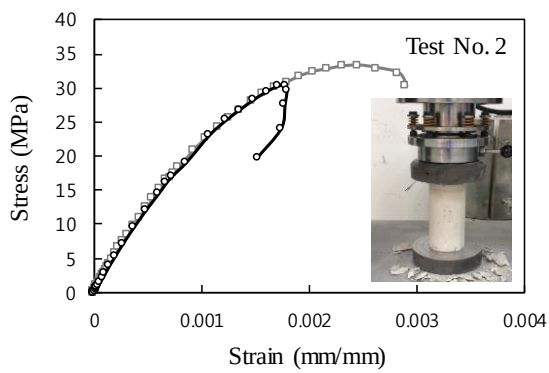

Figure 4-36 Stress and strain curves of concrete cylinders

4.2.5 Test setup and loading plan

Figure 4-37 and Figure 4-38 show a test setup for lateral cyclic loading of a beam and column exterior connection. A hinge support and a roller support were used at the bottom of the column and the end of the beam, respectively. Lateral supports on the sides of the beam and the column were installed to restrain out-of-plane movement. The support details are given in Figure 4-38. To simulate the roller support, two hinges were used at both sides of the support bar. A load cell was attached to measure the end reaction force.

The cyclic lateral loading was performed by controlling the displacement of the actuator (maximum stroke ± 250 mm) placed at a height of 3060 mm from the hinge support of column. As an axial load is relatively low in low-rise buildings, and the axial load has a positive effect by restraining joint shear cracks to the development of beam longitudinal bars, column axial load was not considered.

Figure 4-39 shows the displacement history for the cyclic lateral loading. Load cycles were repeated three times at each displacement step. The loading protocol was planned with increasing of 1.2 ~ 1.5 times previous drift ratio and three steps at every drift ratio specified in ACI 374.1. The lateral displacement of the columns was increased from 0.25% in the elastic range to the drift ratio at 80% of peak loads in the descending branch.

The lateral load (P) and lateral displacement (Δ) were measured from the load cell in the Actuator and the line LVDT at the top of the column, respectively. Horizontal and vertical slips measured at the hinge and roller supports were calibrated to compute the actual lateral displacement applied in the connection specimens.

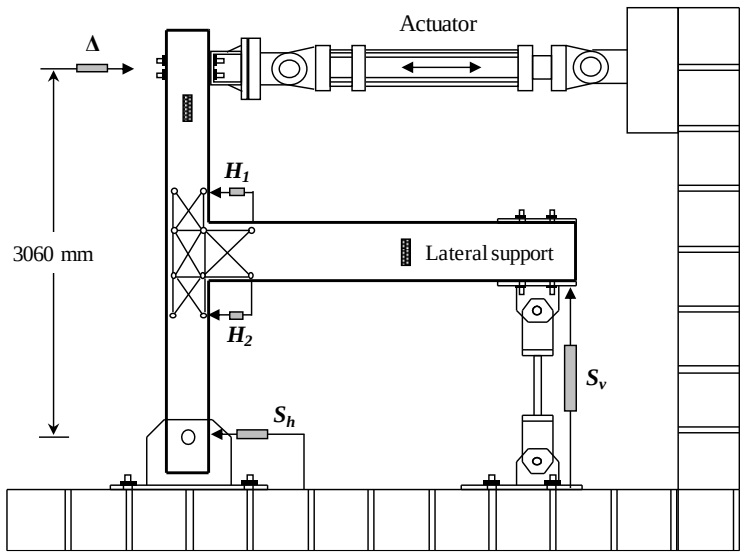

Figure 4-37 Schematic test setup of a beam-column exterior connection

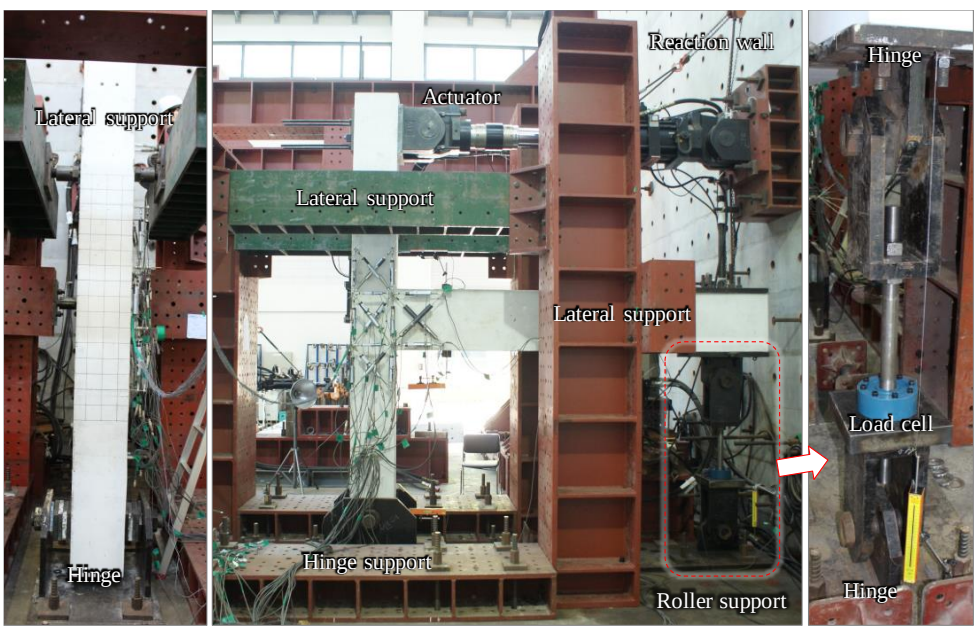

< Side view > < Front view of test setup > < Roller support >

Figure 4-38 Photograph of test setup of an exterior connection

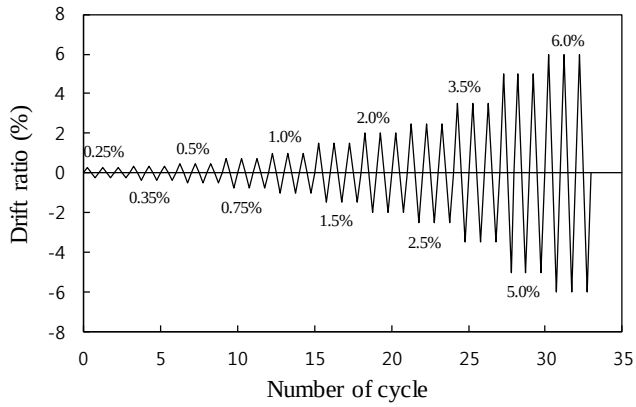

Figure 4-39 Displacement history for cyclic lateral loading

4.3 Predicted Failure Mode and Estimation of Nominal Strength

In this study, the failure modes of beam-column connections were classified into flexural yielding of beams or columns, joint shear failure, and anchorage failure of beam bars. The load capacity of the connections was evaluated according to the failure mode.

4.3.1 Flexural yielding of beams or columns

Figure 4-40 presents Actuator lateral load (P_n), end reaction forces (V_c, V_b, V_{b1}, V_{b2}), and flexural moments at the faces of the joint (M_c, M_b, M_{b1}, M_{b2}) in exterior and interior beam-column connections. In the case of the interior connection, since the magnitude and direction of the flexural moment are different at left and right faces of the joint, the vertical reaction force and flexural moment of beams are classified as V_{b1}, V_{b2} and M_{b1}, M_{b2}, respectively.

If the column yields ($M_c = M_{nc}$) before the beam yields at the faces of the joint, the nominal strength of the joint P_{nc} (Maximum actuator load) is equal to M_{nc} divided by the shear span ($a = [l_c - h_b] / 2$).

$$P_{nc} = \frac{2M_{nc}}{l_c - h_b} \tag{4-21}$$

where, P_{nc} is the nominal joint strength due to column flexural yielding, M_{nc} is the nominal flexural strength of column framing into joint, and l_c is the length of column from loading point to the bottom hinge support (= 3060 mm).

However, if the beam yields first ($M_b = M_{nb}$, $M_{b1} = M_{nb1}$, $M_{b2} = M_{nb2}$) than the column, the nominal joint strength P_{nb} is calculated from the force equilibrium condition of end reaction forces as shown in Figure 4-40.

$$P_{nb} = \left(\frac{M_{nb}}{l_b - 0.5h_c} \right) \frac{l_b}{l_c} \quad \text{for exterior connections} \tag{4-22}$$

$$P_{nb} = \left(\frac{M_{nb1} + M_{nb2}}{l_b - 0.5h_c} \right) \frac{l_b}{l_c} \quad \text{for interior connections} \tag{4-23}$$

where, P_{nb} is the nominal joint strength due to beam flexural yielding, M_{nb}, M_{nb1}, M_{nb2} are the nominal flexural strength of beam framing into joint, and l_b is the length of beam from the column centerline to the roller support (= 2880 mm).

Table 4-7 presents predicted strengths P_{nb} and P_{nc} of beam and column yielding. M_{nc}, M_{nb1} (beam bottom bar yielding), and M_{nb2} (beam top bar yielding) are obtained from the sectional analysis using the actual material strength shown in Table 4-5 and Table 4-6. In the case of the exterior connection, P_{nb} is divided into positive and negative forces because P_{nb} is different depending on the direction of the force. As shown in Table 4-7, in the exterior connection connecting only one beam to the right joint face, P_{nb} is smaller than P_{nc} despite the small column section dimensions (strong column and weak beam behavior). This is because the exterior connection is connected to two columns (ΣM_{nc}) and one beam (M_{nb}) at the joint. On the other hand, in the case of the interior connection, P_{nb} is larger than P_{nc}; thereby, a weak column and strong beam behavior was expected.

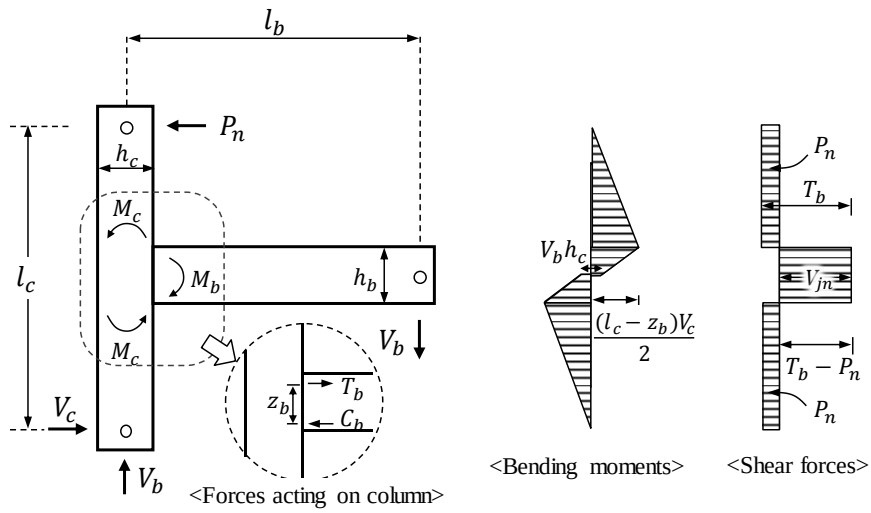

(a) Exterior beam-column connection

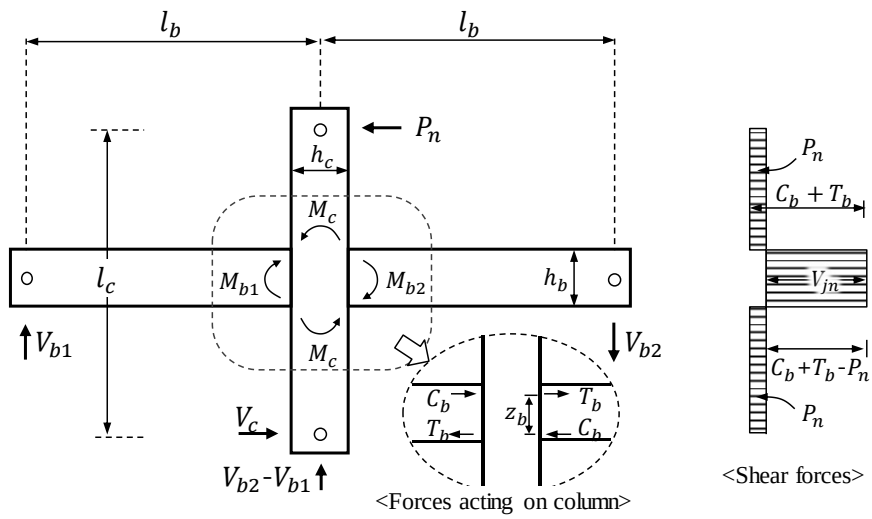

(b) Interior beam-column connection

Figure 4-40 Internal and external forces acting on beam-column connections

Table 4-7 Prediction of nominal strengths depending on failure modes

Speci-men	Column yielding		Beam yielding				Joint shear failure				Failure mode [4]		Anchorage length	
					P_{nb} (kN) [2]		Conforming		Non-conforming				l_{al}[5] [h_c] (mm)	l_{al} / l_{dh} [6] [h_c / d_b]
	M_{nc} (kN·m)	P_{nc}[1] (kN)	M_{nb1} (kN·m)	M_{nb2} (kN·m)	Positive	Negative	V_{jn}^{C}(kN)	P_{nj}^{C} (kN)[3]	V_{jn}^{NC} (kN)	P_{nj}^{NC}(kN)[3]	Positive	Negative		
EUN	196	**152**	209	392	**136**	**73**	-	-	273	**39.5**	J	J	300	**0.59**
EU2R	196	**152**	209	392	**136**	**73**	-	-	273	**39.5**	J	J	300	**0.59**
EU2U	196	**152**	209	392	**136**	**73**	-	-	273	**39.5**	J	J	300	**0.59**
EU4R	220	**171**	252	387	**135**	**88**	679	**99.1**	-	-	J	BJ	300	**0.96**
EU4U	220	**171**	252	387	**135**	**88**	679	**99.1**	-	-	J	BJ	300	**0.96**
EU4UC	369	**286**	252	387	**137**	**89**	873	**130**	-	-	J	BJ	400	**1.28**
IN	220	**171**	252	387	**222**	**222**	-	-	776	**82.6**	J	J	[350]	[18.4]
IU	220	**171**	252	387	**222**	**222**	1165	**124**	-	-	J	J	[350]	[18.4]

1) P_{nc} : Nominal joint strength due to column flexural yielding
2) P_{nb} : Nominal joint strength due to beam flexural yielding
3) P_{nj} : Nominal joint strength due to joint shear failure
4) J : Joint shear failure before beam and column flexural yielding , BJ : Joint shear failure after beam flexural yielding
5) l_{al} : Actual anchorage length provided in tests
6) l_{dh} : Required anchorage length specified in ACI 318-14

4.3.2 Joint shear failure

Joint shear strength considering the effect of transverse reinforcement was evaluated by using the nominal joint shear strength of ASCE 41-13 (FEMA 356) as follows.

$$V_{jn} = 0.083\gamma\sqrt{f_c'}A_j \tag{4-24}$$

where, γ is a factor considering the effect of confined joint concrete by transverse beams and joint transverse reinforcement ratio. According to ASCE 41-13 (FEMA 356 in parenthesis), for interior connections, γ = 15 [conforming] is used for joints with hoop spacing $s \le h_c/2$ (a transverse reinforcement volume ratio $\rho'' \ge 0.003$), and γ = 10 [non-conforming] is used for $s > h_c/2$ ($\rho'' < 0.003$). For exterior connections, γ = 12 [conforming] is used for $s \le h_c/2$ ($\rho'' \ge 0.003$), and γ = 6 [non-conforming] is used for $s > h_c/2$ ($\rho'' < 0.003$). h_c is dimension of column core in the direction of joint shear, and A_j is the effective horizontal joint area with dimensions.

In the case of exterior connections (see Figure 4-40(a)), vertical reaction force $V_b = P\cdot(l_c/l_b)$ is generated at the beam end due to the actuator lateral load on the top of the column. Thus, the beam flexural moment acting at the joint face is $M_b = P\cdot(l_c/l_b)\cdot(l_b - 0.5h_c)$. The nominal horizontal joint shear V_{jn} is the value obtained by subtracting the shear force (= P) of the column from tension force T_b (=M_b/z_b) in beam longitudinal reinforcement. It is noted that z_b is the value of moment arm of beam section. Therefore, the nominal strength P_{nj} of the exterior connection corresponding to the joint shear strength according to Equation (4-24) is determined as follows.

$$V_{jn} = T_b - P_{nj} = P_{nj}\left(\frac{l_c}{l_b}\right)\left(\frac{l_b - 0.5h_c}{z_b}\right) - P_{nj} \tag{4-25}$$

$$P_{nj} = \frac{V_{jn}}{\left(\frac{l_c}{z_b}\right) - \frac{1}{2}\left(\frac{l_c h_c}{l_b z_b}\right) - 1} \tag{4-26}$$

In the case of interior connections (see Figure 4-40(b)), vertical reaction forces V_{b1} and V_{b2} at both ends of the beam are generated due to the actuator lateral load on the column. Thus, the beam flexural moments $M_{b1} = V_{b1} \cdot (l_b - 0.5h_c)$ and $M_{b2} = V_{b2} \cdot (l_b - 0.5h_c)$ are applied to the left and right faces of the joint. The nominal horizontal joint shear V_{jn} is equal to the sum of T_{b1} ($=M_{b1}/z_b$) and C_{b2} ($=M_{b2}/z_b$), minus the column shear force P. The sum of the vertical reaction forces ($= V_{b1} + V_{b2}$) is equal to $P \cdot (l_c/l_b)$, depending on the force equilibrium condition of the joint. Therefore, the nominal joint shear strength V_{jn} and the corresponding nominal strength P_{nj} of the exterior connection according to Equation (4-24) is determined as follows.

$$\begin{aligned} V_{jn} &= C_{b2} + T_{b1} - P_{nj} = (V_{b1} + V_{b2})\left(\frac{l_b - 0.5h_c}{z_b}\right) - P_{nj} \\ &= P_{nj}\left(\frac{l_c}{l_b}\right)\left(\frac{l_b - 0.5h_c}{z_b}\right) - P_{nj} \end{aligned} \tag{4-27}$$

As the nominal strength of the interior connection from Equation (4-27) is equivalent to Equation (4-26), Equation (4-26) can be used for interior connections as well as exterior connections.

Table 4-7 presents nominal joint shear strengths P_{nj}^{C} and P_{nj}^{NC} due to joint shear failure. In this study, the strengths P_{nj}^{C} and P_{nj}^{NC} are classified according to conforming and non-conforming joint shear reinforcement of the ASCE 41-13 method. Specimens **EUN**, **EU2R**, **EU2U**, and **IN** correspond to non-conforming joint reinforcement, and specimens **EU4R**, **EU4U**, **EU4UC**, and **IU** correspond to conforming joint reinforcement. When calculating the nominal joint strength from (4-25) and (4-26), the moment arm z_b is assumed to be approximately 0.87 d_b (Park and Mosalam, 2012), where d_b is the effective depth of beam section. The moment arm z_b of 420 mm is used for all specimens.

4.3.3 Anchorage failure of beam longitudinal bars

If the joint depth h_c (or column section dimension) is small, the bond strength required for the yielding of the flexural reinforcement anchored with 90º standard hooks in the exterior joint may be insufficient. According to ACI 318-14, the minimum anchorage length of 90º standard hooks is as follows.

$$l_{dh} = \frac{f_y d_b}{4.2\sqrt{f_c'}} \cdot 0.7 \tag{4-28}$$

Equation (4-28) is the basic anchorage length of tensile deformed bars with standard hooks of ACI 318-14 multiplied by a correction factor of 0.7 for concrete cover thickness over 50 mm beyond hooks.

Table 4-7 shows the required anchorage length l_{dh} and actual anchorage length l_{al} of the beam flexural reinforcement for each exterior connection specimen. As shown in the table, specimens **EUN**, **EU2R**, and **EU2U** using D25 reinforcing bars had a significantly shortened anchorage length of beam reinforcement at l_{al} / l_{dh} = 0.59 in the joint area. This indicates that joint failure caused by anchorage failure with excessive slip of beam rebars can be occurred, and the load carrying capacity of the joints may be deteriorated. On the other hand, in specimens **EU4R**, **EU4U**, and **EU4UC** with D19 beam reinforcement (l_{al} / l_{dh} = 0.96 ~ 1.28), anchorage demand required by design criteria can be obtained, despite the small column depth and high yield strength (f_y = 577 MPa).

In the case of the interior connections **IN** and **IU** where the beam flexural reinforcement penetrates the joint and is anchored to the concrete compression zone of the opposite beam, the anchorage length of the reinforcing bar required for the flexural strength development of the beam is secured. However, h_c/d_b (=18.4) was significantly smaller than 20.0 required for joints in special moment frames as specified in ACI 318-14 chapter 18 (Table 4-3). When concrete damage is accumulated in the plastic hinge zone of the beam under the reversed cyclic loading, severe bond slip of the reinforcing bar and large shear deformation can be occurred in the joint region.

According to the preceding, failure modes of test specimens can be predicted. In specimens **EUN**, **EU2R**, and **EU2U**, joint shear failure occurs before beam and column flexural yielding, and bond slip occurs due to the lack of the anchorage length. Specimens **EU4R** and **EU4U** are dominated by joint shear failure in the positive direction and beam flexural yielding in the negative direction. Specimen **EU4UC** is subjected to beam flexural yielding in the negative direction due to increase of the effective joint area, and joint shear failure and beam flexural yielding simultaneously occurred in the positive direction. Since the interior connection specimens **IN** and **IU** have a small effective joint area, joint shear failure occurs before beam and column flexural yielding.

4.4 Load - Displacement Relations and Failure Modes

4.4.1 Exterior beam and column connections

Figure 4-41 shows the lateral load (P) and drift ratio (δ) relations of exterior beam and column connections. P is the actuator load acting on the upper part of the column, and δ is drift ratio obtained by dividing the column lateral displacement by the net column height (= 3060 mm) between the loading point and the hinge support. Positive load ($P > 0$) is the state where negative moment (tension in the beam top bars) is applied in the beam. The maximum positive and negative loads P_u are indicated with circular marks on the P - δ cyclic curves. For comparison, the nominal strengths P_{nb}, P_{nc}, and P_{nj} calculated for failure modes in section 4.3 are also marked as horizontal dashed lines in Figure 4-41.

Test strength, predicted strength by actual failure mode, and ductility are summarized in Table 4-8. The ductility is the value obtained by dividing the maximum drift ratio δ_u by the yield drift ratio δ_y. The yield drift ratio δ_y is defined as the point at which the maximum load reaches 60% of the maximum load and the secant stiffness of the origin, and the maximum drift ratio δ_u is defined as the smaller of the positive and negative maximum drift ratios corresponding to 80% of the maximum load.

Cracking patterns and failure modes of exterior connection specimens at drift ratio of 1.5, 2.0, 2.5, 3.5, and 5.0% are shown in Figure 4-42. For a clear view of fine cracks, the crack patterns were reproduced until drift ratio of 2.5%. From drift ratio of 3.5%, as the major cracks were clearly visible, the photographs were compared.

For detailed evaluation of each specimen, the front and side crack patterns at drift ratio of 0.75, 1.5, 2.0, 2.5, 3.5, 5.0% and final failure patterns were illustrated, and the lateral load and drift ratio relations with the same axis scale were presented in Figure 4-43 ~ Figure 4-54.

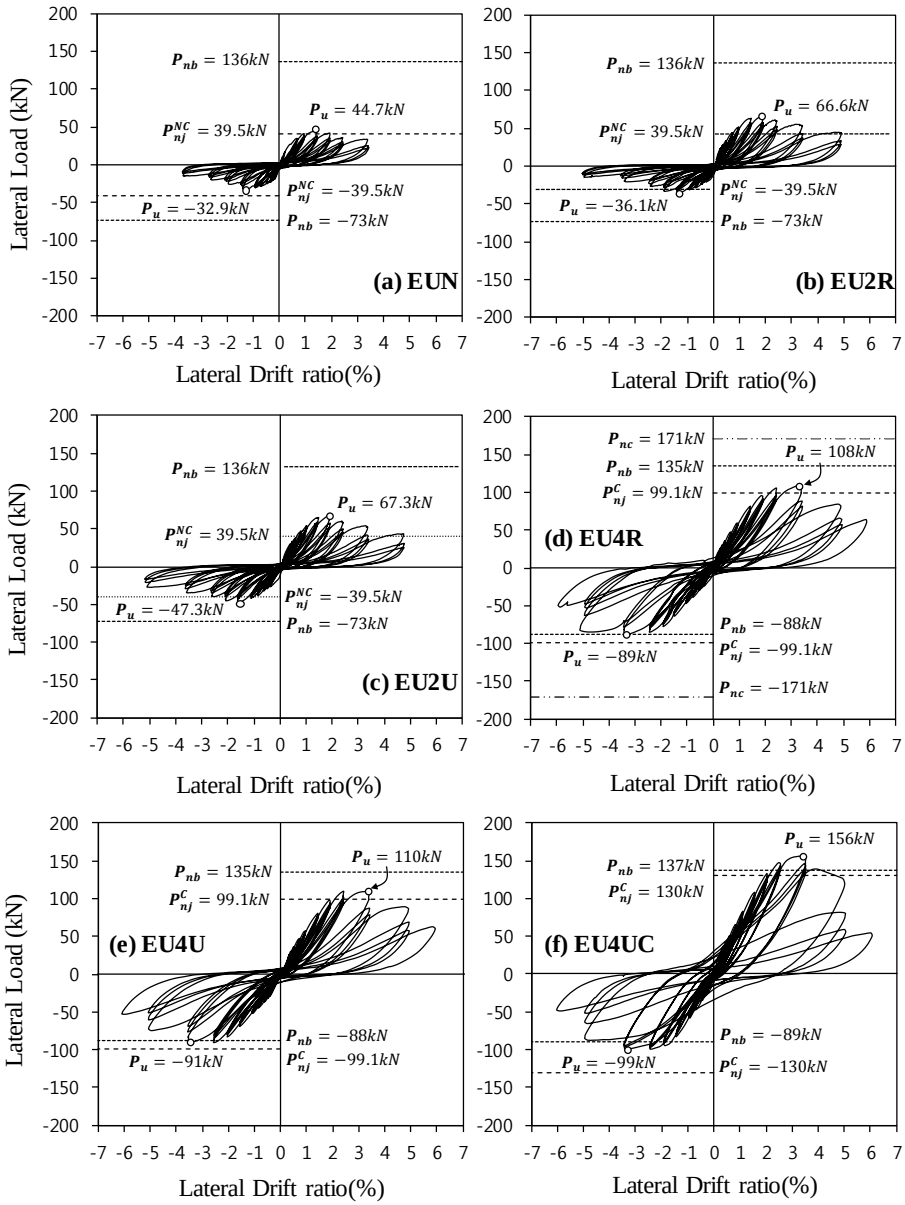

Figure 4-41 Lateral load and drift ratio relationship of exterior connection specimens

Table 4-8 Summary of test results (strength, failure mode, and ductility)

Specimen	Test strength (P_u) [1]		Predicted strength (P_n) [2]		Strength ratio(P_u / P_n)		Failure mode [3]		Average drift ratio (%)		Ductility (δ_u / δ_y)
	Positive	Negative	Positive	Negative	Positive	Negative	Positive	Negative	Yield (δ_y) [4]	Ultimate (δ_u) [5]	
EUN	44.7	32.9	39.5	39.5	1.13	0.83	J	J	0.58	2.48	4.28
EU2R	66.6	36.1	39.5	39.5	1.69	0.91	J	J	0.78	2.93	3.78
EU2U	67.3	47.3	39.5	39.5	1.70	1.20	J	J	0.87	3.34	3.86
EU4R	108	89	99.1	88	1.09	1.01	J	BJ	1.84	5.21	2.83
EU4U	110	91	99.1	88	1.11	1.03	J	BJ	1.91	4.95	2.59
EU4UC	156	99	137	89	1.14	1.11	BJ	BJ	1.88	5.03	2.75
IN	144	137	82.6	82.6	1.74	1.66	J	J	1.81	3.92	2.17
IU	162	154	124	124	1.31	1.24	J	J	2.10	5.13	2.44

1) P_u : Ultimate test loads
2) P_n : Nominal strengths calculated for failure modes in 4.3
3) J : Joint shear failure before beam and column flexural yielding , BJ : Joint shear failure after beam flexural yielding
4) δ_y : Yield drift ratio defined as the point at which the maximum load reaches 60% of the maximum load and the secant stiffness of the origin
5) δ_u : Ultimate drift ratio defined as the smaller of the positive and negative maximum drift ratios corresponding to 80% of the maximum load

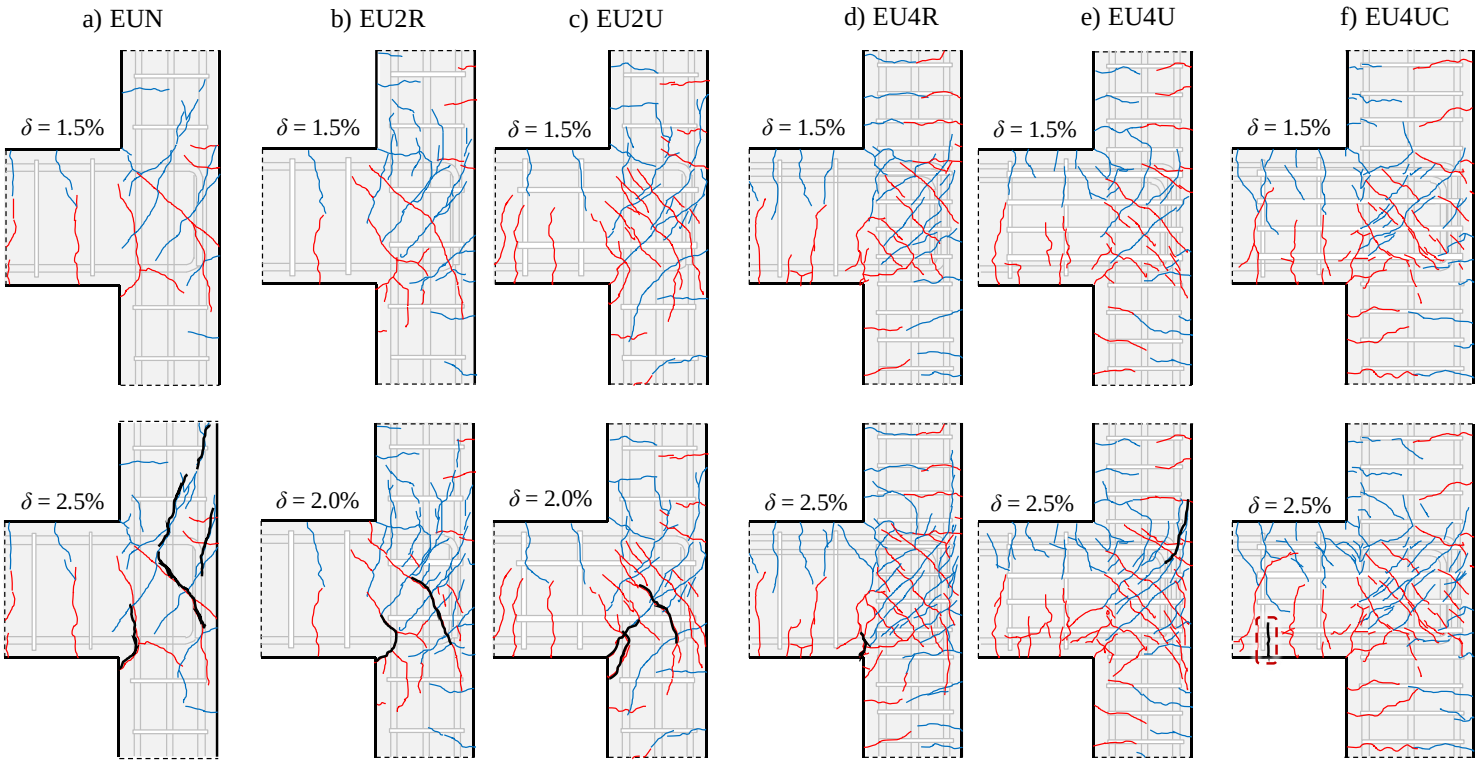

Figure 4-42 Cracking patterns and failure modes of exterior connection specimens at each drift ratio (Continued)

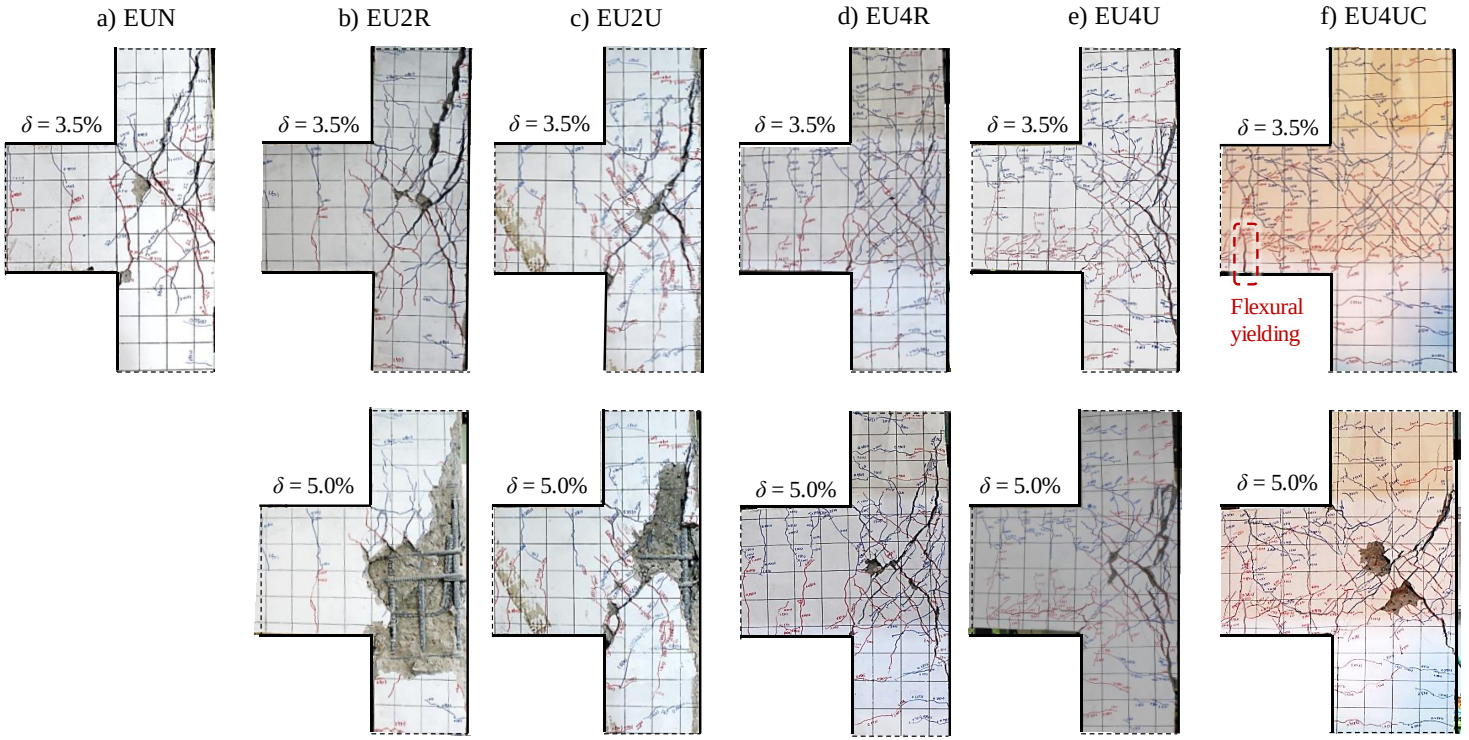

Figure 4-42 Cracking patterns and failure modes of exterior connection specimens at each drift ratio

(1) Non-conforming exterior connections (**EUN**, **EU2R**, and **EU2U**)

As shown in Figure 4-41(a) ~ (c) and Figure 4-42(a) ~(c), specimens **EU2R** and **EU2U** with joint shear reinforcement volume ratio ρ'' of less than 0.003 showed similar cyclic behavior and failure modes to specimen **EUN** without joint shear reinforcement. The specimens showed the maximum load at the drift ratio of 1.5 ~ 2.0%, and then the joint shear crack was enlarged with a decrease in strength. Finally, the anchorage failure of beam longitudinal rebars with severe diagonal shear cracks occurred at the drift ratio of 3.5%. On the other hand, in the adjacent beams and columns, relatively fewer shear cracks were developed than joints. Also, pinching occurred significantly under cyclic loads, thereby decreasing energy dissipation capacity. These results demonstrate that failure modes and cyclic behaviors of **EUN**, **EU2R**, and **EU2U** were dominated by joint shear behavior.

The positive and negative loads P_u of **EUN**, **EU2R**, and **EU2U** were over 50% smaller than P_{nb} due to flexural yielding (= +136 kN and -73 kN), indicating that joint shear failure occurred before beam flexural yielding. For **EN** without joint shear rebars, the maximum positive and negative loads P_u (= +44.7 kN and -32.9 kN) were similar to the nominal joint shear strength P_{nj}^{NC} (= ±39.5 kN, non-conforming). On the other hand, the maximum positive load P_u (= +66.6~67.3 kN) of **EU2R** and **EU2U** with joint shear rebars increased about 50% from **EN** as the joint shear strength is increased by the influence of joint shear reinforcement. However, the maximum negative load P_u (= +36.1~47.3 kN) of **EU2R** and **EU2U** was significantly smaller than the positive direction, which related to the lack of the anchorage length of 90º standard hooks in the joint (l_{al} / l_{dh} = 0.59, see Table 4-7).

In order to analyze the failure sequence and the effect of test parameters on each specimen, specimens **EUN**, **EU2R**, and **EU2U** were investigated in Figure 4-43 ~ Figure 4-48.

A. Specimen EUN

The Specimen **EUN** has no joint shear reinforcement and insufficient anchorage length of beam longitudinal bars in the joint (l_{al} / l_{dh} = 0.59). Joint shear failure is expected in both positive and negative directions.

1. Since the force (moment and shear) transfer through the joint was not successful, a relative small number of cracks were developed, so the crack width increased. Crack patterns in Figure 4-44 support this.

2. The maximum negative load did not reach the nominal joint shear strength P_{nj}^{NC} because the anchorage length of 90º standard hooks of beam rebars in the joint was insufficient. At drift ratio of 1.5% reached maximum load, side vertical crack was developed due to 90º hooks of beam rebars.

3. As the drift ratio increased, vertical cracks on the side were propagated to the column, and the crack width became larger, leading to the anchorage failure of **EUN** with severe shear cracks in the joint.

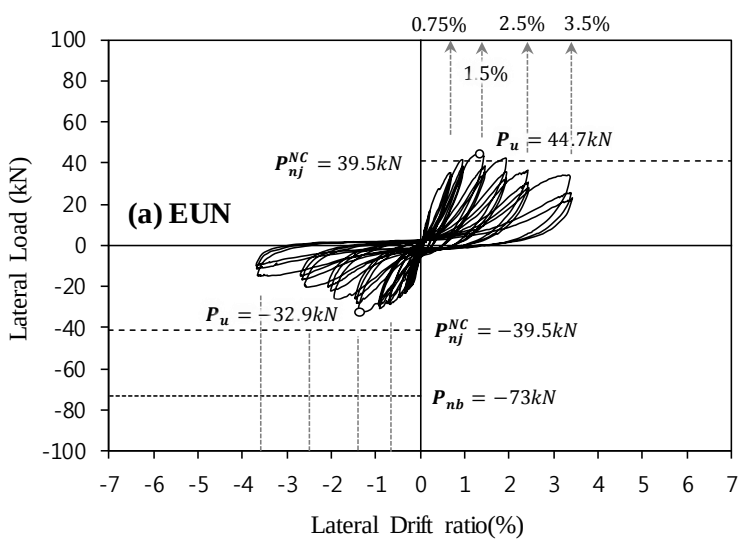

Figure 4-43 Lateral load and drift ratio relationship of specimen EUN

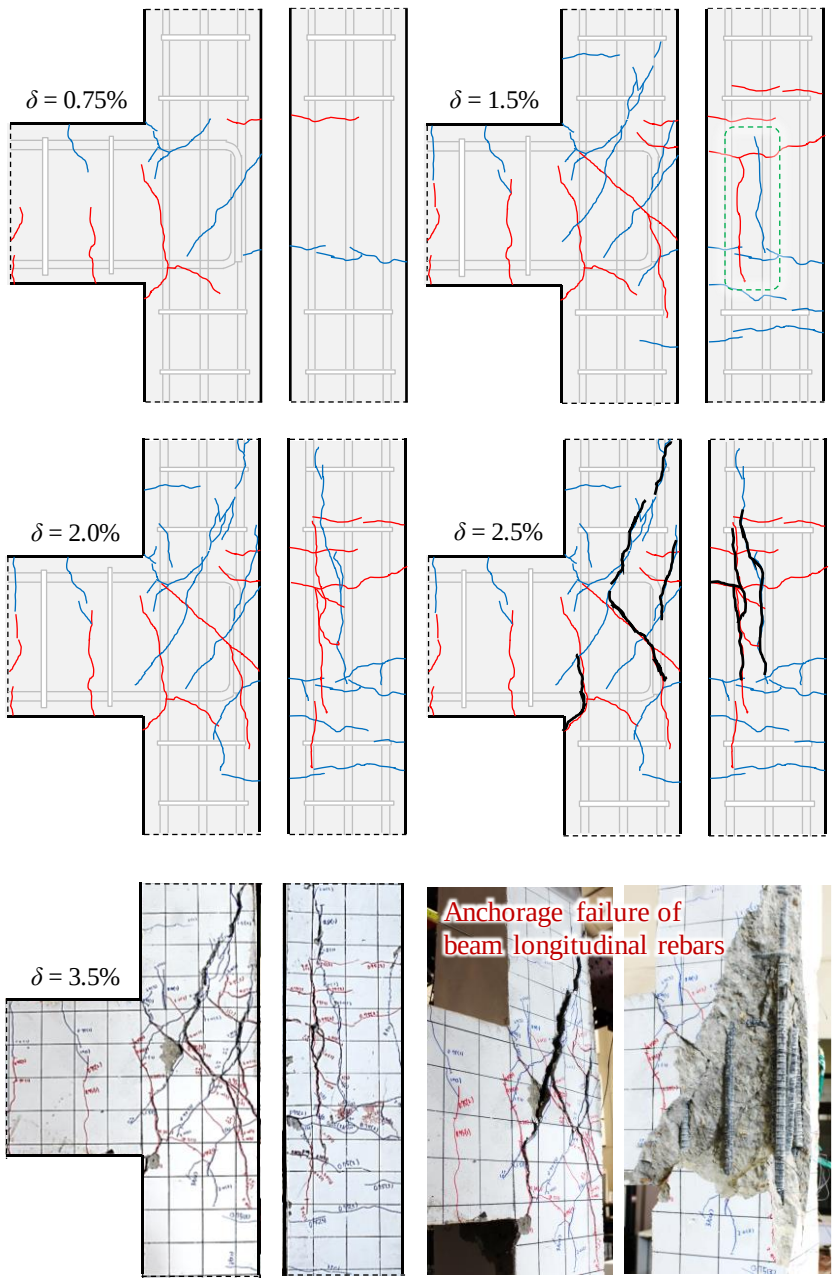

Figure 4-44 Failure sequence and final failure mode of specimen EUN

B. Specimen EU2R

The Specimen **EU2R** has joint shear reinforcement of less than 0.003 (Non-conforming) and insufficient anchorage length of beam longitudinal bars in the joint ($l_{al} / l_{dh} = 0.59$). Joint shear failure is expected in both positive and negative directions.

1. The maximum positive load increased by 49% with the use of joint shear reinforcement; on the other hand, the increase of the maximum negative load was insignificant. Joint shear reinforcement showed a large reinforcing effect in the positive direction with large beam flexural reinforcement ratio.

2. As the joint shear reinforcement was used, the number of cracks in the joints increased compared to specimen **EUN**. In addition, the side vertical cracks caused by 90º hooks were delayed to drift ratio of 2.0% at maximum load.

3. Similar to specimen **EUN**, vertical cracks on the side were propagated to the column, and concrete cover in the joint was spalled off at drift ratio of 5.0%. The 90º hooks was loosened and anchorage failure of beam bars occurred at the end.

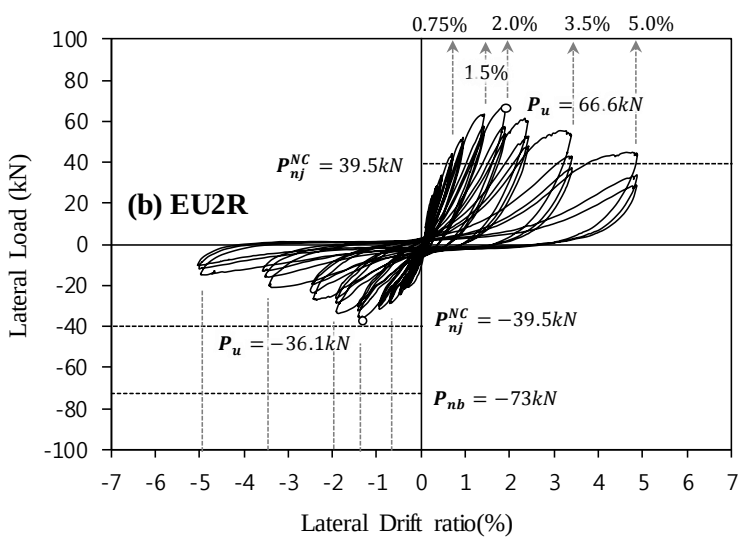

Figure 4-45 Lateral load and drift ratio relationship of specimen EU2R

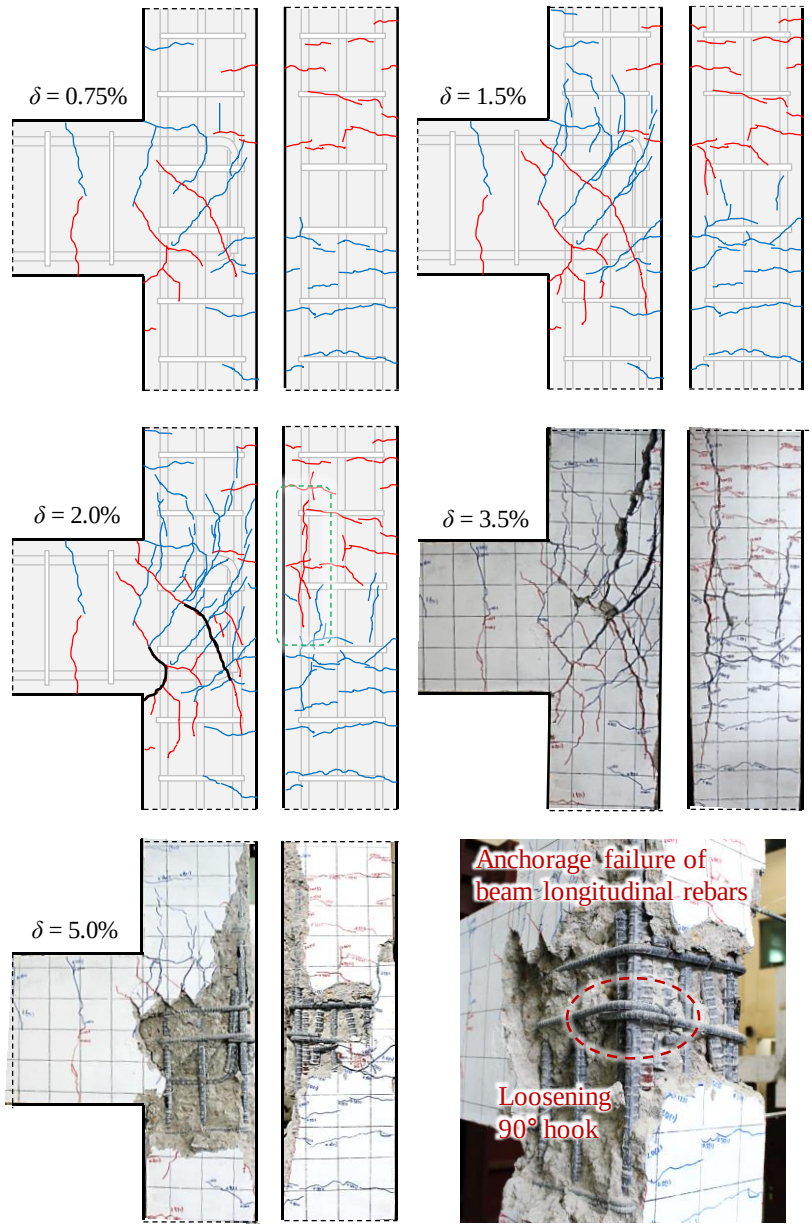

Figure 4-46 Failure sequence and final failure mode of specimen EU2R

C. Specimen EU2U

The Specimen **EU2U** has joint shear reinforcement of less than 0.003 (Non-conforming) and insufficient anchorage length of beam longitudinal bars in the joint (l_{al} / l_{dh} = 0.59). The U shaped bars were used for joint shear reinforcement. Joint shear failure is expected in both positive and negative directions.

1. Compared with **EU2R**, specimen **EU2U** has slightly increased maximum load in the positive direction, and maximum negative load increased more than 30%, thereby exceeding the nominal joint shear strength P_{nj}^{NC} in the negative direction. As a result, diagonal shear cracks in the joints increased as shown in Figure 4-48. In negative direction, U-bar acts as a flexural reinforcement and increases to maximum load as it is anchored into the beam.

2. Similar to **EU2R**, at maximum load (drift ratio of 2.0%), the side vertical cracks initiated due to 90º hooks of beam rebars. The vertical cracks were propagated to the column, and concrete cover in the joint was spalled off at drift ratio of 5.0%. Nevertheless, the U-bar was firmly anchored in the adjacent beam.

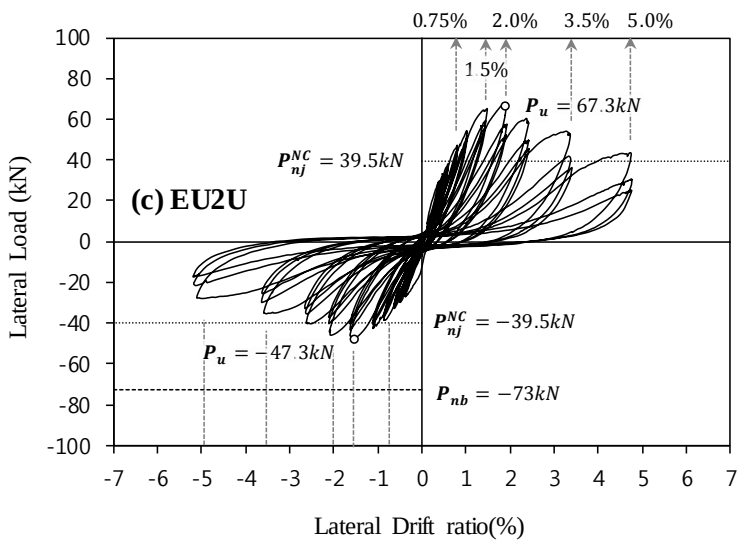

Figure 4-47 Lateral load and drift ratio relationship of specimen EU2U

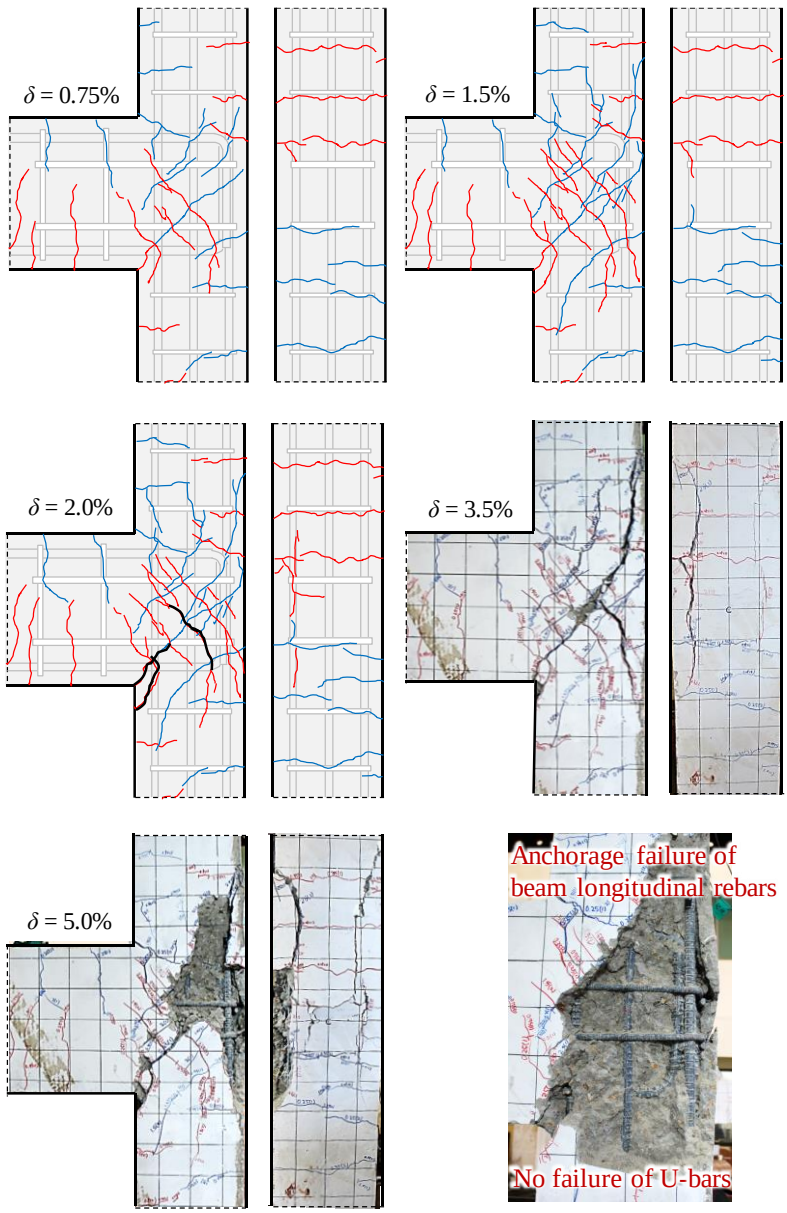

Figure 4-48 Failure sequence and final failure mode of specimen EU2U

(2) Conforming exterior connections (**EU4R**, **EU4U**, and **EU4UC**)

Figure 4-41(d) ~ (f) and Figure 4-42(d) ~ (f) present specimens **EU4R**, **EU4U**, and **EU4UC** with joint shear reinforcement volume ratio ρ'' of greater than 0.003 and joint reinforcement spacing reduced to 100 mm. Specimens **EU4R** and **EU4U** showed almost the same cyclic behavior and failure modes. As shown in Figure 4-42(d) and (e), compared with **EU2R** and **EU2U**, joint concrete cracks and damage were not large even at the maximum load when the joint shear reinforcement restrained the shear cracks at drift ratio of ±3.0 ~ 3.5%. The specimens were failed with joint concrete crushing and excessive shear cracking at drift ratio of 5.0%. Pinching occurred significantly during cyclic loading because **EU4R** and **EU4U** were dominated by joint shear deformation.

As the joint shear reinforcement ratio increased and sufficient anchorage length of beam rebars was secured (l_{al} / l_{dh} = 0.96 ~ 1.28), the maximum loads of specimens **EU4R** and **EU4U** increased by more than 60% compared to those of **EU2R** and **EU2U**. The maximum positive load P_u (= 108 ~ 110 kN) was smaller than the nominal joint strength P_{nb}^{+} (= 135 kN) due to beam flexural yielding, but the maximum negative load P_u (= 89 ~ 91 kN) was almost the same as P_{nb}^{-} (= 88 kN). This indicates that the beam yielded in the negative direction but not in the positive direction. The maximum positive load P_u (= 108 ~ 110 kN) are closely related to the nominal strength P_{nj}^{C} due to joint shear failure by Equations (4-25) and (4-26).

The specimen **EU4UC** with the column depth increased to 450 mm yielded at drift ratio of 2.0% and reached maximum loads P_u (=+156 kN and -99 kN) at drift ratio of 3.5%. As the joint area increased, the maximum positive load increased by 43% compared to specimens **EU4R** and **EU4U** by increased joint shear strength in Equation (4-24). Joint shear cracking was not significant until the maximum load occurred, but joint damage rapidly expanded and finally failed at drift ratio of 5.0% by excessive shear cracking. Such failure mode can be deduced from the load and drift ratio curve in Figure 4-41(f). In **EU4UC**, energy dissipation capacity was large because pinching was not large before drift ratio of 3.5%; however, at drift ratio of 3.5% where joint shear cracks increased significantly, pinching and strength degradation occurred, thereby decreasing energy dissipation capacity.

In specimen **EU4UC**, the maximum positive and negative loads P_u (=+156 kN and -99 kN) were greater than the nominal joint strength P_{nb} (=+137 kN and -89 kN) due to beam flexural yielding, which indicates that joint shear failure occurred after flexural yielding of beam top and bottom longitudinal reinforcement.

In order to analyze the failure sequence and the effect of test parameters on each specimen, specimens **EU4R**, **EU4U**, and **EU4UC** were investigated in Figure 4-49 ~ Figure 4-54.

D. Specimen EU4R

The Specimen **EU4R** has joint shear reinforcement of greater than 0.003 (Conforming) and almost satisfied anchorage length of beam longitudinal bars in the joint (l_{al} / l_{dh} = 0.96). Joint shear failure is predicted for positive direction and beam flexural yielding for negative direction.

1. As the maximum loads were significantly increased, the nominal joint shear strength $P_{nj}{}^{C}$ was exceeded in the positive direction and the the nominal strength P_{nb} for beam flexural yielding was reached in the negative direction. Because of the small joint size, joint shear failure occurred before reaching beam flexural yielding in the positive direction.

2. Side vertical cracks initiated at drift ratio of 2.5% were restrained by sufficient joint shear reinforcement and did not propagate to the adjacent column. Therefore, the load reduction did not occur up to drift ratio of 3.5%.

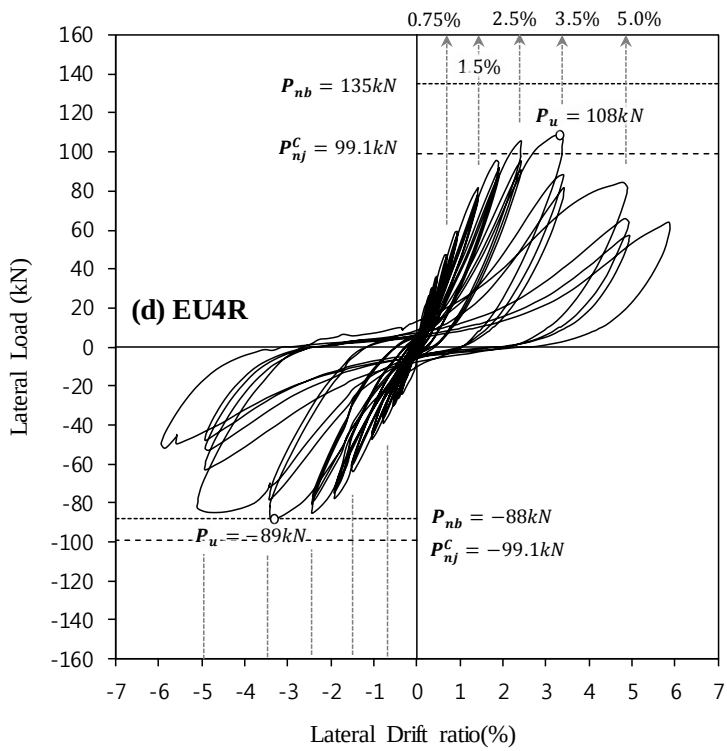

Figure 4-49 Lateral load and drift ratio relationship of specimen EU4R

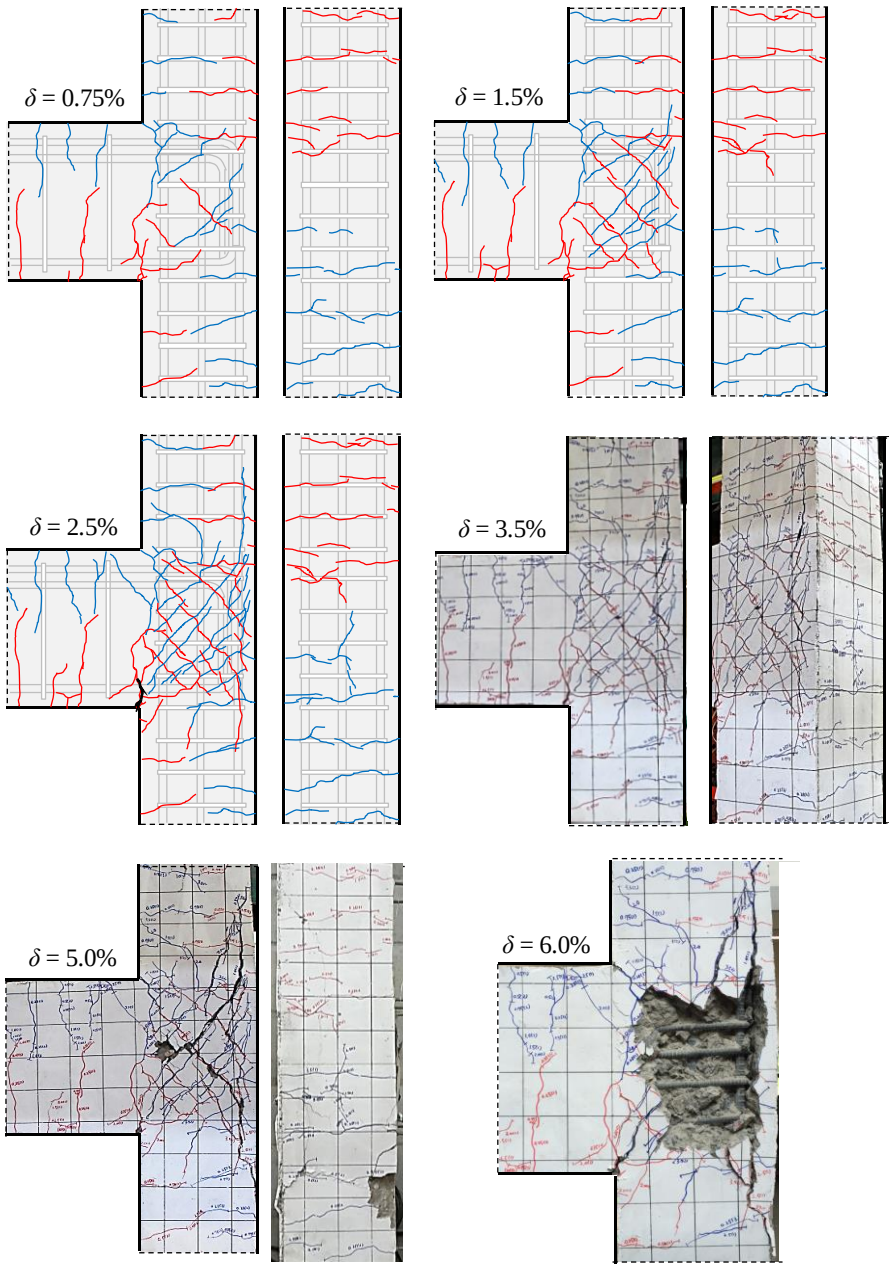

Figure 4-50 Failure sequence and final failure mode of specimen EU4R

E. Specimen EU4U

The Specimen **EU4U** has joint shear reinforcement of greater than 0.003 (Conforming) and almost satisfied anchorage length of beam longitudinal bars in the joint (l_{al} / l_{dh} = 0.96). The U shaped bars were used for joint shear reinforcement. Joint shear failure is predicted for positive direction and beam flexural yielding for negative direction.

1. Compared with **EU4R**, specimen **EU4U** showed almost the same load and drift ratio relationship and failure sequence. As joint shear failure occurred before beam flexural yielding in the positive direction, the shear strength of conforming exterior joints can be predicted with the maximum positive load in the test.

2. Excessive diagonal shear damage was accumulated in the joint until drift ratio of 5.0% and concrete cover was spalled off at drift ratio of 6.0%, but U-bar was sufficiently anchored into the beam at the end of test.

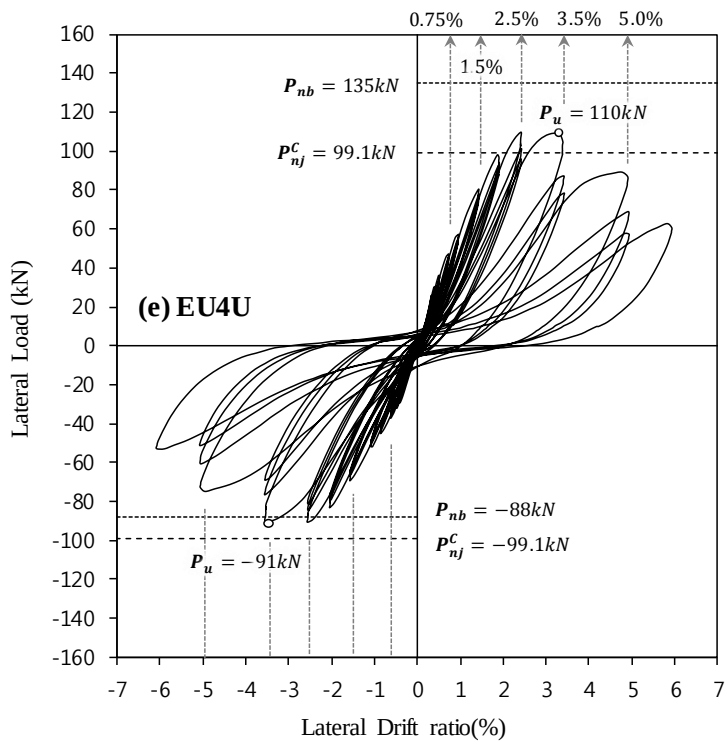

Figure 4-51 Lateral load and drift ratio relationship of specimen EU4U

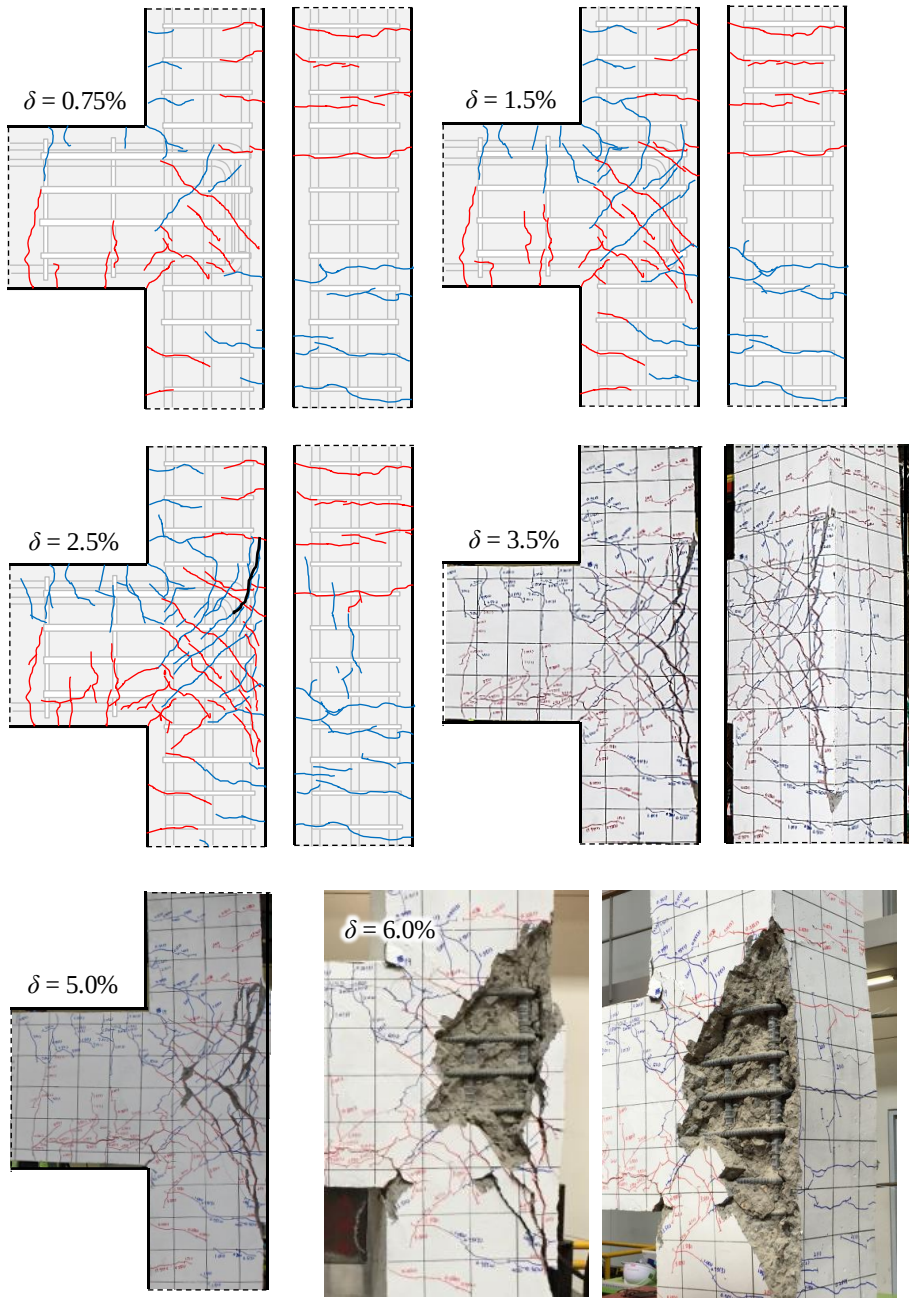

Figure 4-52 Failure sequence and final failure mode of specimen EU4U

F. Specimen EU4UC

The Specimen **EU4UC** has joint shear reinforcement of greater than 0.003 (Conforming) and sufficient anchorage length of beam longitudinal bars in the joint (l_{al} / l_{dh} = 1.28). The U shaped bars were used for joint shear reinforcement and the column depth was increased to 450 mm to increase the joint effective area. Beam flexural yielding before joint shear failure is expected for both positive and negative directions.

1. After beam flexural yielding occurred in both directions, joint shear failure occurred because join shear capacity increased and sufficient anchorage length of beam bars was secured. As flexural yielding occurred, the major flexural cracks occurred at the end of U-bar at drift ratio of 2.5% in Figure 4-54 .

2. Though severe diagonal shear crack and concrete cover spalling off were occurred in the joint at drift ratio of 5.0% and 6.0%, respectively, U-bar was anchored in the beam.

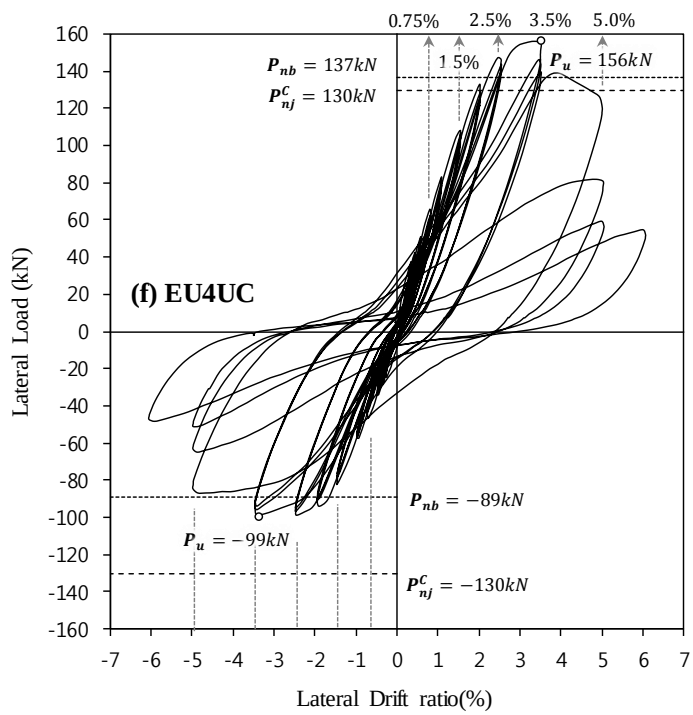

Figure 4-53 Lateral load and drift ratio relationship of specimen EU4UC

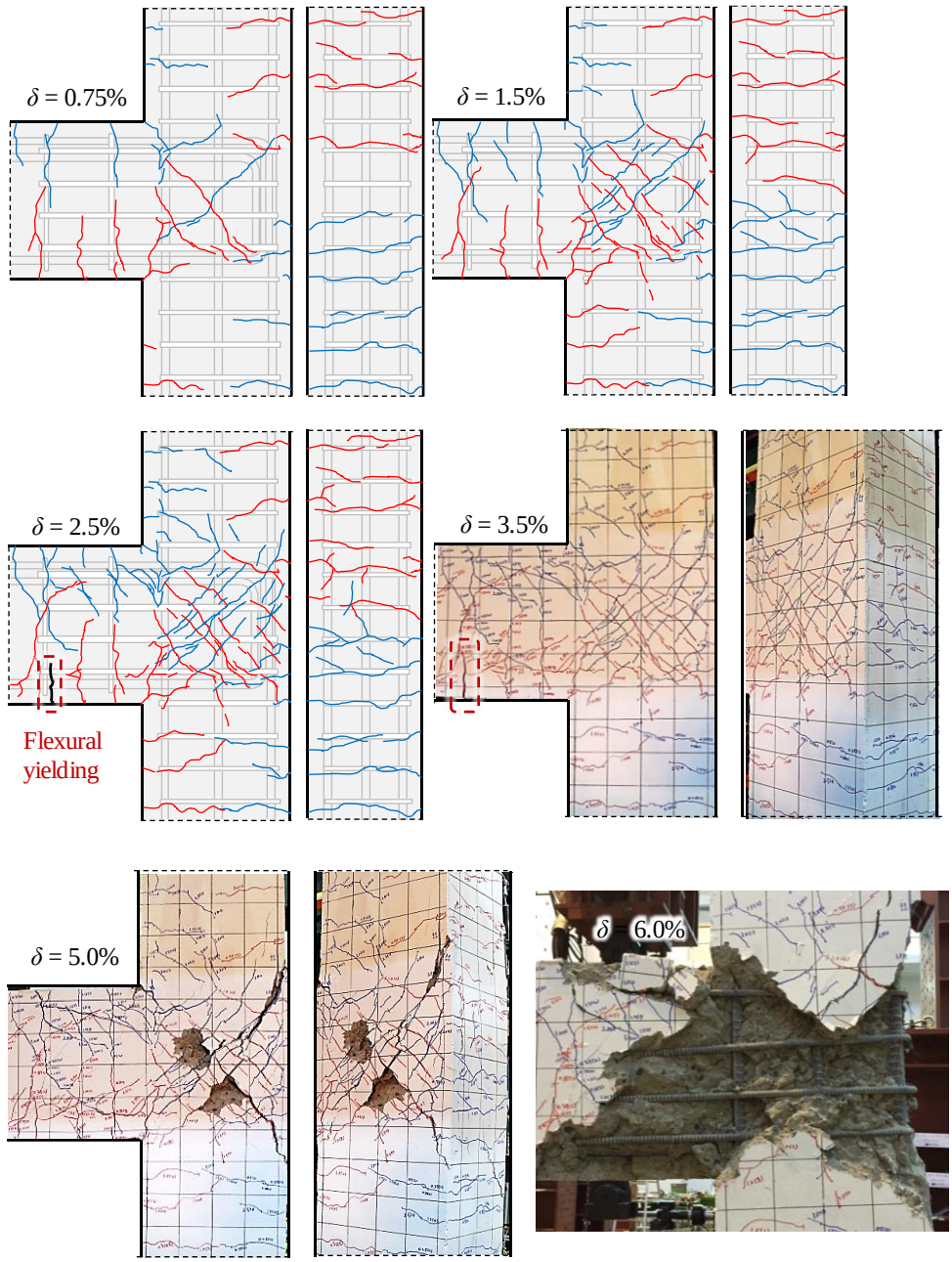

Figure 4-54 Failure sequence and final failure mode of specimen EU4UC

4.4.2 Interior beam and column connections

Figure 4-55 compares the lateral load (P) and drift ratio (δ) relations of interior beam and column connection specimens **IN** and **IU**. Each load and drift ratio relation was presented in Figure 4-56 and Figure 4-58. The crack patterns at drift ratio of 0.75, 1.5, 2.5, 3.5, 5.0, 6.0% and final failure patterns were illustrated in Figure 4-57 and Figure 4-59.

Specimen **IN** without joint shear reinforcement reached maximum load at drift ratio of 2.5% and then failed at drift ratio of 3.5% due to concrete crushing and shear cracking in the joint (See Figure 4-57). On the other hand, specimen **IU** with joint shear reinforcement of s = 100 mm reached maximum load at drift ratio of 3.5% and joint concrete crushed at drift ratio of 5.0%. Because of the small effective joint area, both specimens **IN** and **IU** developed excessive shear cracks and concrete crushing in joints, but cracks and damage in beams and columns were relatively insignificant.

In specimens **IN** and **IU**, the joint shear failure occurred before column flexural yielding because the maximum load was smaller than the nominal joint strength P_{nc} (= 171 kN, See Table 4-7) due to column yielding. Specimen **IN** showed maximum loads P_u (= +144 kN and -137 kN) about 70% larger than the nominal joint shear strength P_{nj}^{NC} (= ±82.6 kN, non-conforming), despite the absence of joint shear reinforcement. Specimen **IU** showed P_u (= +162 kN and -154 kN) about 23% greater than the joint shear strength P_{nj}^{C} (= ±124 kN, conforming). However, it was about 5~10% smaller than P_{nc} (= 171 kN).

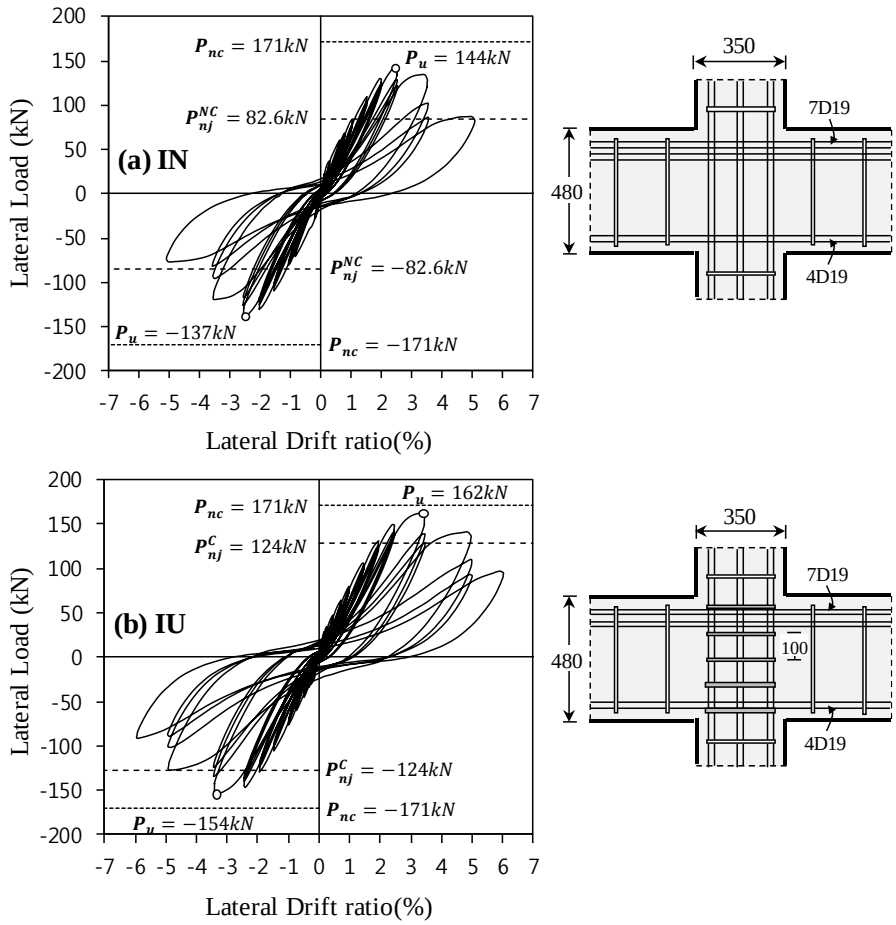

Figure 4-55 Lateral load and drift ratio relationship of exterior connection specimens

A. Specimen IN

The Specimen **IN** has no joint shear reinforcement. Joint shear failure is expected in both directions. Unlike exterior connections, the force transfer through the joint was successful. A number of joint shear cracks were developed until drift ratio of 2.5%, and then joint concrete was crushed at drift ratio of 3.5%. As the drift ratio increased to drift ratio of 5.0%, the joint concrete cover spalled off. Finally, shear failure occurred in the joint.

The diagonal crack width gradually increased and concrete crushing initiated at drift ratio of 2.5% at which the maximum load occurred, and the load was no longer increased.

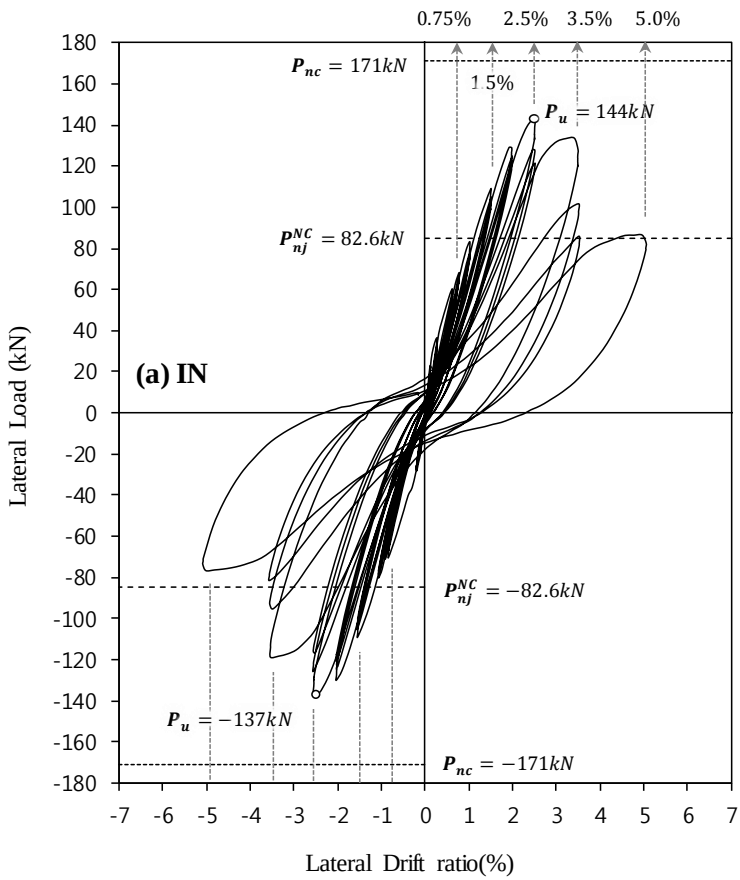

Figure 4-56 Lateral load and drift ratio relationship of specimen IN

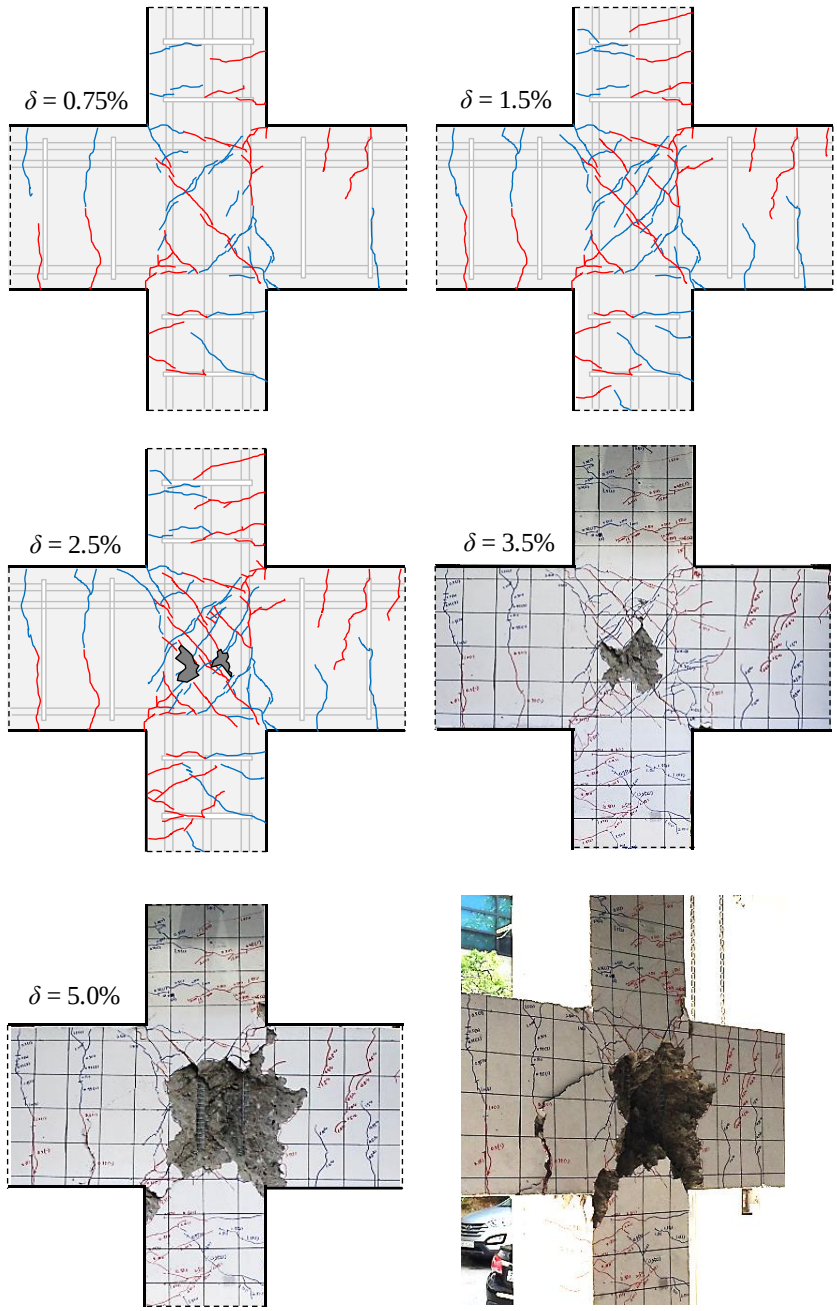

Figure 4-57 Failure sequence and final failure mode of specimen IN

B. Specimen IU

The Specimen **IU** has joint shear reinforcement at a spacing of 100 mm. Joint shear failure is expected in both directions as shown in Table 4-8. As compared with specimen **IN**, the number of joint shear cracks was significantly increased, which leading to increase loading capacity by 13% and displacement ductility by 12%. It is noted that the joint reinforcement improved the force transfer through the joint.

Although the joint reinforcement was sufficient, the joint shear failure occurred before beam and column flexural yielding due to the small effective joint area. This indicates that the effective area plays an important role in the joint behavior than the joint shear reinforcement.

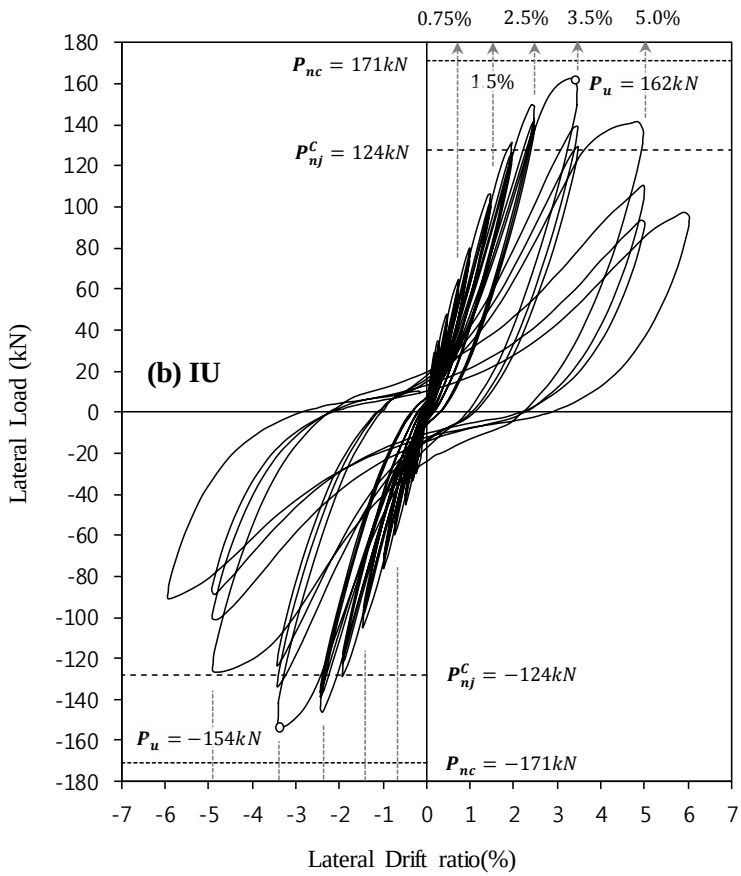

Figure 4-58 Lateral load and drift ratio relationship of specimen IU

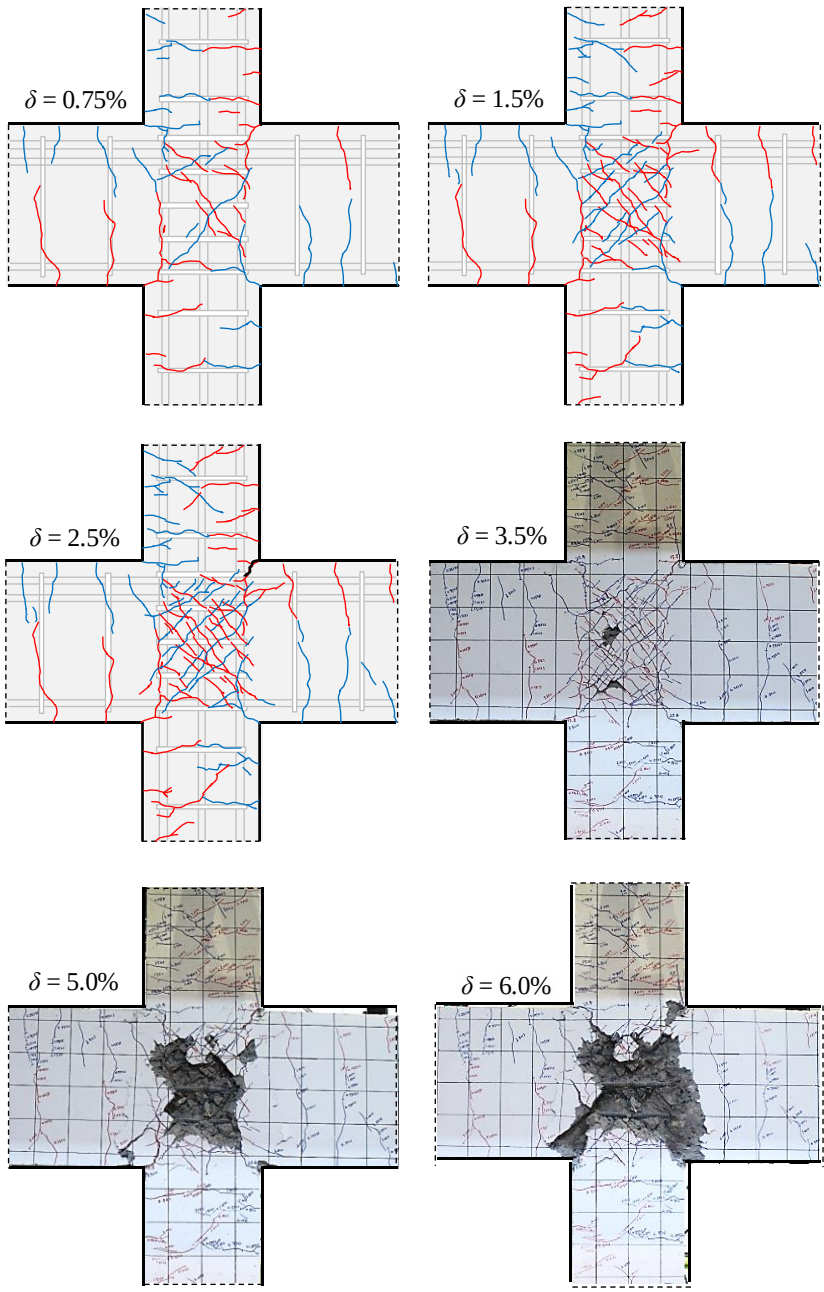

Figure 4-59 Failure sequence and final failure mode of specimen IU

4.5 Strain of Steel Reinforcing Bars

4.5.1 Exterior beam and column connections

4.5.1.1 Strains of beam longitudinal bars

Figure 4-60 shows strains of beam flexural bars at the joint of exterior connection specimens. The horizontal and vertical axes denote lateral drift ratio of columns and measured strains, respectively. The location of strain measurement for each specimen is shown in the figure.

In the case of **EUN** and **EU2R** using D25 reinforcing bars as the flexural reinforcement (l_{al} / l_{dh} = 0.59), the anchorage failure of beam bars occurred with the sudden increase or rapid decrease of the strain at drift ratio of 1.5 ~ 2.0% due to the short anchorage length. Such measurement implies that the anchorage failure and slip occurred significantly in D25 reinforcing bars with 90º standard hooks inside the joint after drift ratio of ±1.5%. The anchorage failure of beam bars was also observed in specimen **EU2U**. On the other hand, in the case of **EU4R** and **EU4U** using D19 reinforcing bars as the flexural reinforcement (l_{al} / l_{dh} = 0.96), the beam bottom bars exceeded the tensile yield strain (= 0.00275 mm/mm) up to ±3.5 ~ 5.0%.

In **EU4UC** where the column depth was increased to 450 mm and the anchorage length of beam bars was sufficiently secured (l_{al} / l_{dh} = 1.28), the strains of beam top and bottom bars retained its tensile strain higher than the yield strain (= 0.00275 mm/mm) to drift ratio of ±5.0%. The strain curves were more stable than those of other specimens as the effective joint area increased. Figure 4-60 (c) ~ (f) showed that the beam longitudinal bars using relatively small diameter D19 retained their anchorage performance until the end of tests.

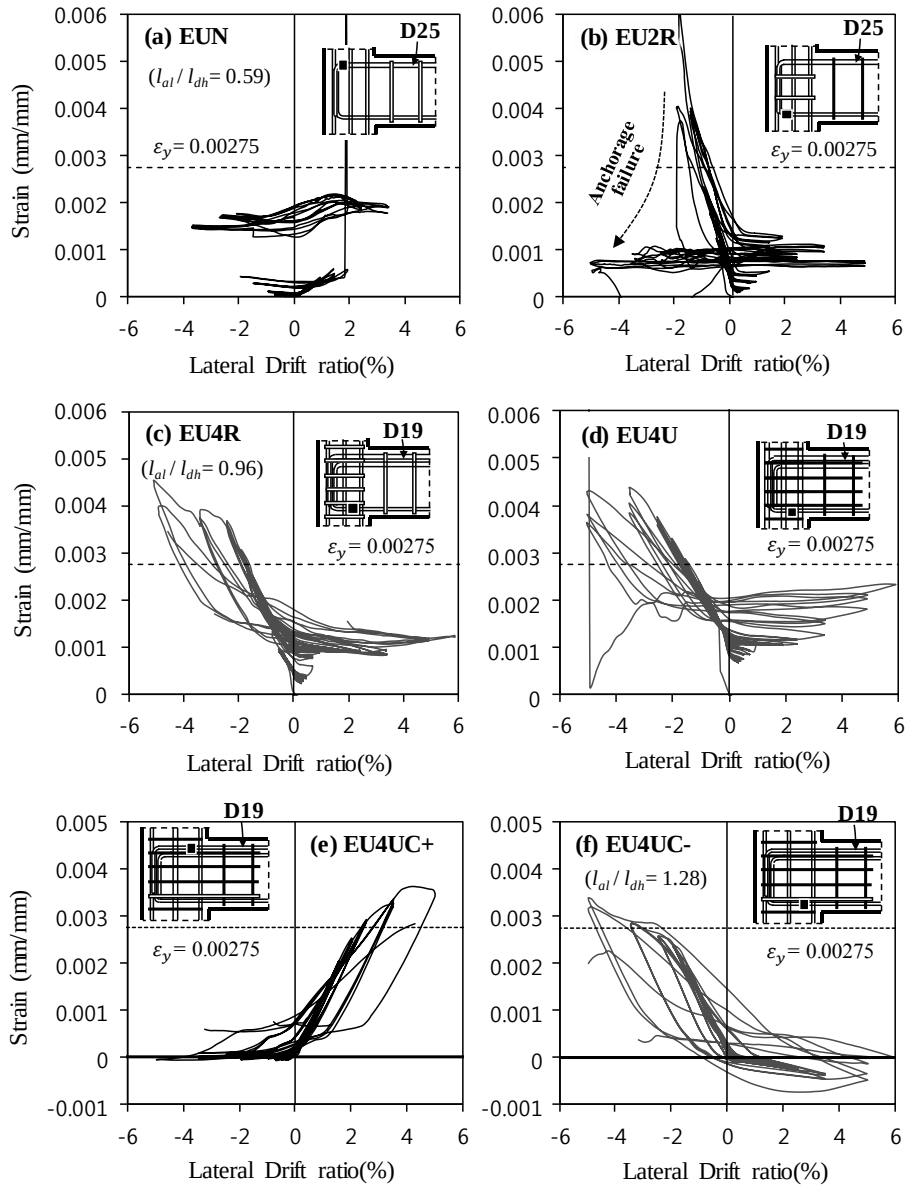

Figure 4-60 Strains of beam bars at the joints of exterior connections

4.5.1.2 Strains of joint shear reinforcement

Figure 4-61 shows the measured strains at joint shear reinforcement. The strains were measured at a perimeter tie in **EU2R**, at a cross tie in **EU4R**, and at U-bars in **EU2U**, **EU4U**, and **EU4UC**. The following results can be obtained from the strain measurement.

1. In the case of **EU2R** and **EU2U** with insufficient joint shear reinforcement ($\rho'' < 0.003$, non-conforming), the shear reinforcement began to increase sharply from drift ratio of 0.5 ~ 1.0% at which the joint shear cracks initiated, and yielded at drift ratio of 2.0 ~ 2.5% where the maximum load was reached. The yielded shear reinforcement cannot increase the joint shear resistance even if the bar strain increases. Thus, the load capacity of **EU2R** and **EU2U** decreased gradually after drift ratio of 2.5% (see Figure 4-41(b) ~ (c)). Further, specimens **EU4R** and **EU4U** with increased joint shear reinforcement ($\rho'' > 0.003$, conforming) also yielded at the maximum load when drift ratio was 3.5%, and then the load capacity began to decrease after drift ratio of 3.5%.

2. For **EU4UC** with increased joint shear strength V_{jn} as calculated from Equation (4-24) by increasing column depth, the joint shear reinforcement reached to the yield strain at drift ratio of 3.5%, and then the load capacity was gradually decreased from 3.5% to 5.0% as shown in Figure 4-41(f). This indicates that the concrete shear resistance of the joint decreases as the drift ratio increases.

3. The strains of **EU2U** and **EU4U** with U-bars increased sharply after reaching the yield strain, compared to **EU2R** and **EU4R** with ties (see Figure 4-61(a) ~ (d)). This means that the closed tie exhibits more stable behavior than the U-bar for joint shear reinforcement after bar yielding. However, despite these different behaviors, **EU2U** and **EU4U** showed almost the same seismic performance as **EU2R** and **EU4R** (see Figure 4-41(b) ~ (e)).

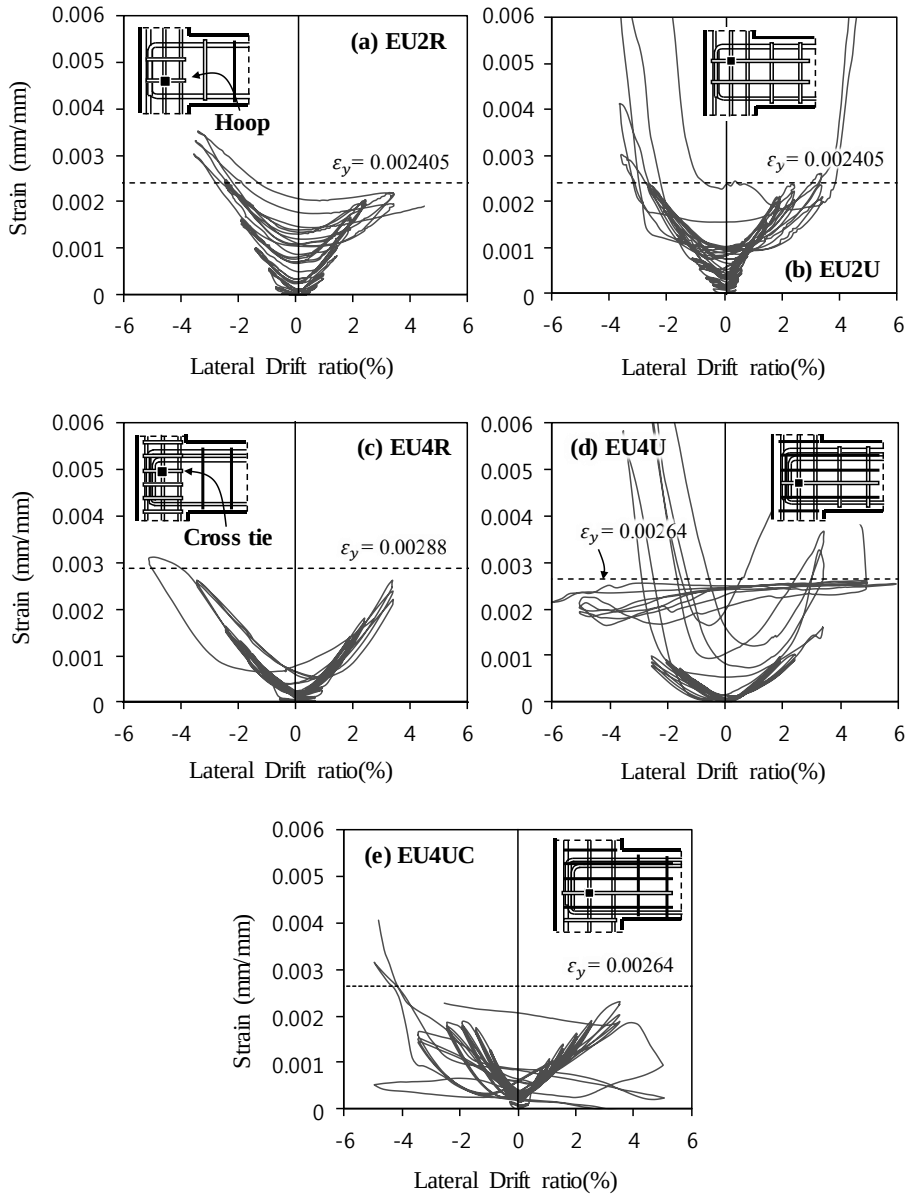

Figure 4-61 Strains of joint shear reinforcement in exterior connections

4.5.2 Interior beam and column connections

4.5.2.1 Strains of beam longitudinal bars

Figure 4-62 shows strain distributions of beam flexural bars near the joint of interior connection specimens. The horizontal and vertical axes, respectively, denote the distance from the column centerline where the strains were measured and the measured bar strains. The bar strain in Figure 4-62 were the maximum values that each bar underwent during the load cycles repeated at each lateral drift ratio. The bar strains are denoted with bars, triangles, circles, squares, and crosses corresponding to drift ratio of 0.25%, 1.0%, 2.0%, 3.5%, and 5.0%, respectively.

The beam longitudinal bars at the face of columns reached yield strain though the maximum loads were smaller than the nominal joint strength due to beam flexural yielding ($P_u < P_{nb}$). This is because the shear cracks and shear deformation in the joint further increase the strain of beam bars

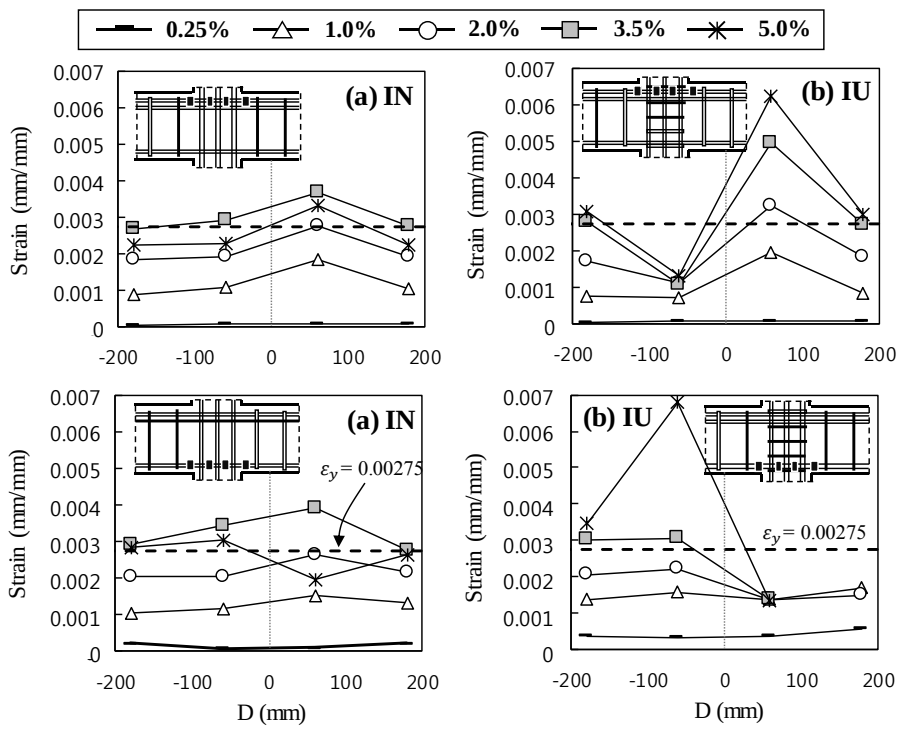

Figure 4-62 Strain distributions of beam bars in interior connections

4.5.2.2 Strains of column longitudinal bars

Figure 4-63 shows the strains of the column longitudinal bars measured at the face of beams. A slightly larger strain was applied to IU specimen using joint transverse reinforcement, but both specimens showed similar strain behavior. Specimens **IN** and **IU** yielded at drift ratio of 2.5 ~ 3.5% and 2.0 ~ 2.5%, respectively, even though joint shear failure occurred prior to column flexural yielding ($P_u < P_{nc}$). Similar to the beam bars, excessive joint diagonal shear cracks further increased the strain of the column bars.

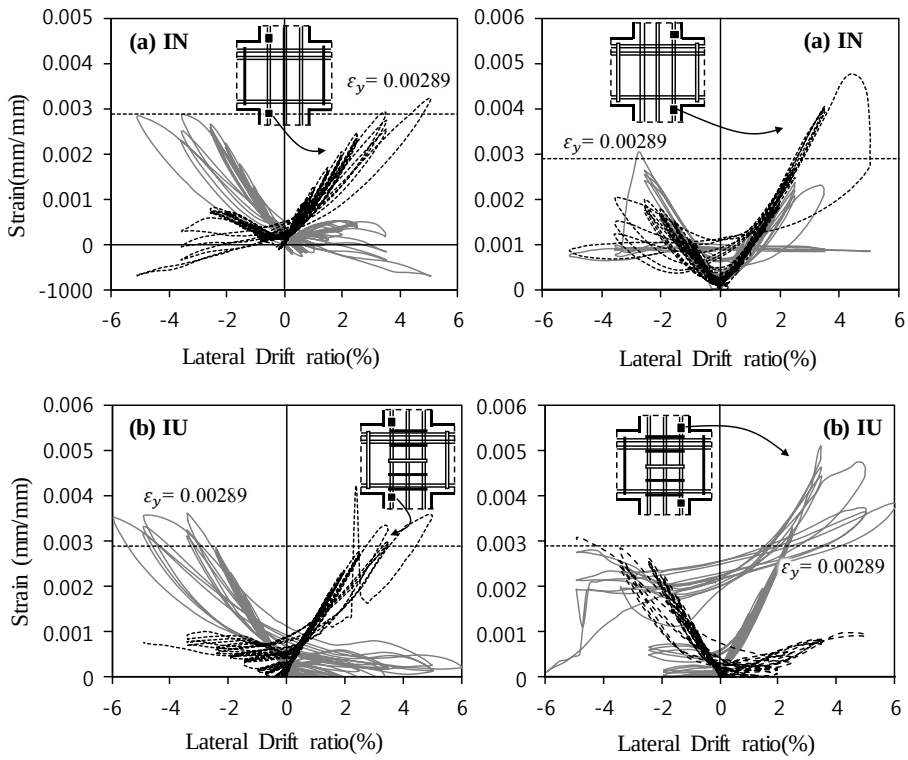

Figure 4-63 Strains of column bars in interior connections

4.5.2.3 Strains of joint shear reinforcement

Figure 4-64 shows strains of the joint shear reinforcement measured in specimen **IU**. The strains were measured in lap spliced U-bar (left graph) and cross-tie (right graph) located in the center of the joint. The U-bar exceeded yield strain at drift ratio of 3.5% at which maximum load was reached as shown in Figure 4-58. Thereafter, the strain of the U-bar was continued to increase, resulting in a gradual decrease in strength due to the expansion of the joint concrete and diagonal shear cracking as shown in Figure 4-58 and Figure 4-59. The lap spliced U-bars used for improving workability have successfully contributed to the joint shear resistance.

The cross-tie strain in the right graph of Figure 4-64 increased rapidly up to drift ratio of 0.35% and reached yield strain at drift ratio of 2.0 ~ 2.5%, which implies that the cross-tie inside the joint was more resistance to joint shear cracking. In addition to the outer tie, the inner cross-tie also plays a major role in joint shear resistance.

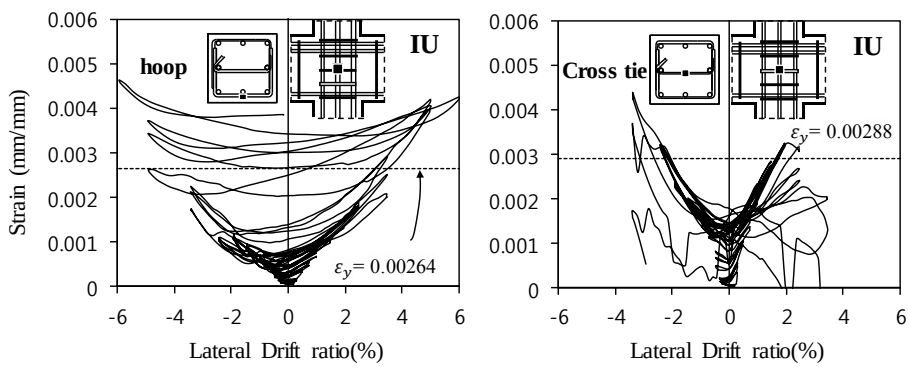

Figure 4-64 Strains of joint shear reinforcement in interior connections

4.6 Factors Affecting Joint Performance

4.6.1 Joint shear reinforcement ratio

In order to evaluate the effect of joint shear reinforcement ratio on exterior joint shear strength, the normalized joint shear stress ($v_j/\sqrt{f_c'}$ or v_j/f_c') and joint shear reinforcement ratio (ρ'' or ρ_j) relations are presented in Figure 4-65. Current design codes define joint shear strength equations in different ways, such as $v_j = k_a\sqrt{f_c'}$ in ACI 318, FEMA 356, and ASCE 41-13, $v_j = 0.2f_c'$ in NZS 3101, and $v_j = k_b(f_c')^{0.7}$ in AIJ 2010 (See section 4.1.3.2). Such joint shear strength equation can be used when the requirements for transverse reinforcement ratio is satisfied as explained in section 4.1.3.4.

FEMA 356 classifies exterior joint shear stresses into non-conforming ($0.5\sqrt{f_c'}$) and conforming ($1.0\sqrt{f_c'}$) depending on the volumetric ratio of transverse reinforcement in the joint (ρ''= 0.003). Similarly, in ASCE 41-13, exterior joint shear stresses are classified as a spacing of joint transverse reinforcement ($s = h_c/2$). On the other hand, ACI 318 and NZS 3101 define joint shear strength only when sufficient joint shear reinforcement is provided for confinement of joint concrete.

Normalized shear stress by $\sqrt{f_c'}$ with the variation of ρ'' is compared with FEMA 356, ASCE 41-13 and ACI 318 in the left graph of Figure 4-65; on the other hand, normalized shear stress by f_c' with the variation of ρ_j is compared with NZS 3101 in the right graph of Figure 4-65.

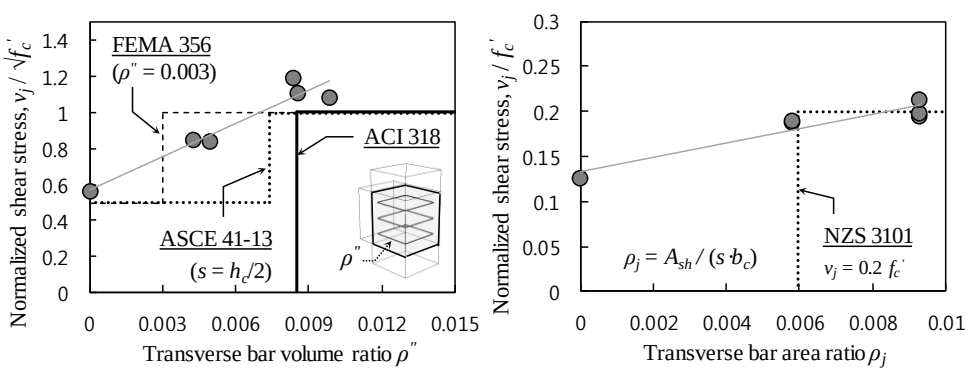

Figure 4-65 Normalized joint shear stresses with the variation of transverse bar ratio

The exterior joint specimens in this study used the maximum loads only in the positive direction at which the joint shear failure occurred prior to beam flexural yielding. In the negative direction, as shear failure occurred after anchorage failure of beam bars or beam flexural yielding, test results were not used. The test results are marked with dark grey circles.

ACI 318 and NZS 3101 accurately predict shear strength of exterior joints using sufficient (conforming) shear reinforcement with $v_{j,\ test}$ / $v_{j,pred}$ ratio of 1.09 ~ 1.19 and 0.95 ~ 1.05, respectively; however, such design codes do not predict unreinforced exterior joints or joints with non-conforming shear reinforcement. Thus, ASCE 41-13 (Seismic evaluation and retrofit of existing buildings) and FEMA 356 (Seismic rehabilitation of buildings) were used to predict exterior joint specimens with non-conforming shear reinforcement.

ASCE 41-13 predicts joint shear stresses of all test specimens in a safe side, especially for the specimen without joint shear reinforcement and conforming joint specimens ($v_{j,\ test}$ / $v_{j,ASCE}$ = 1.09 ~ 1.19). However, the specimens with non-conforming joint shear reinforcement are greatly overestimated ($v_{j,\ test}$ / $v_{j,ASCE}$ = 1.7). Further, FEMA 356 overestimates joint shear stress of the specimens with non-conforming joint shear reinforcement. These results indicate that the joint shear strength variation should be defined in the non-conforming reinforcement zone where sufficient joint shear reinforcement is not provided for concrete confinement.

In order to evaluate the shear stresses of exterior joints with non-conforming shear reinforcement, the joint specimens with J failure (Joint failure before beam or column flexural yielding) were collected from several previous studies including Ehsani and Wight (1985), Tsonos et al. (1992), Murty et al. (2003), and Kuang and Wong (2013). The test results were summarized in Table 4-9, and presented in Figure 4-66. The test results of Ehsani and Wight, Tsonos et al., Murty et al., and Kuang and Wong are marked with white diamonds, grey diamonds, white triangles, and grey squares, respectively.

The normalized joint shear stress is linearly proportional to joint shear reinforcement area ratio. Since shear stress of joint specimens with non-conforming shear reinforcement is mainly influenced by joint shear reinforcement ratio ρ_j, the joint shear stress can be defined as follows.

$$v_j / \sqrt{f_c'} = \min(0.5 + 60\rho_j, 1.0) \quad (4\text{-}29)$$

$$v_j / f_c' = \min(0.07 + 40\rho_j^{1.2}, 0.2) \quad (4\text{-}30)$$

where, ρ_j is joint transverse reinforcement area ratio ($=A_{sh}/[s \cdot b_c]$). The maximum joint shear stresses in Equations (4-29) and (4-30) are defined as $1.0\sqrt{f_c'}$ in ACI 318 and $0.2f_c'$ in NZS 3101, respectively.

As shown in Figure 4-66, the proposed equation predicts joint shear stress of all test specimens in a safe side. Especially, for non-conforming joint specimens, the joint shear stress v_j can be accurately predicted with the variation of joint shear reinforcement area ratio ρ_j. Further, the exterior joint without shear reinforcement can resist joint shear stress at least $0.5\sqrt{f_c'}$ and $0.07f_c'$.

Joint shear stress is influenced by joint transverse bar spacing as well as joint shear reinforcement ratio. Thus, further study is needed to investigate the effect of joint transverse bar spacing (s) on joint shear strength, though the specimens in present and previous studies have various spacing s of joint transverse reinforcement ranged from $0.26h_c$ to $1.08h_c$.

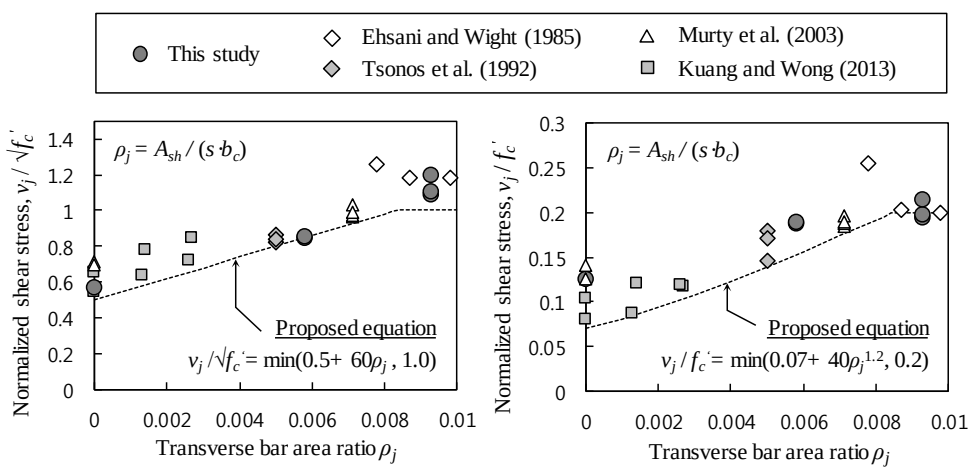

Figure 4-66 Normalized joint shear stresses compared with proposed equations

Table 4-9 Summary of present and existing test results of exterior joints (J failure)

Specimen		f_c' (MPa)	$v_j / \sqrt{f_c'}$ [1]	v_j / f_c'	ρ'' (%) [2]	ρ_j (%) [3]	s/h_c [4]
This Study	EUN	20	0.56	0.13	0	0	-
	EU2R	20	0.84	0.19	0.49	0.58	0.55
	EU2U	20	0.85	0.19	0.43	0.58	0.55
	EU4R	31	1.09	0.19	0.98	0.93	0.34
	EU4U	31	1.11	0.20	0.85	0.93	0.34
	EU4UC	31	1.19	0.21	0.84	0.93	0.26
	IN	31	1.45	0.26	0	0	-
	IU	31	1.63	0.29	1.23	0.93	0.34
Ehsani and Wight (1985)	1B	33.6	1.18	0.20	1.33	0.89	0.67
	2B	35.0	1.18	0.20	1.50	0.98	0.67
	5B	24.3	1.26	0.26	1.18	0.78	0.67
Tsonos et al. (1992)	S4	21	0.82	0.18	0.75	0.5	0.625
	S5	25	0.86	0.17	0.75	0.5	0.625
	S6	33	0.84	0.15	0.75	0.5	0.625
Murty et al. (2003)	Q1	25.6	0.71	0.14	0	0	-
	Q2	27.2	0.96	0.18	1.08	0.71	0.375
	Q3	26.9	0.97	0.19	1.08	0.71	0.375
	R1	30.2	0.69	0.13	0	0	-
	R2	27.3	1.03	0.20	1.08	0.71	0.375
	R3	27.1	0.99	0.19	1.08	0.71	0.375
Kuang and Wong (2013)	BSL450	38.6	0.65	0.10	0	0	-
	BSL450-H1	41.6	0.77	0.12	0.21	0.14	1.08
	BSL450-H2	52.6	0.85	0.12	0.40	0.27	0.72
	BSL600	45.5	0.54	0.08	0	0	-
	BSL600-H1	52.7	0.64	0.09	0.19	0.13	0.8
	BSL600-H2	37.1	0.72	0.12	0.38	0.26	0.5

1) v_j = Joint shear stress at joint shear failure before beam flexural yielding (J failure)

2) ρ'' = Joint transverse reinforcement volume ratio

3) ρ_j = Joint transverse reinforcement area ratio (= A_{sh} / [$s \cdot b_c$])

4) h_c = dimension of column core in the direction of joint shear

4.6.2 Anchorage length of beam longitudinal reinforcement

(1) Test results of exterior joints with anchorage failure

It is often difficult to distinguish a joint shear failure and an anchorage failure of beam longitudinal bars for exterior beam-column connection tests; however, the anchorage failure often exhibits bearing crushing of concrete at the bend, or splitting along the reinforcement. In this section, the joint specimens subjected to failure due to the loss of bond capacity in beam longitudinal bars prior to joint shear failure were analyzed to evaluate the effect of anchorage failure on joint behaviors.

In order to estimate joint shear strength affected by anchorage length (l_{dh}) and diameters (d_b) of beam longitudinal bars, test results of specimens **EUN** and **EU2R**, which failed with bond deterioration of beam bars under negative loadings, were compared in Figure 4-67. The load carrying capacity in both specimens decreased sharply before attaining the nominal joint shear strength P_{nj}^{NC} in negative directions, despite joint shear reinforcement used in specimen **EU2R**. On the other hand, maximum strengths in positive directions could reach the nominal joint shear strength P_{nj}^{NC}, and the specimen **EU2R** was increased load capacity with 49% by joint shear reinforcement. These results demonstrate that the specimens **EUN** and **EU2R** were dominated by joint shear strength in the positive directions, and by bond deterioration of beam bottom bars in the negative directions.

Similar aspect can be observed in crack patterns of the specimens as shown in Figure 4-67. In the crack pattern of specimen **EU2R**, the number of joint diagonal cracks was increased due to improved internal load transfer by joint shear reinforcement in the positive direction, while the number of joint cracks was identical to specimen **EUN** in the negative direction. In side crack patterns, vertical splitting crack was restrained by joint shear reinforcement, resulting in significant increase on the positive maximum load. However, the negative maximum load was not increased significantly (increase only in 10%) because bond capacity of beam bars was deteriorated due to short anchorage length.

When the top bars were stressed in tension (positive direction), the nominal shear strength P_{nj}^{NC} was exceeded prior to bond failure with relatively higher load though the top reinforcing bars in beams had the same anchorage length (l_{al}) and

beam diameter (d_b) as the bottom bars. This is because the bond stress applied on each top reinforcing bar was half of bottom bar under a same moment demand. The bond stress on beam reinforcements in exterior joint specimens are important factor for anchorage length of beam bars.

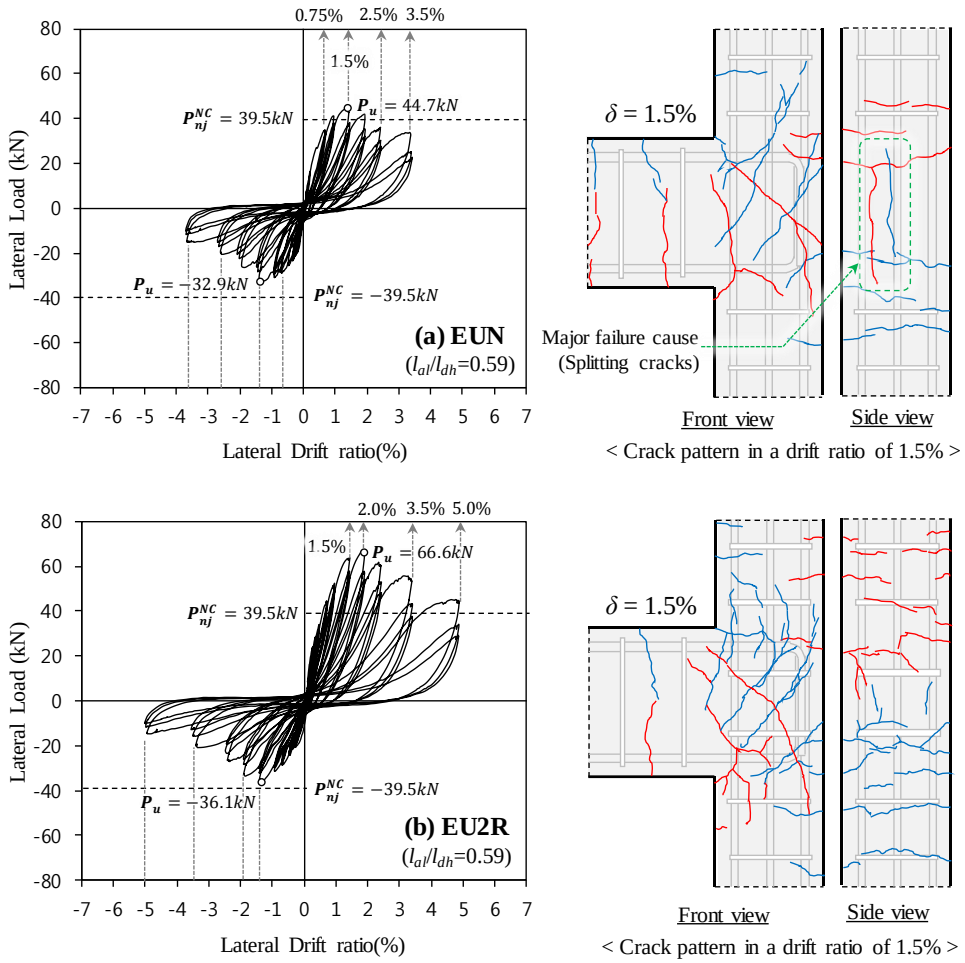

Figure 4-67 Test results of specimens EUN and EU2R with anchorage failure

(2) Bond stress on beam longitudinal bars

In order to evaluate the bond stress acting on each beam longitudinal bar, the normalized bond stress by concrete strength $\sqrt{f_c'}$ depending on failure modes of test specimens is presented in Figure 4-68 and Table 4-10. We assume that the bond stress u is constant along the anchorage length l_{dh}, equilibrium of the beam bar is as follows.

$$T_b = u\ \pi\ d_b\ l_{dh} \tag{4-31}$$

where, T_b is a tensile force of a beam longitudinal bar at a peak load.

Except for the positive direction in specimen **EUN** and the negative direction in specimen **EU2U**, the exterior joint specimens exhibited joint shear failure and anchorage failure at bond stress of $1.22\sqrt{f_c'} \sim 1.36\sqrt{f_c'}$ (MPa) regardless of failure mode. This result indicates that exterior joint specimens with joint shear failure were affected by bond deterioration of beam bars. In the positive direction of **EUN**, due to no joint shear reinforcement, the joint shear failure occurred before bond deterioration of beam bars. In the negative direction of **EU2U**, U-bars in the joint increased flexural stiffness, thereby increasing the peak load and the normalized bond stress $u/\sqrt{f_c'}$.

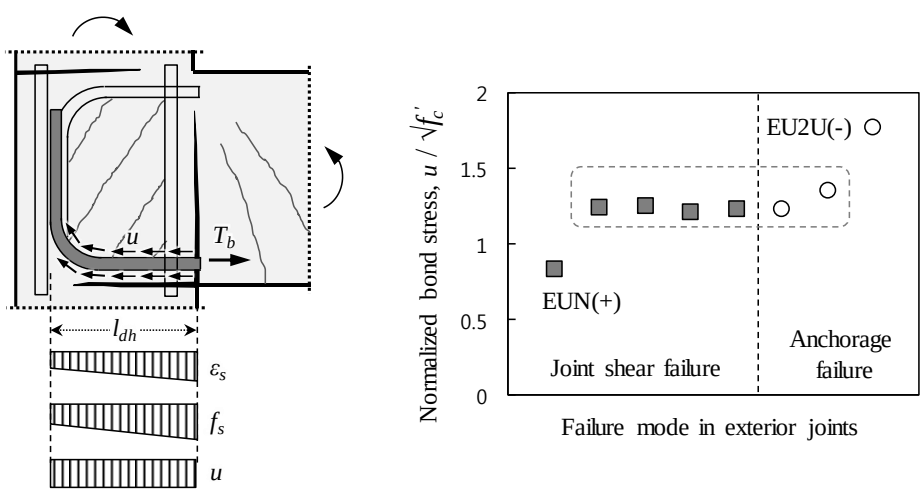

Figure 4-68 Normalized bond stress acing on beam longitudinal bars

Table 4-10 Average bond stress applied in beam longitudinal bars

Specimen		f_c' (MPa)	T_{bt} 1) (kN)	Number of beam bars	T_b 2) of each bars	u 3) (MPa)	$u/\sqrt{f_c'}$	Failure mode
EUN	Positive	20	354	4	88	3.75	0.84	Joint shear
	Negative	20	260	2	130	5.52	**1.24**	**Anchorage**
EU2R	Positive	20	527	4	132	5.59	1.25	Joint shear
	Negative	20	286	2	143	6.06	**1.36**	**Anchorage**
EU2U	Positive	20	533	4	133	5.65	1.26	Joint shear
	Negative	20	374	2	187	7.94	**1.78**	**Anchorage**
EU4R	Positive	31	848	7	121	6.77	1.22	Joint shear
	Negative	31	699	4	175	7.42	1.33	Beam flexure
EU4U	Positive	31	864	7	123	6.89	1.24	Joint shear
	Negative	31	715	4	179	7.59	1.36	Beam flexure
EU4UC	Positive	31	1203	7	172	7.20	1.29	Beam flexure
	Negative	31	763	4	191	6.07	1.09	Beam flexure

1) T_{bt} = Total tensile forces applied in beam longitudinal bars at peak loads

2) T_b = a tensile force of a beam longitudinal bar at a peak load

3) u is an applied average bond stress in beam longitudinal bars (= T_b / [$\pi d_b l_{dh}$])

(3) Measured strain distributions of beam bottom bars

The measured strains of beam bottom longitudinal bars with anchorage failure or flexural yielding were compared in Figure 4-69 to analyze the behaviors of beam hooked bars anchored into the exterior joints. The horizontal and vertical axes denote the distance from the leftmost gauge and the bar strains, respectively. The bar strains were the maximum values that each bar underwent during the load cycles repeated at each lateral drift ratio. The bar strains corresponding to drift ratio of 0.25%, 0.5%, 1.0%, 1.5%, 2.0%, and 3.5% are denoted with bars, crosses, triangles, diamonds, circles, and squares, respectively. Strains at the peak load of each specimen were marked with grey. Yield strain of bars is indicated with horizontal dashed lines, and the critical section (column face) is indicated with vertical dashed lines.

The specimens **EUN**, **EU2R**, and **EU2U** with insufficient anchorage length (l_{al}/l_{dh} = 0.59) in the negative direction (bottom bars in tension) did not reach yield strain at the critical section when the peak load was attained at drift ratio of 1.5%. In **EUN** and **EU2R**, as the strains penetrated into the joint, the measured strains of beam bars in the joints were increased. On the other hand, in **EU2U**, the measured strains of beam bars in the joints were similar due to the effect of the U-bar anchored into the beam. After drift ratio of 1.5%, the measured strain values of beam bars were rapidly increased or decreased by the beam anchorage failure. This result indicates that the specimens **EUN**, **EU2R**, and **EU2U** failed with bond deterioration of beam hooked bars in the joints before beam flexural yielding.

The specimens **EU4R**, **EU4U**, and **EU4UC** with sufficient anchorage length (l_{al}/l_{dh} = 0.96 ~ 1.28) in the negative direction reached yield strain at the critical section when the maximum load was attained at drift ratio of 3.5%. Thus, the specimens exhibited beam flexural yielding before anchorage failure of beam bars or joint shear failure. **EU4R** and **EU4U** with anchorage length ratio l_{al}/l_{dh} of 0.96 showed a strain penetration of beam bars into the joint, resulting in higher strains of beam bars in the joint. On the other hand, **EU4UC** with anchorage length ratio l_{al}/l_{dh} of 1.28 showed the largest strain at the critical section.

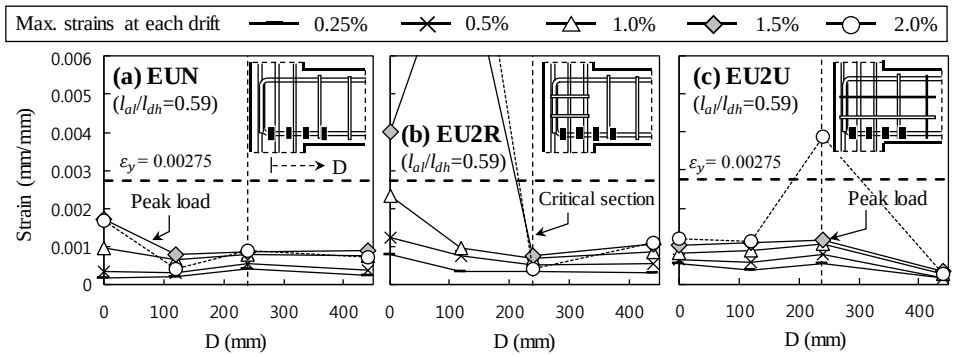

< **Anchorage failure** of beam bottom longitudinal bars>

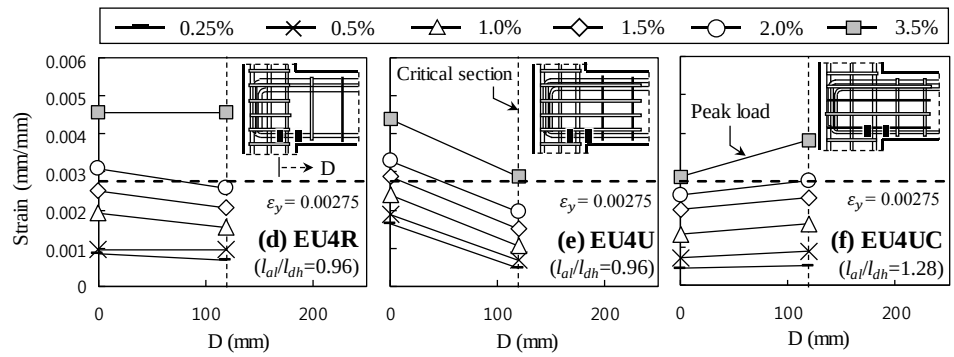

< **Flexural yielding** of beam bottom longitudinal bars>

Figure 4-69 Measured strain distributions of beam bottom longitudinal bars

4.6.3 Effective joint area

In current design codes of section 4.1.3.2, the joint strength (V_{jn}) is proportionally increased to the effective joint area (A_j). According to section 4.1.3.3, the effective joint area is determined by the width of beam or column (b_b or b_c), and the column depth (h_c). To investigate the effect of such effective joint area, specimens **EU4U** and **EU4UC** with same variables except for the column depth (350 mm and 450 mm, respectively) were compared in Figure 4-70.

In the positive direction, the strength increment was 42% by increasing the effective joint area with 29%. In specimen **EU4U**, bond deterioration of beam bars was occurred at drift ratio of 3.5% after joint shear failure occurred at drift ratio of 2.5%. In crack pattern at drift ratio of 3.5%, the severe vertical cracks with diagonal shear cracks were developed along the concrete cover outside the exterior joint. On the other hand, specimen **EU4UC** occurred joint shear failure at drift ratio of 5.0% after beam flexural yielding at drift ratio of 3.5%. As shown in crack pattern at drift ratio of 3.5%, joint concrete damage was relatively less because the specimen was dominated by flexural yielding of beam bars before joint shear failure. However, at drift ratio of 5.0%, joint shear failure occurred with sharply decreasing load carrying capacity.

In the negative direction, both specimens were subjected to beam flexural yielding, resulting in no strength increase despite the increase in the joint area. However, due to the increased joint area in **EU4UC**, the load reduction after peak load was not relatively large from drift ratio of 3.5% to 5.0%.

The joint shear strength was increased proportional to the effective joint area as shown in Figure 4-71. However, specimen **EU2U** with insufficient anchorage length of beam bars (l_{al}/l_{dh} = 0.59) failed before attaining the joint shear strength V_{jn} specified in ACI 318 (See white square in Figure 4-71). When the effective joint area is reduced by the ratio (l_{al}/l_{dh}) of provided anchorage length to required length of ACI 318, ACI 318 predicts the joint shear strength well into the safe side (See grey circle).

$$A_{j,proposed} = A_{j,ACI318}\,(l_{al} / l_{dh}) \tag{4-32}$$

where, the anchorage length ratio of beam bars l_{al} / l_{dh} is smaller than 1.0.

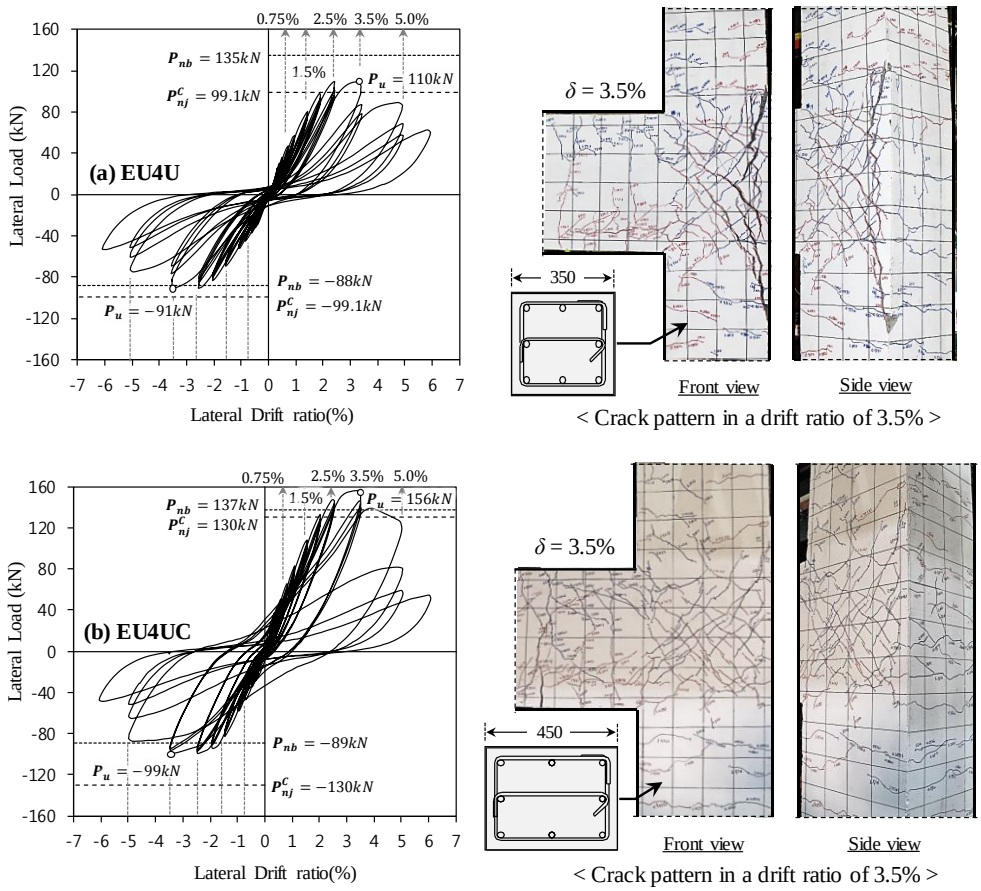

Figure 4-70 Test results of specimens EU4U and EU4UC with different effective joint area

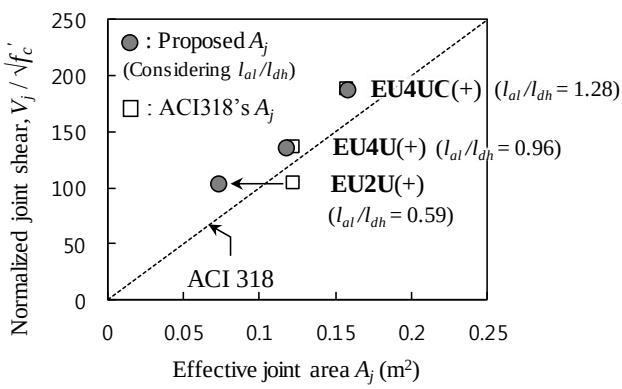

Figure 4-71 Joint shear strength and proposed effective joint area relationship

4.6.4 Joint types between exterior and interior joints

Specimens **EU4R** and **IU** with same test variables except for the joint type are compared in Figure 4-72 to evaluate the seismic behavior of the exterior joint and the interior joint. In the exterior joint, the beam longitudinal bars are anchored inside the joint with 90º hook. In the interior joints, on the other hand, the beam bars are anchored in the beam at the opposite side without hook anchorage.

In both specimens, the maximum loads were attained with the join shear failure at drift ratio of 3.5% (Beam flexural yielding in negative direction of **EU4R**). However, the maximum load P_u and joint shear demand V_{ju} of the interior joint were 50% higher than those of the exterior joint. When the dimension and length of beam and column are the same, the shear force V_{ju} acting in the joint is identical in the interior and exterior joints (Refer to section 4.3.2). Since the interior joint is connected with adjacent beams at both sides, the joint can be confined more effectively than the exterior joint with an adjacent beam at one side. Further, as the 90º hook of beam bars are anchored in the exterior joint, the stiffness of the joint can be rapidly decreased due to the additional outward force from the hook. The outward force resulted in the side vertical cracks in the joint as shown in Figure 4-72.

As shown in the crack patterns at drift ratio of 2.5%, a number of diagonal shear cracks were developed in both exterior and interior joint. Such shear cracks were concentrated in the interior joint between the outmost longitudinal bars of the beam and the column, and in the entire exterior joint.

In current design codes (See section 4.1.3.2), considering such different seismic performances depending on the joint types, the shear strength of the interior joint is larger than that of the exterior joint by 1.25 times in ACI 318 and EC8, and 1.43 times in AIJ.

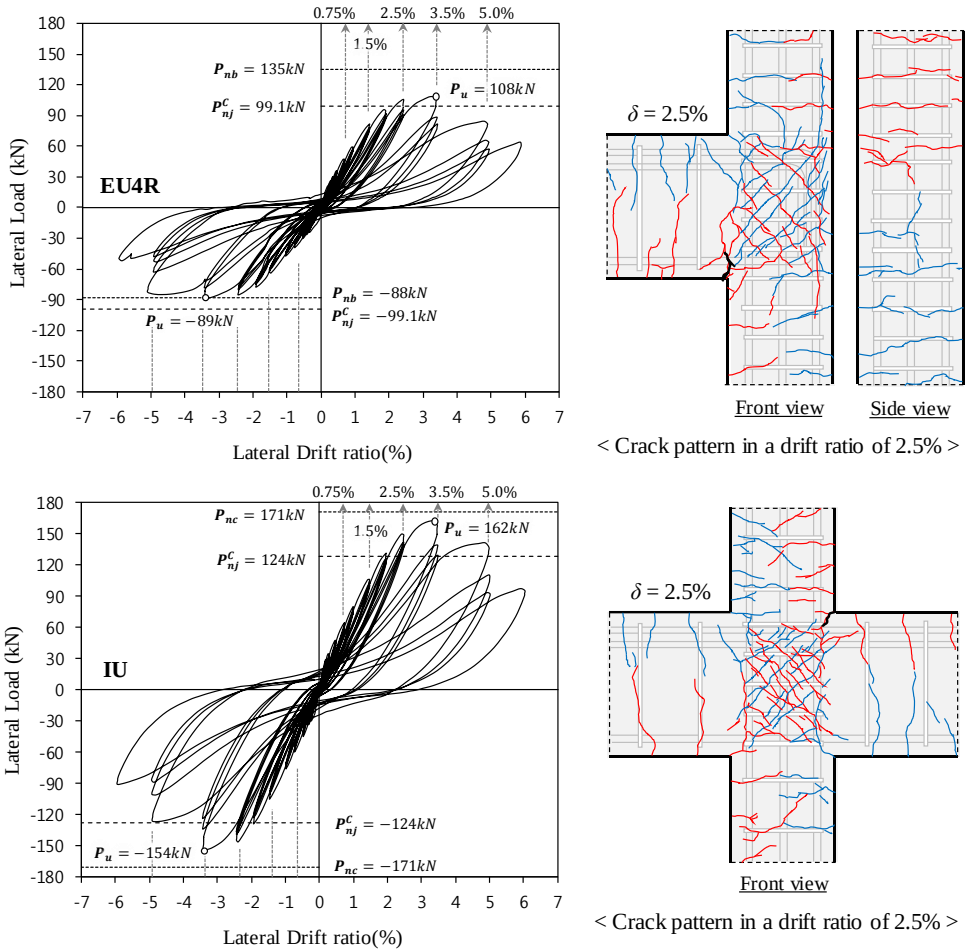

Figure 4-72 Test results of specimens EU4R and IU with different joint type

4.6.5 Joint reinforcement details of closed ties and U-bars

Joint reinforcement details of closed ties and U-bars were compared to investigate the reinforcing effect of the alternative U-bar detail in Figure 4-73 and Figure 4-74. The left figures show test results of non-conforming joint specimens **EU2R** and **EU2U**, where the amount of joint shear reinforcement and the anchorage length of beam bars are smaller than those specified in ACI 318. The right figures show test results of conforming joint specimens **EU4R** and **EU4U**, where the joint shear reinforcement and the anchorage length are satisfied with ACI 318. Specimens **EU2R** and **EU4R** have closed tie with 90º hook in joints, and specimens **EU2U** and **EU4U** have U-bars with $30d_b$ anchorage length into beams.

Load and drift ratio envelope curves and cumulative energy dissipations were presented in Figure 4-73. The envelope curve is a multiple straight line connecting maximum loads of first cycles at each drift ratio according to ACI 374.1-05. The cumulative energy dissipation is expressed as the total area (ΣE_D) enclosed by the load and displacement hysteresis curves. Test specimens with joint shear failure prior to beam flexural yielding showed little difference of strength and energy dissipations depending on joint shear reinforcement details. However, **EU2R** with anchorage failure of beam bars before nominal joint shear strength P_{nj}^{NC} showed maximum strength and energy dissipation capacity lower than those of **EU2U**.

Figure 4-74 shows crack patterns of test specimens with different joint shear reinforcement details at the maximum load or ultimate drift ratio. At maximum load (δ = 1.5% in **EU2R** and **EU2U**, δ = 2.5% in **EU4R** and **EU4U**), the shear crack patterns in the joints were similar with regardless of joint details. However, in **EU2R**, the diagonal shear cracks were relatively less due to the anchorage failure of beam bottom bars. At ultimate drift ratio (δ = 5.0% in **EU2R** and **EU2U**, δ = 6.0% in **EU4R** and **EU4U**), the U-bars were sufficiently anchored into the adjacent beams even after joint concrete cover spalling off, resulting in same residual joint shear strength compared to closed tie with 90º hook.

The alternative U-bar detail could be used as a joint shear reinforcement when sufficient anchorage length ($l_a \geq 30d_b$) is secured into an adjacent beam.

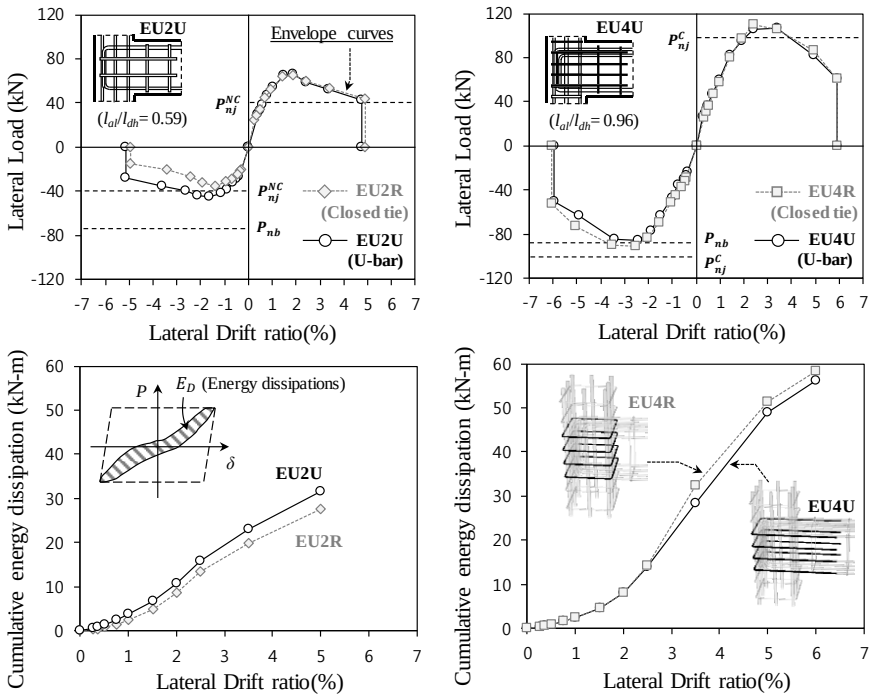

Figure 4-73 Test results of exterior joints according to joint details

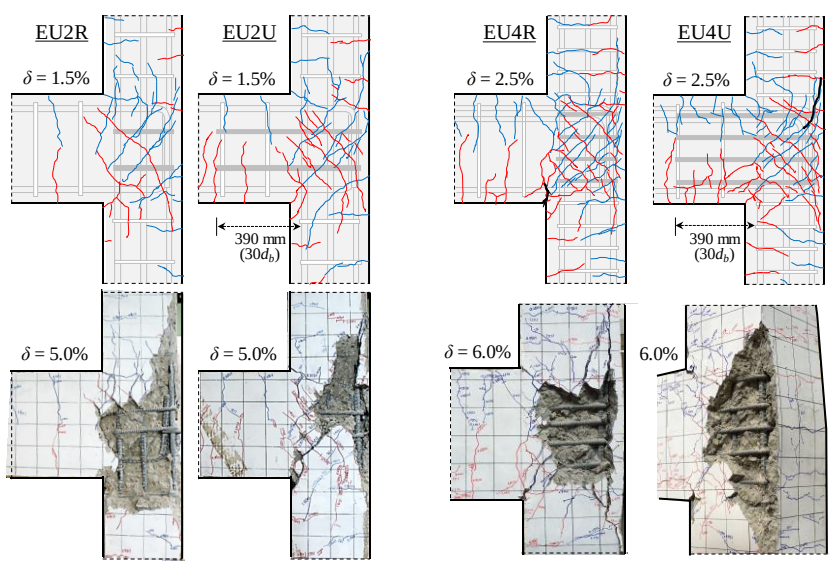

(a) Non-conforming exterior joints (b) Conforming exterior joints

Figure 4-74 Crack patterns of exterior joints according to joint details

4.7 Discussion

In this chapter, the seismic performance of beam-column connections using small effective joint area was evaluated. With the reversed cyclic load test results of exterior and interior connections, the influence of the test parameters on the joint behavior such as joint shear strength, deformation capacity, and failure mode was investigated in terms of the joint types (exterior joint and interior joint), joint shear reinforcement details, and joint shear reinforcement ratio. The main conclusions were summarized as follows.

1) The exterior joints were mainly affected by joint shear reinforcement ratio and the anchorage length of beam longitudinal bars. The maximum joint shear strength was increased proportionally with the increase of joint shear reinforcement ratio, but the joint shear strength was not sufficiently developed due to the bond deterioration of beam bars when the anchorage length of beam bars was not secured. The exterior joint with increased effective joint area improved the joint shear strength, resulting in the beam flexural yielding before the joint shear failure due to increased joint shear strength and sufficient anchorage length of beam bars.

2) For beam flexural yielding before joint failure in exterior joints, sufficient effective joint area and shear reinforcement ratio are needed. On the other hand, when minimum joint reinforcement is used in joints, the joint shear failure occurs, but limited ductility can be attained. However, the joint has no shear reinforcement and the anchorage length of beam bars is insufficient, brittle failure occurred, and both strength and deformation capacity are greatly reduced.

3) The interior joints with the small joint effective area showed the joint shear failure before column flexural yielding. The load carrying capacity of the interior joint even without joint shear reinforcement was superior to the exterior joints with joint shear reinforcement. The maximum loads were 23 ~ 70% greater than the joint shear strength specified in ASCE 41-13. The deformation capacity was more than drift ratio of 3.5 ~ 5.0%.

4) Alternative reinforcement detail using U-bar with improved workability showed similar load - displacement relations and failure mode to the closed tie with 90º hook though the strain of joint shear reinforcement increased rapidly after

reaching the yield strain.

5) Generally, in low-rise buildings with small column size, small joint area does not satisfy the existing seismic design criteria, and thus such buildings are vulnerable to seismic loads. Therefore, the joint shear reinforcement should be used to secure required seismic performance of exterior joints. Particularly, since the exterior joints are influenced not only by the joint shear reinforcement ratio but also by the anchorage length of beam bars, it is necessary to consider two points.

Chapter 5. Effects of Anchorage Details of Beam Bars on RC Exterior Joints

5.1 Introduction

5.1.1 General problems in beam bar anchorage into joint

Low-rise moment frames designed mainly for gravity loads have smaller size of columns and joints than that of beams. In such smaller beam-column joints, it is difficult to secure the joint shear resistance, and it may be vulnerable to bond and anchorage failure in the beam reinforcement. In particular, at an exterior joint where a hook of a beam reinforcement is anchored, the exterior joint behavior can be affected by anchorage details of the beam reinforcement.

Figure 5-1 shows anchorage details of the beam bars in the exterior joints. For convenient bar placement, the beam bottom bar is anchored with a straight line or using a 90º standard hook directed downward (See Figure 5-1(a) and (c)). However, when using such anchorage details, the load transfer of the strut action in the joint is not smooth, so the joint shear resistance can be reduced (Paulay and Priestley 1992).

The seismic provisions of ACI 318-14 and JSCE show that a 90º standard hook shall be located within the confined core concrete of a column with the hook bent into the joint, which indicates that the anchorage detail of Figure 5-1(d) is only allowed. In contrast, the seismic provisions of CSA and EC8 specify that the part of beam longitudinal reinforcement bent inside joints for anchorage shall be placed inside the corresponding column hoops (confined column core), regardless of the hook direction of beam bars, which indicates that the anchorage details of Figure 5-1(c) and (d) are allowed. As shown in different design specifications, the anchorage details of beam bars at the exterior joints may still be controversial, and further researches are needed.

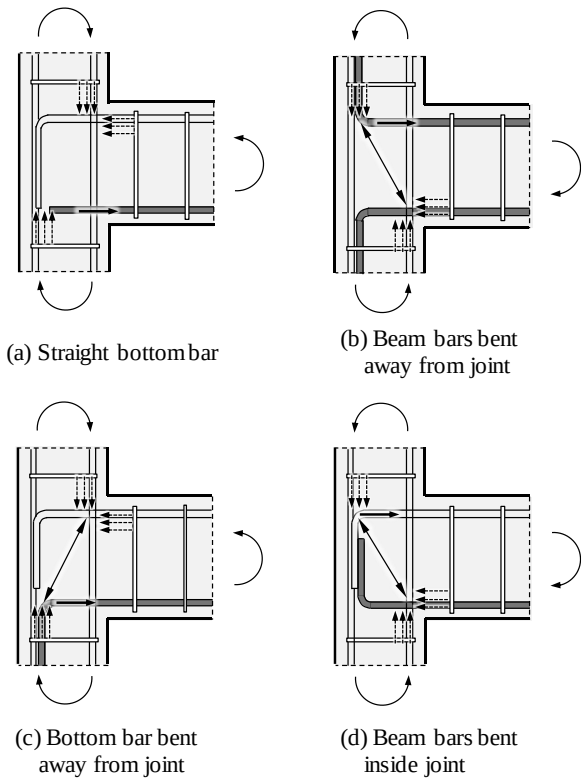

Figure 5-1 Anchorage details of unreinforced exterior joints

5.1.2 Comparison of current design codes for beam bar anchorage

The provisions of current design codes for hook directions of beam longitudinal reinforcement anchored into joints are as follows. The ACI standard was revised in 2014 to include design code about hook direction of beam bars into joints, which differs from previous ACI standard. Previous standard ACI 318-11 (21.7.5.1) specified that the 90-degree hook shall be located within the confined core of a column or of a boundary element. On the other hand, in ACI 318-14 (18.8.5.1), the hook shall be located within the confined core of a column or of a boundary element, with the hook bent into the joint. In commentary, the requirement for the hook to project into the joint is to improve development of a diagonal compression strut across the joint. The requirement applies to beam and column bar terminated at a joint with a standard hook. Similarly, JSCE recommends that primary reinforcement in a beam or a column be fully anchored to the joint of these members as shown in Figure 5-2(a).

In CSA, EC8, and AIJ, it is suggested that beam longitudinal bars can be anchored inside the confined column. In CSA (21.5.5.1), hooks, shall be standard 90 degree hooks and shall be located within the confined column core. EC8 (5.6.2.2) specifies that the part of beam longitudinal reinforcement bent in joints for anchorage shall always be placed inside the corresponding column hoops. AIJ (17.1 (5)) recommends that the beam bottom bars be anchored to the joint, but permits that beam bars are placed inside the confined column if construction is difficult as shown in Figure 5-2(b).

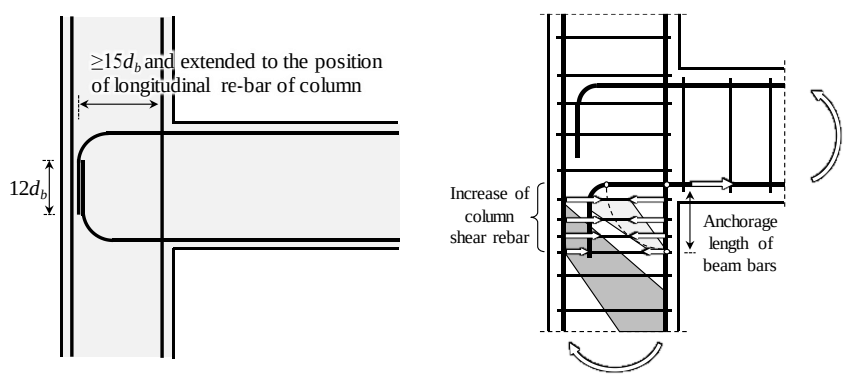

(a) Anchorage of beam longitudinal bar (JSCE) (b) AIJ 2010

Figure 5-2 Japanese design codes for beam rebar anchorage (JSCE and AIJ)

5.1.3 Previous studies for beam bar anchorage

Many researchers (Priestley, 1997; Scott, 1996; Hakuto et al., 2000; Cha et al, 2003; Kuang and Wong, 2006; and Lee et al., 2009) investigated that the effect of the anchorage details of beam bars on the joint shear performance at the exterior joints. According to these studies, when the beam bars are anchored to the outside of the joint (Figure 5-1 (b)), joint shear cracks occur early. After joint shear cracks, the joint shear performance deteriorates because a node for compression strut (CCT node) is not formed. On the other hand, as shown in Figure 5-1 (d), the direct strut mechanism improves the joint shear strength due to the beam bottom bars anchored inside the joint even after shear cracking.

Priestley (1996) proposed that the concrete tensile strengths in the principle stress direction in which the joint shear failure occurs are $0.29\sqrt{f_c'}$ and $0.42\sqrt{f_c'}$ (MPa), respectively, for beam anchorage details in Figure 5-1 (b) and (d). In the case of beam bars bent away from a joint without joint shear reinforcement, diagonal strut in the joint cannot be stabilized, and joint failure occurs at early stage.

In the studies of Scott (1996), when the beam reinforcement is anchored to the outside of the joint (Figure 5-1 (b) and (c)), the load-carrying capacity of the joint decreases, and brittle shear failure can occur when the joint shear cracks extend to the column along beam bars.

Hakuto et al. (2000) suggested that since the details of Figure 5-1 (b) and (c) do not provide an effective node point at beam bars bent away from the joints, a large amount of column hoops exists adjacent to the joint core to equilibrate the horizontal component of force of compressive strut as shown in Figure 5-2(b). Further, in Figure 5-1 (d), as the bearing stresses at the bend act in the joint, the diagonal strut effectively engages the beam longitudinal bars.

Kuang and Wong (2006) tested full scale RC exterior beam-column joints with non-seismic details and different anchorage details of beam longitudinal bars. The anchorage details of beam reinforcement have a significant effect on hysteretic behavior and shear strength of exterior joints (See Figure 5-3). When compared with specimen **BS-L**, the seismic performance of specimens **BS-OL** and **BS-LL** are worse in terms of maximum shear strength and displacement ductility. It is

recommended that the anchorage details of beam bars used in **BS-OL** and **BS-LL** not be used in practice.

As described above, according to the previous studies, when the beam bottom bar is anchored to the outside of the joint rather than the inside of the joint, the joint performance is greatly deteriorated; thus, it is recommended that the beam bar be anchored inside the joint. However, such previous studies performed tests for exterior joints where transverse reinforcement is not used inside the joint. If transverse reinforcement is placed inside the joint, the effect of the anchorage details of beam bars on joint shear performance may differ. In this study, the influence of the anchorage details of beam bars on the joint seismic behavior was investigated through cyclic tests on the exterior joints with joint shear reinforcement.

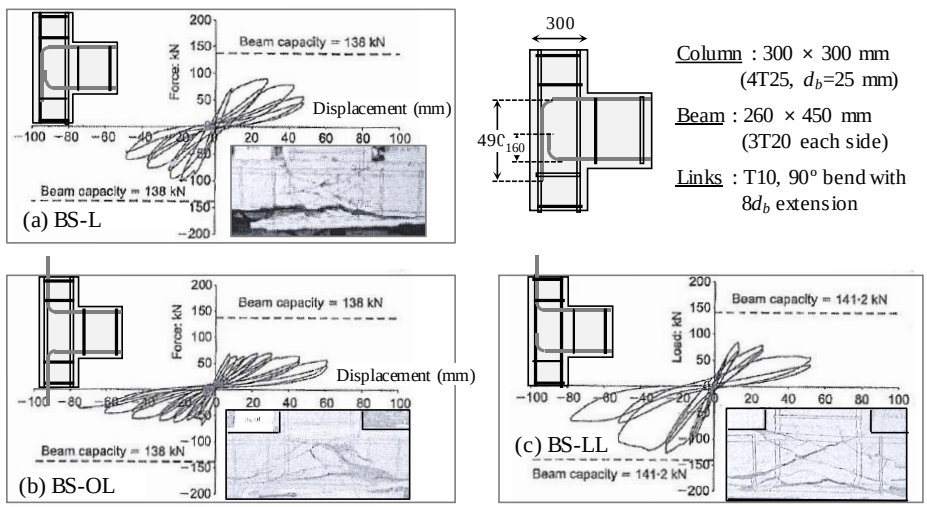

Figure 5-3 The effect of beam bar anchorage details in the study of Wong and Kuang (2006)

5.2 Test Program

5.2.1 Major design parameters

Table 5-1 and Figure 5-4 show the details and the test parameters of the exterior connections. The hook tail direction of beam bottom bars and joint shear reinforcement details were considered as major test parameters. Specimens **EUN**, **EU2R**, **EU2U**, **EU4U**, and **EU4UC** which have presented in Chapter 4 were used for comparison with test specimens in Chapter 5, such as **EDNNI**, **ED2R**, **ED2U**, **ED2UNI**, **ED4U**, and **ED4UC**. In the specimen name. the first letters 'E' indicates the Exterior connections; the following letters 'U' and 'D' denote the hook tail directions of beam bottom bars; the numbers '2' and '4' indicate the number of joint shear reinforcement; 'N', 'R', and 'U' denote the joins shear reinforcement details, no shear reinforcement, 90º hook, and U-bar, respectively; and the letters 'NI' and 'C' indicate no intermediate column bar, and the different column size used in **ED4UC**, respectively.

Table 5-1 Test variables of exterior joint specimens

Specimen[1)]	Hook tail direction of beam bottom bar	Beam-column joints		Beam bar anchorage length	
		Details	Spacing	l_{al}	l_{al} / l_{dh} [4)]
EUN	Upward	-	-	300 mm (l_{al} / d_b = 11.8)	0.59
EDNNI[3)]	Downward				
EU2R	Upward	Perimeter tie (D13) & Cross-tie (D10)	160 mm (ρ_j =0.58%)[2)]		
ED2R	Downward				
EU2U	Upward	U-bar (D13) & Cross-tie (D10)			
ED2U	Downward				
ED2UNI[3)]	Downward				
EU4U	Upward		100 mm (ρ_j =0.93%)	300 mm (15.7)	0.96
ED4U	Downward				
EU4UC	Upward		100 mm (ρ_j =0.93%)	400 mm (20.9)	1.28
ED4UC	Downward				

1) **EUN**, **EU2R**, **EU2U**, **EU4U**, and **EU4UC** have presented in Chapter 4

2) Joint reinforcement ratio, $\rho_j = A_{s,j} / (b_j \cdot s)$ = (127 x 2 + 71)/(350 x 160) x 100 = 0.58%

3) **E**(Exterior)/ **D**(Downward)/ **N**(No joint bar)/ **NI**(No intermediate column bar)
E(Exterior)/ **D**(Downward)/ **2**(Number of joint bar)/ **U**(U-bar) / **NI**(No intermediate column bar)

4) l_{dh} is the required anchorage length of hook bars in tension specified in ACI 318

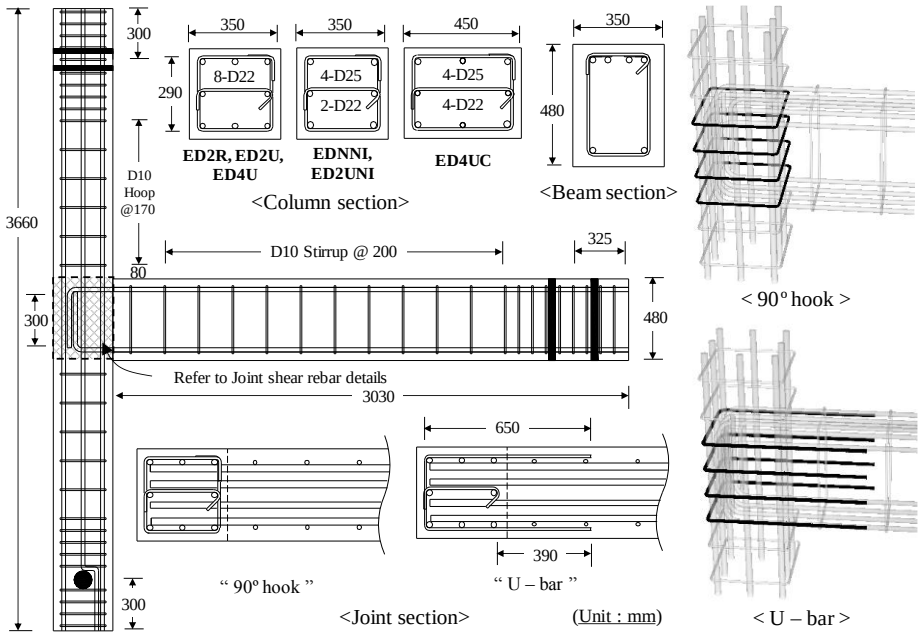

Figure 5-4 Dimensions and reinforcement details of exterior joint specimens

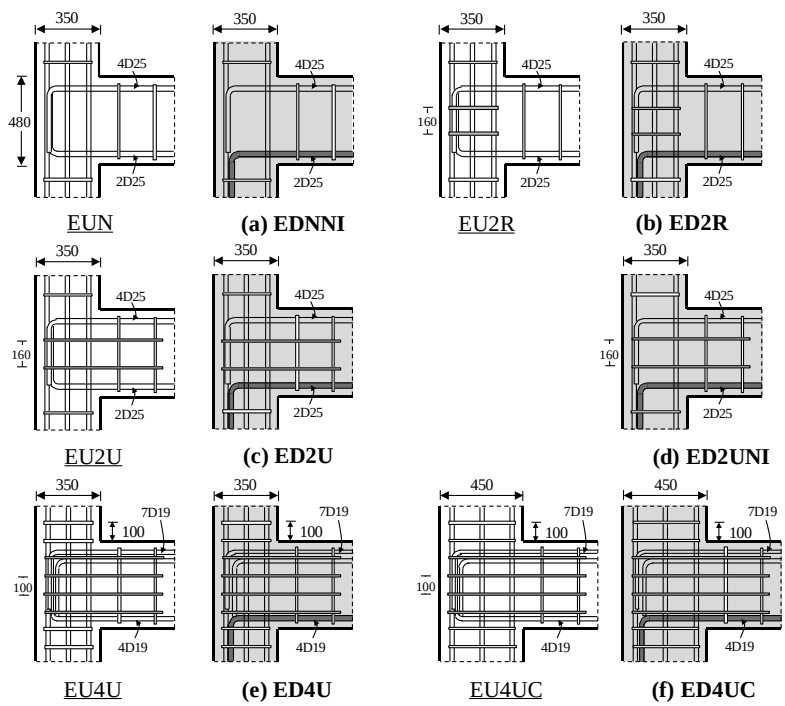

Figure 5-5 Details of joint shear reinforcement

5.2.2 Test specimens

In Figure 5-4, the column span length and the overall beam length are 3660 mm and 3030 mm, respectively. the dimension of the column section was $b_c \times h_c$ = 350 mm × 350 mm and that of the beam section was $b_b \times h_b$ = 350 mm × 480 mm except for **EU4UC** (column section $b_c \times h_c$ = 350 mm × 450 mm). For considering the structural characteristics of the low-rise moment frame structure designed for gravity loads, beam depth h_b (=480 mm) was designed to be larger than column depth h_c (=350 mm or 450 mm).

As the longitudinal reinforcing bars, 8D22 was used for the columns of **ED2R**, **ED2U**, and **ED4U** (ρ_c = 2.53%), 4D25 and 2D22 were used for **EDNNI** and **ED2UNI** (ρ_c = 2.28%), and 4D25 and 4D22 were used for the columns of **ED4UC** (ρ_c = 2.27%). For transverse reinforcement, all columns are provided with closed perimeter ties (D10) with 90º hook and cross-tie with 90º hook at one end and 135º hook at the other hand. The transverse bars were used at a spacing of 170 mm.

For the beams of **EDNNI**, **ED2R**, **ED2U**, and **ED2UNI**, the top reinforcing bars 4D25 (ρ_t = 1.21%, d_b = 25.4 mm) and the bottom reinforcing bars 2D25 (ρ_b = 0.60%) were used. For the beams of **ED4U** and **ED4UC**, the top reinforcing bars 7D19 (ρ_t = 1.20%, d_b = 19.1 mm) and the bottom reinforcing bars 4D19 (ρ_b = 0.68%) were used. The reason for using D25 and D19 reinforcing bars with different diameters is to investigate the influence of the bond performance of the beam reinforcing bars on the joint behavior inside the joint.

Table 5-1 shows the ratio of the anchorage length (l_{al}) to the diameter (d_b) of beam bars. The ratio l_{al} / d_b = 11.8 for **EDNNI**, **ED2R**, **ED2U**, and **ED2UNI**, l_{al} / d_b = 15.7 for **ED4U**, and l_{al} / d_b = 20.9 for **ED4UC**. In all specimens, the anchorage hooks of beam top bars were placed in the gravity direction and embedded in the joint. On the other hand, the anchorage hooks of beam bottom bars were embedded in the joints (**EUN**, **EU2R**, **EU2U**, **EU4U**, and **EU4UC** which have presented in Chapter 4) or in the adjacent lower columns (**EDNNI**, **ED2R**, **ED2U**, **ED2UNI**, **ED4U**, and **ED4UC** in Chapter 5).

For the joint shear reinforcement, a closed tie with 90º hook and a U-shaped bar were used for specimen **ED2R**, and specimens **ED2U**, **ED2UNI**, **ED4U**, and

ED4UC, respectively (See Figure 5-5). U-bar is an improved construction detail and can be used for joint shear reinforcement in low and moderate seismic zones according to ACI 315-99 (Figure 4-11). Both the close tie and the U-bar were made of D13 reinforcing bars. In addition, cross ties with D10 reinforcing bars were additionally used for joint shear reinforcement. For **ED2R**, **ED2U**, and **ED2UNI** where the shear reinforcement is placed at a spacing of 160 mm, the joint shear reinforcement ratio ρ_j is 0.46% (a transverse reinforcement volume ratio $\rho'' = 0.29\%$). For **ED4U** and **ED4UC** where the shear reinforcement is placed at a spacing of 100 mm, the joint shear reinforcement ratio ρ_j is 0.93% ($\rho'' = 0.58\%$ and 0.63%). In the case of low-rise buildings, the compressive force acting on the column is small, so the joint shear reinforcement plays a major role of shear resistance rather than concrete confinement. Thus, the amount of joint shear reinforcement in Table 5-1 is expressed as shear reinforcement ratio, not volume ratio.

5.2.3 Material strengths

Table 5-2 presents the yield and tensile strengths (f_y and f_u) of the reinforcing steel bars used for beam and column connection specimens. As cyclic tests were performed two separate times, f_y (= 481 ~ 588 MPa) and f_u (= 605 ~ 720 MPa) of D10 to D25 bars used in each test were differed as shown in Table 5-2. In the table, SD400 and SD500 denote the nominal yield strength of deformed bars, 400 and 500 MPa, respectively, and D10, D13, D19, D22, and D25 denote the diameters of deformed bars, d_b = 9.53, 12.7, 19.1, 22.2, and 25.4 mm, respectively. The yield and tensile strengths in Table 5-2 are average values of three test results of reinforcing bars.

Table 5-3 shows the mix proportioning of the concrete. The maximum aggregate size was 25.4 mm. In each material test, three concrete cylinders of a diameter 100 mm and a height 200 mm were prepared and the compression tests of the cylinders were performed on the first day of testing. The compressive strengths of the concrete were f_c' = 20, 31 MPa on average.

Table 5-2 Properties of steel reinforcing bars

Test No.	Bar type	d_b (mm)	f_y (MPa)	f_u (MPa)	ε_y (mm/mm)
1	SD400 D10	9.53	552	676	0.00276
	SD400 D13	12.7	481	605	0.00241
	SD500 D22	22.2	565	688	0.00283
	SD500 D25	25.4	550	664	0.00275
2	SD400 D10	9.53	576	689	0.00288
	SD400 D13	12.7	528	656	0.00264
	SD500 D19	19.1	550	685	0.00275
	SD500 D22	22.2	577	720	0.00289
	SD500 D25	25.4	588	702	0.00294

Note: Test No. 1 contains specimens **EDNNI**, **ED2R, ED2U**, and **ED2UNI**
Test No. 2 contains specimens **ED4U** and **ED4UC**

Table 5-3 Mix design of concrete

Test No.	Compressive strength	W/C	Unit weigh, kgf/m^3							Slump
			W	C	FS	S	FA	CA	SP	
1	20 MPa	54.2%	167	200	46	62	873	806	1.54	120 mm
2	31 MPa	48.4%	155	192	64	64	904	909	2.24	120 mm

Note: W = water; C = cement; FS = fly ash; S = blast furnace slag; FA = fine aggregate; CA = coarse aggregate; SP = superplasticizer

5.2.4 Test setup and loading plan

Figure 5-6 shows a test setup for lateral cyclic loading of a beam and column exterior connection. Since the details of test setup are same as the test setup in Chapter 4, please refer to the test setup in Figure 4-38. The displacement history for the cyclic lateral loading is also same as Figure 4-39. The loading protocol was planned with increasing of 1.2 ~ 1.5 times previous drift ratio and three steps at every drift ratio specified in ACI 374.1. The lateral displacement of the columns was increased from 0.25% in the elastic range to the drift ratio at 80% of peak loads in the descending branch.

The lateral load (P) and lateral displacement (Δ) were measured from the load cell in the Actuator and the line LVDT at the top of the column. Horizontal and vertical slips (s_h and s_v) measured at the hinge and roller supports were calibrated to compute the actual lateral displacement applied in the exterior connection. The strain gauges and LVDT locations in test specimens were illustrated in Figure 4-32 and Figure 4-33 (Chapter 4), respectively.

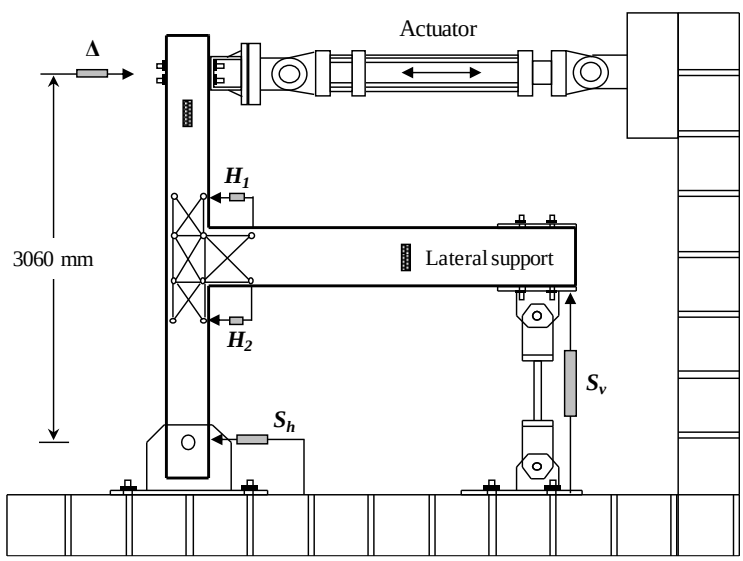

Figure 5-6 Schematic test setup of a beam-column exterior connection

5.3 Load - Displacement Relations and Failure Modes

In this study, the failure modes of exterior connections were classified into flexural yielding of beams or columns, joint shear failure, and anchorage failure of beam bars. The load capacity of the connections was evaluated according to the failure mode. Prediction of failure mode and nominal strength is referred to section 4.3 in Chapter 4.

5.3.1 Non-conforming exterior connections (EDNNI, ED2R, ED2U, ED2UNI)

Figure 5-7 shows the lateral load (P) and drift ratio (δ) relationship for each specimen. P is the actuator load acting on the upper part of the column, and δ is drift ratio obtained by dividing the column lateral displacement by the net column height (= 3060 mm) between the loading point and the hinge support. Positive load ($P > 0$) is the state where negative moment (tension in the beam top bars) is applied in the beam. The maximum positive and negative loads P_u are indicated with circular marks on the P - δ cyclic curves. For comparison, the nominal strengths P_{nb} and P_{nj} are also marked as horizontal dashed lines in Figure 5-7. Figure 5-8 shows cracking patterns and failure modes of exterior connection specimens at each drift ratio. For comparison, the test specimens in Chapter 4 were also presented in Figure 5-7 and Figure 5-8.

Specimen **EDNNI** without joint shear reinforcement showed similar cyclic behavior and failure modes to specimen **EUN** in Chapter 4. The maximum loads were reached at drift ratio of ±1.5%, and then the major joint shear crack was enlarged with a decrease in strength and side vertical crack was developed. Because of no joint shear reinforcement, side vertical cracks were easily developed. Finally, the anchorage failure of beam bars with concrete cover spalling off occurred at drift ratio of 5.0%. In the absence of joint shear reinforcement, the force was not smoothly transmitted through the joint, and the strength was greatly reduced compared to other specimens with joint shear reinforcement. A relatively small number of diagonal cracks resulted in the enlarged major diagonal shear crack width.

In the case of **ED2R**, **ED2U**, and **ED2UNI** where D25 reinforcing bars were used as beam longitudinal reinforcement, the $P - \delta$ relations and failure mode were similar to **EU2R** and **EU2U** in Chapter 4 regardless of the hook direction of beam bottom bars. The maximum loads were reached at drift ratio of 1.5 ~ 2.0%, and the load capacity dropped to 80% of maximum loads at drift ratio of 3.5%. Pinching occurred during cyclic behavior, thereby decreasing energy dissipation capacity. As shown in Figure 5-8, diagonal shear cracks and concrete damage were mainly concentrated in the joint region compared to column and beam, which indicates that the exterior connections were dominated by joint behavior.

The maximum loads of **ED2R**, **ED2U**, and **ED2UNI** were 48 ~ 64% of P_{nb} due to flexural yielding (= +136 kN and -73 kN), which indicating that the joint failure occurred before beam flexural yielding. The maximum load was 66 ~ 71% greater than the nominal joint shear strength P_{nj}^{NC} (= ±39.5 kN, non-conforming) in the positive direction, but it was almost similar to that in the negative direction. The difference between the positive and negative directions is due to the anchorage failure of the beam longitudinal reinforcement in the joint region (l_{al} / l_{dh} = 0.59, see Table 5-1). The tensile stress acting on the beam bottom reinforcing bars was about 2 times the tensile stress of the beam top bars, even though the actuator loads in both positive and negative directions were the same. Thus, early anchorage failure occurred in the beam bottom bars with smaller maximum negative load than maximum positive load.

The reason for such anchorage failure of beam bars is as follows. First, the ratio of positive and negative maximum loads to nominal strength for beam flexural yielding (P_u / P_{nb} = 48 ~ 65%) is similar to the ratio of provided anchorage length to required anchorage length (l_{al} / l_{dh} = 0.59). Second, as shown in Figure 5-8 (c) and (d), joint diagonal shear cracks propagated along the hook tail direction of beam bars, which is disadvantageous to strut action and truss mechanism in the joint.

In order to analyze the failure sequence and the effect of test parameters on each specimen, specimens **EDNNI**, **ED2R**, **ED2U**, and **ED2UNI** were investigated in Figure 5-9 ~ Figure 5-16.

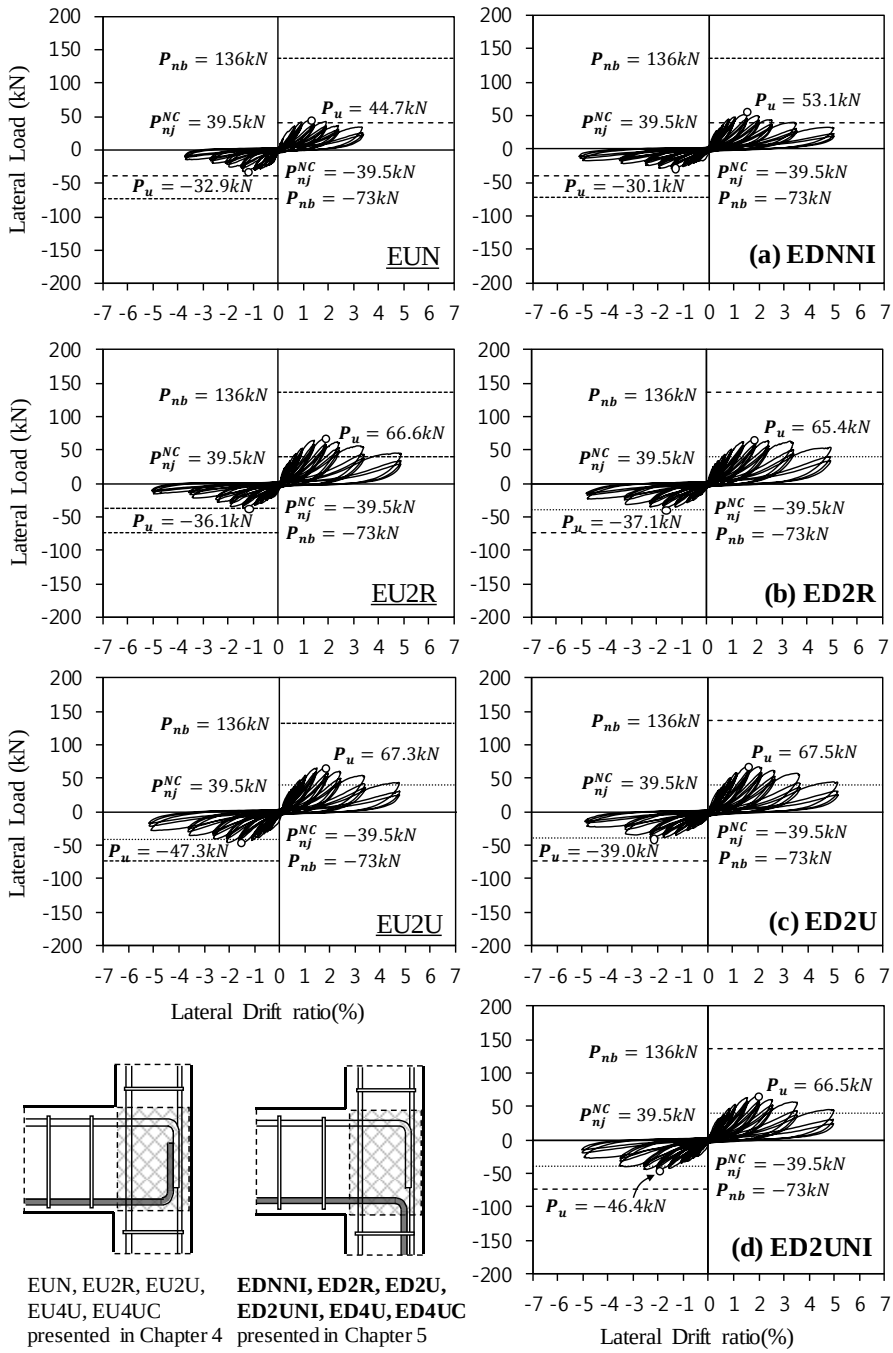

Figure 5-7 Comparison on lateral load - drift ratio relationship of non-conforming exterior connection specimens

Table 5-4 Summary of test results (strength, failure mode, and ductility)

Specimen	Test strength (P_u) [1]		Predicted strength (P_n) [2]		Strength ratio (P_u / P_n)		Failure mode [3]		Average drift ratio (%)		Ductility (δ_u / δ_y)
	Positive	Negative	Positive	Negative	Positive	Negative	Positive	Negative	Yield (δ_y) [4]	Ultimate (δ_u) [5]	
EUN	44.7	32.9	39.5	39.5	1.13	0.83	J	J	0.58	2.48	4.28
EDNNI	53.1	30.1	39.5	39.5	1.34	0.76	J	J	0.67	2.96	4.45
EU2R	66.6	36.1	39.5	39.5	1.69	0.91	J	J	0.78	2.93	3.78
ED2R	65.4	37.1	39.5	39.5	1.66	0.94	J	J	0.89	4.32	4.88
EU2U	67.3	47.3	39.5	39.5	1.70	1.20	J	J	0.87	3.34	3.86
ED2U	67.5	39.0	39.5	39.5	1.71	0.99	J	J	0.98	3.88	3.96
ED2UNI	66.5	46.4	39.5	39.5	1.68	1.17	J	J	1.04	3.92	3.79
EU4U	110	91	99.1	88	1.11	1.03	J	BJ	1.91	4.95	2.59
ED4U	115	91	99.1	88	1.16	1.03	J	BJ	1.99	5.14	2.58
EU4UC	156	99	137	89	1.14	1.11	BJ	BJ	1.88	5.03	2.68
ED4UC	143	97	137	89	1.04	1.09	BJ	BJ	1.78	4.31	2.42

1) P_u : Ultimate test loads
2) P_n : Nominal strengths calculated for failure modes in 4.3 (Chapter 4)
3) J : Joint shear failure before beam and column flexural yielding , BJ : Joint shear failure after beam flexural yielding
4) δ_y : Yield drift ratio defined as the point at which the maximum load reaches 60% of the maximum load and the secant stiffness of the origin
5) δ_u : Ultimate drift ratio defined as the smaller of the positive and negative maximum drift ratios corresponding to 80% of the maximum load

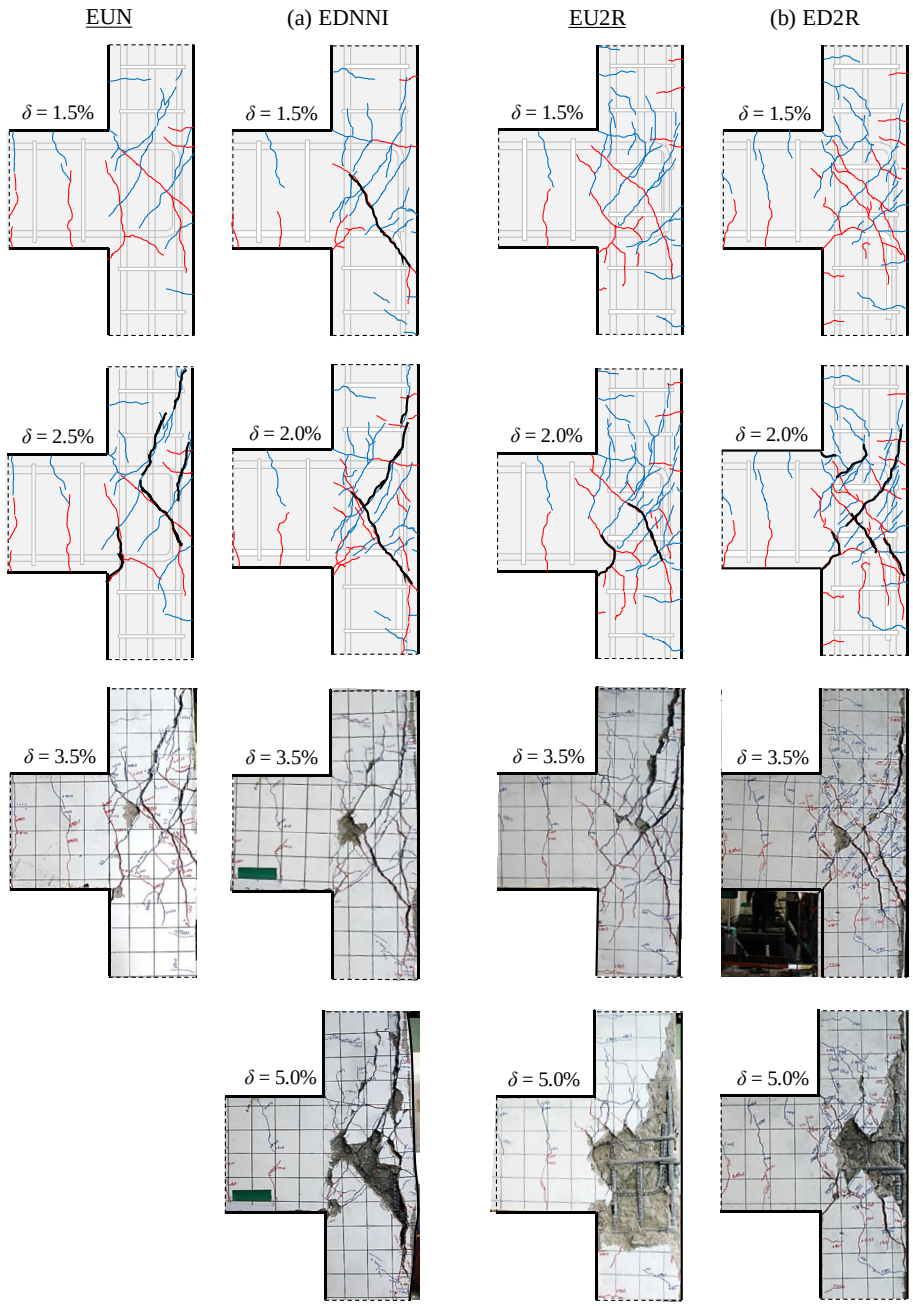

Figure 5-8 Comparison on cracking patterns and failure modes of non-conforming exterior connection specimens at each drift ratio (Continued)

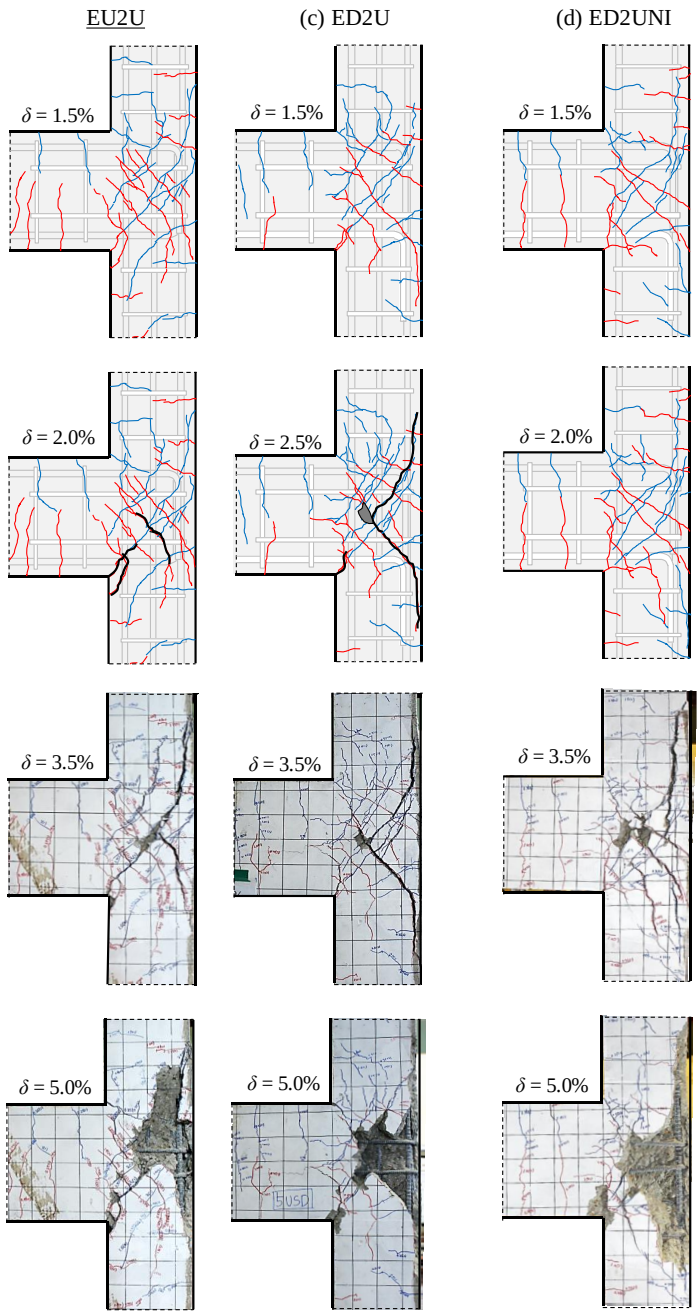

Figure 5-8 Comparison on cracking patterns and failure modes of non-conforming exterior connection specimens at each drift ratio

A. Specimen EDNNI

The specimen **EDNNI** has no joint shear reinforcement, insufficient anchorage length of beam longitudinal bars in the joint (l_{al} / l_{dh} = 0.59), and no intermediate column bars. The hook direction of beam bottom bars is downward. Joint shear failure is expected in both directions.

1. A similar failure mode to specimen **EUN** was observed. In the absence of joint shear reinforcement, the force transfer through the joint was not smooth, so a relatively small number of cracks were developed with wide crack width. Especially, a wide diagonal shear crack occurred in the negative loading at drift ratio of 1.5%.

2. Loads were no longer increased by the diagonal cracks and side vertical cracks at drift ratio of 1.5%. When the beam bottom bars are subjected to tensile stress at drift ratio of 1.5%, a major joint diagonal crack enlarged due to the effect of hook tail direction.

3. The effect of column intermediate bars was not significant. As the column depth was small, the force transfer was affected by the horizontal joint shear reinforcement rather than vertical bars of the columns. Thus, sufficient horizontal shear reinforcement in the joint is required to form the diagonal strut mechanism.

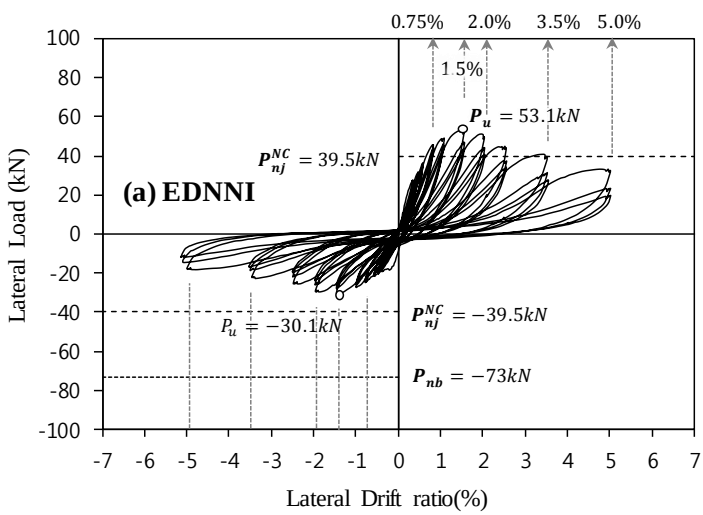

Figure 5-9 Lateral load and drift ratio relationship of specimen EDNNI

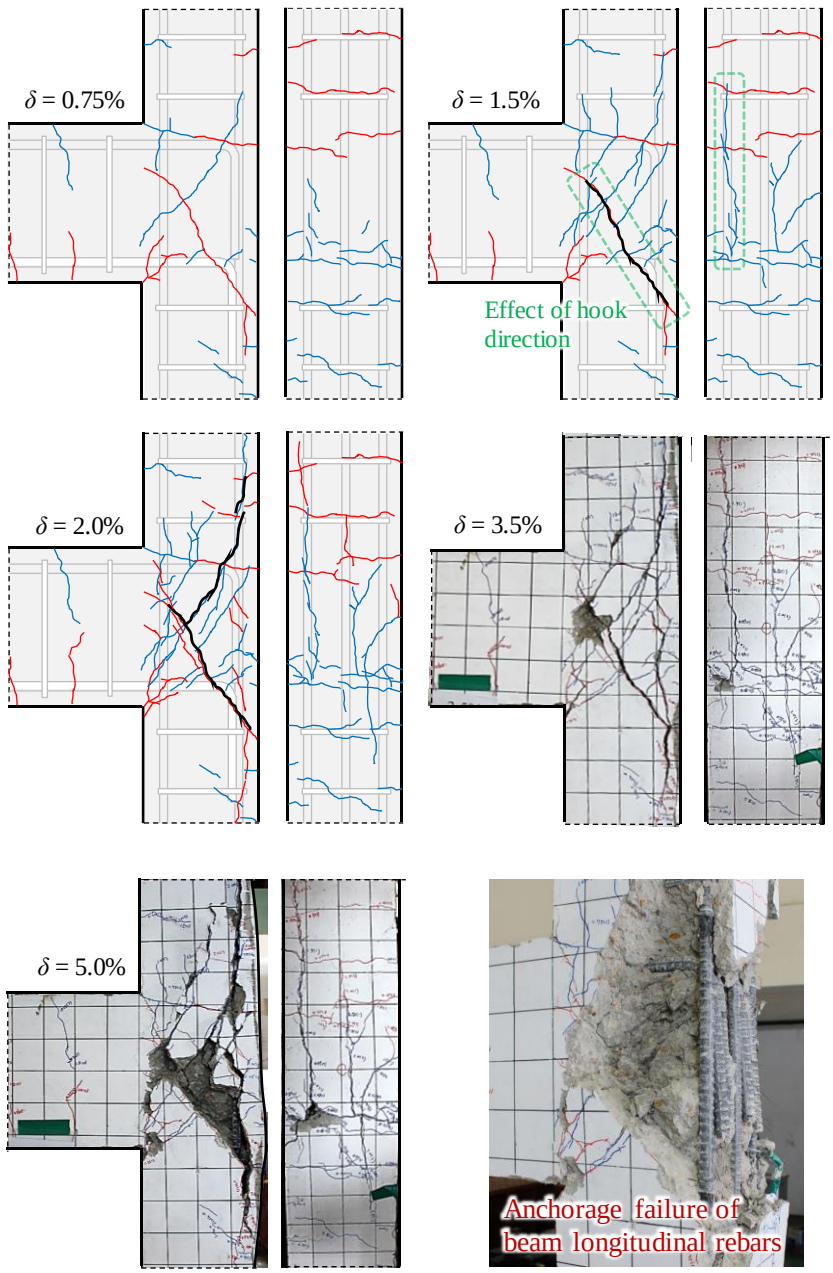

Figure 5-10 Failure sequence and final failure mode of specimen EDNNI

B. Specimen ED2R

The specimen **ED2R** has joint shear reinforcement volume ratio of less than 0.003 (Non-conforming, s = 160 mm) and insufficient anchorage length of beam longitudinal bars in the joint (l_{al} / l_{dh} = 0.59). The hook direction of beam bottom bars is downward. Joint shear failure is expected in both directions.

1. The load-drift ratio relations and failure mode until maximum load (δ = 2.0%) was almost similar to specimen **EU2R**. After drift ratio of 2.0%, the influence of the hook direction gradually occurred. Side vertical cracks occurred when the beam top bars were stressed in tension, but vertical cracks did not occur when tensile stress was applied to the beam bottom bars where the hooks were anchored to the lower column. At drift ratio of 3.5%, thus, the damage of the side vertical cracks was relatively smaller than that of specimen **EU2R**.

2. Finally, the joint shear failure and anchorage failure of the beam bottom bars occurred with concrete cover spalling off at the front and side of the joint. The residual strength at the end of test (δ = 5.0%) was greater than that of **EU2R**.

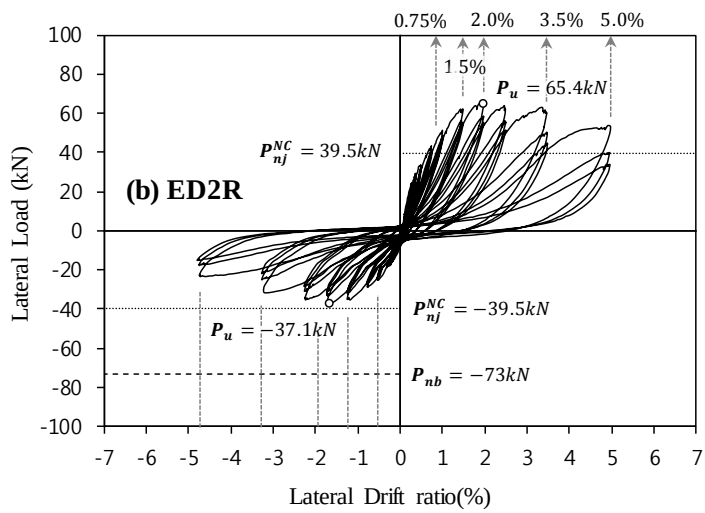

Figure 5-11 Lateral load and drift ratio relationship of specimen ED2R

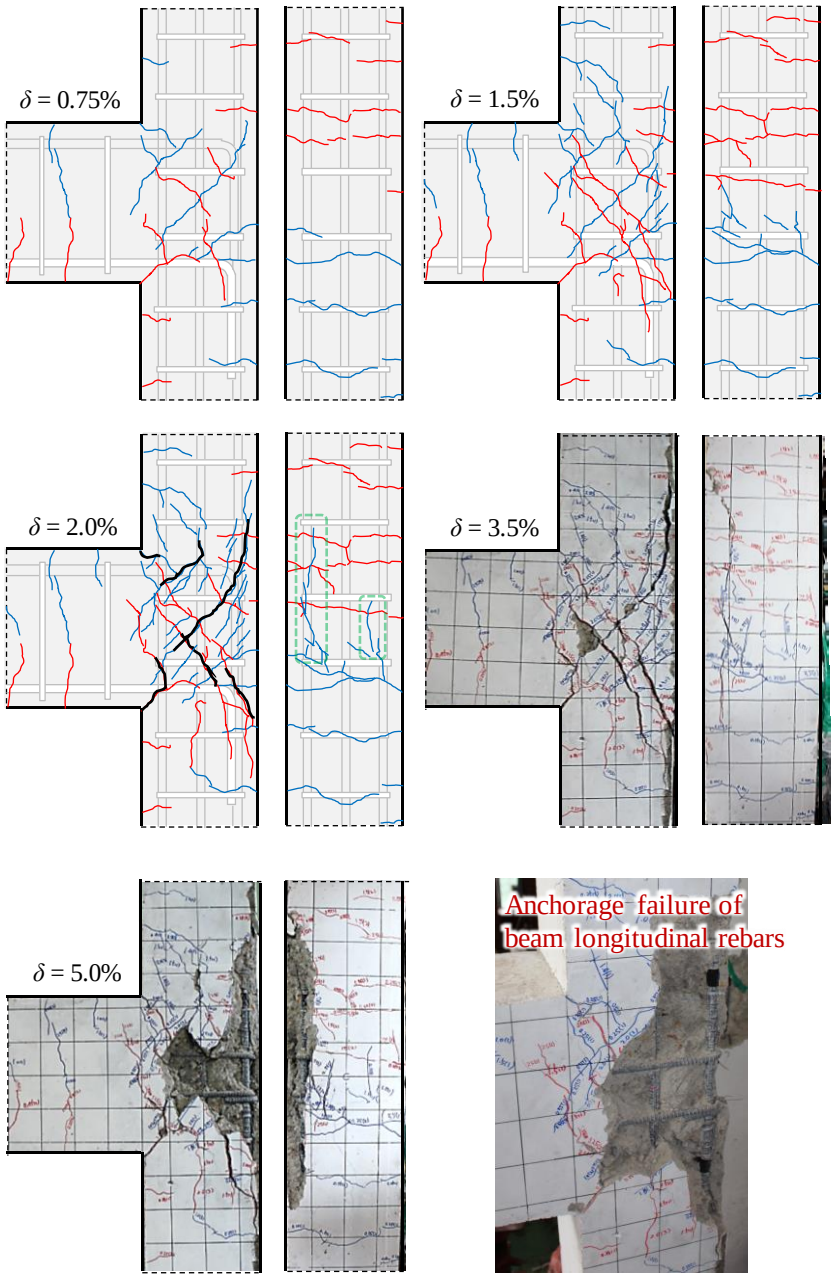

Figure 5-12 Failure sequence and final failure mode of specimen ED2R

C. Specimen ED2U

The specimen **ED2U** has joint shear reinforcement volume ratio of less than 0.003 (Non-conforming, s = 160 mm) and insufficient anchorage length of beam longitudinal bars in the joint (l_{al} / l_{dh} = 0.59). The hook direction of beam bottom bars is downward. The U shaped bars were used for joint shear reinforcement. Joint shear failure is expected in both directions.

1. For positive direction, the same load-drift ratio relation and failure mode as **EU2U** was shown, but not for the negative direction. In Figure 5-13, the initial stiffness decreased sharply in the negative direction, thereby decreasing maximum load. This is because the diagonal strut action in the joint did not work smoothly due to joint diagonal shear crack propagated along the hook tail direction of beam bottom bars as shown in Figure 5-14.

2. Nevertheless, since similar final failure mode and the load-drift ratio relations to closed ties using 90º hooks, the U-bar can be alternative details for joint shear reinforcement for improving workability.

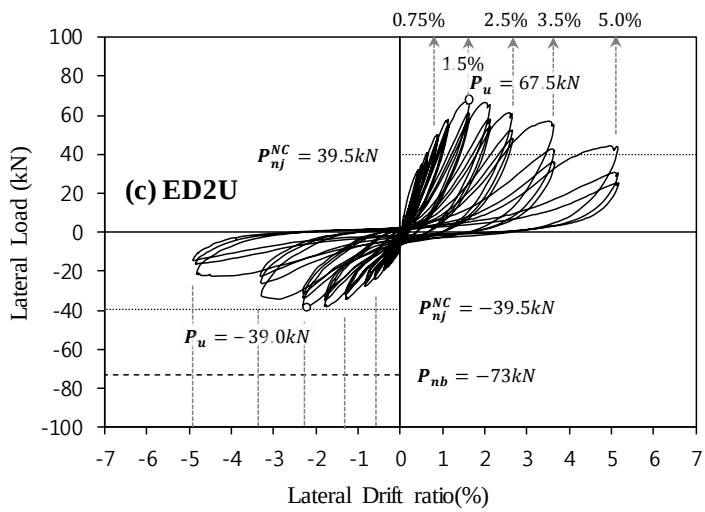

Figure 5-13 Lateral load and drift ratio relationship of specimen ED2U

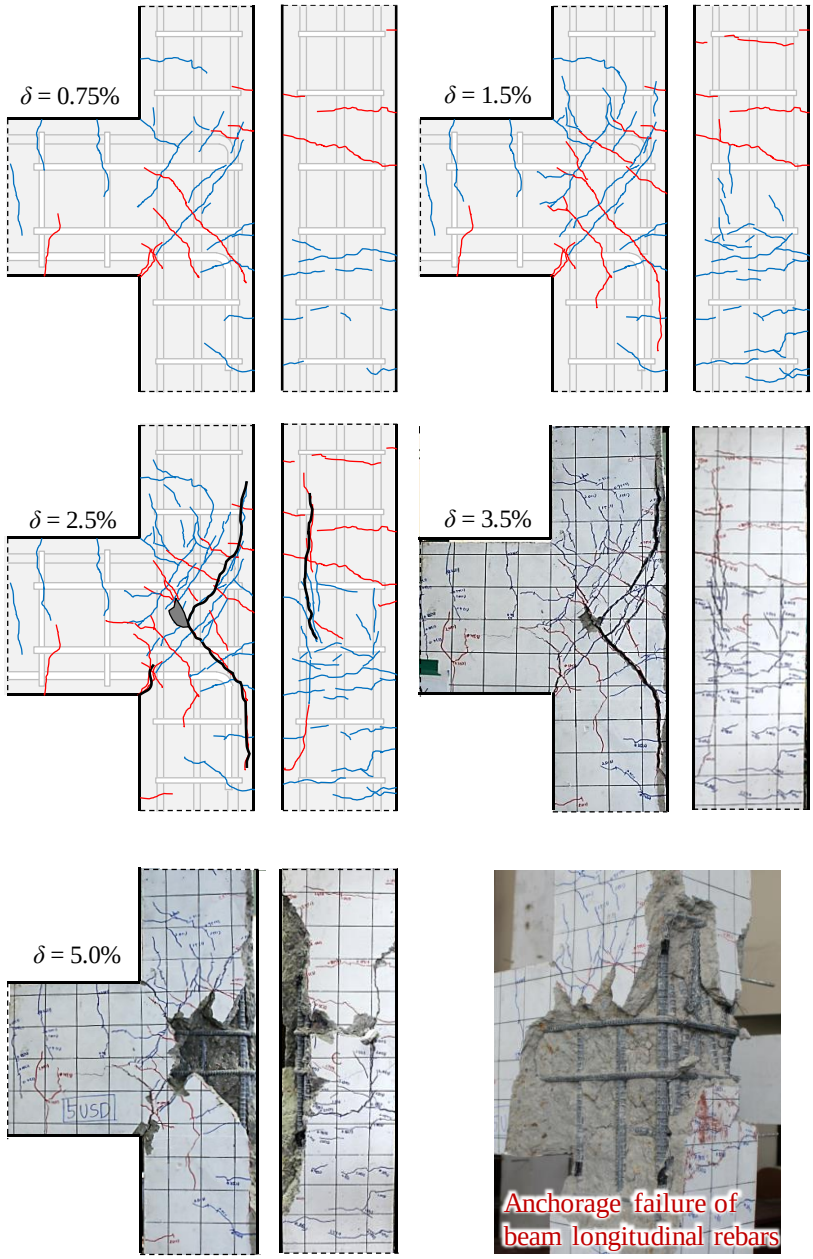

Figure 5-14 Failure sequence and final failure mode of specimen ED2U

D. Specimen ED2UNI

The specimen **ED2UNI** has joint shear reinforcement volume ratio of less than 0.003 (Non-conforming, s = 160 mm), insufficient anchorage length of beam longitudinal bars in the joint (l_{al} / l_{dh} = 0.59), and no intermediate column bars. The hook direction of beam bottom bars is downward. The U shaped bars were used for joint shear reinforcement. Joint shear failure is expected in both directions.

1. In spite of the absence of the column intermediate bars and different hook direction of beam bottom bars, **ED2UNI** showed similar load-drift ratio relation and failure mode to **EU2U**. This indicates that the effect of column intermediate bars and hook direction of beam bottom bars was not significant in the small column (joint) depth.

2. Compared with the specimen **EDNNI** in Figure 5-9, the joint diagonal cracks were restrained by joint horizontal shear reinforcement, thereby increasing load-carrying capacity and deformation capacity. Exterior joints with small column depth can increase joint shear strength by horizontal shear reinforcement.

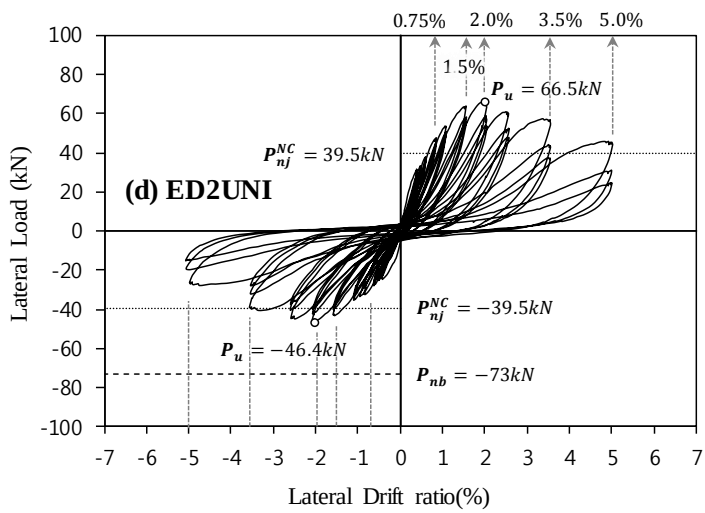

Figure 5-15 Lateral load and drift ratio relationship of specimen ED2UNI

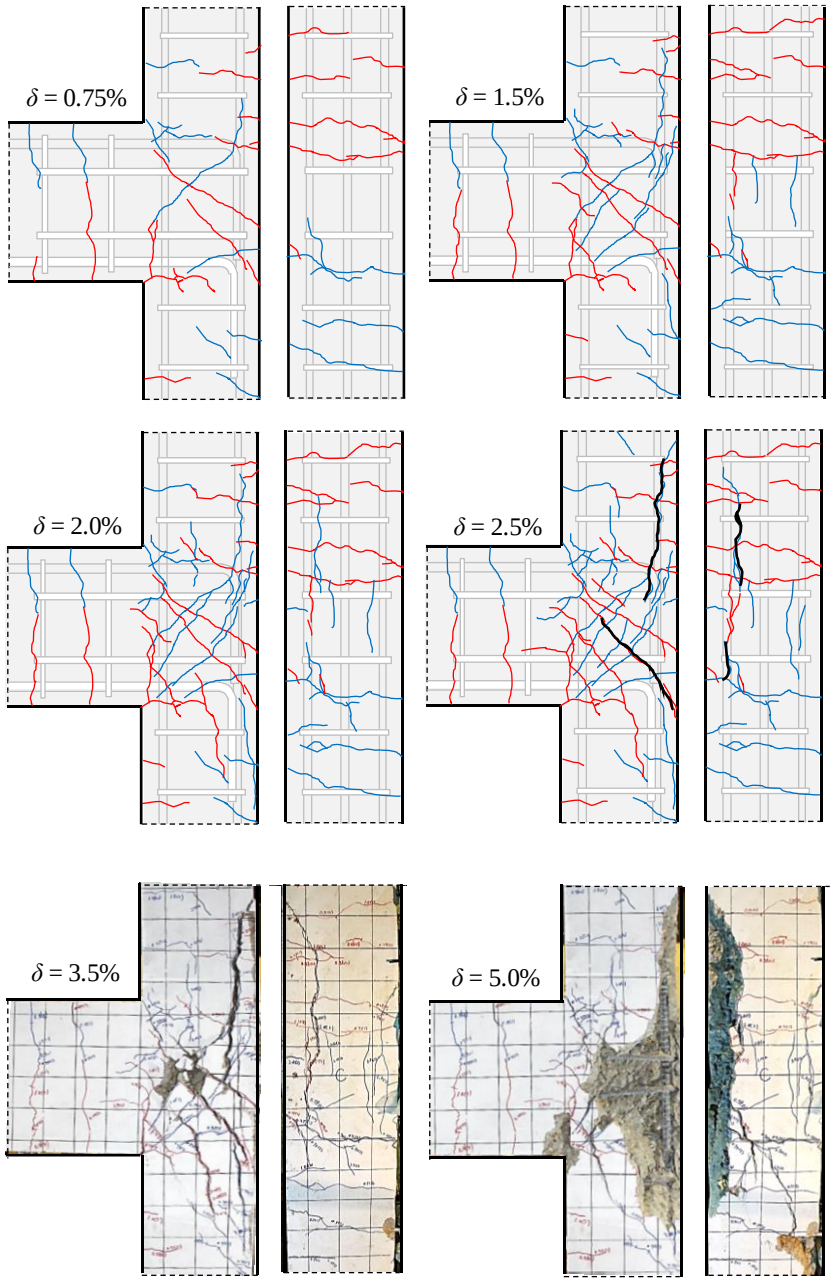

Figure 5-16 Failure sequence and final failure mode of specimen ED2UNI

5.3.2 Conforming exterior connections (ED4U and ED4UC)

Figure 5-17 shows the lateral load (P) and drift ratio (δ) relationship for **ED4U** and **ED4UC** compared with test results of **EU4U** and **EU4UC** presented in Chapter 4. For specimen **ED4U** where D19 reinforcing bars were used as beam reinforcements and a spacing of joint shear reinforcement decreased to 100 mm, maximum positive and negative loads were greatly increased by 70% in the positive direction and 133% in the negative direction compared to specimen **ED2U**. The maximum load was reached at drift ratio of 2.5 ~ 3.5%, and then the load-carrying capacity gradually decreased to less than 80% of the maximum load at drift ratio of 5.0%.

A large number of diagonal cracks occurred at drift ratio of 1.5%, but the diagonal crack width did not significantly increase until drift ratio of 3.5% as a result of restraining the diagonal cracks in the joint shear reinforcement (See Figure 5-18). The concrete cracks and damages were not significant in the adjacent beams and columns. However, severe diagonal cracks occurred with concrete cover spalling off in the joint region.

In the case of **ED4U**, the maximum positive load P_u (= 115 kN) was 16% larger than nominal joint strength P_{nj}^C (= 99.1 kN), but the maximum negative load P_u (= 91 kN) was smaller than P_{nj}^C. This is because the failure modes of **ED4U** were different according to the loading direction. In the case of negative loading when beam bottom bars were stressed in tension, since P_{nb} (= 88 kN) is smaller than P_{nj}^C (= 99.1 kN), beam flexural yielding preceded the joint shear failure. In the case of positive loading when beam top bars were stressed in tension, on the other hand, since P_{nb} (= 135 kN) is greater than P_{nj}^C (= 99.1 kN), the joint shear failure occurred before beam flexural yielding.

For specimen **ED4UC**, where the column depth h_c was increased to 450 mm, the maximum positive load P_u (= 143 kN) increased significantly compared to specimen **ED4U**, but the maximum negative load P_u (= -97 kN) was almost similar. The increase in the positive direction is due to the increase of the effective joint area A_j (= $h_c \cdot b_c$). As a result, although P_{nj}^C (= 130 kN) was slightly smaller than P_{nb} (= 137 kN), specimen **ED4UC**, unlike other specimens, underwent beam flexural yielding prior to joint shear failure even under positive loading. It can be seen from

the test results that the concrete cracking and damages were accumulated not only in the joint but also in the beam at drift ratio of 3.5% as shown in Figure 5-18.

As a result of increasing the effective joint area, the energy dissipation of **ED4UC** was greatly increased as shown in Figure 5-17 (f). The concrete cracks and damage in the joint were not significant at drift ratio of 3.5% as shown in Figure 5-18 (f). However, after drift ratio of 3.5%, the diagonal crack width rapidly increased, thereby decreasing joint shear resistance. Finally, joint shear failure occurred.

EU4UC and **ED4UC** showed different hysteretic behaviors according to the hook direction of beam bottom bars, unlike other specimens. The maximum load of **EU4UC**, in which the beam bottom bars anchored inside the joint, was higher than that of **ED4UC**, anchored in the adjacent column. As a result, the deformation capacity of **EU4UC** was improved, and the energy dissipation was also increased by 18% and 41% at drift ratio of 3.5% and 5.0%, respectively.

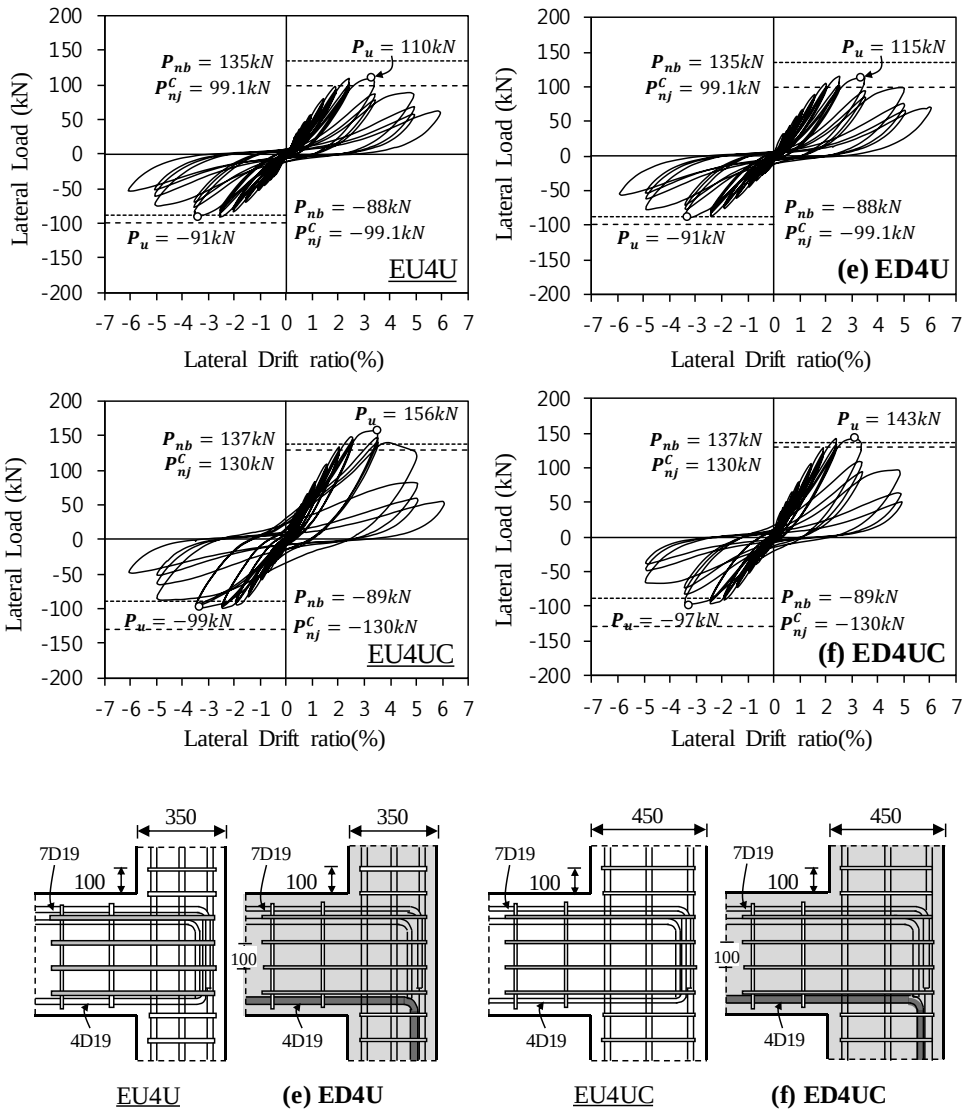

Figure 5-17 Comparison on lateral load - drift ratio relationship of conforming exterior connection specimens

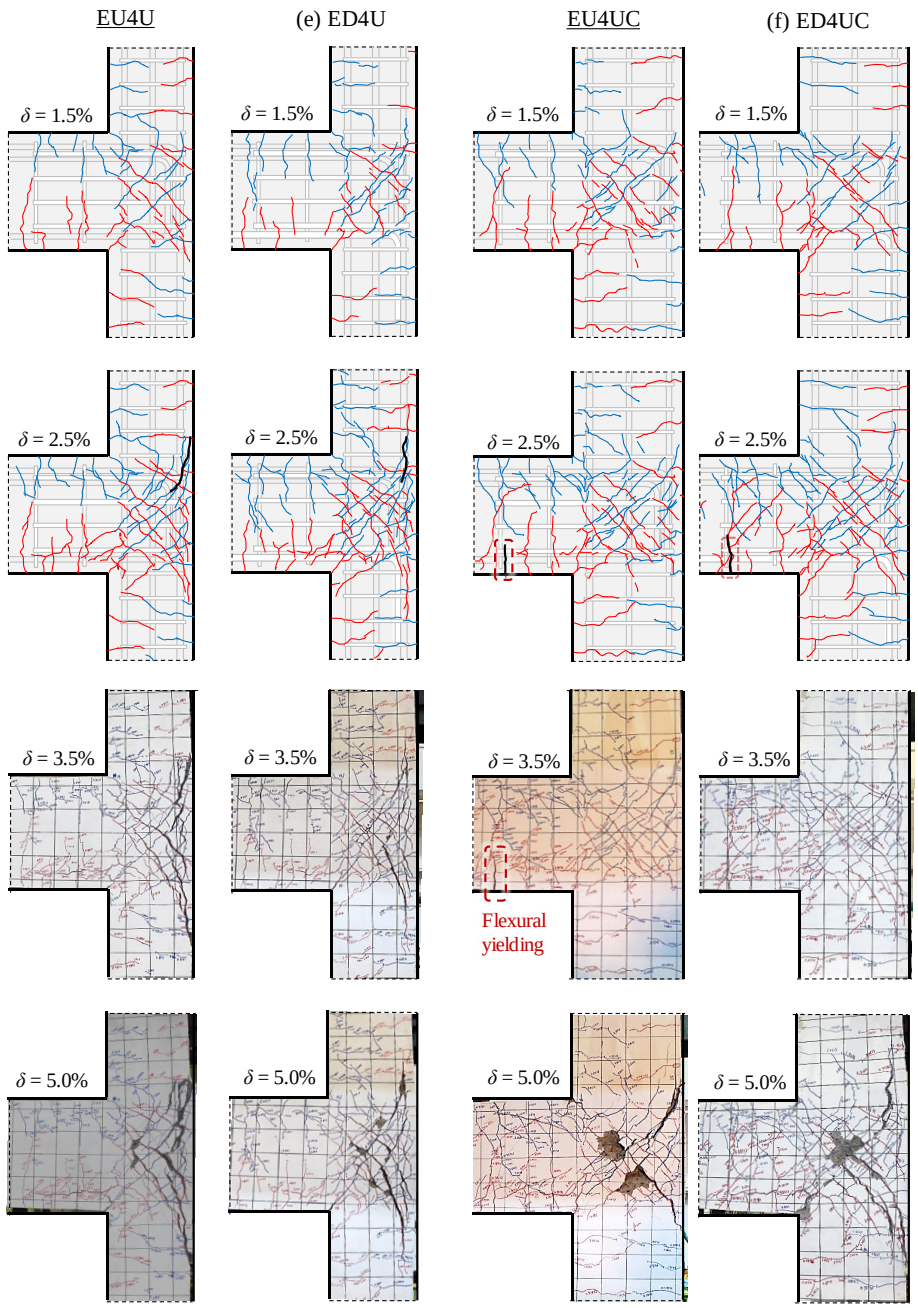

Figure 5-18 Comparison on cracking patterns and failure modes of conforming exterior connection specimens at each drift ratio

E. Specimen ED4U

The specimen **ED4U** has joint shear reinforcement of greater than 0.003 (Conforming) and almost satisfied anchorage length of beam longitudinal bars in the joint (l_{al} / l_{dh} = 0.96). The hook direction of beam bottom bars is downward. The U - bars were used for joint shear reinforcement. Joint shear failure is predicted for positive direction and beam flexural yielding for negative direction.

When compared with **EU4U**, specimen **ED4U** showed the same load-drift ratio relation and failure sequence. This means that there is almost no influence of hook direction of beam bottom bars when column depth is relatively small. The four joint shear reinforcing bars greatly contributed to the joint mechanism and showed a great difference from **ED2U** using two shear reinforcing bars in the joint. Though concrete cover was spalled off at drift ratio of 6.0%, U-bar was sufficiently anchored into the beam at the end of test.

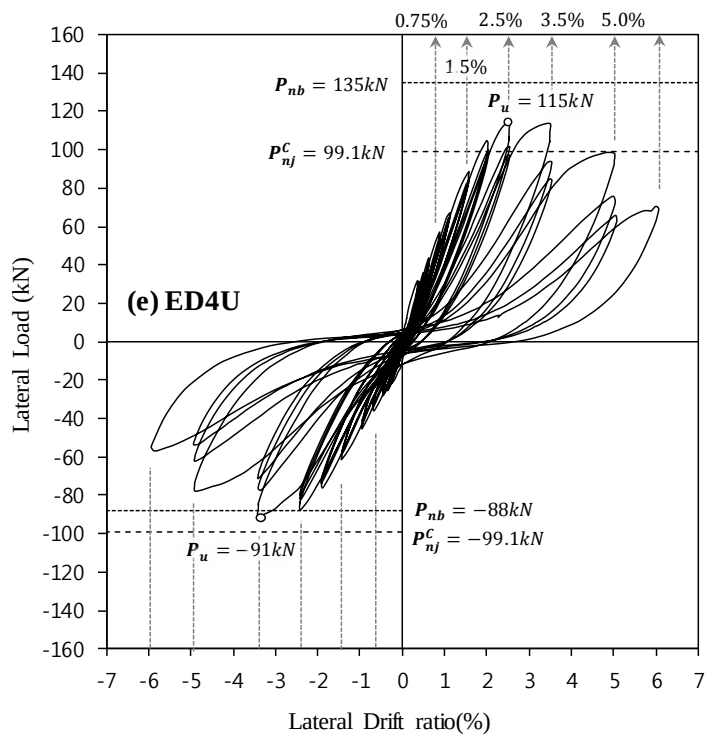

Figure 5-19 Lateral load and drift ratio relationship of specimen ED4U

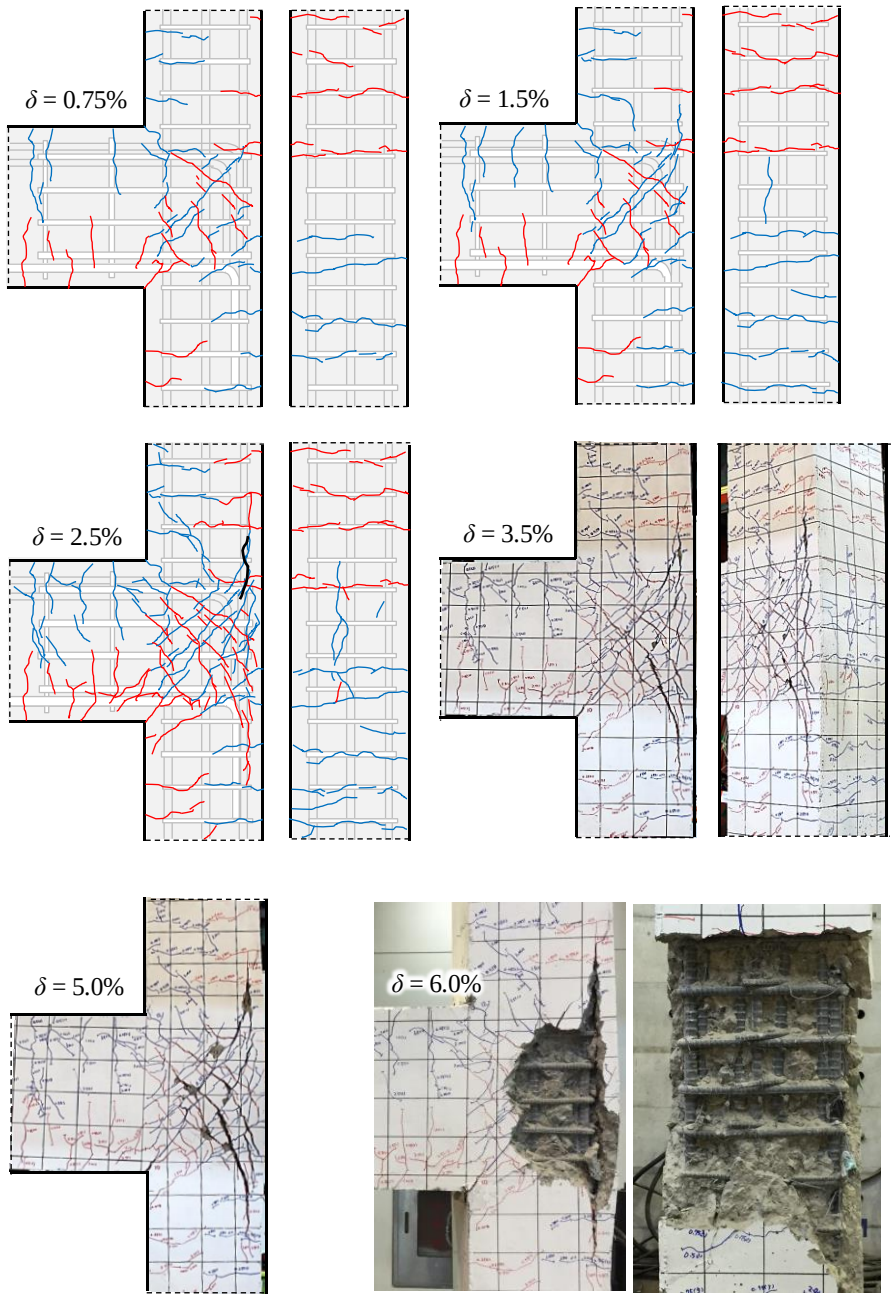

Figure 5-20 Failure sequence and final failure mode of specimen ED4U

F. Specimen ED4UC

The specimen **ED4UC** has joint shear reinforcement of greater than 0.003 (Conforming) and sufficient anchorage length of beam longitudinal bars in the joint (l_{al} / l_{dh} = 1.28). The hook direction of beam bottom bars is downward. The U shaped bars were used for joint shear reinforcement, and the column depth was increased to 450 mm to increase the joint effective area. Beam flexural yielding before joint shear failure is expected for both positive and negative directions.

As the joint area increased, the joint behavior was affected by the hook direction of beam bottom bars. The load-drift ratio relation and energy dissipation capacity of **ED4UC** were similar to **EU4UC** until drift ratio of 2.5%, but they showed a gradual difference after drift ratio of 3.5%.

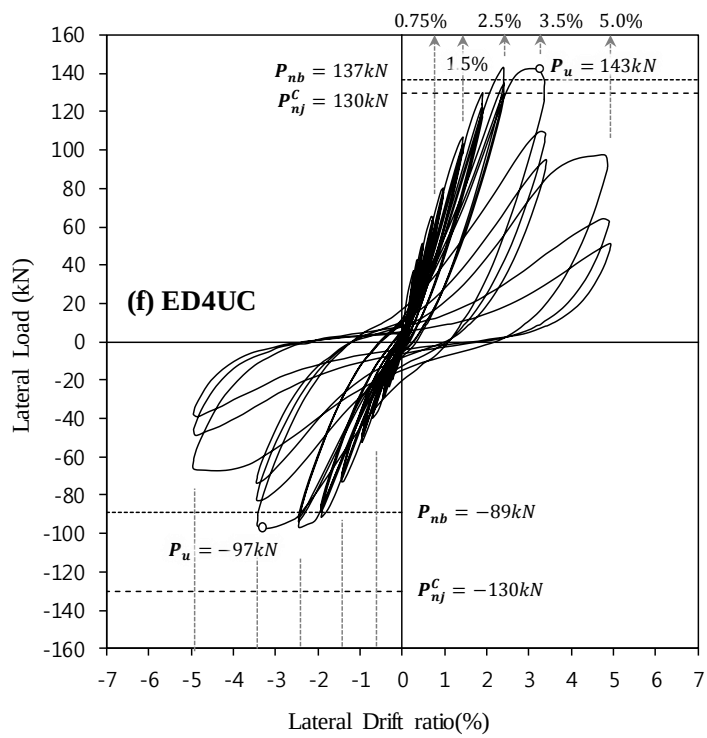

Figure 5-21 Lateral load and drift ratio relationship of specimen ED4UC

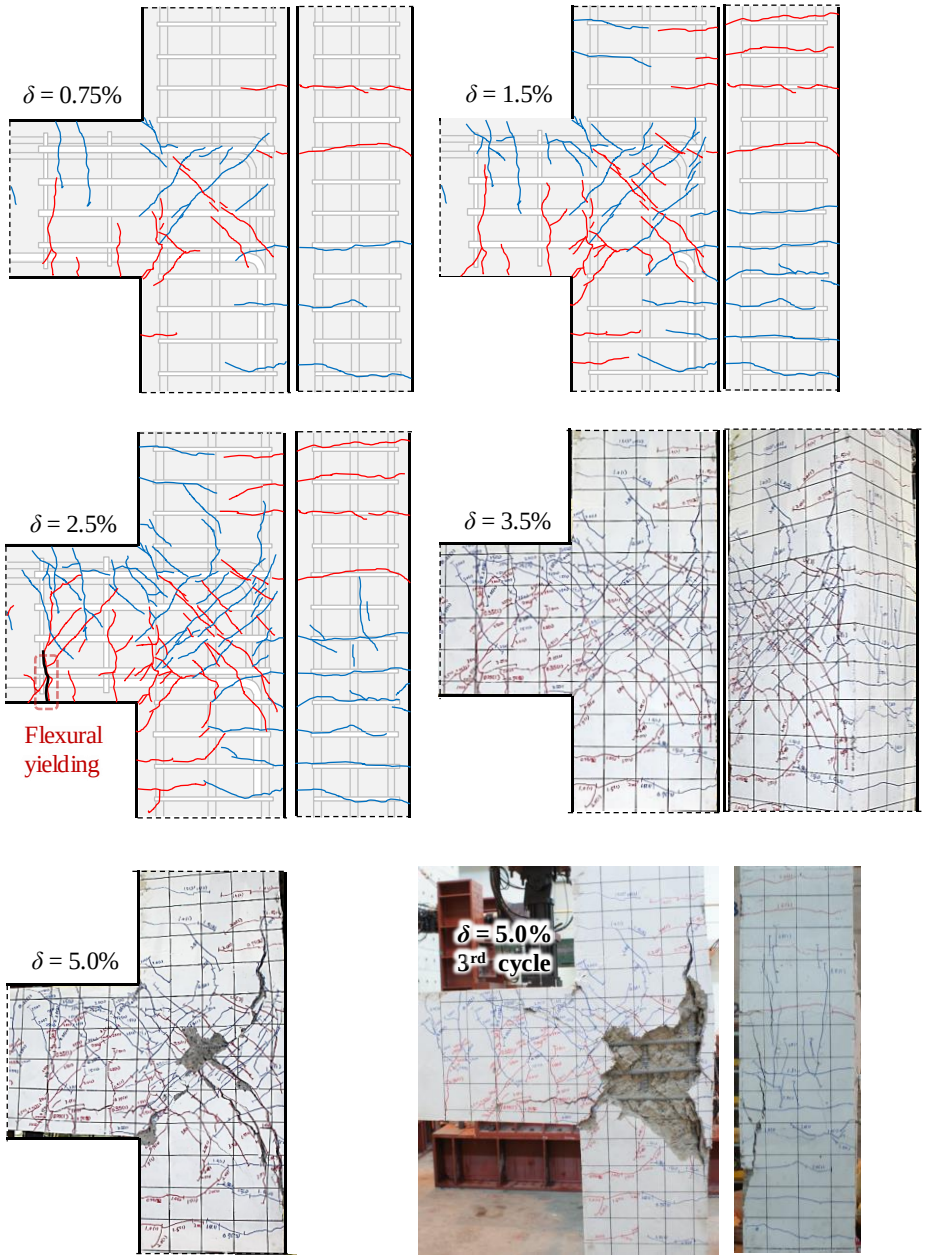

Figure 5-22 Failure sequence and final failure mode of specimen ED4UC

5.4 Strain of Steel Reinforcing Bars

5.4.1 Strains of beam longitudinal bars

Figure 5-23 shows the strains of beam flexural reinforcement measured at specimens **EDNNI**, **ED2R**, **ED2U**, **ED2UNI**, **ED4U**, and **ED4UC** compared to specimens **EUN**, **EU2R**, **EU2U**, **EU4U**, and **EU4UC** in Chapter 4. The strains of the top and bottom bars are both measured at the face of columns. For comparison, the yield strain of the bars is indicated by the horizontal dashed line. The different strain behaviors of beam bars were presented due to joint diagonal shear cracks and anchorage failure of the beam bars.

In specimens **EDNNI**, **ED2R**, **ED2U**, and **ED2UNI** where anchorage failure occurred prior to beam flexural yielding, the strain of beam bars was not increased from drift ratio of 1.0 ~ 1.5% where diagonal shear cracks occurred in the joint. Thus, the top and bottom bars of beams did not reach the yield strain (= 0.00275 mm/mm). In particular, the specimens **EDNNI** and **ED2UNI** without column intermediate bars showed much smaller strains than the other specimens. This results indicate that the bond slip of beam bars was largely occurred before yielding the bars.

On the other hand, in specimen **ED4U** where the joint shear failure occurred before and after the beam flexural yielding, respectively, in positive and negative directions, the strains of beam bars reached yield strain at drift ratio of 3.5%. However, even if the drift ratio increased to over 3.5%, the tensile strains of beam bars did not increase any more. This is because the lateral displacement of the column was absorbed by the shear deformation of the joint after the joint shear failure at drift ratio of 3.5%.

In specimen **ED4UC** where the joint shear failure occurred after beam flexural yielding, the strains of beam bars reached the yield strain at drift ratio of 2.0%. Unlike **ED4U**, the strains continued to increase to drift ratio of 3.5% when the maximum loads were attained. The joint shear strength increased with increasing joint effective area, so the beam bars can resist higher tensile stress after beam flexural yielding.

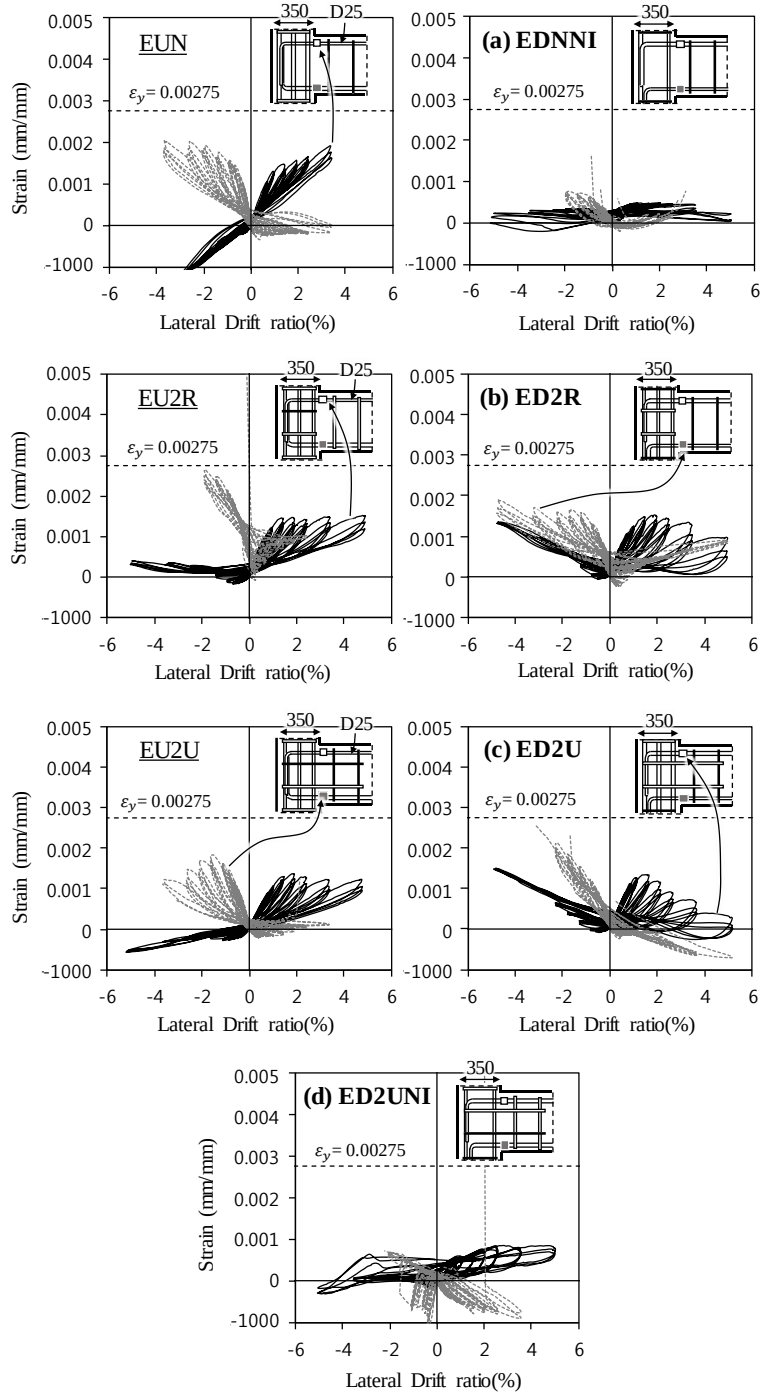

Figure 5-23 Strains of beam top and bottom longitudinal bars (Continued)

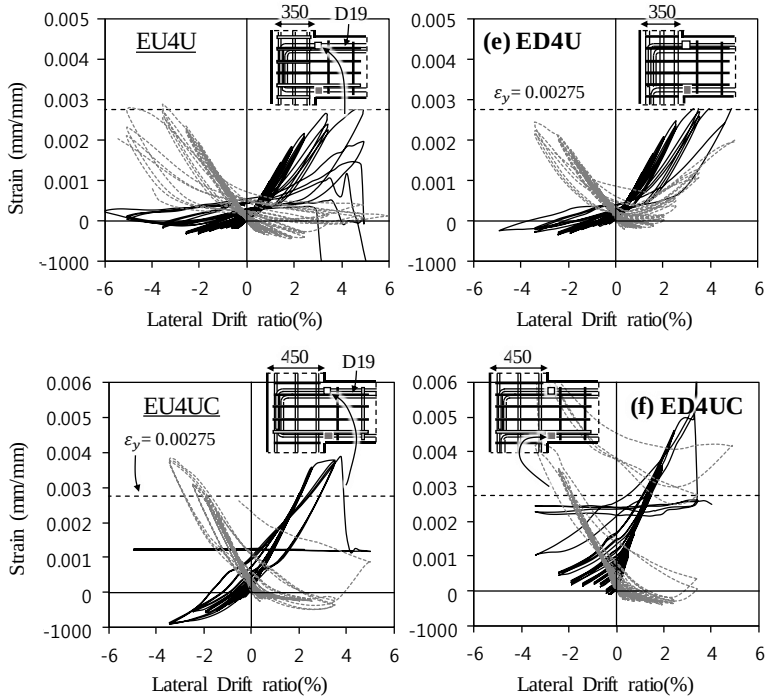

Figure 5-23 Strains of beam top and bottom longitudinal bars

In summary, the strain of beam flexural reinforcement varies greatly depending on the joint shear reinforcement ratio and the diameters of beam bars (D19 and D25). However, when column (joint) depth is so small to secure anchorage length of beam bars, the strain is not related to the hook direction of beam bottom bars because anchorage failure of beam bars has a great influence on the overall behavior.

When column depth is enough to secure anchorage length, on the other hand, the hook direction of beam bottom bars affects the overall behavior of exterior connections. As shown in Figure 5-23(f), the strain of the beam bottom bar of **ED4UC** was similar to that of **EU4UC**, but the strain of the beam top bar was different. This affected the load-drift ratio relations, in which the maximum positive load of **EU4UC** was larger than that of **ED4UC**. When **ED4UC** was in the positive directions (the beam top bar was subjected to tensile stress) at drift ratio of 3.5%, the load-carrying capacity was suddenly decreased with side vertical cracks as shown in Figure 5-21 and Figure 5-22.

5.4.2 Strains of joint shear reinforcement

Figure 5-24 shows the strain of the joint shear reinforcement according to the lateral drift ratio. Specimens **ED2R** and **ED2U** presented strains measured at perimeter ties and U-bars, respectively. Specimens **ED4U** and **ED4UC** have simultaneously measured the strain at U-bars and cross-ties. Strains of U-bars and cross ties are indicated by the black solid line and the grey dashed dotted line, respectively. The yield strain of the joint shear reinforcement is indicated by the horizontal dotted line.

In the case of **ED2R** and **ED2U** where the joint shear reinforcement was spaced at 160 mm, the yield strain was reached at drift ratio of 1.5 ~ 2.5%. This indicates that the shear resistance of the joint shear reinforcement increases approximately linearly with the column drift ratio during the drift ratio ranged from 0.5% to 2.5%. After the joint shear reinforcement yielded at drift ratio of 2.0 ~ 3.5%, the strain increased or decreased rapidly, which means that the joint shear reinforcement did not restrain the width of the joint shear cracks.

On the other hand, in the case of **ED4U** where the joint shear reinforcement was spaced at 100 mm, the cross-tie reached the yield strain, but the perimeter tie did not. Specimen **EU4U** showed a similar strain profile up to drift ratio of 2.5%, but thereafter the strain of U-bar increased sharply with severe diagonal cracks in the joint.

In the specimen **ED4UC** where the joint effective area increased, the yield strain of the cross-tie was reached at drift ratio of 2.5 ~ 3.5% when the beam flexural yielding occurred. This is because the increased joint shear strength increases the shear contribution of the joint shear reinforcement. In particular, the cross-tie reached yield strain at drift ratio of 2.5%, and the strain increased rapidly after yield strain; on the other hand, the perimeter tie strain was relatively small, which indicated that the shear contribution was relatively small. On contrary, the specimen **EU4UC** showed similar strain behavior with reaching the yield strain in both U-bar and cross-tie. The U-bar also contributed to the force transfer.

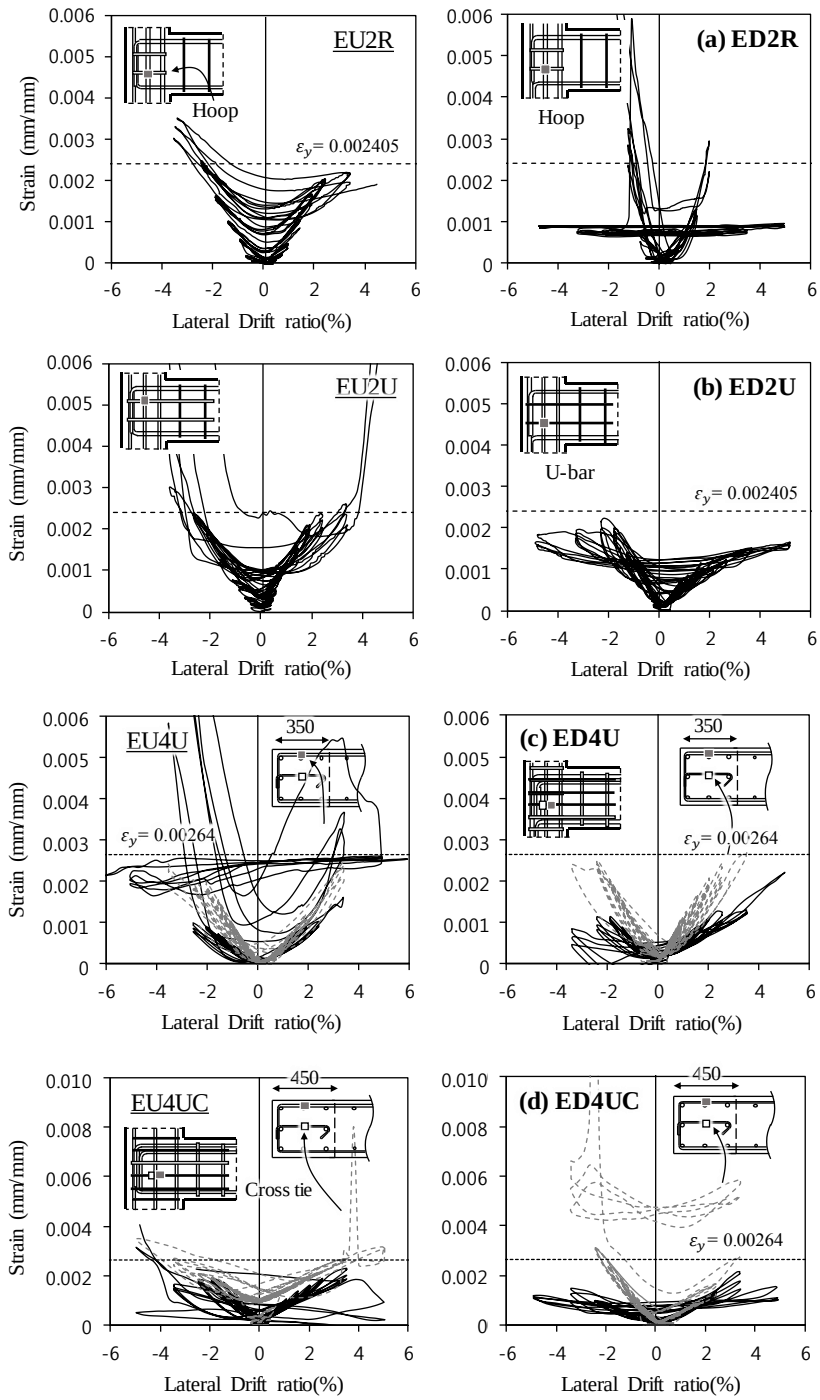

Figure 5-24 Strains of joint shear reinforcement at perimeter ties and cross-ties

5.4.3 Strain distributions of U shaped bars

In order to investigate the performance of U-bars anchored in the adjacent beam, strains were measured along the U-bars. Figure 5-25 shows the strain distributions of the U-bar at the joint. The bar strains were the maximum values that each bar underwent during cyclic loading at each lateral drift ratio. The bars corresponding to δ = 0.5%, 1.0%, 1.5%, 2.0%, and 3.5% are denoted with crosses, triangles, diamonds, circles, and squares, respectively.

In all specimens except for **ED4U** and **EU4UC**, the closer to the joint, the greater strain in the U-bar. In particular, the strain difference was large in non-conforming connection specimens **ED2U** and **ED2UNI** depending on the location of gauges in U-bars compared to conforming connection specimens **ED4U** and **ED4UC**. Further, in the non-conforming specimens, the U-bar did not have a significant effect on increase of flexural strength of beams as the strain at the farthest position of the U-bar from the joint did not increase significantly with increasing the drift ratio.

When the column (joint) depth is enough to secure anchorage length of beam bars, the strain of joint shear reinforcement was affected by the hook direction of beam bars. Figure 5-26 shows the stress transfer of reinforcing bars and concrete around 90º hook. The tensile stress of the reinforcing bar is transferred to the concrete through the bonding stress and the bearing stress of the hook. The bearing stress causes opposite concrete stresses at the hook tail. In particular, when the hook of the beam bottom bar is anchored in the joint (see Figure 5-26(c)), the concrete stress applied to the ends of the joints induces additional tensile stresses in the joint shear reinforcement.

Such U-bar in the joints not only acts as a shear reinforcement against the joint diagonal cracks but also against the bearing stresses on the hook tail of beam longitudinal bars. Thus, in order to investigate the effect of U-bar more closely, it is necessary to examine not only the shear contribution of U-bar but also resistance against the bearing stress due to hook tail of beam bars.

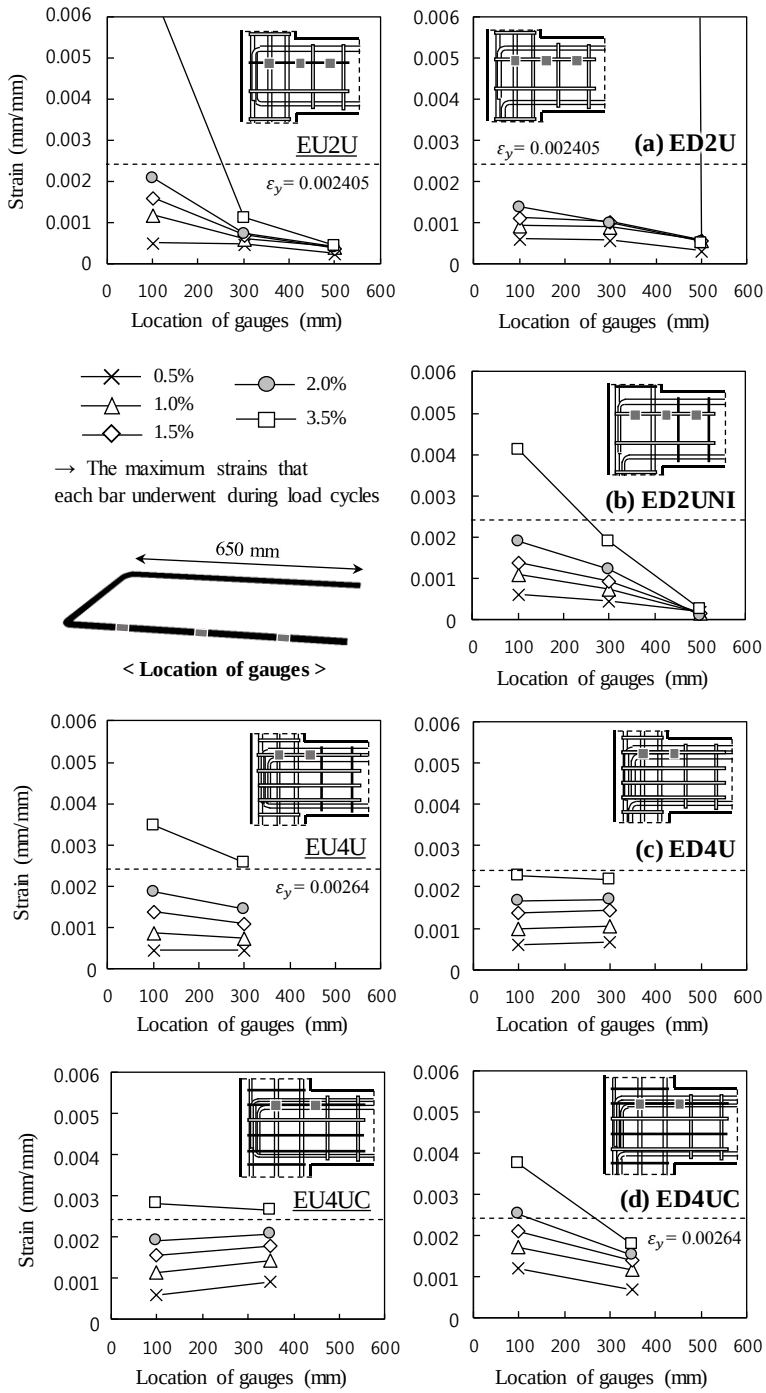

Figure 5-25 Strain distributions of U-bars at the joint

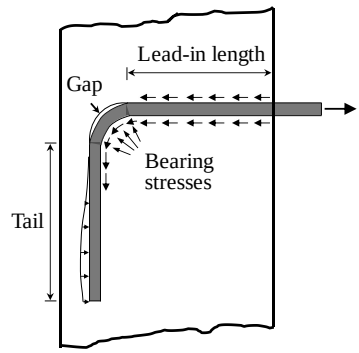

(a) Forces acting on 90°hook bar

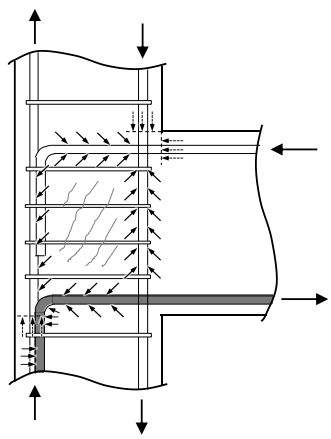

(b) Hook bar bent away from joint

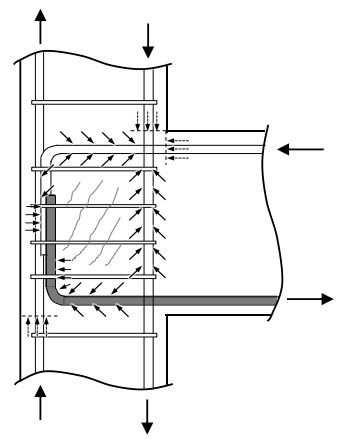

(c) Hook bar bent inside joint

Figure 5-26 Concrete bond resistance acting on 90º hook of beam bars

5.5 Effects of Anchorage Directions of Beam Bars

The anchorage detail of a beam longitudinal bar into an exterior joint has a great influence on the joint shear behavior according to joint shear reinforcement ratio and anchorage length of beam bars. As shown in a gravity load designed joint of Figure 5-1 (a), the load capacity and energy dissipation capacity are significantly reduced by the large slip of beam bottom bars with insufficient anchorage length. According to the previous studies, in the case of exterior joints without joint shear reinforcement, the anchorage direction of beam bars affected the joint behavior. When the 90º hooks of beam bars were anchored in adjacent columns rather than inside joints (Figure 5-1 (b) and (c)), the joint shear strength was reduced because a node for compression strut could not be formed after joint shear cracks occurred. Therefore, according to AIJ (Figure 5-2(b)), in the case of exterior joints with beam bottom bars bent downward into a lower column, a large amount of transverse reinforcements at the lower column are required to form the node point for the compression strut.

In this section, in order to investigate the effect of the hook anchorage direction of beam bars, the specimens in which the beam bottom bars were anchored in columns (Chapter 5) were compared to the specimens in which the beam bars were hooked inside joints (Chapter 4). Since the anchorage length of beam bars affects the exterior joint behavior, load - drift ratio relations and crack patterns at peak loads of test specimens with insufficient (l_{al}/l_{dh} = 0.59) and sufficient anchorage lengths (l_{al}/l_{dh} = 0.96, 1.28) of beam bars were compared in Figure 5-27 and Figure 5-28, respectively.

(1) Test specimens with insufficient anchorage length of beam bars

The test results of specimens **EUN**/**EDNNI** and **EU2U**/**ED2U** with insufficient anchorage length (l_{al}/l_{dh} = 0.59) were compared in Figure 5-27. Specimen details except for the anchorage direction of beam bottom bars are identical to each specimen group. Though the specimen **EDNNI** has no intermediate column bar, the column longitudinal bar ratio is almost same as specimen **EUN**. Specimens **EUN** and **EDNNI** have no joint shear reinforcement; on the other hand, specimens **EU2U** and **ED2U** have joint shear reinforcement of ρ_j = 0.0058 (s/h_c = 0.55).

In specimens **EUN**/**EDNNI** without joint shear reinforcement, the load did not increase after side vertical cracks occurred at drift ratio of 1.5%. In **EUN**, since the beam top and bottom bars were anchored into the joint, vertical cracks were developed by the anchorage hooks of beam top and bottom bars stressed in tension. On the other hand, **EDNNI** only developed a side vertical crack when beam top bars were stressed in tension (Positive direction). Along the anchorage hook direction of beam bottom bars in **EDNNI**, a diagonal shear crack was propagated and enlarged.

Specimens **EU2U**/**ED2U** with joint shear reinforcement showed higher maximum load at drift ratio of 2.0 ~ 2.5% with less damage by side vertical cracks compared to specimens **EUN**/**EDNNI** because the 90º hook of beam bars was restrained by the joint shear reinforcement (U-bars). The maximum loads in positive direction were same in **EU2U** and **ED2U**, but the maximum load in negative direction of **ED2U** was 18% smaller than that of **EU2U** because a join shear crack in **ED2U** was propagated along the hook direction of beam bottom bars similar to **EDNNI**.

According to the anchorage directions of beam bottom bars with insufficient anchorage length, the crack patterns in joints were different, resulting in slightly reducing the load carrying capacity of joints. Owing to lack of anchorage length of beam bars and joint shear reinforcement, it is difficult to evaluate the effect of the anchorage direction of beam bottom bars. Therefore, the following section compares the specimens with sufficient anchorage length of beam bars and joint shear reinforcement.

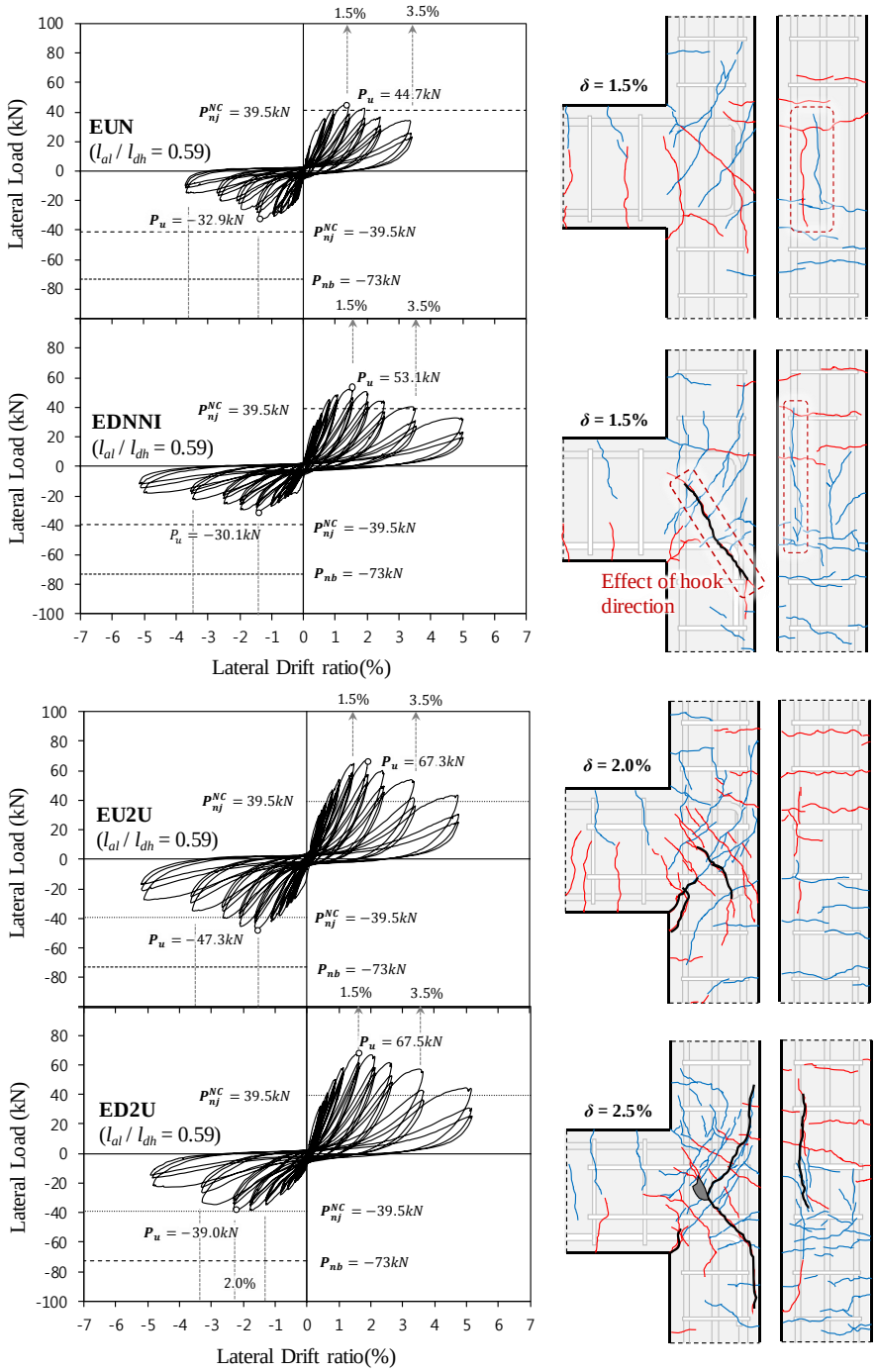

Figure 5-27 Comparison on test results of specimens with insufficient anchorage length

(2) Test specimens with sufficient anchorage length of beam bars

The test results of specimens **EU4U**/**ED4U** and **EU4UC**/**ED4UC** with sufficient anchorage length (l_{al}/l_{dh} = 0.96 and 1.28) were compared in Figure 5-28. Specimen details except for the anchorage direction of beam bottom bars are identical to each group. Specimens **EU4U**/**ED4U** and **EU4UC**/**ED4UC** have joint shear reinforcement of ρ_j = 0.0093 (s/h_c = 0.34 in **EU4U**/**ED4U** and 0.26 in **EU4UC**/**ED4UC**).

The joint shear strength was significantly increased in the case of exterior joints with sufficient anchorage length of beam bars and joint shear reinforcement ratio. The maximum load was attained at drift ratio of 3.5%; further, a larger number of flexural cracks in beams and columns, and joint shear cracks were developed. In specimens **EU4U**/**ED4U** with anchorage length (l_{al}/l_{dh} = 0.96) and joint shear reinforcement (ρ_j = 0.0093 and s/h_c = 0.34), no influence of the anchorage directions of beam bottom bars were observed in both the positive direction where the joint shear failure occurred, and the negative direction where the joint shear failure occurred after beam flexural yielding. As well as the load and drift ratio relations, failure crack patterns at drift ratio of 3.5% when the maximum load was attained were similar.

On the other hand, the specimens **EU4UC**/**ED4UC** with increased column depth to 450 mm showed a difference in the joint behavior according to the anchorage directions of beam bottom bars. Both specimens exceeded beam flexural yielding strength in both positive and negative directions before joint shear failure. Nevertheless, the maximum load in positive direction of **EU4UC** was 10% greater than that of **ED4UC**, and the maximum load in negative direction was the same. Failure crack patterns were also different from each specimen. In specimen **ED4UC**, the joint diagonal cracks propagated down to column along the anchorage direction of beam bottom bars when the bottom bars were stressed in tension. Furthermore, side vertical cracks occurred at drift ratio of 3.5% in positive direction, resulting in relatively smaller positive maximum load in **ED4UC**. Nevertheless, the specimen **ED4UC** showed satisfactory joint performance with a maximum load greater than the beam flexural yielding strength P_{nb} in both positive and negative directions, and a deformation capacity of drift ratio of 3.5%.

In the case of a joint with sufficient anchorage length of beam bars and joint shear reinforcement, a satisfactory joint performance can be attained though beam bottom bars are anchored to an adjacent column instead of inside a joint. For such joint behavior, a large number of transverse reinforcement should be placed in the column where beam bottom bars are anchored.

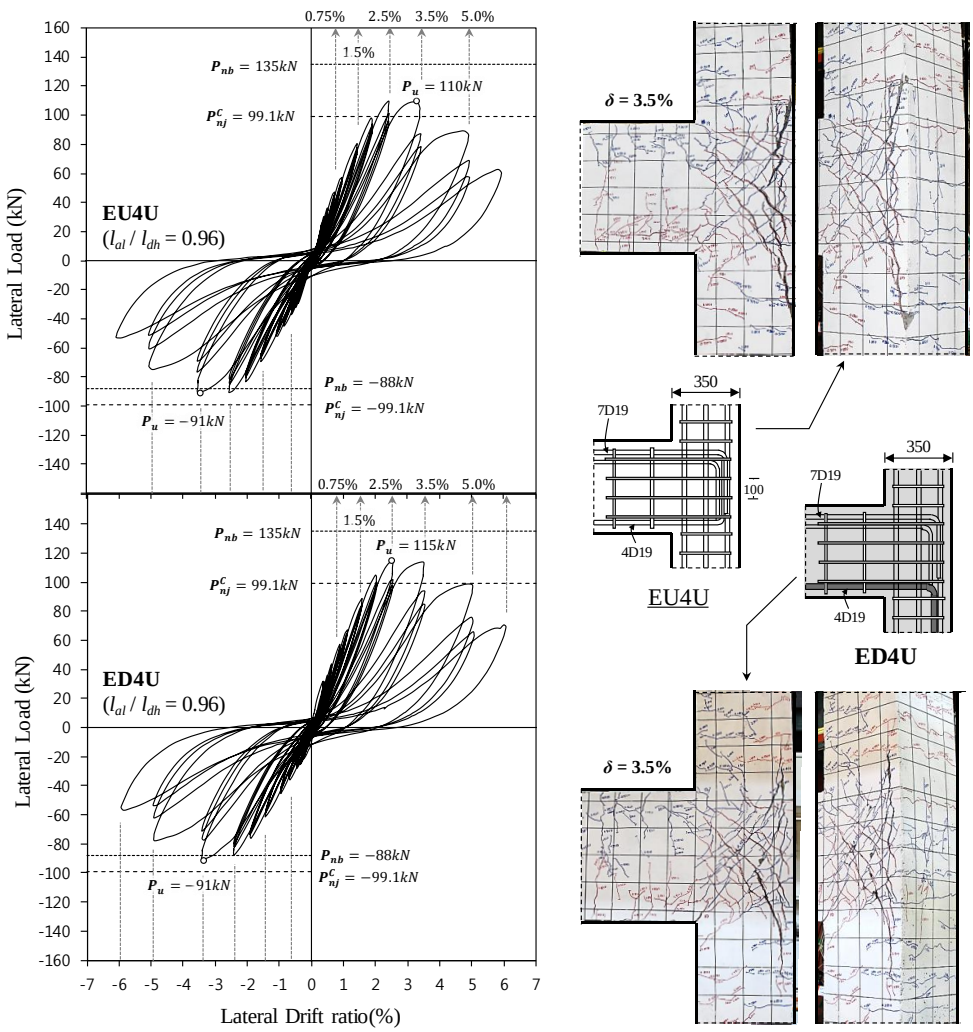

Figure 5-28 Comparison on test results of specimens with sufficient anchorage length (Continued)

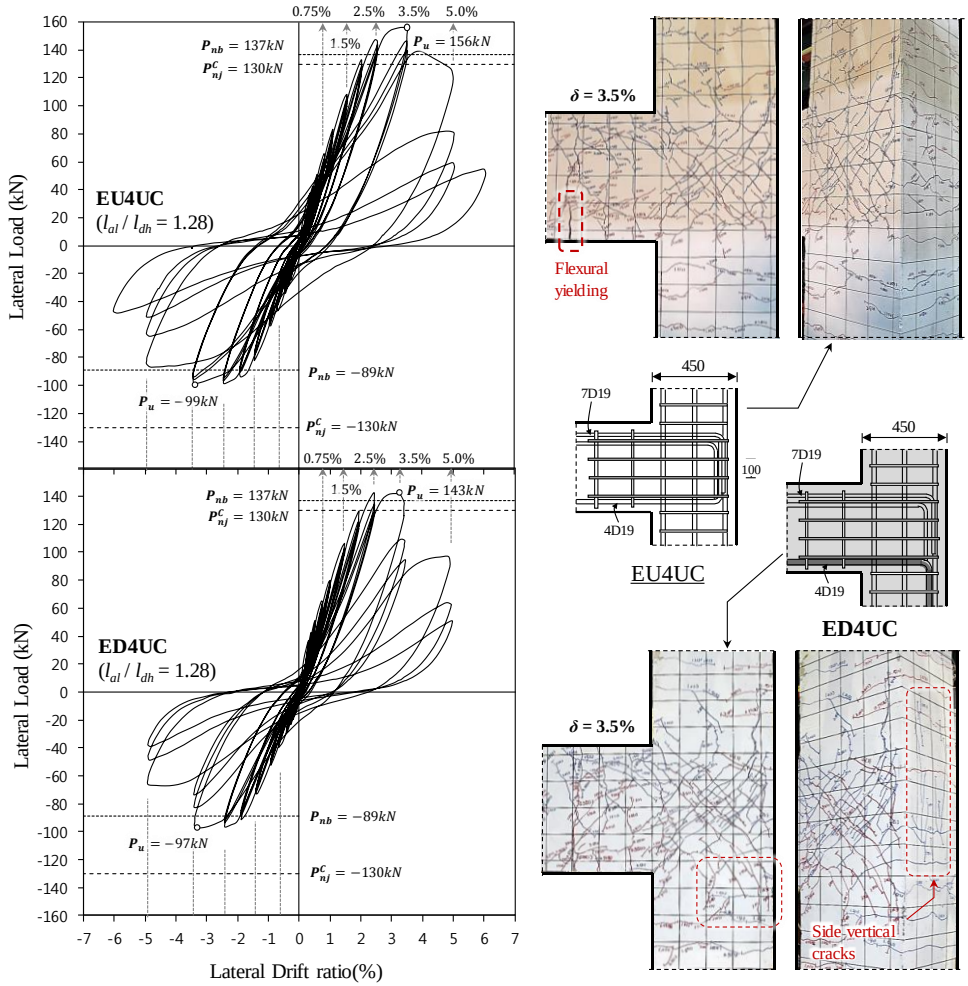

Figure 5-28 Comparison on test results of specimens with sufficient anchorage length

(3) Force transfer mechanisms according to anchorage directions of beam bars

As shown in Figure 5-27 and Figure 5-28, the joint behavior differed according to the anchorage length of beam bars and the joint shear reinforcement ratio. The effect of anchorage directions of beam bottom bars was different, accordingly. In order to investigate force transfer mechanisms in unreinforced and reinforced exterior joints, diagonal strut mechanism and truss mechanism according to anchorage directions of beam bottom bars were illustrated in Figure 5-29.

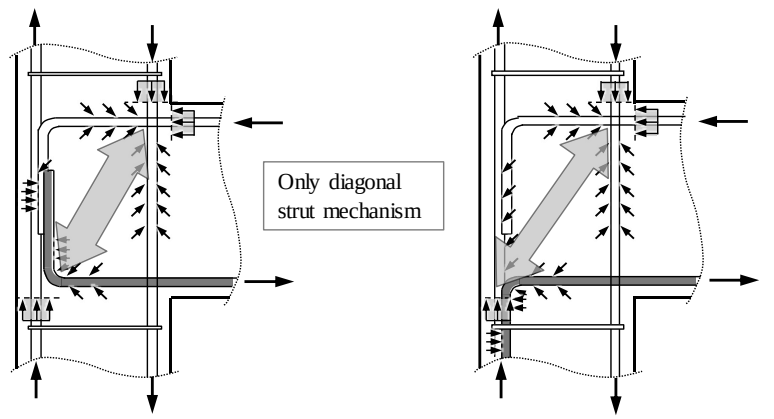

(a1) Bottom bar bent inside joint (a2) Bottom bar bent away from joint

(a) Unreinforced exterior joint

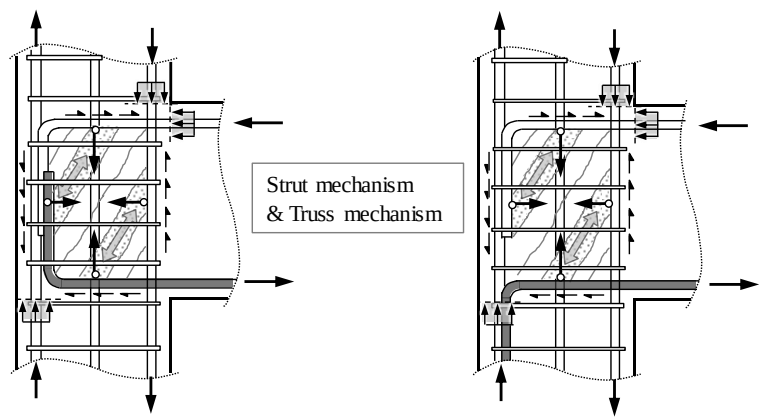

(b1) Bottom bar bent inside joint (b2) Bottom bar bent away from joint

(b) Reinforced exterior joint

Figure 5-29 Force transfer mechanisms in unreinforced and reinforced exterior joints

In the case of unreinforced exterior joints (**EUN** and **EDNNI** in Figure 5-27), joint shear forces were transmitted only by the diagonal strut mechanism, so that the number of joint diagonal cracks was relatively small and the major diagonal crack width rapidly increased, resulting in joint shear failure prior to beam flexural yielding. On the other hand, in the case of reinforced exterior joints (Figure 5-28), the truss mechanism as well as strut mechanism was acted by sufficient joint shear reinforcement and adequate bond of beam bars in the joint. As a result, a joint shear capacity and a deformation capacity were increased with the larger number of joint diagonal cracks. However, specimens **EU2U** and **ED2U** in Figure 5-27 did not significantly increase the joint shear strength due to bond deterioration of beam bars with insufficient anchorage length (l_{al} / l_{dh} = 0.59).

An unreinforced exterior joint with beam bottom bars bent away from the joint (See Figure 5-29(a2)) cannot form a node for compression strut obtained from bearing stress acting on the 90º hook (bending part) of the beam bars. On the other hand, a reinforced exterior joint with beam bottom bars bent away from the joint (See Figure 5-29(b2)) is capable of forming a node for compression strut by the transverse reinforcement located immediately adjacent to the beam bottom bars. Further, since joint shear forces are also transferred by a truss mechanism with joint shear reinforcement and bond of beam bars, the influence of anchorage directions of beam bottom bars is not significant. Thus, satisfactory joint behavior could be attained in specimens **ED4U** and **ED4UC** though the beam bottom bars were anchored in the confined columns.

(4) Recommendation for anchorage directions of beam bars

In order to facilitate force transfers in a joint, it is recommended that beam bars be bent inside the joint. However, if construction is difficult, beam bottom bars can be anchored inside an adjacent confined column. In this case, sufficient shear reinforcement and anchorage length of beam bars should be secured inside the joint so that the truss mechanism can be formed.

5.6 Discussion

The effect of anchorage directions of beam bottom bars on joint behaviors was evaluated by performing reversed cyclic load tests of exterior beam-column connections. The major test parameters include anchorage directions and anchorage lengths of beam bars, and joint shear reinforcement ratio. The main conclusions were summarized as follows.

1) The effect of the anchorage directions of beam bars on joint behaviors is mainly influenced by the amount of joint shear reinforcement and anchorage length of beam bars. It was confirmed that since joint shear forces in exterior joints without shear reinforcement were transmitted only by the diagonal strut mechanism, the joint behaviors were affected by anchorage directions of beam bottom bars. Unreinforced exterior joints with beam bottom bars bent away from the joints were not able to form a node for compression strut, resulting in smaller load capacity with major diagonal shear cracks along hook anchorage of the beam bottom bars. In previous studies, similar joint behaviors were observed when joint reinforcement was not used.

2) Exterior joints with joint shear reinforcement were not significantly affected by anchorage directions of beam bottom bars. By the transverse reinforcement placed adjacent to the beam bottom bars, a node for compression strut can be formed even in exterior joints with beam bottom bars bent away from the joint. Further, joint shear forces are also transferred by a truss mechanism with sufficient joint shear reinforcement and adequate bond of beam bars. Thus, the effect of anchorage directions of beam bottom bars is insignificant for reinforced exterior joints.

3) Beam bars bent inside an exterior joint are recommended to facilitate force transfer in the joint. If construction is difficult, the beam bottom bars can be anchored inside an adjacent confined column with sufficient joint shear reinforcement and anchorage length of beam bars.

Chapter 6. Effects of Alternative Reinforcement Details on RC Frames

6.1 Introduction

6.1.1 Research needs

Frame tests were planned to evaluate the applicability of the alternative reinforcing bar details verified by member tests in Chapter 2 ~ Chapter 5. Since frame specimens have almost same reinforcing bar details as actual buildings, constructability (efficiency of bar placement) of seismic details, alternative details, and non-seismic details can be indirectly investigated during specimen constructions. Further, as concrete is separately poured in pedestal, first story, and second story, the effect of concrete interface in frame specimens can be considered.

Through cyclic tests of frame structures, the overall behavior of low-rise buildings can be investigated in system level. The failure sequence and crack patterns of indeterminate frame specimens may be significantly different from those of determinate column and joint specimens. The failure mechanism varies depending on locations of plastic hinges such as beam sidesway mechanism and column sidesway mechanism.

In additions, in low-rise buildings, shear walls are often used for perimeter walls or space partitions with frame members. Though such shear walls can resist most of lateral forces owing to their high stiffness, brittle failure can occur with relatively low ductility. Thus, the seismic behavior and role of a shear wall should be examined in a frame structure.

6.1.2 Research direction

Low-rise buildings are not required to have large displacement ductility (Special moment frame in ACI 318) because satisfactory seismic performance can be achieved only with limited ductility (Intermediate moment frame in ACI 318). However, since reinforcement details used in an intermediate moment frame are not compatible with the characteristics of low-rise buildings, the reinforcing bar details specified in current design codes should be alternated considering the several characteristics in low-rise buildings. The major characteristics of low-rise buildings are summarized as follows.

1) As the low-rise buildings are subjected to weak-column and strong-beam behavior under earthquake, plastic hinges can be formed at both ends of columns, more attention should be paid to the reinforcing bar details of columns. On the other hand, reinforcing bar details in beams can be relieved compared to current design code requirements.

2) For convenient bar placements in construction fields, various reinforcing bar details are used without any verification, such as transverse reinforcements with non-seismic details in columns and lap splices of column longitudinal bars at plastic hinge regions.

3) Joint shear reinforcement is hardly used in low-rise buildings due to difficult bar placement and steel congestion in beam-column joint. The effective joint area is too small to transmit moment and shear forces between beams and columns.

Accordingly, the alternative reinforcing bar details were proposed for convenient bar placement and structural safety in low-rise buildings. The frames with alternative details were designed to have similar seismic performance as the intermediate moment frame in ACI 318.

6.1.3 Previous studies for RC frames

6.1.3.1 Seismic performance of non-ductile RC frames

(1) Calvi et al. (2002)

Calvi et al. tested a three story RC frame designed for gravity load only under a quasi-static cyclic test. The test frame with smooth reinforcing bars, inadequate bar details, deficient anchorage details, and the absence of capacity design showed brittle local and global damage mechanism. In particular, severe damages were accumulated in the unreinforced exterior joints (Figure 6-1). The shear hinge mechanism due to shear cracking in the joint redistributed the deformation demand within the beam-column joint system. This effect delayed soft story mechanism but high inelastic rotation capacity should be achieved.

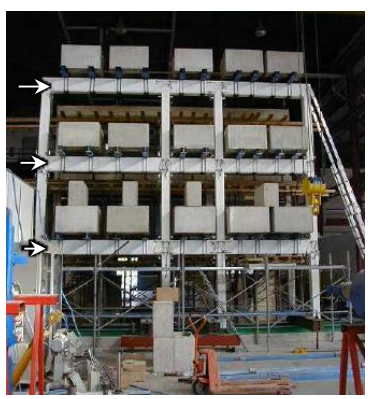

< Test setup for RC frames >

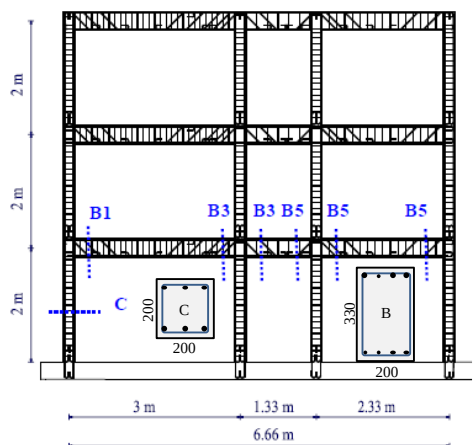

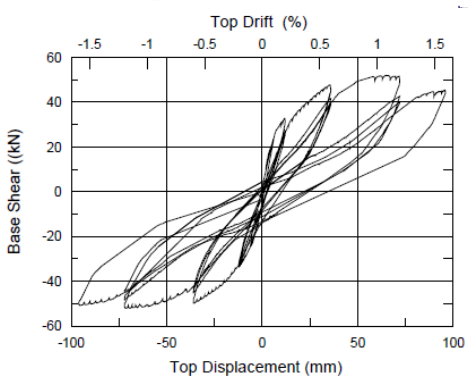

< Base shear and displacement relations >

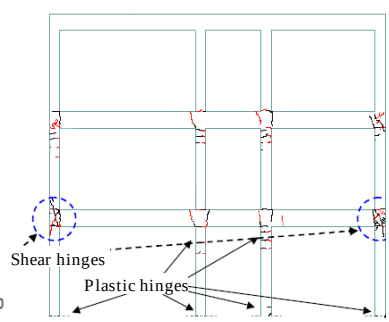

< Crack pattern at a drift ratio of 1.6% >

Figure 6-1 A static cyclic test of a three story RC frame in Calvi et al. (2002)

(2) Wu et al. (2009)

Wu et al. tested shaking table tests of a single-story and three-bay RC frame with two ductile columns and two non-ductile columns as shown in Figure 6-2. When subjected to a scaled earthquake loading from 1999 Chi-Chi EQ, the non-ductile columns sustained shear and axial failure. After non-ductile failed, vertical loads were redistributed to the ductile columns, leading to column overload and collapse of the entire frame. Such test result indicated that axial load variation from overturning moment and load redistribution plays an important role in seismic behaviors of columns.

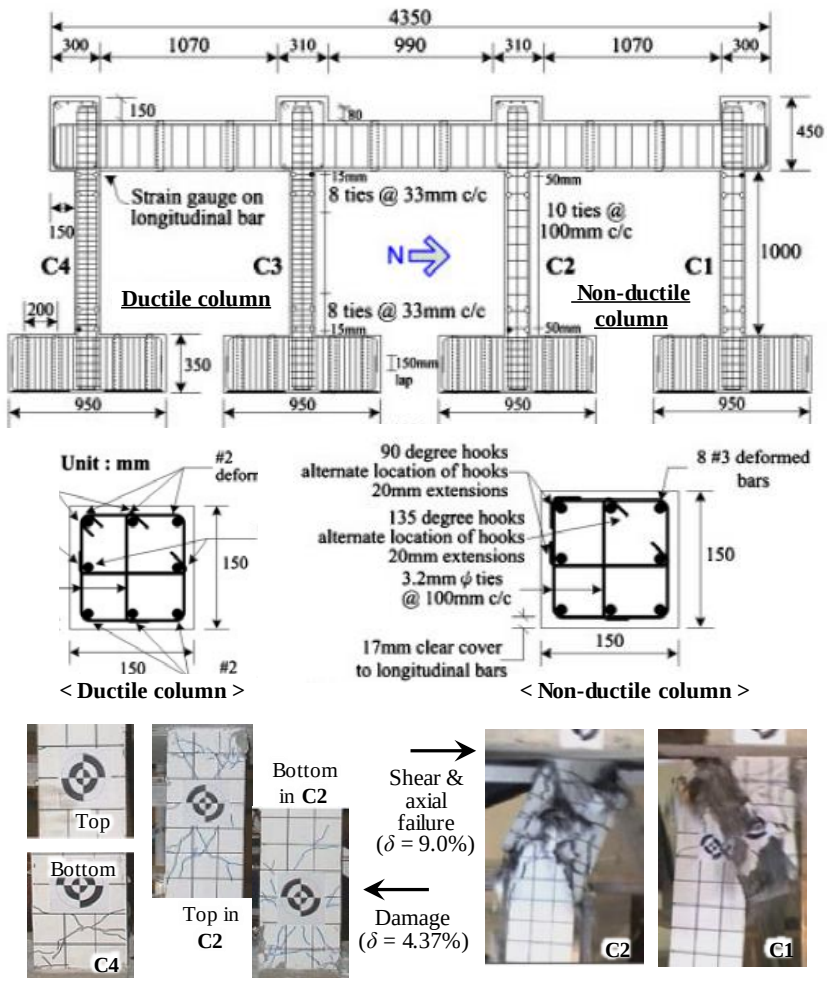

Figure 6-2 Reinforcement details of frame specimen in Wu et al. (2009)

(3) Bayhan et al. (2015)

In the study of Bayhan et al., two-story and two-bay RC fame with weak beam-column joints (without joint shear reinforcement) was tested under earthquake simulations on a shaking table. The frame responded elastically during the first shaking test (0.25g peak base acceleration). In the 0.84g test, flexural cracks developed in the bottom of 1st columns and diagonal cracks developed in the joint as shown in Figure 6-3. During the 1.11g test, the cover concrete in the bottom of B1 column spalled off and joint damages increased. In the final test (1.36g), inclined cracking in joints B1 and C1 increased. Inelastic behavior was primarily concentrated in the first story column and joint.

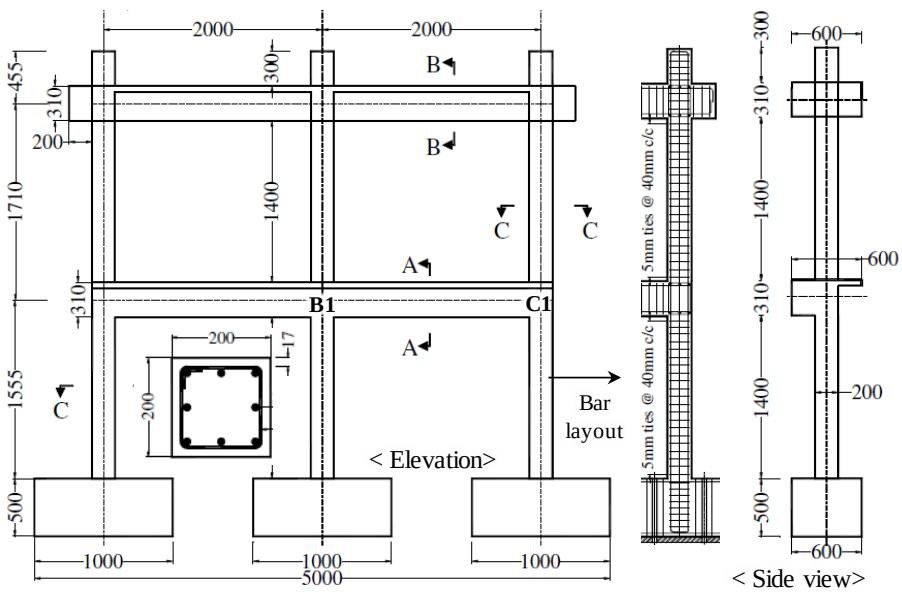

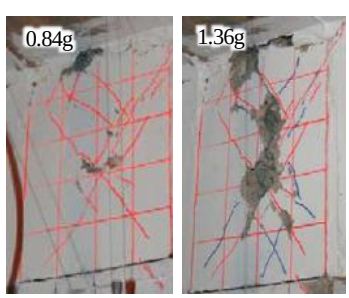

Crack patterns in interior joint B1

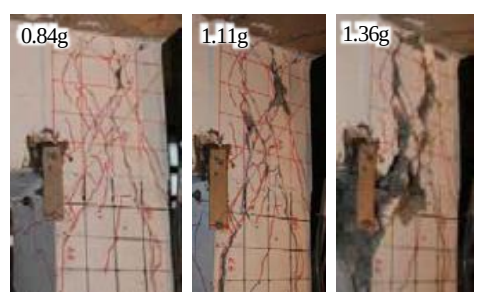

Crack patterns in Exterior joint C1

Figure 6-3 Shaking table test frame in Bayhan et al. (2015)

6.1.3.2 Seismic behavior of RC frames with RC partial infills

(1) Kara and Altin (2006)

Kara and Altin tested one-bay and two-story frames with partial infills to investigate the behavior of non-ductile RC frame strengthened by shear walls. Test results showed that partially infilled frames exhibited higher load carrying capacity (3~7.8 times), stiffness (6 ~ 28 times), and energy dissipation capacity (3~10 times), but lower deformation capacity than the non-ductile frame. The infilled shear wall ratio is proportional to ultimate shear strength but inversely proportional to maximum drift ratio.

In the failure mode of Figure 6-5, the non-ductile frame exhibited flexural shear failure in the 1st columns and shear failure in the joints. The frame with infilled shear wall developed web shear crushing and shear sliding failure at the bottom. Shear cracks were concentrated in short beams located between infilled walls. Diagonal shear cracks developed in the joint not connected to the infilled shear wall due to relative large rotation demand. The most satisfactory seismic behavior was obtained from RC frame with partially infilled wall connected to both the beams and columns in the frame.

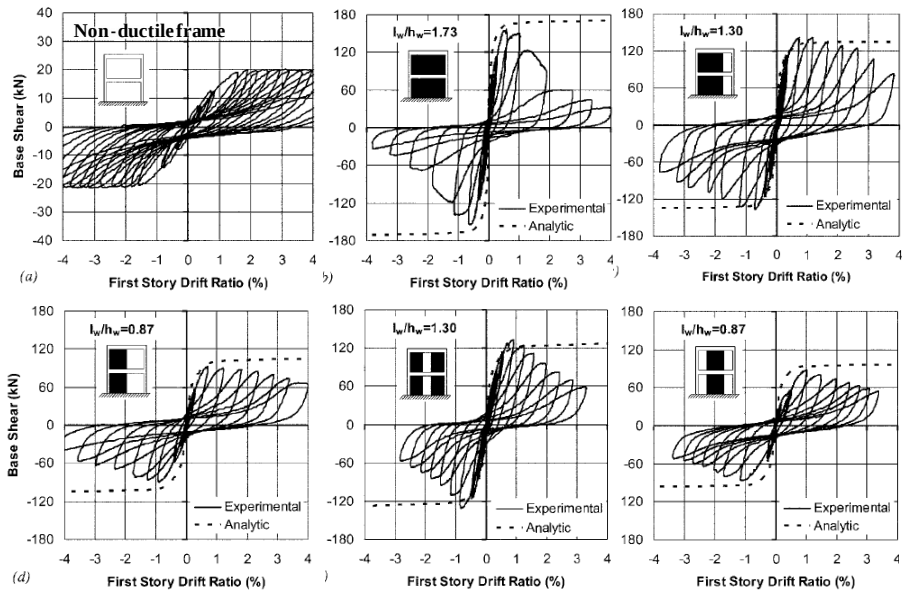

Figure 6-4 The effect of RC infilled shear wall ratio and location in Kara and Altin (2006)

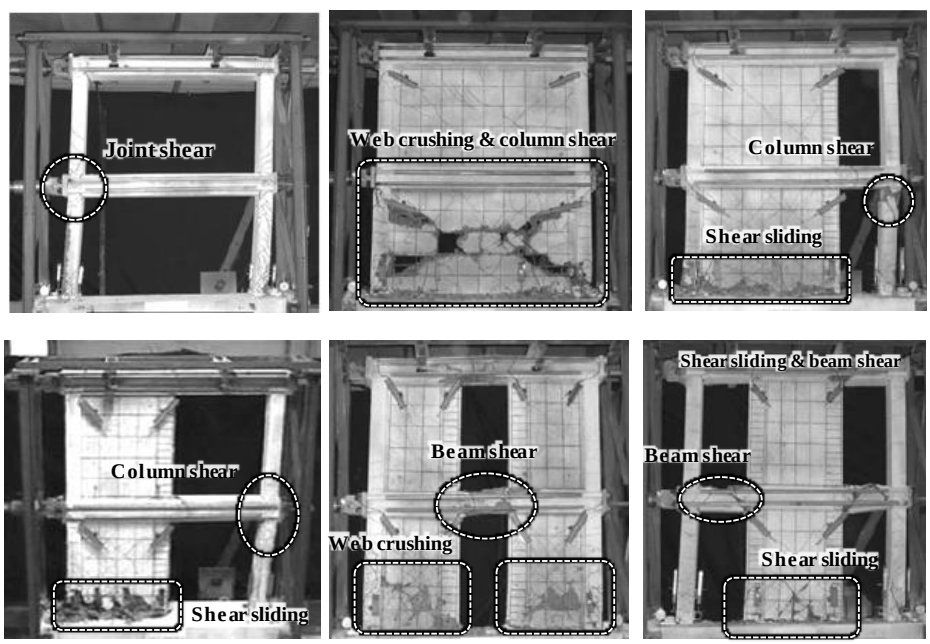

Figure 6-5 Failure modes of frame test results in Kara and Altin

(2) Canbay et al. (2003)

Canbay et al. performed two-story and three-bay RC frame tests to investigate the internal force distribution in RC frames with RC walls. RC infilled walls were added in the middle bay of the frame, which was previously damaged under reversed cyclic loading. Frame specimen details and test results were presented in Figure 6-6.

The bare frame without seismic details showed maximum lateral load 13.9 kN at a displacement of 40 mm. At drift ratio of 1.9%, a diagonal shear crack in the exterior joint was developed with cover spalling at the exterior face of the exterior joint due to outward force of the 90º hook of the beam top bar. On the other hand, the infilled frame yielded in the 1st infilled wall at a lateral load of 45 kN, and the maximum lateral load increased to be 53.2 kN with a displacement of 39 mm. During the test, no cracks were observed on the 2nd infilled wall. The initial stiffness of the infilled frame was about 15 times that of the bare frame, thereby increasing the maximum lateral load by 3.8 times. Prior to failure, 90% of the lateral load was carried by the infilled wall.

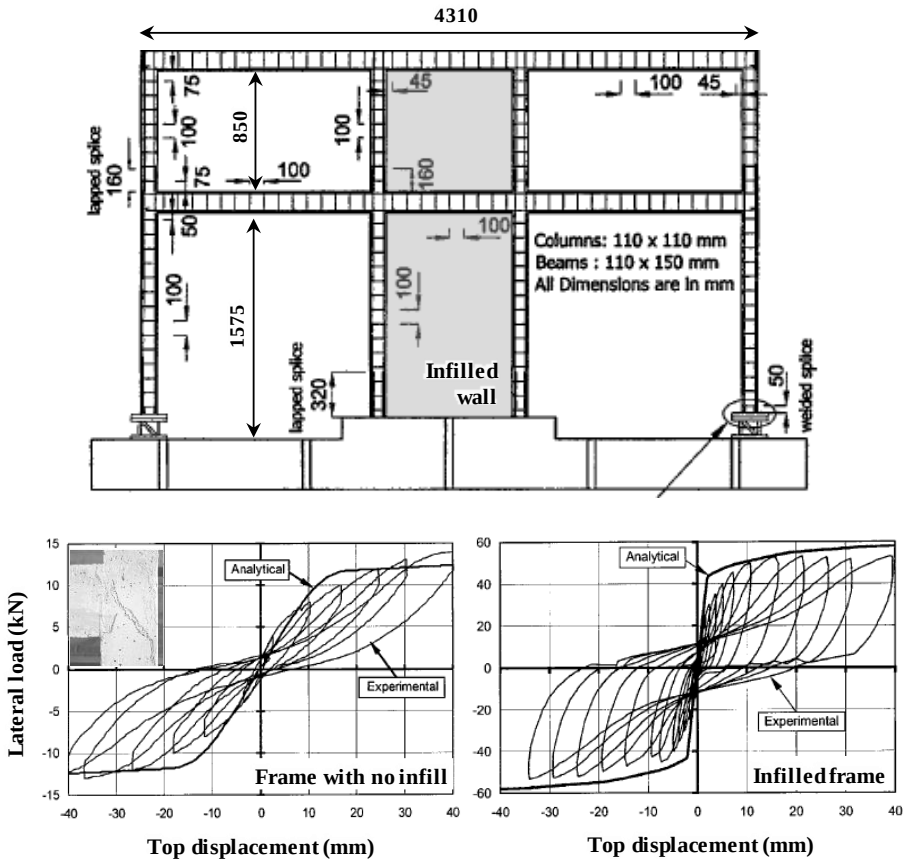

Figure 6-6 The effect of RC infilled shear wall in Canbay et al. (2003)

6.1.3.3 Test investigations for external RC shear wall

In Turkey, as most RC buildings are vulnerable to earthquake, strengthening methods of existing buildings have been being actively developed and studied for safety. The most preferable strengthening method is the application of RC infilled walls due to cost efficiency. When considering the limitation of space for construction and additional heavy costs, the method of external shear wall applied on the external surface of the building can be good strengthening technique.

Kaltakci et al. (2010a, 2011) studied seismic performance of non-ductile frames strengthened with external RC shear walls considering various test variables, such as axial load ratio (10 ~ 20% / 50 ~ 60%) and column reinforcement ratio (ρ_c = 1.3 / 2.3%). The shear wall was added at the right columns of non-ductile frames with dowel bars (See Figure 6-7).

The bare frame without shear wall showed the maximum lateral load (40 ~ 50 kN) at drift ratio of 1.0 ~ 2.0% and gradually decreased lateral load carrying capacity after peak load. The strengthened frame significantly increased maximum lateral load in 3.5 ~ 4.5 times with increased stiffness, thereby increasing energy dissipation capacity.

The bare frames exhibited severe diagonal shear cracks in exterior joint at a lateral load of 20 ~ 25 kN. The damages were accumulated in the joints, resulting in the global failure in the frames. In strengthened frames, as the lateral force resisted by the external shear walls, the walls exhibited flexural cracks from the bottom and diagonal shear cracks propagated to the second floor. Further, as rotation demands in the joint increased, diagonal shear cracks developed in the joint. Under high axial load applied, relatively small number of cracks were developed in the shear wall.

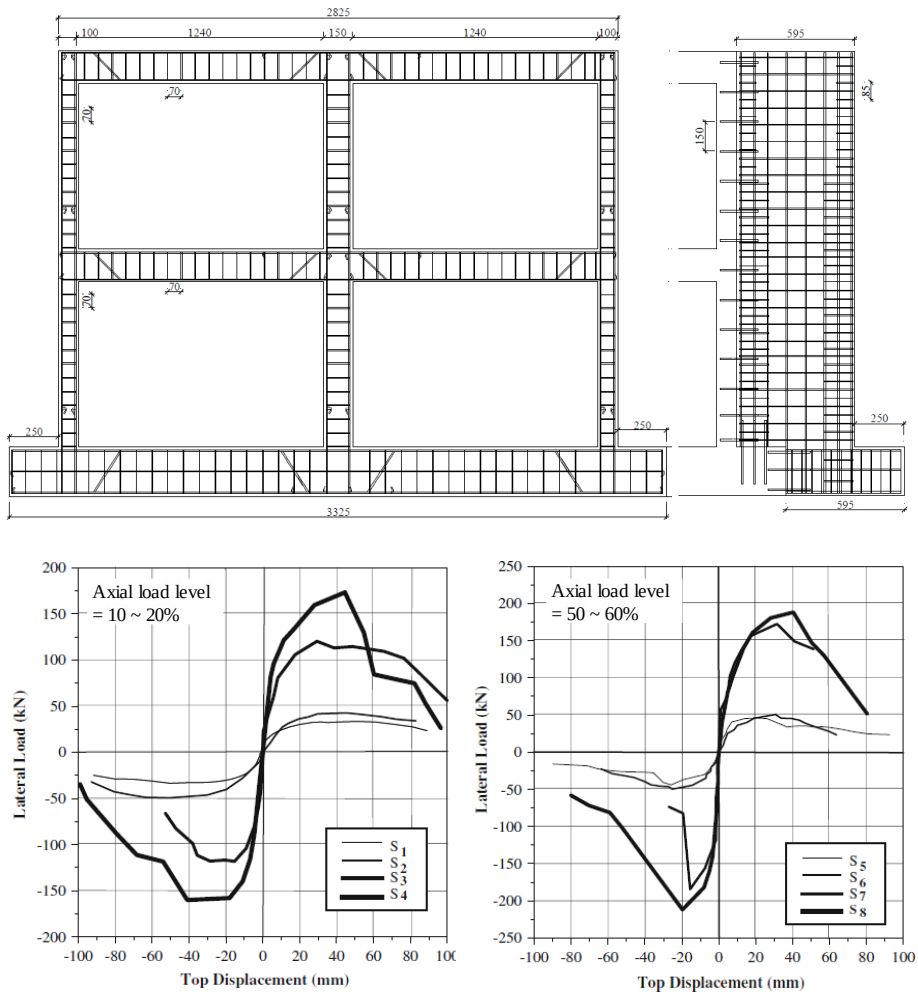

Figure 6-7 The effect of external RC walls in Kaltakci et al. (Continued)

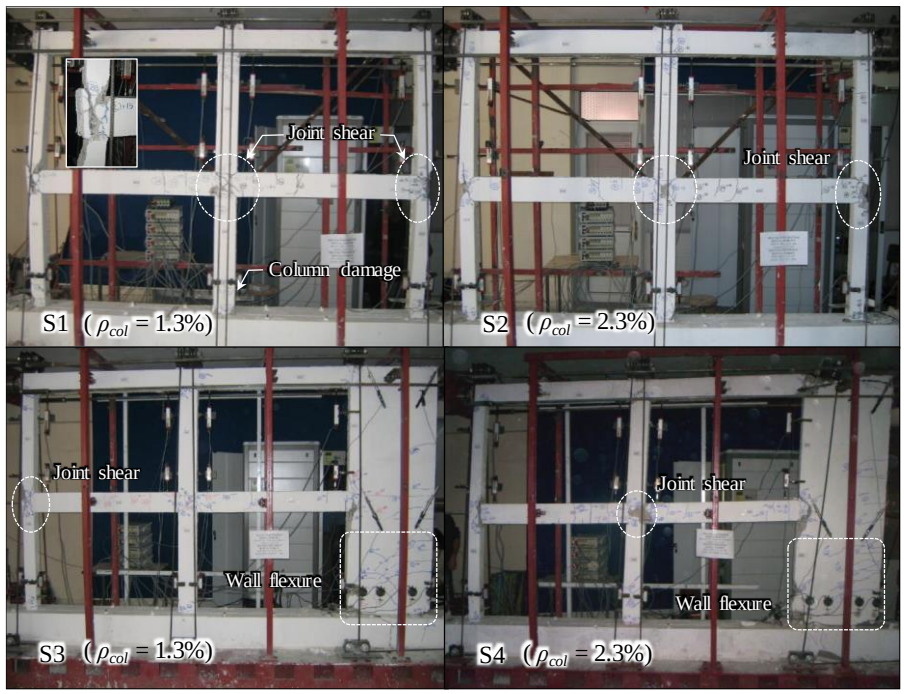

(a) Low axial load (10 ~ 20%)

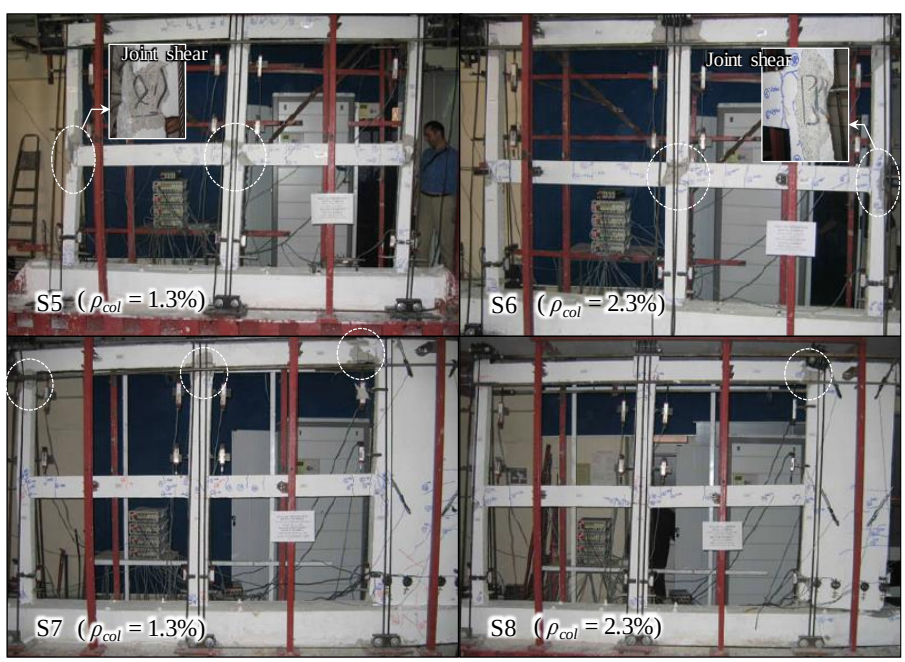

(b) High axial load (50 ~ 60%)

Figure 6-7 The effect of external RC walls in Kaltakci et al. (2010a, 2011)

Kaltakci et al. (2010b) tested two-story and two-bay RC frames to compare the effectiveness of internal and external shear wall locations on strengthened RC frames. In external shear wall (ESW type) and internal shear wall (PISW type), no serious damage was observed on the frames until the maximum latera load was applied. The ESW exhibited many flexural cracks in the shear wall, while the PISW failed by extensive horizontal shear crack developed between the wall and the basement without flexural cracks. Such different failure modes indicate the contribution of shear wall on the overall behavior of the frames.

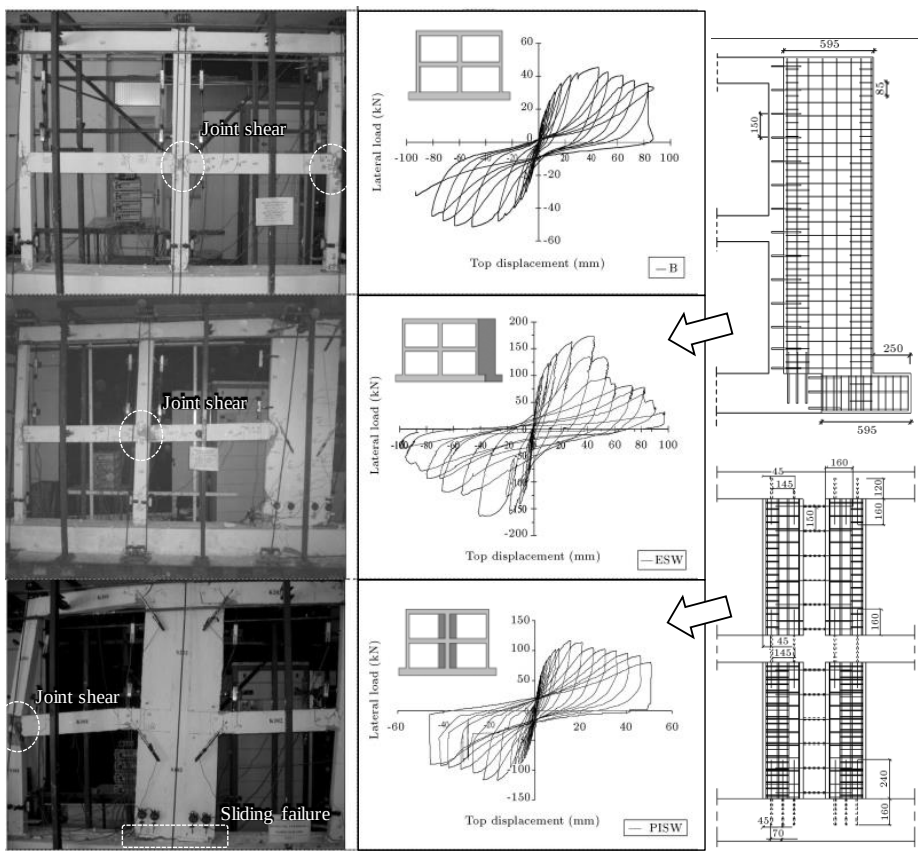

Figure 6-8 The effect of internal and external shear wall location in Kaltakci et al. (2010b)

6.2 Test Program

6.2.1 Major design parameters

Four specimens were planned for RC frame tests (Intermediate moment frame, Alternative 1 moment frame, Alternative 2 moment frame, and moment frame with shear wall). Table 6-1 presents design criteria and test parameters of RC frame specimens. As the major test parameters, reinforcement details of each member (beam, column, and joint) and shear wall were considered.

In order to compare the performance of frames using alternative details, the intermediate moment frame (**IMF**) is designed considering the response modification factor (R= 5.0) according to the current KBC 2016 code. The column shear design was calculated using the capacity design. The shear reinforcement details of columns are hoops with 135º hook at both ends, and ties with 90º hook at the center. The shear reinforcement details of beams are 135º - 135º stirrups with a spacing of *d/4* at both ends, and stirrups with a spacing of *d/2* at the center. Hoops with 135º hook were used for the exterior and interior joints with a spacing of *d/4* (= 70 mm).

Alternative 1 moment frame (**A1F**) used alternative reinforcement details verified by member tests in Chapter 2 ~ Chapter 5 and designed to have the same target strength as specimen **IMF**. Alternative 2 moment frame (**A2F**) was planned to evaluate the seismic performance of the alternative reinforcement details by increasing column and beam flexural strength (longitudinal reinforcement ratio) than **A1F**. The shear reinforcement details of columns and beams are ties with 90º hook and 90º - 90º stirrups with a spacing of *d/2* at both ends and the center, respectively. U shaped bars were used only for the exterior joints with a spacing of *d/4* (= 70 mm).

Moment frame with shear wall (WF) was designed to secure the seismic resistance by a shear wall and the gravity load resistance by a moment frame. This is to alleviate the reinforcement details of the moment frame through the shear wall.

Table 6-1 Design criteria and test parameters of moment frame specimens

Specimen	Intermediate Moment Frame (IMF)	Alternative 1 Moment Frame (A1F)	Alternative 2 Moment Frame (A2F)	Wall and Moment Frame (WF)
Specimen Design	· KBC2016, R= 5.0 (Intermediate moment frame) · Use current details of bars	· Designed with same lateral force to IMF · Use Alternative details	· 40% increase in beam and column flexural bars than A1F · Use Alternative details	· Gravity load design · Ordinary RC shear wall & Ordinary moment frame
Column Shear design	· Shear using capacity design · Shear reinforcement details - Hoop with 135º hook(End) - Tie with 90º hook (Center)	· Shear using capacity design · Shear reinforcement details - Tie with 90º hook (End & Center), $s = 0.5\ H_{min}$	· Shear using capacity design · Shear reinforcement details - Tie with 90º hook (End & Center), $s = 0.5\ H_{min}$	· Gravity load design · Shear rebar details - Tie with 90º hook (End & Center), $s = 1.0\ H_{min}$
Beam Shear design	· Current design code (KBC) - 135º Stirrups $s = d/4$ (End) - Stirrups $s = d/2$ (Center)	· Minimum shear rebars - 90º Stirrups $s = d/2$ (End & Center), No plastic hinge in beam	· Minimum shear rebars - 90º Stirrups $s = d/2$ (End & Center), No plastic hinge in beam	· Gravity load design - 90º Stirrups $s = d/2$ (End & Center)
Joint Shear design	· Exterior and interior joints - Hoop with 135º hook - $s = d/4$ (= 70 mm)	· Exterior joint only - U shaped bar - $s = d/4$ (= 70 mm)	· Exterior joint only - U shaped bar - $s = d/4$ (= 70 mm)	· Exterior joint only - U shaped bar - $s = d/3$ (= 100 mm)
Other features	Details of intermediate moment frame with seismic design according to KBC standard.	Verification of seismic resisting performance for alternative details by designing same target strength as IMF.	- Increase of required shear force in column and beam. -Verification of alternative detail.	-Improved seismic resistance with ordinary RC shear wall of gravity load designed ordinary moment frame

6.2.2 Test specimen design

The design of the test specimen was based on low-rise building prototype (Gross area = 400 m^2) as shown in Figure 6-9. The member size and reinforcement details of the specimens IMF, A1F, and A2F were designed through equivalent static analysis method with response modification factor R = 5.0 (for intermediate moment frame in KBC2016).

$$V = C_s\, W \tag{6-1}$$

$$C_s = \frac{S_{DS}}{\left[\frac{R}{I_E}\right]} \tag{6-2}$$

where V = Base shear, C_s = Seismic response coefficient, W = Total weight of a structure, S_{DS} = Design spectral acceleration at short periods, I_E = Important factor for earthquake load, R = Response modification coefficient, T = Fundamental period of a structure. The base shear force V of low-rise buildings was 10 ~ 25% of the effective building weight W depending on the size of building and the type of ground.

The member size and reinforcement design were determined based on the MIDAS analysis (Equivalent static analysis). The load conditions used in MIDAS are as follows.

1. Dead load (D) : 5.5 kN/m^2 (2^{nd} floor), 6.55 kN/m^2 (roof), self-weight of beams and columns
2. Live load (L) : 2.0 kN/m^2 (2^{nd} floor), 1.0 kN/m^2 (roof)
3. Seismic load (E) : Site coefficient (0.22), Site class (S_c), Response modification coefficient (R = 5.0), Important factor (I_E = 1.0)

All load combinations (1.2D+1.6L, 1.2D+1.0E+1.0L, 0.9D+1.0E, ...) for concrete design were examined, and the most extreme loading conditions were used for each member design. Member dimensions and reinforcement details of each member were presented in Table 6-2 ~ Table 6-3 and Figure 6-10 ~ Figure 6-13. A 70% scale model was designed considering the experimental environment of the seismic simulation test center in Pusan National University to carry out the RC frame test.

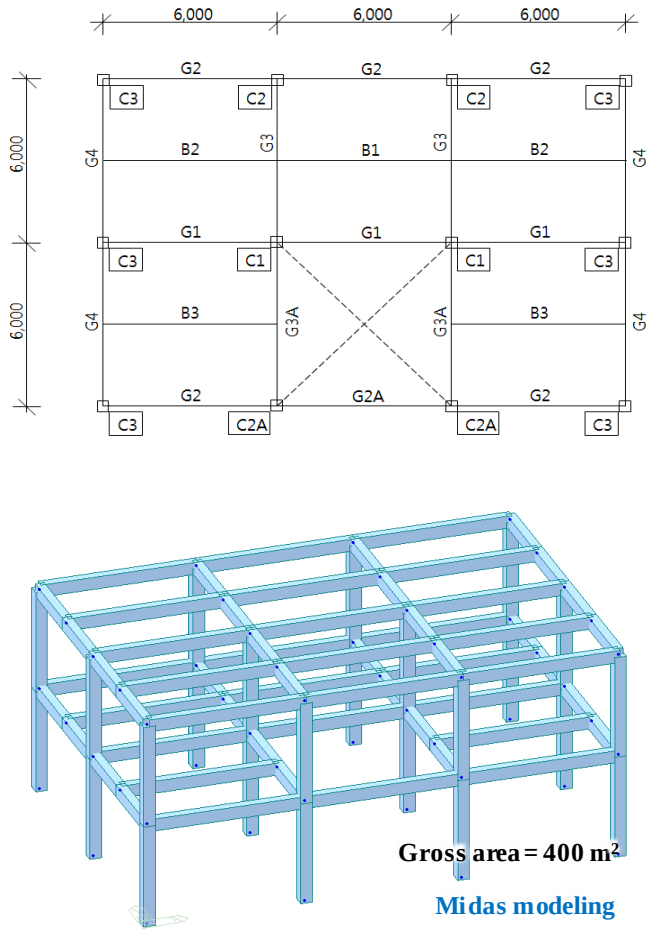

Figure 6-9 Low-rise building prototype for test specimen design

Table 6-2 Details of RC fram specimens

Specimen		IMF	A1F	A2F	WF
Design criteria		Seismic load (R = 5.0)	Seismic load (R = 5.0)	Seismic load (R = 5.0)	Gravity load
Column	Size	400 x 400	400 x 400	400 x 400	350 x 350
	Rebar	8-D19 (ρ_l=1.4%)	8-D19 (ρ_l=1.4%)	6-D22 (ρ_l=1.9%)	4-D22 (ρ_l=1.3%)
Beam	Size	350 x 450	350 x 450	350 x 450	350 x 450
	Top bar	[End] 7-D19 (ρ_t= 1.28%) [Center] 2-D19 (ρ_t= 0.36%)	[End] 7-D19 (ρ_t= 1.28%) [Center] 2-D19 (ρ_t= 0.36%)	[End] 7-D19 (ρ_t= 1.28%) [Center] 2-D19 (ρ_t= 0.36%)	[End] 7-D19 (ρ_t= 1.28%) [Center] 2-D19 (ρ_t= 0.36%)
	Bottom bar	[End] 3-D19 (ρ_b= 0.55%) [Center] 5-D19 (ρ_b= 0.91%)	[End] 3-D19 (ρ_b= 0.55%) [Center] 5-D19 (ρ_b= 0.91%)	[End] 3-D19 (ρ_b= 0.55%) [Center] 5-D19 (ρ_b= 0.91%)	[End] 3-D19 (ρ_b= 0.55%) [Center] 5-D19 (ρ_b= 0.91%)
Wall	Size	-	-	-	1500 x 180
	Rebar	-	-	-	8-D16 & 8-D13 (ρ_l= 0.97%)
↓ 70% scale test model					
Column	Size	280 x 280	280 x 280	280 x 280	250 x 250
	Rebar	6-D16 (ρ_l=1.5%)	6-D16 (ρ_l=1.5%)	6-D19 (ρ_l=2.2%)	4-D16 (ρ_l=1.3%)
Beam	Size	280 x 320	280 x 320	280 x 320	250 x 320
	Top bar	[End] 8-D13 (ρ_t= 1.13%) [Center] 2-D13 (ρ_t= 0.28%)	[End] 8-D13 (ρ_t= 1.13%) [Center] 2-D13 (ρ_t= 0.28%)	[End] 10-D13 (ρ_t= 1.42%) [Center] 2-D13 (ρ_t= 0.28%)	[End] 8-D13 (ρ_t= 1.27%) [Center] 2-D13 (ρ_t= 0.32%)
	Bottom bar	[End] 4-D13 (ρ_t= 0.57%) [Center] 6-D13 (ρ_t= 0.85%)	[End] 4-D13 (ρ_t= 0.57%) [Center] 6-D13 (ρ_t= 0.85%)	[End] 6-D13 (ρ_t= 0.85%) [Center] 6-D13 (ρ_t= 0.85%)	[End] 4-D13 (ρ_t= 0.64%) [Center] 6-D13 (ρ_t= 0.95%)
Wall	Size	-	-	-	1000 x 130
	Rebar	-	-	-	8-D13 & 6-D10 (ρ_l= 1.11%)

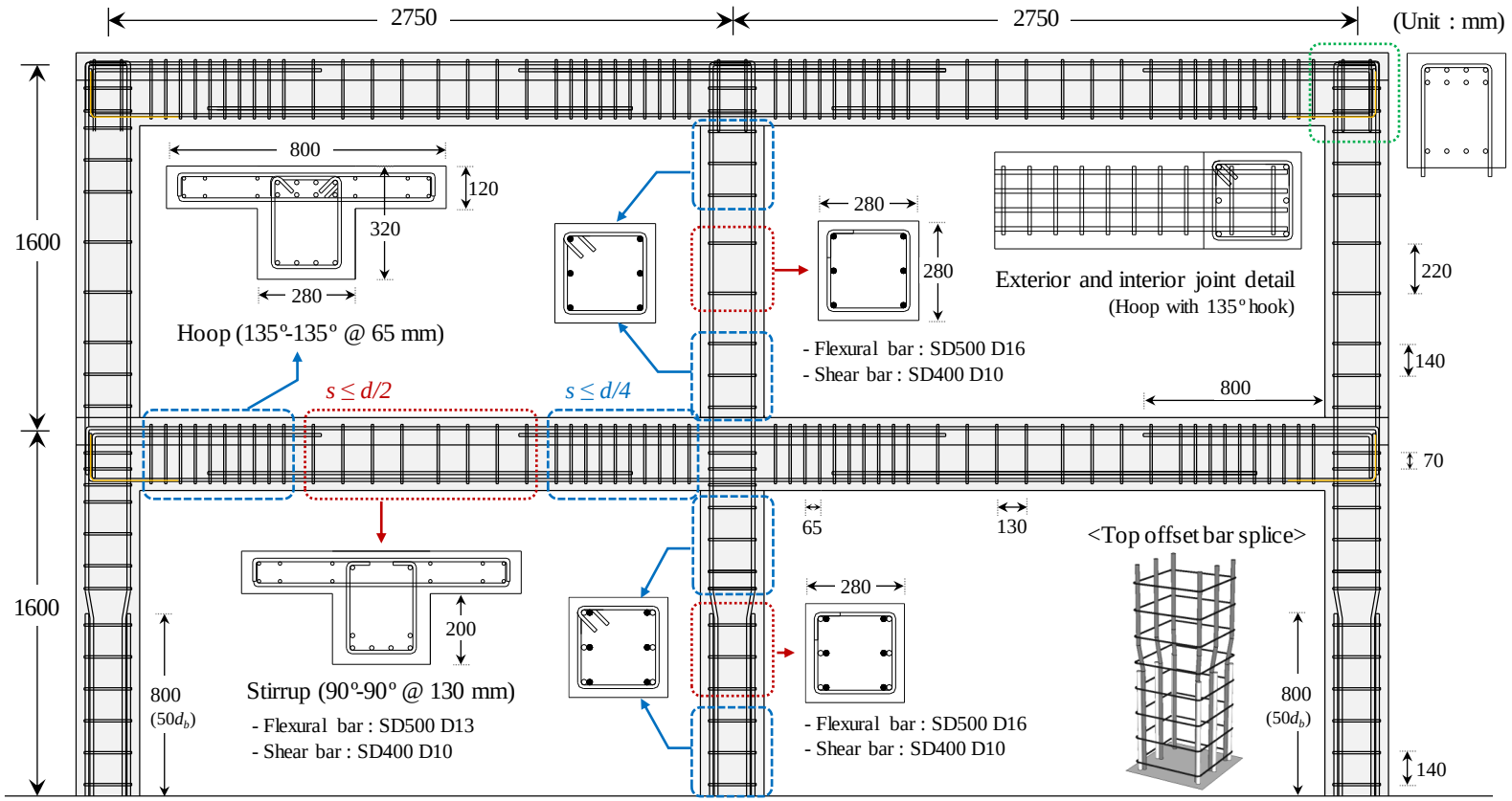

Figure 6-10 Dimensions and reinforcement details of the intermediate moment frame specimen (IMF)

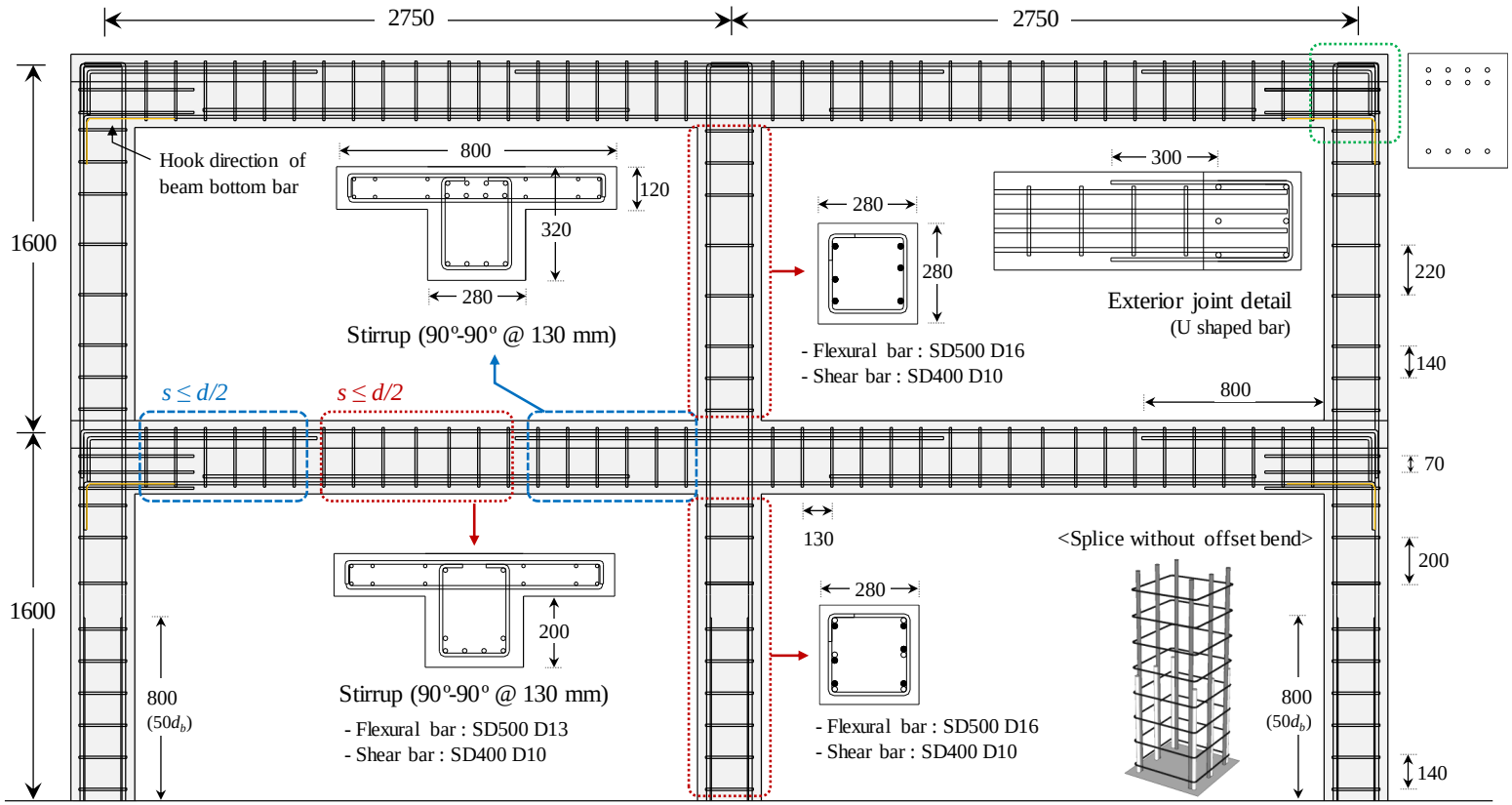

Figure 6-11 Dimensions and reinforcement details of the intermediate moment frame specimen (A1F)

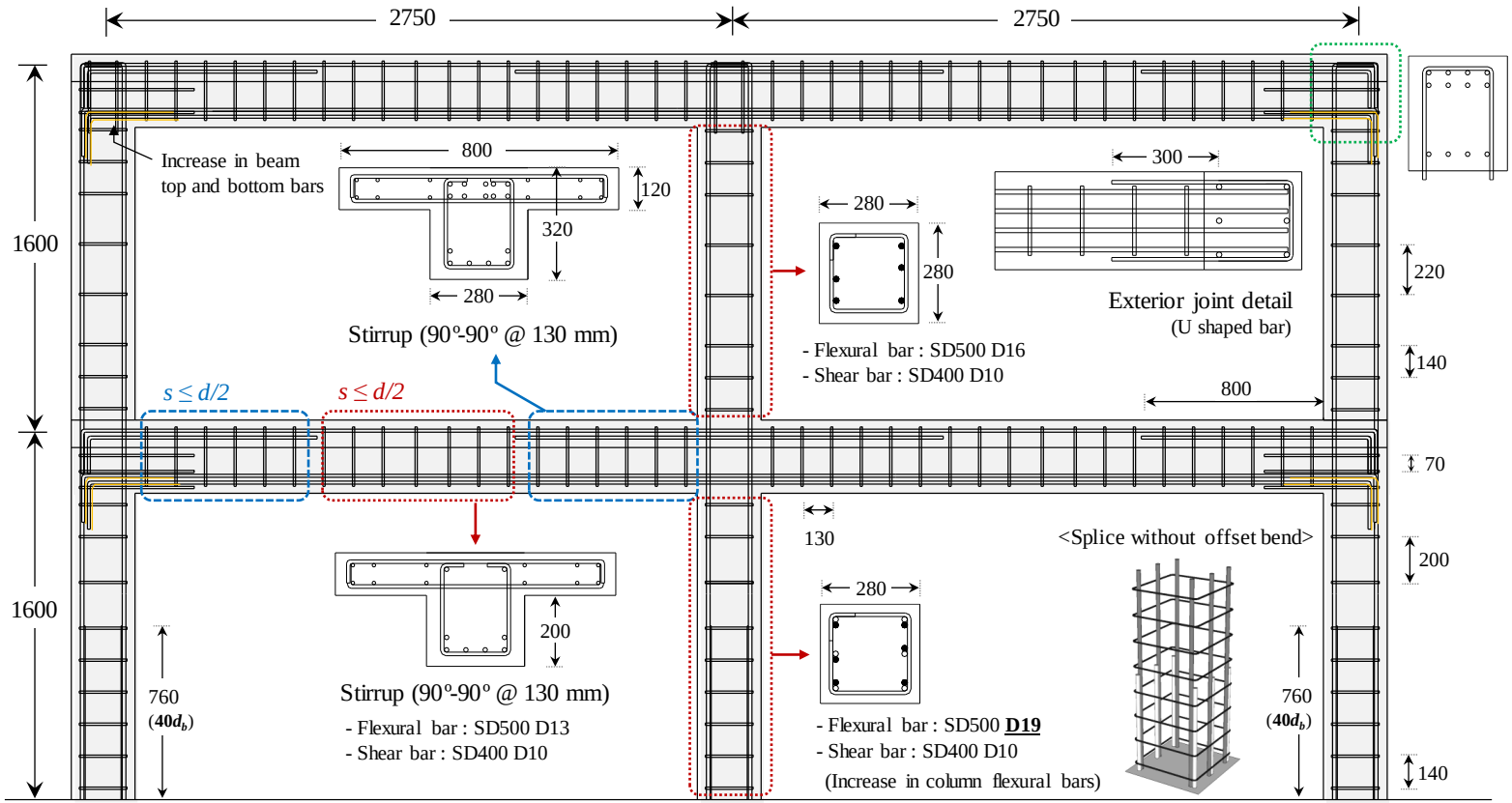

Figure 6-12 Dimensions and reinforcement details of the intermediate moment frame specimen (A2F)

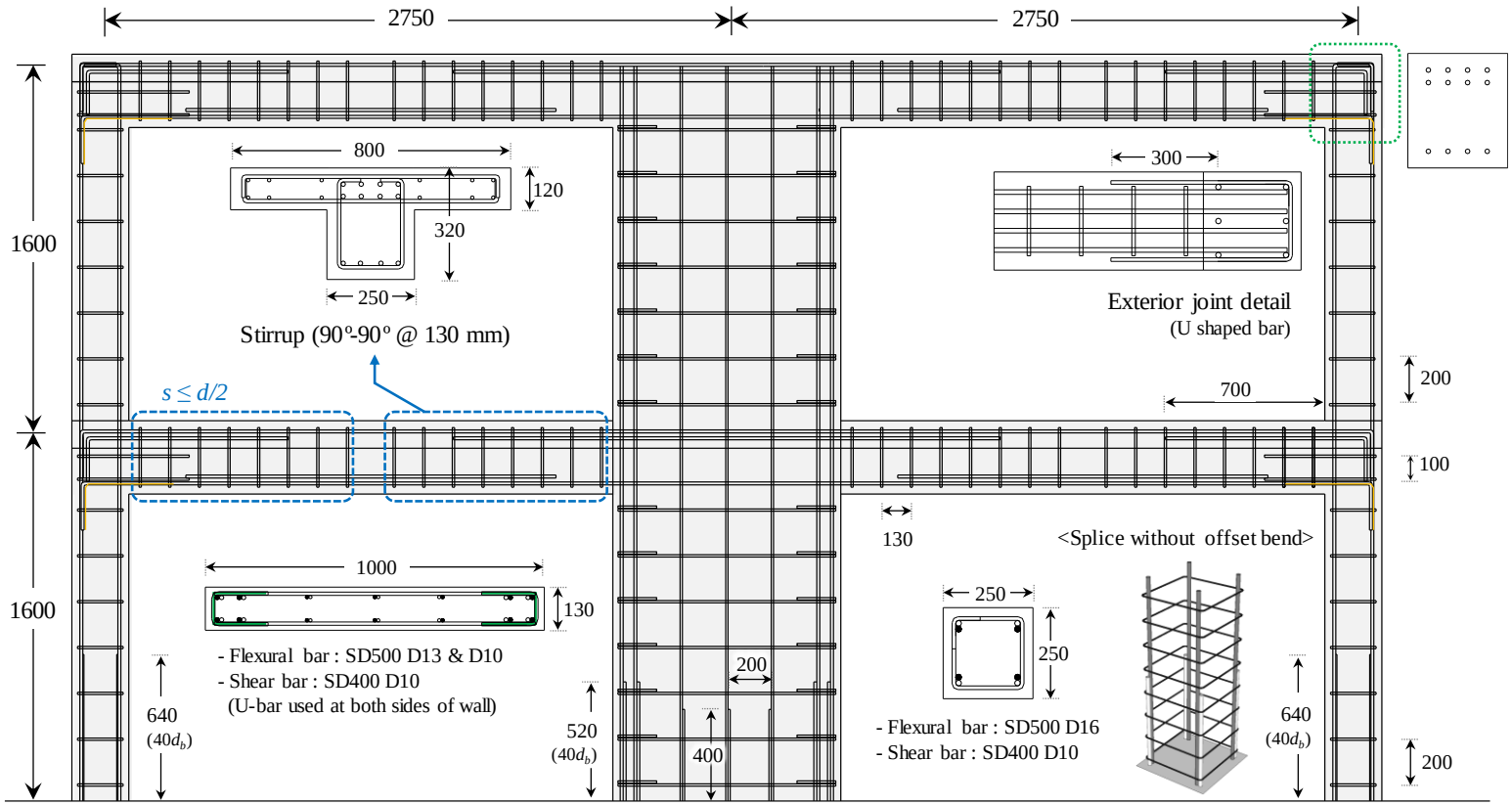

Figure 6-13 Dimensions and reinforcement details of the intermediate moment frame specimen (WF)

Table 6-3 Reinforcement details of RC frame specimens

Specimen	Intermediate Moment Frame (IMF)	Alternative 1 Moment Frame (A1F)	Alternative 2 Moment Frame (A2F)	Wall and Moment Frame (WF)
Column splice details of flexural bars	· Detail : Top offset bar splice · Length : $50d_b$ (KBC 2016)	· Detail : Splice w/o offset bend · Length : $50d_b$ (KBC 2016)	· Detail : Splice w/o offset bend · Length : $40d_b$ (Eq. (3-3))	· Detail : Splice w/o offset bend · Length : $40d_b$ (Eq. (3-3))
Shear rebar details and spacing	[Both ends] P.H zone ·Hoop w/ 135º hook ($s = 0.5H_{min}$) [Center] ·Tie w/ 90º hook ($s = 1.0H_{min}$)	[Both ends] P.H zone ·Tie w/ 135º hook ($s = 0.5H_{min}$) [Center] ·Tie w/ 90º hook ($s = 1.0H_{min}$)	[Both ends] P.H zone ·Tie w/ 135º hook ($s = 0.5H_{min}$) [Center] ·Tie w/ 90º hook ($s = 1.0H_{min}$)	· Gravity load design [Both ends and Center] · Tie with 90º hook ($s = 1.0H_{min}$)
Beam rebar details and spacing	[Both ends] · 135º-135º hoop ($s = 0.25d$) [Center] · 90º-90º stirrup ($s = 0.5d$)	[Both ends and Center] · 90º-90º stirrup ($s = 0.5d$) · D13 bar for beam flexural bar to secure anchorage length	[Both ends and Center] · 90º-90º stirrup ($s = 0.5d$) · D13 bar for beam flexural bar to secure anchorage length	[Both ends and Center] · 90º-90º stirrup ($s = 0.5d$) · D13 bar for beam flexural bar to secure anchorage length
Hook details of beam bottom bars	· Hook anchorage direction of beam bottom bar is upward	· Hook anchorage direction of beam bottom bar is downward (For convenient bar placement)	· Hook anchorage direction of beam bottom bar is downward (For convenient bar placement)	· Hook anchorage direction of beam bottom bar is downward (For convenient bar placement)
Joint reinforcement	· Detail : Hoop w/ 135º hook · $s = 0.25h_c$ (Three joint bars) ·Both interior and exterior joints	· Detail : U-bar · $s = 0.25h_c$ (Three joint bars) · Only exterior joint	· Detail : U-bar · $s = 0.25h_c$ (Three joint bars) · Only exterior joint	· Detail : U-bar · $s = 0.40h_c$ (Two joint bars) · Only exterior joint

6.2.3 Estimation of test strength

6.2.3.1 Strength demand of each member

The strength demand (M_u, V_u) were compared with the member strengths (M_n, V_n) through the section analysis to predict strength of each test specimen. To calculate strength demand of each member, hand calculation method and elastic analysis using MIDAS Gen can be used. The hand calculation method is superposition of each member force after calculating the member reaction force for the lateral load and the gravity load as shown in Figure 6-14(a). However, since the hand calculation is difficult to calculate accurately, MIDAS Gen was used to calculate the strength demand. As shown in Figure 6-14(b), the section size and length of beams and columns were specified, and then the bottom of columns was set to be fixed end. Horizontal load (P1, P2) and vertical load (N) was applied at the same position as the experimental plan.

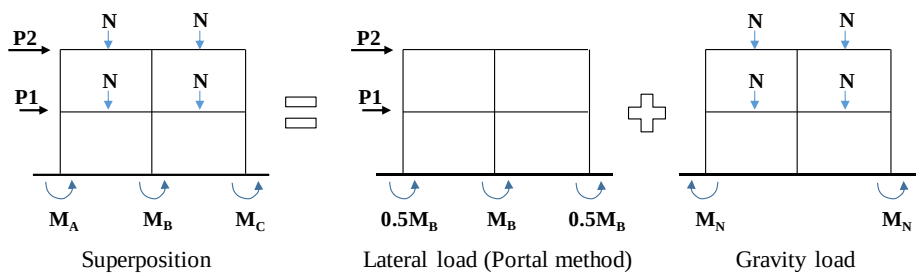

(a) Hand calculation (Portal method)

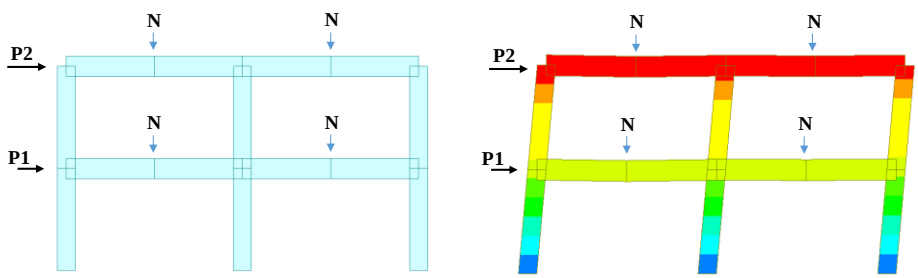

(b) Elastic analysis of MIDAS Gen

Figure 6-14 Estimation of strength demand of each member

6.2.3.2 Member strength of each member (Section analysis)

In order to predict the test strength, both the strength demand and the member strength (capacity) of each member should be calculated. Member strength was calculated by section analysis considering the location of the longitudinal reinforcement in the section. Because the axial force was applied on a column and a wall, the moment strengths of the members were calculated through the P-M interaction as shown in Figure 6-15. The actual material strength was used in calculating the flexural moment strength.

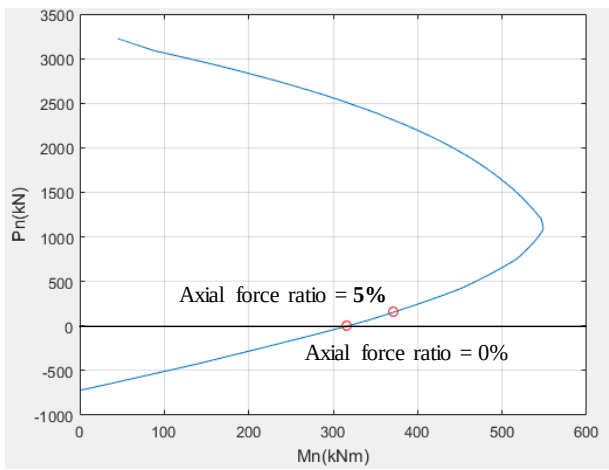

<P-M interaction of wall section>

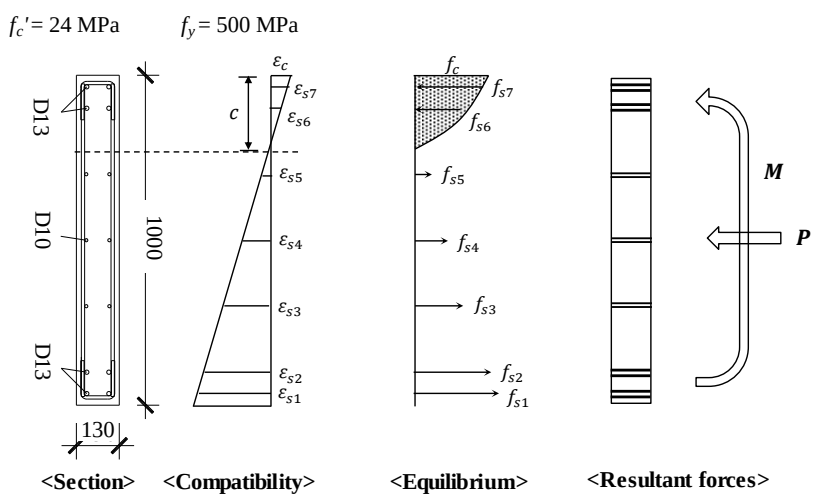

Figure 6-15 Sectional analysis process of a wall member

Member strength through section analysis are presented in Table 6-4. Based on the elastic analysis of MIDAS in the previous section 6.2.3.1, it is assumed that the column has an axial load ratio of 5%. For specimens **IMF** and **A1F**, the column moment strength is 86.5 kN·m, and the beam moment strengths are 213 kN·m and 106 kN·m in top and bottom sections, respectively. For specimen **A2F**, the column moment strength is 105.4 kN·m, and the beam moment strengths are 231 kN·m and 133 kN·m in top and bottom sections, respectively. For specimen **WF**, the column moment strength is 47.5 kN·m, the wall moment strength is 441.7 kN·m, and the beam moment strengths are 201 kN·m and 104 kN·m in top and bottom sections, respectively.

Table 6-4 Member strength of each specimen (Section analysis)

Specimen		IMF	A1F	A2F	WF
Column	Size	280 x 280	280 x 280	280 x 280	**250 x 250**
	Rebar	6-D16 (ρ_l=1.5%)	6-D16 (ρ_l=1.5%)	6-**D19** (ρ_l=2.2%)	4-D16 (ρ_l=1.3%)
	Flexural moment	86.5 kN·m	86.5 kN·m	105.4 kN·m	47.5 kN·m
Beam	Size	280 x 320	280 x 320	280 x 320	250 x 320
	Rebar (End)	[Top] 8-D13 (ρ_t= 1.13%) [Bottom]4-D13 (ρ_b= 0.57%)	[Top] 8-D13 (ρ_t= 1.13%) [Bottom]4-D13 (ρ_b= 0.57%)	[Top] 10-D13 (ρ_t= 1.42%) [Bottom]6-D13 (ρ_b= 0.85%)	[Top] 8-D13 (ρ_t= 1.27%) [Bottom]4-D13 (ρ_b= 0.64%)
	Flexural moment (End)	[Top]213 kN·m [Bot]106 kN·m	[Top]213 kN·m [Bot]106 kN·m	[Top]231 kN·m [Bot]133 kN·m	[Top]201 kN·m [Bot]104 kN·m
Wall	Size	-	-	-	1000 x 130
	Rebar	-	-	-	8-D13 & 6-D10 (ρ_l= 1.11%)
	Flexural moment	-	-	-	441.7 kN·m

6.2.3.3 Predicted test load

In order to estimate the predicted test load for each specimen, the moment strength demand and the strength capacity of each member were compared. If columns or wall in the first story show sufficient rotational ductility after member yielding, it may resist additional lateral forces by plastic mechanism as shown in Figure 6-16.

Columns in low-rise moment frames are subjected to small axial compression force and bending moment while beams are subjected to large bending moments at their ends and mid-span. It means that the cross section of the columns is usually smaller than that of the beams. Accordingly, such moment frame may show a weak column-strong beam behavior with limited ductility during earthquake loading.

The frame yields to the column at the bottom of the outer columns (2) after reaching the yield load at the bottom of the center column (1) at the first story, and then the top of the center column (3) yields, and ultimately collapses with yielding of the top of the outer columns (4). For plastic hinge mechanism of the RC frame, the concrete members (columns) should have sufficient ductility as the steel frame.

In the case of the specimen **IMF**, the flexural yielding in both top and bottom of columns at the first story can be attained with additional lateral load of 80 kN after reaching flexural yielding at the center column with lateral load of 250 kN, as shown in Figure 6-17. This plastic behavior can be possible when the first-story column exhibits sufficient ductility (reaching the required deformation without degrading strength). However, as RC frames have lower ductility than steel frames, ductility details should be used for the columns and joints to exhibit plastic mechanism. The load-carrying capacity decreases as the deformation increases after reaching the yield strength due to concrete crushing and rebar development failure. The predicted test loads in this chapter were estimated using the plastic mechanism (See Table 6-5).

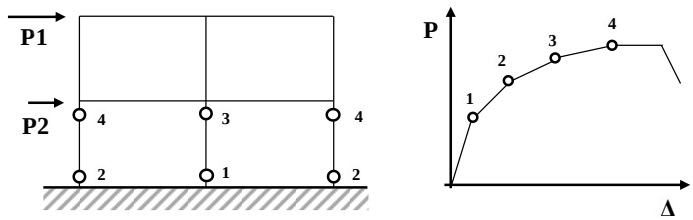

Figure 6-16 Plastic mechanism of RC frames

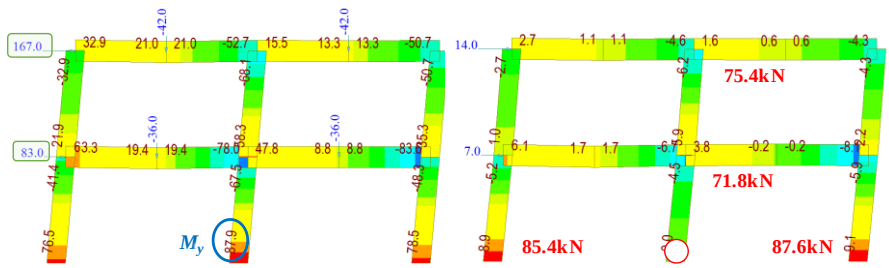

***P* = 250 kN** (Column '1' flexural yielding)

***P* =271 kN** (Column '2' flexural yielding)

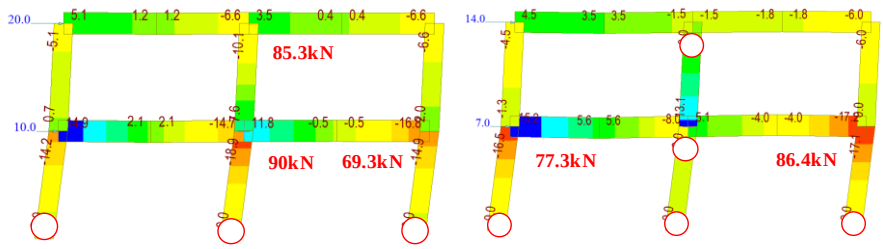

***P* = 301 kN** (Column '3' flexural yielding)

***P* = 323 kN** (Column '4' flexural yielding)

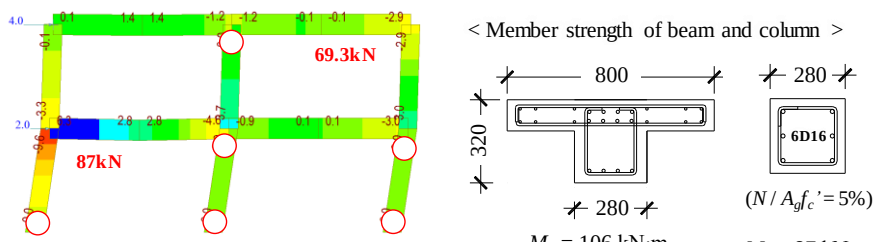

***P* = 330kN** (Column '4' flexural yielding)

Figure 6-17 Plastic mechanism using MIDAS Gen

Table 6-5 Predicted test load of each specimen

Specimen	IMF	A1F	A2F	WF
M_y of column	87 kN·m	87 kN·m	105 kN·m	442 kN·m
M_y	$M_y = P/2.84$ kN·m			$M_y = P/0.776$
P_1 due to 1st column flexural yielding	250 kN	250 kN	300 kN	343 kN
P_n according to plastic mechanism	330 kN	330 kN	396 kN	660 kN

6.2.3.4 Shear design of beam and column

According to ACI 318-14, a beam will yield in flexure due to a major earthquake unless the beam do not have a moment strength more than three to four times the design moment. Therefore, the design shear force should be obtained by approximating the maximum shear force that can be developed in a member. In order to prevent shear failure of frame members, the required shear strength is to be calculated based on the flexural strength of the design members, not factored shear forces indicated by lateral load analysis, as shown in Figure 6-18.

Since the actual yield strength of the longitudinal reinforcement may exceed the specified yield strength and strain hardening of the reinforcement may occur at the face of the joint subjected to large rotations, the required shear strength should be determined using a stress of at least $1.25f_y$ in the longitudinal reinforcement (in the case of special moment frame). In this study, a stress of $1.0f_y$ in longitudinal reinforcement was used because the test specimens were designed to have same target strength to the intermediate moment frame.

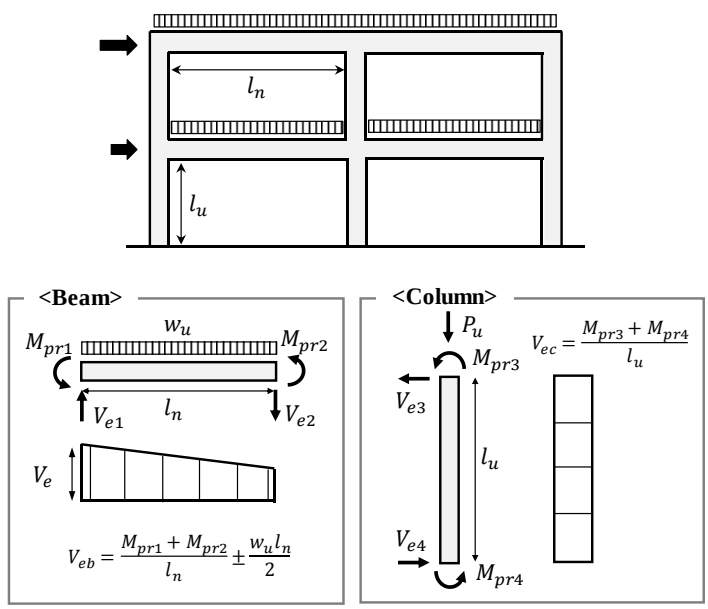

Figure 6-18 Shear design of beam and column using capacity design concept

Table 6-6 compares the required shear strength (demand) calculated from the flexural strength of the design members and the shear capacity of the members. In order to prevent shear failure prior to flexural yielding, shear reinforcement was sufficiently used so that the shear demand was not greater than the shear capacity of members.

Table 6-6 Comparison of shear demand and capacity of beam and column

Specimen			IMF	A1F	A2F	WF	Unit
Beam	Shear demand	M_{pr1}	213	213	231	201	kN·m
		M_{pr2}	106	106	133	104	kN·m
		l_n	2470	2470	2470	2125	mm
		$W_u \cdot l_n$	35	35	35	35	kN
		V_{eb}	146.6	146.6	164.9	161.0	kN
	Shear capacity	V_n	360.7	217.5	217.5	209.6	kN
		V_c	74.4	74.4	74.4	66.4	kN
		s/d	0.25	0.5	0.5	0.5	-
		V_s	286.3	286.3	286.3	286.3	kN
Column	Shear demand	M_{pr3}	86	86	105	48	kN·m
		l_u	1280	1280	1280	1280	mm
		V_{ec}	135.1	135.1	164.7	74.2	kN
	Shear capacity	V_n	197.3	197.3	197.3	133.4	kN
		V_c	74.6	74.6	74.6	58.3	kN
		s/H	0.5	0.5	0.5	0.8	-
		V_s	122.7	122.7	122.7	75.1	kN

6.2.3.5 Shear design of exterior and interior joints

Shear strength of the exterior and interior joints was evaluated because brittle failure occurred due to joint shear when shear failure occurred in the joint before column flexural yielding. The joint shear strength when flexural yielding of the bottom column in the first story was calculated based on elastic analysis of MIDAS Gen.

The shear force acting on the joint can be calculated by subtracting the shear force (P) acting on the top of column from the beam tensile force (T_b) by the moment strength (M_b) acting on the beam as shown in Figure 6-19(a). The shear force (V_{ju}) acting on the joint is as follows.

$$V_{ju} = T_b - P_n = \frac{M_b}{z_b} - P_n \quad \text{(Exterior joints)} \tag{6-3}$$

$$V_{ju} = C_b + T_b - P_n = \frac{M_{b1} + M_{b2}}{z_b} - P_n \quad \text{(Interior joints)} \tag{6-4}$$

Joint shear strength was evaluated according to ASCE41-13. The joint shear strength in ASCE41-13 shall be classified into conforming ($s \leq h_c/2$) and non-conforming ($s > h_c/2$) details according to the joint shear reinforcement spacing as follows.

$$V_{jn} = 0.083\gamma\sqrt{f_c'}A_j \tag{6-5}$$

where γ is a factor considering the effect of confined joint concrete by transverse beams and joint transverse reinforcement ratio. According to ASCE41-13, for interior connections, γ = 15 is used for conforming details, and γ = 10 is used for non-conforming details. For exterior connections, γ = 12 is used for conforming details, and γ = 6 is used for non-conforming details. A_j is the effective horizontal joint area with dimensions.

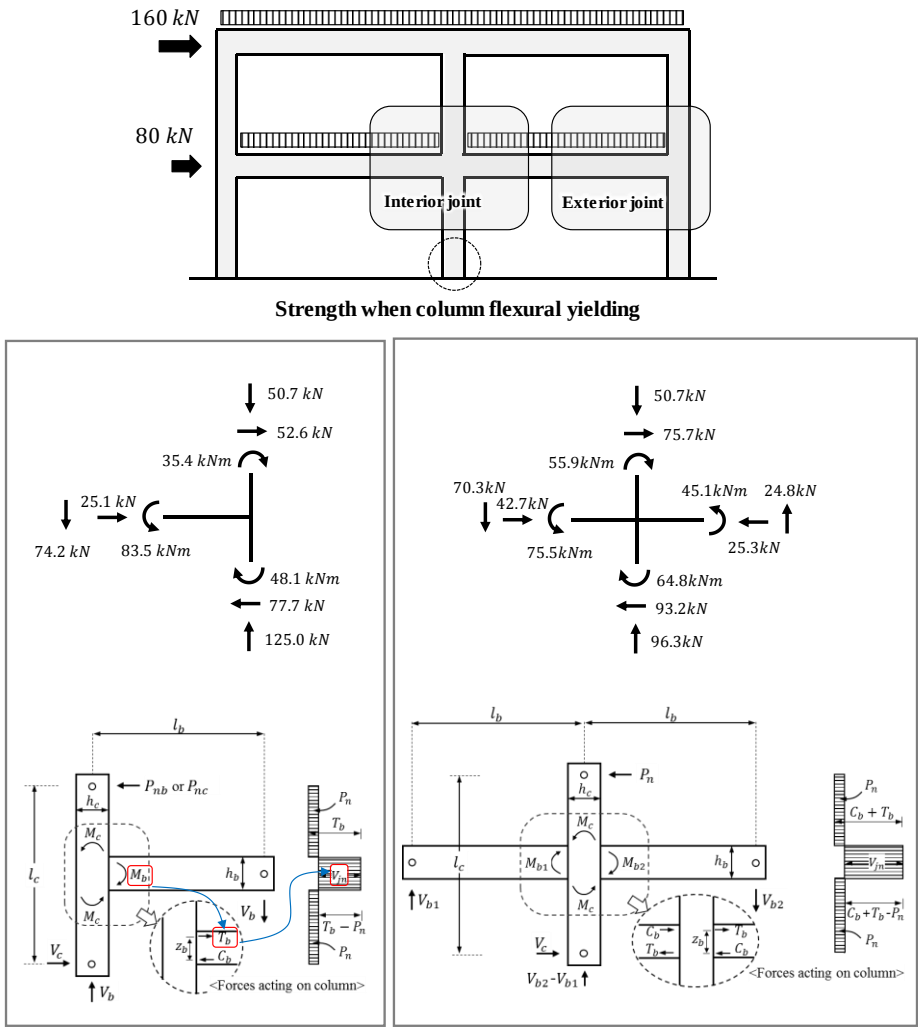

Figure 6-19 Shear design of exterior and interior beam-column joints

Table 6-7 presents the shear demand and shear capacity of exterior and interior joints. Since the required shear force (demand) was greater than the joint shear strength ($V_{jn,NC}$) of the non-conforming details, the joints in specimens **IMF**, **A1F**, and **A2F** required sufficient joint shear reinforcement. On the other hand, the exterior joint in specimen **WF** did not require sufficient joint shear reinforcement because the shear demand is not high. The interior joints also showed the similar pattern. However, because the equations in ASCE41-13 were defined based on a number of test results related to exterior and interior joint specimens with strong-column and weak-beam behavior, it is difficult to apply the ASCE41-13 standard directly to these test specimens. Therefore, in this study, the joint reinforcement details were planned based on the test results in Chapter 4.

As test results in Chapter 4, the exterior joints with a shear bar spacing of smaller than $0.3h_c$ (ρ_j= 0.93%) showed shear strength of $V_{jn,C}$, but the exterior joints with a shear bar spacing of $0.45h_c$ (ρ= 0.58%) showed shear strength of $V_{jn,NC}$. On the other hand, the interior joint specimens showed the joint shear strength larger than $V_{jn,C}$ regardless of joint shear reinforcement. This is because the exterior joint was difficult to secure the anchorage length of beam bars owing to the small column size, thus the 90º hook of beam bars had a great influence on the exterior joint behavior. On the other hand, since the interior joint was connected to the opposite side of the joint without the anchorage hook, it was not influenced by the 90º hook of beam bars.

Therefore, specimens **A1F** and **A2F** used shear reinforcement only in the exterior joint with a spacing of $0.25h_c$. According to ASCE41-13, the joint shear reinforcement in specimen **WF** was not necessary, but the minimum shear reinforcement used in the exterior joint with a spacing of $0.4h_c$ for ductile behavior of the moment frame.

Table 6-7 Joint shear strength of each specimen

Specimen			IMF	A1F	A2F	WF	Unit
Exterior joint	Shear demand	M_b	83.4	83.4	97.9	50.7	kN·m
		P_n	52.9	52.9	61.5	42.4	kN
		V_{ju}	**294.6**	**294.6**	**346.4**	**168.9**	kN
	Shear capacity	$V_{jn,C}$	**478.8**	**478.8**	**478.8**	381.7	kN
		$V_{jn,NC}$	239.4	239.4	239.4	**190.9**	kN
Interior joint	Shear demand	M_{b1}	78.1	78.1	90.7	71.7	kN·m
		M_{b2}	47.7	47.7	60.1	43.8	kN·m
		P_n	79	79	94.7	147	kN
		V_{ju}	**445.2**	**445.2**	**533.6**	**334.3**	kN
	Shear capacity	$V_{jn,C}$	**598.5**	**598.5**	**598.5**	992.4	kN
		$V_{jn,C}$	399.0	399.0	399.0	**661.6**	kN

6.2.4 Test setup of RC frames

6.2.4.1 Test setup for lateral loading

In order to apply static lateral cyclic load to a two-story frame, test setups for lateral loading on previous studies were examined. As the lateral loads (F_1 and F_2) per each floor are determined by the floor weights (w_1 and w_2) and the floor heights (h_1 and h_2) shown in Figure 6-20(a), the method of applying only second floor by a single actuator is excluded from discussion.

There are two ways to apply lateral loads to each floor in a two-story frame. As shown in Figure 6-20(c) and (d), one method is to apply loads directly to each floor with two actuators, the other is to apply loads to first and second floors at the same time with one actuator using a jig. Since the former uses two actuators, a larger load can be applied to the frame, but it is difficult to control the actuator. The latter, on the other hand, is relatively easier to control actuator, but the maximum lateral load applied to the frame is relatively small. In addition, since one loading point must be dispersed into two loading points, a jig for the lateral load distributions should be prepared. In this study, for safe and precise testing setup, one actuator with a jig is used as shown in Figure 6-20(d).

Figure 6-21 shows the test setup for applying lateral loading. Since the floor weights of the first and second floors were almost same ($w_1 \approx w_2$), and the height of the second floor from the bottom was twice that of the first floor ($h_2 = 2h_1$), the actuator was installed so that the lateral loads acting on second-story and first-story slabs were 2:1. The actuator used in this study is able to apply 1000 kN with maximum stroke of ±250 mm.

In detail of the loading point as shown in Figure 6-21, two hinges were provided for each floor to facilitate the distribution of lateral loads. Load cells were installed to individually measure two different loads applied on each floor. The lateral loads were transferred through slabs rather than beams because vulnerable exterior joints were not affected by the confinement effect of jigs, and crack patterns of exterior joints were observed in detail.

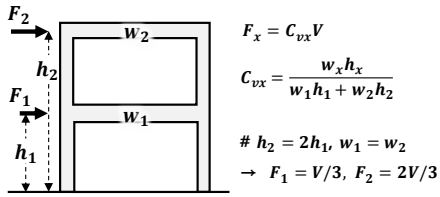

(a) Vertical distribution of seismic force

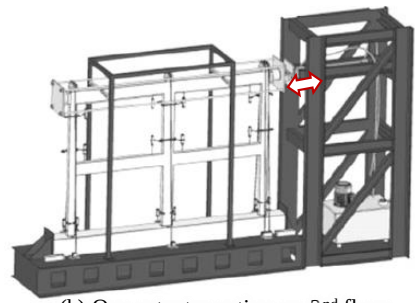

(b) One actuator acting on 2nd floor (Kaltakci et al., 2010b)

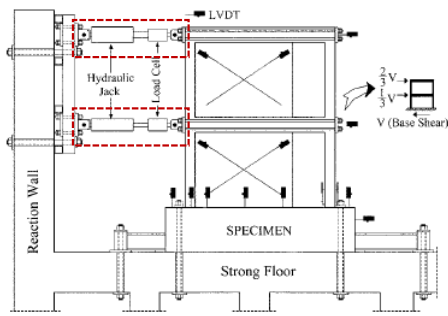

(c) Two actuators acting on 1st and 2nd floors (Kara and Altin, 2006)

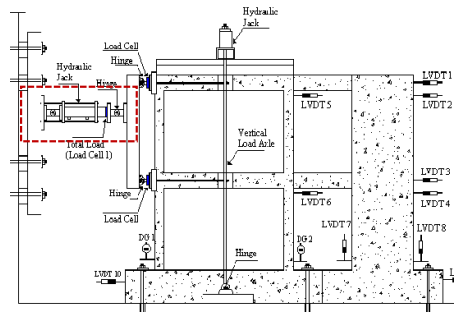

(d) One actuator acting on 1st and 2nd floors (Kaltakci et al., 2010a)

Figure 6-20 Test setups of RC frames on previous studies

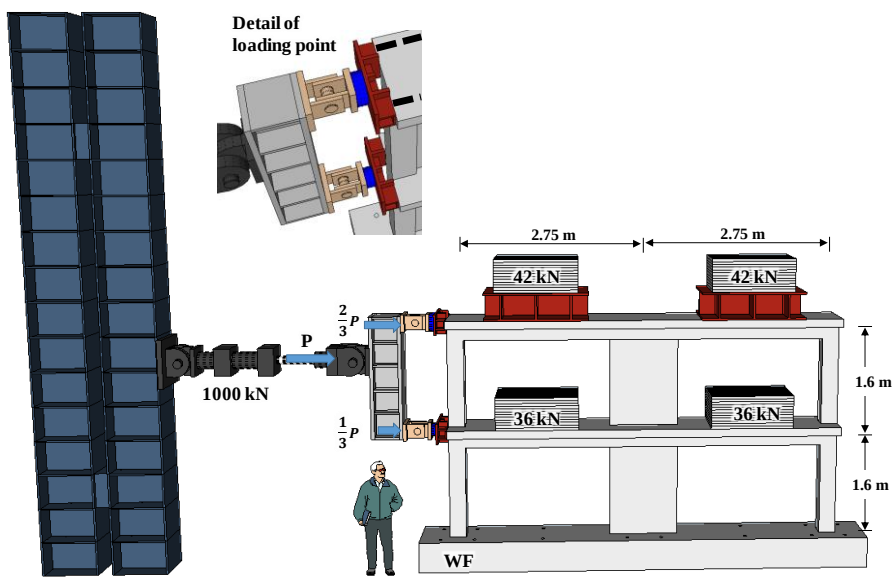

Figure 6-21 Schematic test setup for cyclic test of RC frame

6.2.4.2 Connection between loading point and test frame

In order to transmit lateral loads to all the columns constantly, a detail of the connection between a loading point and a test frame is significant. As shown in previous studies (Figure 6-22), the steel plate was attached to the exterior joint of the test frame to evenly distribute the lateral load over the entire frame, so that the lateral load acted on each column equally. However, such a setup is not preferable because the steel plate increased in confinement of the exterior joint, and exerted an advantage on the exterior joint behavior.

In this study, to minimize the effect of confinement of the exterior joint by the jig, steel rods were inserted into slabs, and the loading jig was connected with the frame. As shown in Figure 6-23, crack patterns of exterior joints could be examined through a certain space between the loading zig (U shape) and the frame (slab and beam).

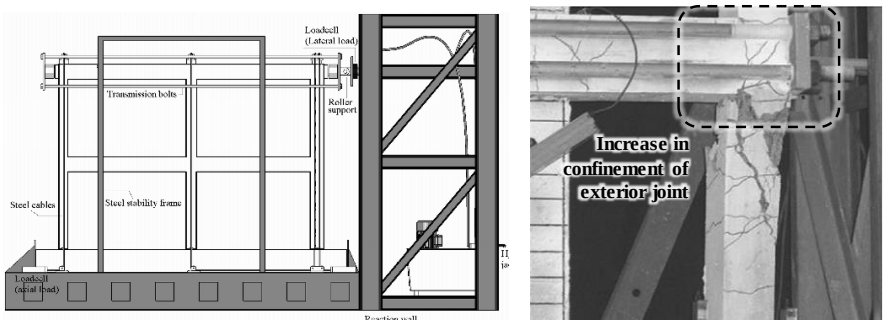

(a) Kaltakci et al. (2010b) (b) Kara and Altin (2006)

Figure 6-22 Connection between loading point and specimens in previous studies

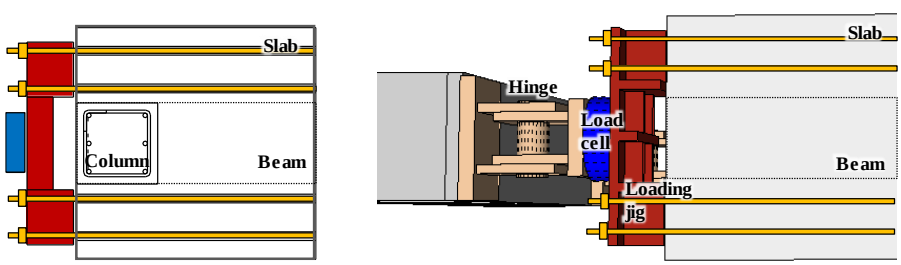

Figure 6-23 Idea for connection between loading point and specimen in this study

6.2.4.3 Lateral support of test specimen

Since the test frames were two-dimensional, deformation might occur in the out-of-plane direction perpendicular to the direction of the actuator load during cyclic tests. If the out-of-plane deformation occurs, the test frame may be twisted, which affects the test result. In order to prevent the out-of-plane deformation, the four ball jigs were installed to support the first and second story slabs. Figure 6-24 shows the lateral support detail of a test specimen.

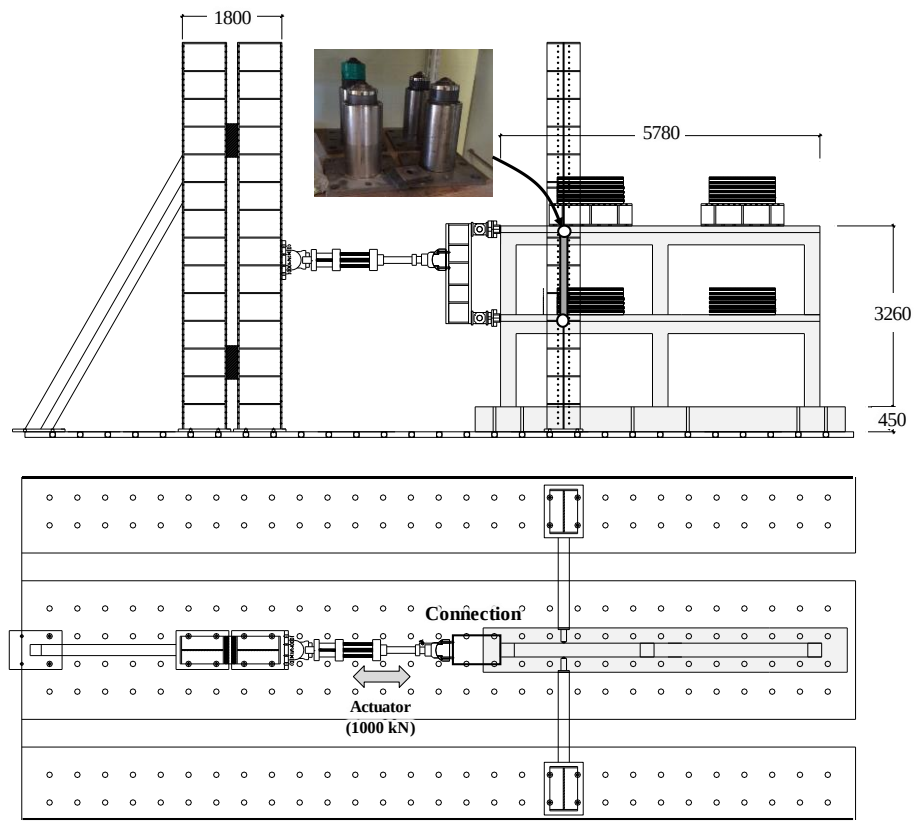

Figure 6-24 Lateral support for preventing out of plane deflection

6.2.4.4 Displacement measuring plan

As shown in Figure 6-25, the installation of the LVDTs was planned to measure lateral displacement, shear deformation (diagonal displacement) and flexural deformation (rotation angle) of columns, joints, and walls. Slip deformation was also measured at the bottom of first-story columns.

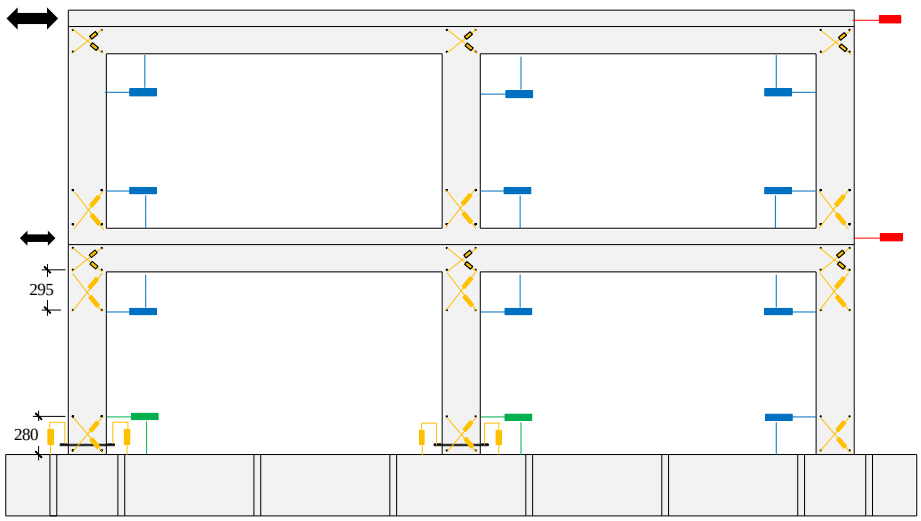

(a) Specimens **IMF, A1F, A2F**

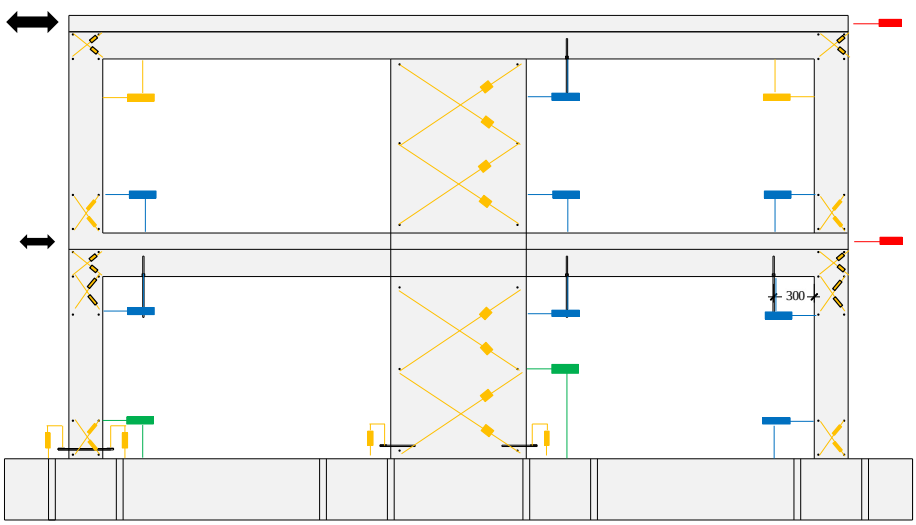

(b) Specimen **WF**

Figure 6-25 Displacement measuring plan of test specimens

6.2.4.5 Strain measuring plan

In order to evaluate splice performance according to the detail of first story columns using lap splices, steel gauges were attached to both top and bottom splice bars at a spacing of 250 mm. Gauges were also attached to flexural bars and shear reinforcing bars to determine the flexural yielding of columns, beams, and walls, and the role of the shear bars. Figure 6-26 shows the location of steel gauges in test specimens.

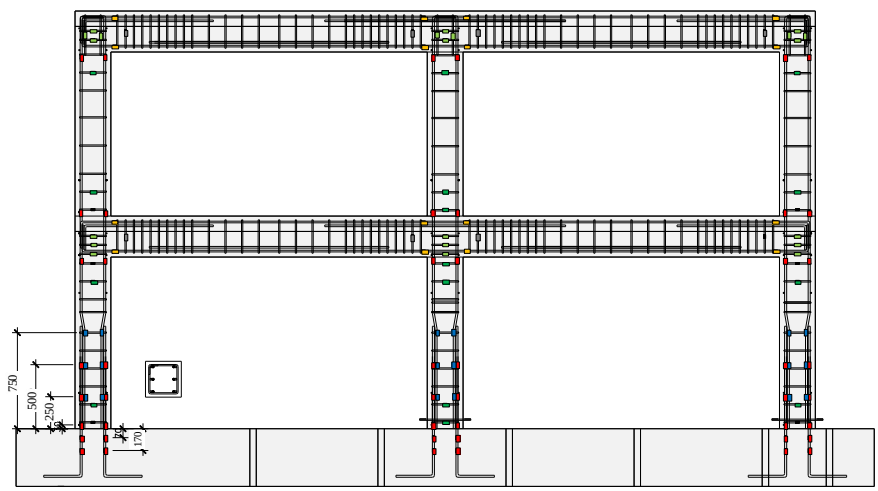

(a) Specimens **IMF, A1F, A2F**

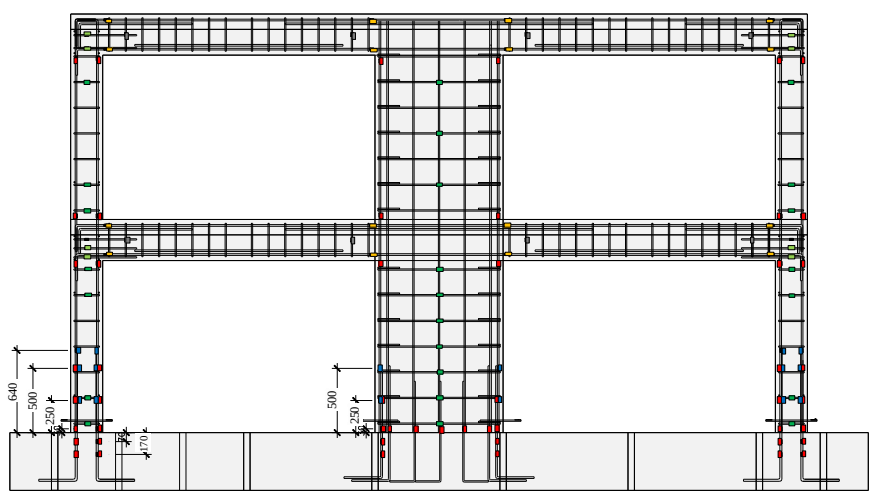

(b) Specimen **WF**

Figure 6-26 Strain measuring plan of test specimens

6.2.5 RC frame specimen construction process

Concrete in RC test frames was poured at three different times. The pedestals connected to the strong floor in the laboratory were made much larger than the columns or walls of the frames with sufficient flexural and shear reinforcement so that cracks and deformations did not occur. As shown in Figure 6-27(a) and (b), plastic pipes were pre-installed to connect the pedestal with the strong floor using steel rods, and first concrete was poured in the pedestal. Since the lap splices of the column longitudinal bars located between the pedestal and the first-story column, the bottom splice bars were located on the surface of the pedestal considering the lap splice length and detail. In order to improve the shear friction capacity, the interface of the pedestal was roughened as shown in Figure 6-27(c).

Since columns and walls between first-story and second-story were constructed without lap splices, column reinforcing bars were arranged to be anchored on the top of second-story columns as shown in Figure 6-27(d). Formworks for first-story columns and walls were installed, and beam rebars were arranged on beam formworks (Figure 6-27(e) and (f)). As shown in Figure 6-27(g), the slab formworks were installed, and the slab reinforcement was arranged. After the reinforcing bar work was completed, second concrete in the first-story members (columns, walls, and beams) was poured at once (Figure 6-27(h)). The reinforcing bars in the second-story members were arranged in the same manner as the first-story members. Third concrete was poured in the second-story members at once. The detailed construction process is illustrated in Figure 6-27.

(a) Formwork installation and rebar arrangement of pedestal
(2016. 4. 1 ~ 4. 10)

Figure 6-27 RC frame specimen construction process (continued)

(b) Concrete pouring in pedestal (2016. 4. 11)

(c) Roughening interface of pedestal

(d) Rebar arrangement of columns and walls in 1st and 2nd stories (2016. 4. 12 ~ 4. 15)

(e) Formwork installation of columns and walls in 1st story (2016. 4. 16 ~ 4. 17)

Figure 6-27 RC frame specimen construction process (continued)

(f) Rebar arrangement of beams in 1st story
(2016. 4. 18 ~ 4. 24)

(g) Formwork installation and rebar arrangement of slabs in 1st story
(2016. 4. 24 ~ 4. 29)

(h) Concrete pouring in columns, walls, beams, and slabs in 1st story
(2016. 4. 30)

Figure 6-27 RC frame specimen construction process (continued)

(i) Rebar arrangement of beams in 2nd story
(2016. 5. 4 ~ 5. 7)

(j) Formwork installation and rebar arrangement of slabs in 2nd story
(2016. 5. 8 ~ 5. 11)

(k) Concrete pouring in columns, walls, beams, and slabs in 2nd story
(2016. 5. 12)

(l) Completion of test specimens

Figure 6-27 RC frame specimen construction process

6.2.6 Loading plan

Figure 6-28 shows the test setup for the cyclic loading of frame specimen and the drift (Δ/a, a = the height of second floor = 3200 mm) history of the actuator for cyclic loading (displacement controlled test). The frame specimen was fixed on the pedestal, and the actuator was connected between the test specimen and the reaction frame to apply lateral load. According to ACI 374.1, the drift ratio for each loading step was increased from 0.25% to 1.2 ~ 1.5 times of the previous load drift ratio. The load cycles were repeated three times for each loading step.

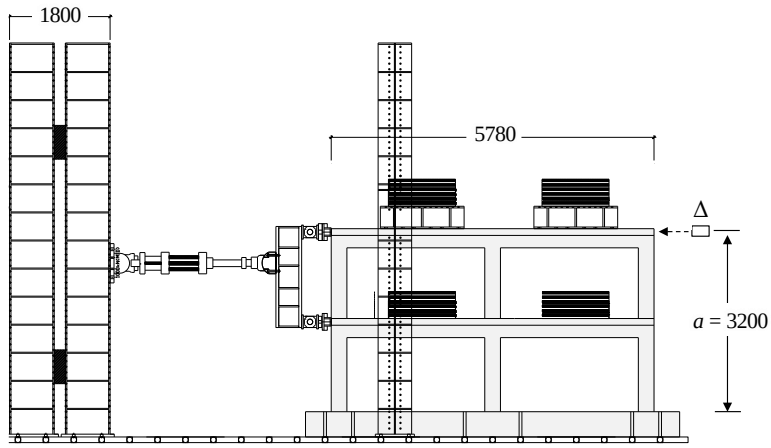

(a) Test setup for RC frame specimen

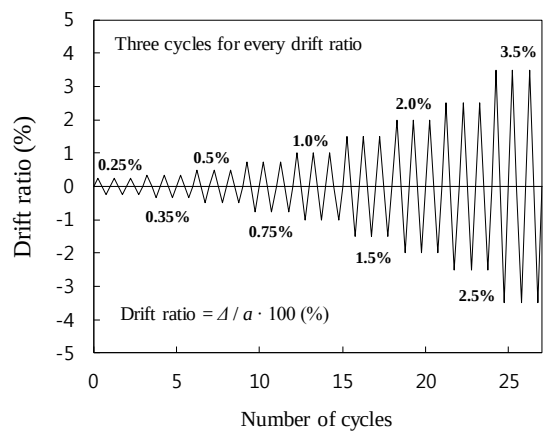

(b) Loading protocol for cyclic loading (ACI 374.1)

Figure 6-28 RC frame specimen construction process

6.3 Test Results and Observations

6.3.1 Material strengths

6.3.1.1 Concrete compressive strengths

Since the frame specimen were poured at three times as shown in Figure 6-29, the concrete cylinders were prepared for every members, the pedestal, the first-story, and the second-story members. Table 6-8 and Figure 6-30(a) show the concrete compressive strength variations according to curing periods.

The first frame test was conducted on June 10, 2016 (**IMF**= June 10, **A1F** = June 20, **A2F** = June 22, **WF** = June 15). As shown in Figure 6-30(a), the concrete strength did not increase anymore at the day of frame tests. The concrete strengths at one week before the first frame test were 26.7 MPa (Pedestal), 37.6 MPa (First story), and 26.9 MPa (Second story) as shown in Figure 6-30. The concrete strengths at 40 days after frame tests showed a slight decrease in strength but no significant change.

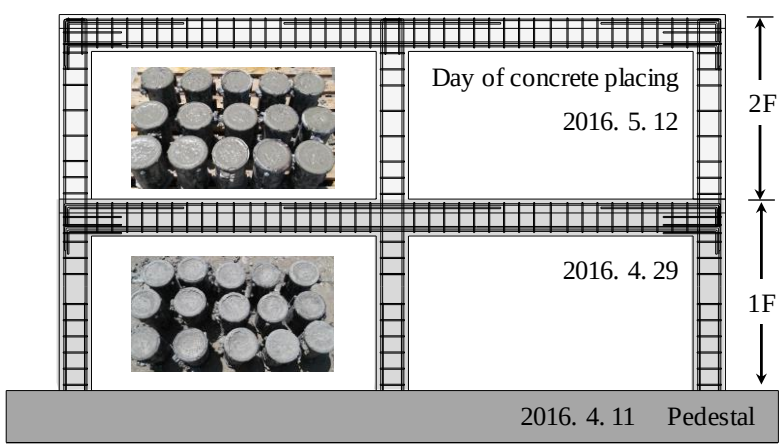

Figure 6-29 Schedule and location of concrete placing

Table 6-8 Average concrete strengths according to curing periods

Test No.	Test date	Curing period	Test 1	Test 2	Test 3	Average
Pedestal	2016. 4. 21	10	16	16	16	16.0
	2016. 5. 9	28	18	18	18	18.0
	2016. 5. 31	50	24	24	24	24.0
	2016. 6. 2	52	26.7	-	-	**26.7**
	2016. 8. 3	114	26.3	24.7	26.5	25.8
1F	2016. 5. 9	10	28	29	32	29.7
	2016. 5. 19	20	32	34	34	33.3
	2016. 5. 31	32	40	35	38	37.7
	2016. 6. 2	34	37.6	-	-	**37.6**
	2016. 8. 3	96	35.8	36.8	36.1	36.3
2F	2016. 5. 19	7	19	20	21	20
	2016. 5. 31	19	27	26	25	26
	2016. 6. 2	21	26.9	-	-	**26.9**
	2016. 8. 3	83	29.2	25.5	22.8	25.9

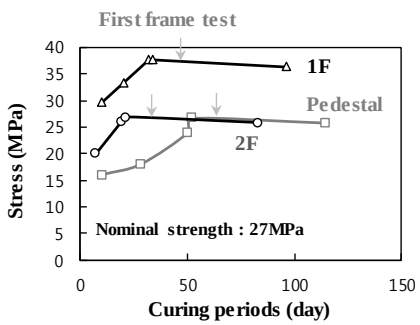

(a) Concrete strength variations according to curing periods

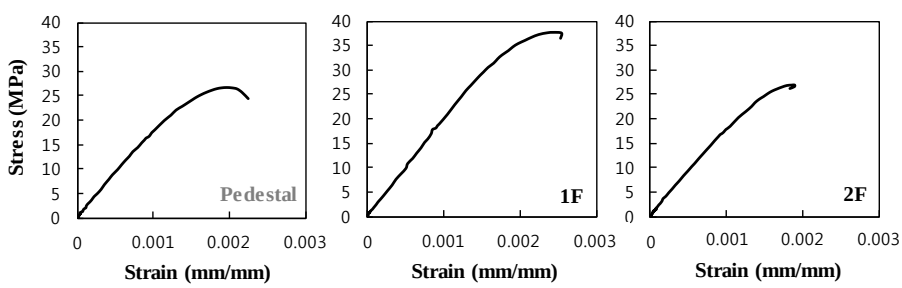

(b) Stress and strain curves of concrete cylinders

Figure 6-30 Test results of concrete cylinders

6.3.1.2 Steel rebar tensile strength

The reinforcing bars used in the test specimens were D10, D13, D19 with nominal strength of 400 MPa for shear reinforcement, and D10, D13, D16, D19 with nominal strength of 500 MPa for flexure reinforcement. Table 6-9 shows the yield strength, tensile strength, and yield strain of rebars used in the test specimens. The strengths are the average values of test strength obtained from the three specimens.

The yield strength of the SD400 D10 reinforcing bar used as shear reinforcement was 504 MPa, and the yield strengths of SD500 reinforcing bars used as flexure reinforcement were 542 ~ 601 MPa. The stress and strain curves of reinforcing bars are presented in Figure 6-31.

Table 6-9 Average strengths of steel reinforcing bars

Specimens	Location	d_b (mm)	f_y (MPa)	f_u (MPa)	ε_y (mm/mm)
SD400 D10	B/C/W Shear	9.53	504	614	0.00252
SD400 D13	Pedestal shear	12.7	510	615	0.00255
SD400 D19	Pedestal flexure	19.1	512	635	0.00256
SD500 D10	Wall flexure	9.53	542	631	0.00271
SD500 D13	Beam flexure	12.7	548	653	0.00274
SD500 D16	Column flexure	15.9	601	697	0.00301
SD500 D19		19.1	586	726	0.00293

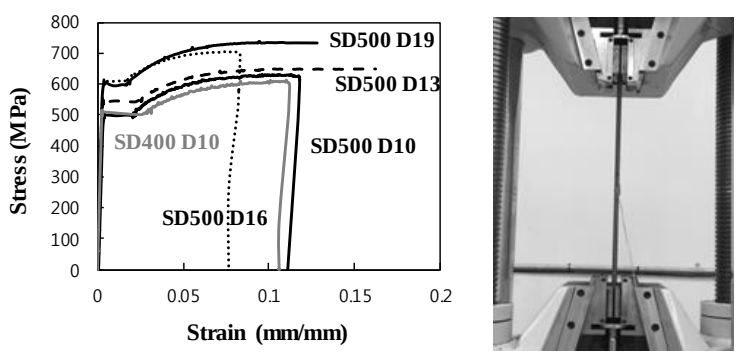

Figure 6-31 Test results of steel reinforcing bars

6.3.2 Comparison of lateral load and displacement measurements

6.3.2.1 Displacement difference in the left and right columns

In order to verify that the actuator load was transmitted to the entire members of the frame (left and right columns), the first and second floor displacements ($\Delta_{1,L}$ and $\Delta_{2,L}$ in Figure 6-32(a)) measured at the actuator position (left column) were compared with those ($\Delta_{1,R}$ and $\Delta_{2,R}$ Figure 6-32(a)) measured at the end of the frame (right column). In particular, the displacement difference measured in left and right columns were analyzed to verify that the actuator load was transmitted to the rightmost column farthest from the actuator when the actuator pulled the frame.

Figure 6-32(b) shows the displacement difference measured in left and right columns of specimen **A1F** according to the data scanning. The maximum displacement difference measured at the left and right sides of the first-story slab ($\Delta_{1,L}$ - $\Delta_{1,R}$) was -4.6 mm ~ 1.4 mm, and that of the second-story slab ($\Delta_{2,L}$ - $\Delta_{2,R}$) was -6.6 mm ~ 6.2 mm. Although the displacement difference in the second-story slab seems relatively larger, it is not a big differenced considering that the displacement of the second-story slab is twice that of the first-story slab. Further, when the actuator was pulled (Y axis in Figure 6-32(b) was minus), the displacement difference was larger in the first floor, but almost the same in the second floor.

The ratio of the left and right displacement difference ($\Delta_{n,L} - \Delta_{n,R}$) divided by the displacement value ($\Delta_{n,R}$) measured from the right side is presented according to the data scanning steps in Figure 6-32(c). In the initial stage of the test, the displacement difference ratio was about 40%. However, as the total displacement increased, the displacement difference decreased to 10% ~ 20% of the total displacement. This indicates that the actuator load was well transmitted with the test setup used in this study.

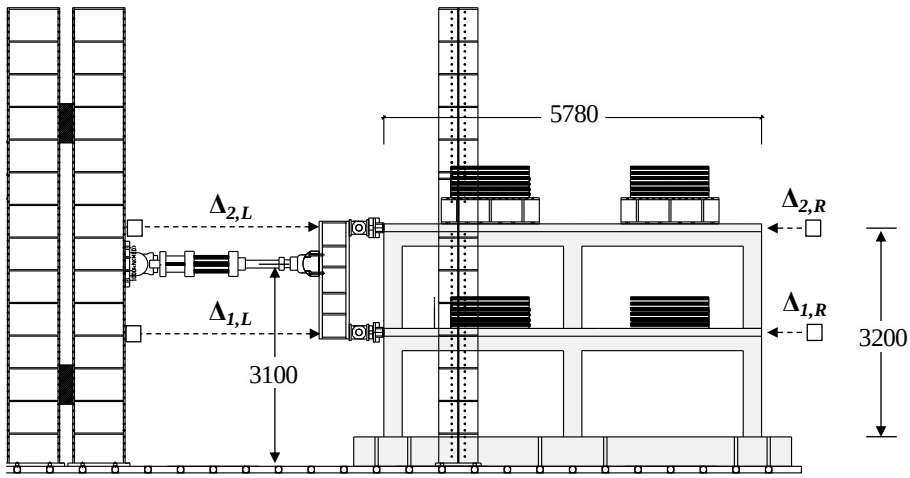

(a) Measuring location of lateral displacements

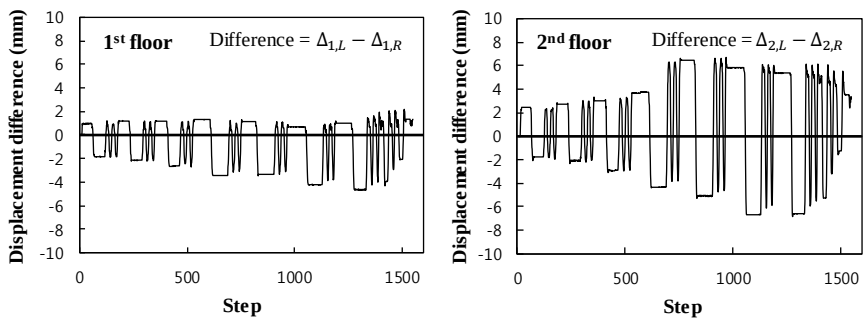

(b) Displacement difference measured in left and right columns

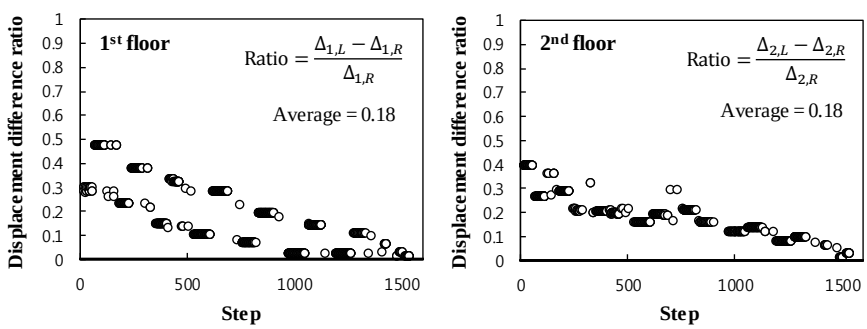

(c) Displacement difference ratio

Figure 6-32 Comparison of displacement difference measured in specimen A1F

6.3.2.2 Load and displacement acting on first and second floors

(1) Comparison of lateral load acting on first and second floors

In this study, two different loads ($F_2 = 2F_1$) were applied to both first and second-story slabs through a single actuator and a jig as shown in Figure 6-33(a). The load values measured from load cells at the first and second floor slabs were investigated to verify that the actuator load was successfully transferred with $F_2 = 2F_1$.

Figure 6-33(b) and (c) show the measured lateral load values of F_1 and F_2, and the ratio of two loads (F_2 / F_1) in specimens **A1F** and **A2F**. The load ratio of the first and second floor slabs was 1:2. However, the ratio (F_2 / F_1) in specimen **A1F** was 2.5 or more in the first cycle with drift ratio of 1.0%, 1.5%, and 2.0% because the load value F_1 was not accurately measured by the load cell. In the case of specimen **A1F**, the positive direction load of the first floor was not increased after drift ratio of 1.0%, but the negative direction load was increased. On the other hand, in specimen **A2F**, the load was constantly transferred with $F_2 = 2F_1$ until the end of test.

If the lateral loads were accurately measured by the load cells, the actuator load (F_A) should be equal to the sum of the loads acting on the first and second floors ($F_1 + F_2$). Figure 6-33(d) shows the result of comparing the actuator load and the load cell values. Since the ratio of F_A to ($F_1 + F_2$) was 1.0, the actuator load value was almost the same as the sum of the load cell values measured from first and second floors. However, in specimen **A1F**, the actuator load (F_A) was about 10% larger at drift ratio of 1.0%, 1.5%, and 2.0% because the load F_1 was not accurately measured by the load cell installed on the first-story slab as described above.

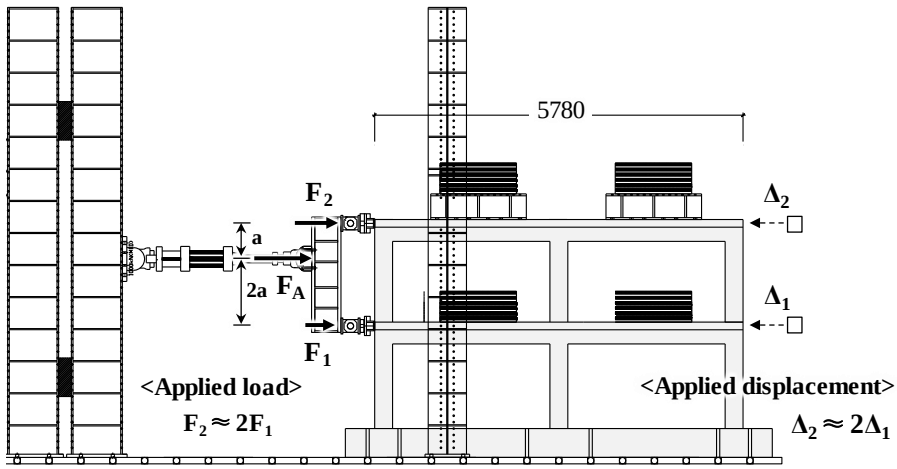

(a) Load and displacement measurement acting on first and second floors

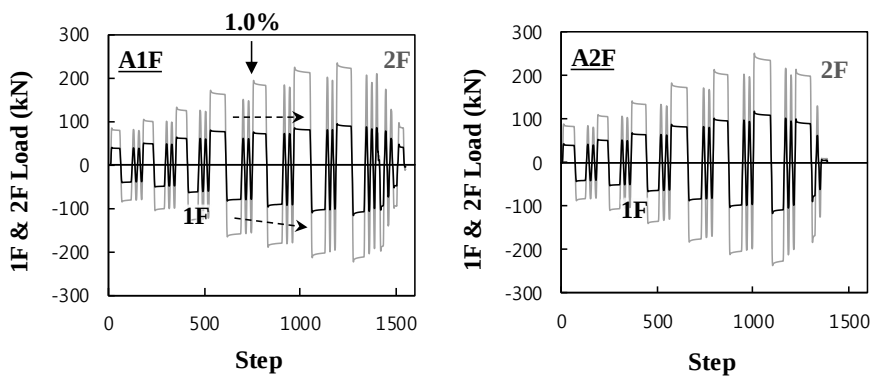

(b) Comparison of lateral loads acting on first and second floors

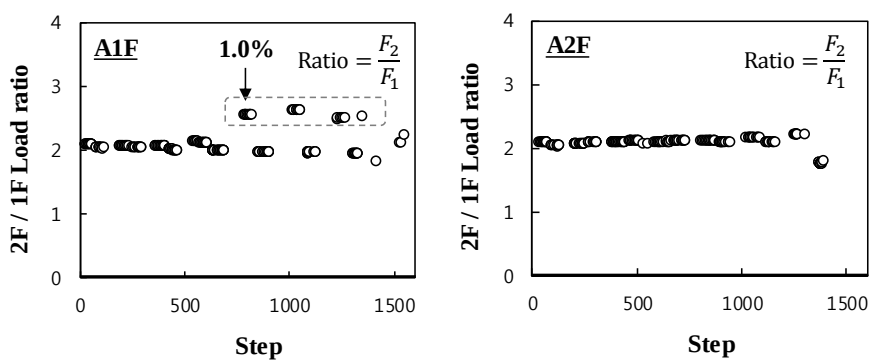

(c) Lateral load ratio acting on first and second floors

Figure 6-33 Comparison of load measurements in specimens A1F and A2F (Continued)

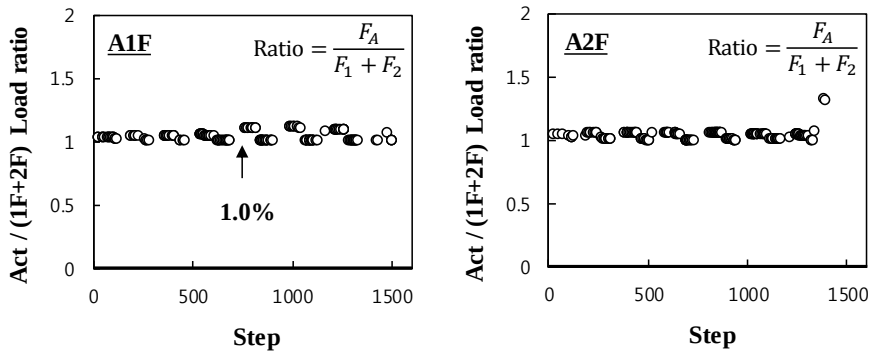

(d) Comparison of lateral load measured from the actuator and load cells

Figure 6-33 Comparison of load measurements in specimens A1F and A2F

(2) Comparison of lateral displacement on first and second floors

The displacement values (Δ_1 and Δ_2) measured at the first and second-story slabs were investigated in Figure 6-34. In the initial stage, the displacement of the second floor was about twice that of the first floor as the load twice larger than the first floor acted on the second floor ($F_2 = 2F_1$). The soft story mechanism occurred at the first floor as the plastic hinge zone progressed along with the yielding at the bottom of first-story columns. As a result, the displacement ratio (Δ_2 / Δ_1) gradually decreased from 2.0 to 1.0 with increasing the displacement Δ_1.

Such displacement measurement indirectly showed that the specimens failed with weak-column and strong-beam behavior. The displacement ratio (Δ_2 / Δ_1) decreased rapidly in specimen **A2F** with relatively small deformation capacity compared to specimen **A1F**.

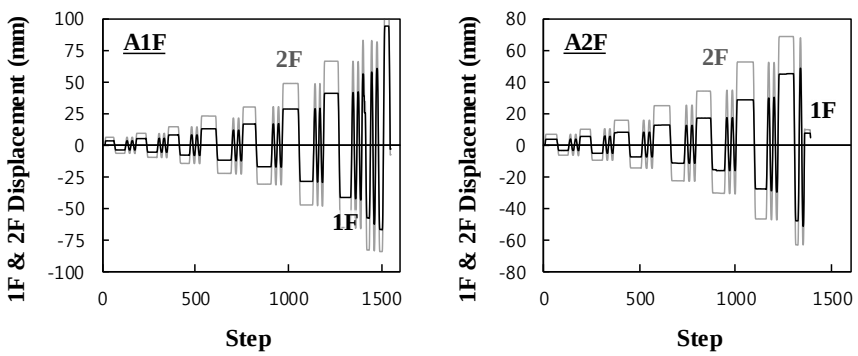

(a) Comparison of lateral displacements on first and second floors

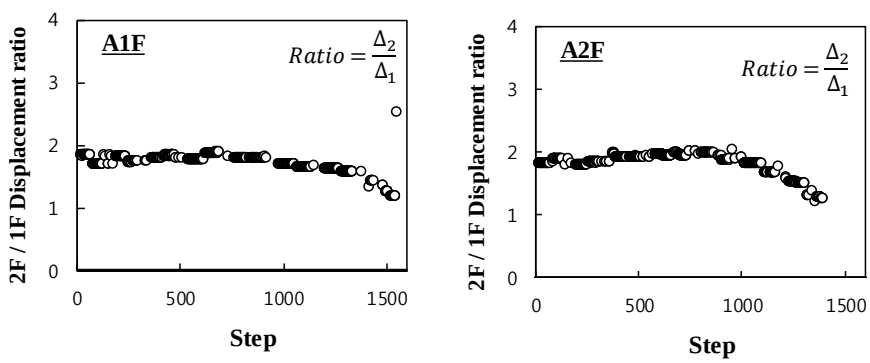

(b) Lateral displacement ratio on first and second floors

Figure 6-34 Comparison of displacement measurements in specimens A1F and A2F

6.3.3 Test Results

6.3.3.1 Intermediate moment frame (IMF)

The intermediate moment frame (**IMF**) was designed using the response modification factor R = 5.0 according to the KBC2016 design code. The lateral load and drift ratio relationship, and failure sequence with crack patterns are presented in Figure 6-35 and Figure 6-36, respectively.

In Figure 6-35, the horizontal axis indicates the drift ratio of second floor displacement ($\Delta_{2,b}$) divided by the second floor height from the pedestal (L_2= 3200 mm), and the vertical axis denotes the actuator load. The P_u marked with white circles represents the maximum load values in the positive and negative directions. The predicted strength P_n estimated based on the plastic mechanism of columns as shown in Figure 6-17 is indicated by a thick dashed line. The predicted load at which the first-story center column attains its yield strength is denoted by P_{n1} with a thin dotted line. Figure 6-36 shows a failure sequence and crack patterns of the whole test frame at drift ratio of 0.5%, 0.75%, 1.0%, 1.5%, 2.0%, 2.5%, and 3.5%.

The specimen **IMF** exceeded the yield strength of first-story center column P_{n1} at drift ratio of 0.75% to 1.0%, and reached the maximum load (346.8 kN and -336.7 kN) at drift ratio of 2.5%. During second cycle positive loading at drift ratio of 3.5%, the load carrying capacity was decreased to 80% of the maximum load, so the test was terminated. The test results are summarized in Table 6-10. The maximum load P_u (346.8 kN and -336.7 kN) was about 4% larger than the predicted load P_n (330.0 kN) obtained by the plastic mechanism. This indicates that even after the first-story center column yields (P_{n1}), it is sufficiently resistant to additional lateral loads by the plastic mechanism (See Figure 6-16).

The displacement ductility of specimen **IMF** was 4.41. The ductility is δ_u / δ_y by calculating the yield drift ratio (δ_y) and the ultimate drift ratio (δ_u) based on the envelop curve for the first cycle. The yield drift ratio δ_y was calculated as P_{max} / K_y where P_{max} is the maximum load and K_y is the secant stiffness, connecting the origin and the pre-peak point of $0.6P_{max}$. The ultimate drift ratio δ_u was calculated as the drift ratio at the point where the load carrying capacity was decreased to 80% of P_{max}. The yield drift ratio δ_y was 0.84%, and the ultimate drift ratio δ_u was 3.71% in

specimen **IMF**.

As shown in Figure 6-36, at drift ratio of 0.5%, flexural cracks occurred at the top and bottom of the first-story columns and initial diagonal cracks developed at joints. The flexural cracks also occurred in the beam connected to the exterior joints in the first story. At drift ratio of 0.75% ~ 1.0% when the first-story center column yielded, cracks were concentrated in the column plastic hinge zone as the flexural cracks developed into diagonal cracks, and diagonal cracks were also concentrated in the joints. Compared to the second-story columns, a relatively large number of cracks occurred in the first-story columns. At drift ratio of 1.5% ~ 2.0%, the number of cracks rapidly increased in the plastic hinge zone of the first-story columns and the second-story center column due to plastic mechanism of columns. Since specimen **IMF** showed weak-column and strong-beam behavior, relatively few cracks were observed in beams compared to columns and joints.

In drift ratio of 2.5%, as the width of diagonal cracks at the center and right columns in the first story increased, the load carrying capacity decreased significantly. Finally, at drift ratio of 3.5%, splitting failure occurred due to diagonal shear cracks in plastic hinge zones and splitting cracks along the lap splice region of column longitudinal bars.

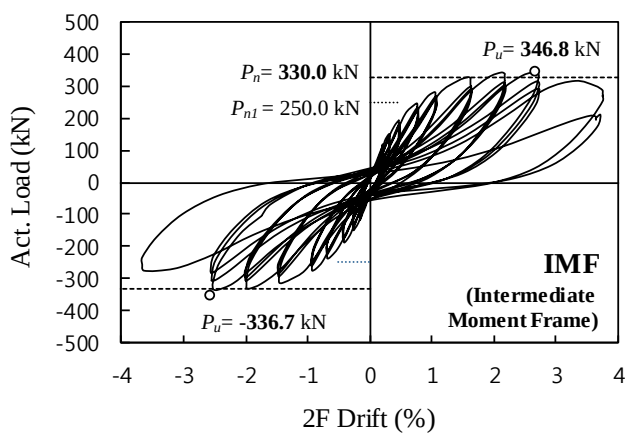

Figure 6-35 Lateral load and drift ratio relationship of specimen IMF

Table 6-10 Test results of RC frame specimens

Specimen		IMF	A1F	A2F	WF
Predicted strength	P_n (kN) [1]	330	330	396	660
	P_{n1} (kN) [2]	250	250	300	343
Test results	P_{test}^+ (kN)	346.8	367.0	390.1	471.5
	P_{test}^- (kN)	336.7	346.4	362.2	440.8
	P_u (kN)	341.8	356.7	376.2	456.2
	P_u / P_n	1.04	1.08	0.95	0.69
	P_u / P_{n1}	1.37	1.43	1.25	1.33
Ductility	δ_y (%) [3]	0.84	0.84	0.84	0.41
	δ_u (%) [4]	3.71	2.68	1.96	1.55
	Δ_u / δ_y	4.41	3.21	2.33	3.83
Initial stiffness (kN/mm)	Positive	19.01	20.98	20.32	42.18
	Negative	22.27	21.08	21.24	42.81
	Average	20.64	21.03	20.78	42.50
Cumulative energy dissipation (kN·m)	0.5%	8.9	5.3	6.0	8.6
	1.0%	27.9	19.1	22.3	34.9
	1.5%	53.5	42.7	47.5	67.8
	2.5%	145.0	124.7	70.5	-
	3.5%	188.3	134.5	-	-

1) Predicted strength of frames considering plastic mechanism
2) Yield strength of 1st columns located in the center of frames
3) Yield drift ratio = P_{max} / K_y where P_{max} is the maximum strength and K_y is the secant stiffness, connecting the origin and the pre-peak point of $0.6P_{max}$
4) Ultimate drift ratio when the loading capacity is decreased to 80% of maximum strength

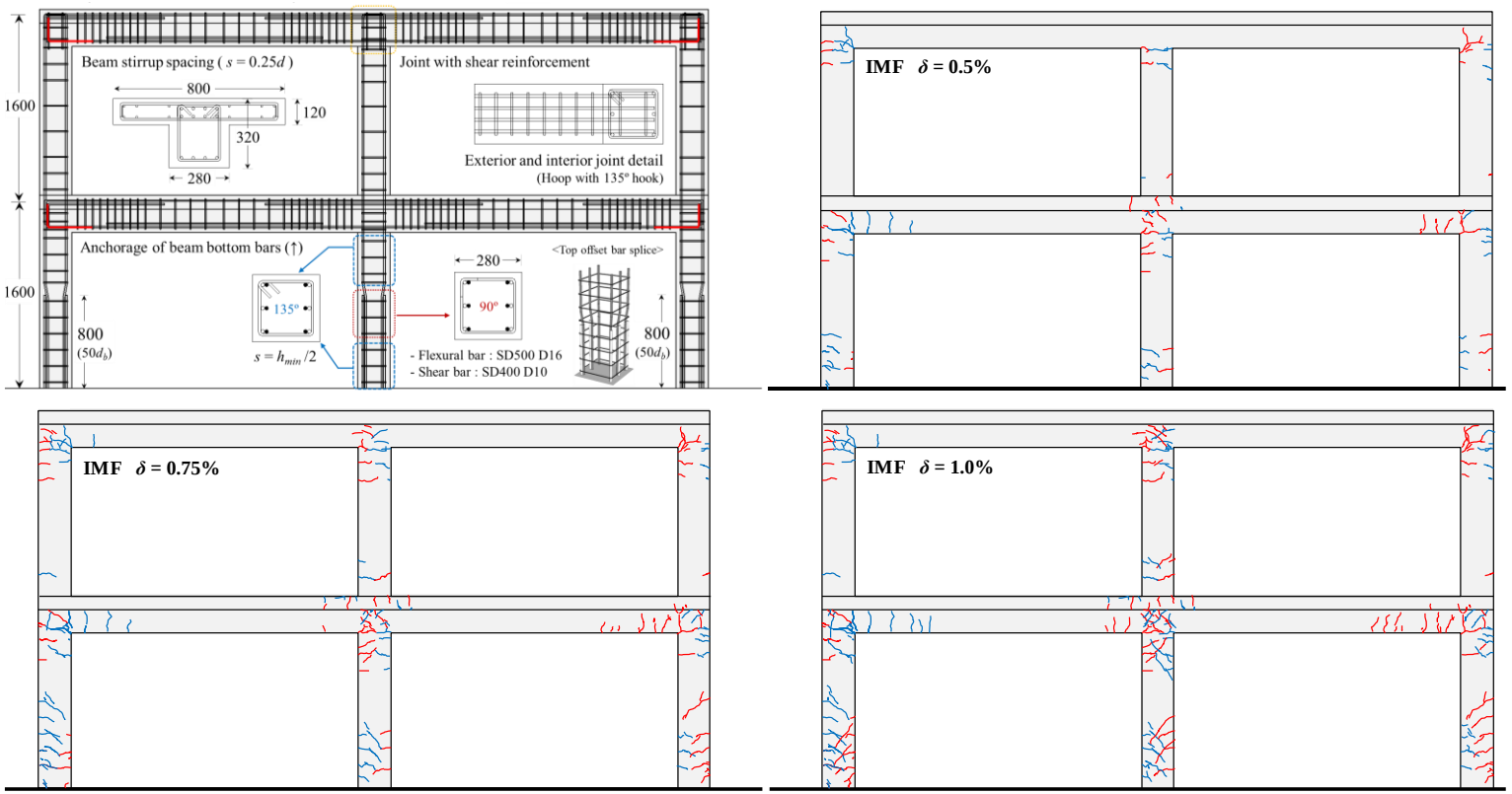

Figure 6-36 Failure sequence and crack patterns of specimen IMF (Continued)

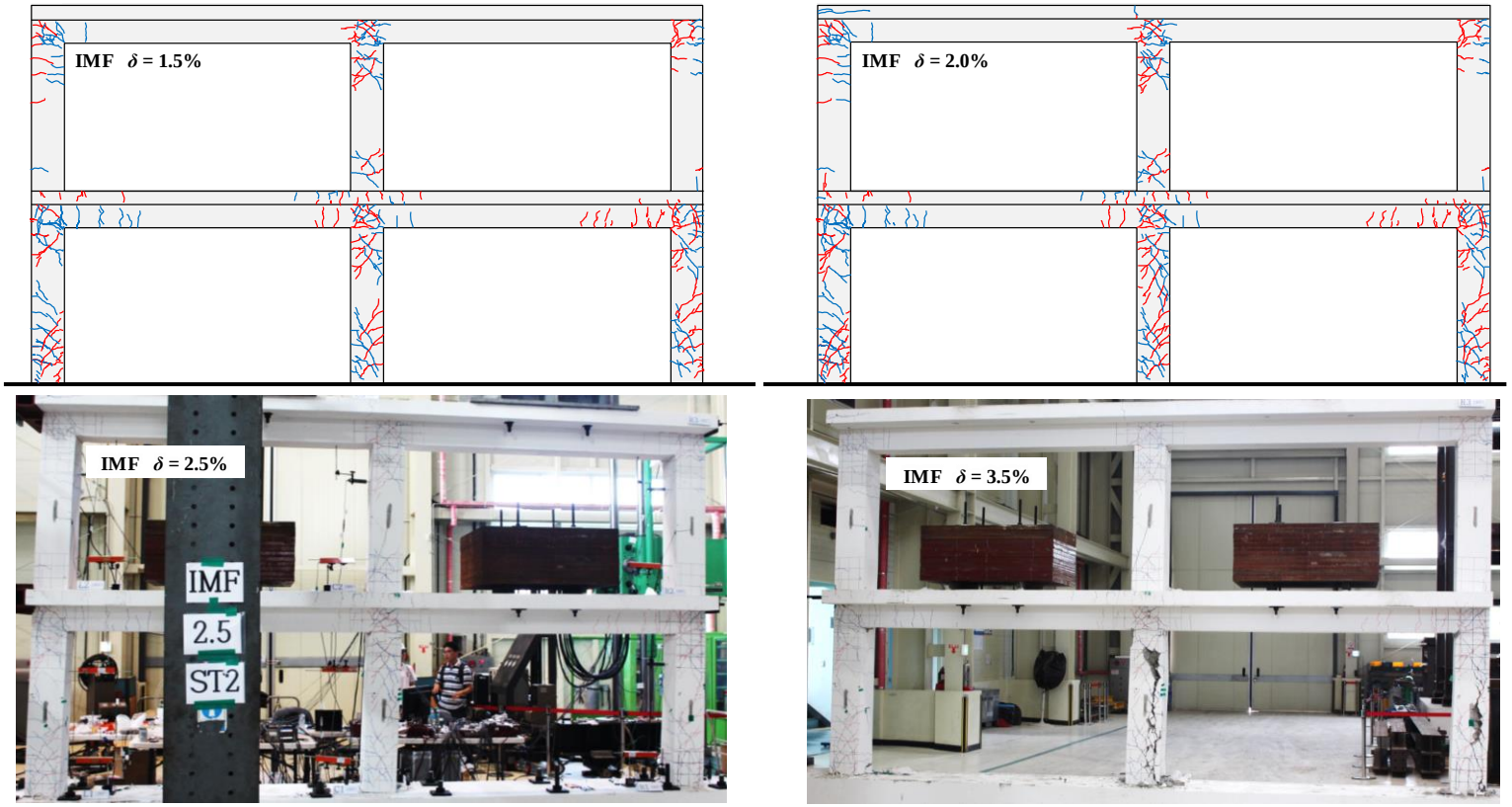

Figure 6-36 Failure sequence and crack patterns of specimen IMF according to drift ratio

For the thorough investigation of the final failure mode in specimen **IMF**, after the end of test, concrete cover was removed, and reinforcement details inside concrete was examined. Figure 6-37 shows the final failure mode and reinforcement details of first-story center and right columns after failure. The 135º hooks of the transverse bars used in the top and bottom of columns were anchored in the core concrete, and were not released even after spalling concrete cover off. On the other hand, the 90º hooks of the transverse bars used in the middle of columns were loosened. Such anchorage failure of transverse bars in column resulted in splitting failure of columns with severe diagonal shear cracking. Both the center and right columns in the first story showed similar final failure mode.

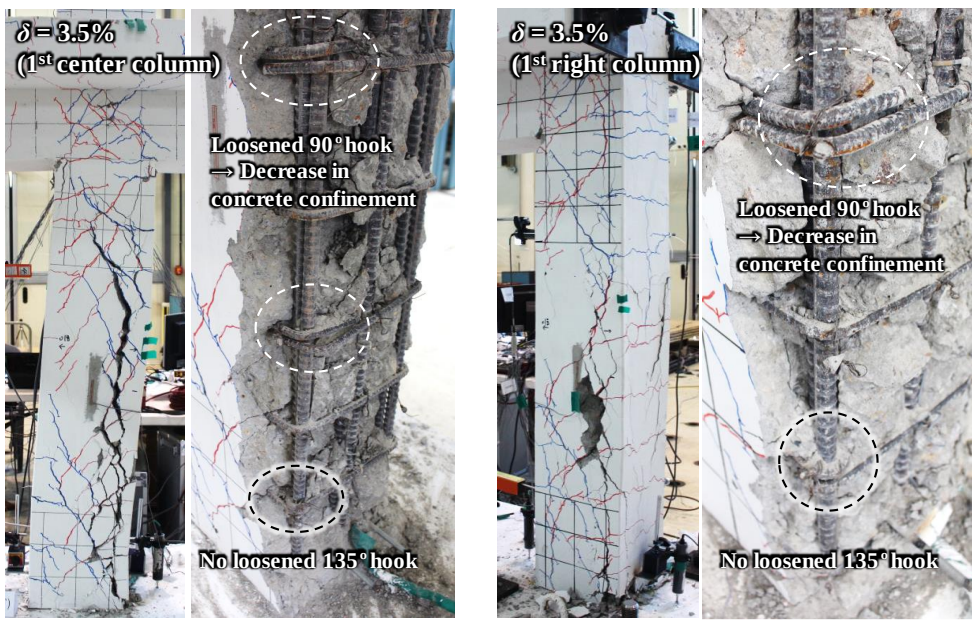

Figure 6-37 Final failure mode of specimen IMF

6.3.3.2 Alternative 1 moment frame (A1F)

The alternative 1 moment frame (**A1F**) was designed with the same target strength as the specimen **IMF**, and used alternative reinforcement details verified through member tests in Chapter 2 ~ Chapter 5. The lateral load and drift ratio relationship, and failure sequence with crack patterns are presented in Figure 6-38 and Figure 6-39, respectively.

The specimen **A1F** exceeded the yield strength of first-story center column P_{n1} at drift ratio of 0.75%, and reached the maximum load (367.0 kN and -346.4 kN) at drift ratio of 2.0%. During first cycle positive loading at drift ratio of 3.5%, the load carrying capacity was suddenly decreased to 80% of the maximum load, so the test was terminated. The test results are summarized in Table 6-10. The maximum load P_u (367.0 kN and -346.4 kN) was about 8% larger than the predicted load P_n (330.0 kN) obtained by the plastic mechanism. This indicates that even after the first-story center column yields (P_{n1}), it is sufficiently resistant to additional lateral loads by the plastic mechanism.

Since specimen **A1F** was designed with the same target strength as **IMF**, the maximum load was almost the same. On the other hand, the ductility of specimen **A1F** (δ_y = 0.84% and δ_u = 2.68%) was 3.21, which was about 27% lower than that of specimen **IMF**. Specimen **A1F** was somewhat inferior in terms of deformation capacity by simplifying and relaxing the reinforcement details (Hook detail and spacing of transverse reinforcement, etc.) compared to specimen **IMF**.

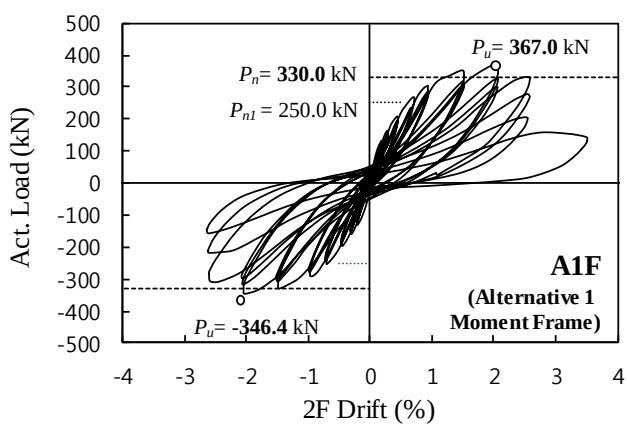

Figure 6-38 Lateral load and drift ratio relationship of specimen A1F

The failure sequence and crack patterns of specimen **A1F** was similar to specimen **IMF** up to drift ratio of 2.0%. At drift ratio of 0.5%, flexural cracks occurred at the top and bottom of the first-story columns and initial diagonal cracks developed at joints. At drift ratio of 0.75% when the first-story center column yielded, cracks were concentrated in the column plastic hinge zone as the flexural cracks developed into diagonal cracks, and diagonal cracks were observed in the joints. At drift ratio of 1.0% ~ 2.0%, cracks rapidly increased in the plastic hinge zone of the first-story columns and the second-story center column due to plastic mechanism of columns.

In the first cycle at drift ratio of 2.5%, splitting cracks were occurred along the lap splice region of the first-story center column. In the first-story left and right columns, the width of diagonal cracks increased significantly, thereby decreasing the load carrying capacity. Finally, at drift ratio of 3.5%, splitting failure occurred with severe diagonal shear cracking.

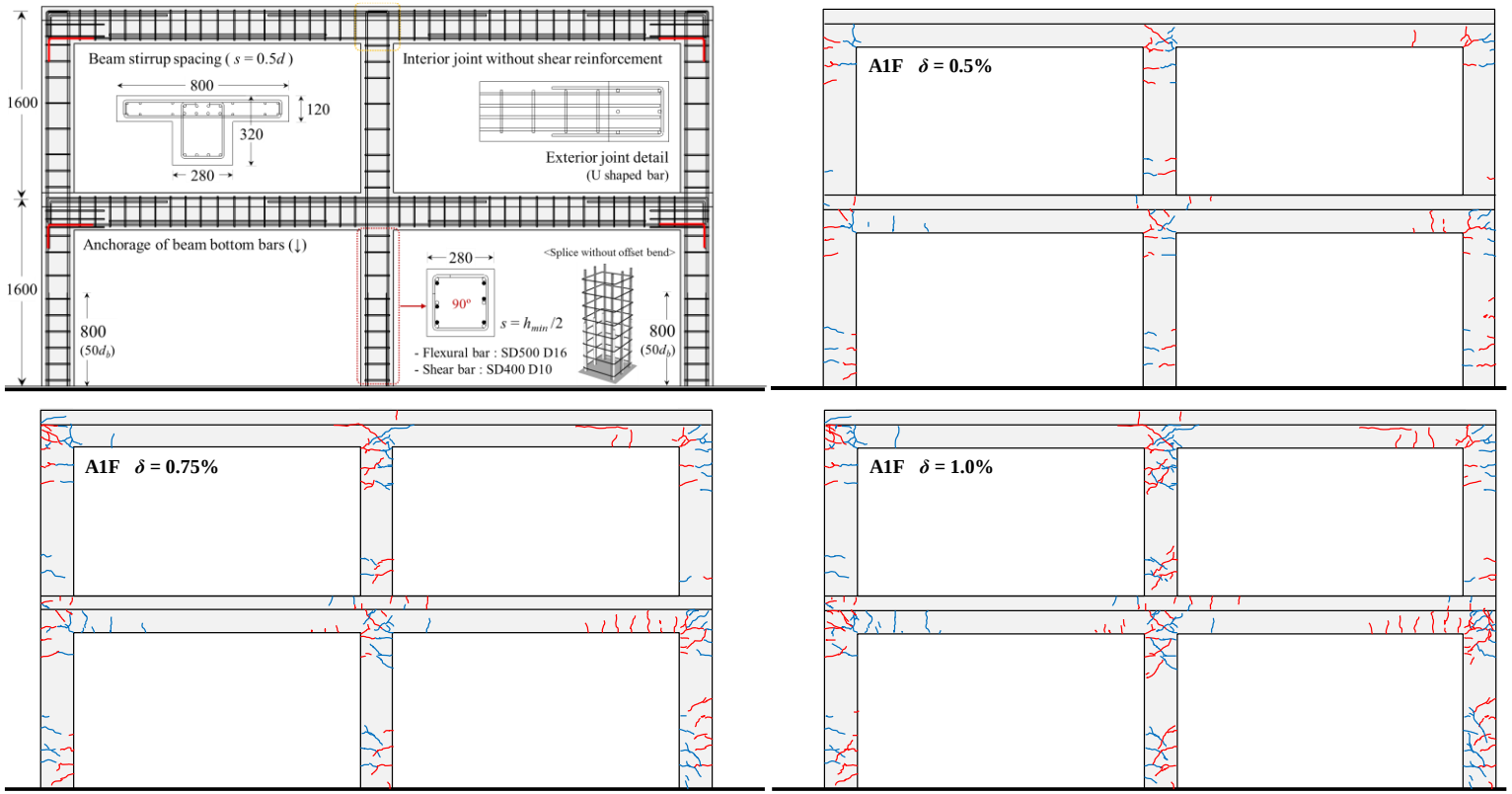

Figure 6-39 Failure sequence and crack patterns of specimen A1F according to drift ratio (Continued)

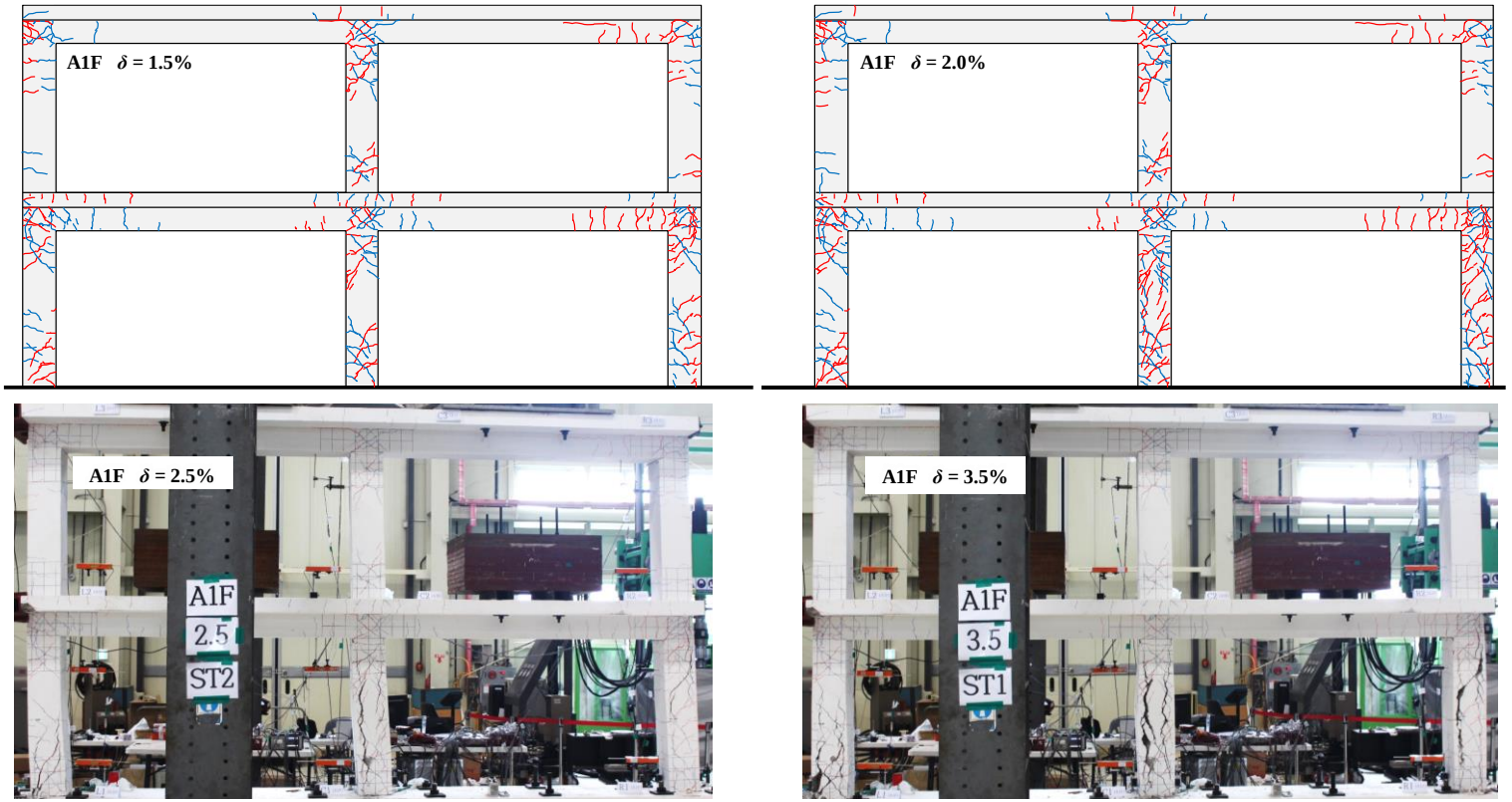

Figure 6-39 Failure sequence and crack patterns of specimen A1F according to drift ratio

In order to investigate the main cause of final failure mode, the reinforcement details inside concrete was examined by removing concrete cover after the end of test. Figure 6-40 shows the final failure mode and reinforcement details of first-story left, center, and right columns after failure. Because specimen **A1F** used transverse reinforcement with 90º hooks in the whole columns, the hooks were easily loosened after concrete cover spalling off. As a result, splitting cracks occurred along lap splice region of center column longitudinal bars in specimen **A1F**, and the crack width was enlarged as the drift ratio increased. In the right column of the first story, splitting failure occurred with severe diagonal shear cracking in the middle of the right column.

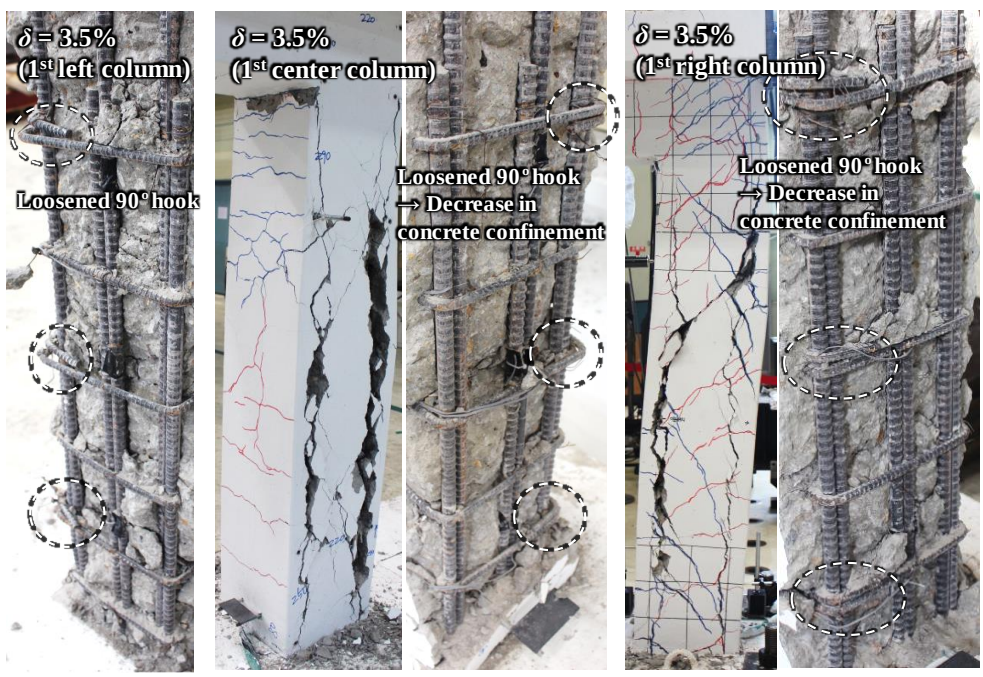

Figure 6-40 Final failure mode of specimen A1F

6.3.3.3 Alternative 2 moment frame (A2F)

The alternative 2 moment frame (**A2F**) was designed to increase the required shear forces applied in columns and joints by increasing the flexural reinforcement ratio of columns and beams by 40% over specimen **A1F**. The same alternative reinforcement details as specimen **A1F** were used. The lateral load and drift ratio relationship, and failure sequence with crack patterns are presented in Figure 6-41 and Figure 6-42, respectively.

The specimen **A2F** exceeded the yield strength of first-story center column P_{n1} at drift ratio of 0.75% ~ 1.0%, and reached the maximum load (390.1 kN and -362.2 kN) at drift ratio of 1.5%. During second cycle positive loading at drift ratio of 2.0%, the load carrying capacity was suddenly decreased to 80% of the maximum load, so the test was terminated. The test results are summarized in Table 6-10.

The maximum load P_u (390.1 kN and -362.2 kN) was about 5% smaller than the predicted load P_n (396.0 kN) obtained by the plastic mechanism. As the flexural reinforcement ratio increased, the maximum strength P_n increased by 20%. As a result, due to increased column shear demand, the load carrying capacity was suddenly decreased before attaining the predicted strength P_n, resulting in brittle failure. Though specimen **A2F** exceeded the yield strength of first-story center column (P_{n1}) and resisted additional lateral loads, but did not reach the target load (P_n) due to insufficient column shear capacity compared to the increased shear demand.

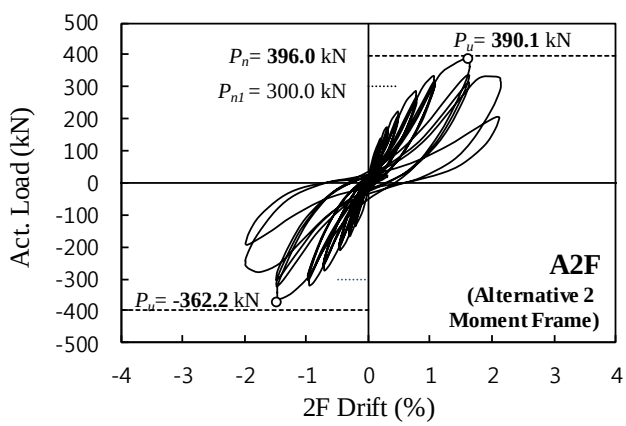

Figure 6-41 Lateral load and drift ratio relationship of specimen A2F

The ductility of specimen **A2F** (δ_y = 0.84% and δ_u = 1.96%) was 2.3, which was about 27% lower than that of specimen **A1F**. As brittle failure occurred after the maximum load, the ductility decreased significantly.

The failure sequence and crack patterns of specimen **A2F** was similar to those of specimens **IMF** and **A1F** up to drift ratio of 1.0%. At drift ratio of 0.5%, flexural cracks occurred at the top and bottom of the first-story columns and initial diagonal cracks developed at joints. At drift ratio of 0.75% when the first-story center column yielded, cracks were concentrated in the column plastic hinge zone as the flexural cracks developed into diagonal cracks, and diagonal cracks were observed in the joints.

At drift ratio of 1.5%, the failure sequence progressed rapidly due to the higher load (shear) applied to columns than the previous specimens. Figure 6-43 compares the crack patterns of the first-story center columns at drift ratio of 1.5% and 2.0%. In specimen **A2F**, splitting cracks occurred at drift ratio of 1.5%, and bond splitting failure occurred at drift ratio of 2.0%. On the other hand, splitting cracks occurred in the lap splice region of column longitudinal bars at drift ratio of 2.0% for specimen **A1F** and 2.5% for specimen **IMF**. This is because specimen **A2F** has higher shear force demand at the same drift ratio than the previous specimens.

To analyze the main cause of final failure mode, the concrete cover was removed after the end of test to examine the reinforcement details inside concrete. Figure 6-44 shows the final failure mode and reinforcement details of first-story left, center, and right columns after failure. Specimen **A2F** used transverse reinforcement with 90º hooks in the entire section of columns, resulting in loosening of 90º hooks after spalling concrete cover off. As a result, splitting cracks occurred along lap splice region of center column longitudinal bars at drift ratio of 1.5%, and the crack was widened as the drift ratio increased. The left and right columns on the first story were failed due to the severe diagonal shear cracks at the middle of the columns.

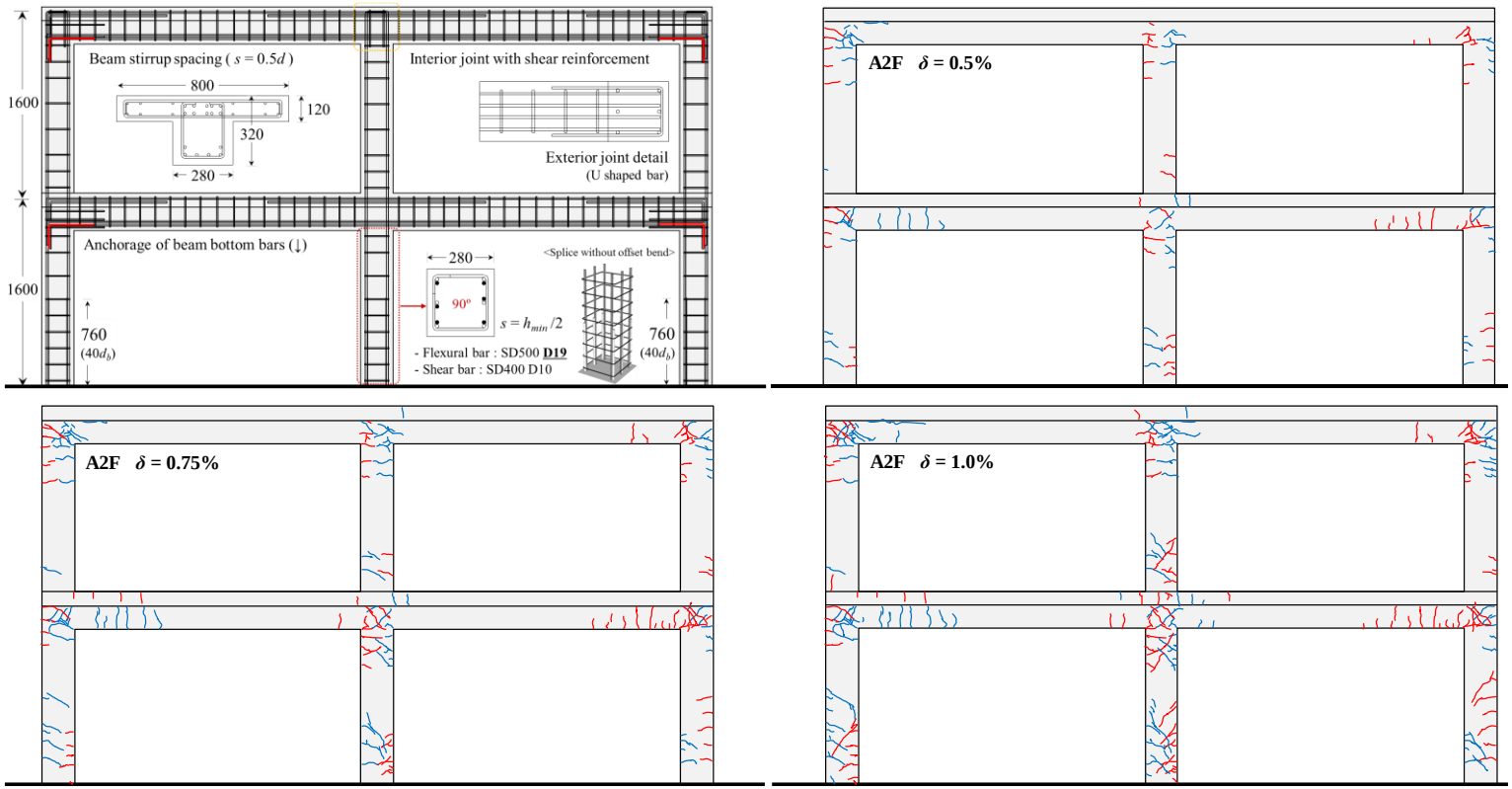

Figure 6-42 Failure sequence and crack patterns of specimen A2F according to drift ratio (Continued)

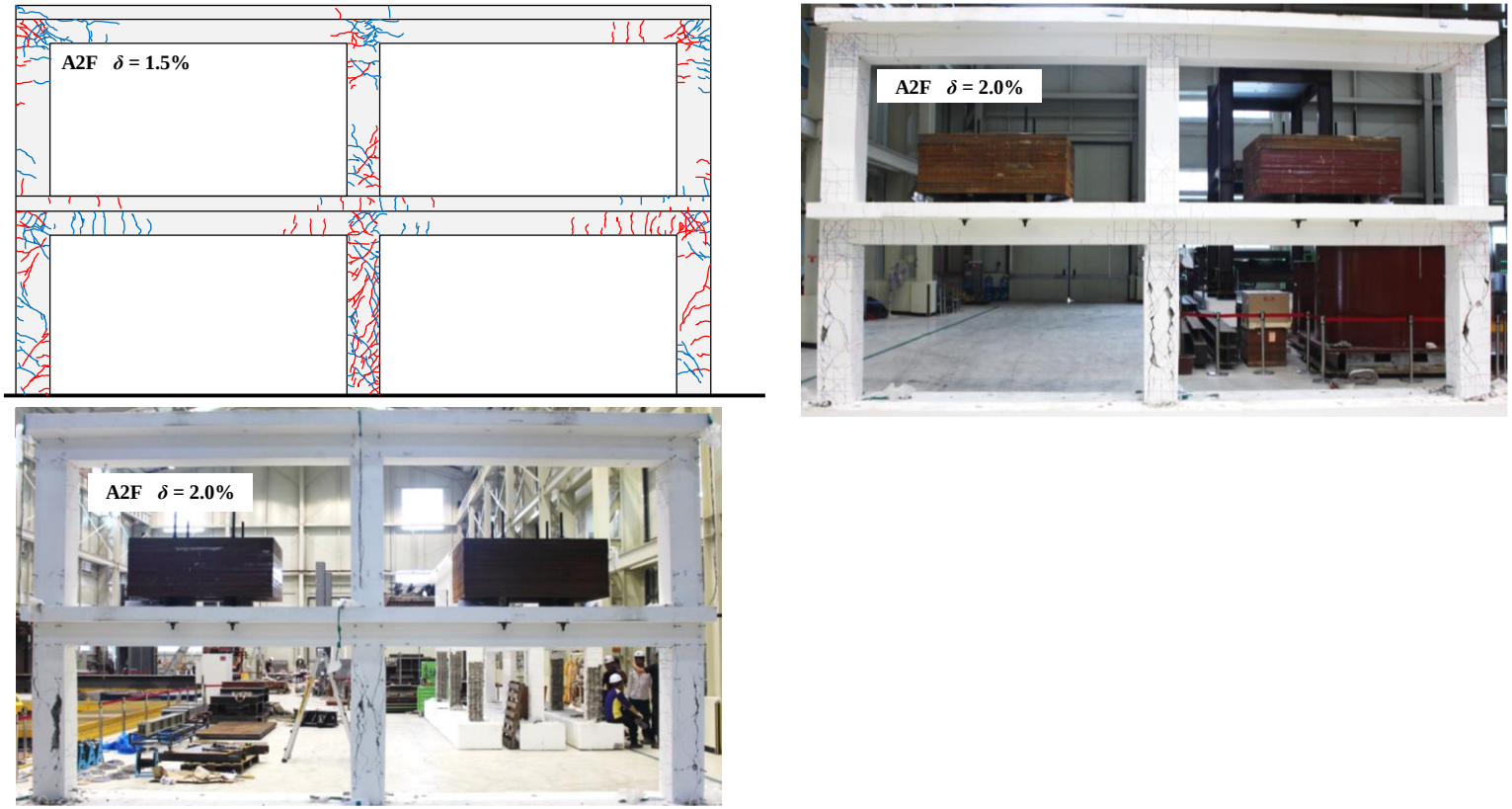

Figure 6-42 Failure sequence and crack patterns of specimen A2F according to drift ratio

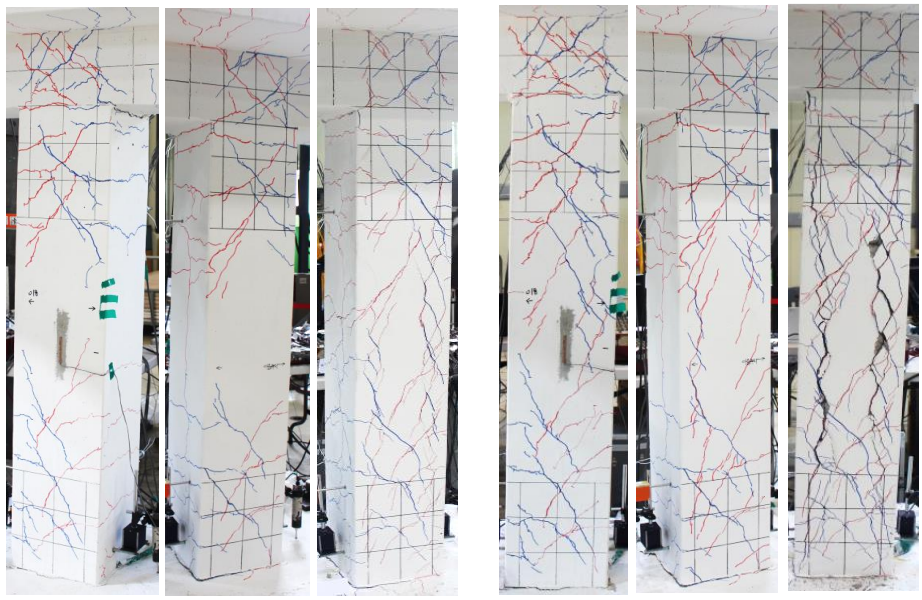

< IMF > < A1F > < A2F > < IMF > < A1F > < A2F >

(a) Drift ratio = 1.5% (b) Drift ratio = 2.0%

Figure 6-43 Crack patterns of 1st center columns at drift ratio of 1.5% and 2.0%

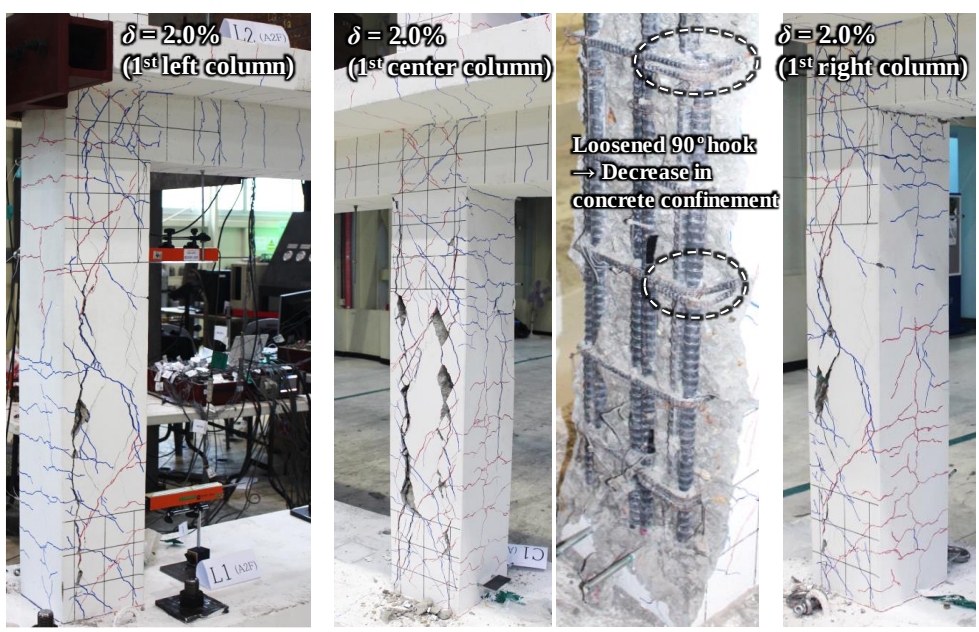

Figure 6-44 Final failure mode of specimen A2F

6.3.3.4 Wall and Moment frame (WF)

The specimen Wall and moment frame (**WF**) was designed to secure the lateral load-resisting performance only with shear wall and gravity load with moment frame. The lateral load and drift ratio relationship, and failure sequence with crack patterns are presented in Figure 6-45 and Figure 6-46, respectively.

The specimen **WF** exceeded the yield strength of first-story center wall P_{n1} (343.0 kN) at drift ratio of 0.5% ~ 0.75%, and reached the maximum load (471.5 kN and -440.8 kN) at drift ratio of 1.0%. During second cycle negative loading at drift ratio of 1.5%, the load carrying capacity was suddenly decreased, so the test was terminated. The test results are summarized in Table 6-10. The maximum load P_u (471.5 kN and -440.8 kN) was 69% of the predicted load P_n (660.0 kN) obtained by the plastic mechanism. As unexpected failure (horizontal shear failure) occurred at the upper part of the second-story shear wall, specimen **WF** did not resist additional lateral loads by the plastic mechanism.

The ductility of specimen **WF** (δ_y = 0.41% and δ_u = 1.55%) was 3.83, which was 19% and 64% larger than that of specimens **A1F** and **A2F**, respectively. The ductility of specimen **WF** was larger than that of other specimens because the ultimate drift ratio δ_u was small, but the yield drift ratio δ_y was less than half of other specimens due to high initial stiffness.

The specimen **WF** showed completely different crack patterns and failure mode from the previous specimens. At the drift ratio of 0.25%, the diagonal cracks occurred in the lower part of the first-story shear wall; on the other hand, cracks were hardly occurred in columns. This is because the shear wall resisted most of the lateral loads. At drift ratio of 0.35% ~ 0.5%, the diagonal shear cracks were progressed to the upper part of the first-story shear wall, and the horizontal shear cracks were initiated in the upper part of the second-story shear wall.

At drift ratio of 0.75% when the applied load exceeded P_{n1}, the compressive concrete crushing in the first-story shear wall began to occur, and the diagonal shear cracks rapidly increased in the second-story shear wall. As the flexural yielding of the first-story shear wall occurred, the flexural cracks in the first and second-story shear wall progressed greatly, and the diagonal shear cracks developed in the exterior

joints.

At drift ratio of 1.0% when the maximum load was reached, severe cracks were concentrated on the upper part of the two-story shear wall. The horizontal shear crack in the upper part of the second-story shear wall widened with diagonal shear cracks. Finally, the load carrying capacity decreased rapidly due to horizontal sliding failure with severe horizontal cracks at drift ratio of 1.5%. Figure 6-47 and Figure 6-48 show the failure sequences of the second-story and first-story shear walls according to drift ratio.

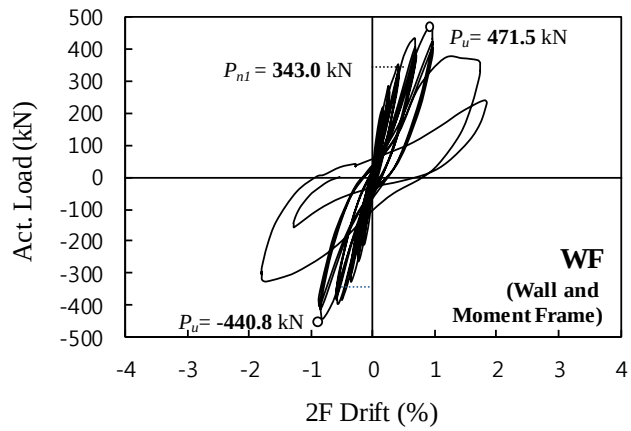

Figure 6-45 Lateral load and drift ratio relationship of specimen WF

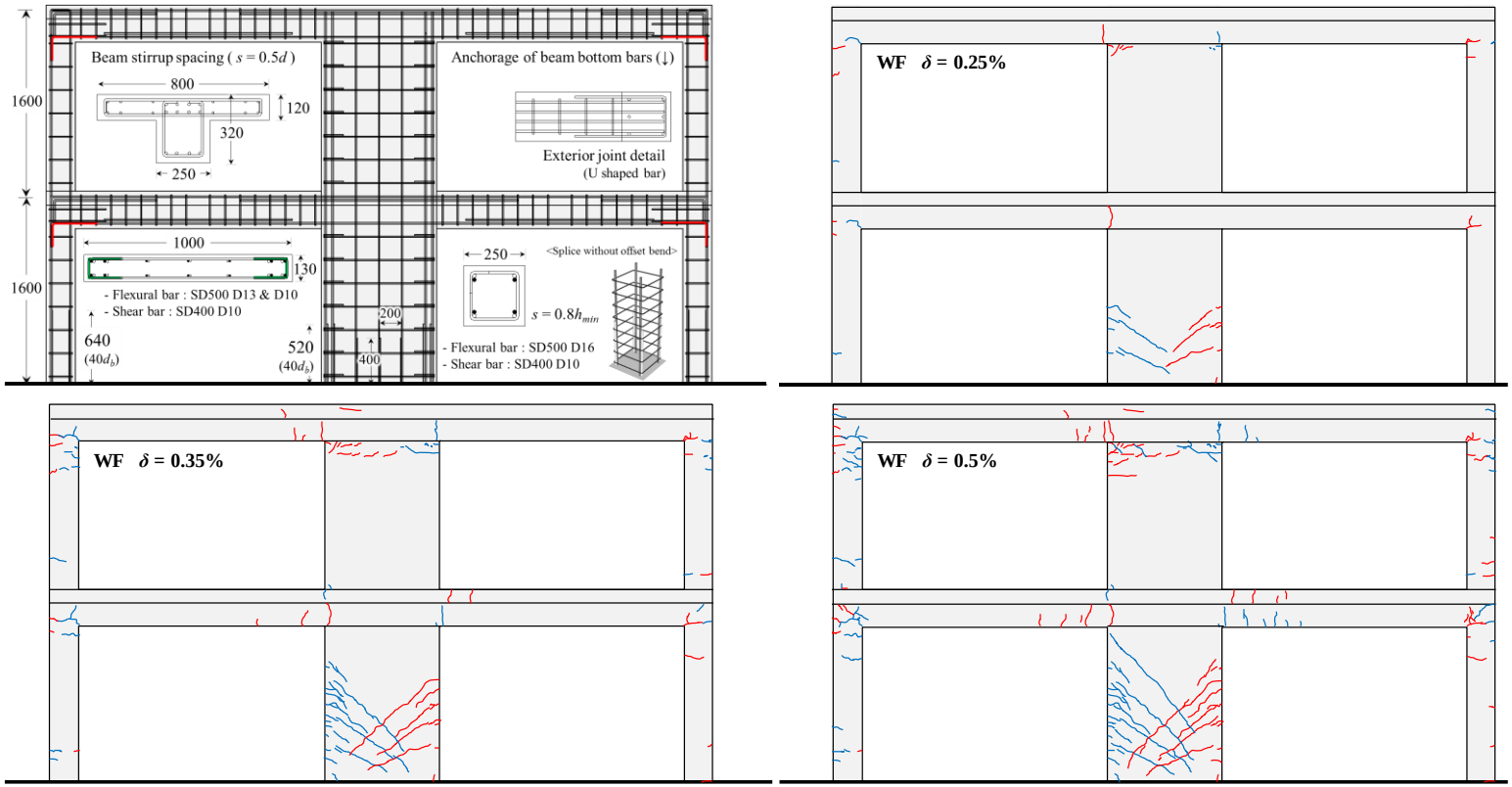

Figure 6-46 Failure sequence and crack patterns of specimen WF according to drift ratio (Continued)

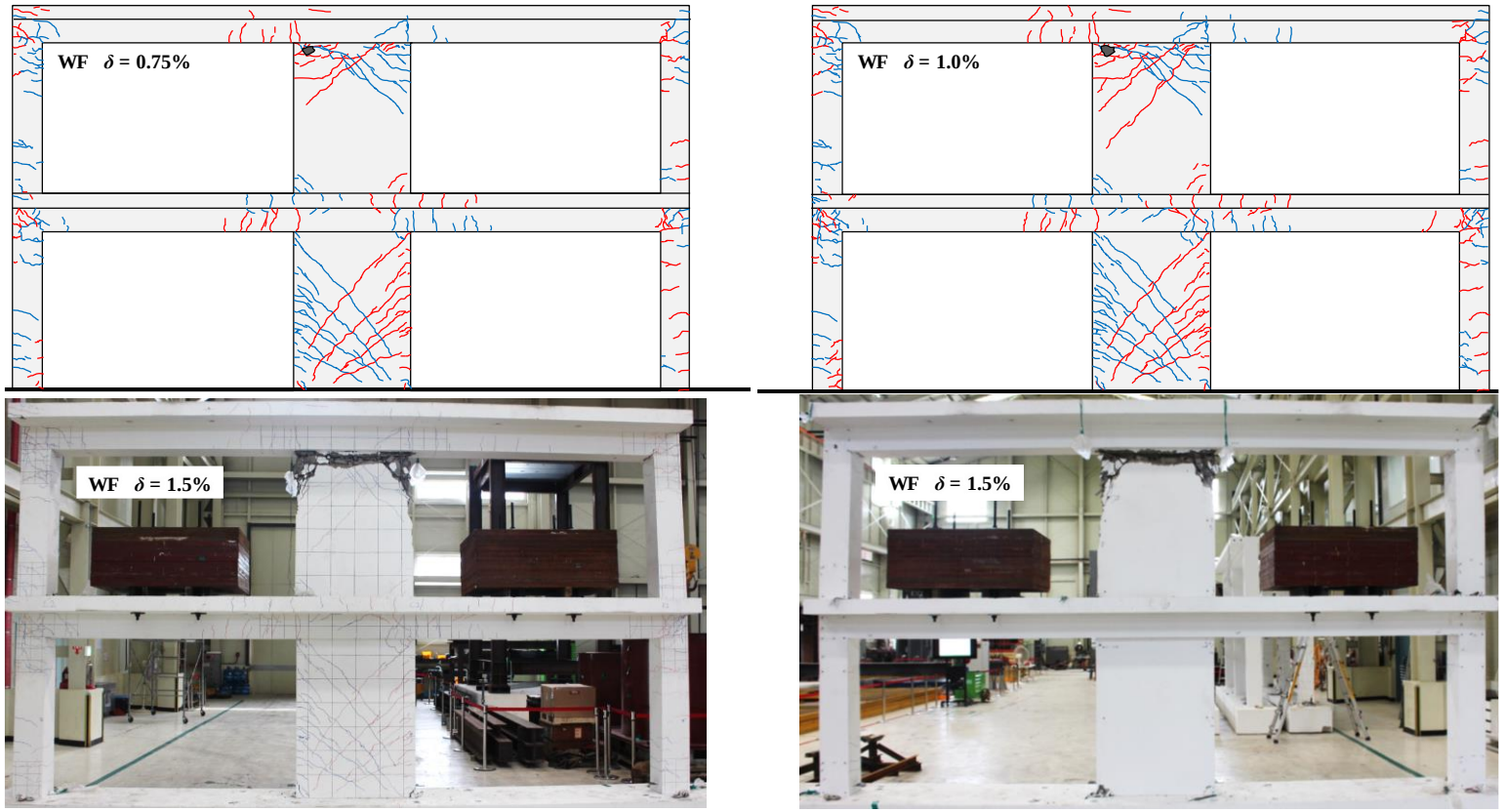

Figure 6-46 Failure sequence and crack patterns of specimen WF according to drift ratio

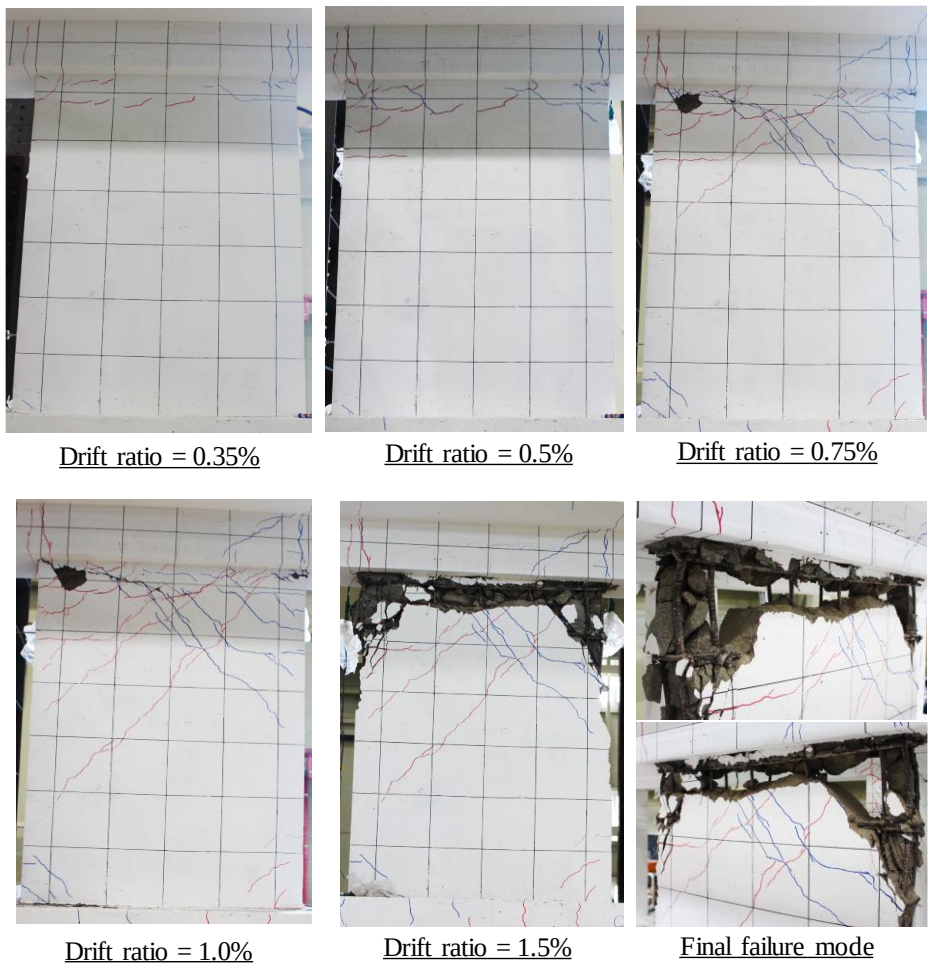

Figure 6-47 Failure sequence of 2nd story shear wall according to drift ratio

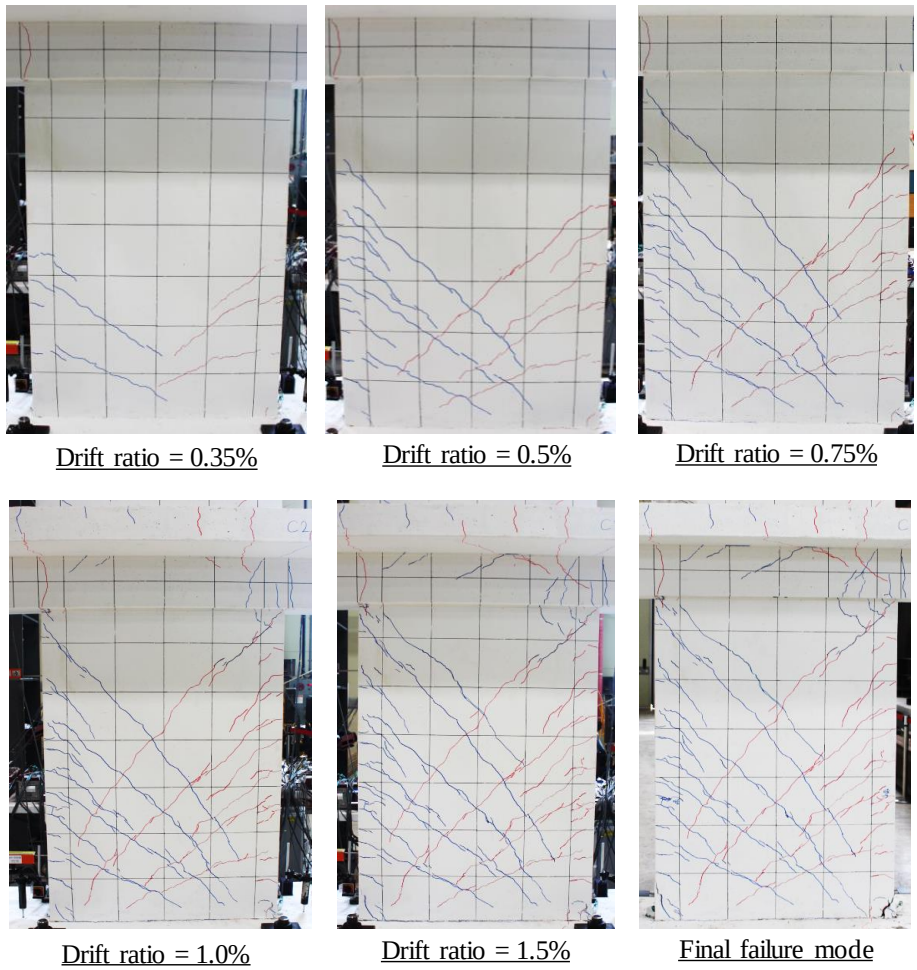

Figure 6-48 Failure sequence of 1st story shear wall according to drift ratio

6.4 Test Analysis

6.4.1 Comparison on load - drift ratio envelope curves

Figure 6-49 shows the envelope curves for each specimen in order to compare the load and drift ratio relationship. The envelope curve is a multiple straight line connecting maximum loads of first cycles at each drift ratio according to ACI 374.1-05. The test specimens **IMF**, **A1F**, **A2F**, and **WF** are denoted with circles, squares, triangles, and diamonds, respectively.

The initial stiffness of the specimens was greatly influenced by structural systems. Specimen **WF** using shear wall showed initial stiffness two times larger than other frame specimens. The initial stiffness was 42.5 kN/mm for specimen **WF** and 20.64 ~ 21.03 kN/mm for other frame specimens. The frame specimens (**IMF**, **A1F**, and **A2F**) showed similar stiffness up to drift ratio of 0.5%. After drift ratio of 0.5%, the specimen **A2F** showed highest stiffness among the frame specimens because of higher column and beam flexural reinforcement ratio.

The maximum strength of the specimens was also affected by structural systems. Specimen **WF** with shear wall showed 21 ~ 33% greater strength than other specimens because of high stiffness of the shear wall. However, the load did not increase anymore because horizontal sliding failure occurred at drift ratio of 1.0%. Among the framed specimens, specimen **A2F** with higher column and beam longitudinal reinforcement ratio showed the largest load which was 5% and 10% greater strength than specimens **IMF** and **A1F**, respectively. However, the specimen **A2F** did not show a significant increase in maximum load considering the increased column and beam longitudinal reinforcement ratio by 40%. This is because the load carrying capacity was suddenly decreased due to splitting failure with severe diagonal shear cracks in columns at drift ratio of 1.5%.

Though specimen **A1F** showed 4% higher load than specimen **IMF**, the deformation capacity decreased slightly compared to specimen **IMF** by decreasing rapidly the load capacity after drift ratio of 2.0%.

6.4.2 Comparison on cumulative energy dissipation capacity

The energy dissipation capacity is the ability of a structure to absorb energy during cyclic loading, expressed as the area (E_D) enclosed by the load and displacement hysteresis curves as shown in Figure 6-50. The amount of energy dissipation during cyclic loading is an important factor to evaluate seismic performance of structures. Figure 6-50 shows cumulative energy dissipation capacity for each specimen. The test specimens **IMF**, **A1F**, **A2F**, and **WF** are denoted with circles, squares, triangles, and diamonds, respectively.

The cumulative energy dissipation capacity was affected by the maximum deformation capacity and load carrying capacity of test specimens. Specimen **IMF** with highest displacement ductility showed the highest energy dissipation capacity with the ultimate drift ratio of 3.71%. Specimen **A1F** showed the second highest energy dissipation capacity with the ultimate drift ratio of 2.68%. Specimen **A2F** showed a higher ultimate drift ratio than specimen **WF**, but two specimens showed the similar cumulative energy dissipation capacity due to the high stiffness and maximum strength of specimen **WF**.

Specimen **A1F** showed the energy dissipation capacity similar to specimen **IMF** up to drift ratio of 2.5%. This indicates that the structural performance differences between the reinforcement details in **IMF** and alternative details in **A1F** were not significant until the maximum load was reached (Drift ratio of 2.0 ~ 2.5%). The cumulative energy dissipation at drift ratio of 2.5% was 145 kN·m for specimen **IMF**, and 124.7 kN·m for specimen **A1F**. On the other hand, a large difference in energy dissipation capacity of specimen **A2F** was shown with a sudden decrease in strength at drift ratio of 2.0% though similar energy dissipation to other specimens was shown up to drift ratio of 1.5%. Up to drift ratio of 1.0% ~ 1.5%, specimen **WF** with shear wall showed higher energy dissipation capacity than specimen **IMF** because of high stiffness and high strength. However, the expected horizontal shear failure occurred at drift ratio of 1.5%, resulting in the lowest cumulative energy dissipation capacity.

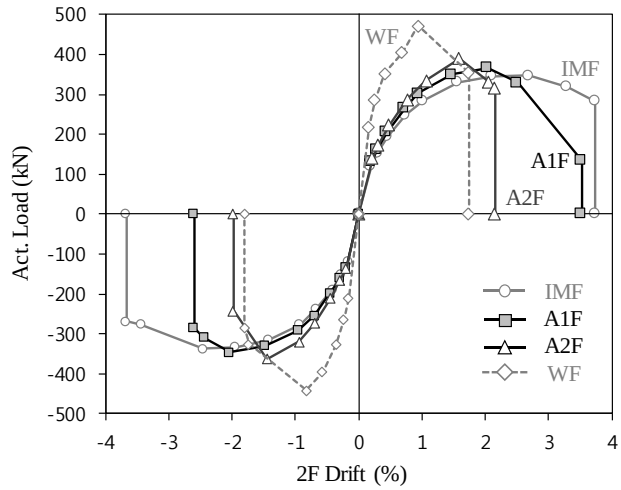

Figure 6-49 Comparison on load – drift ratio envelope curves

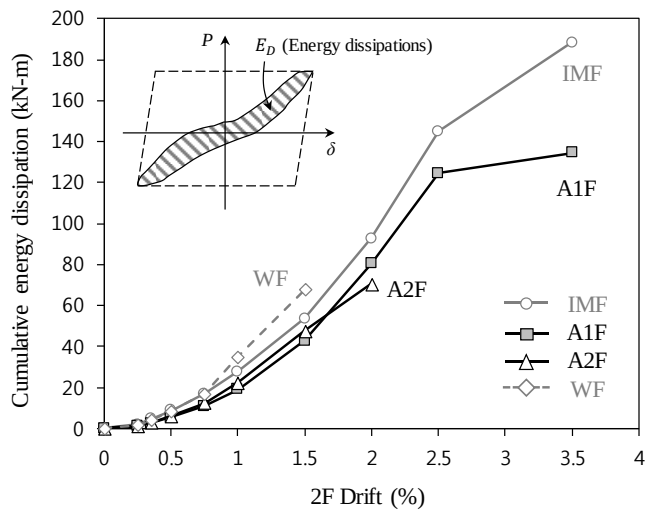

Figure 6-50 Comparison on cumulative energy dissipation capacity

6.4.3 Strains of column reinforcement

Most major cracks were concentrated on the columns compared with beams and joints in the frame specimens, which indicates typical weak-column and strong-beam behavior. In particular, vertical splitting cracks and diagonal shear cracks were concentrated on the first-story columns with the soft story behavior. Further, the behavior of each member (columns, beams, joints etc.) in the frames was important because the tests were performed in the system level rather than the member level. Thus, strains measured in each column were mainly analyzed to evaluate seismic performance of the frames.

The strains measured from longitudinal bars in plastic hinge regions of first-story and second-story columns, transverse bars of first-story columns, and lap splice regions of first-story columns were examined.

6.4.3.1 Strains of column longitudinal bars according to column position

The test results of the frame specimens (**IMF**, **A1F**, and **A2F**) showed that the bond failure occurred in lap splice regions of the first-story columns after the nominal strength (P_n) according to plastic mechanism of columns has been reached. Such plastic mechanism of columns in the frame specimens was verified by measured strains from longitudinal bars in plastic hinge regions of first-story and second-story columns as shown in Figure 6-51 ~ Figure 6-54. The strains measured at all the plastic hinge regions (12 locations) of columns were shown at each location. The horizontal axis of the graphs indicates the drift ratio measured at the second-story slab, and the vertical axis indicates the measured strains of column longitudinal bars. The black dotted line and the grey solid line represents the strains measured at the left and right column longitudinal bars in the plastic hinge zones. For comparison, the yield strain of the bars is indicated by the horizontal dashed line and the yield point is marked with a white circle. The load - drift ratio envelop curves of each specimen (for positive load directions only) are also shown in the Figures.

Specimens **IMF** and **A1F**, in which the maximum loads exceeded P_n according to plastic mechanism, yielded the first-story columns and the second-story center column as shown in Figure 6-51 and Figure 6-52. The sequence of plastic hinge mechanism in columns was similar to the result of MIDAS Gen in Figure 6-17: The bottom of the first-story(1^{st}) center column → the bottom of the 1^{st} left and right columns → the top of the 1^{st} center column → the top of the second-story(2^{nd}) center column → the top of the 1^{st} left and right columns → the bottom of the 2^{nd} center column. Though specimens **IMF** and **A1F** showed a slight difference in the sequence of plastic hinge mechanism, the overall plastic mechanism was similar.

On the other hand, specimen **A2F**, which failed before reaching P_n according to plastic mechanism, yielded only the bottom of the 1^{st} columns as shown in Figure 6-53. This is because the load carrying capacity was decreased due to the anchorage failure and the diagonal shear failure before the load by plastic hinge mechanism of columns was smoothly transmitted. The additional shear reinforcement can result in increasing both load and deformation capacities.

Specimen **WF**, in which horizontal shear failure occurred at the top of the 2^{nd} shear wall, yielded the bottom of the 1^{st} shear wall and 1^{st} left/right columns because the specimen was unexpectedly failed at drift ratio of 1.0%. Dowel bars to prevent horizontal shear failure at the top of the 2^{nd} shear wall can provide higher load and deformation capacities than the current test result.

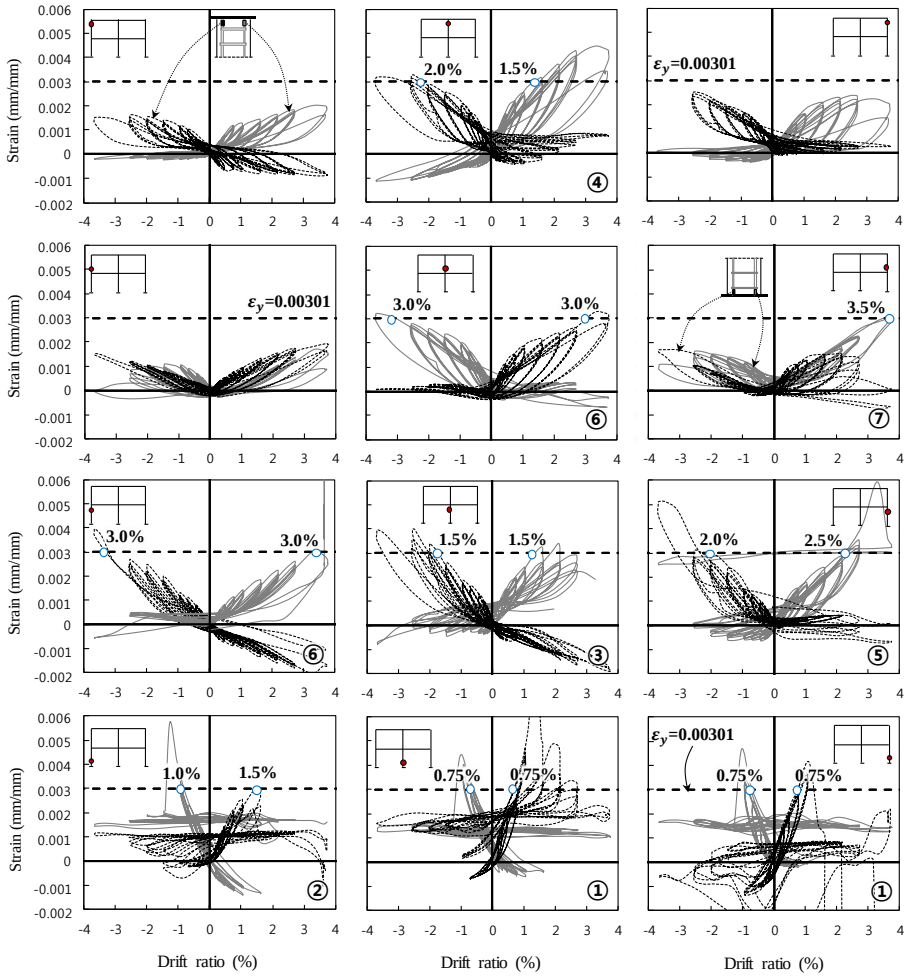

(a) Measured strains in column longitudinal bars

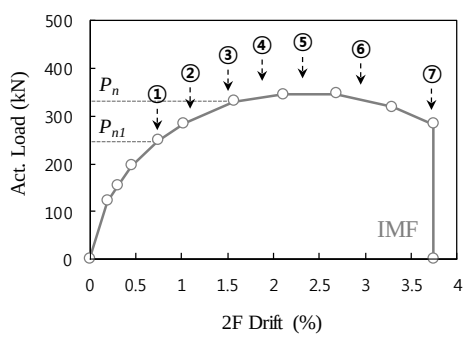

(b) Envelope curve for load and drift ratio relations

Figure 6-51 Strains of column longitudinal bars in specimen IMF

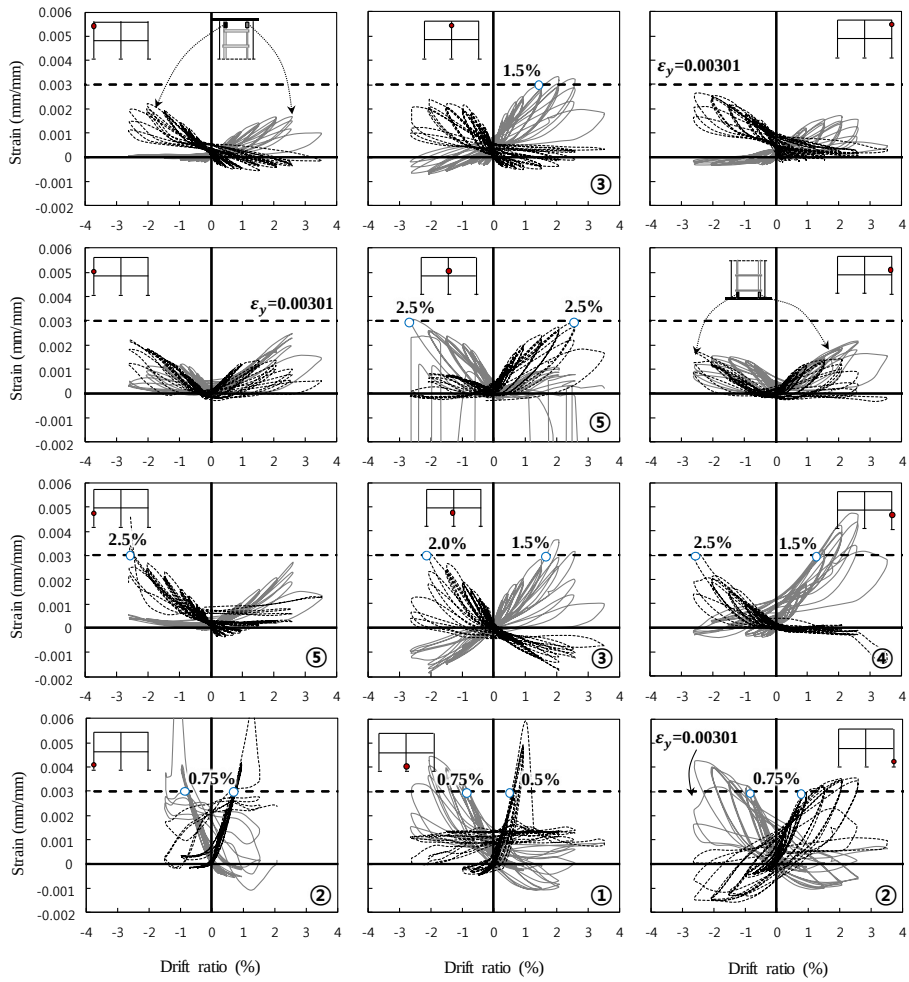

(a) Measured strains in column longitudinal bars

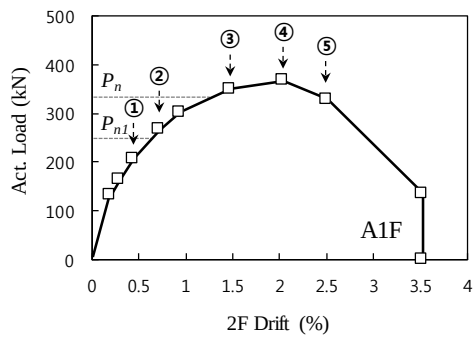

(b) Envelope curve for load and drift ratio relations

Figure 6-52 Strains of column longitudinal bars in specimen A1F

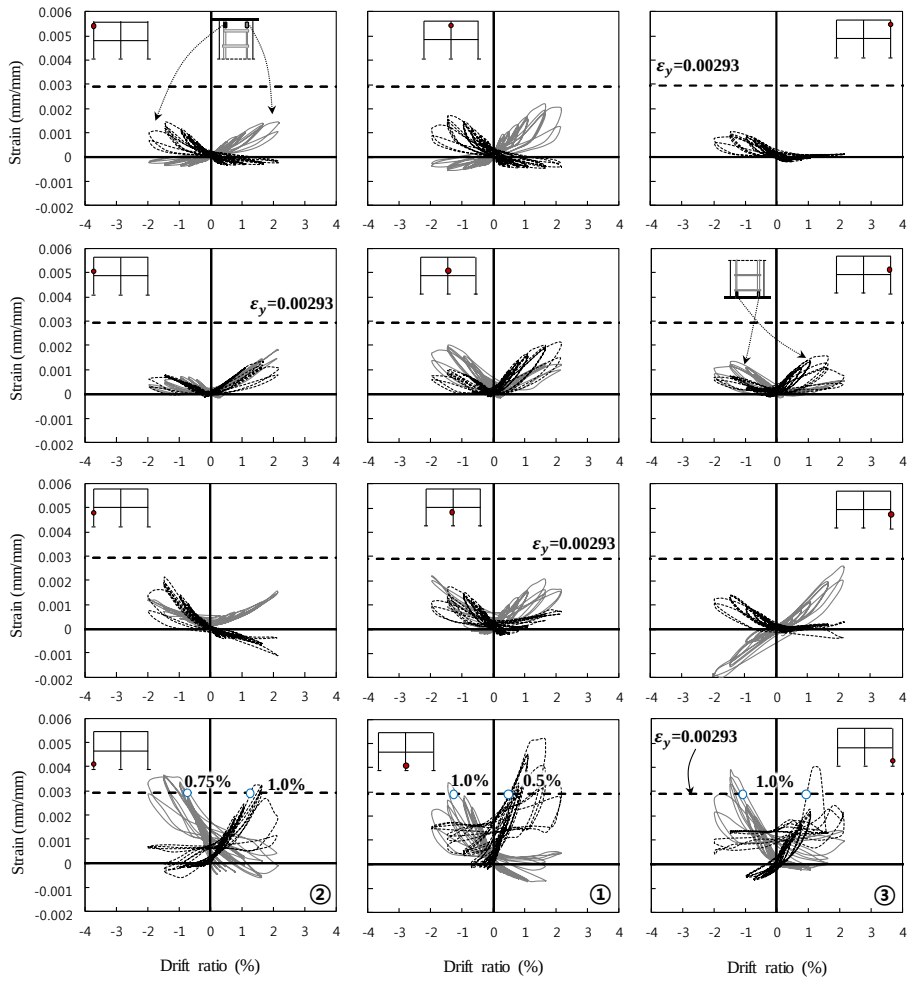

(a) Measured strains in column longitudinal bars

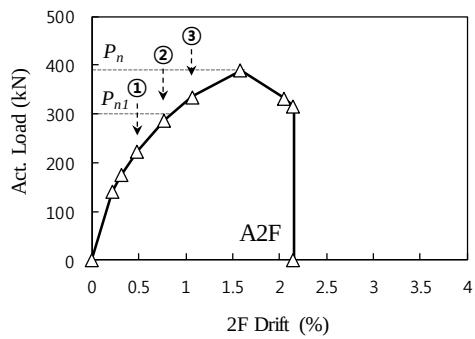

(b) Envelope curve for load and drift ratio relations

Figure 6-53 Strains of column longitudinal bars in specimen A2F

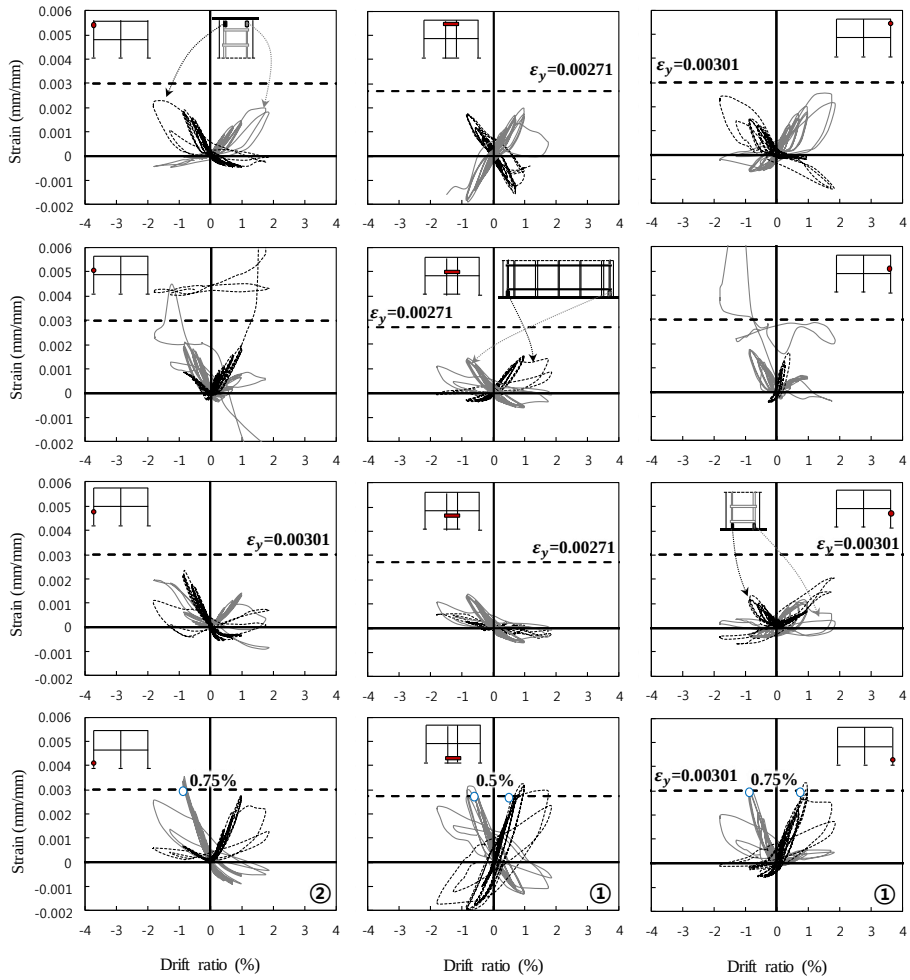

(a) Measured strains in column longitudinal bars

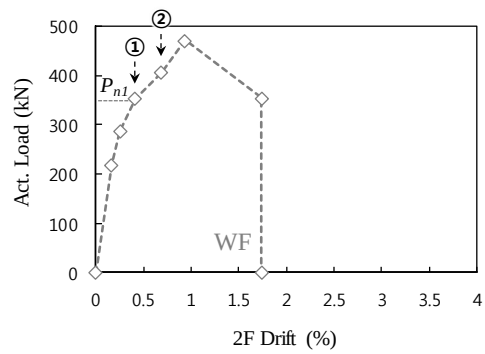

(b) Envelope curve for load and drift ratio relations

Figure 6-54 Strains of column longitudinal bars in specimen WF

6.4.3.2 Strains of column transverse reinforcing bars according to column position

In the frame specimens, the major failure modes were bond failure and diagonal shear failure in the first-story columns. Since such failure modes were significantly influenced by transverse bars of columns, the strains measured from transverse bars in plastic hinge zones of the first-story columns were compared in Figure 6-55. The strains at the second transverse bars from the top and bottom of columns were used considering a 45º angle of a diagonal shear crack. The horizontal axis of the graphs indicates the drift ratio measured at the second-story slab, and the vertical axis indicates the measured strain of column transverse bars. For comparison, the yield strain of the bars is indicated by the horizontal dashed line.

The effect on hook details of column transverse bars was investigated by the strain values measured at the bottom of the 1st center columns in specimens **IMF** and **A1F**. Specimens **IMF** and **A1F** used transverse bars with 135º hook and 90º hook in plastic hinge regions, respectively. As a result of strains, the 135º hook was not loosened until drift ratio of 3.5%, but the 90º hook was loosened at drift ratio of 2.0%. In specimen **A1F**, the rapid decrease of load capacity at drift ratio of 2.0% was attributed to reduced concrete confinement effect of transverse bars due to loosening the 90º hook.

The strain values at 1st center columns were larger than that at 1st left and right columns. This is because larger shear forces applied on the center columns during cyclic loading. In additions, not only the vertical splitting cracks but also severe diagonal cracks developed at 1st center columns, thereby increasing tensile stresses applied in transverse bars. On the other hand, the strains at the left and right columns were relatively small, which was influenced not only by the applied shear forces but also by final failure modes. In the final failure modes of each specimen, the diagonal cracks were located at the middle of left and right columns, not in plastic hinge zones.

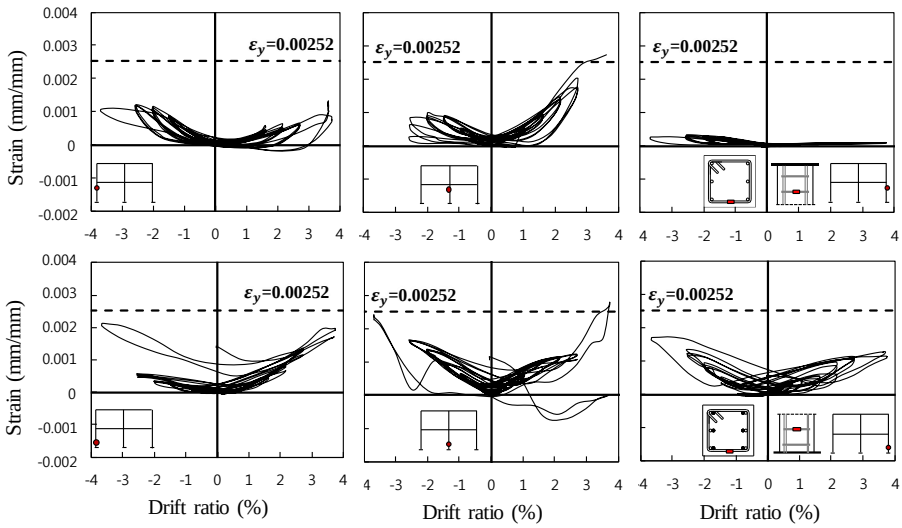

(a) Specimen **IMF**

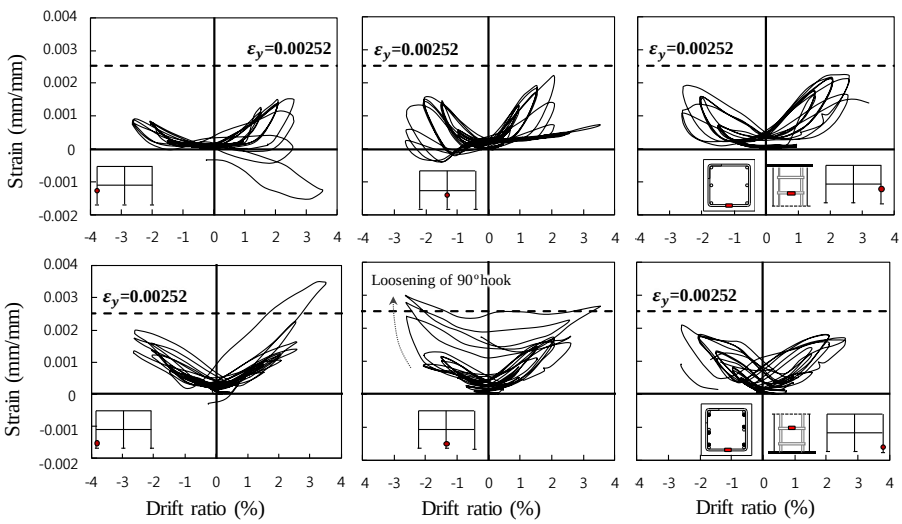

(b) Specimen **A1F**

Figure 6-55 Strains of column transverse bars at plastic hinge zone in a first story **(**Continued**)**

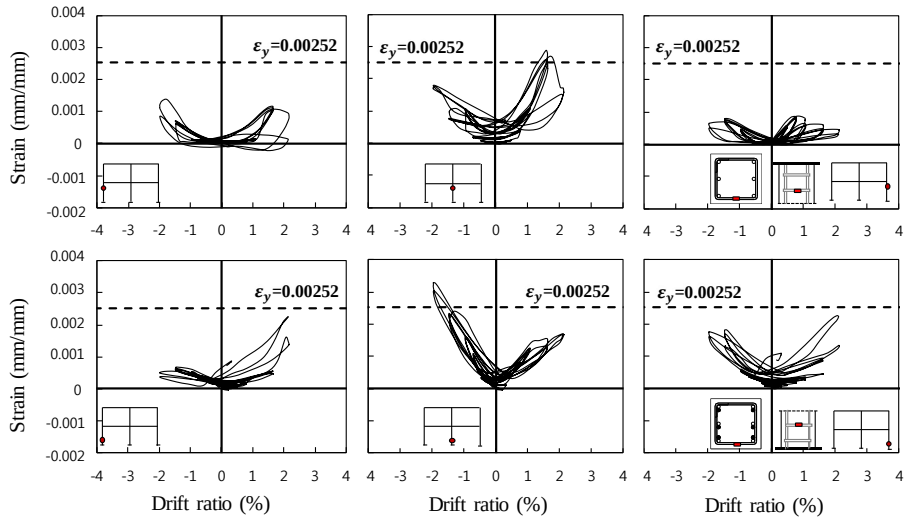

(c) Specimen **A2F**

Figure 6-55 Strains of column transverse bars at plastic hinge zone in a first story

6.4.3.3 Strains of column longitudinal bars in lap splice zones

The major failure mode of the 1st columns is the bond failure with severe vertical splitting cracks along lap splice regions of the columns when specimens **IMF**, **A1F**, and **A2F** reached the ultimate drift ratio of 3.5%, 2.5%, and 2.0%, respectively. In order to investigate such bond failure, strain distributions measured from the 1st center column longitudinal bars in lap splice zones were plotted in Figure 6-56. In each specimen, the strains of the top and bottom splice bars were plotted in the right and left figures, respectively. The horizontal and vertical axes, respectively, denote the bar strains and the height from the base where the strains were measured. The bar strains were the maximum values that each spliced bar underwent during the load cycles repeated at each lateral drift ratio. For clarity, the bar strains corresponding to δ = 0.25%, 0.5%, 1.0%, 1.5%, 2.0%, and 3.5% are denoted with bars, crosses, triangles, diamonds, circles, and squares, respectively.

The strains of the bottom splice bars increased as the strains were closer to the pedestal, while the strains of the top splice bars did not vary significantly along the lap splice region. Further, the maximum strains in the splice region were much greater in the bottom splice bars than in the top splice bars. The strain measurements indicate that the tensile stress of the bottom splice bars was transferred to the top splice bars through bond between bars and surrounded concrete. As the variation of tensile stress in the bottom splice bars of the splice region was large, the larger bond demand was required in the bottom bars.

The strains of the bottom splice bars extended from pedestals exceeded the yield strain ε_y before and after drift ratio of 1.0%. The strains increased constantly up to drift ratio of 1.0%; however, after drift ratio of 1.0%, the strains rather decreased or increased slightly. This indicates that the load transfers at the splice regions of the 1st center columns decreased sharply after reaching yield strength P_{n1} of 1st center columns at drift ratio of 1.0%. After the plastic hinge of the 1st center columns occurred, the load and deformation were concentrated on plastic hinge zones of the 1st left and right columns.

There was no significant difference according to lap splice details of column longitudinal bars. Specimen **IMF** used the top offset bar splice detail, and specimens **A1F** and **A2F** used the splice without offset bend as shown in Figure 6-56. Since the

location of the bottom splice bars was the same in both splice details, the strain distributions along the splice regions was not significantly different. On the other hand, the top splice bars were located inside the concrete in specimen **IMF**, and adjacent to transverse bars in specimen **A1F** and **A2F**. Since such top splice bars did not exert large tensile stresses during column flexural stress transfer, they did not affect the behavior of specimens. However, in the case of both splice details (**IMF**, **A1F**, **A2F**), since the location of the bottom splice bars where the large column flexural stress was applied was adjacent to the cover concrete, the bond failure by vertical splitting cracks occurred along lap splice regions after spalling concrete cover off.

Using the strain distributions of the top and bottom splice bars in the 1st center columns, tensile stress distributions and moment gradient of column longitudinal bars were illustrated in Figure 6-57. Since the column moment by the lateral load decreased linearly from the bottom ($h = 0$) to the end of the splice zone ($h = l_s$), the corresponding flexural tensile stresses (sum of the top and bottom splice bar stresses) decreased to the end of the splice zone.

Figure 6-56 shows that the strains of the bottom splice bars and the corresponding stresses decreased sharply toward the end of the splice zone, and the stresses of the top splice bars were almost constant along the splice length. Based on such strain distribution pattern, the tensile stress distribution of column longitudinal bars can be presented as shown in Figure 6-57(b).

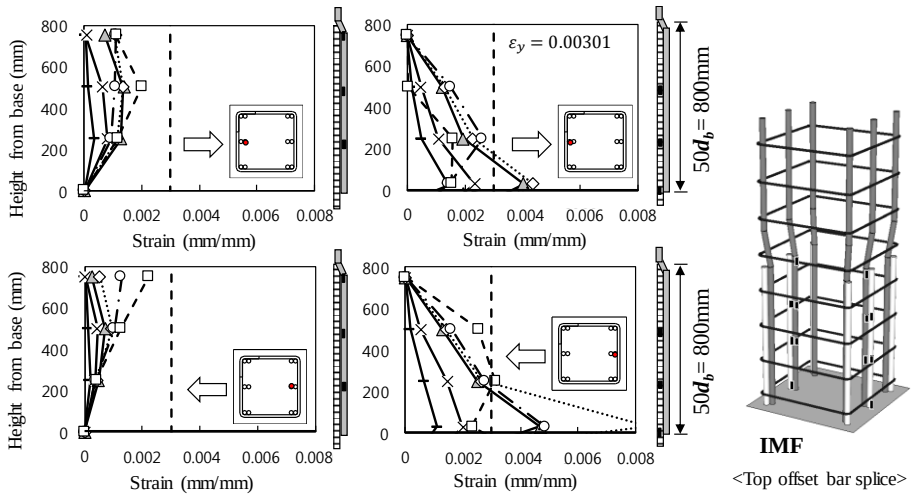

(a) Specimens **IMF**

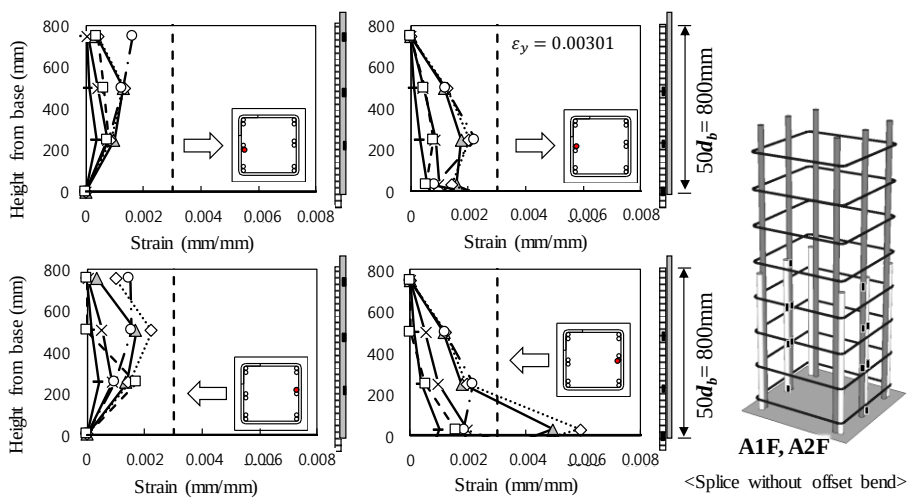

(b) Specimens **A1F**

Figure 6-56 Strain distributions of column longitudinal bars in lap splice zones (Continued)

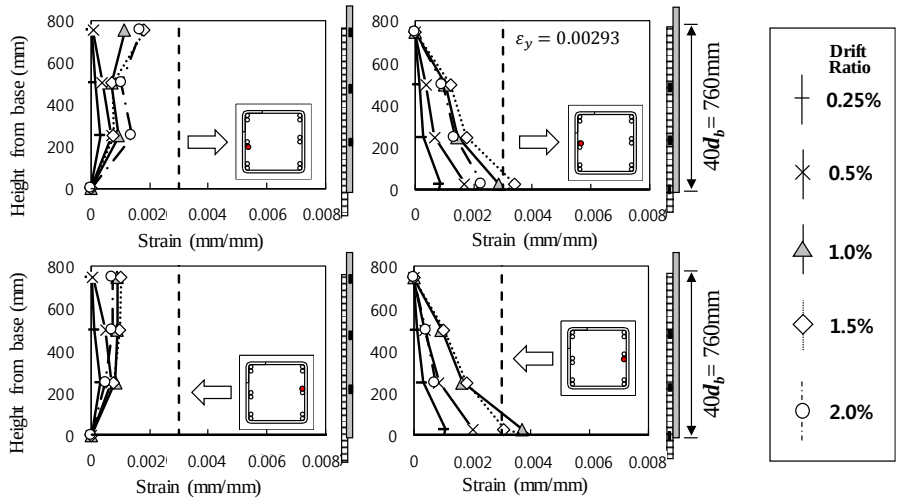

(c) Specimens **A2F**

Figure 6-56 Strain distributions of column longitudinal bars in lap splice zones

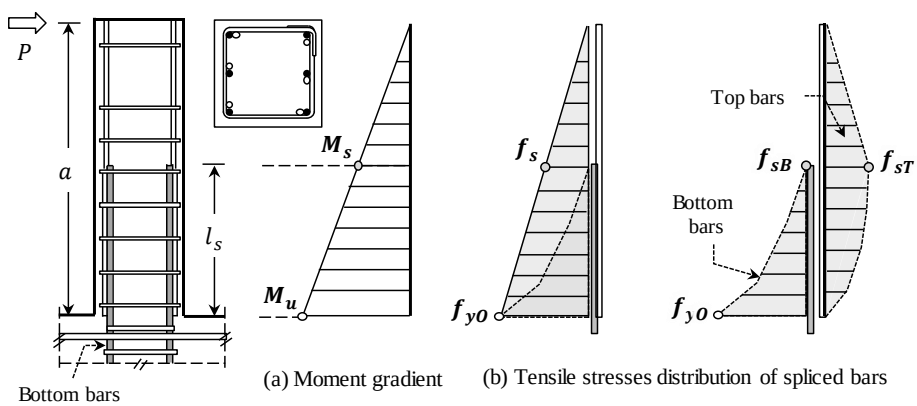

Figure 6-57 Moment gradient and tensile stress distribution of spliced bars

6.4.4 Strains of wall reinforcement

6.4.4.1 Strain distributions of wall vertical bars

The overall behavior of specimen **WF** was changed due to the shear wall located at the center of the specimen. The highest load was observed due to high initial stiffness of the shear wall, but unexpected failure occurred at drift ratio of 1.5% due to severe horizontal shear cracks at the upper part of the second-story shear wall.

In order to analyze the structural behavior of the wall, the strain profile of the first-story wall under negative loading direction was presented in Figure 6-58. The horizontal axis indicates the location of vertical bars in the 1st wall measuring the strains, and the vertical axis indicates the strain values. The strains are the maximum values measured in the points C, R2, and R1, and the minimum values in the points L1 and L2 at drift ratio of 0.25%, 0.35%, 0.75%, 1.0%, and 1.5%.

The strains at the outermost vertical bars (L1 and R1) were relatively smaller than those at the bars located 60 mm inside (L2 and R2) because of gauge damage by spalling concrete cover off and bond slip between vertical bars and concrete. As the drift ratio increased, the strains of L1 and R1 were not varied, but the strains of L2 and R2 were varied.

Until the drift ratio of 0.75%, the strain profile measured from the specimen was similar to the strain distribution shown in Figure 6-15. However, after yielding vertical bars, the strain in the tension side increased sharply and the strain in the compression side changed to tensile strain. This is because the sliding deformation was occurred at the interface between the wall and the pedestal after the 1st shear wall yielded at drift ratio of 0.75% (See Figure 6-59). As such sliding deformation initiated, the number of diagonal shear cracks in the 1st shear wall hardly increased as shown in Figure 6-48. On the contrary, after drift ratio of 0.75%, the diagonal cracks and horizontal shear cracks propagated in the 2nd shear wall, resulting in sliding failure at drift ratio of 1.5%. Most lateral loads were transmitted to the 2nd shear wall while the sliding deformation occurred in the 1st shear wall after drift ratio 0.75%.

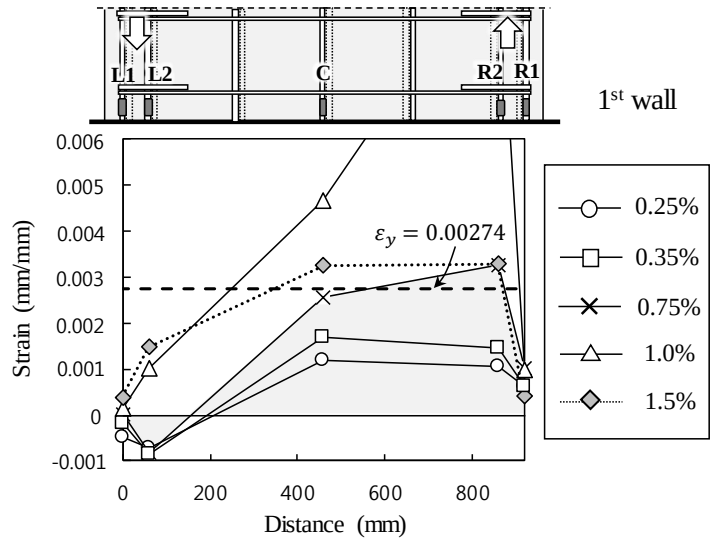

Figure 6-58 Strain distributions of bottom vertical bars in the first-story wall

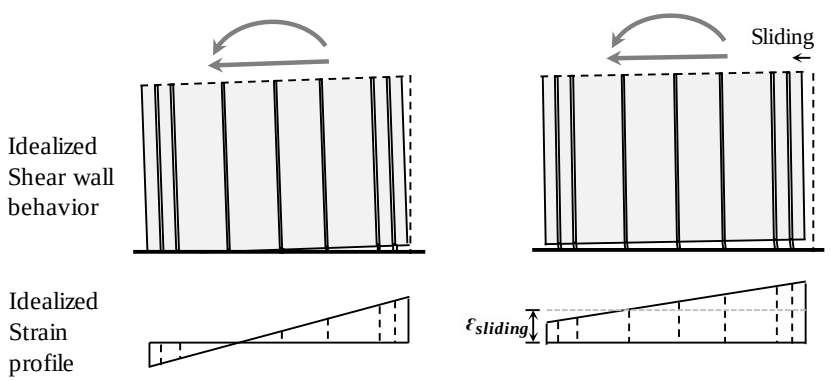

Figure 6-59 Shear wall behavior and strain profile before and after drift ratio of 0.75%

6.4.4.2 Strain distributions of wall horizontal bars

Figure 6-60 shows the strain distributions measured at horizontal reinforcements in the 1st and 2nd shear walls according to each drift ratio. The horizontal axis indicates measured strains, and the vertical axis indicates the height of the wall from the base and the beam. The bar strains were the maximum values that each spliced bar underwent during the load cycles repeated at each lateral drift ratio. For clarity, the bar strains corresponding to δ = 0.25%, 0.35%, 0.5%, 1.0%, and 1.5% are denoted with bars, squares, crosses, triangles, and diamonds, respectively.

In the strain distributions of horizontal bars in the 1st shear wall (Figure 6-60(b)), At drift ratio of 0.25%, the first deformation observed in reinforcement B2, and the strains in reinforcements B2 and B3 increased at drift ratio of 0.35%. As the diagonal shear cracks propagated to the top of the 1st shear wall (See Figure 6-48), deformation occurred in reinforcements C and T3 at drift ratio of 0.5%. At drift ratio of 1.0%, the strain in reinforcement B3 exceeded the yield strain (ε_y = 0.00252). As the load carrying capacity decreased at drift ratio of 1.5%, the strains also decreased. No deformation was observed in reinforcements B1 and T1 located at both ends of the wall.

In the strain distributions of horizontal bars in the 2nd shear wall (Figure 6-60(a)), At drift ratio of 0.5%, the first deformation observed in reinforcement T. As the diagonal shear cracks propagated to the bottom of the 2nd shear wall (See Figure 6-47), the strains in reinforcements T and C increased at drift ratio of 1.0%. As the load carrying capacity decreased at drift ratio of 1.5%, the strains also decreased. No deformation was observed in reinforcement B.

The strains from the horizontal shear reinforcement were shown to be the same pattern as the diagonal shear crack propagation of the wall. In the 1st wall where the diagonal cracks developed throughout the wall, deformations concentrated at the middle of the wall. In the 2nd wall with diagonal cracks only at the upper part of the wall, most deformations occurred at the upper part of the wall.

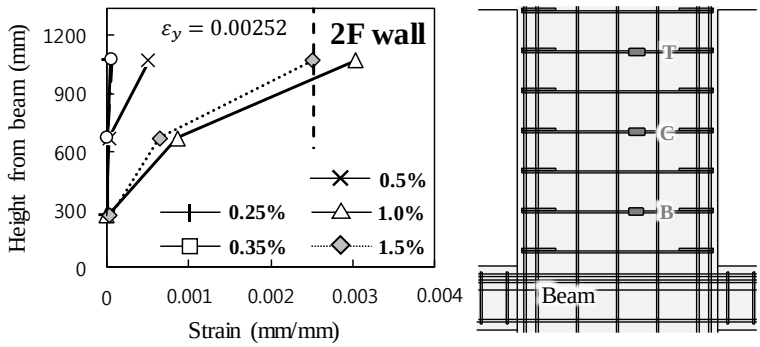

(a) Second-story shear wall

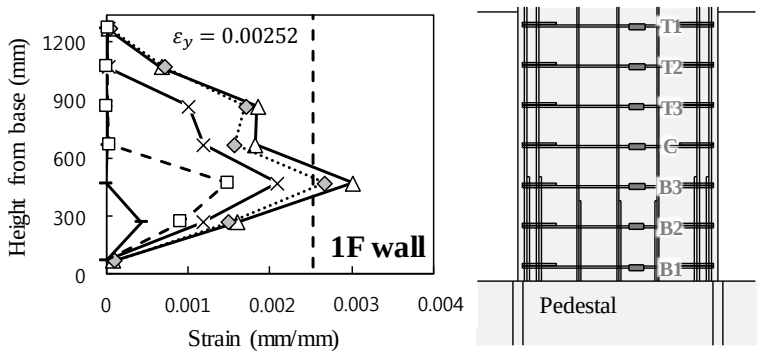

(b) First-story shear wall

Figure 6-60 Strain distributions of horizontal bars in shear wall

6.4.5 Deformation contributions of bar slip, flexure, and shear

In order to evaluate the effect of the deformations at each member location on the lateral displacement of the entire frame, the LVDTs were installed to measure the flexure (including column bar slip) and shear deformations as shown in Figure 6-25 and Figure 6-61(a). Since test frames showed the weak column and strong beam behavior, the flexural and shear deformations of columns at plastic hinge regions were mainly measured. Further, shear deformation of joints and bar slip deformation at the bottom of the 1st column were also measured.

As the total horizontal deformation of frames was contributed by column bar slip deformation, flexural deformation, and shear deformation at the plastic hinge zone (See Figure 6-61(b) ~ (d)), the results of each deformation measurement were compared according to test specimens.

Figure 6-62 shows the contribution of column bar slip deformation, flexural deformation, and shear deformation measured at the bottom left column of the first story in specimen **IMF**. Until drift ratio of 0.5%, most of deformations were caused by flexure and column bar slip without shear deformation. In particular, the bar slip deformation was about 60% of the total deformation. After drift ratio of 0.75% when diagonal cracks initiated, the contribution of shear deformation was increased steadily until the end of test. At drift ratio of 3.5%, as the diagonal crack width at the plastic hinge zone of the bottom column became wide, the contribution of shear deformation was increased to over 50% of the total deformation.

The specimen **IMF** had more than 80% of the total deformation due to flexural and bar slip deformations of the column. In particular, the bar slip deformation was more than half of the total deformation because of the relatively low axial force applied on the column, resulting in large column bar slip at the interface between the column and the pedestal.

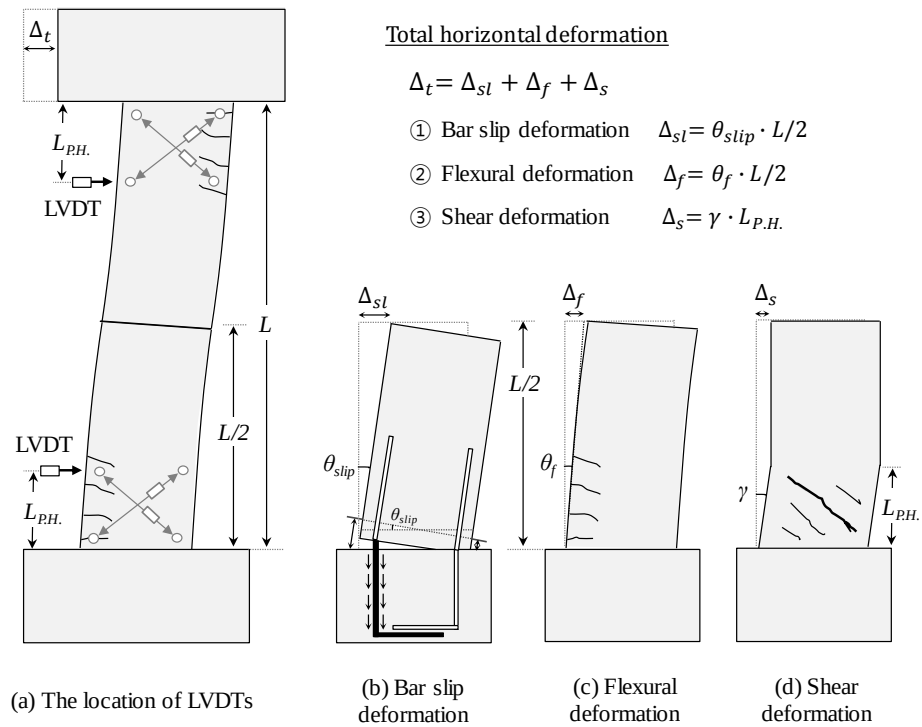

Figure 6-61 Components of flexibility in columns

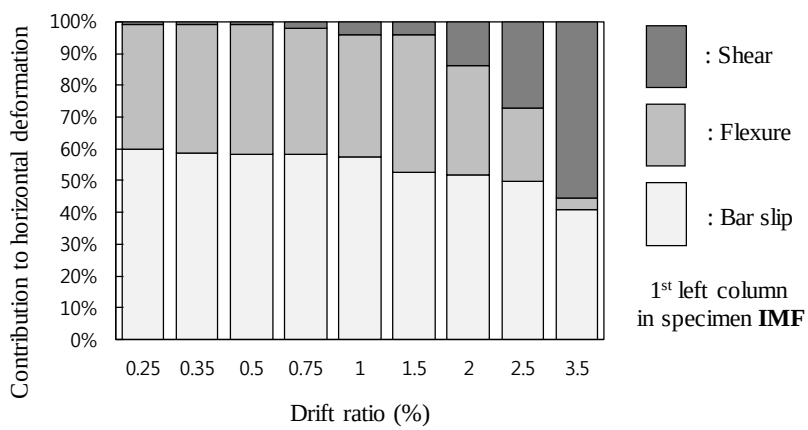

Figure 6-62 Deformation contribution of bar slip, flexure, and shear

6.4.5.1 Bar slip deformations

From drift ratio of 0.25%, cracks occurred at the interface of the column and the pedestal before the flexural cracks propagated to the middle of the column, and the crack width slightly increased by column bar slip. Such crack openings at the bottom of 1st column in specimen **A1F** were observed as shown in Figure 6-63(a). In other specimens, similar crack openings were also observed. The bar slip deformation (rotation angle, θ_{slip}) was calculated by the vertical displacement (d_l and d_r) measured at a distance of 70 mm from the pedestal (See Figure 6-63(b)).

The column bar slip (s_a) occurred as much as the sum of strains measured along anchored column bar into the pedestal. Figure 6-64 shows the strain distributions of the column bars measured in the pedestals of each specimen. The horizontal and vertical axes denote the bar strains and the depth to the pedestal where strains were measured, respectively. The bar strains were the maximum values that each spliced bar underwent during the load cycles repeated at each lateral drift ratio. For clarity, the bar strains corresponding to δ = 0.25%, 0.5%, 1.0%, 1.5%, and 2.0% are denoted with bars, crosses, triangles, diamonds, and circles, respectively.

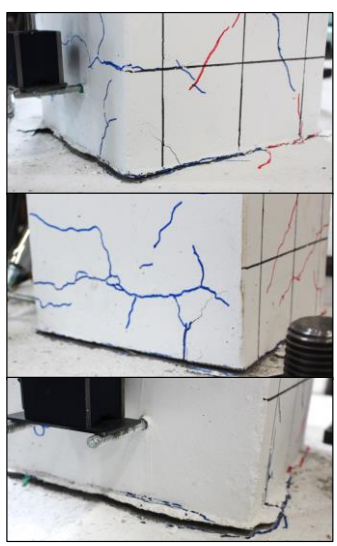

(a) Observed crack opening by bar slip

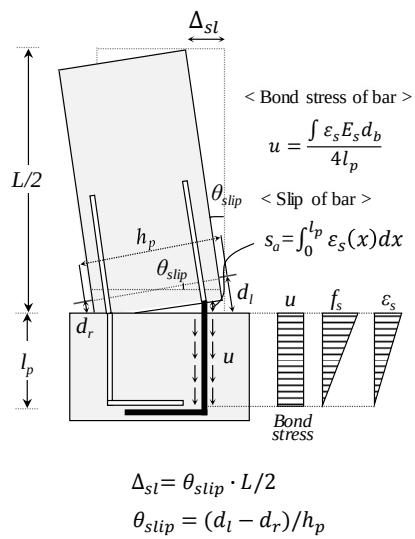

(b) Measurements of column bar slip

Figure 6-63 Effect on column bar slip

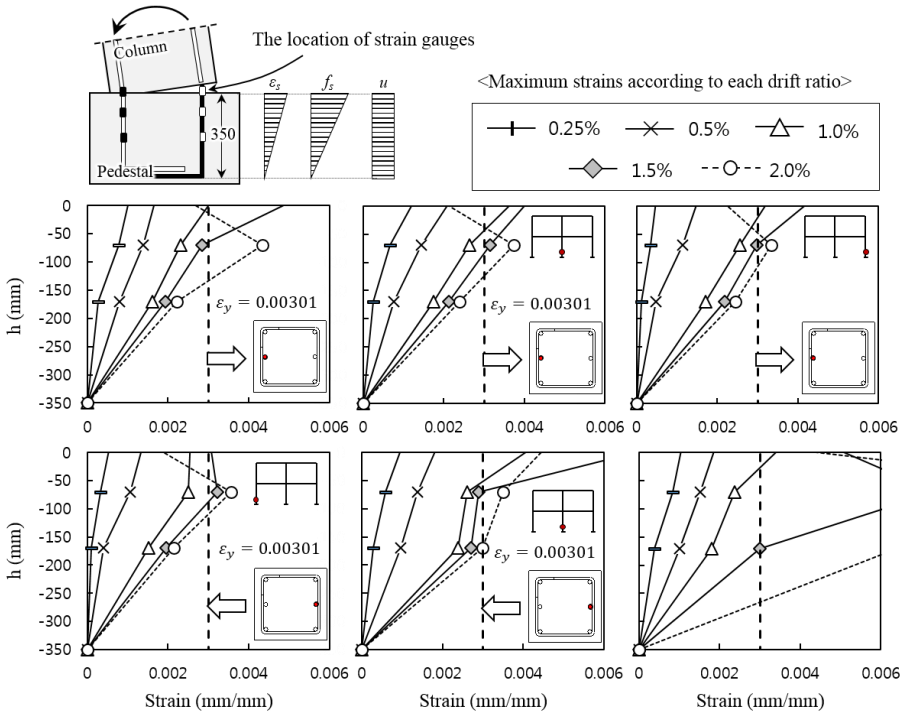

(a) Specimen **IMF**

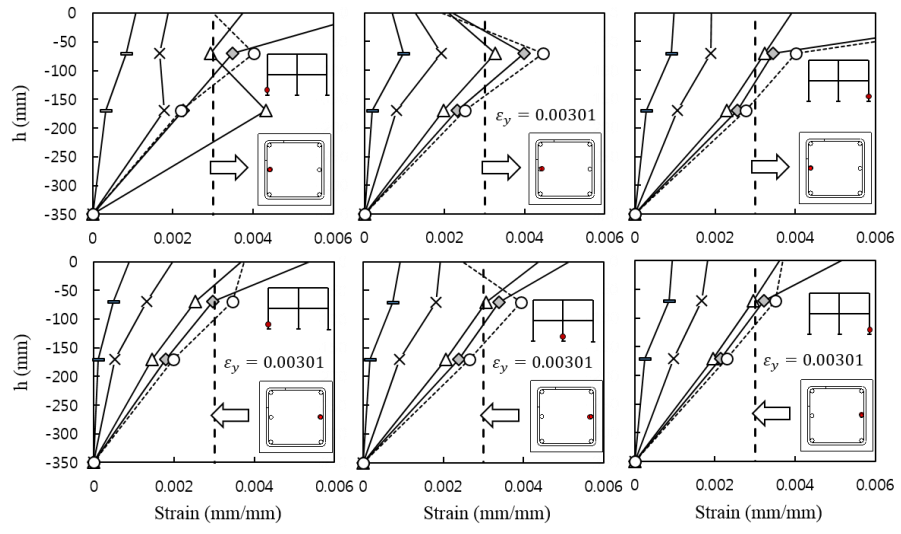

(b) Specimen **A1F**

Figure 6-64 Strain distributions of column bars in pedestals (Continued)

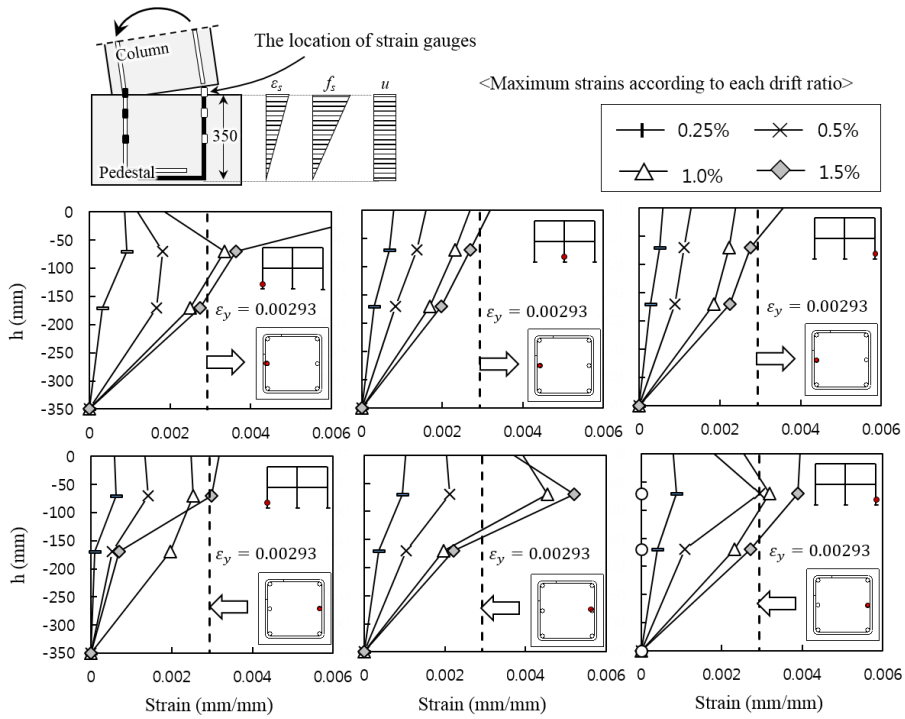

(c) Specimen **A2F**

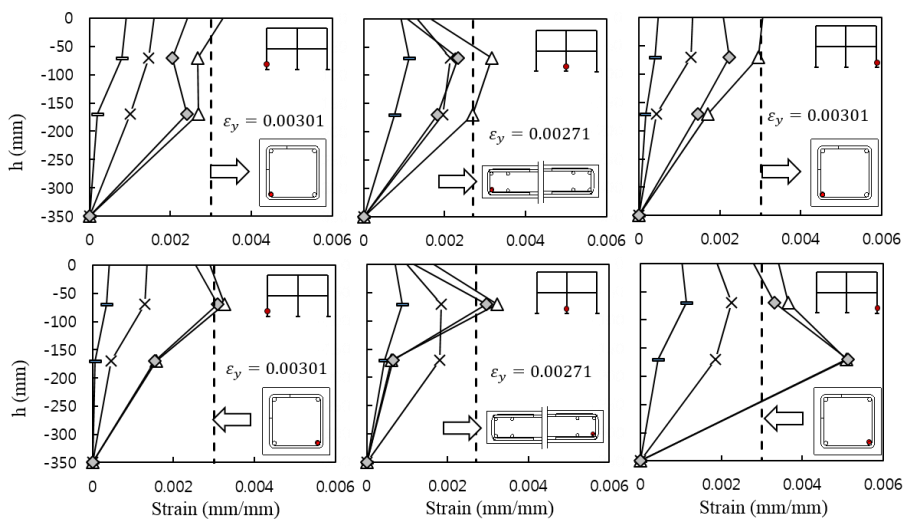

(d) Specimen **WF**

Figure 6-64 Strain distributions of column bars in pedestals

Though there was a slight difference between the locations of strain measurement, as expected, the strains decreased linearly from the pedestal. As strain penetration occurred inside the pedestal, the strains at a distance of 70 mm below the pedestal reached the yield strain around drift ratio of 1.5% (δ=1.0% in specimen **WF**).

Through the measured strain values, the bond stresses of the column bars at the pedestal were calculated as shown in Figure 6-65. If we assume the bond stress u is constant along the anchorage length, equilibrium of the anchored bar is as follows.

$$T = f_s \pi \frac{d_b^{\,2}}{4} = u \pi d_b l_p \tag{6-6}$$

Solving for the bond stress,

$$u = \frac{\int \varepsilon_s E_s d_b}{4 l_p} \tag{6-7}$$

Figure 6-65 shows the bond stresses applied on column bars in pedestals at drift ratio of 1.0% and 1.5% using the strain measurements in Figure 6-64. The bond stresses were ranged from $0.6\sqrt{f_c'}$ (MPa) to $1.25\sqrt{f_c'}$ (MPa) with the mean value of $0.93\sqrt{f_c'}$ and the standard deviation of 0.45. In previous studies, Sozen et al. (1992) recommended using $u = 0.5\sqrt{f_c'}$ (MPa); Elwood and Eberhard (2009) recommended $u = 0.8\sqrt{f_c'}$ (MPa); Lehman and Moehle (2000), and Setzler and sezen (2008) recommended $u = 1.0\sqrt{f_c'}$ (MPa) for the average bond stress values in elastic response.

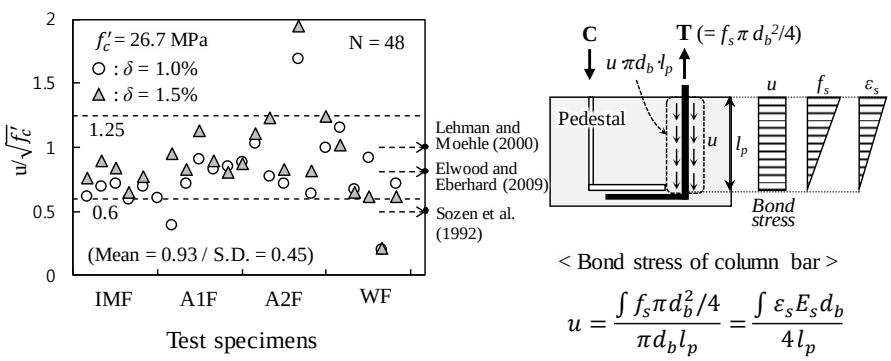

Figure 6-65 Bond stresses applied on column bars in pedestals at δ =1.0% and 1.5%

6.4.5.2 Flexural deformations

The flexural deformations measured at plastic hinge zone of each column were compared with the lateral displacement at the 2nd slab. As shown in Figure 6-66, the LVDT displacements measured horizontally in the column plastic hinge zone were used for flexural deformation. Hereafter, the value of flexural deformation is a sum of a bar slip deformation and a pure flexural deformation (Δ_{sl} and Δ_f). A method for predicting flexural deformation using LVDT measurements is given in **Appendix A**.

Figure 6-67 compares the lateral displacement values due to flexural deformations measured at the top and bottom of 1st and 2nd columns and the lateral displacement values at the 2nd slab (horizontal solid line in Figure 6-67). The contributions of flexural deformations in 2nd top column, 2nd bottom column, 1st top column, and 1st bottom column were indicated by a black bar, a dark grey bar, a grey bar, and a light grey bar. In each specimen, the contributions in positive and negative directions of the left column were plotted in the right and left figures, respectively.

The sum of the flexural deformations for top and bottom of each column showed 80 ~ 100% of the lateral displacements measured in the 2nd slabs except for negative directions in specimen **IMF** and specimen **WF** (over 100%). This result indicates that the column flexural deformations were predominant in the frame specimens. At the last drift ratio when failure occurred, the value of flexural deformation became sharply smaller than that of the previous drift ratio, because the effect of shear deformation was increased.

The flexural deformations between 1st columns and 2nd columns were similar in the initial stage. However, as the drift ratio increased, the flexural deformations of the 1st columns were relatively increased. When the drift ratio was 1.5%, the flexural deformation of the 1st columns was higher than that of the 2nd columns by 8 ~ 47% in **IMF** an **A1F**. This is because the flexural deformations increased greatly with the plastic hinge developed at the 1st columns.

As the shear cracks and shear deformations were not large in the left column of specimen **WF**, the flexural deformation was relatively large. At drift ratio of 1.5%, the flexural deformation in the 2nd left column rapidly increased as the sliding failure occurred in the upper part of the 2nd wall.

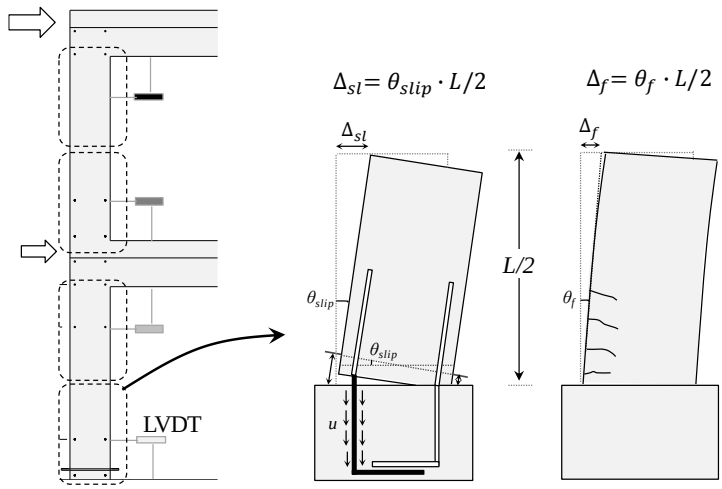

(a) Locations of LVDTs for flexural deformations (b) Bar slip deformation (c) Flexural deformation

Figure 6-66 Flexural deformation measurements

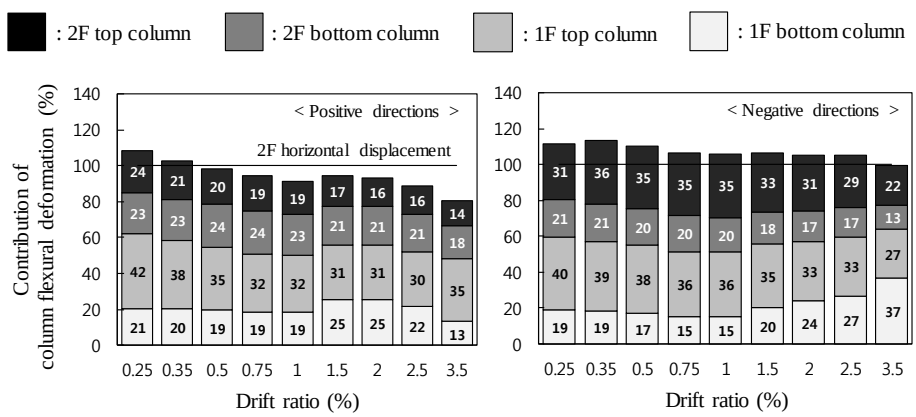

(a) Specimen **IMF**

Figure 6-67 Flexural deformation contributions of left columns (Continued)

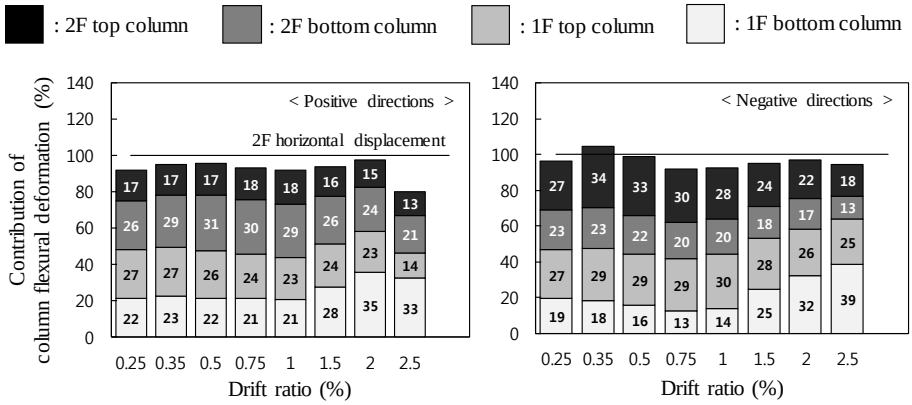

(b) Specimen **A1F**

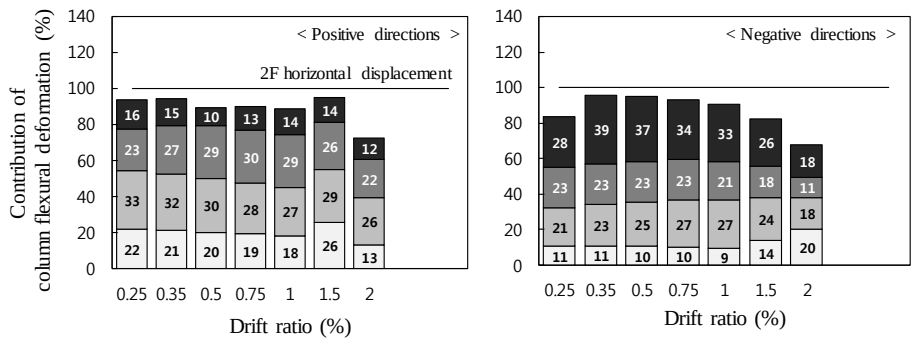

(c) Specimen **A2F**

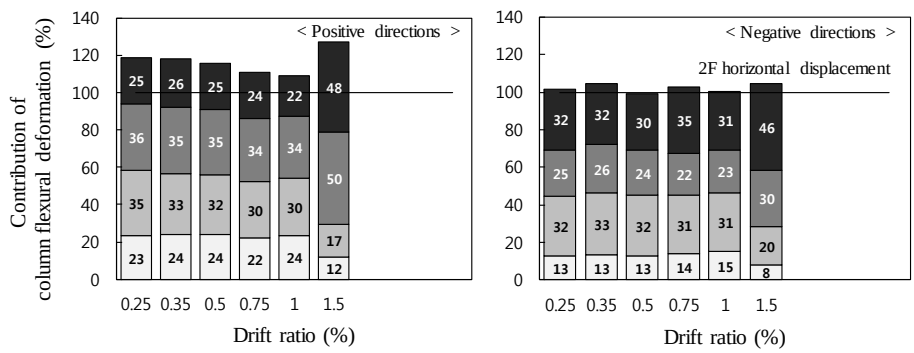

(d) Specimen **WF**

Figure 6-67 Flexural deformation contributions of left columns

6.4.5.3 Shear deformations

Since the horizontal displacement of frames was affected not only by the flexural deformations of members but also by shear deformations, the shear deformations measured at the column and the joint as shown in Figure 6-68. The shear deformations were calculated on the basis of shear distortions measured in the column plastic hinge regions and the joints. No measurements were made in the upper plastic hinge region of 2nd columns where shear deformations were relatively low. A method for predicting shear distortions using LVDT measurements is given in **Appendix A**.

Figure 6-69 and Figure 6-70 compare the flexural and shear deformations measured at the center and right columns, respectively, and the lateral displacement values at the 2nd slab (horizontal solid line). The contributions of shear deformations in joints and columns were indicated by a black bar and a dark grey bar, respectively. The contributions of flexural deformations in 2nd column and 1st column were presented by a grey bar and a light grey bar, respectively. In each specimen, the contributions in positive and negative directions of the columns were plotted in the right and left figures, respectively. Deformation contributions of shear wall in specimen **WF** were evaluated in 6.4.5.4.

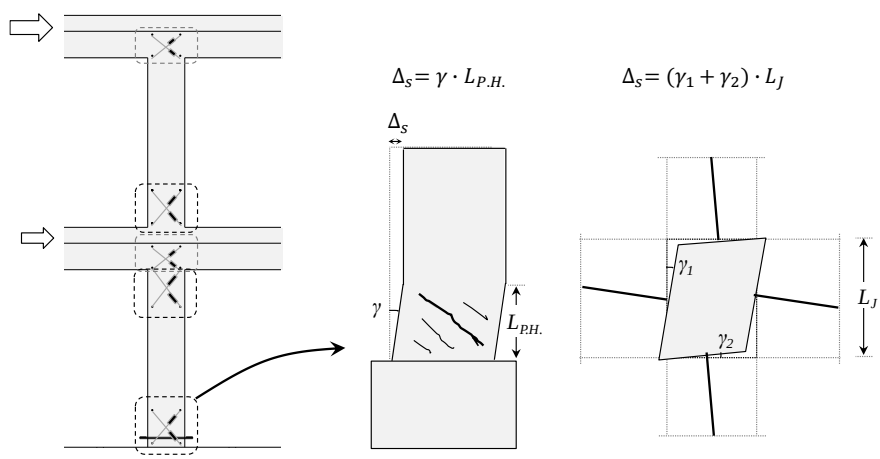

Figure 6-68 Shear deformation measurements

In Figure 6-69 and Figure 6-70, the sum of flexural and shear deformations of most columns showed 100 ~ 120% of the lateral displacements measured in the 2nd slab. In particular, the shear deformations were very small compared to the flexural deformations. The ratio of the shear deformations to the total deformations was shown with grey solid line, and the contribution value was shown on the right vertical axis. The contribution of shear deformation was initially 5%, and steadily increased as the drift ratio increased, showing 10 ~ 20% at the ultimate drift ratio.

Joint shear deformations were initiated from drift ratio of 0.25% due to joint diagonal shear cracks as shown in crack patterns of each specimen. The joint shear deformations did not increase rapidly with increasing drift ratio, but showed almost constant. On the other hand, column shear deformations hardly occurred at the initial stage, but increased sharply as the drift ratio increased. This indicates that the shear deformations were dominated after column flexural yielding in the frame specimens.

The frame specimens showed flexural dominated behaviors by analyzing flexural and shear deformations measured at each member. In particular, as weak-column and strong-beam behavior, the column flexural deformations were more than 80% of the total deformations. The shear failure finally occurred in the column plastic hinge zone, and splitting failure with severe vertical cracks occurred in the lap splice zone of columns.

Even after the occurrence of diagonal shear cracks, the joint shear deformations were not significantly increased due to the shear reinforcement in the exterior joints. Thus, joint shear failure did not occur.

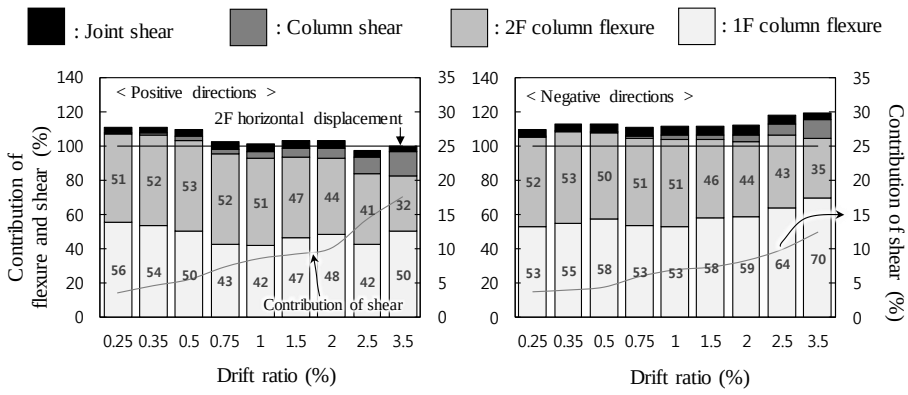

(a) Specimen **IMF**

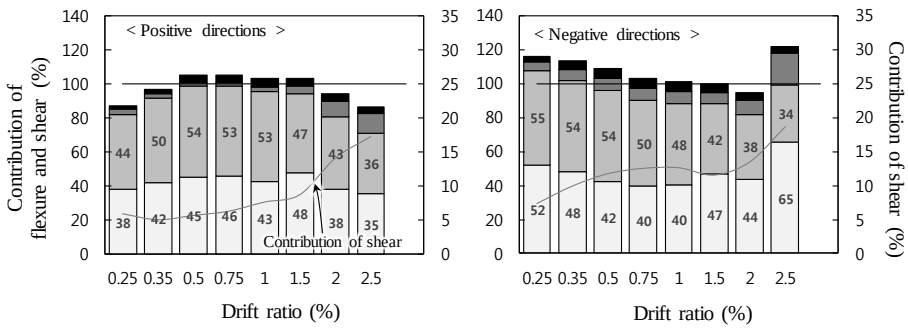

(b) Specimen **A1F**

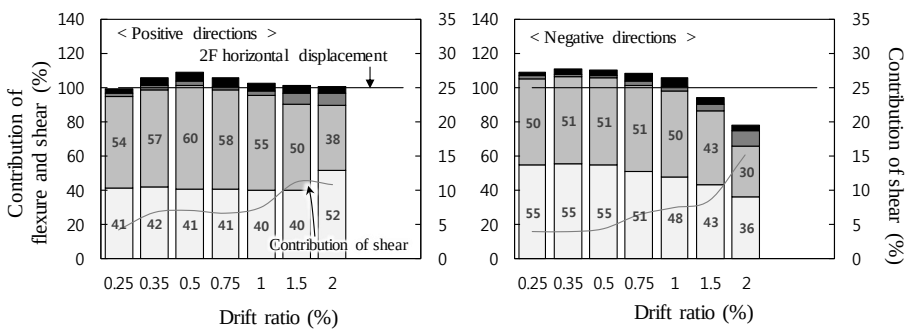

(c) Specimen **A2F**

Figure 6-69 Flexural and shear deformation contributions of center columns

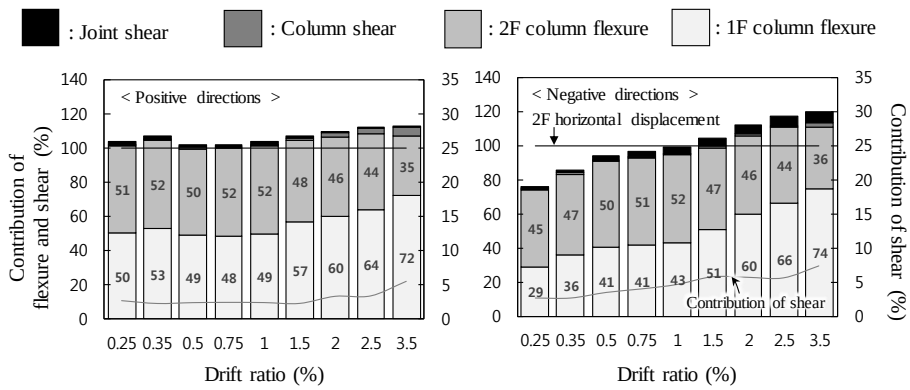

(a) Specimen **IMF**

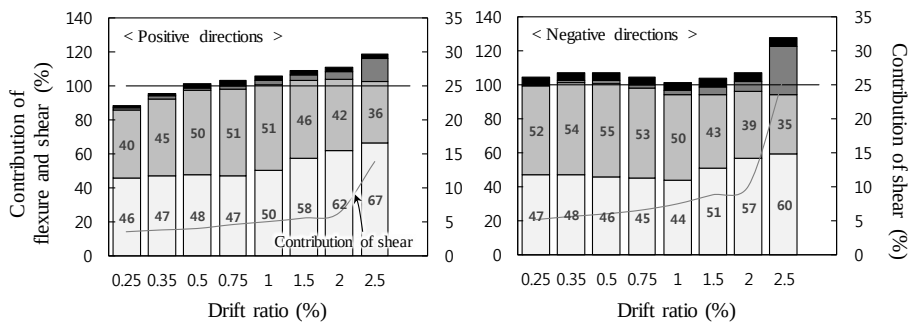

(b) Specimen **A1F**

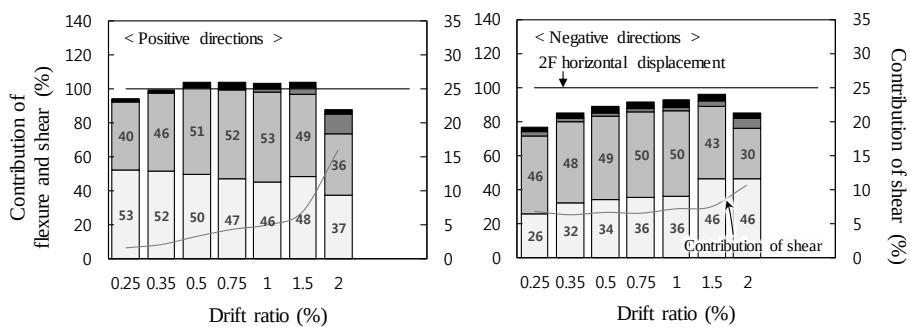

(c) Specimen **A2F**

Figure 6-70 Flexural and shear deformation contributions of right columns

6.4.5.4 Deformation contribution of shear wall

To measure flexural and shear deformations in shear wall, LVDTs were installed as shown in Figure 6-71. The flexural and shear deformations were calculated as the horizontal and diagonal displacements, respectively. A method for predicting flexural and shear deformations using LVDT measurements is given in **Appendix A**.

Figure 6-72 compares the lateral displacement values due to flexural and shear deformations and the lateral displacement values at the 2nd slab (horizontal solid line in Figure 6-72). The contributions of shear and flexural deformations in 2nd wall were indicated by a black bar and a dark grey bar, respectively. The contributions of shear and flexural deformations in 1st wall were presented by a grey bar and a light grey bar, respectively. In each specimen, the contributions in positive and negative directions of the left column were plotted in the right and left figures, respectively.

The shear wall also showed a large flexural deformation similar to that of columns. The shear deformation of the 1st shear wall was only 10 ~ 20% of the total deformation, and the flexural deformations of the 1st and 2nd shear wall were 80% of the total deformation. In the 2nd shear wall, shear deformation slightly increased from drift ratio of 0.5% due to horizontal shear cracks. At drift ratio of 1.5% when horizontal sliding failure occurred in the 2nd shear wall, the deformations in the 2nd shear wall were abruptly increased.

In order to examine the column bar slip deformation at the bottom of the 1st shear wall, the slip deformation was indicated by a light grey bar in Figure 6-73. The column bar slip deformation was 20% of the total deformation, which was smaller than the flexural deformation in the 1st shear wall.

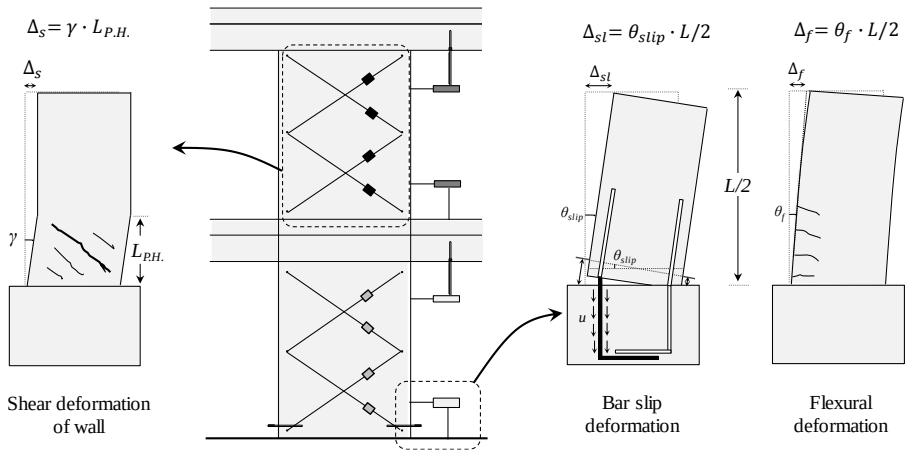

Figure 6-71 Components of flexibility in shear wall

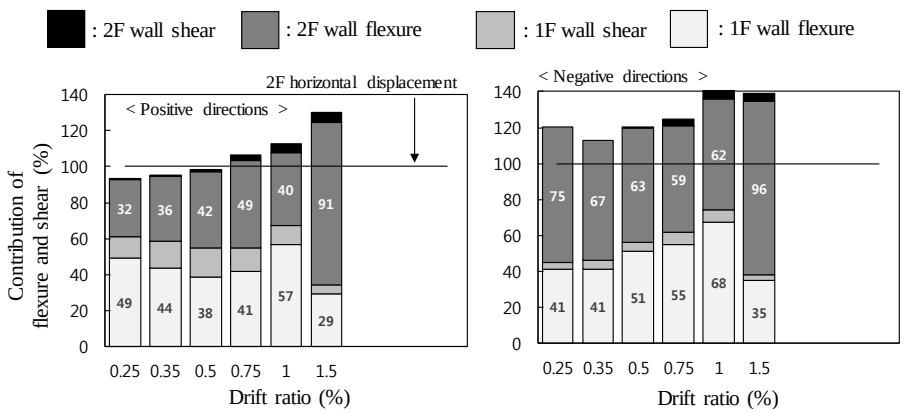

Figure 6-72 Flexural and shear deformation contributions of shear wall

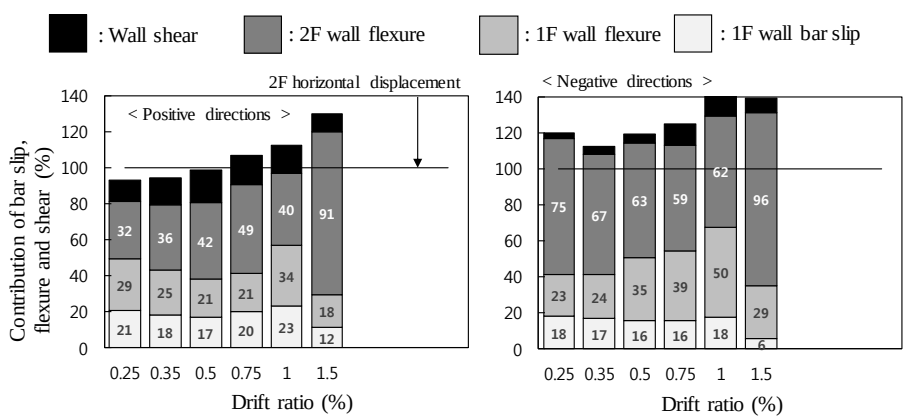

Figure 6-73 Contributions of bar slip, flexural and shear deformations in shear wall

6.5 Main Causes of Failure in Specimen WF

6.5.1 Final failure mode of specimen WF

Specimen **WF** experienced horizontal sliding failure with diagonal shear cracks at the upper part of the 2nd shear wall. In order to analyze the main causes of failure, the load - drift ratio relations and failure pattern were examined in Figure 6-74. Until 3rd cycle in drift ratio of 1.0%, diagonal cracks and horizontal shear cracks occurred without significant load reduction. However, in 1st cycle positive loading at drift ratio of 1.5%, severe horizontal sliding cracks with major diagonal shear crack were developed, thereby decreasing load carrying capacity. In 1st cycle negative loading at drift ratio of 1.5%, severe horizontal sliding cracks with major diagonal shear crack were also occurred.

The major cracks which have had a significant impact on the final failure are shown in Figure 6-75 with horizontal and vertical bar details (grey dashed lines). The grey arrows indicate the loading directions acting along the crack surface. Horizontal loads applied on the 2nd wall at drift ratio of 1.0% are also presented in Figure 6-75. In the 1st cycle positive loading at drift ratio of 1.5%, horizontal shear cracks occurred in the tension zone with severe diagonal shear cracks in the compression zone. Similar behavior was observed in the negative loading. Such cracks eventually resulted in horizontal sliding failure at the upper part of the 2nd shear wall.

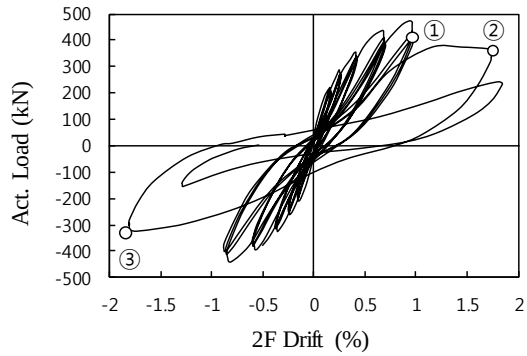

(a) Load - drift ratio relations of specimen **WF**

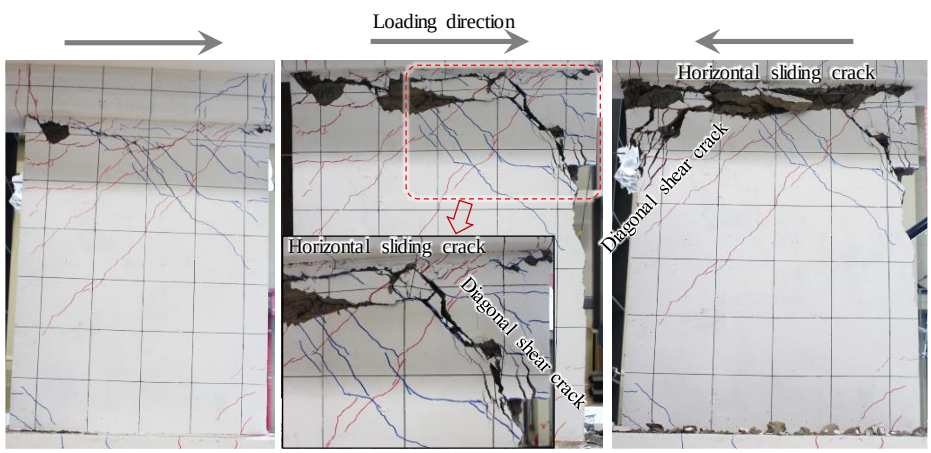

< 1.0% 3rd cycle> < 1.5% 1st cycle (+) > < 1.5% 1st cycle (-) >

(b) Failure sequence of second-story shear wall

Figure 6-74 Load - drift ratio relations and final failure mode of specimen WF

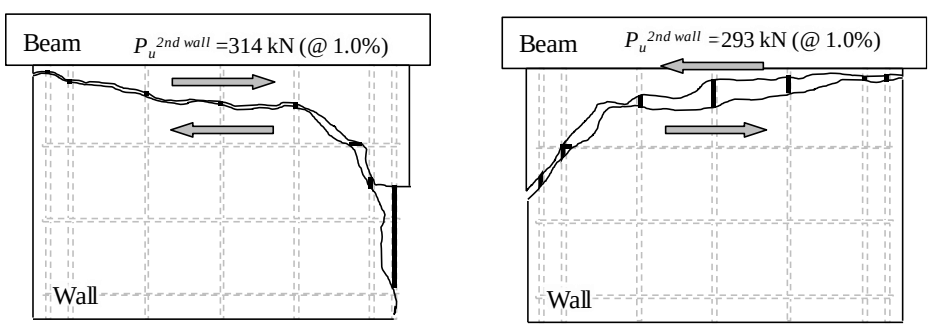

< 1.5% 1st cycle (+) > < 1.5% 1st cycle (-) >

Figure 6-75 Failure mode of second-story shear wall in specimen WF

6.5.2 Shear friction strength and vertical shear strength

In order to investigate the causes of horizontal sliding failure, horizontal shear forces acting on the 2nd shear wall and shear friction strength specified in ACI 318-14 were compared. The shear forces at drift ratio of 1.0% were 314 kN ($2/3P_u^+$) in the positive direction, and 293 kN($2/3P_u^-$) in the negative direction. The shear friction strength equation in ACI 318-14 is as follows.

$$V_n = A_{vf} f_y \mu \tag{6-8}$$

where the coefficient of friction μ is 1.4 for concrete placed monolithically, 1.0 for the hardened concrete with intentionally roughened surface (a full amplitude of 6 mm), and 0.6 for the hardened concrete without intentionally roughened surface. As the 2nd shear wall in specimen **WF** was placed monolithically, the coefficient of friction μ was used to be 1.4.

Assuming that all vertical bars resist shear friction, V_n = (72×6+127×8) ×542×1.4 = 1099 kN. However, as shown in Figure 6-75, since the shear frictional resistance was insignificant due to flexural bar yielding and flexural cracks in the tension zone and severe diagonal cracks in the compression zone, only the vertical reinforcement in the middle can resist most shear friction, V_n = (72×6)×542×1.4 = 327 kN. In this case, the applied horizontal shear forces (314 kN and 293 kN) are similar to the shear friction strength (327 kN).

Vertical shear strength was also investigated because diagonal shear cracks occurred in the compression zone. The vertical shear strength specified in ACI 318-14 is consisted of the shear strengths by concrete (V_c) and by shear reinforcement(V_s) as follows.

$$V_n = V_c + V_s \tag{6-9}$$

$$V_c = (\sqrt{f_c'}/6)hd \tag{6-10}$$

$$V_s = A_{vh} f_y d/s_h \tag{6-11}$$

where A_{vh} is the cross-sectional area of the horizontal shear reinforcement, and d can be calculated as $0.8l_w$(wall length). The vertical shear strength (380 kN) of the 2nd

shear wall calculated as V_c = 0.167×√26.7×130×800 = 90 kN, and V_s = 72×2×504×800×200 = 290 kN was higher than the applied shear forces (314 kN, 293 kN).

6.5.3 Anchorage details of wall vertical bars

The wall vertical bars should be anchored in the 2nd slab for sufficient stress transfer. Figure 6-76 shows the anchorage details and length used in the 2nd shear wall. The vertical bars penetrated the beam and anchored inside the slab with 90º hook. The anchorage length was 260 mm, which was 26d_b for D10 reinforcing bars and 20d_b for D13 reinforcing bars. As the development length of standard hooks specified in ACI 318-14 was 25d_b, the D10 bars had a sufficient length, but D13 bars did not.

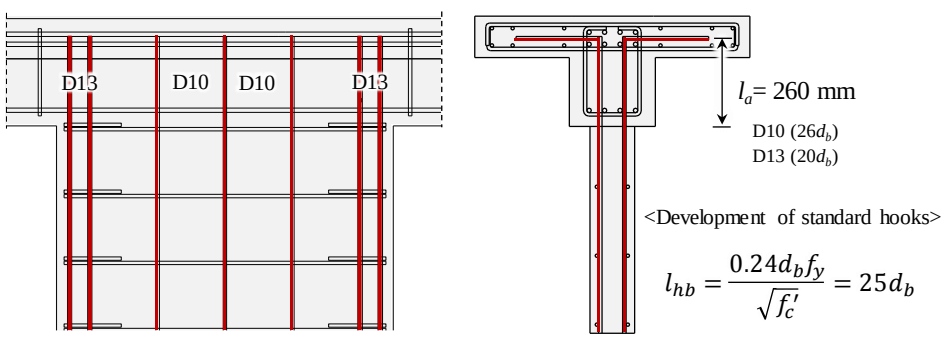

Figure 6-76 Anchorage length of wall longitudinal bars

As a result of the analysis of the main causes of failure in specimen **WF**, horizontal sliding failure occurred at the upper part of the 2nd shear wall with severe diagonal cracks in compression zone. The horizontal shear crack and sliding failure occurred at the shear friction strength calculated by the vertical reinforcement at the middle of the shear wall. This indicates that the vertical bars in the compression zone and tension zone do not play a significant role in the lateral force resistance because flexural bar yielding and flexure/shear cracks. Further, the D13 reinforcing bars were calculated to be insufficient anchorage length to the 2nd shear wall.

6.6 Discussion

In this study, two-story and two-bay frame tests were performed with the variation of reinforcement details verified by column and beam-column connection tests in Chapter 2 ~ Chapter 5. The test results showed that the alternative details could be applicable to low-rise buildings, and the structural performance of the alternative details was verified through frame tests. Four frame tests were conducted with the major parameters of reinforcement details and shear wall; Intermediate Moment frame according to KBC standard (**IMF**), Alternative detail frame (**A1F**), another Alternative detail frame with increased column and beam flexural bar ratio (**A2F**), and gravity load dominated frame with shear wall (**WF**). The main test results are summarized as follows.

1) In the case of moment frames without a shear wall, weak-column and strong-beam behaviors in the 1st story were observed. Since small gravity load is generally applied in low-rise buildings, the depth of columns is much smaller than that of beams, and flexural strength can be designed in beams larger than columns due to the slab effect. As a result of the frame test, plastic hinges were occurred in the 1st columns with the weak-column and strong-beam behavior.

2) In low-rise buildings, lap splices of column longitudinal bars can be used in the plastic hinge region of columns, and the offset bar details should not be applied for convenient bar placement. As the required shear force by earthquake is relatively small, the lap splices of column bars used in the plastic hinge region is not great problem. However, lap splice length of column bars should be sufficiently secured ($50d_b$ for SD500 bars), and spacing of transverse bars in the splice region should be less than $d/2$. When splice without offset bend was used in the plastic hinge region, vertical splitting cracks occurred along the splice region even at low deformations.

3) The most vulnerable members in low-rise buildings are exterior and interior beam-column connection because the moments and shear forces acting on columns and beams are transmitted through the joints in the beam-column connections. Since the joints should smoothly transmit the moments and shear forces, transverse bars are necessarily required. However, in the joints where the column and beam reinforcements are overlapped, it is difficult to place the closed hoops due to the steel

congestion. Thus, when the U shaped bars are used for the joints, the workability can be greatly improved, and the structural performance can be ensured. In order to use U-bars, the width of beams should be equal to or larger than the column width, and the U-bars recommend to be anchored to adjacent beams by $23d_b$ or more.

4) When a shear wall is used in a moment frame building, sliding failure can be occurred horizontally in the upper part of the top shear wall. In order to prevent such sliding failure, a dowel reinforcement should be additionally provided between the upper wall and the beam (or slab) to secure a sufficient shear friction strength. When designing shear wall, consideration should be given not only to the vertical shear force but also shear friction strength.

Chapter 7. Alternative Rebar Details for Low-rise Buildings

7.1 Column

7.1.1 Transverse reinforcement details

The vertical spacing of transverse reinforcement is to be less than half of the minimum column height as shown in Figure 7-1.

(Commentary) In low-rise buildings, since column dimensions are smaller than beams due to low gravity load, column shear demand is increased by weak-column and strong-beam behavior under seismic loading. Therefore, to resist the increased shear demand, the minimum spacing of the column transverse reinforcement is limited to half of the minimum column height ($s \leq h_{min}/2$).

The transverse reinforcement details of columns include ties with 90º hooks, lap spliced ties at one side, and U-bars as well as hoops with 135 º hooks as shown in Figure 7-2. In addition, the location of the anchorage of the transverse bars should be alternated vertically so that the anchorage bars are not concentrated at one location.

(Commentary) Since relatively low axial forces are applied on columns in low-rise buildings and large inelastic deformations are not required, alternative transverse reinforcements in Figure 7-2 can be used for enhancing construction workability. In the spliced tie and the U-bar, the lap splice length is required greater than 300 mm. Further, additional cross-tie in the splice tie should be used to prevent buckling of longitudinal reinforcement. The end extension with $6d_b$ at the end of U-bar is recommended to enhance anchorage performance of the U-bar after concrete cover spalling.

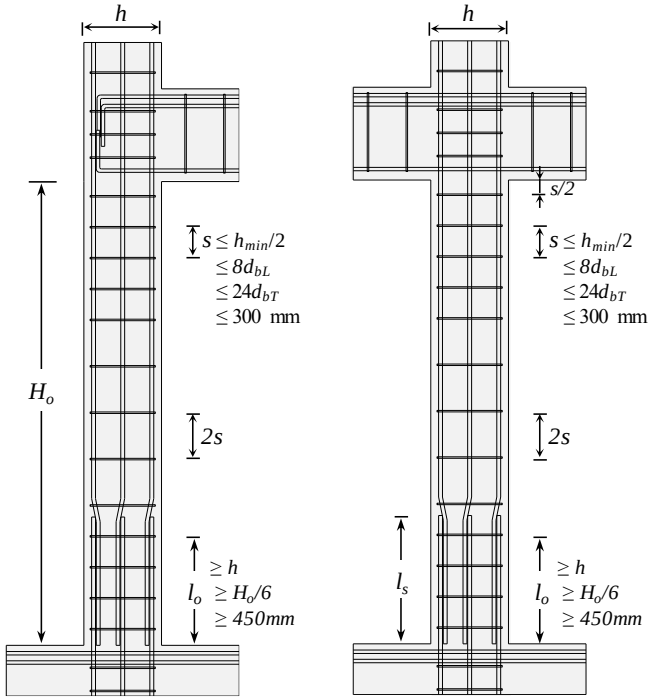

(a) Exterior column (b) Interior column

Figure 7-1 Transverse reinforcement details of columns

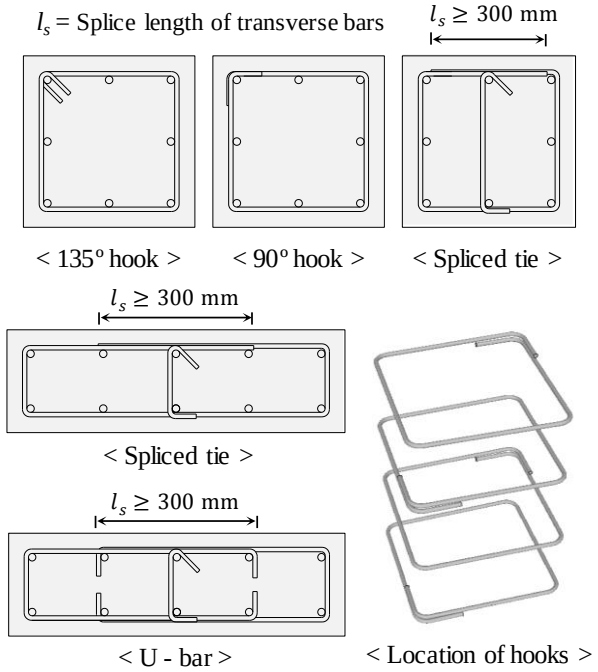

Figure 7-2 Anchorage details of transverse reinforcement

7.1.2 Lap splice details of column longitudinal bars

For lap splice details of column longitudinal bars in low-rise buildings, as shown in Figure 7-3, bottom offset bar splice, top offset bar splice, and splice without offset bend can be used.

(Commentary) In the bottom offset bar splice, the bottom bars from the lower story are offset inside. In the top offset bar splice, on the other hand, the top bars are offset inside. Alternatively, in low-to-moderate seismic zone, the splice without offset bend (Figure 7-3(c)) is used due to construction efficiency. Such non-offset bar detail results in weak bond performance and difficult positioning of column longitudinal bars at the column corner.

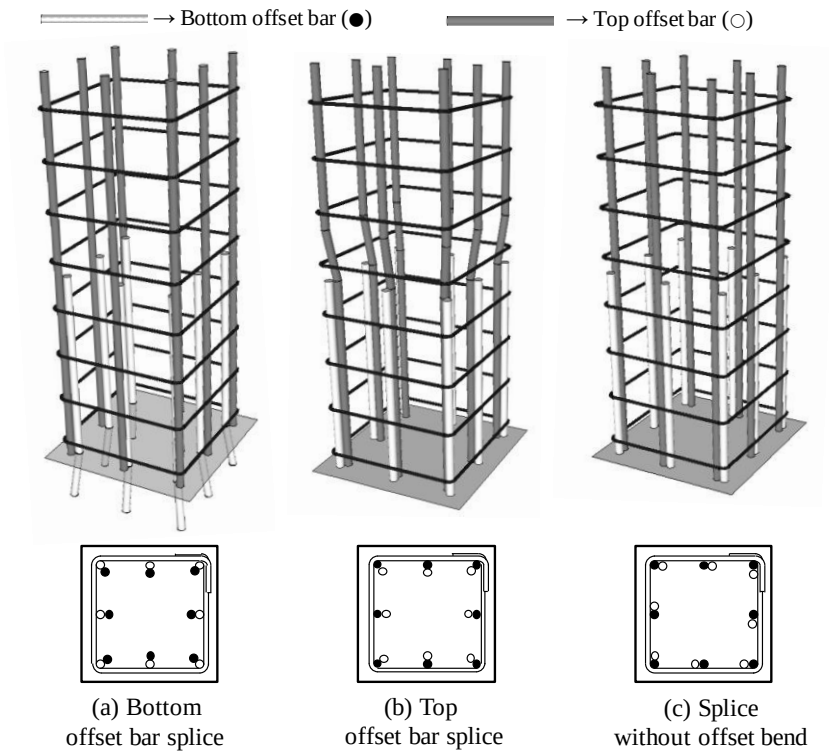

Figure 7-3 Lap splice details of column longitudinal bars

The detail of lap splice between a pedestal and 1st column is illustrated in Figure 7-4.

(Commentary) In a low-rise building, since lap splices of column longitudinal bars are used between a pedestal and 1st column, the detail of splice without offset bend can be used. When the bottom bars are located inside the concrete core, bottom offset bar ratio is increased by 10% to secure flexural strength of the column.

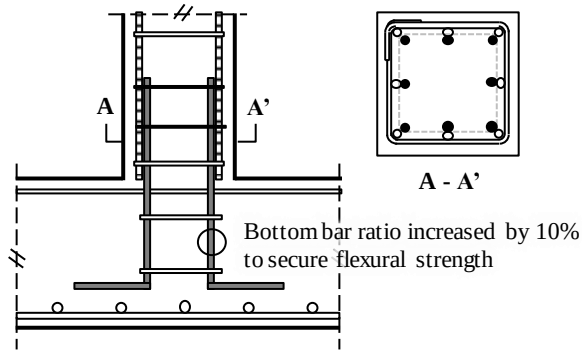

Figure 7-4 Lap splice detail between a pedestal and a 1st column

7.1.3 Lap splice length of column longitudinal bars

The lap splice length of column longitudinal bars is to be 40 times the diameter of column bars when the transverse bars are spaced at smaller than half of the minimum column height with 90º hook, and yield strength of reinforcement equal to 400 MPa (f_y = 400 MPa).

(Commentary) In previous structural design criteria for low-rise buildings, the lap splice length has a simple form (proportional to the bar diameter), so the requirement for lap splice length is conservative. According to existing test results on the lap splice length of column bars, sufficient splice performance for low-rise buildings can be achieved with only 80% of required lap splice length. Therefore, the required splice length of column bars in low-rise buildings is decreased to be $40d_b$, provided that the spacing of transverse bars is smaller than half of the minimum column height, and 90º or 135º hooks are used.

7.2 Beam-column connection

7.2.1 Joint shear reinforcement details

Joint shear reinforcement in beam-column corner and exterior connections should be used as shown in Figure 7-5.

(Commentary) As low-rise buildings designed only for gravity load do not contain joint shear reinforcement, beam-column connections are vulnerable to earthquake. Thus, the connections should be reinforced by joint shear reinforcement for earthquake load resistance. According to test results, the exterior connections are more vulnerable compared to the interior ones. The seismic performance of exterior connections is determined by joint shear reinforcement ratio and anchorage length of beam bars.

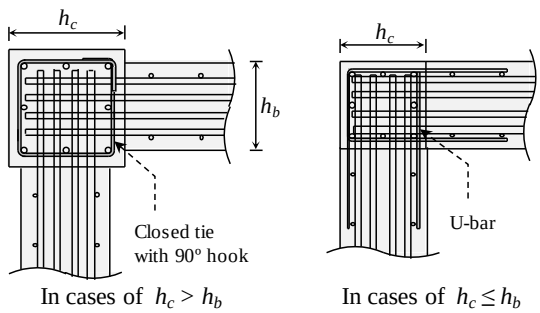

(a) Beam-column corner joint

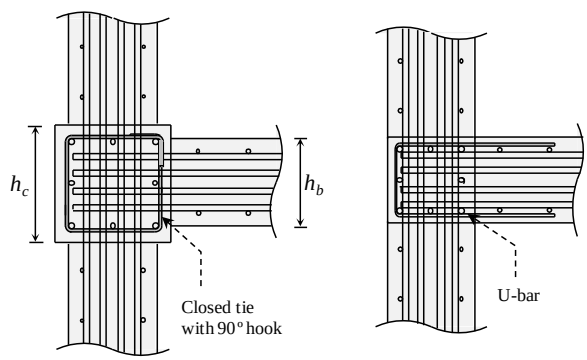

(b) Beam-column exterior joint

Figure 7-5 Joint shear reinforcement details according to beam and column depths

7.2.2 Joint shear reinforcement ratio

For the details of joint shear reinforcement, ties with 90º hook and U-bar can be used as shown in Figure 7-6. Alternative detail U-bar for convenient bar placement can be used when the beam width is equal to or greater than the column width, and anchorage length of U-bar into the adjacent beam from the column should be secured with greater than $25d_b$.

The vertical spacing of joint shear reinforcement is not greater than $0.3h_c$ at corner joints, and $0.5h_c$ at the exterior joints where three sides of a column are connected to beams (See Figure 7-7). The interior joints confined on all four vertical faces do not require joint shear reinforcement.

(Commentary) In low-rise buildings with low axial load, ties with 90º hook and U-bar can be used for joint shear reinforcement. Since the closed ties with 90º hook are located with beam and column longitudinal bars, the workability of bar placement is greatly reduced. On the other hand, U-bar detail can significantly improve the workability by inserting the U-bars after arrangement of beam and column reinforcements (See Figure 7-6). However, the U-bar detail can be used only when the beam width is greater than the column width, and the U-bar is necessary to secure an anchorage length of $25d_b$ or more from the column. In order to secure the joint shear performance, sufficient joint shear reinforcement should be ensured. Based on test results related to the effect of joint shear reinforcement ratio, the vertical spacing of joint shear reinforcement and volumetric ratio of joint shear reinforcement according to the joint location are recommended in Table 7-1.

7.2.3 Details of beam bars anchored into joints

If the column depth in the direction parallel to beam longitudinal bars is not greater than 500 mm, the maximum bar diameter of beams is limited to D19.

(Commentary) Since the column depth used in low-rise buildings is generally 400 mm or less, small size reinforcing bars should be used to secure the anchorage length of bam bars. In the previous test, when the column depth was 350 mm, and SD500 D19 bars were used for beam bars, anchorage failure or bond deterioration were not observed along beam anchorage bars.

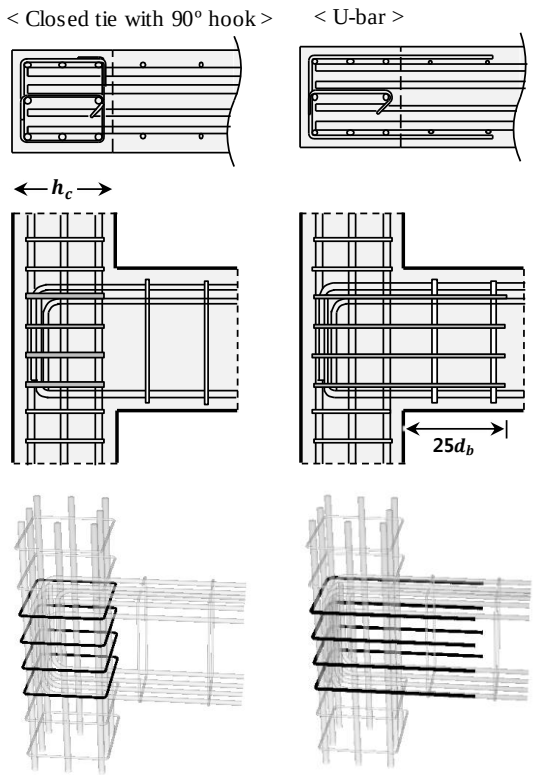

Figure 7-6 2D and 3D joint shear reinforcement details

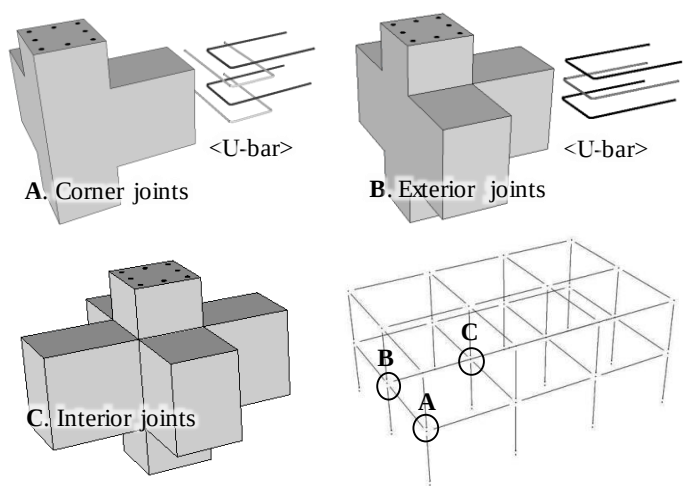

Figure 7-7 Joint shear reinforcement details in each joint location

Table 7-1 Definition of effective joint width according to desgin codes

Joint geometry	A	B	C
Spacing of shear reinforcement	$s \leq 0.3h_c$	$s \leq 0.5h_c$	Non
Shear reinforcement volume ratio	$\rho'' > 0.006$ 1)	$\rho'' > 0.003$	Non

1) ρ'' indicates volumetric ratio of horizontal confinement reinforcement in the joint

Chapter 8. Summary and Conclusions

The seismic performance of various alternative reinforcing bar details which can ensure construction efficiency and structural safety of low-rise buildings was verified through a series of experimental studies in this dissertation. In additions, seismic reinforcement details specified in current design codes and non-seismic details used in construction fields of low-rise buildings were also compared to evaluate seismic performance level of alternative bar details. Considering characteristics of low-rise buildings, a number of cyclic loading tests were conducted on columns, beam-column connections, and two-story and two-bay frames using various types of reinforcing bar details. Through column tests, the effects of transverse reinforcement details and lap splice details of column longitudinal bars on seismic performance of columns were investigated. Beam-column connection tests were conducted to examine seismic performance of U-shaped bar detail, and to evaluate the effect of joint shear reinforcement ratio and anchorage details of beam longitudinal bars. Finally, the application and seismic performance of alternative bar details were evaluated in system level through two-story and two-bay frame tests.

Based on test results of present and existing researches, several analytical models were developed. To investigate a post yield deformation capacity of column, a shear strength degradation model for columns was proposed on the basis of test results of columns with various tie details and tie spacing. Also, a modified lap splice length model for column longitudinal bars was proposed to consider moment gradient and reduced average bond demand of lap spliced bars along splice regions. Finally, this dissertation empirically presented a shear strength model for exterior beam-column connections considering the effect of joint shear reinforcement ratio ρ_j, even less than seismic code requirements.

In this dissertation, each chapter deals with slightly different main subjects, so major findings and conclusions are divided into the following sections.

8.1 Effects of Tie Details and Shear Strength Degradation Model for Columns (Chapter 2)

Cyclic load tests were conducted to evaluate seismic performance of square and rectangular columns with various tie spacing ($s = d/2$, $d/3$, and $d/4$) and tie details such as hoops with 135º hook, ties with 90º hook, lap-spliced ties, and U-bars. The effects of spacing and anchorage details of ties on the inelastic deformation capacity after column flexural yielding were investigated. Further, a post-yield shear strength degradation model for columns was proposed and verified on the basis of a number of previous and existing test results. The major findings are summarized as follows.

1) The anchorage details of column transverse reinforcement significantly affected the inelastic deformation after flexural yielding. Immediately after concrete cover spalling off, premature anchorage failure of 90º hooked and lap-spliced ties occurred, leading to relatively less ductility of columns when compared to the column with 135º hooked hoops. This result indicates that the end of transverse bar anchorages should be fully anchored inside core concrete to attain sufficient deformation capacity.

2) The post-yield failure mode and ductility of columns were affected by spacing of column transverse bars, especially by the ratio of shear resistance by transverse bars V_s to the applied shear force V_u. After column flexural yielding, the columns designed to have $V_s / V_u < 1.0$ were abruptly failed by excessive diagonal shear cracks at plastic hinge regions; on the other hand, the columns satisfying $V_s / V_u \geq 1.0$ showed large inelastic deformations with limited web shear cracks.

3) Since shear resistance by concrete V_c is gradually degraded with increasing column deformation, a post-yield deformation capacity of columns is primarily influenced by transverse reinforcement of columns. When closely spaced transverse reinforcement ($V_s / V_u \geq 1.0$) or a seismic hoop with 135º hook are used, large inelastic deformation can be achieved even after severe concrete cover damages by column flexural yielding.

4) The post-yield shear failure of columns is attributed to the degradation of concrete shear resistance V_c, so a shear degradation model for columns was proposed

as $V_{nr} = \eta V_c + V_s$, where η ($0 \leq \eta \leq 1$) is a reduction factor depending on column ductility μ and anchorage detail of transverse reinforcement. The proposed model was verified with a number of present and existing test results of columns with shear failure after flexural yielding. The results showed that the proposed model predicted the post-yield strength degradation and inelastic deformation capacity of columns with reasonable precision.

8.2 Effects of Lap Splice Length/Details and Modified Splice Length Model for Column Longitudinal Bars (Chapter 3)

In this chapter, the effects of lap splice length and details (Bottom offset bar splice, Top offset bar splice, and Splice without offset bend) of column longitudinal bars were evaluated when lap splices were used at plastic hinge regions of columns. Further, a modified lap splice length model for lap-spliced columns was proposed considering moment gradients along splice regions. The main conclusion was presented as follows.

1) According to provided lap splice lengths of column bars ($30d_b \sim 50d_b$), seismic performance of columns was different. In spliced column with $l_s = 50d_b$ satisfying ACI 318 requirement, the test strength reached the nominal flexural strength with ductile behavior despite the lap splice being located in the plastic hinge region. However, the inelastic deformation and energy dissipations of spliced columns gradually degraded when provided lap splice length was decreased to $40d_b$ or $30d_b$, less than the ACI 318 requirement.

2) The shear span to depth ratio (a/h) and transverse reinforcement ratio (V_s) also affect seismic performance of spliced columns. When shear span ratio (a/h) was 3.0, the test strength reached the nominal flexural strength, despite short splice lengths. On the other hand, columns with shear span ratio of 6.0 showed maximum test strength less than the nominal strength ($M_u = 0.95M_n$), but relatively large post-yield deformation. Lap-spliced columns with a larger tie spacing (smaller V_s) exhibited smaller inelastic deformation capacity due to early splitting failure along splice regions.

3) The lap splice details of column bars significantly influenced nominal flexural strength, post-yield deformation capacity, energy dissipations, and failure mode of spliced columns. Bottom offset bar splice showed lower flexural strength but greater ductility and energy dissipation (Flexural failure mode); on the other hand, top offset bar slice and splice without offset bend showed greater flexural strength but lower ductility and energy dissipation (Splitting failure mode). Top offset bar splice showed similar seismic behavior to splice without offset bend.

4) When lap splice is used in the plastic hinge zone, it is recommended that the spliced bars extended from the bottom members be offset inside and the moment strength at the lap splice be calculated using the actual location of the bottom splice bars. Further, to ensure a ductile behavior without splitting failure at a lap splice region, the shear strength of the transverse reinforcement alone needs to be not less than shear demand ($V_s > V_u$) and the spacing of the transverse bars confining the spliced bars should be not greater than $d/2$.

5) Since tensile stresses of spliced bars significantly vary along splice regions in columns, the average bond demand of spliced bars decreases with increasing moment gradient of columns. Thus, a modified lap splice length model for lap-spliced columns considering moment gradient along splice regions was proposed to reduce splice length required in current design codes. The reduced splice length correlated well with the present and existing cyclic test results of columns with lap splices.

8.3 Effects of Joint Reinforcement Details and Shear Strength Model for Exterior Beam-Column Connections (Chapter 4)

Cyclic tests of beam-column connections using small effective joint area were performed to evaluate the effects of joint shear reinforcement ratio, anchorage length of beam bars, U-shaped bars for joint shear reinforcement, and joint types (exterior and interior joints). Based on test results of exterior joints, a shear strength model for exterior joints was empirically presented. The main conclusions were summarized as follows.

1) Seismic performance of exterior joints was mainly affected by joint shear reinforcement ratio and provided anchorage length of beam bars. The maximum joint shear strength was increased proportionally with the increase of joint shear reinforcement ratio. However, when the anchorage length of beam bars was not secured, the joint shear strength was not proportional to joint shear reinforcement due to bond deterioration of beam bars. The exterior joints with relatively large effective joint area improved joint shear behavior due to increased joint shear strength and sufficient anchorage length of beam bars.

2) An alternative joint reinforcement, U-bar, was verified by comparison with the closed tie with 90º hook used in exterior joints. Even after concrete cover spalled off with excessive diagonal shear cracks in the joints, the U-bars fully anchored into adjacent beam could sustain joint shear resistance without anchorage failure.

3) Interior joints with small joint effective areas showed joint shear failure before column flexural yielding, while exterior joints exhibited joint shear failure before/after beam flexural yielding, or anchorage failure of beam bars. The maximum load of an interior joint even without joint shear reinforcement was greater than that of exterior joints with joint shear reinforcement. Further, the interior joints showed maximum loads 23 ~ 70% greater than joint shear strength specified in ASCE 41-13, and deformation capacity more than drift ratio of 3.5 ~ 5.0%.

4) Generally, in low-rise buildings with small column size, such buildings are vulnerable to earthquake because of small effective joint area not satisfying existing seismic design codes. Therefore, sufficient joint shear reinforcement should be used to secure seismic performance of exterior joints. Particularly, since the exterior joints are mainly influenced not only by the joint shear reinforcement ratio, but also by anchorage length of beam bars, it is necessary to consider these two points.

5) The current seismic design codes (ACI 318 or NZS 3101) define joint shear capacity only for the case when the amount of joint shear reinforcement is satisfied with the code requirements. However, according to test results of exterior joints, the joint shear strength was proportionally increased to joint shear reinforcement ratio even when the amount of joint shear reinforcement is less than the code requirements. Thus, a shear strength model for exterior joints was empirically presented, based on present and existing test results of joint specimens only with joint shear failure.

8.4 Effects of Anchorage Details of Beam Reinforcement on Exterior Joints (Chapter 5)

In this chapter, the effect of anchorage directions of beam bottom bars on exterior joint behavior was evaluated by cyclic load tests of exterior beam-column connections. The major test parameters include anchorage directions and anchorage lengths of beam bars and joint shear reinforcement ratio. Exterior connections with only beam bottom bars bent away from the joints were compared to those with both top and bottom beam bars bent inside the joints in Chapter 4. The main conclusions were summarized as follows.

1) Since joint shear forces in exterior joints without shear reinforcement were transmitted only by the diagonal strut mechanism, the joint behaviors were affected by anchorage directions of beam bottom bars. Unreinforced exterior joints with beam bottom bars bent away from the joints were not able to form a node for compression strut, resulting in low joint shear capacity with diagonal shear cracks along hook anchorage direction of beam bottom bars.

2) On the other hand, exterior joints with joint shear reinforcement were not significantly influenced by anchorage directions of beam bottom bars. When joint transverse reinforcement is located close to beam bottom bars, a node for compression strut can be formed in an exterior joint even with beam bottom bars bent away from the joint. Further, joint shear forces are also transferred by a truss mechanism with sufficient joint shear reinforcement and adequate bond stress on beam bars. Thus, the effect of anchorage directions of beam bottom bars is not significant for exterior joints with joint shear reinforcement.

3) Beam bars bent inside an exterior joint are recommended to facilitate force transfer in the joint. If construction is difficult, however, the beam bottom bars can be anchored inside an adjacent confined column with sufficient joint shear reinforcement and anchorage length of beam bars.

8.5 Effects of Alternative Reinforcement Details on Two-Story and Two-bay Frames (Chapter 6)

Two-story and two-bay frame tests were performed to verify the application of reinforcing bar details verified by column tests (Chapters 2 and 3) and beam-column connection tests (Chapters 4 and 5). The overall seismic behavior of low-rise buildings was also investigated in system level whether the buildings were controlled by beam sidesway mechanism or column sidesway mechanism. In additions, the seismic behavior and role of a shear wall in a frame were also examined. Through four frame tests, major findings are summarized as follows.

1) Moment frames without a shear wall showed weak-column and strong-beam behaviors (i.e., column sidesway mechanism). Since flexural strength of beams was designed to be greater than that of columns due to larger size of beams than columns and slab effect, plastic hinges were primarily developed in the 1st columns. In the seismic design of low-rise buildings, therefore, more attention should be paid to the reinforcing bar details of columns than those of beams.

2) Since a final failure mode of frames without a shear wall was severe vertical splitting cracks along splice regions, structural designers should take lap splice length and details of column longitudinal bars into account, especially when lap splices are used at plastic hinge regions. Though shear demand in spliced columns is relatively small in low-rise buildings under earthquake, splice length of column bars ($50d_b$ for SD500 bars) should be sufficiently secured with seismic details and adequate spacing of transverse reinforcement (at least $s \leq d/2$).

3) As moments and shear forces acting on columns and beams are transmitted through joints in beam-column connections, sufficient joint shear reinforcement is required for satisfactory seismic performance of the entire moment frame. However, in joints where column and beam reinforcements are overlapped, it is difficult to place joint shear reinforcement due to steel congestion. Through an alternative detail of U shaped bar, workability can be greatly improved, and satisfactory seismic performance can be ensured.

4) When a shear wall is used in a moment frame building, sliding failure can be occurred horizontally in the upper part of shear wall at top floor. In order to prevent such sliding failure, dowel reinforcement should be additionally provided between a wall and a beam (or a slab) to secure a sufficient shear friction strength. In design of shear walls, consideration should be given not only to vertical shear force but also shear friction strength.

References

Aboutaha, R. S., Engelhardt, M. D., Jirsa, J. O., and Kreger, M. E. (1999). "Experimental Investigation of Seismic Repair of Lap Splice Failures in Damaged Concrete Columns." *ACI Structural Journal*, 96(2), 297-306.

ACI Committee 315. (1999). *Details and Detailing of Concrete Reinforcement*, American Concrete Institute. Farmington Hills, MI.

ACI Committee 318. (2014). *Building Code Requirements for Structural Concrete (ACI 318-14) and Commentary*, American Concrete Institute. Farmington Hills, MI.

ACI Committee 318. (2011). *Building Code Requirements for Structural Concrete (ACI 318-11) and Commentary*, American Concrete Institute. Farmington Hills, MI.

ACI Committee 352. (2002). *Recommendations for Design of Beam-Column Connections in Monolithic Reinforced Concrete Structures*. American Concrete Institute. Farmington Hills, MI.

ACI Committee 374. (2005). *Acceptance Criteria for Moment Frames Based on Structural Testing and Commentary*, American Concrete Institute, Farmington Hills, MI.

AIJ. (2010). *Standard for Structural Calculation of Reinforced Concrete Structures*, Architectural Institute of Japan, Tokyo. Japan.

ASCE/SEI 41-13. (2013). *Seismic Rehabilitation of Existing Buildings*. American Society of Civil Engineers, Reston, VA.

Ascheim, M., and Moehle, J. P. (1992). “Shear Strength and Deformability of RC Bridge Columns Subjected to Inelastic Cyclic Displacements.” *UCB/EERC Rep. 1992/03*, University of California, Berkeley, CA.

Bayhan, B., Moehle, J. P., Yavari, S., Elwood, K. J., Lin, S. H., Wu, C. L., and Hwang, S. J. (2015). “Seismic Response of a Concrete Frame with Weak Beam-Column Joints.” *Earthquake Spectra*, 31(1), 293-315.

Bournas, D. A., Triantafillou, T. C., Zygouris, K., and Stavropoulos, F. (2009). “Textile-reinforced Mortar versus FRP Jacketing in Seismic Retrofitting of RC Columns with Continuous or Lap-spliced Deformed bars.” *Journal of Composites for Construction*, 13(5), 360-371.

Boyes, A., Bull, D. K., and Pampanin, S. (2008). “Seismic Performance of Concrete Columns with Inadequate Transverse Reinforcement.”.

Calvi, G., Magenes, G., and Pampanin, S. (2002). “Experimental Test on a Three Storey Reinforced Concrete Frame Designed for Gravity only.” *12th European Conference on Earthquake Engineering*.

Canbay, E., Ersoy, U., and Ozcebe, G. (2003). “Contribution of Reinforced Concrete Infills to Seismic Behavior of Structural Systems.” *ACI Structural Journal*, 100(5), 637-643.

Cha, B. G., Ko, D. W., Woo, W. S., and Lee, H. S. (2003). “Cyclic Loading Tests of RC Exterior Beam-Column Joints with Non-Seismic Detailing.” *Journal of the Korea Concrete Institute*, 15(1), 11-16.

Chun, S. C., and Shin, Y. S. (2014). “Cyclic Testing of Exterior Beam-Column Joints with Varying Joint Aspect Ratio.” *ACI Structural Journal*, 111(3), 693-704.

Chung, L., and Shah, S. P. (1989). "Effect of Loading Rate on Anchorage Bond and Beam-Column Joints." ACI Structural Journal, 86(2), 132-142.

CSA. (2004). *CSA A23.3-04 Design of Concrete Structures*, Canadian Standard Association, Mississauga, Ontario.

Ehsani, M. R., and Wight, J. K. (1985). "Exterior Reinforced Concrete Beam-to-Column Connections Subjected to Earthquake-type Loading." *ACI Journal Proceedings*, 82(4), 492-499.

ElGawady, M., Endeshaw, M., McLean, D., and Sack, R. (2010). "Retrofitting of Rectangular Columns with Deficient Lap Splices. Journal of Composites for Construction." *Journal of Composites for Construction*, 14(1), 22-35.

Elwood, K. J., and Eberhard, M. O. (2009). "Effective Stiffness of Reinforced Concrete Columns. *ACI Structural Journal*, 106(4), 476-484.

Elwood, K. J., and Moehle, J. P. (2005a). "Drift Capacity of Reinforced Concrete Columns with Light Transverse Reinforcement." *Earthquake Spectra*, 21(1), 71-89.

Elwood, K. J., and Moehle, J. P. (2005b). "Axial Capacity Model for Shear-damaged Columns." *ACI Structural Journal*, 102(4), 578-587.

Elwood, K. J., and Moehle, J. P. (2006). "Idealized Backbone Model for Existing Reinforced Concrete Columns and Comparisons with FEMA 356 Criteria." *Structural Design of Tall and Special Buildings*, 15(5), 553-569.

Esaki, F. (1996). "Reinforcing effect of steel plate hoops on ductility of R/C square columns." *Procedings of 11th World Conference on Earthquake Engineering*.

European Standard EN 1992-1. (2004). *Eurocode 2: Design of Concrete Structures: Part 1-1: General Rules and Rules for Buildings*, European Committee for Standardization. Brussels.

European Standard EN 1998-1. (2004). *Eurocode 8: Design of Structures for Earthquake Resistance*, European Committee for Standardization. Brussels.

FEMA. (1997). *NEHRP Guidelines for the Seismic Rehabilitation of Buildings*. Publication 273, Washington, DC.

FEMA. (2000). *Prestandard and Commentary for the Seismic Rehabilitation of Buildings*. Publication 356, Washington, DC.

Ferguson, P. M., and Krishnaswamy, C. (1971). "Tensile Lap Splices - Part 2: Design Recommendations for Retaining Wall Splices and Large Bar Splices." *Rep. 1971/04*, Univ. of Texas, Austin, TX.

Ghee, A. B., Priestley, MJN., and Paulay, T. (1989). "Seismic Shear Strength of Circular Reinforced Concrete Columns." *ACI Structural Journal*, 86(1), 45-59.

Gill, W. D. (1979). "Ductility of Rectangular Reinforced Concrete Columns with Axial Load." Master thesis, Univ. of Canterbury, Christchurch, New Zealand.

Hakuto, S., Park, R., and Tanaka, H. (2000). "Seismic Load Tests on Interior and Exterior Beam-Column Joints with Substandard Reinforcing Details." *ACI Structural Journal*, 97(1), 11-25.

Harajli, M. (2008). "Seismic Behavior of RC Columns with Bond-Critical Regions: Criteria for Bond Strengthening Using External FRP Jackets." *Journal of Composites for Construction*, 12(1), 69-79.

Haroun, M. A., and Elsanadedy, H. M. (2005). "Fiber-reinforced Plastic Jackets for Ductility Enhancement of Reinforced Concrete Bridge Columns with Poor Lap-splice Detailing." *Journal of Bridge Engineering*, 10(6), 749-757.

Harries, K. A., Ricles, J. M., Pessiki, S., and Sause, R. (2006). "Seismic Retrofit of Lap Splices in Nonductile Square Columns using Carbon Fiber-reinforced Jackets." *ACI Structural Journal*, 103(6), 874-884.

Ichinose, T. (1992). "A Shear Design Equation for Ductile R/C Members." *Earthquake Engineering and Structural Dynamics*, 21(3), 197-214.

Jirsa, J. O. (1991). "Design of Beam-Column Joints for Seismic Resistance." *Special Publication of ACI Journal*, 123, 1-518.

JSCE (2007). *Standard Specifications for Concrete Structures*, Japan Society of Civil Engineers, No.15, Tokyo, Japan.

Kaku, T., and Asakusa, H. (1991). "Bond and Anchorage of Bars in Reinforced Concrete Beam-Column Joints." *Special Publication of ACI Journal*, 123, 401-424.

Kaltakci, M. Y., Ozturk, M., and Arslan, M. H. (2010a). "An Experimental Investigation for External RC Shear Wall Applications." *Natural Hazards and Earth System Sciences*, 10(9), 1941-1950.

Kaltakci, M. Y., Arslan, M. H., and Yavuz, G. (2010b). "Effect of Internal and External Shear Wall Location on Strengthening Weak RC Frames." *Scientia Iranica Transaction a-Civil Engineering*, 17(4), 312-323.

Kaltakci, M. Y., Arslan, M. H., and Yilmaz, U. S. (2011). "Experimental and Analytical Analysis of RC Frames Strengthened Using RC External Shear Walls." *Arabian Journal for Science and Engineering*, 36(5), 721-747.

Kara, M. E., and Altin, S. (2006). “Behavior of Reinforced Concrete Frames with Reinforced Concrete Partial Infills.” *ACI Structural Journal*, 103(5), 701-709.

KBC2016. (2016). *Korean Building Code and Commentary*, Architectural Institute of Korea, Kimoondang.

Kuang, J. S., and Wong, H. F. (2006). “Effects of Beam Bar Anchorage on Beam-Column Joint Behaviour.” *Proceedings of the Institution of Civil Engineers-Structures and Buildings*, 159(2), 115-124.

Kuang, J. S., and Wong, H. F. (2013). “Horizontal Hoops in Non-seismically Designed Beam–column Joints.” *HKIE Transactions*, 20(3), 164-171.

Lam, S., Wu, B., Wong, Y., Wang, Z., Liu, Z., and Li, C. (2003). “Drift Capacity of Rectangular Reinforced Concrete Columns with Low Lateral Confinement and High-axial Load.” *Journal of structural engineering*, 129(6), 733-742.

Lee, C. H., Park, J. H., Kim, T. J., Kim, S. Y., and Kim, D. K. (2016). “Damage Potential Analysis and Earthquake Engineering-related Implications of Sep. 12, 2016 M5.8 Gyeongju Earthquake.” *Journal of the Earthquake Engineering Society of Korea*, 20(7), 527−536.

Lee, J. Y., and Watanabe, F. (2003). “Shear Deterioration of Reinforced Concrete Beams Subjected to Reversed Cyclic Loading.” *ACI Structural Journal*, 100(4), 480-489.

Lee, Y. W., Park, H. G., and Choi, D. B. (2009). “An Experiment to Enhance the Deformation Capacity of RC Exterior Joint with the Non-seismic Detials.” *Journal of the Architectural Institute of Korea*, 25(8), 27-34.

Lehman, D. E., and Moehle, J. P. (1998). “Seismic Performance of Well-Confined Concrete Bridge Columns.” *PEER-1998/01, Pacific Earthquake Engineering*

Research Center, Univ. of California, Berkeley, CA, 316 pp.

Lukkunaprasit, P., and Sittipunt, C. (2003). "Ductility Enhancement of Moderately Confined Concrete Tied Columns with Hook-clips." *ACI Structural Journal*, 100(4), 422-429.

Lynn, A. C., Moehle, J. P., Mahin, S. A., and Holmes, W. T. (1996). "Seismic Evaluation of Existing Reinforced Concrete Building Columns." *Earthquake Spectra*, 12(4), 715-739.

Melek, M., and Wallace, J. W. (2004). "Cyclic Behavior of Columns with Short Lap Splices." *ACI Structural Journal*, 101(6), 802-811.

Mo, Y. L., and Wang, S. J. (2000). "Seismic Behavior of RC Columns with Various Tie Configurations." *Journal of Structural Engineering*, 126(10), 1122-1130.

Moehle, J. P., and Cavanagh, T. (1985). "Confinement Effectiveness of Crossties in RC." *Journal of structural engineering*, 111(10), 2105-2120.

Muguruma, H., Watanabe, F., and Komuro, T. (1989). "Applicability of High Strength Concrete to Reinforced Concrete Ductile Column." *Transactions of the Japan Concrete Institute*, 11(1), 309-316.

Murty, C., Rai, D. C., Bajpai, K., and Jain, S. K. (2003). "Effectiveness of Reinforcement Details in Exterior Reinforced Concrete Beam-column Joints for Earthquake Resistance." *ACI Structural Journal*, 100(2), 149-156.

Nagasaka, T. (1982). "Effectiveness of Steel Fiber as Web Reinforcement in Reinforced Concrete Columns." *Transactions of the Japan Concrete Institute*, 4, 493-500.

NRC. (2005). *National Building Code of Canada and Commentary*, National research Council of Canaada, Ottawa, Ontario.

Ono, A., Shirai, N., Adachi, H., and Sakamaki, Y. (1989). "Elasto-plastic Behavior of Reinforced Concrete Column with Fluctuating Axial Force." *Transactions of the Japan Concrete Institute*, 11, 239-246.

Park, H. G., Yu, E. J., and Choi, K. K. (2012). "Shear-strength Degradation Model for RC Columns Subjected to Cyclic Loading." *Engineering Structures*, 34, 187-197.

Park, R. (1997). "A Static Force-based Procedure for the Seismic Assessment of Existing Reinforced Concrete Moment Resisting Frames." *Bulletin of the New Zealand National Society for Earthquake Engineering*, 30(3), 213-226.

Park, S., and Mosalam, K. M. (2012). "Analytical Model for Predicting Shear Strength of Unreinforced Exterior Beam-column Joints." *ACI Structural Journal*, 109(2), 149-160.

Paulay, T. (1982). "Lapped Splices in Earthquake-resisting Columns." *ACI Journal Proceedings*, 79(6), 458-469.

Paulay, T., Park, R., and Preistley, M. (1978). "Reinforced Concrete Beam-Column Joints under Seismic Actions." *ACI Journal Proceedings*, 75(11), 585-593.

Paulay, T., and Priestly, MJN. (1992). *Seismic Design of Reinforced Concrete and Masonry Buildings*, John Wiley & Sons.

Priestley, MJN. (1997). "Displacement-based Seismic Assessment of Reinforced Concrete Buildings." *Journal of Earthquake Engineering*, 1(01), 157-192.

Priestley, MJN., Verma, R., and Xiao, Y. (1994). "Seismic Shear-Strength of Reinforced-Concrete Columns." *Journal of Structural Engineering*, 120(8), 2310-2327.

Saatcioglu, M., and Ozcebe, G. (1989). "Response of Reinforced-Concrete Columns to Simulated Seismic Loading." *ACI Structural Journal*, 86(1), 3-12.

Sakai, Y., and Kyōkai, N. K. K. (1990). "Experimental Studies on Flexural Behavior of Reinforced Concrete Columns Using High-strength Concrete" *Transactions of Japan Concrete Institute*.

Scott, R. H. (1996). "Intrinsic Mechanisms in Reinforced Concrete Beam-Column Connection Behavior." *ACI Structural Journal*, 93(3), 1-11.

Setzler, E. J., and Sezen, H. (2008). "Model for the Lateral Behavior of Reinforced Concrete Columns including Shear Deformations." *Earthquake Spectra*, 24(2), 493-511.

Sezen, H. (2002). "Seismic Behavior and Modeling of Reinforced Concrete Building Columns." Ph.D. dissertation, Univ. of California, Berkeley, CA.

Sezen, H., and Moehle, J. P. (2004). "Shear Strength Model for Lightly Reinforced Concrete Columns." *Journal of Structural Engineering*, 130(11), 1692-1703.

Sezen, H., and Moehle, J. P. (2006). "Seismic Tests of Concrete Columns with Light Transverse Reinforcement." *ACI Structural Journal*, 103(6), 842-849.

Shiohara, H. (2001). "New Model for Shear Failure of RC Interior Beam-column Connections." *Journal of structural engineering*, 127(2), 152-160.

Soesianawati, M.T. (1986). "Limited Ductility Design of Reinforced Concrete Columns." Master thesis, Univ. of Canterbury, Christchurch, New Zealand.

Sozen, M., Monteiro, P., Moehle, J., and Tang, H. (1992). "Effects of Cracking and Age on Stiffness of Reinforced Concrete Walls Resisting in-Plane Shear." *Proceedings of the 4th Symposium on Current Issues Related to Nuclear Power Plant Structures, Equipment and Piping,* Orlando, FL.

Standards New Zealand. (2004). *Structural Design Actions, Part 5: Earthquake Actions, NZS 11705:2004*, Wellington, New Zealand.

Standards New Zealand. (2006). *Concrete Structures Standard, NZS 3101*, Wellington, New Zealand.

Tanaka, H. (1990). "Effect of Lateral Confining Reinforcement on the Ductile Behaviour of Reinforced Concrete Columns." Ph.D. dissertation, Univ. of Canterbury, Christchurch, New Zealand.

Tsonos, A. G., Tegos, I. A., and Penelis, G. G. (1992). "Seismic Resistance of Type-2 Exterior Beam-Column Joints Reinforced with Inclined Bars." *ACI Structural Journal*, 89(1), 3-12.

Wight, J. K., and Sozen, M. A. (1973). "Shear Strength Decay in Reinforced Concrete Columns Subjected to Large Deflection Reversals." *Rep. 1973/08*, Univ. of Illinois, Urbana-Champaign, IL.

Wong, H. F., and Kuang, J. S. (2008). "Effects of Beam-column Depth Ratio on Joint Seismic Behaviour." *Proceedings of the Institution of Civil Engineers-Structures and Buildings*, 161(2), 91-101.

Wu, C. L., Kuo, W. W., Yang, Y. S., Hwang, S. J., Elwood, K. J., Loh, C. H., and Moehle, J. P. (2009). "Collapse of a Nonductile Concrete Frame: Shaking Table Tests." *Earthquake Engineering & Structural Dynamics*, 38(2), 205-224.

Hwang, S. J., Lee, H. J., Liao, T. F., Wang, K. C., and Tsai, H. H. (2005). Role of hoops on shear strength of reinforced concrete beam-column joints. *ACI Structural Journal*, 102(3), 445-453.

Hwang, S. J., and Lee, H. J. (1999). "Analytical Model for Predicting Shear Strengths of Exterior Reinforced Concrete Beam-column Joints for Seismic Resistance." *ACI Structural Journal*, 96(5), 846-858.

Appendix

Methods for predicting flexural and shear deformations using LVDT measurements

1. Column (Wall) deformations

In order to predict deformations in column (wall) plastic hinge zone, LVDTs can be installed and measured as show in Fig. A-1(a) and Fig. A-2(a). In Fig. A-1(a), the rotational angle (θ_P) at plastic hinge region was estimated from the horizontal displacement (Δ_P) measured at the end of plastic hinge zone, and the shear distortion (γ) was measured by the diagonal displacement values in the plastic hinge zone. However, such method cannot directly measure column bar slip rotation (deformation). On the other hand, the method in Fig. A-2(a) can measure column bar slip deformation, flexural deformation, and shear deformation, individually. The bar slip deformation is obtained by using the rotation angle (θ_A) measured at the point A adjacent to the interface, and the flexural deformation can be obtained by subtracting the rotation angle of the point A from the rotation angle measured at the point B ($\theta_B - \theta_A$). If the rotation angles at points C and D are measured, more accurate flexural deformations can be predicted, but such rotation angles are relatively smaller than the rotation angle at point B, and most deformation concentrates in the plastic hinge zone.

As shown in Fig. A-3, the shear distortion of the plastic hinge zone is calculated using the displacements (δ_1 and δ_2) measured in the diagonal direction, and the lengths of the LVDT (a and b) installed in the horizontal and vertical directions.

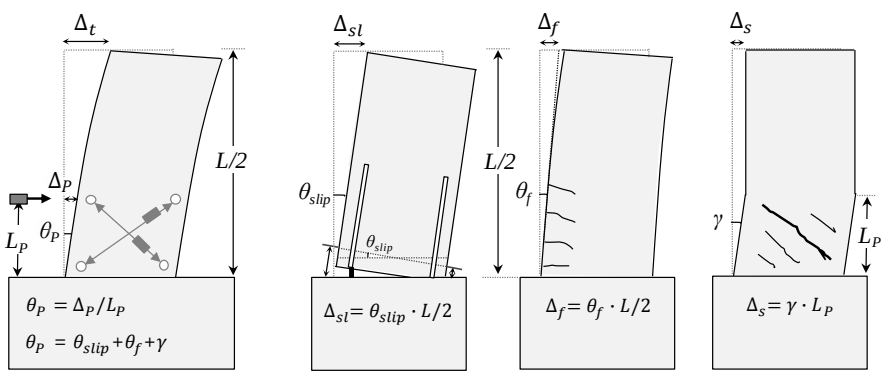

(a) LVDT measurements (b) Bar slip rotation (c) Flexural rotation (d) Shear distortion

Figure A-1 Measuring method of column deformations

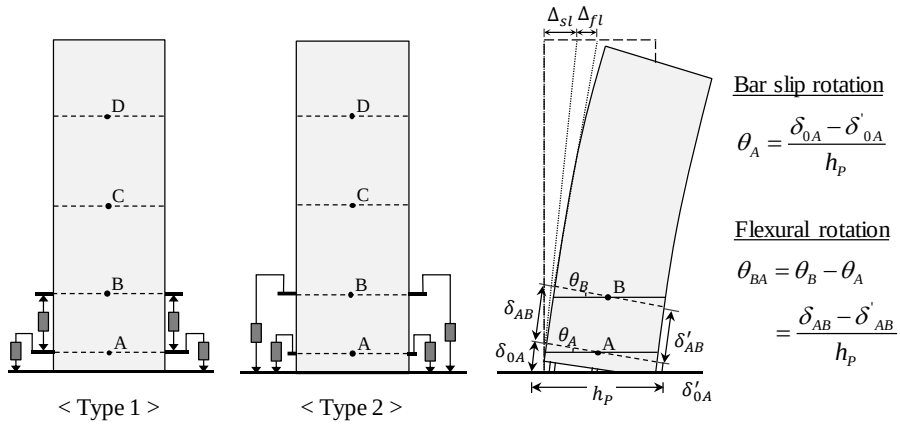

(a) LVDT for flexure and bar slip deformations (b) Flexural and bar slip rotations

Figure A-2 Measuring method of column bar slip and flexural deformations

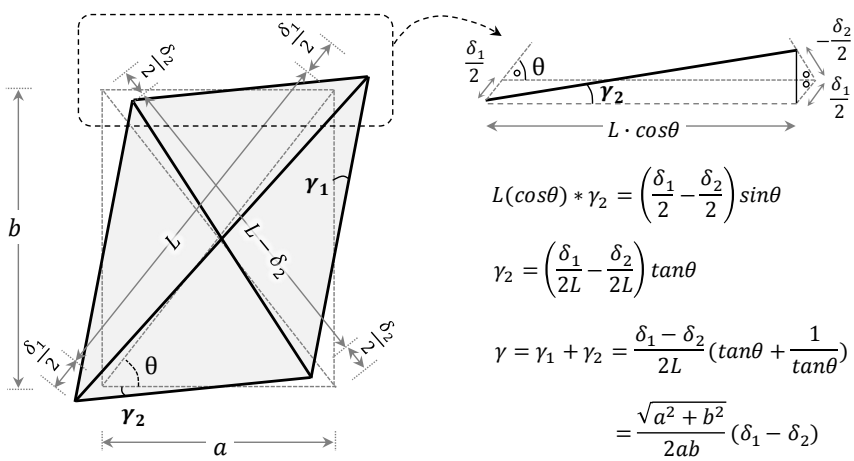

Figure A-3 Measurement of shear distortion

초 록

층수 2층 이하의 소규모 건축물은 국내 전체 건물 동수의 약 80% 이상을 차지하고 있으나, 구조 전문가에 의한 내진 설계나 구조 성능에 대한 구체적인 검토 없이 설계되는 경우가 많아 지진 발생시 큰 피해가 발생할 수 있다. 2016년 9월 12일 경주에서 발생한 지진은 국내 기상청 관측 이래 가장 큰 규모(리허터 규모 5.8)로, 지진파의 에너지가 고주파수 대역에 집중되어 내진설계가 안된 소규모 건축물에 피해가 주로 집중되었다. 경주지진 발생 이후 소규모 건축물의 내진설계에 대한 관심이 높아짐에 따라, 2017년 2월에 내진설계 대상 건물에 대한 건축법 시행령이 변경되었다. 내진설계 대상 건물의 범위가 층수 3층 이상이거나 연면적 1000 m^2 이상 건축물에서 층수 2층 이상이거나 연면적 500 m^2이상 건축물로 확대되었다. 또한, 내진설계 대상 소규모 건축물은 일반 건축물에 적용되는 건축구조기준(KBC 2016)이나 소규모 건축물에만 적용되는 소규모 건축구조기준 중 선택적으로 적용할 수 있도록 하였다. 하지만, 현행 소규모 건축구조기준은 비구조전문가가 별도의 구조계산없이 부재의 철근 상세를 결정할 수 있도록 제정되었고, 철근 상세는 일반 건축물에 적용되는 복잡한 KBC의 철근 상세를 그대로 따르고 있다. 이러한 복잡한 철근 상세는 시공 관리가 제대로 이뤄지지 않는 소규모 건축물에서 준수되지 않는 경우가 많고, 소규모 건축물의 구조 특성상 KBC의 내진 철근 상세보다 완화된 비내진 철근 상세를 주로 사용된다. 따라서, 본 논문에서는 소규모 건축물의 구조안전성과 시공성 향상을 위해 소규모 건축물의 특징을 반영한 철근 상세를 개발하였고, 다양한 대안 철근 상세의 내진성능을 실험적으로 검증하였다.

본 논문의 주요 목적은 소규모 콘크리트 건축물에 특화된 철근 상세의 내진성능과 적용성 검증으로, 기둥, 보-기둥 접합부, 2층 2경간 골조에 대한 반복가력실험을 수행하였다. 소규모 건축물의 목표 내진성능 수준은 제한된 연성능력을 가지는 KBC의 중간 모멘트 골조 수준으로 정하였다. 대안 철근 상세와의 성능 비교를 위해, 현행 설계 기준의 내진 철근 상세와 현장에서 성능 검증 없이 무분별하게 사용되는 비내진 철근 상세도 함께 고려하였다. 다양한 실험결과를 바탕으로 소규모 건축물의 내진설계시 각 부재별 설계 주의 사항 및 대안 철근 상세를 제시하였고, 실험결과 분석과정에서 개발된 기둥과 보-기둥 접합부에 대한 해석 모델도 함께 논의하였다. 실험 및 해석 연구를 통해 얻은 주요 결론은 다음과 같다.

소규모 콘크리트 건축물은 기둥에 작용하는 중력하중이 크지 않기 때문에 기둥 단면 크기가 일반 건축물에 비해 작다. 따라서, 소규모 건축물은 지진 발생시 약기둥-강보 거동을 보일 수 있으며, 기둥 단부에서 소성힌지가 먼저 발생할 가능성이 크기 때문에 기둥 횡철근 상세가 중요하다. 이에 다양한 기둥 횡철근 상세(135도 갈고리, 90도 갈고리, 대안상세)와 횡철근 간격(s = d/2, d/3, d/4)을 변수로 정사각형 기둥과 직사각형 기둥 반복 가력 실험을 수행하였다. 실험 결과, 횡철근 갈고리가 내부 콘크리트에 정착이 된 상세(135도 갈고리와 갈고리 정착되는 U-bar)는 피복 콘크리트 탈락 이후에도 충분한 변형능력을 보였지만, 90도 갈고리와 이음된 횡철근 상세는 피복 탈락 이후 횡철근 풀림에 의해 상대적으로 낮은 변형능력을 보였다. 또한, 기둥의 변형능력은 횡철근에 의한 전단강도 V_s와 요구전단력 V_u의 비에 큰 영향을 받았다. V_s / V_u가 1.0보다 작은 기둥은 휨 항복 이후 급격히 하중이 감소하면서 전단파괴가 발생하였지만, V_s / V_u가 1.0보다 큰 기둥은 휨 항복 이후 횡철근이 대각균열을 억제하면서 큰 연성 능력을 보였다. 이는 콘크리트에 의한 전단강도 V_c가 전단변형이 증가함에 따라 서서히 감소하기 때문에 비탄성 변형에서의 전단강도는 V_s에 큰 영향을 받았다. 이를 바탕으로, 기둥의 전단강도 감소 모델을 제안하였고, 본 연구 및 기존 실험결과 자료를 통해 제안된 모델을 검증하였다.

소규모 건축물에서는 소성변형이 크게 발생하는 기둥 하부에 주로 겹침 이음이 사용되기 때문에 기둥 주근의 이음길이 및 이음상세는 하중재하능력, 연성능력, 에너지소산능력 등 기둥의 내진성능을 종합적으로 고려하여 결정되어야 한다. 이에 기둥 주근의 다양한 이음길이 (l_s = 30d_b ~ 50d_b)와 이음상세 (하부 오프셋철근 이음, 상부 오프셋철근 이음, 무절곡 이음상세)를 주요 변수로 기둥 반복 가력 실험을 수행하였다. 현행 이음길이 기준을 만족하는 기둥 (l_s = 50d_b)은 휨 항복 이후에도 충분한 연성능력을 보였지만, 이음길이가 40d_b와 30d_b로 감소함에 따라 이음구간에서 발생하는 기둥 주근의 부착파괴(쪼갬 균열)에 의해 내진 성능이 감소하였다. 또한, 기둥 주근의 이음상세에 따라 내진성능 차이를 보였다. 하부 오프셋철근 이음 기둥은 상대적으로 낮은 휨강도를 보였지만, 연성능력과 에너지소산능력은 뛰어났다. 그에 반해, 상부 오프셋철근 이음과 무절곡 이음 기둥은 상대적으로 높은 휨강도를 보였지만, 낮은 연성능력과 에너지 소산능력을 보였다. 기둥 주근의 이음구간에는 횡력에 의한 모멘트 기울기가 발생하기 때문에 일정한 모멘트가 작용하는 이음구간 (보 주근 이음 실험)에 비해 평균 부착 요구량이 작다. 이를 반영하기 위해 모멘트 기울기를 고려한 기둥 주근의 이음길이 모델을 개발하였고, 본 연구 및 기존 실험결과 자료로 제안된 모델을 검증하였다.

일반적으로 기둥 크기가 작은 소규모 건축물은 작은 보-기둥 조인트 크기에 의해 조인트 전단강도가 작으므로 보 또는 기둥이 휨 항복하기 전 조인트 전단파괴가 발생할 수 있다. 또한, 보 주근의 90도 갈고리 정착길이 확보가 어렵기 때문에 소규모 건축물 설계시 조인트 철근상세에 주의해야 한다. 본 연구에서는 작은 조인트 크기를 가지는 보-기둥 접합부 반복가력 실험을 통해 조인트 전단철근량, 보 주근 정착길이, 조인트 형상(내부/외부)의 영향을 살펴보았고, 대안상세인 U형 전단철근의 성능을 실험적으로 검증하였다. 외부 조인트 전단강도는 조인트 전단철근량에 따라 비례적으로 증가하였지만, 보 주근의 정착길이가 짧은 경우는 부착파괴에 의해 조인트 강도가 결정되었다. 조인트 크기가 증가한 접합부는 조인트 전단강도와 보 주근 정착길이가 증가함에 따라 조인트 내진성능이 향상되었다. 또한, 조인트 전단파괴가 발생한 외부 접합부 실험결과를 바탕으로 조인트 전단철근비를 반영한 조인트 전단강도 모델을 제안하였다.

외부 조인트에 정착되는 보 주근 갈고리 방향이 접합부 거동에 미치는 영향을 살펴보기 위해 보 하부 주근이 조인트 외부에 정착되는 접합부와 조인트 내부에 정착되는 접합부를 비교하였다. 조인트 무횡보강 접합부는 대각 스트럿 메커니즘에 의해 조인트 전단력이 전달되기 때문에 보 하부 주근 갈고리 방향에 영향을 크게 받았다. 그에 반해, 조인트 횡보강 접합부는 대각 스트럿 메커니즘뿐만 아니라 트러스 메커니즘에 의해 전단력이 전달되기 때문에 보 하부 주근 갈고리 방향이 미치는 영향은 미비하였다. 따라서, 조인트 전단철근과 보 주근 정착길이가 충분한 접합부에서는 보 하부 주근을 횡보강된 기둥으로 정착할 수 있다.

기둥과 접합부 실험을 통해 검증된 철근 상세와 횡하중 작용시 소규모 건축물의 시스템 수준에서의 거동을 평가하기 위해 2층 2경간 골조 실험을 수행하였다. 또한, 골조와 함께 사용되는 전단 벽체의 성능과 역할을 살펴보기 위해 전단 벽체 보강 골조 실험도 함께 수행하였다. 실험결과를 살펴보면, 전단 벽체가 없는 골조는 1층 양단부에 소성힌지가 발생하였고, 최종적으로 약기둥-강보 거동을 보이면서 기둥 주근의 이음부에서 쪼갬 균열과 함께 부착 파괴가 발생하였다. 외부 조인트는 U형 전단철근 보강으로 만족스러운 내진성능을 보였다. 전단 벽체가 보강된 골조는 2층 벽체 상부에서 예상치 못한 수평 미끄러짐 파괴가 발생하여 예상 하중에 도달하기 전 취성파괴가 발생하였다. 이러한 수평 파괴를 막기위해서는 2층 벽체와 보 사이에 추가적인 다우얼 철근을 배근하여야 한다.

본 학위 논문에서는 소규모 건축물에 특화된 대안 철근 상세를 검증하기 위해 다양한 부재실험 (기둥 30개와 접합부 14개) 및 2층 2경간 골조실험 (4개)을 수행하였고, 실험결과를 바탕으로 기둥 및 접합부에 대한 해석 모델을 개발하였다. 또한, 새롭게 개정되는 소규모 건축구조기준에 반영할 주요 부재들의 철근 대안 상세에 대한 설계기준 및 해설을 제시하였다.

주요어 : 소규모 건축물; 대안 철근 상세; 제한된 연성상세; 띠철근 상세; 겹침 이음; 조인트 횡보강; 보 주근 정착상세; 2층−2경간 골조

학 번 : 2013-30931